Tony L. Schmitz
K. Scott Smith

Mechanical Vibrations

Modeling and Measurement

Second Edition

Springer

Mechanical Vibrations

Tony L. Schmitz • K. Scott Smith

Mechanical Vibrations

Modeling and Measurement

Second Edition

Springer

Tony L. Schmitz
Mechanical, Aerospace, and
Biomedical Engineering
University of Tennessee, Knoxville
Knoxville, TN, USA

K. Scott Smith
Manufacturing Demonstration Facility
Machining and Machine Tools Research Group
Oak Ridge National Laboratory
Knoxville, TN, USA

ISBN 978-3-030-52343-5 ISBN 978-3-030-52344-2 (eBook)
https://doi.org/10.1007/978-3-030-52344-2

This Springer imprint is published by the registered company Springer Nature Switzerland AG
The registered company address is: Gewerbestrasse 11, 6330 Cham, Switzerland

To our children, Jake, BK, Kellye, and Kyle

Preface

In this second edition textbook, we describe essential concepts in the vibration analysis of mechanical systems. The book incorporates the fundamentals of modal analysis, beam theory, and finite element analysis, as well as the required mathematics and experimental techniques, into a unified framework that is written to be accessible to undergraduate students, researchers, and practicing engineers alike. This book is based on undergraduate courses in mechanical vibrations that we have previously offered and developed the text to be applied in a traditional 15-week course format. It is appropriate for undergraduate engineering students who have completed the basic courses in mathematics (through differential equations) and physics and the introductory mechanical engineering courses including statics, dynamics, and mechanics of materials.

We organized the book into ten chapters. The chapter topics are summarized here.

- Chapter 1—We introduce the types of mechanical vibrations, damping, and periodic motion.
- Chapter 2—We explore topics in single degree of freedom free vibration, including the equation of motion, the damped harmonic oscillator, and unstable behavior.
- Chapter 3—We introduce single degree of freedom forced vibration and discuss the frequency response function, rotating unbalance, base motion, and the impulse response.
- Chapter 4—We extend the analysis in Chap. 2 to consider two degrees of freedom free vibration. This includes the eigensolution for the equations of motion and modal analysis.
- Chapter 5—We extend the analysis in Chap. 3 to consider two degrees of freedom forced vibration. We describe complex matrix inversion, modal analysis, and the dynamic absorber.
- Chapter 6—We analyze model development by modal analysis. This incorporates the peak picking approach for identifying modal parameters from a system frequency response measurement and mode shape measurement.

- Chapter 7—We describe frequency response function measurement techniques. Impact testing is highlighted.
- Chapter 8—The topic of this chapter is continuous beam modeling. We develop closed-form frequency response function expressions for transverse beam vibration, torsion vibration, and axial vibration of beams.
- Chapter 9—We provide an introduction to finite element analysis. Beam models for axial and transverse vibration are derived and implemented; this includes the mass and stiffness matrices. Examples are provided to evaluate model convergence as elements are added. This chapter is new to the second edition.
- Chapter 10—We introduce the concept of receptance coupling, where frequency response functions (receptances) are coupled to predict assembly dynamics.

To demonstrate and unify the various concepts, the beam experimental platform (BEP) is used throughout the text. Engineering drawings for the BEP are included in Appendix A, so that instructors can provide their own demonstrations in the classroom. Additionally, MATLAB® programming solutions are integrated into the text through many numerical examples.

Special features of the book include: (1) MATLAB® MOJO code examples; (2) *By the Numbers* numerical solutions; (3) problems and solutions, including MATLAB® code; (4) non-mathematical *In a Nutshell* explanations that summarize selected concepts in layman's terms; and (5) discussions and numerical examples of model uncertainty.

We conclude by acknowledging the many contributors to this text. They naturally include our instructors, colleagues, collaborators, and students. Among these, we would like to particularly recognize the contributions of J. Tlusty, M. Davies, T. Burns, J. Pratt, and H.S. Kim.

Knoxville, TN Tony L. Schmitz
Knoxville, TN K. Scott Smith
April 2020

Contents

Chapter 1
Introduction

> The last thing one discovers in composing a work is what to put first.
> —Blaise Pascal

1.1 Mechanical Vibrations

The subject of mechanical vibrations deals with the oscillating response of elastic bodies to disturbances, such as an external force or other perturbation of the system from its equilibrium position. All bodies that possess mass and have finite stiffness are capable of vibrations. While some vibrations are desirable, such as the "silent ring" mode for cell phones, it is often the engineer's objective to reduce or eliminate vibrations. Examples include:

- automobile vibrations, which can lead to passenger discomfort
- building vibrations during earthquakes
- bridge vibrations due to high winds
- cutting tool vibrations during machining operations
- print head vibrations during additive manufacturing.

In a Nutshell
Vibration can be thought of as a periodic exchange of potential and kinetic energy (stored energy and the energy of motion). All mechanical systems that vibrate have mass and stiffness. The mass is the part of the system that relates force and acceleration. When the mass is in motion, the system has kinetic energy. The stiffness is the part of the system that relates force and displacement. When the stiffness element is displaced, the system has potential energy. All real physical systems also possess damping, which is the part of the system that dissipates energy. Damping may be caused by friction between moving elements, flow of a fluid through a restriction, or other means, but whatever the source damping converts kinetic and potential energy into heat, which is lost.

(continued)

T. L. Schmitz, K. S. Smith, *Mechanical Vibrations*,
https://doi.org/10.1007/978-3-030-52344-2_1

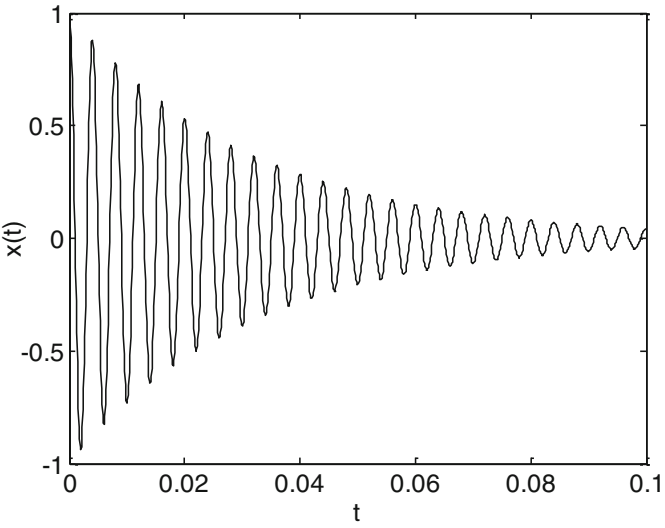

Fig. 1.1 Example of free vibration. The magnitude of the oscillating motion decays over time and the periodic vibration occurs at the natural frequency

During vibration, energy is periodically transformed back and forth between kinetic and potential until all the energy is lost through damping.

1.2 Types of Vibrations

Mechanical vibrations can be classified into three general categories. These are: **free vibration**, **forced vibration**, and **self-excited vibration** (or **flutter**). In the following paragraphs, the three vibration types are described in more detail.

1.2.1 Free Vibration

Free vibration is encountered when a body is disturbed from its equilibrium position and a corresponding vibration occurs. However, there is no long-term external force acting on the system after the initial disturbance. When describing the motion of a vibrating body that can be modeled as a simple spring-mass-damper system, for example, free vibration results when some initial conditions are applied, such as an initial displacement or velocity, to obtain the solution to its homogeneous second-order differential equation of motion [1].

Free vibration is observed as an exponentially-decaying, periodic response to the initial conditions as shown in Fig. 1.1. This periodic motion occurs at the system's

(damped) natural frequency. We will discuss these concepts in more detail in Sect. 2.4. A good example of free vibration is the motion and resulting sound of a guitar string after it is plucked. The pitch of the sound (the natural frequency of vibration) depends on the string's length and diameter; a shorter string produces a higher natural frequency for a selected diameter, while a larger diameter string produces a lower natural frequency for a given length. The pitch also depends on the tension in the string; tighter strings produce higher frequencies.

1.2.2 Forced Vibration

In this case, a continuing periodic excitation is applied to the system. After some initial transients (i.e., the homogeneous solution to the differential equation), the system reaches steady-state behavior (i.e., the particular solution). At steady state, the system response resembles the forcing function and the vibrating frequency matches the forcing frequency.

A special situation arises when the forcing frequency is equal to the system's natural frequency. This results in the largest vibration magnitude (for the selected force magnitude) and is referred to as **resonance**. Unlike free vibration, where the response of the system to the initial conditions is typically plotted as a function of time, forced vibration is most often described as a function of the forcing frequency. See Fig. 1.2, where the peak corresponds to resonance.

Rotating unbalance represents a common type of forced vibration. Consider a wheel/tire assembly on an automobile, for example. If the mass of the wheel/tire is

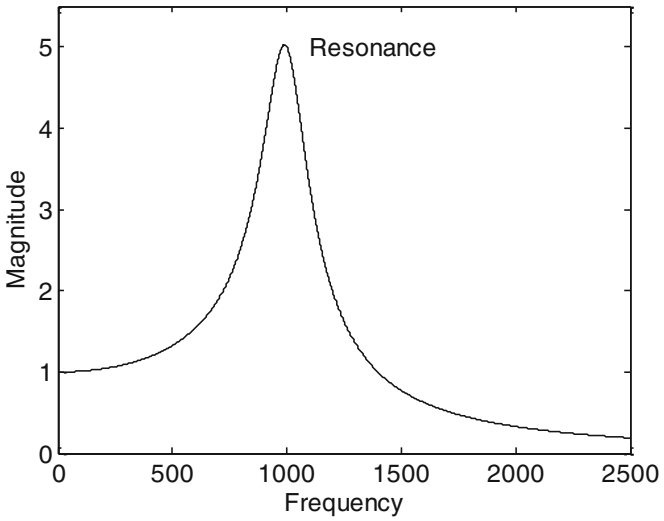

Fig. 1.2 Forced vibration is often described in the frequency-domain, rather than the time-domain. Resonance is identified where the forcing frequency is equal to the natural frequency

not distributed evenly around the circumference, then a once-per-revolution forcing function is produced by the unbalanced mass. This periodic forcing function (whose frequency depends on the rotating speed of the wheel/tire) can serve to excite one of the car frame or drive train natural frequencies and can lead to significant vibration magnitude. For this reason, it is common practice to balance wheel/tire assemblies before installing them on a vehicle. We will discuss rotating unbalance more in Sect. 3.5.

In a Nutshell
Almost all forced vibrations are man-made. The vibration persists as long as the excitation is present. When the excitation stops, the vibration becomes a free vibration and dies away due to damping. Many readers will be intuitively familiar with the frequency-dependent nature of forced vibrations and the concept of resonance. If the automobile with the unbalanced tire is driven very slowly, then vibration is not felt. As the car speeds up, the amplitude of the vibration increases, but if the driver continues to increase the speed, then after a certain speed, the vibration amplitude diminishes. The largest vibration amplitude occurs at resonance. As another example, shower singers may have noticed that there is a particular note that is very loud when singing in a shower stall. That frequency corresponds to a resonance of the enclosure.

1.2.3 Self-Excited Vibration

Self-excited vibration, or flutter, occurs when a steady input force is modulated into vibration at the system's natural frequency. An intuitive example is whistling. Here, the steady blowing of air across your lips produces sound (vibration) at a frequency which depends on the tension in your lips (which governs the natural frequency). The diaphragm does not move at the high frequency of the sound, but rather the steady push of air is converted into a vibration of the "structure". Similarly, the steady pull of the bow across a violin string causes sound at the string's natural frequency (which, like the guitar example, depends on the string's length, diameter, and tension).

In a Nutshell
The rosin on a violin bow has an interesting characteristic—the coefficient of friction between the bow and the string changes depending on the relative velocity between them. When the string and the bow move in the same direction, the relative velocity is low and the coefficient of friction is high. Energy is put into the string motion during this phase. When the string and the bow move in opposite directions, the relative velocity is high, and the

(continued)

coefficient of friction is low. Less energy is lost here than was input during the first part of the motion and the difference is enough to sustain the vibration over the damping losses.

This behavior differentiates self-excited vibrations from both free and forced vibrations. Unlike free vibration, a long-term external force is present. Contrary to forced vibration, the excitation in a self-excited vibration is steady rather than periodic and the vibration occurs near the natural frequency. An example time-domain response for self-excited vibration is provided in Fig. 1.3.

The term **flutter** is based on the common presence of self-excited vibrations in aeroelastic applications. It occurs due to the air (fluid) flow over wings during flight. This steady flow is modulated into vibration near the wing's natural frequency. This vibration can be minor (a small magnitude vibration manifested as in-flight "buzz") or can be catastrophic in extreme cases. The phenomenon is not limited to aircraft structures, however. A well-known example is the destruction of the Tacoma Narrows Bridge on November 7, 1940 in Washington state [2].

Another common example of self-excited vibration is **chatter** in machining processes. Chatter in milling occurs when the steady forced excitation caused by the teeth impacting the workpiece (and removing material in the form of small chips) is modulated into vibration at the system's natural frequency. This modulation can occur due to the inherent feedback mechanism which is present in milling. The feedback is the result of the dependence of the thickness of the chip being removed on not only the tool's current vibration state, but also on the vibration state of the

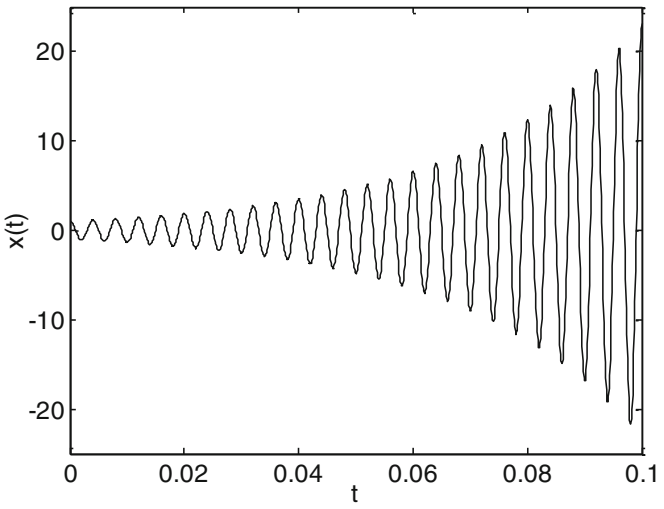

Fig. 1.3 The magnitude of self-excited vibration can increase over time until limited in some way (typically by a nonlinear effect). The oscillating frequency is close to the system's natural frequency

previous tooth when removing material at the same angular location. Because the cutting force is proportional to the chip thickness, the variable chip thickness causes variation in the cutting force. This force variation, in turn, also affects the corresponding tool vibration. This phenomenon is referred to as "regeneration of waviness" and results in a time-delayed differential equation of motion for milling. If chatter occurs, the resulting large forces and vibrations can lead to poor surface finish and damage to the tool, workpiece, and/or spindle [3].

In a Nutshell
The three classes of vibration are distinguished not by the physical characteristics of the vibrating components, but rather by the nature of the excitation and the character of the resulting motion. Vibration problems have different solutions depending on the class. For example, free vibration problems are often solved by modifying the initial conditions or by increasing the damping so that the transient vibration attenuates more quickly. Forced vibration problems are often solved by reducing the external excitation or changing the system so that the excitation is not close to resonance. Self-excited vibration problems are often solved by disturbing or eliminating the self-excitation mechanism. Table 1.1 summarizes the three vibration types.

1.3 Damping

All vibrating systems are subject to **damping**, or energy dissipation due to fluid motion, friction at contacting surfaces, or other mechanisms. This causes the response to decay over time for free vibration. In forced vibration, the input force must overcome the damping in order to sustain the constant magnitude response. We will discuss types of damping and their mathematical models in more detail in Sect. 2.4.

1.4 Modeling

As noted previously, it is often the responsibility of the engineer to model vibrating systems to determine their response to arbitrary inputs or decide how to modify a structure to mitigate the effects of a particular forcing function. Regardless, each system requires a certain number of independent coordinates to adequately describe its motion. These coordinates are the **degrees of freedom**.

For a particle in three-dimensional space, three coordinates are necessary—one for each of the three translation directions. A rigid body, on the other hand, requires six degrees of freedom to describe its motion: three translations and three rotations. See Fig. 1.4.

Table 1.1 Vibration classification

Vibration class	Excitation	Frequency of resulting motion	Characteristic
Free vibration	Initial conditions	(Damped) natural frequency	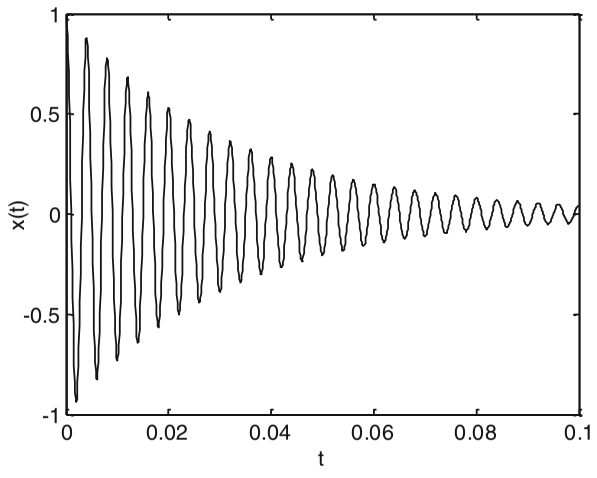
Forced vibration	Persistent, periodic external source	Frequency of the external source	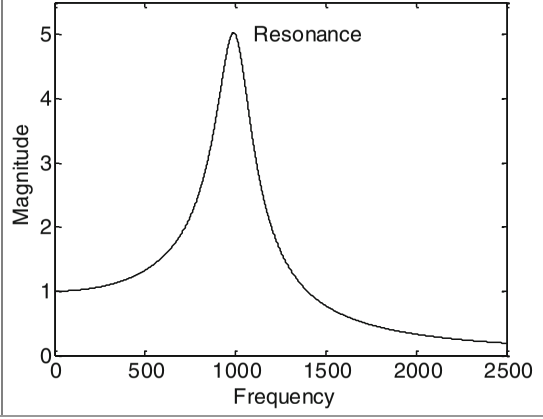

(continued)

Table 1.1 (continued)

Vibration class	Excitation	Frequency of resulting motion	Characteristic
Self-excited vibration	Persistent, steady external source	Self-selected and usually close to the natural frequency	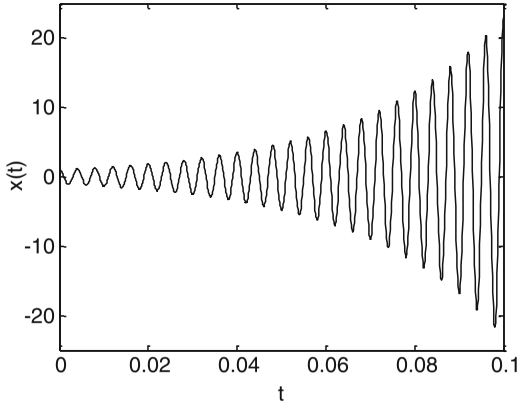

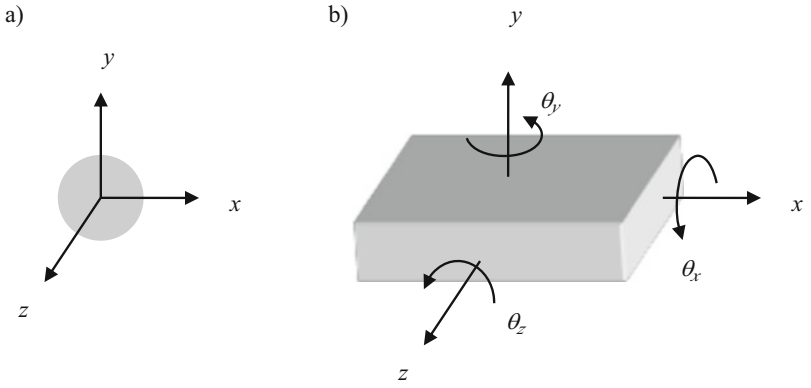

Fig. 1.4 (**a**) Three degrees of freedom for a particle; and (**b**) six degrees of freedom for a rigid body

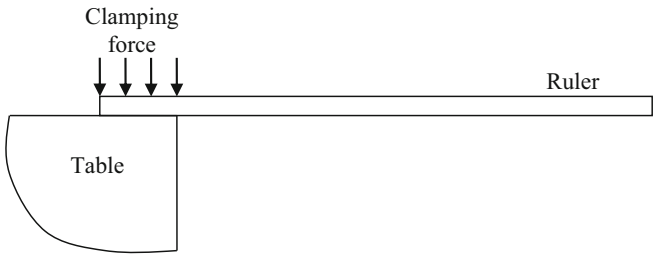

Fig. 1.5 A ruler clamped against the edge of a table

For an elastic body, or one that possesses mass and has finite stiffness, an infinite number of coordinates is required to fully describe its motion. To demonstrate this, let's imagine a ruler overhung from the edge of a table and clamped flat; see Fig. 1.5. We can consider each tick mark as a point on the beam. Naturally, the motion of each of these points differs as a function of time in response to the end of the ruler being displaced and released. Therefore, we require a coordinate at each of the tick marks. If we switched that ruler with another ruler of identical geometry and overhang length, but with twice as many tick marks, we could repeat the experiment and see that a coordinate was again required at each tick mark. At the limit, we could assign an infinite number of coordinates to an infinite number of tick marks. An infinite number of coordinates, however, means we would have an infinite number of degrees of freedom. We could make the same argument about any other structure we might consider.

This poses a problem for our modeling efforts. Must all our models possess an infinite number of degrees of freedom? Luckily, it is often acceptable to use only a few degrees of freedom when describing a body's vibration behavior. For the cantilever beam (clamped ruler) shown in Fig. 1.5, we might be interested in only the lowest, or fundamental, natural frequency. The shape of the beam as it vibrates at this natural frequency, referred to as a mode shape, is shown in Fig. 1.6. If we are

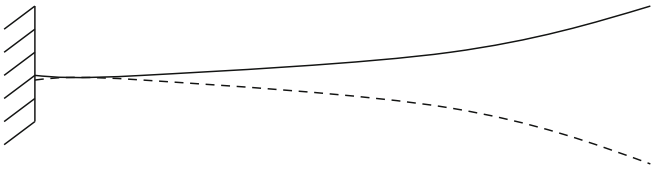

Fig. 1.6 Fundamental mode shape for a cantilever beam

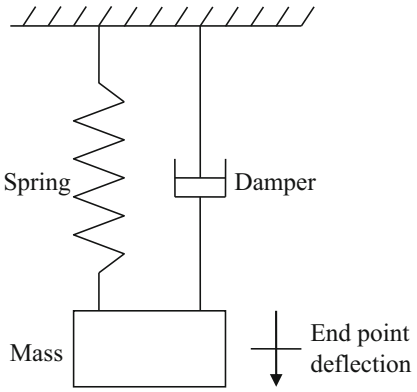

Fig. 1.7 Single degree of freedom spring-mass-damper model used to approximate the cantilever beam behavior

only interested in motion that occurs in this single mode shape (and corresponding natural frequency), we could pick a single point on the beam (at its end, for example) and describe the motion using this single degree of freedom. We could then approximate the continuous beam with a (discrete) single degree of freedom model as shown in Fig. 1.7. We will discuss how to determine the parameters for this spring-mass-damper model in Sects. 3.4 and 6.2.

1.5 Periodic Motion

To this point, we've mentioned that vibrations are oscillatory in nature. Let's now add some definitions to this discussion. A signal that repeats at regular intervals in time is referred to as **periodic**. An example is shown in Fig. 1.8. The simplest form of periodic motion is **harmonic motion**. Common examples of harmonic motion are the sine and cosine functions.

Figure 1.9 shows the sine function $x(t) = Asin(\omega t)$, where A is the magnitude with the units of x (if x is a displacement, then units of millimeters or micrometers may be appropriate, for example) and ω is the circular frequency expressed in radians/second (or rad/s). As shown in figure, the function repeats every τ seconds and we can write that $x(t + \tau) = x(t)$. The variable τ is referred to as the **time period** (or just the period) of the signal $x(t)$. It is related to ω (rad/s) as shown in Eq. 1.1. There is

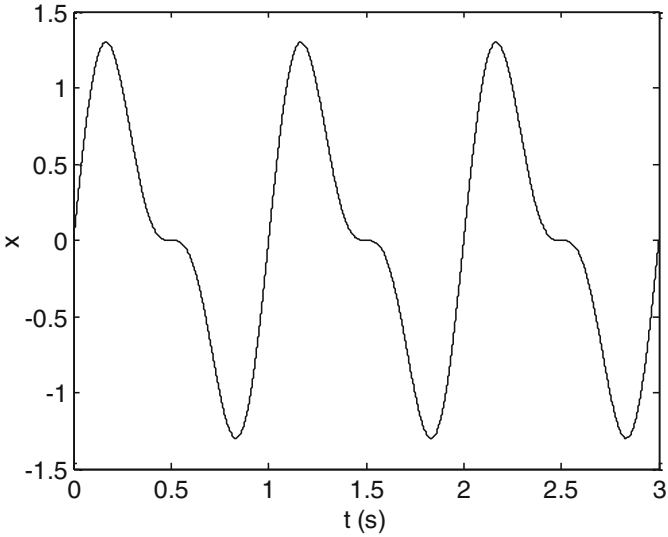

Fig. 1.8 Periodic motion example, $x(t)$. The signal repeats over an interval of 1 s. Three full periods are shown

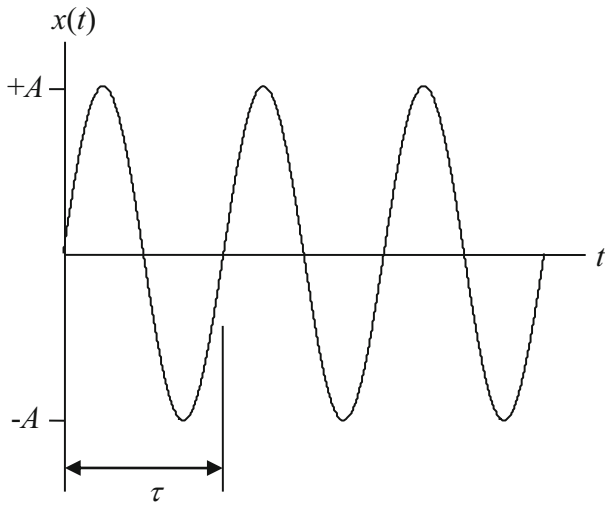

Fig. 1.9 The sine function is an example of harmonic motion

really no mystery to this relationship. It is simply based on two facts: (1) there are 2π rad per one cycle of vibration; and (2) τ gives the number of seconds per one cycle.

$$\tau = \frac{2\pi}{\omega} \tag{1.1}$$

In a Nutshell
Many readers may be more familiar with expressing vibration frequencies in cycles/s, or Hertz (Hz). The vibration motion repeats each cycle, or whenever the sine or cosine argument changes by 2π. For that reason, there are 2π rad per cycle. We will use the Greek letter ω to represent a vibration frequency in rad/s and the letter f to indicate a vibration frequency in cycles/s. The conversion between the two is provided in Eq. 1.4

The reason we refer to ω as the circular frequency is that we can represent $x(t)$ as a vector rotating in the complex (real-imaginary) plane with the frequency ω. The **Argand** diagram[1] in Fig. 1.10 shows that the sine function is the projection of the counter-clockwise rotating vector with a length (magnitude) A on the horizontal (or real) axis. The angle of the vector at any instant is the product ωt.

The French physicist and mathematician Jean-Baptiste Joseph Fourier made an important observation about periodic functions. He found that a periodic function $x(t)$ can be represented by an infinite sum of sine and cosine terms as shown in Eq. 1.2, where $\omega_2 = 2\omega_1$, $\omega_3 = 3\omega_1$, etc. This is referred to as the **Fourier series** and the coefficients a_0, a_1, b_1, a_2, b_2, etc. are called the Fourier coefficients [1].

$$x(t) = a_0 + a_1 \cos(\omega_1 t) + b_1 \sin(\omega_1 t) + a_2 \cos(\omega_2 t) + b_2 \sin(\omega_2 t) + a_3 \cos(\omega_3 t) + b_3 \sin(\omega_3 t) + \cdots \tag{1.2}$$

Let's take another look at Fig. 1.8. This signal is actually the sum of two sine functions, $x(t) = x_1 + x_2 = \mathit{sin}(2\pi t) + 0.5\ \mathit{sin}(2 \cdot 2\pi t)$. All three signals, x_1, x_2, and $x(t)$, are shown in Fig. 1.11. Comparing this function to Eq. 1.2, we see that $\omega_1 = 2\pi$ rad/s, $b_1 = 1$, $b_2 = 0.5$, and the remaining coefficients are zero. Also, from the figure we see that the period of $x(t)$ is 1 s. Let's use MATLAB®[2] to see how we can define and plot this function. See MATLAB® MOJO 1.1.

MATLAB® MOJO 1.1

```
% matlab_mojo_1_1.m

clear
close all
clc

% Define variables
t = 0:0.001:3;        % s
omega1 = 2*pi;        % rad/s
omega2 = 2*omega1;      % rad/s
```

[1] A plot of complex numbers as points in the complex plane is referred to as an Argand diagram [4]; we will use this description throughout the text.

[2] MATLAB® and Simulink® are registered trademarks of The MathWorks, Inc.

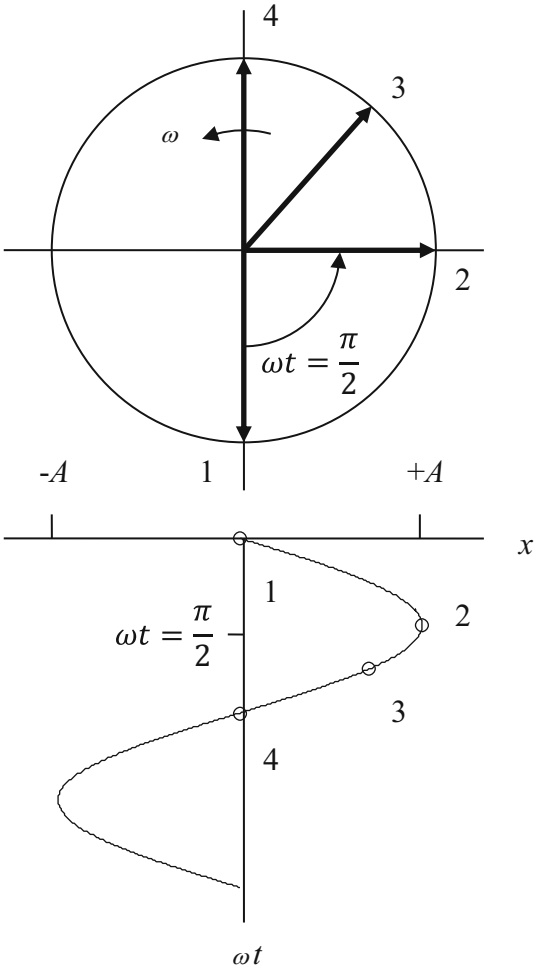

Fig. 1.10 Argand diagram for the function $x(t) = Asin(\omega t)$

```
b1 = 1;
b2 = 0.5;

% Define functions
x1 = b1*sin(omega1*t);
x2 = b2*sin(omega2*t);
x = x1 + x2;

figure(1)
plot(t, x1, 'k:', t, x2, 'k--', t, x, 'k-')
set(gca,'FontSize', 14)
xlabel('t (s)')
ylabel('x')
legend('x_1', 'x_2', 'x')
```

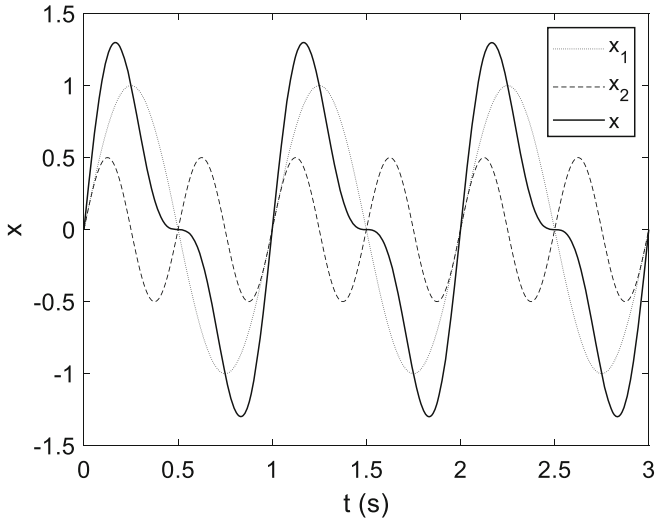

Fig. 1.11 The periodic motion in Fig. 1.8 is the sum of two sine functions, x_1 and x_2

Next, consider the square wave shown in Fig. 1.12. We see that this function is also periodic with a period of 1 s. Can it be represented using Eq. 1.2? The answer is yes—its Fourier series is the sum of the odd sine harmonics:[3] $x(t) = b_1 \, sin \, (\omega_1 t) + b_3 \, sin \, (\omega_3 t) + \ldots$ This makes sense when we observe that the square wave is an **odd function**, which means that $x(t) = -x(-t)$. In other words, the function does not simply mirror about the $t = 0$ point, it must also be inverted. Based on the period of 1 s and using Eq. 1.1, we can find that $\omega_1 = \frac{2\pi}{\tau} = \frac{2\pi}{1} = 2\pi$ rad/s . Furthermore, the Fourier coefficients are given by: $b_n = \frac{4}{n\pi}$, where n represents the odd integers. These odd integers can be represented by the expression $n = 2k - 1$, where $k = 1, 2, 3, \ldots$

The top panel of Fig. 1.13 shows the square wave and Fourier series approximation using the first three term ($k = 1$, 2, and 3, so $n = 1$, 3, and 5). As with any Fourier series, increasing the number of terms tends to increase its ability to reproduce the signal in question. The bottom panel of Fig. 1.13 shows the result for 20 terms. In this case, the square wave is reproduced quite accurately. However, if we look closely, we see oscillations near the discontinuities in the piecewise continuous square wave. This reflects the inherent challenge in representing a discontinuous function by a finite series of continuous sine and cosine functions and is referred to as **Gibbs' phenomenon** [5]. Figure 1.13 was produced using the m-file provided in MATLAB® MOJO 1.2.

MATLAB® MOJO 1.2.

[3] "Harmonics" is used to indicate the terms in the Fourier series.

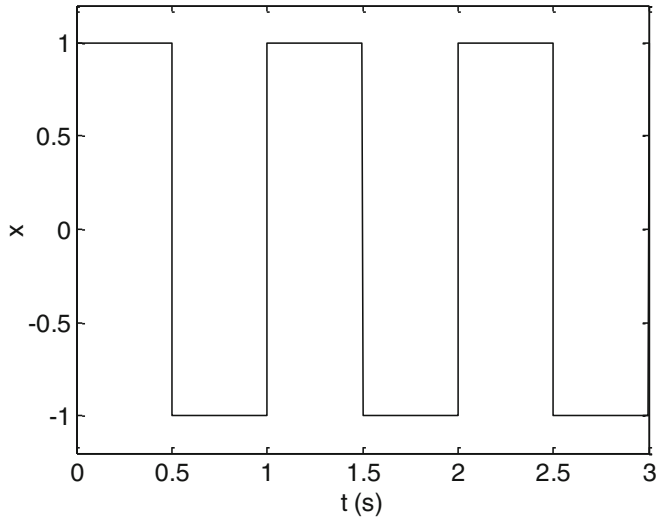

Fig. 1.12 Square wave for $t \geq 0$

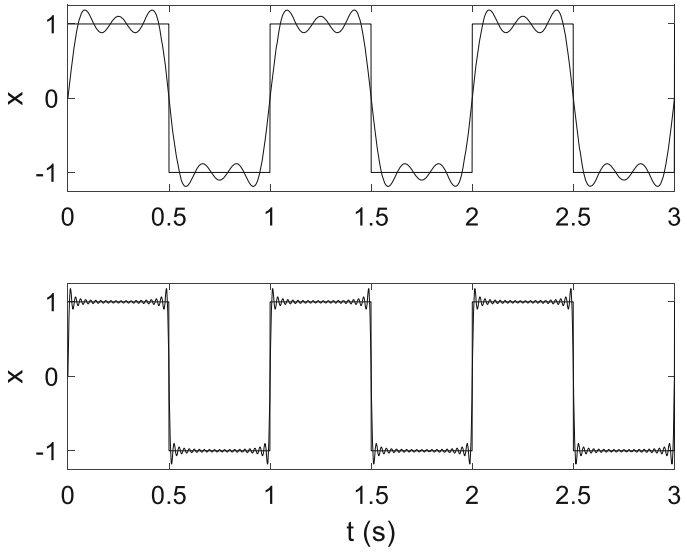

Fig. 1.13 Square wave and Fourier series approximations for (top) 3 terms and (bottom) 20 terms

```
% matlab_mojo_1_2.m

clear
close all
clc

% Define variables
t = 0:0.001:3;        % s
omega1 = 2*pi;        % rad/s

% Define square wave as a piecewise function
for cnt = 1:length(t)
  if t(cnt) < 0.5
    x_ref(cnt) = 1;
  elseif t(cnt) >= 0.5 && t(cnt) < 1
    x_ref(cnt) = -1;
  elseif t(cnt) >= 1 && t(cnt) < 1.5
    x_ref(cnt) = 1;
  elseif t(cnt) >= 1.5 && t(cnt) < 2
    x_ref(cnt) = -1;
  elseif t(cnt) >= 2 && t(cnt) < 2.5
    x_ref(cnt) = 1;
  elseif t(cnt) >= 2.5 && t(cnt) < 3
    x_ref(cnt) = -1;
  elseif t(cnt) >= 3
    x_ref(cnt) = 1;
  end
end

% Define square wave using its Fourier series
terms = 3;
x = 0;

for cnt = 1:terms
  b = 4/((2*cnt - 1)*pi);
  omega = (2*cnt - 1)*omega1;
  x = x + b*sin(omega*t);
end

figure(1)
hold on
subplot(211)
plot(t, x_ref, 'k', t, x, 'k')
set(gca,'FontSize', 14)
ylabel('x')
axis([0 3 -1.25 1.25])

% Define square wave using its Fourier series
terms = 20;
x = 0;
```

```
for cnt = 1:terms
  b = 4/((2*cnt - 1)*pi);
  omega = (2*cnt - 1)*omega1;
  x = x + b*sin(omega*t);
end

subplot(212)
plot(t, x_ref, 'k', t, x, 'k')
set(gca,'FontSize', 14)
xlabel('t (s)')
ylabel('x')
axis([0 3 -1.25 1.25])
```

In a Nutshell

Fourier's genius was to recognize that any time-varying signal can be represented as a sum of sine and cosine functions of different frequencies and amplitudes. This means that if we determine how to treat these sine and cosine terms, then we can extend the analysis to any time-varying signal. This will be very useful as we proceed with our study of mechanical vibrations.

Returning to our sine wave in Figs. 1.9 and 1.10, we see in Fig. 1.14 that the path of the rotating vector is repeated every 2π rad in the Argand diagram. Because the

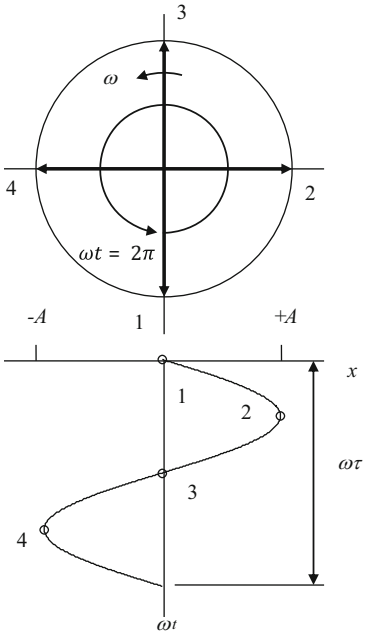

Fig. 1.14 Argand diagram showing the derivation of Eq. 1.3

vector angle at any instant in time is ωt rad and one full cycle of vibration (i.e., one rotation of the vector) takes τ seconds, we can write that $2\pi = \omega\tau$. This equation can be rearranged to give Eq. 1.1 or we can solve for the circular frequency.

$$\omega = \frac{2\pi}{\tau} \text{ rad/s} \tag{1.3}$$

Alternately, we can define the frequency in cycles/s, or **Hertz** (Hz). By convention in this text, we will use the frequency variable f when applying units of Hz and ω when using rad/s. Because there are 2π rad per cycle of vibration, the conversion from ω to f is:

$$f = \frac{\omega}{2\pi}. \tag{1.4}$$

Combining Eqs. 1.3 and 1.4, we can relate the frequency in Hz directly to the vibration period in seconds.

$$f = \frac{1}{\tau} \tag{1.5}$$

If $x(t) = Asin(\omega t)$ in Fig. 1.14 represents position, what can we say about the corresponding velocity, $v(t)$, and acceleration, $a(t)$? For velocity, we calculate the first time derivative of position to obtain:

$$v(t) = \frac{dx}{dt} = \omega Acos(\omega t). \tag{1.6}$$

Acceleration is the time derivative of velocity (or second derivative of position). We can therefore write acceleration as:

$$a(t) = \frac{dv}{dt} = -\omega^2 Asin(\omega t). \tag{1.7}$$

Using the Argand diagrams in Fig. 1.15a–c, we can see that velocity leads position by $\frac{\pi}{2}$ rad (90°) and acceleration leads position by π rad (180°). Although all three vectors are rotating at the circular frequency ω, they have different **phase** values. That is, they reach their maximum values at different instants in time. This is demonstrated in Fig. 1.16, where the three vectors are shown together for an arbitrary instant in time. We can see from this figure that position and acceleration always point in opposite directions. The position reaches its maximum at the moment that the acceleration reaches its minimum. Therefore, with proper scaling the two vectors could be summed to zero for all time, t. Using $x(t) = Asin(\omega t)$ and Eq. 1.7, we see that the required scaling factor is $-\omega^2$. Rewriting Eq. 1.7, we have that:

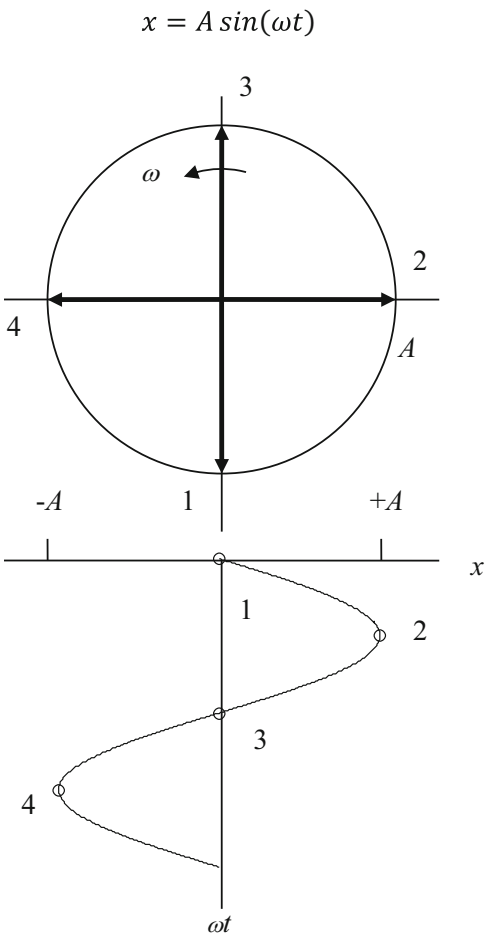

Fig. 1.15 (**a**) Argand diagram showing position. (**b**) Argand diagram showing velocity. (**c**) Argand diagram showing acceleration

$$\ddot{x} = \frac{d^2x}{dt^2} = -\omega^2 A sin(\omega t) = \omega^2 A sin(\omega t + \pi), \tag{1.8}$$

where the second equality emphasizes the π rad phase shift between acceleration and position. Combining Eq. 1.8 and $x(t) = Asin(\omega t)$ with the $-\omega^2$ scaling factor, we can write:

$$\ddot{x} + \omega^2 x = 0 \text{ or} \tag{1.9}$$

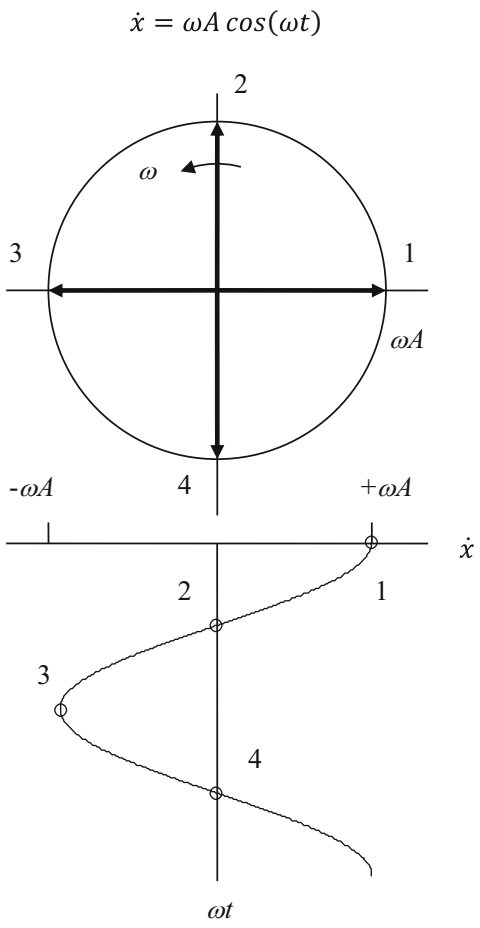

Fig. 1.15 (continued)

$$\frac{d^2x}{dt^2} + \omega^2 x = 0. \tag{1.10}$$

Equation 1.10 is referred to as the **differential equation of harmonic motion**. We'll revisit this equation in Sect. 2.1.

As we mentioned previously, the horizontal projection axis we used for our Argand diagrams is the **real axis**. The vertical axis is the **imaginary axis**. These names do not identify the "existence" of the axes. Rather, given that we can describe an arbitrary vibration as a sum of cosine and sine components, the real part is the cosine component and the imaginary part is the sine component of the signal. We can therefore represent a unit magnitude vector in the complex plane as $x(t) = cos(\omega t) + isin(\omega t)$, where i is the imaginary variable and $i = \sqrt{-1}$. The

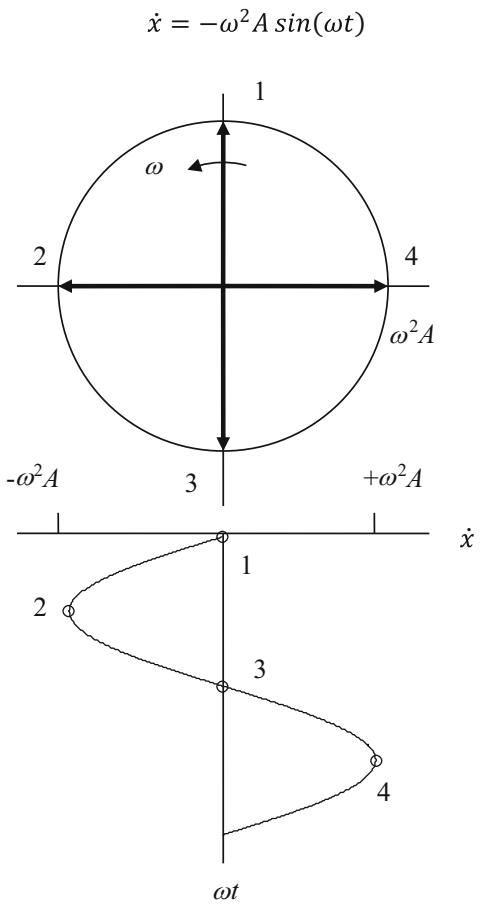

Fig. 1.15 (continued)

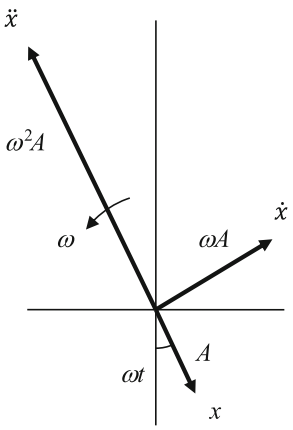

Fig. 1.16 Argand diagram showing position, velocity, and acceleration vectors together

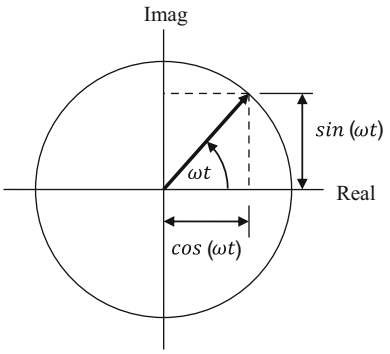

Fig. 1.17 The unit vector in the complex plane with its projections on the real and imaginary axes

projection of this unit vector on the real and imaginary axes is demonstrated in Fig. 1.17.

In a Nutshell
The idea of a real and imaginary axis leads to a mathematical convenience as discussed here. It is sometimes difficult for students to see the reason why this notation would be useful, but it eliminates many trigonometric manipulations that would otherwise be required. Bear with us for a little while and trust that this will be important (and useful) as we proceed.

Exponential notation is often used to describe vectors in the complex plane. In this case, we write the unit vector as $x(t) = e^{i\omega t} = cos\,(\omega t) + isin(\omega t)$. This is referred to as an **Euler's formula**. We can show it is true using three Maclaurin series.[4]

1. $e^y = 1 + y + \frac{y^2}{2!} + \frac{y^3}{3!} + \frac{y^4}{4!} + \ldots$
2. $cos\,(y) = 1 - \frac{y^2}{2!} + \frac{y^4}{4!} - \frac{y^6}{6!} + \frac{y^8}{8!} - \ldots$ Note that cosine is an **even function**, where $x(t) = x(-t)$, so we use the even harmonics in its series expansion.
3. $sin\,(y) = y - \frac{y^3}{3!} + \frac{y^5}{5!} - \frac{y^7}{7!} + \frac{y^9}{9!} - \ldots$

If we equate y in these series with $i\omega t$, then we find that $y^2 = i^2(\omega t)^2 = -(\omega t)^2$, $y^3 = -i(\omega t)^3$, $y^4 = (\omega t)^4$, $y^5 = i(\omega t)^5$, and so on. Substituting into the individual series, we have:

1. $e^{i\omega t} = 1 + i\omega t - \frac{(\omega t)^2}{2!} - \frac{i(\omega t)^3}{3!} + \frac{(\omega t)^4}{4!} + \ldots$
2. $cos\,(i\omega t) = 1 - \frac{(\omega t)^2}{2!} + \frac{(\omega t)^4}{4!} - \frac{(\omega t)^6}{6!} + \frac{(\omega t)^8}{8!} - \ldots$
3. $sin\,(i\omega t) = \omega t - \frac{(\omega t)^3}{3!} + \frac{(\omega t)^5}{5!} - \frac{(\omega t)^7}{7!} + \frac{(\omega t)^9}{9!} - \ldots$

[4] A Maclaurin series is a Taylor series expansion of a function evaluated about zero.

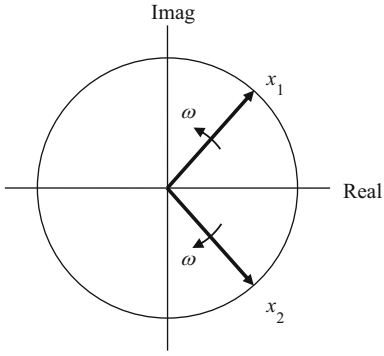

Fig. 1.18 Two counter-rotating unit vectors used to derive additional Euler's formula relationships

By inspection, we see that the sum $cos(\omega t) + isin(\omega t)$ is equal to $e^{i\omega t}$. The conclusion is that we can express harmonic motion using exponential notation and still satisfy the differential equation of harmonic motion.

Let's now look at two additional relationships derived from Euler's formula. Consider the two counter-rotating unit vectors, x_1 and x_2, shown in Fig. 1.18. Both are rotating at the circular frequency ω, but in opposite directions. At $t = 0$, both are horizontal and pointing to the right. We can write these two vectors as: $x_1 = cos(\omega t) + isin(\omega t)$ and $x_2 = cos(\omega t) - isin(\omega t)$. Alternately, we can use exponential notation to write $x_1 = e^{i\omega t}$ and $x_2 = e^{-i\omega t}$. When the two vectors are added, the imaginary parts always cancel so that we are left with:

$$\begin{aligned} x_1 + x_2 &= (\cos(\omega t) + i\sin(\omega t)) + (\cos(\omega t) - i\sin(\omega t)) \\ x_1 + x_2 &= 2\cos(\omega t). \end{aligned} \tag{1.11}$$

Alternately, the sum can be expressed as: $x_1 + x_2 = e^{i\omega t} + e^{-i\omega t}$. The right hand side of this equation can then be equated to the right hand side of the second line in Eq. 1.11 to arrive at the relationship:

$$cos(\omega t) = \frac{e^{i\omega t} + e^{-i\omega t}}{2}. \tag{1.12}$$

Similarly, taking the difference between x_1 and x_2 gives the relationship:

$$sin(\omega t) = i\left(\frac{e^{i\omega t} - e^{-i\omega t}}{2}\right). \tag{1.13}$$

By the Numbers 1.1

Let's complete an example to quantitatively explore the vector representation of vibration using the Argand diagram. Consider the signal $x(t) = 5e^{i2700t} = 5(cos(2700t) + isin(2700t))$. The circular frequency is 2700 rad/s or $\frac{2700}{2\pi} = 429.7$ Hz

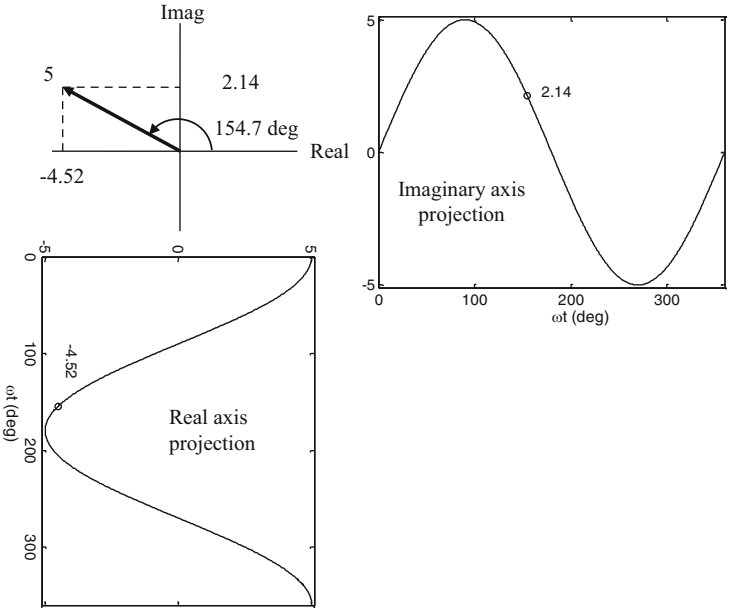

Fig. 1.19 *By the Numbers 1.1*—the vector $x(t) = 5e^{i2700t}$ is shown in the complex plane for $t = 0.001$ s

(according to Eq. 1.4).[5] The angle of the vector in the complex plane is defined by $\omega t = 2700t$ rad, where t is expressed in seconds. For $t = 0.001$ s, the angle is $2.7 \text{ rad} = 2.7\frac{180}{\pi} = 154.7^{\circ}$. The vector at this time is displayed in Fig. 1.19. The projections on the real (cosine component) and imaginary (sine component) axes are also shown. The real axis projection is: $5\ cos\ (154.7) = -4.52$, while the imaginary axis projection is: $5\ sin\ (154.7) = 2.14$. Therefore, for $t = 0.001$ s, we can write: $x\ (0.001) = 5e^{i2.7} = -4.52 + i2.14$.

Chapter Summary

- There are three primary categories of vibration: free, forced, and self-excited. Free vibration occurs at the system's natural frequency when there is no long-term forcing function. Forced vibration is the response to a periodic forcing function; the vibrating frequency matches the forcing frequency under steady-state conditions. Forced vibration is generally described in the frequency domain. Self-excited vibration exists when a steady input force is modulated into vibration at a system natural frequency.
- All physical systems are subject to some form of damping, or energy dissipation.

[5] To give this frequency some frame of reference, middle C on the musical scale has a frequency of 261.63 Hz. The frequency for this example would therefore be well within the audible range if its amplitude was large enough.

- The number of independent coordinates required to describe a body's motion is the number of degrees of freedom. While mechanical systems possess an infinite number of degrees of freedom in general, it is typically possible to adequately describe a system's behavior with a limited set of coordinates. The activity of describing a continuous system by a discrete number of coordinates is referred to as "modeling" the vibratory system.
- Periodic motion repeats at regular intervals; the time for each interval is called the time constant. The vibrating frequency is related to the time constant.
- Examples of harmonic motion are the sine and cosine functions.
- An Argand diagram is the representation of complex numbers as points in the complex plane. The complex plane axes are labeled as "Real" and "Imaginary" to correspond to the real and imaginary parts of complex numbers.
- The Fourier series represents periodic motion as an infinite sum of sine and cosine terms.
- Typical frequency units are rad/s and Hz.
- The exponential function can be used to represent harmonic motion.

Exercises

1. Answer the following questions.

   (a) All bodies which possess _____ and _____ are capable of vibrations.
   (b) Name the three fundamental categories of vibration.
   (c) How many degrees of freedom are necessary to fully describe the vibratory motion of an elastic body?

2. For the waveform shown in Fig. P1.2, answer the following questions.

   (a) Is this motion periodic?
   (b) If the motion is periodic, what is the period of the motion (in seconds)?
   (c) If the motion is periodic, what is the frequency of its motion (express your answer in both rad/s and Hz)?

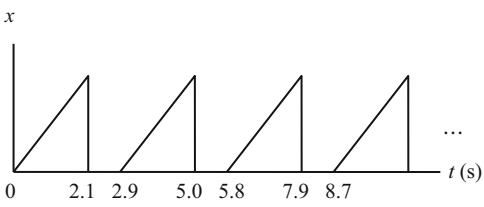

Fig. P1.2 Example waveform

3. To explore the Fourier series representation of signals, complete the following.

   (a) Approximate a square wave by plotting the following function in MATLAB®. Begin a new m-file by selecting File/New/M-File.

$$x = \frac{4}{\pi}\,sin\,(\omega t) + \frac{4}{3\pi}\,sin\,(3\omega t) + \frac{4}{5\pi}\,sin\,(5\omega t) + \frac{4}{7\pi}\,sin\,(7\omega t)$$

   Use $\omega = 2\pi$ rad/s and plot your results from $t = 0$ to 5 s in steps of 0.001 s. You can define your time vector using the following statement.

```
t = 0:0.001:5;
```

   Also, π can be defined in MATLAB® using `pi`. Finally, the argument for sine (or any harmonic function) must be in rad/s in MATLAB® (not degrees). For example, you can define the displacement using the following statement.

```
   x = 4/pi*sin(omega*t) + 4/(3*pi)*sin(3*omega*t) + 4/(5*pi)
*sin(5*omega*t) + 4/(7*pi)*sin(7*omega*t);
```

   To plot the result, you can use the following statements.

```
figure(1)
plot(t, x)
xlabel('t (s)')
ylabel('x(t)')
```

   (b) What is the period (in seconds) of the waveform?
   (c) What is the frequency in Hz?
   (d) Replot the function using 50 terms (following the pattern of odd multiples of ω with the $\frac{4}{n\pi}$ coefficients where $n = 1, 3, 5, \ldots$). What is the effect of including additional terms?

4. If displacement can be described as $x = 5\ cos\ (\omega t)$ mm, where $\omega = 6\pi$ rad/s, complete the following.

   (a) Plot the displacement over the time interval from $t = 0$ to 3 s in steps of 0.02 s. What is the period (in seconds) of the harmonic displacement?
   (b) Plot the velocity (in mm/s) over the same time interval.
   (c) Plot the acceleration (in mm/s^2) over the same time interval.
   (d) Calculate the maximum velocity (i.e., calculate the time derivatives and find the maximum values) and acceleration and verify your results using your plots.

5. The complex exponential function, $x = e^{i\omega t}$, can be used to describe harmonic motion (the function can be defined in MATLAB® using `x = exp (1i*omega*t);`). Complete the following to explore this function.

(a) Plot the real part of the function for $\omega = \pi$ rad/s over a time interval of $t = 0$–10 s using time steps of 0.05 s. Use the command `plot(t, real (x))` to complete this task.
(b) Plot the imaginary part of the function. Use the command `plot(t, imag (x))`.
(c) Describe your results from parts (a) and (b) in terms of sine and cosine functions.
(d) Sketch the Argand diagram for x at $t = 0.25$ s and show its projections on the real and imaginary axes. What is the numerical value of these projections? How do these results relate to parts (a) and (b)?

6. A harmonic motion has an amplitude of 0.2 cm and a period of 15 s.

(a) Determine the maximum velocity (m/s) and maximum acceleration (m/s^2) of the periodic motion.
(b) Assume that the motion expresses the free vibration of an undamped single degree of freedom system and that the motion was initiated with an initial displacement and no initial velocity. Express the motion (in units of meters) in each of the following four forms.

- $Acos(\omega_n t + \Phi_c)$
- $Asin(\omega_n t + \Phi_s)$
- $Bcos(\omega_n t) + Csin(\omega_n t)$
- $De^{i(\omega_n t)} + Ee^{-i(\omega_n t)}$

7. Determine the sum of the two vectors $x_1 = 6e^{i\frac{\pi}{6}}$ and $x_2 = -1e^{i\frac{\pi}{3}}$.
8. If the velocity at a particular point on a body is $v(t) = 250\ sin\ (100t)$, complete the following. $v(t) = \frac{dx}{dt} = \omega Acos(\omega t)$

(a) Plot the velocity in the complex plane at $t = 0.01$ s.
(b) Using the velocity equation, determine the corresponding expression for displacement.

9. In bungee jumping, a person leaps from a tall structure while attached to a long elastic cord. Would the resulting oscillation be best described as free, forced, or self-excited vibration?
10. The sine function can be represented as $sin\,(\theta) = \theta - \frac{\theta^3}{3!} + \frac{\theta^5}{5!} - \frac{\theta^7}{7!} + \frac{\theta^9}{9!} \cdots$. Plot the percent error between $sin(\theta)$ and:

- θ (rad)
- $\theta - \frac{\theta^3}{3!}$ (rad)
- $\theta - \frac{\theta^3}{3!} + \frac{\theta^5}{5!}$ (rad)

for a range of θ values from 0.001 rad to $\frac{\pi}{2}$ rad in steps of 0.001 rad.

Calculate the percent error using $\left(\frac{\theta - sin(\theta)}{sin(\theta)}\right) \cdot 100$ for the θ approximation, $\left(\frac{\left(\theta - \frac{\theta^3}{3!}\right) - sin(\theta)}{sin(\theta)}\right) \cdot 100$ for the $\theta - \frac{\theta^3}{3!}$ approximation, and so on. How do these results relate to the small angle approximation?

References

1. Kreyszig E (1983) Advanced engineering mathematics, 5th edn. Wiley, New York, NY
2. http://en.wikipedia.org/wiki/Tacoma_Narrows_Bridge_(1940)
3. Schmitz T, Smith KS (2009) Machining dynamics: Frequency response to improved productivity. Springer, New York, NY
4. Weisstein EW (2010) "Argand Diagram" from MathWorld—a Wolfram Web Resource. http://mathworld.wolfram.com/ArgandDiagram.html
5. http://en.wikipedia.org/wiki/Gibbs_phenomenon

Chapter 2
Single Degree of Freedom Free Vibration

> The least movement is of importance to all nature. The entire ocean is affected by a pebble.
> —Blaise Pascal

2.1 Equation of Motion

For the discussions in this chapter, we'll use what is referred to as a **lumped parameter model**, to describe free vibration. The "lumped" designation means that the mass is concentrated at a single coordinate (degree of freedom) and it is supported by a massless spring and damper. Recall from Sect. 1.2.1 that free vibration means that the mass is disturbed from its equilibrium position and vibration occurs at the natural frequency, but a long-term external force is not present. The lumped parameter model is typically depicted as shown in Fig. 2.1. Here, the linear spring, k, exerts a force, f, proportional to displacement, x. See Fig. 2.2, where the slope of the line represents the spring constant, k. This linear relationship is referred to as **Hooke's law**. Typical SI units for k are N/m.

$$f = kx \tag{2.1}$$

In a Nutshell
Lumped parameters do not exist in the real world. All springs have some mass. All physical masses deform in the presence of a force and, therefore, have stiffness. However, it is often possible to identify system components where mass, stiffness, or damping is the dominant feature. A lumped parameter model is dramatically simpler and often sufficiently accurate for our purposes. It is the essence of engineering to make the problem simple enough to be tractable, yet sophisticated enough to reasonably represent reality.

T. L. Schmitz, K. S. Smith, *Mechanical Vibrations*,
https://doi.org/10.1007/978-3-030-52344-2_2

A viscous damping model is assumed in Fig. 2.1. For this type of damping, the force is proportional to velocity; see Eq. 2.2, where c is the viscous damping coefficient with units of force per velocity (in SI, the units are N s/m). Physically, viscous damping is observed by forcing a body through a fluid. For example, if you pull your hand through the water in a swimming pool, you will find that the force increases with your hand's speed. Another example is a shock absorber, or dashpot, where fluid is forced though one or more small holes. If you attempt to collapse or expand the shock absorber more rapidly, the force increases proportionally. Damping is discussed in more detail in Sect. 2.4.

$$f = c\dot{x} \tag{2.2}$$

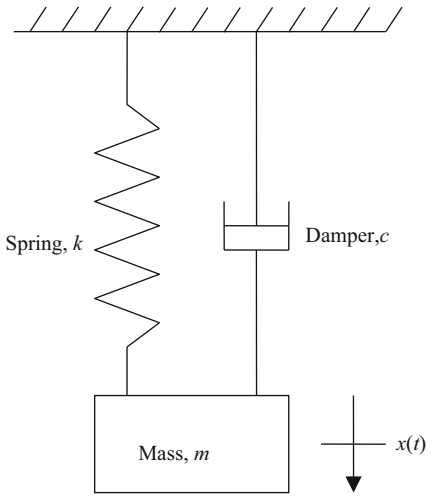

Fig. 2.1 Lumped parameter spring-mass-damper model for single degree of freedom free vibration

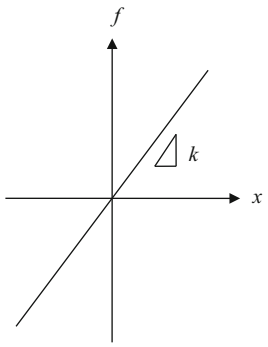

Fig. 2.2 Hooke's law for a linear spring; the spring constant, k, is the slope of the line

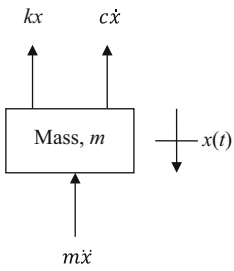

Fig. 2.3 Free body diagram for spring-mass-damper system (d'Alembert's inertial force, $f = m\ddot{x}$, is included)

In a Nutshell
If we assume lumped parameters and viscous damping, then the equations of motion will be ordinary linear differential equations with constant coefficients—one of the few classes of differential equations that we can easily solve. This advantage is so powerful that we often assume "equivalent" viscous damping even when we are certain that the damping is not actually viscous.

To obtain the differential equation of motion for the spring-mass-damper system, let's draw the free body diagram. Figure 2.3 shows three forces acting on the single degree of freedom mass:

- the spring force, kx
- the damping force, $c\dot{x}$, and
- the "inertial force", $m\ddot{x}$.

This transformation of the accelerating body into an equivalent static system by the addition of the inertial force is referred to as **d'Alembert's principle**. It enables us to simply sum the forces and set the result equal to zero (as in the static case). For Fig. 2.3, this "static" force sum is $\sum f_x = -m\ddot{x} - c\dot{x} - kx = 0$, where a positive force is assumed in the $+x$ direction (down in Fig. 2.3). Rewriting gives the familiar form for the equation of motion.

$$m\ddot{x} + c\dot{x} + kx = 0 \tag{2.3}$$

Note that this gives the same result as if we had used $\sum f_x = m\ddot{x}$ and not considered the inertial force. In this case, we would have obtained $\sum f_x = m\ddot{x} = -c\dot{x} - kx$ (where the positive force direction is again down in Fig. 2.3), or $\sum f_x = m\ddot{x} + c\dot{x} + kx = 0$.

To begin our analysis of this equation of motion, let's neglect damping for now so that the new equation is:

$$m\ddot{x} + kx = 0. \tag{2.4}$$

In a Nutshell
We will see that the inclusion of damping typically makes the results surprisingly more complex. For that reason, it is usually easiest to start with the simpler undamped case.

This equation is similar to the "differential equation of harmonic motion" we saw in Eq. 1.10. We've already seen in Sect. 1.5 that the exponential function can be used to describe harmonic motion through Euler's formula. Therefore, let's assume a (harmonic) solution to Eq. 2.4 of the form:

$$x(t) = Xe^{st}, \tag{2.5}$$

where $s = i\omega$ is the Laplace variable. We can then take the first and second time derivatives of Eq. 2.5 to determine the velocity and acceleration, respectively.

$$\dot{x}(t) = sXe^{st} \tag{2.6}$$

$$\ddot{x}(t) = s^2Xe^{st} \tag{2.7}$$

In a Nutshell
The solution to a differential equation is a function which makes it true. The solution to the differential equation described by Eq. 2.4 is a function of time, $x(t)$, such that the sum of its second derivative multiplied by m and the function itself multiplied by k is zero. One solution procedure for ordinary linear differential equations with constant coefficients (like Eq. 2.4) begins with making an assumption of the solution form. Equation 2.5 shows a typical assumption. One instructor somewhere in our past said we should assume $x(t) = Be^{st}$ because that form is the "best" assumption. This may sound corny, but it provides a nice mnemonic. In fact, it turns out that this assumption provides all of the solutions that exist for this differential equation.

We can now substitute for x and $\ddot{x}$ in Eq. 2.4 using Eqs. 2.5 and 2.7.

$$m\left(s^2Xe^{st}\right) + k(Xe^{st}) = 0 \tag{2.8}$$

Grouping terms gives $Xe^{st}(ms^2 + k) = 0$. There are two possibilities for this equation to be true. Since it is a product of two terms, at least one of the two terms must be equal to zero. If $Xe^{st} = 0$, this means that no motion has occurred. Our assumed form leads to all possible solutions and this is a valid solution. However, it is not a very interesting outcome, so it is referred to as the **trivial solution**. We are interested in the alternative:

$$ms^2 + k = 0. \tag{2.9}$$

This is used to obtain our vibration solution and is referred to as the **characteristic equation** for the system. From this equation, we can identify the **natural frequency**, or the frequency at which the system will vibrate if disturbed from equilibrium and released. Because we are not considering damping in this discussion, it is referred to as the undamped natural frequency, ω_n.

Let's solve for s from Eq. 2.9. We see that $s^2 = -\frac{k}{m}$. Taking the square root of both sides gives $s = \pm\sqrt{-\frac{k}{m}} = \pm i\sqrt{\frac{k}{m}}$. We've already stated that $s = i\omega$. Comparing these two equations for s gives the natural frequency of vibration for our undamped single degree of freedom system.

$$\omega_n = \sqrt{\frac{k}{m}} \tag{2.10}$$

Here, we've selected the positive root to give a positive natural frequency. If the stiffness units are N/m and the mass units are kg, then the units of natural frequency are:

$$\sqrt{\frac{\frac{N}{m}}{kg}} = \sqrt{\frac{\frac{kg\frac{m}{s^2}}{m}}{kg}} = \sqrt{\frac{1}{s^2}} = \frac{rad}{s}.$$

Note that the unit radian does not strictly require a unit symbol and is typically omitted in mathematics literature. It has been added here for clarity and to emphasize the description of the rotating vector in the Argand diagram. If we wish to express the natural frequency in units of Hz (or cycles/s), we simply apply Eq. 1.4. In this case, we use the variable f_n to indicate the alternate units of the natural frequency.

$$f_n = \frac{\omega_n}{2\pi} \tag{2.11}$$

In a Nutshell

This makes intuitive sense. We would expect systems that have a high natural frequency to be stiff and have a low mass. The highest pitch guitar strings are thin and tight. We would also expect systems that have a low natural frequency to be more massive and flexible. The lowest pitch guitar strings are the loosest and often have a second string wound around them to increase their mass.

The total solution to the equation of motion is the sum of the two solutions determined from the roots of the characteristic equation: $s_1 = +i\omega_n$ and $s_2 = -i\omega_n$. Using Eq. 2.5, the two solutions are summed to obtain:

$$x(t) = X_1 e^{s_1 t} + X_2 e^{s_2 t} = X_1 e^{i\omega_n t} + X_2 e^{-i\omega_n t}. \tag{2.12}$$

In the right hand side of this equation, the first term, $X_1 e^{i\omega_n t}$, is a counter-clockwise rotating vector in the complex plane and the second term, $X_2 e^{-i\omega_n t}$, is a clockwise rotating vector. To determine the coefficients X_1 and X_2, we use the **initial conditions**. These are typically applied at time $t = 0$ to the system that was originally at equilibrium in order to disturb it from this state. We can describe these initial conditions (or disturbances) as: (1) $x(0) = x_0$, the initial displacement; and (2) $\dot{x}(0) = \dot{x}_0$, the initial velocity. If we let $t = 0$ in Eq. 2.12, we obtain $x(0) = x_0 = X_1 e^0 + X_2 e^0$. Because $e^0 = 1$, we can write this as:

$$x_0 = X_1 + X_2. \tag{2.13}$$

Next, we take the time derivative of Eq. 2.12 to obtain $\frac{dx}{dt} = \dot{x}(t) = i\omega_n X_1 e^{i\omega_n t} - i\omega_n X_2 e^{-i\omega_n t}$. Setting $t = 0$ and substituting the initial velocity gives $\dot{x}(0) = \dot{x}_0 = i\omega_n X_1 e^0 - i\omega_n X_2 e^0$. This result can be rewritten as:

$$\dot{x}_0 = i\omega_n X_1 - i\omega_n X_2. \tag{2.14}$$

We can solve for X_1 by multiplying Eq. 2.13 by $i\omega_n$ and summing this result with Eq. 2.14. The X_2 terms cancel and we are left with $X_1 = \frac{i\omega_n x_0 + \dot{x}_0}{2i\omega_n}$. Let's rationalize the right hand side of this equation by multiplying both the numerator and denominator by i.

$$X_1 = \frac{i^2\omega_n x_0 + i\dot{x}_0}{2i^2\omega_n} = \frac{-\omega_n x_0 + i\dot{x}_0}{-2\omega_n} = \frac{\omega_n x_0 - i\dot{x}_0}{2\omega_n} \tag{2.15}$$

We can now solve for X_2 using Eq. 2.13: $X_2 = x_0 - X_1 = \frac{2\omega_n x_0}{2\omega_n} - X_1$. See Eq. 2.16.

$$X_2 = \frac{2\omega_n x_0 - \omega_n x_0 + i\dot{x}_0}{2\omega_n} = \frac{\omega_n x_0 + i\dot{x}_0}{2\omega_n} \tag{2.16}$$

Because X_1 and X_2 are identical except for the sign of their imaginary parts, they are referred to as **complex conjugates**. We can also write them in exponential form as described in Sect. 1.5. If the real and imaginary parts of X_1 are a and b, then we have that $X_1 = a + ib$, where $a = \frac{\omega_n x_0}{2\omega_n} = \frac{x_0}{2}$ and $b = \frac{-\dot{x}_0}{2\omega_n}$. In exponential notation, the

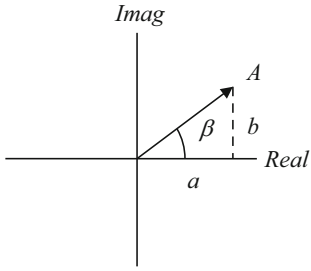

Fig. 2.4 Complex plane representation of $X_1 = Ae^{i\beta}$

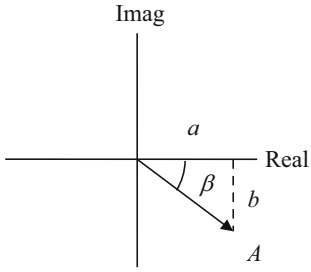

Fig. 2.5 Complex plane representation of $X_2 = Ae^{-i\beta}$

equivalent expression is $X_1 = Ae^{i\beta}$, where $A = \sqrt{a^2 + b^2}$ and $\beta = tan^{-1}\left(\frac{b}{a}\right)$. These relationships are depicted in Fig. 2.4.

Again using a and b, we can express the second complex coefficient as $X_2 = a - ib = Ae^{-i\beta}$. The corresponding graphical relationships between a, b, A, and β are shown in Fig. 2.5.

Substituting for X_1 and X_2 in Eq. 2.12 gives:

$$x(t) = X_1 e^{i\omega_n t} + X_2 e^{-i\omega_n t} = Ae^{i\beta} e^{i\omega_n t} + Ae^{-i\beta} e^{-i\omega_n t}$$
$$x(t) = A\left(e^{i(\omega_n t+\beta)} + e^{-i(\omega_n t+\beta)}\right) \tag{2.17}$$

Rewriting Eq. 1.12, we have that $2\ cos\ (\theta) = e^{i\theta} + e^{-i\theta}$, where θ is an arbitrary argument. Using this relationship, we can rewrite Eq. 2.17 as $x(t) = A\ (2\ cos\ (\omega_n t + \beta)) = 2Acos(\omega_n t + \beta)$. As we've seen, A and β depend on ω_n (i.e., the model parameters k and m) and the initial conditions. Specifically, $A = \sqrt{\left(\frac{x_0}{2}\right)^2 + \left(\frac{-\dot{x}_0}{2\omega_n}\right)^2}$ and $\beta = tan^{-1}\left(\frac{\frac{-\dot{x}_0}{2\omega_n}}{\frac{x_0}{2}}\right) = tan^{-1}\left(\frac{-\dot{x}_0}{\omega_n x_0}\right)$.

We can plot $x(t) = 2Acos(\omega_n t + \beta)$ for two distinct cases: (1) $\dot{x}_0 = 0$ and $x_0 \neq 0$; and (2) $x_0 = 0$ and $\dot{x}_0 \neq 0$. For the first case, $\beta = 0$ and the representation of the counter-clockwise rotating vector x in the complex plane at $t = 0$ is shown in Fig. 2.6a. For the second case, $\beta = \frac{\pi}{2}$ and x is shown at $t = 0$ in Fig. 2.6b. The time-domain representations of these two cases (i.e., the projection of the vectors on the real axis) are included in Fig. 2.7a (first case) and Fig. 2.7b (second case).

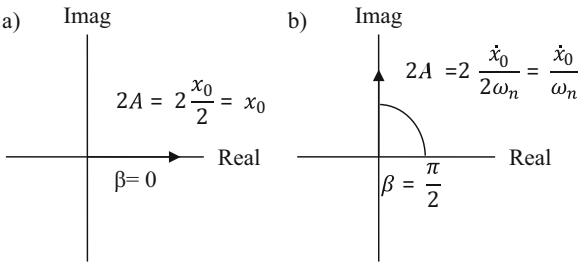

Fig. 2.6 Vector representation of $x(t) = 2Acos(\omega_n t + \beta)$ at $t = 0$ for: (**a**) $\dot{x}_0 = 0$ and $x_0 \neq 0$; and (**b**) $x_0 = 0$ and $\dot{x}_0 \neq 0$

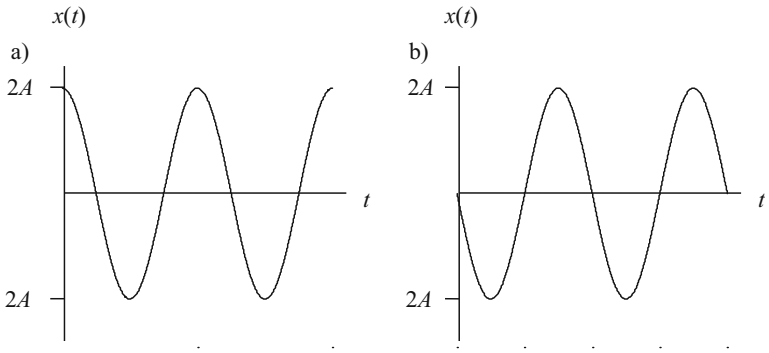

Fig. 2.7 Time-domain representation of $x(t) = 2Acos(\omega_n t + \beta)$ for: (**a**) $\dot{x}_0 = 0$ and $x_0 \neq 0$; and (**b**) $x_0 = 0$ and $\dot{x}_0 \neq 0$

We can express undamped free vibration (i.e., the solution to Eq. 2.4) in several forms. Using somewhat careless notation (the A in the following list is not the same A we just discussed), these forms can be generically written as:

- $x(t) = Acos(\omega_n t + B)$
- $x(t) = Csin(\omega_n t + D)$
- $x(t) = Esin(\omega_n t) + Fcos(\omega_n t)$
- $x(t) = Ge^{i\omega_n t} + He^{-i\omega_n t}$,

where A through F are real-valued (no imaginary part) and G and H are complex.

In a Nutshell

It might seem like a long (mathematical) way to go, but the end result is that free vibration of a single degree of freedom system with no damping is sinusoidal and occurs at the natural frequency of the system. The initial conditions might make the vibration larger or smaller or make it look more like a sine or a cosine. However, the initial conditions do not change the frequency of the motion. The natural frequency is a fundamental property of a single degree of freedom system.

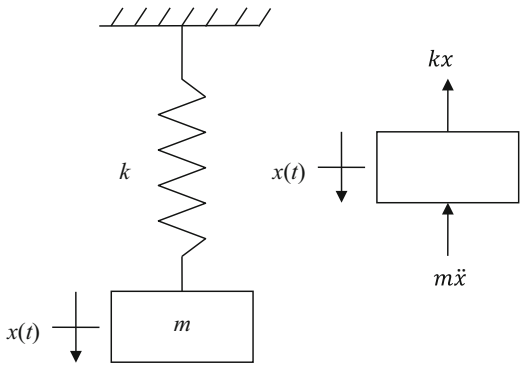

Fig. 2.8 *By the Numbers 2.1*—the example spring-mass system and corresponding free body diagram are shown.

By the Numbers 2.1

Consider the spring-mass system shown in Fig. 2.8, where $k = 5 \times 10^7$ N/m and $m = 0.1$ kg. The free body diagram is also shown. Based on this diagram, the force balance is $\sum f_x = 0 = -m\ddot{x} - kx$. The equation of motion is therefore $m\ddot{x} + kx = 0$, as we have already seen.

Let's consider the spring stiffness and try to make some sense of this value. We can rewrite $k = 5 \times 10^7$ N/m as $k = \frac{5000}{100}\frac{N}{\mu m}$. In other words, it requires 5000 N to deflect the spring by 100 μm. To put 5000 N in more physical terms, let's convert it to pounds-force by dividing by 4.448. The result is $\frac{5000}{4.448} = 1124$ lb_f. This is approximately 2.55 Kawasaki Ninja 500R motorcycles (curb weight 440 lb_f). If we placed these 2.55 motorcycles on top of the spring, it would deflect by 100 μm, which is approximately the diameter of a human hair. This seems like a very stiff spring, but this is actually a typical k value for many mechanical systems, such as the bending stiffness for an endmill clamped in a spindle on a milling machine.

Let's next discuss the mass of 0.1 kg. We can convert this to Newtons by multiplying Earth's gravitational acceleration value of 9.81 m/s^2. The result is $f = 9.81(0.1) = 0.98$ N. Dividing this result by 4.448 to convert it to pounds-force, we obtain $f = \frac{0.98}{4.448} = 0.22\,\text{lb}_\text{f}$. This is about the same as the precooked weight of the beef patty on a McDonald's Quarter Pounder. Relative to the motorcycles from the force description, this is not much weight.

Given the stiff spring and low mass, what does your intuition tell you about the corresponding natural frequency? You would probably expect that this combination would yield a high natural frequency, i.e., if we did deflect the mass (supported by the spring) from its equilibrium position and then let it vibrate, a high oscillating frequency would not be a surprise. Using Eq. 2.10, we find that $\omega_n = \sqrt{\frac{5\times10^7}{0.1}} = 22361$ rad/s. We can express this result in Hz by applying Eq. 2.11: $f_n = \frac{\omega_n}{2\pi} = \frac{22361}{2\pi} = 3559$ Hz. Therefore, if we were to disturb this system from its equilibrium position, it would complete 3559 cycles of oscillation per second. For comparison purposes, the highest note on a standard piano has a frequency of 4186 Hz, where the sound we hear is due to the free vibration of a taut, thin wire which is excited by

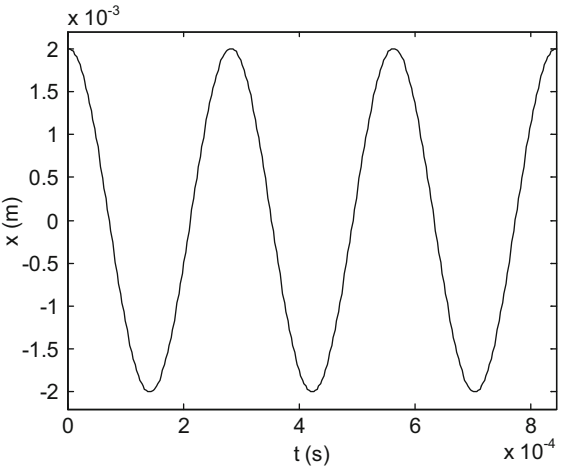

Fig. 2.9 *By the Numbers 2.1*—the free vibration response to an initial displacement of 0.002 m is shown

striking it with a "hammer" (the padded hammer motion is initiated by the pressing the piano key).

To solve the equation of motion for this harmonic vibration, let's select initial conditions of $x_0 = 0.002$ m and $\dot{x}_0 = 0$. This means that we pulled the mass down by 0.002 m and then released it. Although many forms are available to us, let's use $x(t) = Esin(\omega_n t) + Fcos(\omega_n t)$ for the vibration description. To apply both initial conditions and solve for E and F, we'll need the time derivative of the position:

$$\frac{dx}{dt} = \dot{x}(t) = \omega_n Ecos(\omega_n t) - \omega_n Fsin(\omega_n t). \tag{2.18}$$

We can now apply the two initial conditions by setting $t = 0$.

$$x(0) = x_0 = Esin(0) + Fcos(0) = F \tag{2.19}$$

$$\dot{x}(0) = \dot{x}_0 = \omega_n Ecos(0) - \omega_n Fsin(0) = \omega_n E \tag{2.20}$$

From Eqs. 2.19 and 2.20, we see that $F = x_0$ and $E = \frac{\dot{x}_0}{\omega_n}$ so that we can generically write:

$$x(t) = \frac{\dot{x}_0}{\omega_n} \, sin\,(\omega_n t) + x_0 \, cos\,(\omega_n t). \tag{2.21}$$

In a Nutshell

We can always use the solution form provided by Eq. 2.21 for single degree of freedom free vibration problems when the initial conditions are known.

Substituting our initial conditions and natural frequency, Eq. 2.21 simplifies to $x(t) = 0.002\,cos\,(22361t)$ m. The resulting vibration is shown in Fig. 2.9. Note that the period of vibration for this example is $\tau = \frac{1}{f_n} = \frac{2\pi}{\omega_n} = \frac{2\pi}{22361} = 2.81 \times 10^{-4}$ s $= 0.281$ ms.

In practice, we would expect that the free vibration magnitude would decay over time and eventually stop, not persist with a constant magnitude as we see in Fig. 2.9. This is because all physical systems exhibit some level of damping. However, let's continue this undamped example by considering a second form for the harmonic vibration solution $x(t) = Acos(\omega_n t + B)$. The derivative is:

$$\dot{x}(t) = -\omega_n A sin(\omega_n t + B). \tag{2.22}$$

We apply the initial conditions to obtain:

$$x(0) = x_0 = Acos(0 + B) = Acos(B) \tag{2.23}$$

and

$$\dot{x}(0) = \dot{x}_0 = -\omega_n A sin(0 + B) = -\omega_n A sin(B). \tag{2.24}$$

We can divide Eq. 2.24 by Eq. 2.23 to obtain:

$$\frac{-\omega_n A sin(B)}{Acos(B)} = \frac{\dot{x}_0}{x_0}, \tag{2.25}$$

which can be rewritten as $-\omega_n\,tan\,(B) = \frac{\dot{x}_0}{x_0}$. Solving for the phase angle, B, gives:

$$B = tan^{-1}\left(-\frac{\dot{x}_0}{\omega_n x_0}\right). \tag{2.26}$$

Given B, we can solve for A using Eq. 2.23:

$$A = \frac{x_0}{cos\,(B)}. \tag{2.27}$$

For this example, we find that $B = tan^{-1}\left(-\frac{0}{22361(0.002)}\right) = 0$ and $A = \frac{0.002}{cos\,(0)} = 0.002$ m. Substituting into $x(t) = Acos(\omega_n t + B)$ naturally gives the same result we found previously: $x(t) = 0.002\,cos\,(22361t)$ m. We can follow the identical approach for any of the harmonic vibration forms provided.

2.2 Energy-Based Approach

As an alternative to drawing a free body diagram to identify the equation of motion for a vibratory system, we can use an energy-based approach. In this method, we recognize that oscillating systems constantly switch between kinetic and potential energy. For our spring-mass system, we can express the **kinetic energy** of the moving mass as $KE = \frac{1}{2}mv^2$ and the **potential energy** of the spring as $PE = \frac{1}{2}kx^2$. As a check on these equations, let's take a look at the units. For KE, we have $kg\left(\frac{m}{s}\right)^2 = \frac{kg \cdot m}{s^2}m = N \cdot m$. Similarly, PE gives $\frac{N}{m}(m)^2 = N \cdot m$. As expected, these units describe energy/work.

The sum of the kinetic and potential energies is a constant value in time: $KE + PE =$ constant. Substituting for KE and PE considering our spring-mass system and taking the time derivative of this sum gives:

$$\frac{d}{dt}\left(\frac{1}{2}mv^2 + \frac{1}{2}kx^2\right) = 0. \tag{2.28}$$

We now need to calculate the time derivatives of the two terms in Eq. 2.28. Rewriting the velocity, v, as $\dot{x}$, its derivative is:

$$\frac{d}{dt}\left(\frac{1}{2}m\dot{x}^2\right) = \frac{1}{2}m(2\dot{x})\ddot{x} = m\ddot{x}(\dot{x}). \tag{2.29}$$

Similarly, the potential energy derivative is:

$$\frac{d}{dt}\left(\frac{1}{2}kx^2\right) = \frac{1}{2}k(2x)\dot{x} = kx(\dot{x}). \tag{2.30}$$

Substituting Eqs. 2.29 and 2.30 into Eq. 2.28 gives:

$$\dot{x}(m\ddot{x} + kx) = 0, \tag{2.31}$$

which is the same result obtained from the free body diagram approach for this spring-mass system: $m\ddot{x} + kx = 0$. The energy method is particularly useful when the "mass" and "spring" elements are difficult to identify. Let's consider an example [1].

A cylinder with mass, m, rolls without slipping on a concave cylindrical surface as shown in Fig. 2.10. Let's determine the cylinder's differential equation of motion for small oscillations about the lowest point for the concave surface (this is the equilibrium position). For no slipping, the two arc lengths, $R\theta$ and $r\phi$, are equal: $R\theta = r\phi$. Their time derivatives are also equal:

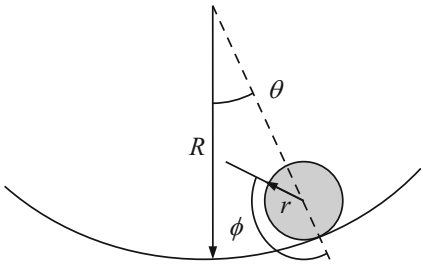

Fig. 2.10 A cylinder rolls without slipping on a concave cylindrical surface

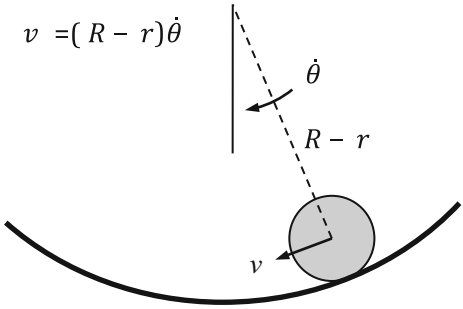

Fig. 2.11 Translational velocity, v, for the rolling cylinder

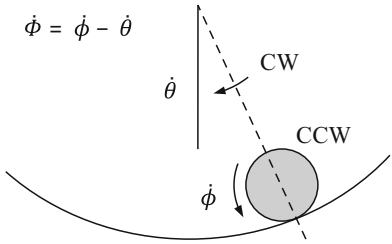

Fig. 2.12 Rotational velocity, $\dot{\Phi}$, for the rolling cylinder

$$R\dot{\theta} = r\dot{\phi}. \tag{2.32}$$

To apply the energy method, we need to write equations for both *KE* and *PE*. For the kinetic energy, there is both translation and rotation of the rolling cylinder. The translational velocity, v, is equal to the product of the radius from the concave surface center to the cylinder center, $R - r$, and the angular velocity about the surface center, $\dot{\theta}$:

$$v = (R - r)\dot{\theta} \tag{2.33}$$

as shown in Fig. 2.11. The rotational velocity for the cylinder itself is $\dot{\Phi} = \dot{\phi} - \dot{\theta}$. We require this difference because $\dot{\phi}$ is counter-clockwise (CCW), while $\dot{\theta}$ is clockwise (CW) as the cylinder rolls from right to left as shown in Fig. 2.12. We

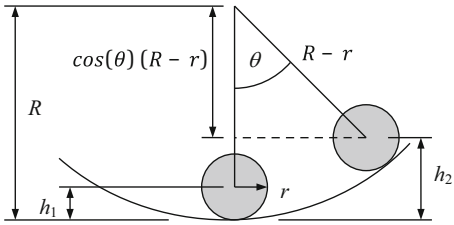

Fig. 2.13 Cylinder height as a function of the angle θ

can express the cylinder's rotational velocity in terms of $\dot{\theta}$ only, however, by applying the no-slipping condition represented by Eq. 2.32. Solving this equation for $\dot{\phi}$ gives $\dot{\phi} = \frac{R}{r}\dot{\theta}$. Substitution in $\dot{\phi} - \dot{\theta}$ yields:

$$\dot{\Phi} = \frac{R}{r}\dot{\theta} - \dot{\theta} = \left(\frac{R-r}{r}\right)\dot{\theta}. \tag{2.34}$$

Given these velocity expressions, we can now write the kinetic energy equation. We again have the $\frac{1}{2}mv^2$ term for the translational kinetic energy, but we also have a $\frac{1}{2}J\dot{\Phi}^2$ term for the rotational kinetic energy, where J is the mass moment of inertia. The kinetic energy equation is:

$$KE = \frac{1}{2}m\left((R-r)\dot{\theta}\right)^2 + \frac{1}{2}J\left(\left(\frac{R-r}{r}\right)\dot{\theta}\right)^2. \tag{2.35}$$

Simplifying Eq. 2.35 gives:

$$\begin{aligned} KE &= \frac{1}{2}m\left((R-r)^2\dot{\theta}^2 + \frac{r^2}{2}\left(\frac{R-r}{r}\right)^2\dot{\theta}^2\right) \\ KE &= \frac{1}{2}m(R-r)^2\left(\dot{\theta}^2 + \frac{\dot{\theta}^2}{2}\right) = \frac{3}{4}m(R-r)^2\dot{\theta}^2, \end{aligned} \tag{2.36}$$

where we substituted for the uniform cylinder's mass moment of inertia: $J = \frac{mr^2}{2}$.

Because there are no springs in this system, the potential energy is based only on the height of the cylinder's center above the lowest position. We can express this in terms of the angle θ as shown in Fig. 2.13, where h_1 is the lowest position height and h_2 is the height that varies with θ. These two heights are:

$$h_1 = r \tag{2.37}$$

and

$$h_2 = R - \cos(\theta)(R - r). \tag{2.38}$$

The gravitational potential energy is then:

$$\begin{aligned} PE = mg(h_2 - h_1) &= mg(R - \cos(\theta)(R - r) - r) \\ PE &= mg(R - r)(1 - \cos(\theta)). \end{aligned} \tag{2.39}$$

Finally, we sum the kinetic and potential energy and calculate the time derivative of this sum. Alternatively, we can first calculate the derivatives of each and then sum them and set this result equal to zero. Note that this sum is set equal to zero because the derivative of a constant is zero, i.e., $\frac{d}{dt}(KE + PE = \text{constant})$ gives $\frac{dKE}{dt} + \frac{dPE}{dt} = 0$. The kinetic and potential energy derivatives are:

$$\frac{d}{dt}(KE) = \frac{d}{dt}\left(\frac{3}{4}m(R - r)^2\dot{\theta}^2\right) = \frac{3}{4}m(R - r)^2(2\dot{\theta})\ddot{\theta} \tag{2.40}$$

and

$$\frac{d}{dt}(PE) = \frac{d}{dt}(mg(R - r)(1 - \cos(\theta))) = mg(R - r)(\sin(\theta))\dot{\theta}. \tag{2.41}$$

Their sum is $m\dot{\theta}\left(\frac{3}{2}(R - r)^2\ddot{\theta} + g(R - r)\sin(\theta)\right) = 0$. For small angles, we can approximate $sin(\theta)$ as θ and rewrite this equation as:

$$\ddot{\theta} + \frac{2}{3}\frac{g}{(R - r)}\theta = 0. \tag{2.42}$$

This is the system equation of motion written in the same form as Eq. 1.10, which is the **standard form** for the **differential equation of harmonic motion**. Using this form, $\frac{d^2x}{dt^2} + \omega^2 x = 0$, we can immediately identify the natural frequency for the system:

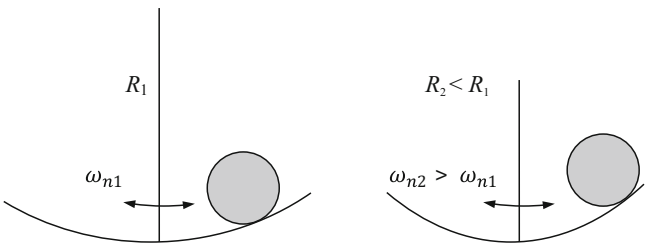

Fig. 2.14 Natural frequency dependence on R for the rolling cylinder example

$$\omega_n = \sqrt{\frac{2}{3}\frac{g}{(R-r)}}. \tag{2.43}$$

This equation tells us that a larger radius, R, of the concave surface should give a lower natural frequency. Using Fig. 2.14, we see that this makes intuitive sense.

Let's return to the spring-mass system and show how to quickly identify the natural frequency using the energy expressions. First, we can recognize that the kinetic energy is maximum when the potential energy is zero since their sum is a constant. In equation form, we have $KE_{max} + 0 =$ constant. For the undamped, single degree of freedom, lumped parameter model, this maximum kinetic energy is identified when the oscillating mass is passing through its $x = 0$ position (where the velocity is maximum, $\dot{x}_{max}$). Naturally, the potential energy is zero at $x = 0$ because the spring extension is zero. Second, we can also see that the potential energy is maximum when the kinetic energy is zero: $0 + PE_{max} =$ constant. The maximum potential energy occurs at the maximum spring extension, x_{max}, where the mass velocity is zero. Because KE_{max} and PE_{max} are both equal to the same constant, we can equate them.

$$\frac{1}{2}m\dot{x}_{max}^2 = \frac{1}{2}kx_{max}^2 \tag{2.44}$$

To determine the $\dot{x}_{max}$ and x_{max} values, we need to select a form for the harmonic solution of the differential equation of motion from our previous list. Let's use $x(t) = A\cos(\omega_n t + B)$. The maximum value is $x_{max} = A$. The velocity is $\dot{x}(t) = -\omega_n A\sin(\omega_n t + B)$ and its maximum value is $\dot{x}_{max} = \omega_n A$. Substituting in Eq. 2.44 gives:

$$\frac{1}{2}m\left(\omega_n^2 A^2\right) = \frac{1}{2}k\left(A^2\right). \tag{2.45}$$

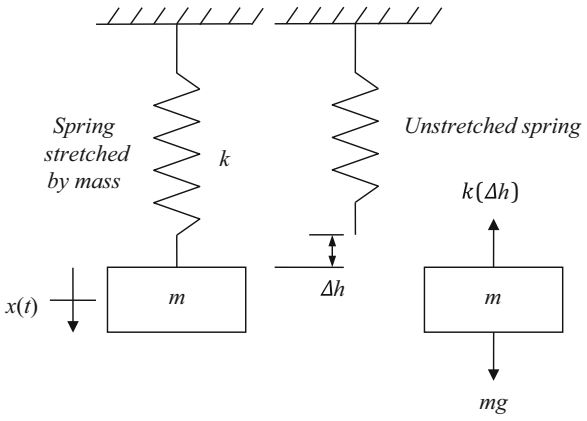

Fig. 2.15 Static free body diagram for spring-mass system

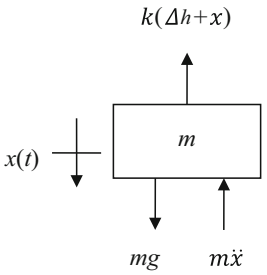

Fig. 2.16 Free body diagram for vibrating spring-mass system including the gravitational force and static spring deflection

Rewriting Eq. 2.45 gives $\omega_n^2 = \frac{k}{m}$. This result is the same as Eq. 2.10 which is based on the free body diagram analysis. Solving for the natural frequency yields $\omega_n = \sqrt{\frac{k}{m}}$.

Given the rolling cylinder and spring-mass examples we've considered in this section, you may be asking the question: "Why didn't we include the gravitational potential energy for the spring-mass example?" This is a great question and its answer resides in how we are defining the $x = 0$ location. In all spring-mass (-damper) examples in this text, we'll set x to be equal to zero at the static equilibrium position of the mass. This means that the spring is actually deflected from its free length by the gravitational force (mass) already. The force balance from the static free body diagram in Fig. 2.15 is $k(\Delta h) = mg$, where Δh is the spring extension due to the weight of the lumped parameter mass, m.

Now let's consider some other position while the mass is vibrating. In this case the spring force is $k(x + \Delta h)$ and the force balance from the free body diagram in Fig. 2.16 is:

$$\sum f_x = mg - k(x + \Delta h) - m\ddot{x} = 0. \tag{2.46}$$

Expanding this equation and substituting $k(\Delta h)$ for mg gives $k(\Delta h) - kx - k(\Delta h) - m\ddot{x} = 0$. Canceling and rewriting gives the expected equation of motion $m\ddot{x} + kx = 0$. Our conclusion is that the gravity potential is canceled by the deflected spring force, so we do not need to consider either.[1]

In a Nutshell

The gravity term does not appear in the spring-mass system because the equations are written about the equilibrium position. This kind of system vibrates with the same frequency and in the same way whether it is aligned with gravity, perpendicular to gravity, or even in the absence of gravity. In the case of the rolling cylinder, it is gravity that supplies the spring component. The cylinder example does not vibrate in the absence of gravity.

[1]This also describes why there is no gravitational force, mg, in Fig. 2.3.

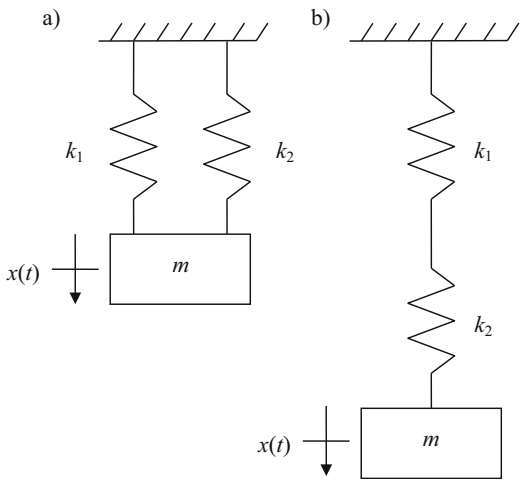

Fig. 2.17 Two springs arranged in: (**a**) parallel; and (**b**) series

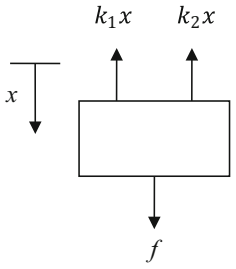

Fig. 2.18 Static free body diagram for two springs in parallel

2.3 Additional Information

Before continuing with the spring-mass-damper (i.e., the damped harmonic oscillator) analysis in the next section, there are three topics that we should explore.

2.3.1 Equivalent Springs

Figure 2.17 shows two possibilities for combining two springs, k_1 and k_2. In Fig. 2.17a, the springs are arranged in **parallel**. What we'd like to do is replace these two parallel springs with a single, **equivalent spring**, k_{eq}. We can find this equivalent spring constant using Fig. 2.18. The total force, f, required to deflect the two springs balances the sum of the two spring forces, f_1 and f_2 in the static case. Because the deflection is the same for both springs, we can write:

$$f = f_1 + f_2 = k_1x + k_2x = (k_1 + k_2)x. \tag{2.47}$$

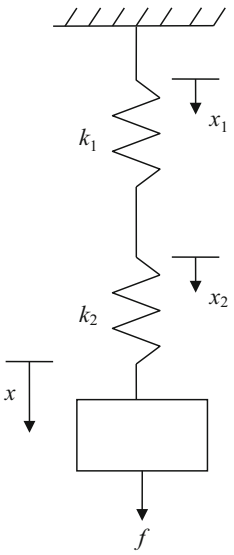

Fig. 2.19 Deflections for two springs in series

By inspection, we see that $k_{eq} = k_1 + k_2$. For n springs in parallel with constants $k_1, k_2, k_3, \ldots, k_n$, the equivalent spring constant is:

$$k_{eq} = \sum_{j=1}^{n} k_j. \tag{2.48}$$

For the springs in **series** shown in Fig. 2.17b, we recognize that a force applied to the end of the two springs will cause a deflection, x, and that the sum of the deflections for the individual springs, x_1 and x_2, must equal the total deflection. Additionally, we know that the individual deflections depend on the force, F, applied at the free end; see Fig. 2.19. These deflections are $x_1 = \frac{f}{k_1}$ for the top spring and $x_2 = \frac{f}{k_2}$ for the bottom spring. The total deflection is therefore $x = x_1 + x_2 = \frac{f}{k_1} + \frac{f}{k_2}$. We find the equivalent spring constant using Eq. 2.49.

$$k_{eq} = \frac{f}{x} = \frac{f}{\frac{f}{k_1} + \frac{f}{k_2}} = \frac{1}{\frac{1}{k_1} + \frac{1}{k_2}} \tag{2.49}$$

In general, for n springs in series with constants $k_1, k_2, k_3, \ldots, k_n$, the equivalent spring constant is calculated using:

$$\frac{1}{k_{eq}} = \sum_{j=1}^{n} \frac{1}{k_j}. \tag{2.50}$$

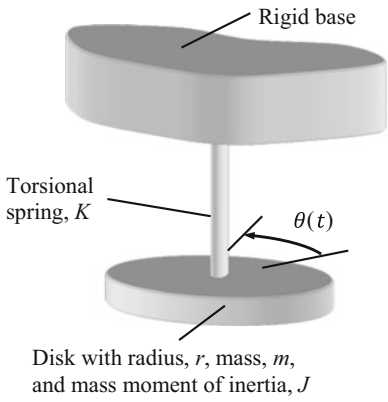

Fig. 2.20 Lumped parameter model for single degree of freedom torsional system

In a Nutshell
The process of determining an equivalent spring means that we apply a "test force" and measure the resulting displacement. This is generally true both in our idealized models and in practice. It is useful because springs very rarely look like our idealized textbook picture. This concept gives us an idea for a physical test we can use to construct an idealized model of a physical system.

2.3.2 Torsional Systems

For single degree of freedom **torsional systems**, the independent coordinate is the rotational angle, θ, rather than position. We'll again assume a lumped parameter system as shown in Fig. 2.20. A massless rod, which serves as a torsional spring, K, is attached to a disk with a mass moment of inertia, J. The spring constant for the rod can be expressed as:

$$K = \frac{GI}{l}, \tag{2.51}$$

where G is the shear modulus, I is the polar moment of inertia, and l is the rod's length. The shear modulus can be written as a function of the elastic modulus, E, and Poisson's ratio, ν: $G = \frac{E}{2(1+\nu)}$. The polar moment of inertia for the rod with diameter, d, is $I = \frac{\pi d^4}{32}$.

The free body diagram, which includes the inertial torque, is shown in Fig. 2.21. Summing the torques (counter-clockwise is assumed positive) gives $\sum T = -J\ddot{\theta} - K\theta = 0$. We can rewrite this to obtain the standard form for the torsional differential equation of harmonic motion:

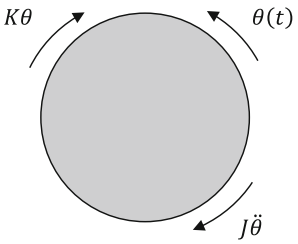

Fig. 2.21 Free body diagram for torsional system (top view through the rigid base in Fig. 2.20). The d'Alembert inertial torque is included

$$\ddot{\theta} + \frac{K}{J}\theta = 0. \tag{2.52}$$

We can now directly identify the natural frequency: $\omega_n = \sqrt{\frac{K}{J}}$.

Let's take a look at the SI units for this system. For the spring constant, G has units of Pa or N/m^2, I has units of m^4, and l has units of m. Combining these, we obtain:

$$\frac{\frac{N}{m^2}m^4}{m} = N \cdot m. \tag{2.53}$$

However, we can see that the stiffness is multiplied by the rotation angle to give the final torque. Therefore, we can include units of radians in the stiffness denominator: $\frac{N \cdot m}{rad}$. Remember that in mathematical "writing", we can include or exclude radians as desired.

We also need units for the disk's mass moment of inertia. As we saw with the rolling cylinder problem, $J = \frac{mr^2}{2} = \frac{md^2}{8}$, where r indicates radius, d is diameter, and m is the disk mass. The units are $kg \cdot m^2$, but we will again include radians in the denominator for compatibility with the equation of motion: $\frac{kg \cdot m^2}{rad}$. Let's now verify the natural frequency units.

$$\omega_n = \sqrt{\frac{\frac{N \cdot m}{rad}}{\frac{kg \cdot m^2}{rad}}} = \sqrt{\frac{kg\frac{m}{s^2}m}{kg \cdot m^2}} = \sqrt{\frac{1}{s^2}} = \frac{rad}{s}. \tag{2.54}$$

2.3.3 Nonlinear Springs

In this text we are only considering vibration of linear systems. However, there are instances where a nonlinear model better describes the system behavior. One way to incorporate nonlinear behavior is through the use of nonlinear springs, or springs where the force is not linear with displacement as we showed in Fig. 2.2. A common nonlinear spring model, referred to as a **Duffing spring**, includes a cubic nonlinearity:

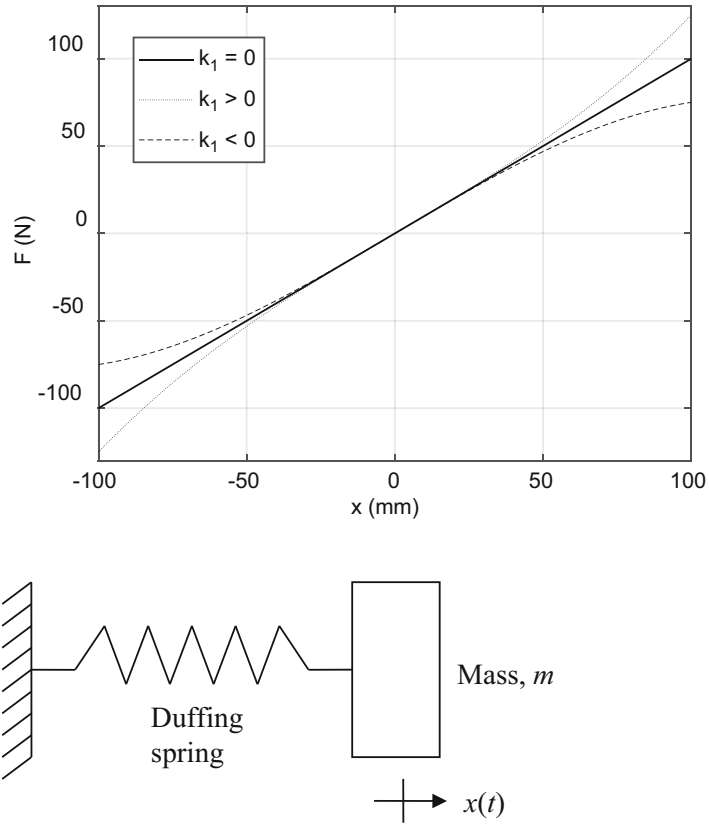

Fig. 2.22 Duffing spring responses for linear, hardening, and softening cases

$$f = k_0 x + k_1 x^3. \tag{2.55}$$

For the Duffing spring, k_0 is the linear spring constant ($k_0 > 0$) and k_1 is the nonlinear spring constant. If k_1 is greater than zero, the spring is a hardening spring. If k_1 is less than zero, it is a softening spring. The (undamped) Duffing differential equation of motion is:

$$m\ddot{x} + k_0 x + k_1 x^3 = 0, \tag{2.56}$$

where the linear spring in Fig. 2.8 has simply been replaced by the Duffing spring. Analytical solutions for such nonlinear differential equations are difficult to obtain, but we do have some tools to help us understand their behavior. Let's explore the Duffing spring in MATLAB® MOJO 2.1. In this example, we'll compare the displacement-force relationships for three cases: (1) $k_1 = 0$ (linear); (2) $k_1 = 2.5 \times 10^4$ N/m^3 (hardening); and (3) $k_1 = -2.5 \times 10^4$ N/m^3 (softening). In all instances, $k_0 = 1 \times 10^3$ N/m. The results are provided in Fig. 2.22. Note that these values were selected for plotting convenience and do not represent a particular physical system.

MATLAB® MOJO 2.1

```
% matlab_mojo_2_1.m

clear
close all
clc

% Define variables
x = -0.1:0.001:0.1;     % m
k0 = 1000;          % N/m

% Define force
F = k0*x;
k1 = 25000;          % N/m^3

Fstiff = F + k1*x.^3;    % stiffening spring
Fsoft = F - k1*x.^3;     % softening spring

figure(1)
plot(x*1e3, F, 'k-', x*1e3, Fstiff, 'k:', x*1e3, Fsoft, 'k--')
set(gca,'FontSize', 14)
xlabel('x (mm)')
ylabel('F (N)')
legend('k_1 = 0', 'k_1 > 0', 'k_1 < 0')
grid
axis([-100 100 -130 130])
```

2.4 Damped Harmonic Oscillator

Let's now include damping in the single degree of freedom spring-mass lumped parameter model. As we mentioned previously, all systems exhibit damping or "losses". There are three main types of damping used to model physical systems.

2.4.1 Viscous Damping

As we discussed previously, the viscous damping model relates force to velocity as shown in Eq. 2.2. In this equation, the proportionality constant c is the viscous damping coefficient with SI units of N s/m. Physically, this model adequately describes the retarding force on a body that is moving at a moderate speed through a fluid. Because it is convenient to implement mathematically, it is the most common selection for modeling vibratory systems.

2.4.2 Coulomb Damping

This type of damping represents the energy dissipation due to dry sliding between two surfaces (or friction). In this case, the force, which always opposes the direction of motion, is described by Eq. 2.57. In this equation, μ is the friction coefficient and N is the normal force between the two bodies, which is perpendicular (normal) to the contacting surfaces.

$$f = \mu N \tag{2.57}$$

2.4.3 Solid Damping

Solid, or structural, damping occurs due to internal energy dissipation within the material of the vibrating body. Consider a steel beam floating in space. If an astronaut were to tap this beam at its end, it would begin to rotate about its center of mass—this is referred to as **rigid body motion**—and it would also begin vibrating. Since nothing is touching the beam and there is no obvious resistance to motion, why does the vibrating motion eventually stop? This is solid damping and we will describe it using a complex elastic modulus for the beam material, E_s, in Sect. 8.3. See Eq. 2.58, where η is the material-dependent solid damping factor.

$$E_s = E(1 + i\eta) \tag{2.58}$$

2.4.4 Damped System Behavior

Since viscous damping is the most common modeling choice, we'll consider it now to represent our single degree of freedom spring-mass-damper system. As shown in Figs. 2.1 and 2.3 from Sect. 2.1, the equation of motion is $m\ddot{x} + c\dot{x} + kx = 0$ (see Eq. 2.3). Because the vibratory response when the system is disturbed from its equilibrium position is again harmonic, we can select a solution of the form $x(t) = Xe^{st}$ with $\dot{x}(t) = sXe^{st}$ and $\ddot{x}(t) = s^2Xe^{st}$. Substituting in the equation of motion and grouping terms gives:

$$\left(ms^2 + cs + k\right)Xe^{st} = 0. \tag{2.59}$$

As with the undamped model, there are two options for Eq. 2.59. If $Xe^{st} = 0$, no motion has occurred and this is referred to as the trivial solution. The characteristic equation is therefore:

$$ms^2 + cs + k = 0. \tag{2.60}$$

The characteristic equation is quadratic in s and has two roots. Dividing by m gives $s^2 + \frac{c}{m}s + \frac{k}{m} = 0$ and the two roots can be determined using the quadratic equation.

$$s_{1,2} = \frac{-\frac{c}{m} \pm \sqrt{\left(\frac{c}{m}\right)^2 - 4(1)\frac{k}{m}}}{2(1)} = -\frac{c}{2m} \pm \sqrt{\left(\frac{c}{2m}\right)^2 - \frac{k}{m}} \tag{2.61}$$

The total solution for the system vibration is the sum of the two harmonic responses defined by the two roots: $x(t) = X_1 e^{s_1 t} + X_2 e^{s_2 t} = X_1 e^{\left(-\frac{c}{2m} + \sqrt{\left(\frac{c}{2m}\right)^2 - \frac{k}{m}}\right)t} + X_2 e^{\left(-\frac{c}{2m} - \sqrt{\left(\frac{c}{2m}\right)^2 - \frac{k}{m}}\right)t}$. This equation can be rewritten as shown in Eq. 2.62, where the first term in the product (i.e., the exponential term) describes the damping envelope that bounds the decaying oscillation and the second term (in parentheses) defines the oscillatory part.

$$x(t) = e^{\left(-\frac{c}{2m}\right)t}\left(X_1 e^{\left(\sqrt{\left(\frac{c}{2m}\right)^2 - \frac{k}{m}}\right)t} + X_2 e^{\left(-\sqrt{\left(\frac{c}{2m}\right)^2 - \frac{k}{m}}\right)t}\right) \tag{2.62}$$

The system behavior depends on the value of the radical expression, $\sqrt{\left(\frac{c}{2m}\right)^2 - \frac{k}{m}}$, and there are three possibilities.

1. If $\left(\frac{c}{2m}\right)^2 - \frac{k}{m} < 0$, the characteristic equation will have complex roots (i.e., s_1 and s_2 will have both real and imaginary parts). In this case, the response is vibratory (see Eq. 2.62).
2. If $\left(\frac{c}{2m}\right)^2 - \frac{k}{m} > 0$, the characteristic equation will have real-valued roots and there is no oscillation. The viscous damping is large enough to prevent vibration.
3. If $\left(\frac{c}{2m}\right)^2 - \frac{k}{m} = 0$, the two roots are real and equal, $s_{1,2} = -\frac{c}{2m}$, and there is just no oscillation. This case is referred to as **critical damping**. If a system with critical damping is displaced, it will return to its equilibrium position as quickly as possible without ever passing through the equilibrium position.

We can determine the damping coefficient required to achieve critical damping, c_c, by rearranging the radical equation for case 3: $\left(\frac{c_c}{2m}\right)^2 - \frac{k}{m} = 0$. We have that $\left(\frac{c_c}{2m}\right)^2 = \frac{k}{m}$ or $c_c = 2m\sqrt{\frac{k}{m}}$. Finally, by simplifying we obtain:

$$c_c = 2\sqrt{km}. \tag{2.63}$$

We can now define a dimensionless parameter, referred to as the **damping ratio**, using the critical damping coefficient. The damping ratio, ζ, is:

$$\zeta = \frac{c}{c_c} = \frac{c}{2\sqrt{km}}. \tag{2.64}$$

In a Nutshell
It is often convenient to describe the damping of a system in comparison to the damping that would just prevent vibration. This is the damping ratio. A damping ratio of, say, 0.3 means that the system has 30% of the damping required to prevent vibration. Unless designers make special efforts, most mechanical structures have very low damping ratios—almost always less than 10% and more typically on the order of 1–5%.

Let's now see how we can rewrite the equation of motion to use the damping ratio. We've already seen the form $s^2 + \frac{c}{m}s + \frac{k}{m} = 0$. We can write the final term, $\frac{k}{m}$, as ${\omega_n}^2$, but what about the $\frac{c}{m}$ coefficient on s? This can be expressed as $\frac{c}{m} = 2\zeta\omega_n$. Solving for ζ gives $\zeta = \frac{c}{2m\omega_n}$. This can be rewritten as $\zeta = \frac{c}{2\sqrt{m^2}\sqrt{\frac{k}{m}}} = \frac{c}{2\sqrt{\frac{km^2}{m}}} = \frac{c}{2\sqrt{km}}$, which validates the $\frac{c}{m} = 2\zeta\omega_n$ equation. We can therefore rewrite the equation of motion in the form shown in Eq. 2.65. We will use this form in many instances as we move forward.

$$s^2 + 2\zeta\omega_n s + {\omega_n}^2 = 0 \tag{2.65}$$

In the same way as we discussed for the radical expression value, there are three possibilities for the damping ratio.

1. If $\zeta < 1$ ($c < c_c$), the response is vibratory with a magnitude that decays exponentially over time. The system that exhibits this behavior is referred to as **underdamped**. This is the situation for most mechanical systems.
2. If $\zeta > 1$ ($c > c_c$), there is no vibration. This is the **overdamped** case.
3. If $\zeta = 1$ ($c = c_c$), the system is **critically damped**.

2.4.5 *Underdamped System*

Let's explore the underdamped case in a little more detail. As stated earlier, the two roots of the characteristic equation will be complex-valued. These roots are calculated using Eq. 2.61, where the term under the radial is negative. Let's verify that the radial term is indeed negative for an underdamped system. We need to show that $\left(\frac{c}{2m}\right)^2 - \frac{k}{m} < 0$. This equation can be rewritten as $\frac{c}{2m} < \sqrt{\frac{k}{m}}$ (or $c < 2m\omega_n$) and

simplified to obtain $c < 2\sqrt{m^2}\sqrt{\frac{k}{m}}$, or $c < 2\sqrt{km}$. Because this is equivalent to $c < c_c$, which indicates underdamped behavior, we have validated our assertion.

Let's rewrite the radical term as $-\left(\frac{k}{m} - \left(\frac{c}{2m}\right)^2\right)$. Using the undamped natural frequency and damping ratio, we can then redefine this expression as $-({\omega_n}^2 - (\zeta\omega_n)^2) = -({\omega_n}^2(1 - \zeta^2))$. We can substitute this result in Eq. 2.61 to obtain a new form for the roots equation as shown in Eq. 2.66.

$$\begin{aligned} s_{1,2} &= -\zeta\omega_n \pm \sqrt{-\left({\omega_n}^2\left(1-\zeta^2\right)\right)} \\ s_{1,2} &= -\zeta\omega_n \pm i\omega_n\sqrt{1-\zeta^2} \end{aligned} \tag{2.66}$$

We can now introduce the **damped natural frequency**, ω_d, which describes the frequency of free vibration when damping is present:

$$\omega_d = \omega_n\sqrt{1-\zeta^2}. \tag{2.67}$$

Because the damping ratio for mechanical systems if typically small ($\zeta < 0.1$), the value of the damped natural frequency is only slightly less than the undamped natural frequency. For example, if $\zeta = 0.05$ (5% viscous damping), then $\omega_d = \omega_n\sqrt{1-0.05^2} = 0.999\omega_n$.

The roots in Eq. 2.66 can now be written in more compact notation: $s_{1,2} = -\zeta\omega_n \pm i\omega_d$. Substitution in the assumed harmonic form enables us to rewrite Eq. 2.62 as shown in Eq. 2.68, where the first term in the product again describes the damping envelope that bounds the oscillation (at the damped natural frequency) defined by the second term in the product. See Fig. 2.23.

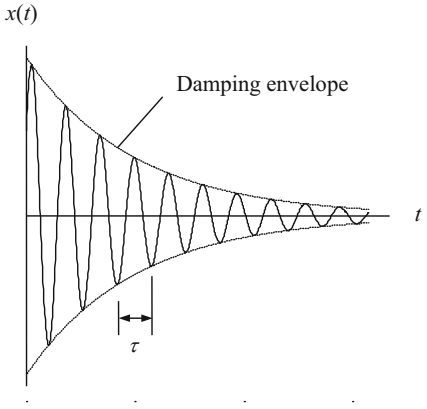

Fig. 2.23 Damped free vibration response

$$x(t) = e^{-\zeta\omega_n t}\left(X_1 e^{i\omega_d t} + X_2 e^{-i\omega_d t}\right) \tag{2.68}$$

For the exponential term in Eq. 2.68, a higher damping ratio gives a more rapid decay rate. For the oscillatory part, if the period of vibration is τ (expressed in seconds), the damped natural frequency (in Hz) is:

$$f_d = \frac{1}{\tau}. \tag{2.69}$$

Also, the relationship between the damped natural frequency in rad/s, ω_d, and Hz is $\omega_d = 2\pi f_d$ as we saw for the undamped case.

By the Numbers 2.2

Let's calculate the free vibration response for a spring-mass-damper system with the following parameters.

- $m = 1$ kg
- $c = 20$ N s/m
- $k = 1 \times 10^4$ N/m
- the initial displacement is: $x_0 = 25$ mm
- the initial velocity is: $\dot{x}_0 = 1000$ mm/s

The undamped natural frequency is $\omega_n = \sqrt{\frac{k}{m}} = \sqrt{\frac{1\times10^4}{1}} = 100$ rad/s. Converting to Hz, we obtain $f_n = \frac{\omega_n}{2\pi} = 15.9$ Hz. The damping ratio is $\zeta = \frac{c}{2\sqrt{km}} = \frac{20}{2\sqrt{1\times10^4(1)}} = 0.1$ (or 10% damping). The damped natural frequency is therefore $\omega_d = \omega_n\sqrt{1-\zeta^2} = 100\sqrt{1-0.1^2} = 99.5$ rad/s.

For this underdamped case, we can use the form for the solution provided in Eq. 2.68. In order to apply the initial conditions, we also need the velocity, which we obtain by calculating the time derivative of Eq. 2.68. See Eq. 2.70.

$$\dot{x}(t) = e^{-\zeta\omega_n t}(i\omega_d)\left(X_1 e^{i\omega_d t} - X_2 e^{-i\omega_d t}\right) - \zeta\omega_n e^{-\zeta\omega_n t}\left(X_1 e^{i\omega_d t} + X_2 e^{-i\omega_d t}\right) \tag{2.70}$$

Substituting $t = 0$ into Eqs. 2.68 and 2.70 gives:

$$x(0) = x_0 = X_1 + X_2 \tag{2.71}$$

and

$$\dot{x}(0) = \dot{x}_0 = i\omega_d(X_1 - X_2) - \zeta\omega_n(X_1 + X_2). \tag{2.72}$$

Using Eq. 2.71, we can substitute for $(X_1 + X_2)$ in Eq. 2.72. This gives $\dot{x}_0 = i\omega_d(X_1 - X_2) - \zeta\omega_n x_0$. Solving this equation for $(X_1 - X_2)$ yields $X_1 - X_2 = \frac{\dot{x}_0 + \zeta\omega_n x_0}{i\omega_d}$. We can rationalize this equation by multiplying both the numerator and denominator by the imaginary variable i:

$$X_1 - X_2 = \frac{\dot{x}_0 + \zeta\omega_n x_0}{i\omega_d}\frac{i}{i} = \frac{-i(\dot{x}_0 + \zeta\omega_n x_0)}{\omega_d}. \tag{2.73}$$

We can now add Eqs. 2.71 and 2.73 to eliminate X_2. The result is:

$$X_1 = \frac{x_0}{2} - i\frac{(\dot{x}_0 + \zeta\omega_n x_0)}{2\omega_d}. \tag{2.74}$$

Using Eq. 2.71, we can then determine X_2.

$$X_2 = \frac{x_0}{2} + i\frac{(\dot{x}_0 + \zeta\omega_n x_0)}{2\omega_d} \tag{2.75}$$

The coefficients X_1 and X_2 are complex conjugates. This is always the case for this form of the underdamped harmonic motion solution. Substituting the values for this example into Eqs. 2.74 and 2.75 gives:

$$X_1 = \frac{25}{2} - i\frac{(100 + 0.1(100)25)}{2(99.5)} = 12.5 - i6.28$$

and

$$X_2 = 12.5 + i6.28.$$

Let's rewrite these expressions in vector notation before substituting in the response equation (Eq. 2.68). The vector representations of these complex conjugates are plotted in Fig. 2.24. Using this figure, we can determine the magnitude and phase for each vector. The magnitude, which is the square root of the sum of the squares of the real (Re) and imaginary (Im) parts, is the same for both vectors and is given by:

$$|X_{1,2}| = \sqrt{Re^2 + Im^2} = \sqrt{12.5^2 + 6.28^2} = 13.99.$$

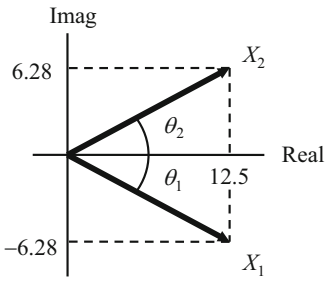

Fig. 2.24 X_1 and X_2 complex conjugates

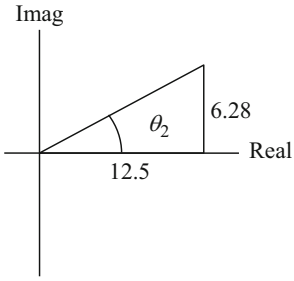

Fig. 2.25 Phase calculation for X_2

The phase is the inverse tangent of the ratio of the imaginary part to the real part; this is evident from Fig. 2.25 which highlights the "triangle" formed by the real and imaginary parts of the X_2 vector. The corresponding phase is $\theta_2 = tan^{-1}\left(\frac{Im}{Re}\right) = tan^{-1}\left(\frac{6.28}{12.5}\right) = 0.466$ rad $= 26.67°$. For the X_1 vector, the phase is $\theta_1 = tan^{-1}\left(\frac{Im}{Re}\right) = tan^{-1}\left(\frac{-6.28}{12.5}\right) = -0.466$ rad $= -26.67°$.

The vector notations for X_1 and X_2 are then $X_1 = 13.99e^{-i0.466}$ and $X_2 = 13.99e^{i0.466}$. We can now substitute in Eq. 2.68, where $\zeta\omega_n = 0.1(100) = 10$ rad/s and $\omega_d = 99.5$ rad/s.

$$x(t) = e^{-\zeta\omega_n t}\left(X_1 e^{i\omega_d t} + X_2 e^{-i\omega_d t}\right) = e^{-10t}\left(13.99e^{-i0.466}e^{i99.5t} + 13.99e^{i0.466}e^{-i99.5t}\right)$$
$$= 13.99e^{-10t}\left(e^{i(99.5t-0.466)} + e^{-i(99.5t-0.466)}\right)$$

Using Eq. 1.12 (derived from Euler's formula), we can rewrite this equation as:

$$x(t) = 2(13.99)e^{-10t}\,cos\,(99.5t - 0.466) = 27.98e^{-10t}\,cos\,(99.5t - 0.466)\text{ mm},$$

where the magnitude is 27.98 mm, the phase is −0.466 rad, and the decay rate is described by the exponential term e^{-10t}. This damped free vibration response is shown in Fig. 2.26, where the initial value $x(0) = 27.98e^{-10(0)}\,cos\,(99.5(0) - 0.466) = 27.98\,cos\,(-0.466) = 25$ mm matches the initial displacement, $x_0 = 25$ mm, and the **period of vibration** is:

$$\tau = \frac{1}{f_d} = \frac{2\pi}{\omega_d} = \frac{2\pi}{\omega_n\sqrt{1-\zeta^2}} = \frac{2\pi}{100\sqrt{1-0.1^2}} = 0.063\text{ s}$$

Figure 2.26 was produced using the code provided in MATLAB® MOJO 2.2.

MATLAB® MOJO 2.2

```
% matlab_mojo_2_2.m

clear
close all
clc
```

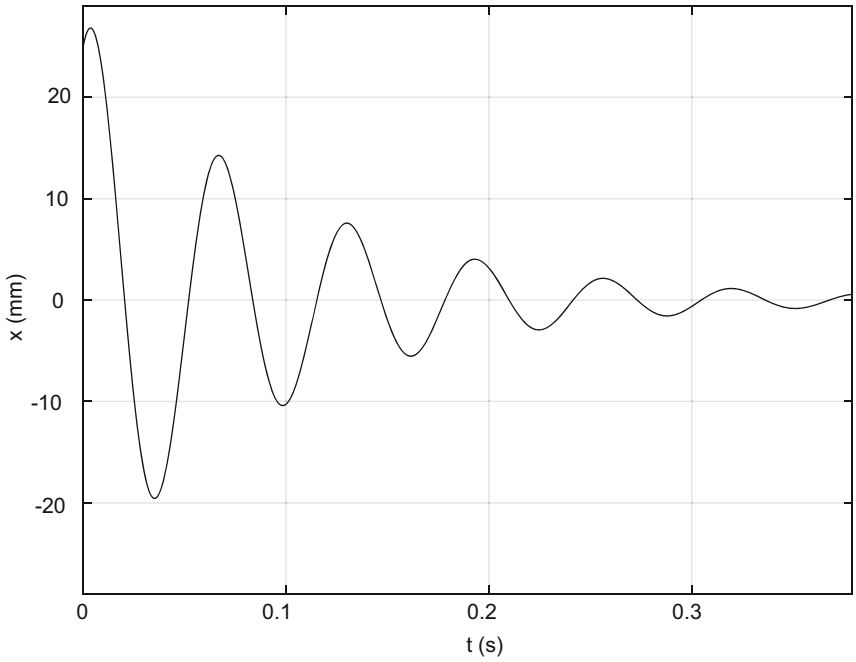

Fig. 2.26 *By the Numbers 2.2*—free vibration response for damped system

```
% Define variables
A = 27.98;          % mm
omegan = 100;        % rad/s
zeta = 0.1;
omegad = omegan*sqrt(1-zeta^2);
fd = omegad/2/pi;      % Hz
tau = 1/fd;         % s
phi = 0.466;         % rad
t = 0:tau/100:6*tau;     % s

% Define displacement
x = A*exp(-zeta*omegan*t).*cos(omegad*t - phi);    % mm

figure(1)
plot(t, x, 'k-')
set(gca,'FontSize', 14)
xlabel('t (s)')
ylabel('x (mm)')
grid
axis([0 max(t) -29 29])
```

By the Numbers 2.3
Let's now consider the free vibration response for a spring-mass-damper system with an initial displacement $x(0) = x_0$ and zero initial velocity for three cases: (1) $\zeta = 2$ (overdamped); (2) $\zeta = 0.2$ (underdamped); and (3) $\zeta = 1$ (critically damped).

Overdamped ($\zeta = 2$)

Because there are two real-valued roots for the characteristic equation, we can write the response in the following form:

$$x(t) = X_1 e^{\left(-\zeta+\sqrt{\zeta^2-1}\right)\omega_n t} + X_2 e^{\left(-\zeta-\sqrt{\zeta^2-1}\right)\omega_n t}. \tag{2.76}$$

The corresponding velocity equation is:

$$\begin{aligned}\dot{x}(t) = &\left(-\zeta + \sqrt{\zeta^2-1}\right)\omega_n X_1 e^{\left(-\zeta+\sqrt{\zeta^2-1}\right)\omega_n t} \\ &+ \left(-\zeta - \sqrt{\zeta^2-1}\right)\omega_n X_2 e^{\left(-\zeta-\sqrt{\zeta^2-1}\right)\omega_n t}.\end{aligned} \tag{2.77}$$

For $\zeta = 2$, the exponent term $-\zeta \pm \sqrt{\zeta^2-1}$ is $-2 \pm \sqrt{2^2-1} = -2 \pm \sqrt{3}$. Substituting gives:

$$x(t) = X_1 e^{\left(-2+\sqrt{3}\right)\omega_n t} + X_2 e^{\left(-2-\sqrt{3}\right)\omega_n t}$$

for position and:

$$\dot{x}(t) = \left(-2+\sqrt{3}\right)\omega_n X_1 e^{\left(-2+\sqrt{3}\right)\omega_n t} + \left(-2-\sqrt{3}\right)\omega_n X_2 e^{\left(-2-\sqrt{3}\right)\omega_n t}$$

for velocity.

We can now apply the initial conditions $x(0) = x_0$ and $\dot{x}(0) = 0$. Substituting gives: $x(0) = \dot{x}_0 = X_1 + X_2$ and $\dot{x}(0) = 0 = \left(-2+\sqrt{3}\right)\omega_n X_1 + \left(-2-\sqrt{3}\right)\omega_n X_2$. The velocity equation can be simplified to be: $\dot{x}(0) = 0 = \left(-2+\sqrt{3}\right)X_1 + \left(-2-\sqrt{3}\right)X_2$ by dividing both sides by ω_n. We now have a system of two linear equations with two unknowns. We could solve for X_1 and X_2 by a variety of methods, but let's use **matrix inversion** here since we'll begin writing our equations of motion in matrix form for the two degree of freedom systems in Sect. 4.1. Our two equations in matrix form are:

$$\begin{bmatrix} 1 & 1 \\ -2+\sqrt{3} & -2-\sqrt{3} \end{bmatrix} \begin{bmatrix} X_1 \\ X_2 \end{bmatrix} = \begin{bmatrix} x_0 \\ 0 \end{bmatrix},$$

where the position equation is the top row of the 2×2 (rows $\times$ columns) matrix multiplied by the 2×1 column vector $\begin{bmatrix} X_1 \\ X_2 \end{bmatrix}$ and set equal to the top, or (1,1), entry, x_0, in the 2×1 column vector on the right hand side of the equal sign $\begin{bmatrix} x_0 \\ 0 \end{bmatrix}$. We perform this term-by-term multiplication to obtain $(1)X_1 + (1)X_2 = x_0$. Similarly, the second row gives the velocity equation. We multiply the (2,1) entry, $-2+\sqrt{3}$, in the 2×2 matrix by X_1 and the (2,2) entry, $-2-\sqrt{3}$, by X_2 and set the result equal to 0, the (2,1) entry in the column vector on the right hand side of the equation. If we rewrite this matrix equation as $A\vec{X} = \vec{B}$, then algebraically we know that we can find $\vec{X}$ by moving A to the right hand side of the equation. For scalar values, we can simply divide both sides by A or, equivalently, multiply both sides by the inverse of A. We can write this as $\vec{X} = A^{-1}\vec{B}$. In our matrix problem, we can perform the same operation, but determining the inverse of the 2×2 A matrix requires a little work.[2] Let's first write the $\vec{X} = A^{-1}\vec{B}$ equation explicitly.

$$\begin{bmatrix} X_1 \\ X_2 \end{bmatrix} = \begin{bmatrix} 1 & 1 \\ -2+\sqrt{3} & -2-\sqrt{3} \end{bmatrix}^{-1} \begin{bmatrix} x_0 \\ 0 \end{bmatrix}$$

Inverting the 2×2 A matrix to determine A^{-1} requires three steps.

1. Switch the on-diagonal terms. This means that we replace the (1,1) entry, 1, by the (2,2) entry, $-2-\sqrt{3}$, and the (2,2) entry by the (1,1) entry.
2. Change the signs of the off diagonal terms. The (1,2) entry becomes -1 and the (2,1) entry becomes $-\left(-2+\sqrt{3}\right) = 2-\sqrt{3}$.
3. Divide each entry in the matrix by the **determinant**. For a 2×2 matrix, the determinant is the difference between the product of the on-diagonal terms and the product of the off-diagonal terms, i.e., $(1,1)(2,2) - (1,2)(2,1)$. For our matrix, this is:

$$(1)\left(-2-\sqrt{3}\right) - (1)\left(-2+\sqrt{3}\right) = -2-\sqrt{3}+2-\sqrt{3} = -2\sqrt{3}.$$

The result for the matrix inversion is:

[2]These matrix manipulations are a subset of the topics covered in a **linear algebra** course.

$$\begin{bmatrix} 1 & 1 \\ -2+\sqrt{3} & -2-\sqrt{3} \end{bmatrix}^{-1} = \frac{1}{-2\sqrt{3}} \begin{bmatrix} -2-\sqrt{3} & -1 \\ 2-\sqrt{3} & 1 \end{bmatrix}$$
$$= \frac{1}{2\sqrt{3}} \begin{bmatrix} 2+\sqrt{3} & 1 \\ -2+\sqrt{3} & -1 \end{bmatrix}.$$

Matrix inversion can also be completed in MATLAB® using the `inv` command. From the command prompt (>>), we first define the 2×2 A matrix. The semicolon indicates the end of the first row in the matrix description.

```
>> A = [1 1;-2+sqrt(3) -2-sqrt(3)]

A =

  1.0000  1.0000
 -0.2679 -3.7321
```

We next determine the matrix inverse. The answer (`ans`) shown below is identical to the result we obtained using the three-step inversion procedure.

```
>> inv(A)

ans =

  1.0774  0.2887
 -0.0774 -0.2887
```

The complete matrix equation is now:

$$\begin{bmatrix} X_1 \\ X_2 \end{bmatrix} = \frac{1}{2\sqrt{3}} \begin{bmatrix} 2+\sqrt{3} & 1 \\ -2+\sqrt{3} & -1 \end{bmatrix} \begin{bmatrix} x_0 \\ 0 \end{bmatrix}.$$

We write the X_1 equation using the top row:

$$X_1 = \frac{1}{2\sqrt{3}} \left(\left(2+\sqrt{3}\right) x_0 + (1)0 \right) = \frac{2+\sqrt{3}}{2\sqrt{3}} x_0 \approx 1.08 x_0.$$

We determine X_2 from the bottom row:

$$X_2 = \frac{1}{2\sqrt{3}} \left(\left(-2+\sqrt{3}\right) x_0 + (-1)0 \right) = \frac{-2+\sqrt{3}}{2\sqrt{3}} x_0 \approx -0.08 x_0.$$

Substituting in Eq. 2.76 gives:
$x(t) = 1.08 x_0 e^{\left(-2+\sqrt{3}\right)\omega_n t} - 0.08 x_0 e^{\left(-2-\sqrt{3}\right)\omega_n t}$ or $\frac{x(t)}{x_0} = 1.08 e^{(-0.27)\omega_n t} - 0.08 e^{(-3.73)\omega_n t}$.

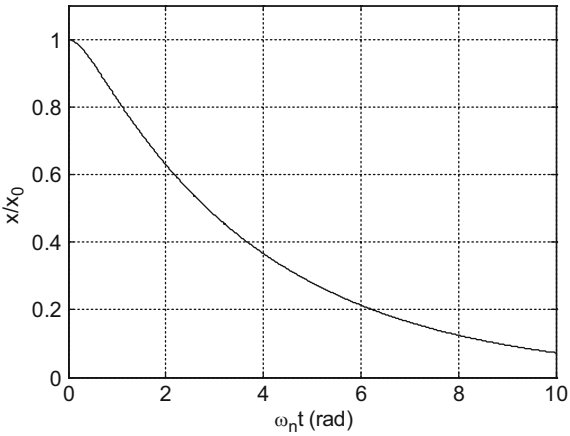

Fig. 2.27 *By the Numbers 2.3*—response for overdamped system with initial displacement only.

The ratio is plotted as a function of $\omega_n t$ in Fig. 2.27.

Underdamped ($\zeta = 0.2$)

We can write the response for the underdamped system with two complex-conjugate roots from the characteristic equation as shown in Eq. 2.68:

$$x(t) = e^{-\zeta\omega_n t}\left(X_1 e^{i\sqrt{1-\zeta^2}\omega_n t} + X_2 e^{-i\sqrt{1-\zeta^2}\omega_n t}\right)$$

or, equivalently, as:

$$x(t) = Xe^{-\zeta\omega_n t}\, sin\left(\sqrt{1-\zeta^2}\omega_n t + \phi\right). \tag{2.78}$$

The velocity equation is:

$$\begin{aligned}\dot{x}(t) = &-\zeta\omega_n X e^{-\zeta\omega_n t}\, sin\left(\sqrt{1-\zeta^2}\omega_n t + \phi\right) \\ &+ \sqrt{1-\zeta^2}\omega_n X e^{-\zeta\omega_n t}\, cos\left(\sqrt{1-\zeta^2}\omega_n t + \phi\right).\end{aligned} \tag{2.79}$$

In this example, $x(0) = x_0$, $\dot{x}(0) = 0$, and $\sqrt{1-\zeta^2} = \sqrt{1-0.2^2} = \sqrt{0.96}$. Substituting gives:

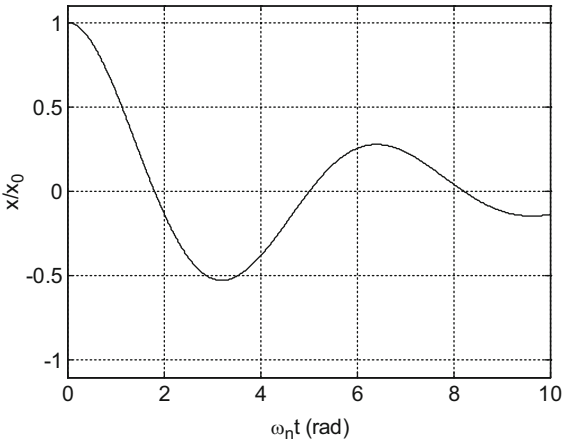

Fig. 2.28 *By the Numbers 2.3*—response for underdamped system with initial displacement only.

$$x(0) = x_0 = Xsin(\phi) \text{ and}$$

$$\dot{x}(0) = 0 = -0.2\omega_n Xsin(\phi) + \sqrt{0.96}\omega_n Xcos(\phi).$$

We can use the velocity equation to determine ϕ. Rewriting gives:

$$0.2\omega_n X \sin(\phi) = \sqrt{0.96}\omega_n X \cos(\phi), \text{ or } \frac{X\sin(\phi)}{X\cos(\phi)} = \tan(\phi) = \frac{\sqrt{0.96}\omega_n}{0.2\omega_n}.$$

This yields $\phi = 1.37$ rad $= 78.5°$. Using the position equation, we solve for X:

$$X = \frac{x_0}{sin(\phi)} = \frac{x_0}{\sqrt{0.96}}.$$

Substituting in Eq. 2.78 gives:

$$\begin{aligned} x(t) &= \frac{x_0}{\sqrt{0.96}} e^{-0.2\omega_n t} \sin\left(\sqrt{0.96}\omega_n t + 1.37\right) \text{ or } \frac{x(t)}{x_0} \\ &= \frac{1}{\sqrt{0.96}} e^{-0.2\omega_n t} \sin\left(\sqrt{0.96}\omega_n t + 1.37\right). \end{aligned}$$

This ratio is plotted in Fig. 2.28. Note that the response is now oscillatory for the underdamped system.

Critically damped ($\zeta = 1$)

The response for this case is written as:

$$x(t) = (X_1 + X_2 t)e^{-\omega_n t} \tag{2.80}$$

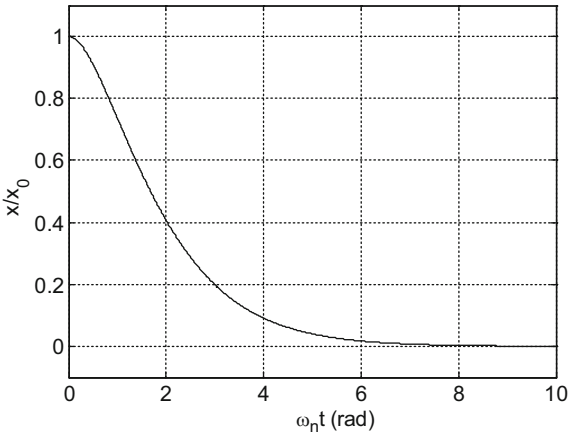

Fig. 2.29 *By the Numbers 2.3*—response for critically damped system with initial displacement only

because there are two repeated, real-valued roots. The corresponding velocity equation is:

$$\dot{x}(t) = -\omega_n(X_1 + X_2 t)e^{-\omega_n t} + X_2 e^{-\omega_n t}. \tag{2.81}$$

Substituting the initial conditions, $x(0) = x_0$, $\dot{x}(0) = 0$, into Eqs. 2.80 and 2.81 gives $x(0) = x_0 = X_1$ and $\dot{x}(0) = 0 = -\omega_n(X_1) + X_2$. From the velocity equation, we obtain $X_2 = \omega_n X_1 = \omega_n x_0$. We can now replace X_1 and X_2 in Eq. 2.80 to find the position as a function of ω_n, x_0, and t. The ratio $\frac{x(t)}{x_0}$ is plotted versus $\omega_n t$ in Fig. 2.29. As a check on this figure, we can see that the value is 1 at $\omega_n t = 0$ as expected, $\frac{x}{x_0} = (1 + 0)e^0 = 1$.

$$x(t) = (x_0 + \omega_n x_0 t)e^{-\omega_n t} \quad \text{or} \quad \frac{x(t)}{x_0} = (1 + \omega_n t)e^{-\omega_n t}$$

2.4.6 *Damping Estimate from Free Vibration Response*

We've said that all physical systems include damping and we've seen that the amount of damping influences the resulting free vibration response. We can now "reverse engineer" this analysis. We'll use the behavior during free oscillation to determine the amount of damping in a system. Quantifying damping is important because it is difficult to predict using models. Designers can use the material properties and dimensions of the components in a structure to predict the natural frequencies using finite element analysis, for example. However, the magnitude of the vibrations that occur when the structure is excited is more challenging to predict

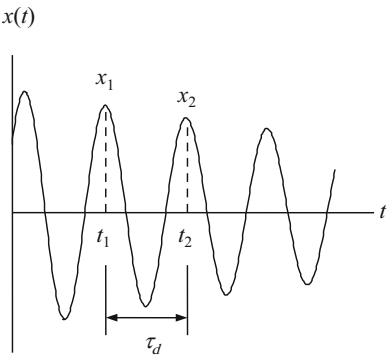

Fig. 2.30 General response for the free vibration of an underdamped single degree of freedom system

based only on first principles. Therefore, damping is typically identified experimentally.

We've already seen in Eq. 2.78 that the free vibration response of an underdamped single degree of freedom system can be written as $x(t) = Xe^{-\zeta\omega_n t}\, sin\left(\sqrt{1-\zeta^2}\omega_n t + \phi\right)$. The general response is shown in Fig. 2.30, where the response value is identified at two time instants, t_1 and t_2, separated by the **damped period of vibration**:

$$\tau_d = \frac{1}{f_d} = \frac{2\pi}{\omega_d} = \frac{2\pi}{\omega_n\sqrt{1-\zeta^2}}. \tag{2.82}$$

We see that the response decreases from x_1 to x_2 over the period, τ_d. For the viscously damped system, we also know that the decay is exponential and depends on the damping ratio, ζ. We can therefore define the **logarithmic decrement**, δ, to describe this amplitude reduction:

$$\delta = ln\left(\frac{x_1}{x_2}\right). \tag{2.83}$$

We can now substitute for x_1 and x_2 in Eq. 2.83 using the expression $x(t) = Xe^{-\zeta\omega_n t}\, sin\left(\sqrt{1-\zeta^2}\omega_n t + \phi\right)$ evaluated at the times, t_1 and t_2:

$$\delta = ln\left(\frac{Xe^{-\zeta\omega_n t_1}\, sin\left(\sqrt{1-\zeta^2}\omega_n t_1 + \phi\right)}{Xe^{-\zeta\omega_n t_2}\, sin\left(\sqrt{1-\zeta^2}\omega_n t_2 + \phi\right)}\right). \tag{2.84}$$

We can simplify Eq. 2.84 by recognizing that $t_2 = t_1 + \tau_d$.

$$\delta = ln\left(\frac{Xe^{-\zeta\omega_n t_1}\, sin\left(\sqrt{1-\zeta^2}\omega_n t_1 + \phi\right)}{Xe^{-\zeta\omega_n(t_1+\tau_d)}\, sin\left(\sqrt{1-\zeta^2}\omega_n(t_1+\tau_d) + \phi\right)}\right) \tag{2.85}$$

Because the sine function is periodic, we know that $sin(t_1) = sin\,(t_1 + \tau_d)$. This enables us to rewrite Eq. 2.85 because the sine terms in the numerator and denominator cancel.

$$\delta = ln\left(\frac{e^{-\zeta\omega_n t_1}}{e^{-\zeta\omega_n(t_1+\tau_d)}}\right) = ln\left(\frac{e^{-\zeta\omega_n t_1}}{e^{-\zeta\omega_n t_1}e^{-\zeta\omega_n\tau_d}}\right) = ln\left(e^{\zeta\omega_n\tau_d}\right) = \zeta\omega_n\tau_d \tag{2.86}$$

We can now experimentally determine the damping ratio by following three steps.

1. Substitute for τ_d in Eq. 2.86 using Eq. 2.82.

$$\delta = \zeta\omega_n\tau_d = \zeta\omega_n\frac{2\pi}{\omega_n\sqrt{1-\zeta^2}} = \frac{2\pi\zeta}{\sqrt{1-\zeta^2}} \tag{2.87}$$

2. Measure x_1 and x_2 during free vibration and calculate δ using Eq. 2.83.
3. Solve for ζ from Eq. 2.87. Rewriting gives $\delta\sqrt{1-\zeta^2} = 2\pi\zeta$. By squaring both sides, we obtain $\delta^2(1-\zeta^2) = 4\pi^2\zeta^2$. Combining terms yields $\zeta^2 = \frac{\delta^2}{4\pi^2+\delta^2}$, which we can write as:

$$\zeta = \sqrt{\frac{\delta^2}{4\pi^2+\delta^2}}. \tag{2.88}$$

Alternately, we can recognize that $\sqrt{1-\zeta^2} \approx 1$ for small ζ so that we can rewrite Eq. 2.87 as $\delta \simeq 2\pi\zeta$. Solving for ζ gives:

$$\zeta \simeq \frac{\delta}{2\pi}. \tag{2.89}$$

In a Nutshell

Equation 2.89 provides a very useful result. In a physical single degree of freedom system we know how to measure the mass, m, using a balance, for example. We can apply a static force and measure the resulting deflection to identify the static stiffness, k. Damping is more difficult to quantify. We often are not even sure about the source of the damping. Is it viscous? Did it come

(continued)

from friction? An easy way to determine the equivalent viscous damping is to initiate vibration and then measure the height of two successive vibration peaks. The natural logarithm of the ratio of the peak heights divided by 2π closely approximates the damping ratio. Experimentally, when the damping ratio is low, the difference in two successive peak heights may be small and, therefore, difficult to measure accurately. However, because this ratio of peak heights holds for any two successive peaks, the accuracy of the estimate may be improved by considering the heights of peaks separated by several cycles, N. That is, $\frac{x_0}{x_N} = \left(\frac{x_0}{x_1}\right)\left(\frac{x_1}{x_2}\right)\left(\frac{x_2}{x_3}\right)\ldots\left(\frac{x_{N-1}}{x_N}\right) = \left(\frac{x_0}{x_1}\right)^N$, so $ln\left(\frac{x_0}{x_N}\right) = Nln\left(\frac{x_0}{x_1}\right) = N\delta$. This means that in order to calculate the damping ratio using the peak height change over several cycles, we compute the natural logarithm of the ratio, divide by 2π, and divide this result by the number of cycles. Additionally, this approach can be used to determine how many cycles of the motion would be required for the vibration to fall below a predetermined amplitude. If the damping ratio is known, then we can solve for N.

2.4.7 Damping Estimate Uncertainty

For any measurement, there is always **uncertainty** associated with the result. For the logarithmic decrement, the combined standard uncertainty in the damping ratio, $u_c(\zeta)$, depends on the standard uncertainties in the measurements of x_1 and x_2, $u(x_1)$ and $u(x_2)$ [2]. To determine how these uncertainties are related, we can perform a first-order Taylor series expansion of Eq. 2.89 after substituting for δ: $\zeta \simeq \frac{1}{2\pi} ln\left(\frac{x_1}{x_2}\right) = \frac{1}{2\pi}(ln(x_1) - ln(x_2))$. If we neglect any potential relationship (or correlation) between the x_1 and x_2 values, represented by the **covariance**, we can find $u_c(\zeta)$ using:

$$u_c{}^2(\zeta) = \left(\frac{\partial\zeta}{\partial x_1}\right)^2 u^2(x_1) + \left(\frac{\partial\zeta}{\partial x_2}\right)^2 u^2(x_2), \tag{2.90}$$

where the partial derivatives are $\frac{\partial\zeta}{\partial x_1} = \frac{1}{2\pi}\frac{1}{x_1}$ and $\frac{\partial\zeta}{\partial x_2} = \frac{1}{2\pi}\frac{1}{x_2}$. Substituting gives:

$$u_c(\zeta) = \frac{1}{2\pi}\sqrt{\frac{u^2(x_1)}{x_1{}^2} + \frac{u^2(x_2)}{x_2{}^2}}, \tag{2.91}$$

where the average (or mean) values of x_1 and x_2 are used to evaluate the combined standard uncertainty.

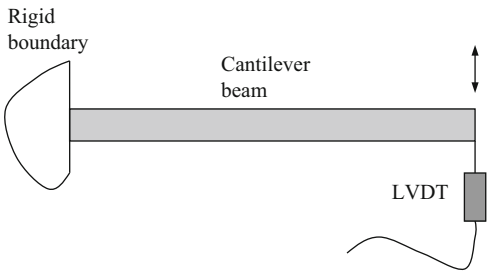

Fig. 2.31 *By the Numbers 2.4*—measurement of free oscillation for a cantilever beam using an LVDT

By the Numbers 2.4

The tip displacement for a freely vibrating cantilever beam was measured as shown in Fig. 2.31. The displacement values, x_1 and x_2, were recorded at two times separated by the damped vibration period of 0.01 s; these values were 0.93 mm and 0.82 mm. The manufacturer-specified measurement uncertainty for the **linear variable differential transformer**[3] (LVDT) used to perform the displacement measurement was 0.01 mm. Let's determine the damped natural frequency, mean value of the damping ratio, and the associated uncertainty in the damping ratio for this measurement activity.

First, we use Eq. 2.82 to find the damped natural frequency, $f_d = \frac{1}{\tau_d} = \frac{1}{0.01} = 100$ Hz. Second, for the mean damping ratio, we use Eq. 2.83 to calculate the logarithmic decrement, $\delta = ln\left(\frac{x_1}{x_2}\right) = ln\left(\frac{0.93}{0.82}\right) = 0.13$. The damping ratio is then $\zeta \simeq \frac{0.13}{2\pi} = 0.02$, or 2%. Third, the uncertainty in this value is determined using Eq. 2.91.

$$u_c(\zeta) = \frac{1}{2\pi}\sqrt{\frac{0.01^2}{0.93^2} + \frac{0.01^2}{0.82^2}} = 0.002$$

This combined standard uncertainty represents one standard deviation of the mean value of ζ. We can interpret it this way. For a normal (or **Gaussian**) distribution of ζ values, we would expect subsequent measurements to appear within the interval of ± 0.002 about the mean value 68.2% of the time. For (approximately) a 95% **level of confidence**, we would expand this interval to $\pm 2u_c(\zeta) = 0.004$.

Before moving to Sect. 2.5 and unstable behavior, let's return to the Argand diagram and compare the undamped and damped cases. The undamped free vibration response described by $x(t) = X_u\, cos\,(\omega_n t + \phi_u)$ is shown in Fig. 2.32, where $\phi_u = tan^{-1}\left(\frac{-\dot{x}_0}{\omega_n x_0}\right)$ and $X_u = \frac{x_0}{cos\,(\phi_u)}$ (the u subscript represents "undamped"). With the addition of damping, the response is $x(t) = X_d e^{-\zeta\omega_n t}\, cos\,(\omega_d t + \phi_d)$, where

[3] An LVDT is a transformer with three coils placed next to one another around a tube. A ferromagnetic core slides in and out of the tube; this cylindrical core usually serves as the moving probe. An alternating current is passed through the center coil and, as the core moves, voltages are induced in the outer coils. These voltages are used to determine the core displacement [3].

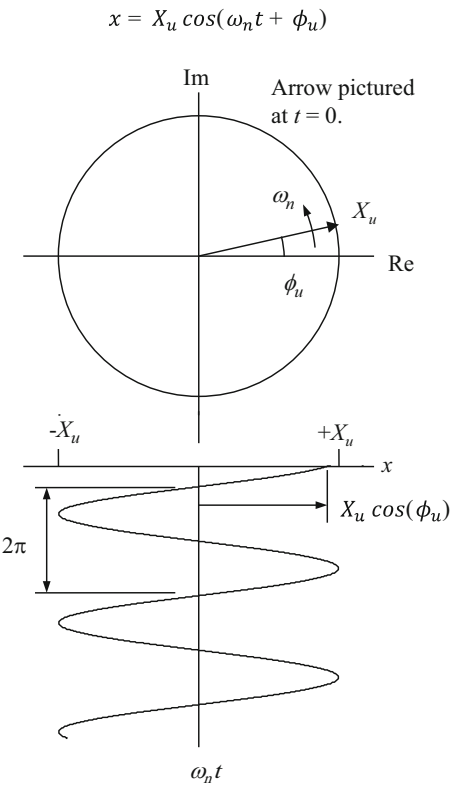

Fig. 2.32 Argand diagram for undamped free vibration response $x(t) = X_u\, cos\,(\omega_n t + \phi_u)$

$\phi_d = tan^{-1}\left(\frac{-\zeta\omega_n x_0 - \dot{x}_0}{\omega_d x_0}\right)$ and $X_d = \frac{x_0}{cos\,(\phi_d)}$ (the d subscript represents "damped"). The damped case is pictured in Fig. 2.33 for comparison purposes. Because the response decays over time, the vector length decreases and the tip traces a "spiral" pattern.

2.5 Unstable Behavior

For the single degree of freedom damped oscillator, we detailed the solution to the equation of motion $m\ddot{x} + c\dot{x} + kx = 0$ with the initial conditions $x(0)$ and $\dot{x}(0)$. We discussed four possible scenarios based on the damping ratio: $\zeta < 1$ (underdamped), $\zeta = 0$ (no damping), $\zeta = 1$ (critically damped), and $\zeta > 1$ (overdamped). For $\zeta < 1$, we saw responses of the type shown in Fig. 2.34. These decaying responses are called **asymptotically stable** because they exponentially approach zero (the equilibrium position) as time progresses. For the $\zeta = 0$ response in Fig. 2.35, the behavior is **marginally stable**; the response neither grows nor decays. The $\zeta = 1$

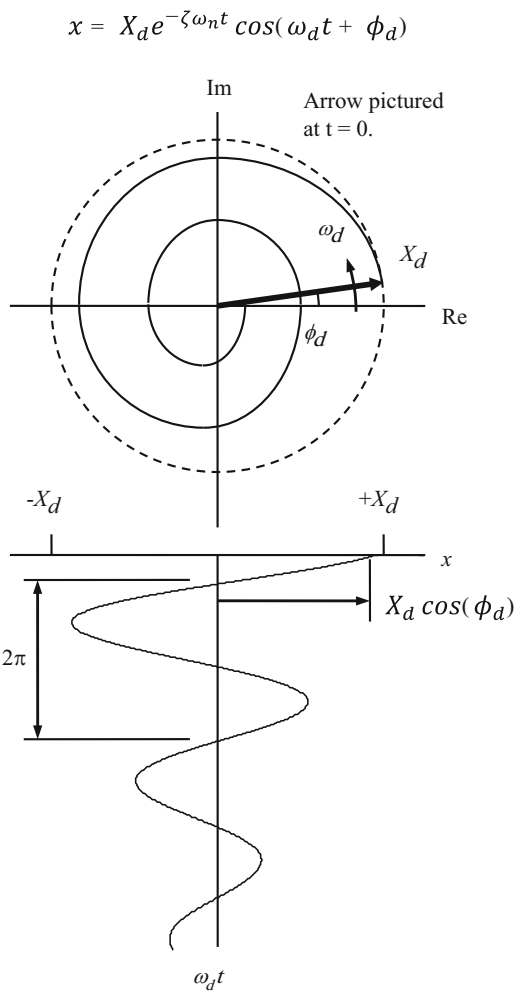

Fig. 2.33 Argand diagram for damped free vibration response $x(t) = X_d e^{-\zeta\omega_n t} cos(\omega_d t + \phi_d)$

and $\zeta > 1$ cases are also stable. Like the $\zeta < 1$ case, these responses approach the equilibrium position as time increases.

What if the response does not approach the equilibrium position? This is called **unstable** behavior. We'll discuss two types: flutter instability (or self-excited vibration) and divergent instability.

2.5.1 Flutter Instability

Let's again consider the equation of motion $m\ddot{x} + c\dot{x} + kx = 0$. For positive mass values ($m > 0$), unstable behavior is obtained if c or k are less than zero. This is

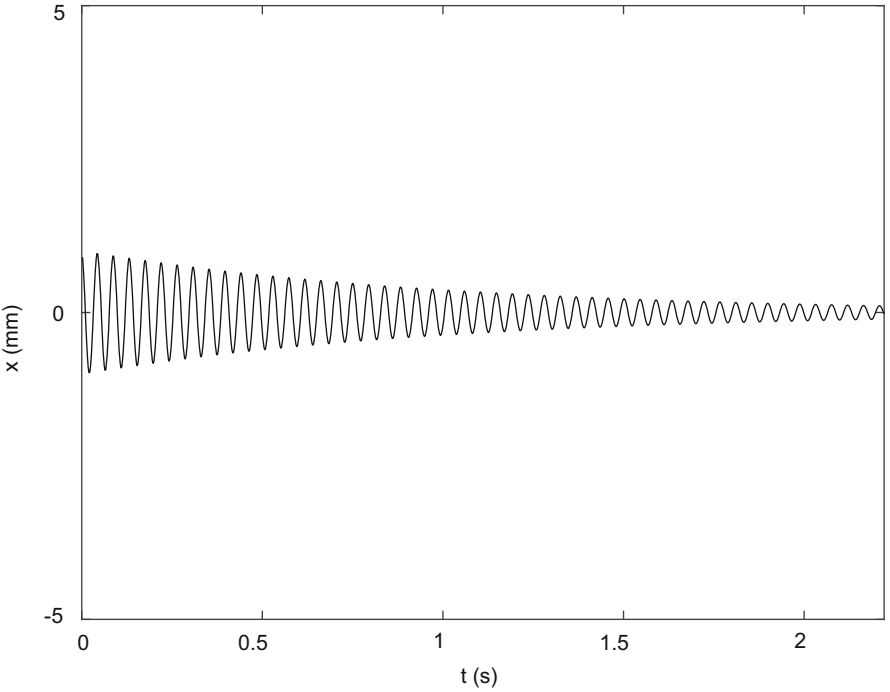

Fig. 2.34 *By the Numbers 2.5*—stable behavior ($c = 1.1c_{\text{lim}}$)

referred to as negative damping or stiffness, respectively. This unstable behavior leads to oscillatory motion that grows, rather than decays, over time. It is referred to as **flutter instability** or **self-excited vibration**.

Consider a structure moving through a fluid, such as an aircraft wing moving through the air, that can be modeled as a single degree of freedom system with a velocity-dependent aerodynamic force, $f = \gamma\dot{x}$, acting on it [4]. The equation of motion is:

$$m\ddot{x} + c\dot{x} + kx = \gamma\dot{x}, \tag{2.92}$$

where we'll specify that m, c, k, and γ are all positive. Rewriting this equation yields $m\ddot{x} + (c - \gamma)\dot{x} + kx = 0$. Now we have two possibilities for the effective damping coefficient, $c - \gamma$. If $c - \gamma > 0$, then $\zeta = \frac{c-\gamma}{2\sqrt{km}} > 0$ and we obtain stable behavior. However, if $c - \gamma < 0$, then $\zeta < 0$ and the response grows exponentially over time (flutter). If $c - \gamma = 0$, the system is marginally stable.

While we have only considered analytical solutions to the differential equations of motion so far, let's now solve Eq. 2.92 numerically. We will implement **Euler integration** in a time-domain simulation to determine the system behavior for various $c - \gamma$ values.

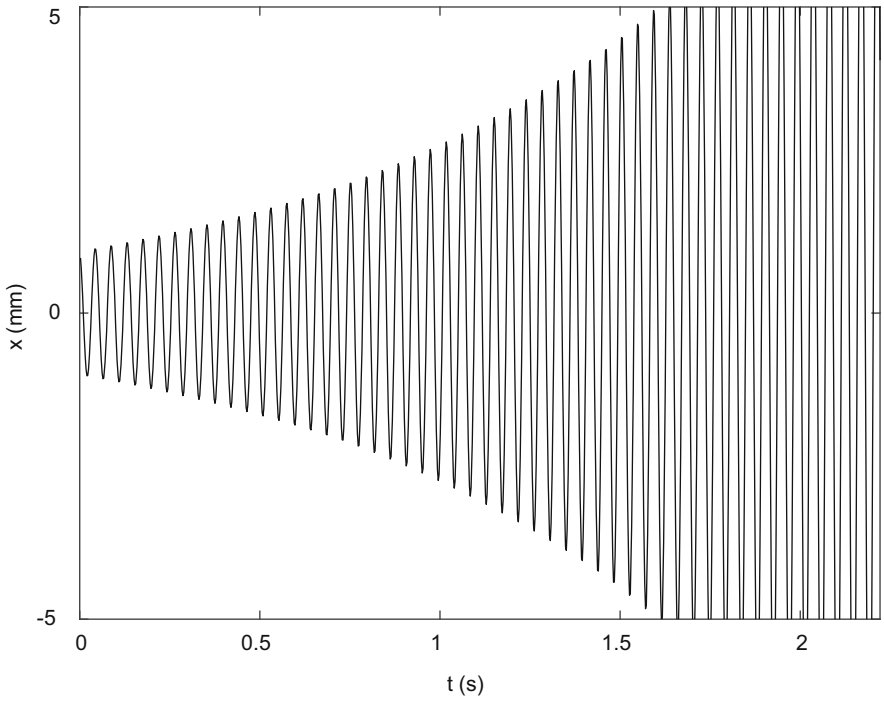

Fig. 2.35 *By the Numbers 2.5*—flutter instability ($c = 0.9c_{\text{lim}}$)

The simulation is carried out in small **time steps**, dt. Because we are numerically integrating the system equation of motion to determine the resulting vibration, care must be exercised in selecting dt. If the value is too large, inaccurate results are obtained. As a rule of thumb, it is generally acceptable to set dt to be at least ten times smaller than the period corresponding to the highest natural frequency in the system's dynamic model.

Given the equation of motion $m\ddot{x} + (c - \gamma)\dot{x} + kx = 0$, the acceleration in the current simulation time step is determined using:

$$\ddot{x} = \frac{-(c - \gamma)\dot{x} - kx}{m},$$

where the velocity, $\dot{x}$, and position, x, from the previous time step are used (for the first time step, they are set equal to the initial conditions). The velocity for the current time step is then determined by Euler integration:

$$\dot{x} = \dot{x} + \ddot{x} \cdot dt,$$

where the velocity on the right hand side of the equation is retained from the previous time step and used to update the current value (on the left hand side of the equation). The current velocity is then applied to determine the current displacement according to:

$$x = x + \dot{x} \cdot dt.$$

Again, the displacement on the right hand side of the equation is retained from the previous time step. Finally, the time-dependent displacement can be written to a vector, y, as:

$$y_n = x,$$

where the n subscript on y indicates the time step. This is used to simplify the "book keeping" in the MATLAB® program; see By the Number 2.5 and MATLAB® MOJO 2.3. The corresponding time is $t_n = n \cdot dt$.

By the Numbers 2.5

Let's choose the following parameters for Eq. 2.92: $m = 500$ kg, $k = 1 \times 10^7$ N/m, and $\gamma = 1 \times 10^4$ N s/m with initial conditions of $x(0) = 1 \times 10^{-3}$ m and $\dot{x}(0) = 0$. At the limit of stability, $c - \gamma = 0$. Therefore, for a given γ value, the associated limiting c value is $c_{lim} = \gamma$. In this case, $c_{lim} = 1 \times 10^4$ N s/m. For $c > c_{\text{lim}}$, the system is stable. If $c < c_{\text{lim}}$, flutter occurs. Using the code provided in MATLAB® MOJO 2.3, the results shown in Figs. 2.34 and 2.35 were obtained. In Fig. 2.34, the system is stable with $c = 1.1c_{\text{lim}}$. Unstable results are seen in Fig. 2.35, where $c = 0.9c_{\text{lim}}$. Exponentially increasing oscillatory behavior is observed. For these figures, the response is plotted over 50 periods of vibration, $\tau = \frac{1}{f_n} = 2\pi\sqrt{\frac{m}{k}} = 0.044$ s, using a time step of $dt = \frac{\tau}{20} = 0.0022$ s.

MATLAB® MOJO 2.3

```
% matlab_mojo_2_3.m

clear
close all
clc

% Define parameters
m = 500;              % kg
k = 1e7;              % N/m
gamma = 1e4;            % N s/m
clim = gamma;           % N s/m
fn = 1/(2*pi)*sqrt(k/m);      % Hz
tau = 1/fn;           % s
c = 0.9*clim;
```

```
% Define simulation variables
dt = tau/20;            % sec/step
steps = round(50*tau/dt);

% Euler integration initial conditions
x = 1e-3;              % m
dx = 0;               % m/s

% Initialize final position and time vectors
y = zeros(1, steps);
time = zeros(1, steps);

for cnt = 1:steps
  ddx = (-(c - gamma)*dx - k*x)/m;       % m/s^2
  dx = dx + ddx*dt;                 % m/s
  x = x + dx*dt;                  % m

  % Write results to vectors
  y(cnt) = x;                    % m
  time(cnt) = cnt*dt;                % s
end

figure(1)
plot(time, y*1e3, 'k')
xlim([0 max(time)])
ylim([-5 5])
set(gca,'FontSize', 14)
xlabel('t (s)')
ylabel('x (mm)')
```

2.5.2 *Divergent Instability*

In order to model and simulate divergent instability we will use the **inverted pendulum**, composed of a mass, m, supported by a massless rod of length, l, that rotates about the frictionless pivot, O. The rod is held in its vertical equilibrium position by springs and dampers as shown in Fig. 2.36. The free body diagram for a rotation, θ, of the mass/rod counter-clockwise from the equilibrium position is provided in Fig. 2.37. The forces that need to be considered include:

- the gravity force, mg
- the two spring forces, $k\delta$, where $\delta = \frac{l}{2} sin(\theta)$ is the horizontal deflection due to rotation of the rod as shown in Fig. 2.38
- the two viscous damping forces, $c\dot{\delta}$, where $\dot{\delta} = \frac{d\delta}{dt} = \frac{l}{2} cos(\theta) \cdot \dot{\theta}$ is the horizontal velocity
- the reaction forces at the pivot in the horizontal, R_x, and vertical, R_y, directions.

In order to sum moments, M, about O, the forces can be redrawn to give the components perpendicular and parallel to the massless rod. Only the perpendicular

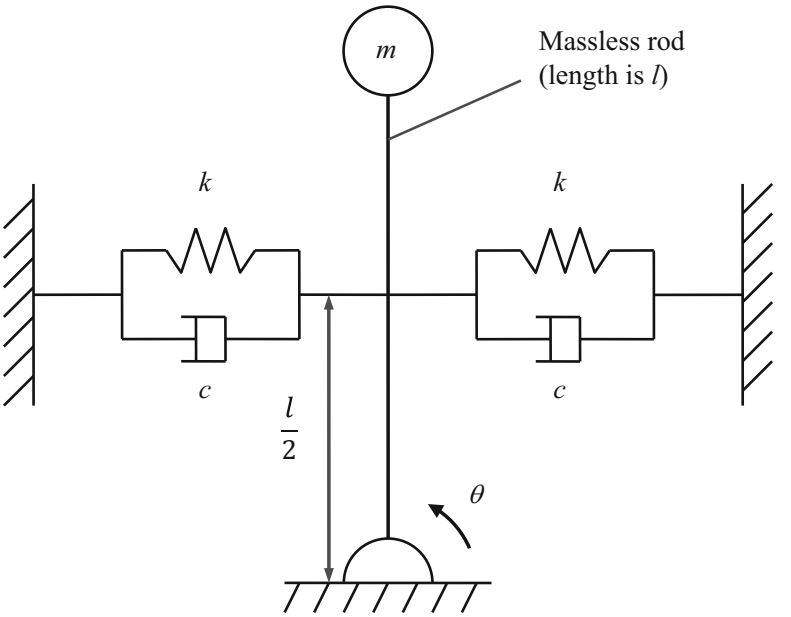

Fig. 2.36 Inverted pendulum

Fig. 2.37 Free body diagram for inverted pendulum

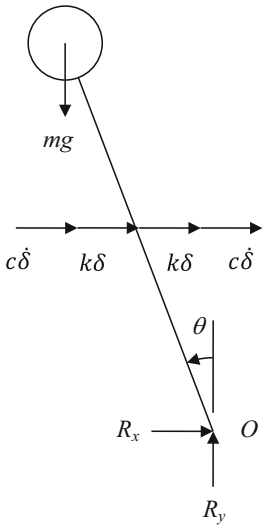

components need to be considered in the moment sum and, because we are summing about O, the reaction components may be neglected. The free body diagram is shown in Fig. 2.39, where d'Alembert's inertial moment, $J\ddot{\theta} = ml^2\ddot{\theta}$, with mass moment of inertia, J, is also included so that $\sum M_O = 0$.

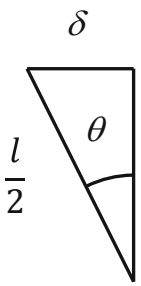

Fig. 2.38 Relationship between δ and θ

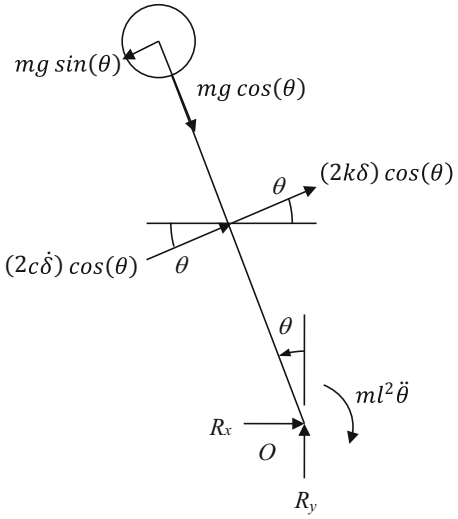

Fig. 2.39 Free body diagram with force components perpendicular and parallel to the massless rod. The d'Alembert inertial moment is also included

Using Fig. 2.39, the moment sum is:

$$ml^2\ddot{\theta} + \left(2c\dot{\delta}\right) cos\,(\theta)\frac{l}{2} + (2k\delta)\, cos\,(\theta)\frac{l}{2} - mgsin(\theta)l = 0.$$

Substituting for δ and $\dot{\delta}$ gives:

$$ml^2\ddot{\theta} + \left(2c\frac{l}{2}\, cos\,(\theta)\cdot\dot{\theta}\right) cos\,(\theta)\frac{l}{2} + \left(2k\frac{l}{2}\, sin\,(\theta)\right) cos\,(\theta)\frac{l}{2} - mgsin(\theta)l = 0.$$

For small rotations, $sin(\theta) \approx \theta$ and $cos(\theta) \approx 1$. Substituting these approximations and combining terms yields:

$$ml^2\ddot{\theta} + c\frac{l^2}{2}\dot{\theta} + \left(k\frac{l^2}{2} - mgl\right)\theta = 0.$$

If $k\frac{l^2}{2} - mgl < 0$, the effective stiffness is negative and divergent unstable behavior is obtained. In this situation, the motion grows without bound and no oscillation occurs when the pendulum is disturbed from its equilibrium position. Physically, this means that the spring force is insufficient to counteract gravity and the pendulum simply falls over for nonzero initial conditions. However, if $k\frac{l^2}{2} - mgl > 0$, the pendulum oscillates around its equilibrium position when disturbed from equilibrium and the response eventually decays to zero due to the viscous dampers. The limiting spring stiffness is found using $k_{lim}\frac{l^2}{2} - mgl = 0$. Rewriting gives $k_{lim} = \frac{2mg}{l}$. If $k < k_{lim}$, divergent instability occurs.

By the Numbers 2.6

Consider the inverted pendulum in Fig. 2.36 with $m = 0.5$ kg, $c = 1$ N s/m, and $l = 0.3$ m. The limiting spring stiffness is $k_{lim} = \frac{2(0.5)9.81}{0.3} = 32.7$ N/m. For initial conditions of $\theta(0) = 5^{\circ}$ and $\dot{\theta}(0) = 0$, let's determine the response $\theta(t)$ using Euler integration. As with the aircraft wing example, the first step is to solve the equation of motion for the acceleration term.

$$\ddot{\theta} = \frac{c\frac{l^2}{2}\dot{\theta} + \left(k\frac{l^2}{2} - mgl\right)\theta}{ml^2}$$

The angular velocity of the pendulum for the current time step is then determined by:

$$\dot{\theta} = \dot{\theta} + \ddot{\theta} \cdot dt,$$

where the angular velocity on the right hand side of the equation is the value from previous time step. This new velocity is then used to calculate the current angle.

$$\theta = \theta + \dot{\theta} \cdot dt$$

Using the code provided in MATLAB® MOJO 2.4, the results displayed in Figs. 2.40, 2.41 and 2.42 were obtained for three k values:

- $k = 0.99k_{lim}$
- $k = k_{lim}$
- $k = 10k_{lim}$.

In Fig. 2.40, the system exhibits divergent instability with $k = 0.99k_{lim}$. The pendulum mass simply falls in the direction of the initial angular offset. Marginal stable results are seen in Fig. 2.41, where $k = k_{lim}$. There is no mass rotation because the spring restoring force exactly offsets the gravity force. Exponentially decaying

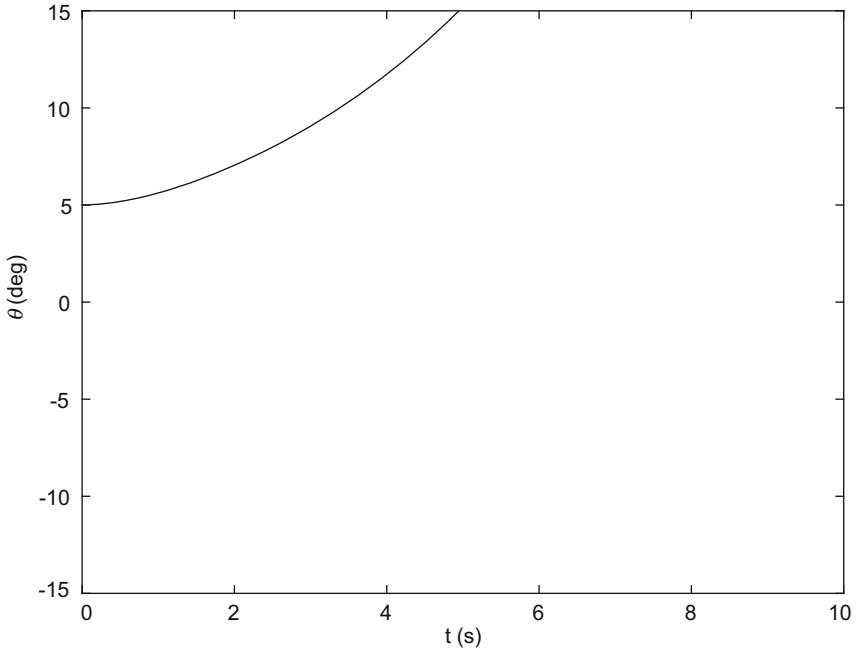

Fig. 2.40 *By the Numbers 2.6*—divergent instability for the inverted pendulum with $k = 0.99k_{lim}$

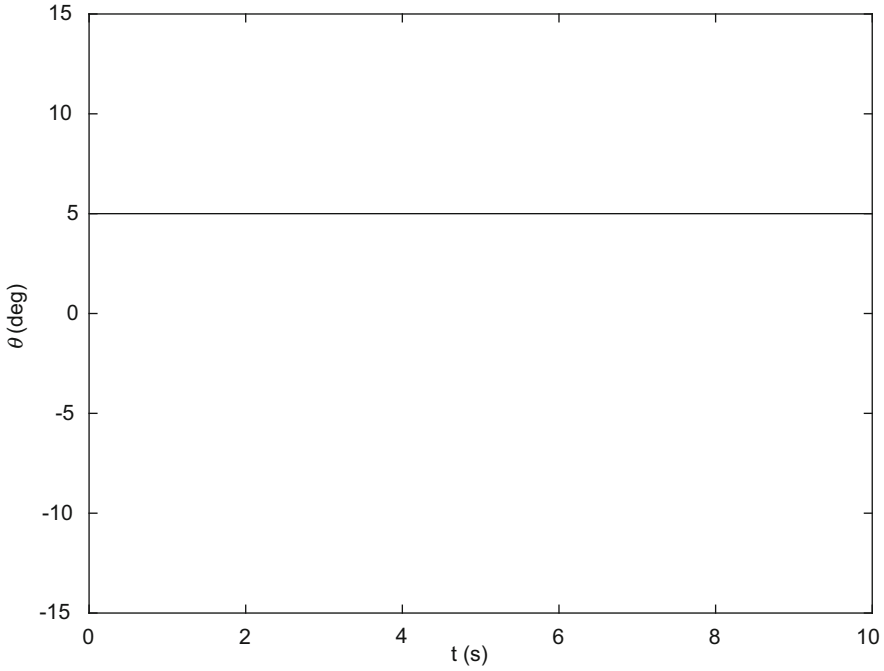

Fig. 2.41 *By the Numbers 2.6*—marginal stability for the inverted pendulum with $k = k_{lim}$

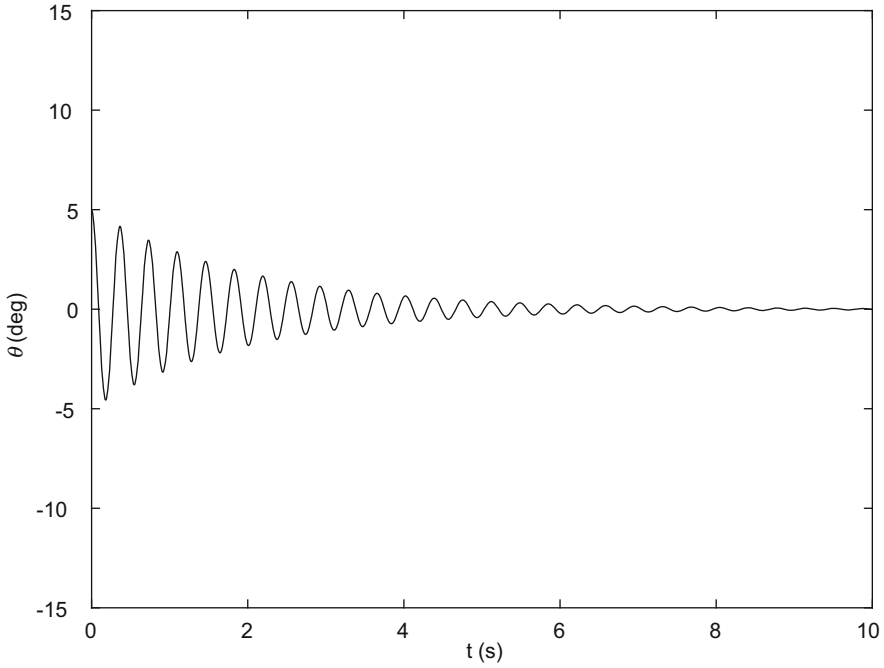

Fig. 2.42 *By the Numbers 2.6*—asymptotic stability for the inverted pendulum with $k = 10k_{lim}$

oscillatory behavior is observed in Fig. 2.42, where $k = 10k_{lim}$. In this asymptotically stabile case, the pendulum's angular position oscillates about the equilibrium position (zero rotation). For these figures, the response is plotted over 2000 steps using a time increment of $dt = 0.005$ s.

MATLAB® MOJO 2.4

```
% matlab_mojo_2_4.m

clear
close all
clc

% Define parameters
m = 0.5;              % kg
c = 1;               % N s/m
g = 9.81;             % m/s^2
l = 0.3;              % m
klim = 2*m*g/l;          % N/m
k = 0.99*klim;

% Define simulation variables
dt = 0.005;     % sec/step
steps = 2000;
```

```
% Euler integration initial conditions
theta = 5*pi/180;        % rad
dtheta = 0;           % rad/s

% Initialize final theta vector and time vector
th = zeros(1, steps);
time = zeros(1, steps);

for cnt = 1:steps
  ddtheta = (-(c*l^2/2)*dtheta-(k*l^2/2-m*g*l)*theta)/(m*l^2);  %
rad/s^2
  dtheta = dtheta + ddtheta*dt;        % rad/s
  theta = theta + dtheta*dt;         % rad

  % Write results to vectors
  th(cnt) = theta;               % rad
  time(cnt) = cnt*dt;              % s
end

figure(1)
plot(time, th*180/pi, 'k')
xlim([0 max(time)])
ylim([-15 15])
set(gca,'FontSize', 14)
xlabel('t (s)')
ylabel('\theta (deg)')
```

2.6 Free Vibration Measurement

To conclude this chapter, let's introduce the **beam experimental platform (BEP)** that we will use to demonstrate various concepts throughout this text. The design dimensions and materials are provided in Appendix A. A photograph of the measurements setup is shown in Fig. 2.43. The 12.7 mm diameter steel rod is clamped in the base with an overhang length of 125 mm. An **accelerometer** is attached to the cantilever beam's free end. This is a piezoelectric measurement transducer that gives a voltage which is proportional to acceleration. We will discuss it in more detail in Sect. 7.3.3. The rod was disturbed from equilibrium by a light tap from a small hammer and the resulting vibration was recorded. A plot of the acceleration, a, versus time, t, is provided in Fig. 2.44, where the hammer impact was applied at 0.005 s. We see that the response resembles the underdamped free vibration results we've already studied; it decays exponentially over time. However, there are also some differences. It doesn't uniformly decay to zero; in fact, it seems to grow and decrease periodically within the overall damping envelope. This is because there are actually multiple natural frequencies of the continuous beam excited simultaneously by the hammer tap. To model this behavior, we need to consider multiple degrees of

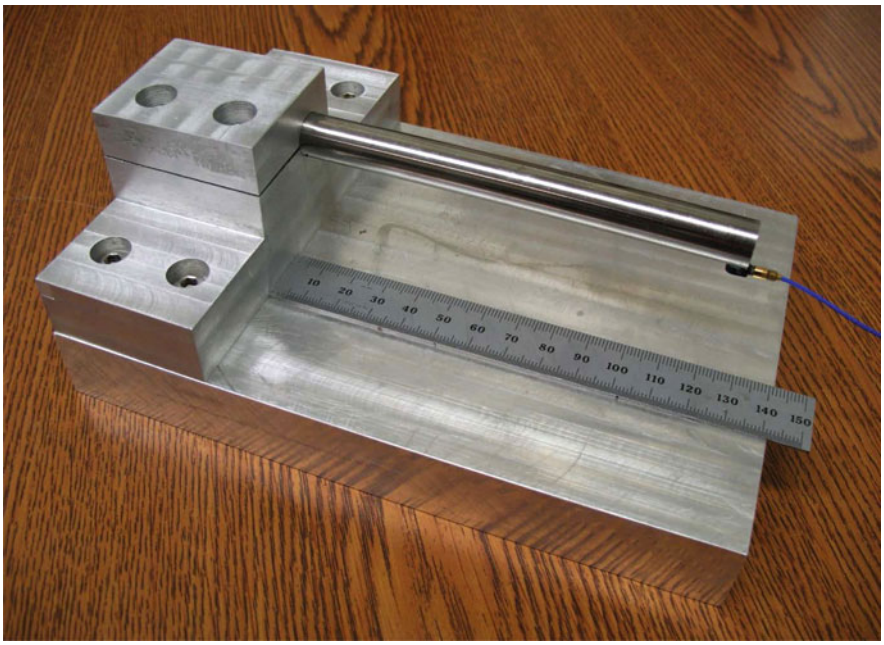

Fig. 2.43 Photograph of free vibration measurement using the BEP

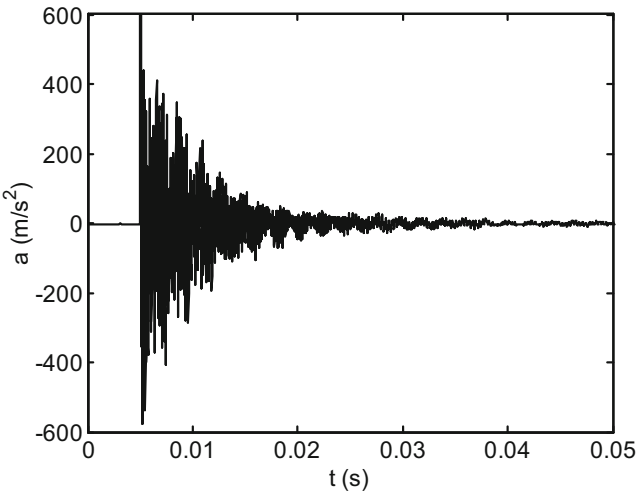

Fig. 2.44 Tip acceleration for the BEP due to a hammer tap disturbance at $t = 0.005$ s

freedom. As we move forward, we will discuss both multiple degree of freedom systems and modeling techniques for continuous beams.

Chapter Summary

- The lumped parameter model, composed of a mass (located at each coordinate) that is supported by massless springs and/or dampers, can be used to represent physical systems.
- D'Alembert's principle can be used to represent a dynamic model as a static system by including the inertial force(s) or moment(s) in the free body diagram.
- A system's characteristic equation is used to determine its natural frequency(s).
- Initial conditions are used to solve the differential equation of motion and determine the time-domain response for free vibration.
- When applying an energy-based approach, the expressions for kinetic and potential energy are used to identify the equation of motion for a system.
- An equivalent spring can be developed for springs in series and springs in parallel.
- The Duffing spring, which includes a cubic nonlinearity, can be used to describe the behavior of nonlinear systems.
- Three primary damping models are viscous, Coulomb, and solid damping.
- The dimensionless damping ratio, ζ, is used to describe the behavior of damped systems.
- For underdamped systems, where $\zeta < 1$, the response is vibratory with a magnitude that decays exponentially over time.
- For overdamped systems, where $\zeta > 1$, there is no vibration.
- Matrix inversion can be used to solve linear systems of equations.
- The logarithmic decrement, which is determined from measurements of free vibration, can be used to estimate the damping ratio.
- All measurement results include uncertainty. Given an equation for the value in question (expressed as a function of other measured inputs), the uncertainty of that value can be determined by a Taylor-series expansion of the equation.
- Two types of instability are: (1) flutter or self-excited vibration; and (2) divergent instability.
- The equation of motion can be solved numerically using Euler integration.
- An accelerometer can be used to measure the vibration of structures.

Exercises

1. For a single degree of freedom spring-mass system with $m = 1$ kg and $k = 4 \times 10^4$ N/m, complete the following for the case of free vibration.
   (a) Determine the natural frequency in Hz and the corresponding period of vibration.
   (b) Given an initial displacement of 5 mm and zero initial velocity, write an expression for the time response of free vibration using the following form.

$$x(t) = X_1 e^{i\omega_n t} + X_2 e^{-i\omega_n t} \text{ mm}$$

(c) Plot the first ten cycles of motion for the result from part (b).

2. For a single degree of freedom spring-mass system, complete the following.
   (a) If the free vibration is described as $x(t) = A\cos(\omega_n t + \Phi_c)$, determine expressions for A and Φ_c if the initial displacement is x_0 and the initial velocity is $\dot{x}_0$.
   (b) If the free vibration is described as $x(t) = A\cos(\omega_n t) + B\sin(\omega_n t)$, determine expressions for A and B if the initial displacement is x_0 and the initial velocity is $\dot{x}_0$.

3. The differential equation of motion for a cylinder rolling on a concave cylindrical surface is
   $\ddot{\theta} + \frac{2}{3}\frac{g}{R-r}\theta = 0$, where g is the gravitational constant (Fig. P2.3).
   (a) Write the expression for the natural frequency, ω_n (rad/s).
   (b) If the free vibration is described as $\theta(t) = A\sin(\omega_n t + \Phi_s)$, determine expressions for A and Φ_s if the initial angle is θ_0 and the initial angular velocity is $\dot{\theta}_0$.
   (c) If $R = 200$ mm, $r = 10$ mm, $\theta_0 = 5^\circ = 0.087$ rad, and $\dot{\theta}_0 = 0$, plot $\theta(t)$ (°) using the function from part (b) for the time interval from $t = 0$ to 5 s in steps of 0.005 s.

4. For a single degree of freedom spring-mass-damper system with $m = 1$ kg, $k = 4 \times 10^4$ N/m, and $c = 10$ N s/m, complete the following for the case of free vibration.
   (a) Calculate the natural frequency (in rad/s), damping ratio, and damped natural frequency (in rad/s).
   (b) Given an initial displacement of 5 mm and zero initial velocity, write the expression for the underdamped, free vibration in the form $x(t) = e^{-\zeta\omega_n t}(A\cos(\omega_d t) + B\sin(\omega_d t))$ mm.
   (c) Plot the first ten cycles of motion.
   (d) Calculate the viscous damping value, c (in N s/m), to give the critically damped case for this system.

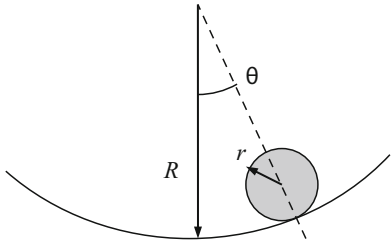

Fig. P2.3 Cylinder rolling on a concave cylindrical surface

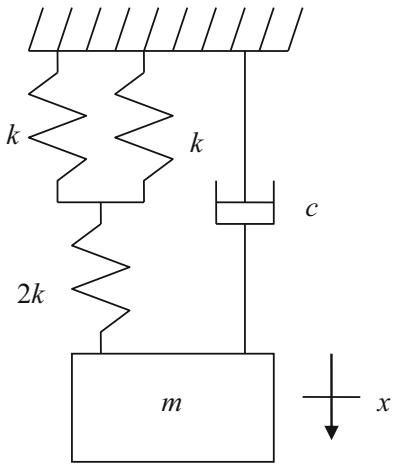

Fig. P2.5 Single degree of freedom spring-mass-damper system under free vibration

5. For a single degree of freedom spring-mass-damper system with $m = 0.2$ lb_m, $k = 2.5 \times 10^3$ lb_f/in, $c = 10.92$ lb_f-s/ft, $x_0 = 0.1$ in, and $\dot{x}_0 = 0$, complete the following for the case of free vibration (Fig. P2.5).

   (a) Determine the equivalent spring constant (in lb_f/in) for the spring configuration shown in the figure.
   (b) Determine the force (in lb_f) required to cause the initial displacement of 0.1 in (assume the system was at static equilibrium prior to introducing the initial displacement).
   (c) Calculate the damping ratio. You will need the units correction factor: (32.2 ft-lb_m)/(lb_f-s^2). Is this system underdamped or overdamped?
   (d) Calculate the damped natural frequency (in Hz).

6. For a single degree of freedom spring-mass-damper system under free vibration, determine the values for the mass, m (kg), viscous damping coefficient, c (N s/m), and spring constant, k (N/m), given the following information.

   - The damping ratio is 0.1.
   - The undamped natural frequency is 100 Hz.
   - The initial displacement is 1 mm.
   - The initial velocity is 5 mm/s.
   - If the system was critically damped, the value of the damping coefficient would be 586.1 N s/m.

7. For a single degree of freedom spring-mass-damper system under free vibration, the following information is known: $m = 2$ kg, $k = 1 \times 10^6$ N/m, $c = 500$ N s/m, $x_0 = 4$ mm, and $\dot{x}_0 = 0$ mm/s.

   Determine the corresponding expression for velocity (mm/s) if position is given in the form $x(t) = Ae^{-\zeta\omega_n t} cos\,(\omega_d t + \varphi_c)$.

   Numerically evaluate all coefficients and constant terms in your final expression.

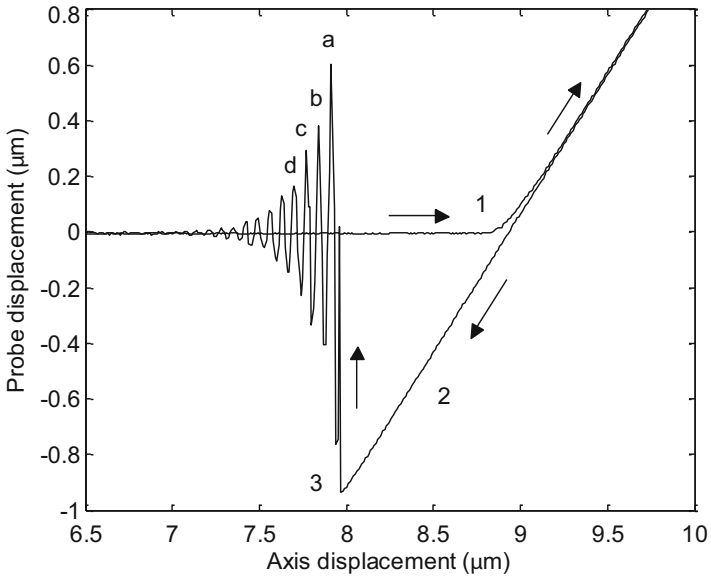

Fig. P2.8 Probe displacement as a function of the axis position

8. The requirement for small features on small parts has led to increased demands on measuring systems. One approach for determining the size of features (such as a hole's diameter) is to use a probe to touch the surface at several locations (e.g., points on the hole wall) and then use these coordinates to calculate the required dimension. To probe small features, small probes are required. However, at small size and force scales, intermolecular forces can dominate.

   An example is the interaction between very small, flexible probes and surfaces. As shown in Fig. P2.8, a 72 μm diameter probe tip comes into contact with a measurement surface (1) and the probe begins to deflect. The attractive (van der Waals) force between the probe and surface causes the tip to "stick" to the surface as it is retracted after contact (2). The motion is provided by an axis which moves the probe relative to the surface. Once the retraction force on the probe overcomes the attractive force, the probe is released from the surface (3) and it oscillates under free vibration conditions. Given the probe's free vibration response, determine the damping ratio using the logarithmic decrement approach. The peaks from the free vibration response are provided in Table P2.8. [The data in Fig. P2.8 is courtesy of IBS Precision Engineering, Eindhoven, The Netherlands.]
9. If the free vibration a single degree of freedom spring-mass system is described as $x(t) = Asin(\omega_n t + \Phi_s)$, determine expressions for A and Φ_s if the initial displacement is x_0 and the initial velocity is $\dot{x}_0$.
10. For a single degree of freedom spring-mass-damper system, the free vibration response shown in the Fig. P2.10a was obtained due to an initial displacement with no initial velocity.

Table P2.8 Peak values for probe free vibration

Peak label	Peak value (μm)
a	0.60
b	0.38
c	0.29
d	0.16

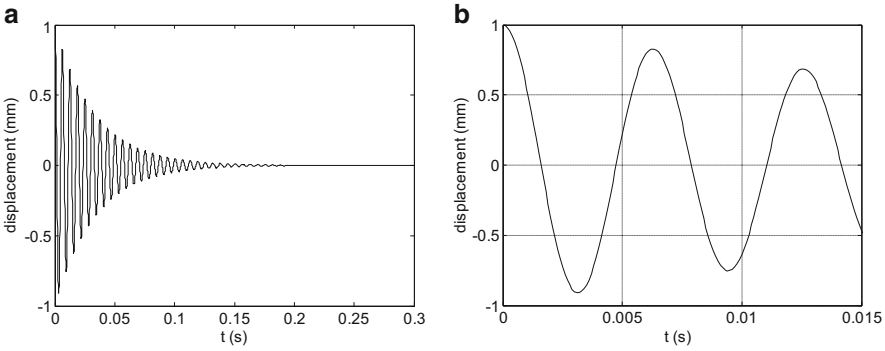

Fig. P2.10 (**a**) Free vibration response for a single degree of freedom spring-mass-damper system. (**b**) First few cycles of free vibration response for a single degree of freedom spring-mass-damper system

(a) Determine the damping ratio using the logarithmic decrement. Figure P2.10b, which shows just the first few cycles of oscillation, is provided to aid in this calculation.
(b) What was the initial displacement for this system?
(c) Determine the period of oscillation and corresponding damped natural frequency (in Hz).
(d) If the system mass is 1 kg, determine the spring constant (in N/m).

References

1. Thomson W, Dahley M (1998) Theory of vibrations with applications, 5th edn. Prentice Hall, Upper Saddle River, NJ
2. Taylor B, Kuyatt C (1994) Guidelines for evaluating and expressing the uncertainty of NIST measurement results, NIST Technical Note 1297, 1994 Edition. National Institute of Standards and Technology, Gaithersburg, MD
3. http://en.wikipedia.org/wiki/Linear_variable_differential_transformer
4. Inman D (2001) Engineering vibration, 2nd edn. Prentice Hall, Upper Saddle River, NJ

Chapter 3
Single Degree of Freedom Forced Vibration

Imagination decides everything.
—Blaise Pascal

3.1 Equation of Motion

Let's continue our study of the lumped parameter spring-mass-damper model, but now consider **forced vibration**. While the oscillation decays over time for a damped system under free vibration, the vibratory motion is maintained at a constant magnitude and frequency when an external energy source (i.e., a forcing function) is present. In Fig. 3.1, a harmonic input force has been added to the model, $f(t) = Fe^{i\omega t}$, where ω is the forcing frequency.

In a Nutshell
We've already seen that the complex exponential notation can be used to represent sine and cosine functions. The addition of the input force in Fig. 3.1 simply means that the system is being excited by a sinusoidal force. Additionally, because any periodic signal can be expressed by a sum of sine and cosine functions with different frequencies and amplitudes and because the system is linear and superposition can be applied, the discussion that follows applies to systems excited by any periodic force.

The free body diagram (including the inertial force) is also provided in Fig. 3.1. By summing the forces in the x direction, $\sum f_x = 0$, the equation of motion is determined:

$$m\ddot{x} + c\dot{x} + kx = Fe^{i\omega t}, \tag{3.1}$$

where viscous damping is included in the model.

T. L. Schmitz, K. S. Smith, *Mechanical Vibrations*,
https://doi.org/10.1007/978-3-030-52344-2_3

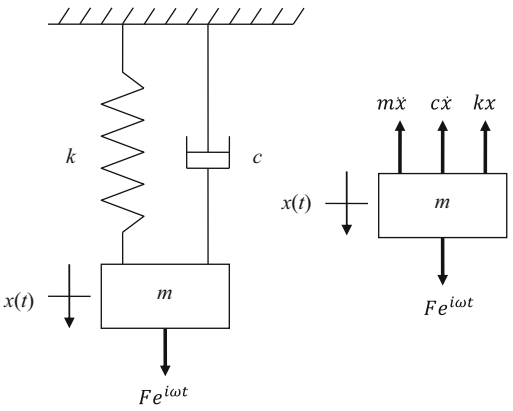

Fig. 3.1 Spring-mass-damper model with a harmonic input force. The free body diagram is included

3.2 Frequency Response Function

The total solution to the forced vibration equation of motion (Eq. 3.1) has two parts: (1) the homogeneous, or **transient**, solution; and (2) the particular, or **steady-state**, solution. The transient portion is the free vibration response, $m\ddot{x} + c\dot{x} + kx = 0$, and, as we saw in Chap. 2, it rapidly decays for damped systems. The steady-state portion remains after the transient has attenuated and it persists as long as the force is acting on the system. The particular solution takes the same form as the forcing function after the transients are damped out. The resulting vibration has the same frequency as the harmonic force. Specifically, given the force $f(t) = Fe^{i\omega t}$, the corresponding steady-state response can be written as $x(t) = Xe^{i\omega t}$. Given this form for the position, the velocity is $\dot{x}(t) = i\omega Xe^{i\omega t}$ and the acceleration is $\ddot{x}(t) = (i\omega)^2 Xe^{i\omega t} = -\omega^2 Xe^{i\omega t}$. Substituting these expressions in Eq. 3.1, we obtain:

$$-m\omega^2 Xe^{i\omega t} + i\omega cXe^{i\omega t} + kXe^{i\omega t} = Fe^{i\omega t}. \tag{3.2}$$

Grouping terms gives:

$$\left(-m\omega^2 + i\omega c + k\right)Xe^{i\omega t} = Fe^{i\omega t}. \tag{3.3}$$

This relates the force to the resulting vibration as a function of the forcing frequency, ω. Both sides of Eq. 3.3 include $e^{i\omega t}$, so we can eliminate it. We are now considering the response in the **frequency domain**, rather than the time domain since t no longer appears in the equation. Let's rewrite Eq. 3.3 so that we have the ratio of the output (the complex-valued vibration, X) to the input (the real-valued force, F). This is referred to as the **frequency response function** (FRF) for physical systems.

$$\frac{X}{F}(\omega) = G(\omega) = \frac{1}{-m\omega^2 + i\omega c + k} \tag{3.4}$$

In a Nutshell
We see in Eq. 3.4 that the relationship between the exciting force and the resulting vibration depends not only on the system parameters (m, k, and c) and amplitude of the exciting force (F), but also on the frequency of the excitation (ω).

In the **Laplace domain** ($s = \sigma + i\omega$), frequencies from negative infinity to positive infinity ($-\infty \leq \omega \leq +\infty$) are considered. In this case, the ratio $\frac{X}{F}(s)$ is referred to as the **transfer function** for the system. We can obtain the transfer function from the forced vibration equation of motion, $m\ddot{x} + c\dot{x} + kx = f(t)$, using the Laplace transforms of $x(t)$ and $f(t)$. These are $Lx(t) = X(s) = \int_0^\infty e^{-st}x(t)dt$ and $Lf(t) = F(s) = \int_0^\infty e^{-st}f(t)dt$. We also need the velocity:

$$L\dot{x}(t) = sX(s) - x(0)$$

and acceleration:

$$L\ddot{x}(t) = s^2X(s) - sx(0) - \dot{x}(0).$$

Substituting into the equation of motion gives:

$$m\left(s^2X(s) - sx(0) - \dot{x}(0)\right) + c(sX(s) - x(0)) + kX(s) = F(s).$$

For the transfer function we are considering the steady-state response so we can neglect the transients and let $x(0) = \dot{x}(0) = 0$. This yields:

$$\left(ms^2 + cs + k\right)X(s) = F(s),$$

which can be rewritten as the transfer function:

$$\frac{X}{F}(s) = \frac{1}{ms^2 + cs + k}.$$

For our purposes, however, we are interested in the measurement and subsequent modeling of physical systems. Therefore, we will limit our discussions to the FRF, which considers only positive frequencies and the system-specific damping.

In a Nutshell
For those with a background in controls, the FRF is a special case of the transfer function. The transfer function is a surface (like a tent) above the s plane (i.e., the plane with a σ axis and an $i\omega$ axis). "Poles" (like tent poles) are where that surface rises very high (to ∞) and "zeroes" are where the tent touches the ground (s plane). The FRF is a slice through the tent fabric along the axis where $\sigma = 0$ (the frequency axis).

Let's check the zero frequency (static or DC) case for Eq. 3.4. Substituting $\omega = 0$, we obtain:

$$\frac{X}{F}(0) = G(0) = \frac{1}{-m(0)^2 + i(0)c + k} = \frac{1}{k}.$$

This is simply Hooke's law that we discussed in Sect. 2.1. For the static case, we see that $F = kX$. In this instance, the response X is not complex; it has no imaginary component. Let's now rewrite the FRF to express it as a function of the natural frequency, ω_n, and damping ratio, ζ, rather than m, c, and k.

$$G(\omega) = \frac{1}{k - m\omega^2 + i\omega c} = \frac{1}{m}\left(\frac{1}{\left(\frac{k}{m} - \omega^2\right) + i\frac{c}{m}\omega}\right)$$

From Chap. 2, we know that $\frac{k}{m} = {\omega_n}^2$ and $\frac{c}{m} = 2\zeta\omega_n$. Substituting gives:

$$G(\omega) = \frac{1}{m}\left(\frac{1}{({\omega_n}^2 - \omega^2) + i2\zeta\omega_n\omega}\right).$$

Multiply this result by $\frac{k}{k}$ to obtain:

$$G(\omega) = \frac{1}{k}\frac{k}{m}\left(\frac{1}{({\omega_n}^2 - \omega^2) + i2\zeta\omega_n\omega}\right) = \frac{1}{k}\left(\frac{{\omega_n}^2}{({\omega_n}^2 - \omega^2) + i2\zeta\omega_n\omega}\right).$$

It is common to rewrite this equation using the frequency ratio, $r = \frac{\omega}{\omega_n}$, which expresses how close the excitation frequency is to the natural frequency of the system. Dividing the numerator and denominator of the term in parentheses by ${\omega_n}^2$, the new FRF form is:

$$G(\omega) = \frac{1}{k}\left(\frac{1}{\left(1 - \left(\frac{\omega}{\omega_n}\right)^2\right) + i2\zeta\left(\frac{\omega}{\omega_n}\right)}\right). \tag{3.5}$$

Substituting the frequency ratio r for $\frac{\omega}{\omega_n}$ yields the more compact FRF equation:

$$G(r) = \frac{1}{k}\left(\frac{1}{(1-r^2)+i2\zeta r}\right). \tag{3.6}$$

In Eq. 3.6, $r = 1$ represents a special case. In this instance:

$$G(1) = \frac{1}{k}\left(\frac{1}{\left(1-(1)^2\right)+i2\zeta(1)}\right) = \frac{1}{k}\left(\frac{1}{i2\zeta}\right).$$

This gives the largest value of $G(r)$ for a fixed value of ζ. It is called **resonance**. Physically, this means that when a system is forced at its natural frequency ($\omega = \omega_n$), the steady-state response is largest and its amplitude depends on the system stiffness and damping ratio. Intuitively, a larger stiffness or damping ratio gives a smaller response. Note that the resonant response is purely imaginary.

In a Nutshell
The resonant response, $G(r = 1)$, is not imaginary in the sense that it does not exist. "Purely imaginary" means that if the excitation is represented by a sine function, then the resulting vibration at resonance is represented by a cosine function. The force and vibration reach their maximum values at different times and, at resonance, the force is maximum when the displacement is zero.

Rather than leaving the FRF in the form shown in Eq. 3.6, let's rationalize by multiplying the numerator and denominator by the complex conjugate of the denominator.

$$G(r) = \frac{1}{k}\left(\frac{1}{(1-r^2)+i2\zeta r}\cdot\frac{(1-r^2)-i2\zeta r}{(1-r^2)-i2\zeta r}\right) = \frac{1}{k}\left(\frac{(1-r^2)-i2\zeta r}{(1-r^2)^2+(2\zeta r)^2}\right). \tag{3.7}$$

This function has both real and imaginary parts. The **real part** is:

$$Re\left(G(r)\right) = \frac{1}{k}\left(\frac{(1-r^2)}{(1-r^2)^2+(2\zeta r)^2}\right) \tag{3.8}$$

and the **imaginary part** is:

$$Im(G(r)) = \frac{1}{k}\left(\frac{-2\zeta r}{(1-r^2)^2+(2\zeta r)^2}\right). \tag{3.9}$$

We can also express Eq. 3.7 in terms of **magnitude** and **phase**. This relates to the vector description we've discussed previously (see Figs. 2.4 and 2.5, for example).

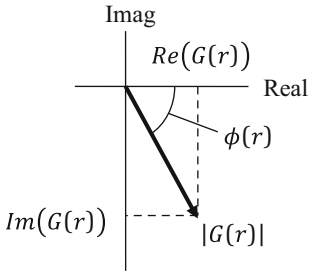

Fig. 3.2 Vector description of the FRF's magnitude and phase

Figure 3.2 demonstrates the relationships between the real and imaginary parts and the magnitude and phase. The magnitude is calculated according to:

$$|G(r)| = \sqrt{(Re\,(G(r)))^2 + (Im(G(r)))^2} = \frac{1}{k}\sqrt{\frac{1}{(1-r^2)^2 + (2\zeta r)^2}} \tag{3.10}$$

and the phase[1] is determined using:

$$\phi(r) = tan^{-1}\left(\frac{Im(G(r))}{Re\,(G(r))}\right) = tan^{-1}\left(\frac{-2\zeta r}{1-r^2}\right). \tag{3.11}$$

Physically, the magnitude gives the size of the vibration response and the phase describes how much the vibration lags the harmonic, oscillating force. To better understand the phase lag, consider the **Slinky**®—a helical spring toy invented by Richard James in the 1940s [1]. By holding the Slinky® vertically and attaching several of the coils at the bottom together (using a rubber band, for example), you can approximate a spring-mass-damper system (although the damping is quite low). Now begin moving your hand up and down very slowly. You will observe that the "mass" at the bottom basically follows your hand's motion. As you increase the frequency of your hand's oscillation, however, you will see that the mass exhibits a different behavior; now its motion directly opposes your hand's motion. For the low forcing frequency, the phase lag is near zero. For the higher frequency, the phase lag is close to 180° (i.e., $\phi \approx -180°$ and the mass's motion is out of phase with your hand's motion). The sharp transition between "in phase" and "out of phase" vibration is observed due to the low damping in the system.

As an alternative to Eqs. 3.10 and 3.11, the magnitude and phase can be expressed in terms of the model parameters m, k, and c. See Eqs. 3.12 and 3.13.

[1] Note that the tangent function exhibits quadrant dependence in the complex plane. In MATLAB® the `atan2` function can be used to respect this quadrant-dependent behavior.

$$|G(r)| = \sqrt{\frac{1}{(k - m\omega^2)^2 + (c\omega)^2}} \tag{3.12}$$

$$\phi = tan^{-1}\left(\frac{-c\omega}{k - m\omega^2}\right) \tag{3.13}$$

3.3 Evaluating the Frequency Response Function

Let's now plot the FRF as a function of the frequency ratio, r (or, equivalently, the forcing frequency, ω). Figure 3.3 shows the FRF magnitude from Eq. 3.10. Results are provided for ζ values of 0.01, 0.05, and 0.1 with $k = 1 \times 10^6$ N/m. We see that the peak height is reduced with increased damping. This "sharpness" of the magnitude peak is sometimes described as the system Q (or **quality factor**). A tall, sharp peak (low damping) represents a system with high Q. The Q can be related to ζ as shown in Eq. 3.14.

$$Q = \frac{1}{2\zeta} \tag{3.14}$$

In Fig. 3.3, the $r = 0$ magnitude is $|G(r = 0)| = \left|\frac{X}{F}\right| = \frac{1}{k} = 1 \times 10^{-6}$ m/N. This DC result is independent of the damping ratio. For the resonant case where $r = 1$:

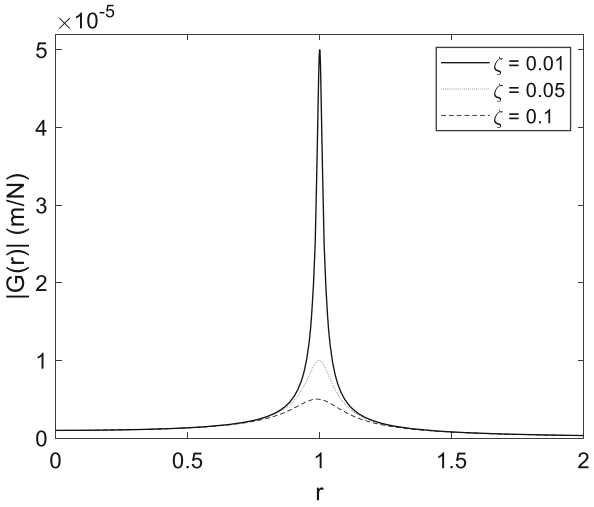

Fig. 3.3 Magnitude vs. r plot for underdamped systems ($\zeta = 0.01$, 0.05, and 0.1 with $k = 1 \times 10^6$ N/m)

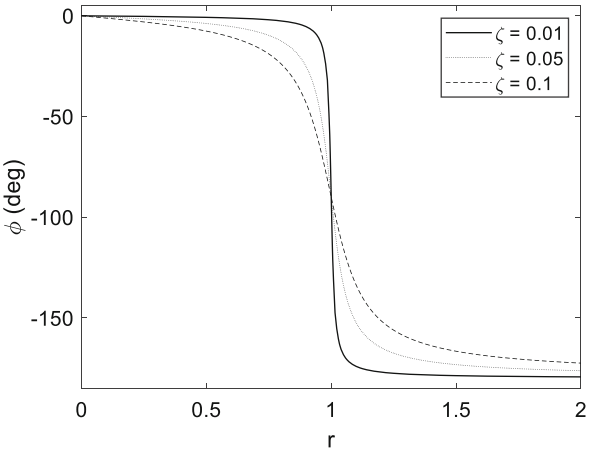

Fig. 3.4 Phase vs. r plot for underdamped systems ($\zeta = 0.01, 0.05$, and 0.1 with $k = 1 \times 10^6$ N/m)

$$|G(r=1)| = \frac{1}{2k\zeta} = \frac{1}{2\left(1 \times 10^6\right)\zeta} = \frac{5 \times 10^{-7}}{\zeta}.$$

The three peak values are $\{5 \times 10^{-5}, 1 \times 10^{-5}$, and $5 \times 10^{-6}\}$ m/N.

The phase plot is typically provided in conjunction with the magnitude plot to fully describe the FRF. The phase for the same system used in Fig. 3.3 is shown in Fig. 3.4; the code used to produce Figs. 3.3 and 3.4 is included in MATLAB® MOJO 3.1. In Fig. 3.4, the phase at $r = 0$ is $\phi = 0$. This is the static result where there is no phase lag between the displacement and force. At $r = 1$ (resonance), the phase is $\phi = tan^{-1}\left(\frac{2\zeta}{0}\right) = -\frac{\pi}{2}$ rad $= -90°$. For $r \gg 1$, the phase approaches $-\pi$ rad $(-180°)$. This is the "out of phase" condition where the force reaches is minimum value while the displacement reaches its maximum value. See the time-domain representations of the force and displacement in Fig. 3.5.

MATLAB® MOJO 3.1

```
% matlab_mojo_3_1.m

clear
close all
clc

% Define variables
r = 0:0.001:2;
k = 1e6;          % N/m

% Define function
zeta1 = 0.01
mag1 = 1/k*(1./((1-r.^2).^2 + (2*zeta1*r).^2)).^0.5;
phase1 = atan2(-2*zeta1*r, (1-r.^2));

zeta2 = 0.05
mag2 = 1/k*(1./((1-r.^2).^2 + (2*zeta2*r).^2)).^0.5;
phase2 = atan2(-2*zeta2*r, (1-r.^2));
```

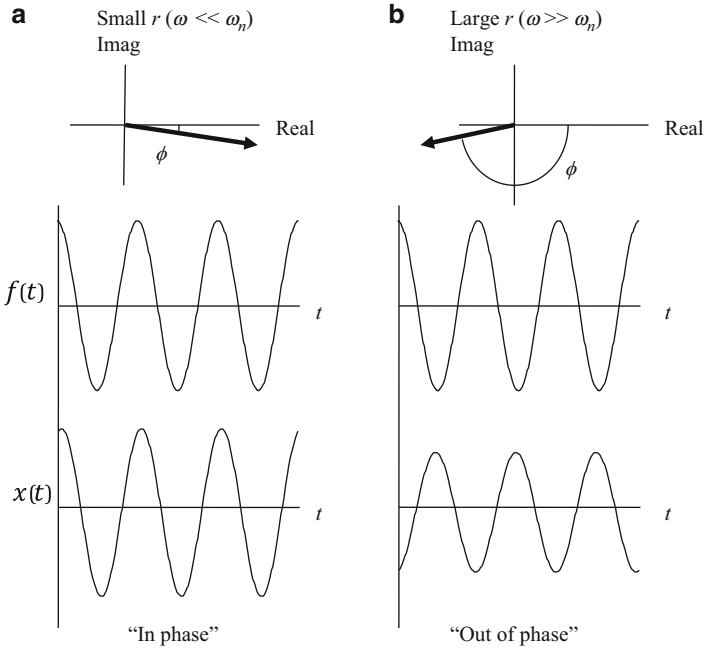

Fig. 3.5 Time-domain representations of phase between force and displacement for: (**a**) small r; and (**b**) large r ($r \gg 1$)

```
zeta3 = 0.1
mag3 = 1/k*(1./((1-r.^2).^2 + (2*zeta3*r).^2)).^0.5;
phase3 = atan2(-2*zeta3*r, (1-r.^2));

figure(1)
plot(r, mag1, 'k-', r, mag2, 'k:', r, mag3, 'k--')
set(gca,'FontSize', 14)
xlabel('r')
ylabel('|G(r)| (m/N)')
axis([0 2 0 5.2e-5])
legend('\zeta = 0.01', '\zeta = 0.05', '\zeta = 0.1')

figure(2)
plot(r, phase1*180/pi, 'k-', r, phase2*180/pi, 'k:', r, phase3*180/pi,
'k--')
set(gca,'FontSize', 14)
xlabel('r')
ylabel('\phi (deg)')
axis([0 2 -185 5])
legend('\zeta = 0.01', '\zeta = 0.05', '\zeta = 0.1')
```

In a Nutshell

The magnitude and phase representations show how the forced vibration is related to the exciting force over a range of frequencies. Let's look at the vibration that results for a given force amplitude as the frequency of the force changes. In all cases, the frequency of the vibration is the same as the frequency of the exciting force. When the excitation frequency is low, the force and displacement go together and reach their maximum values at almost the same time. They are "in phase". As the frequency of the excitation frequency increases, the amplitude of the displacement increases and the displacement begins to fall behind the force (it reaches its peak value a little later than the force reaches its peak value). At resonance (where the excitation frequency equals the natural frequency), the amplitude of the displacement is at its largest value and the displacement reaches its maximum when the force is zero. The force and displacement are phase shifted by 90°. As the excitation frequency continues to increase, the amplitude of the displacement begins to decrease and the displacement lags even farther behind the force. When the excitation frequency is very high, the amplitude of the displacement becomes much smaller and the displacement reaches a positive maximum when the force reaches a negative maximum. They are phase shifted by 180° ("out of phase").

Next, let's plot the real and imaginary parts of the FRF, again as a function of the frequency ratio. Using Eq. 3.8, we obtain Fig. 3.6 for $\zeta = 0.01$, 0.05, and 0.1 with $k = 1 \times 10^6$ N/m. We see that, similar to the magnitude plot in Fig. 3.3, the peak-to-peak height decreases with increasing damping. For the imaginary part (Eq. 3.9), a similar trend is observed in Fig. 3.7. The code used to produce Figs. 3.3 and 3.4 is provided in MATLAB® MOJO 3.2.

MATLAB® MOJO 3.2

```
% matlab_mojo_3_2.m

clear
close all
clc

% Define variables
r = 0:0.001:2;
k = 1e6;          % N/m

% Define function
zeta1 = 0.01
real1 = 1/k*(1-r.^2)./((1-r.^2).^2 + (2*zeta1*r).^2);
imag1 = 1/k*(-2*zeta1*r)./((1-r.^2).^2 + (2*zeta1*r).^2);
```

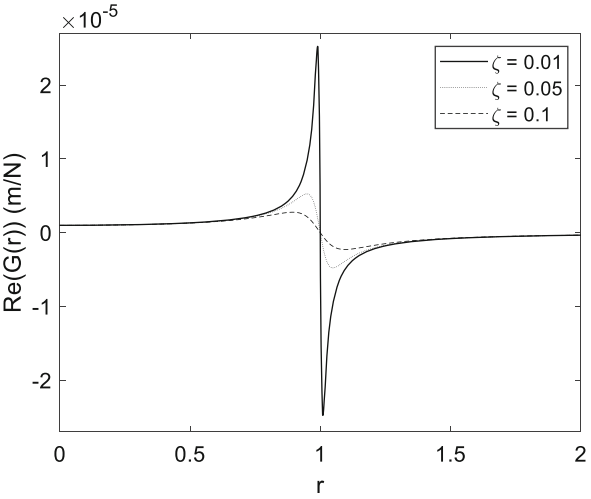

Fig. 3.6 FRF real part vs. r plot for underdamped systems ($\zeta = 0.01$, 0.05, and 0.1 with $k = 1 \times 10^6$ N/m)

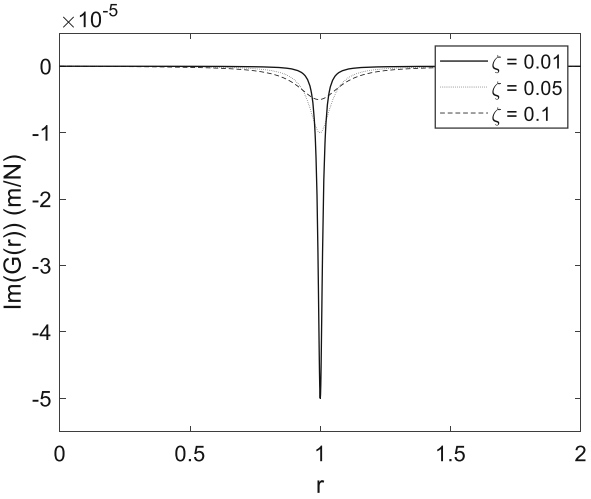

Fig. 3.7 FRF imaginary part vs. r plot for underdamped systems ($\zeta = 0.01$, 0.05, and 0.1 with $k = 1 \times 10^6$ N/m)

```
zeta2 = 0.05
real2 = 1/k*(1-r.^2)./((1-r.^2).^2 + (2*zeta2*r).^2);
imag2 = 1/k*(-2*zeta2*r)./((1-r.^2).^2 + (2*zeta2*r).^2);

zeta3 = 0.1
real3 = 1/k*(1-r.^2)./((1-r.^2).^2 + (2*zeta3*r).^2);
imag3 = 1/k*(-2*zeta3*r)./((1-r.^2).^2 + (2*zeta3*r).^2);

figure(1)
plot(r, real1, 'k-', r, real2, 'k:', r, real3, 'k--')
set(gca,'FontSize', 14)
xlabel('r')
```

```
ylabel('Re(G(r)) (m/N)')
axis([0 2 -2.7e-5 2.7e-5])
legend('\zeta = 0.01', '\zeta = 0.05', '\zeta = 0.1')

figure(2)
plot(r, imag1, 'k-', r, imag2, 'k:', r, imag3, 'k--')
set(gca,'FontSize', 14)
xlabel('r')
ylabel('Im(G(r)) (m/N)')
axis([0 2 -5.5e-5 5e-6])
legend('\zeta = 0.01', '\zeta = 0.05', '\zeta = 0.1')
```

For the single degree of freedom FRF we are considering now, several important points can be identified directly from the real and imaginary plots. As we've already discussed, the zero frequency ($r = 0$) response gives a value of $\frac{1}{k}$ for the real part and zero for the imaginary part. At resonance ($r = 1$), the real part is zero and the imaginary part reaches its minimum value of $-\frac{1}{2k\zeta}$. The maximum real part value of approximately $\frac{1}{4k\zeta(1-\zeta)}$ occurs at a frequency of $r = 1 - \zeta$ ($\omega = \omega_n(1 - \zeta)$). At a frequency of $r = 1 + \zeta$ ($\omega = \omega_n(1 + \zeta)$), the minimum real part is observed with a value of approximately $-\frac{1}{4k\zeta(1+\zeta)}$. We can also note that the peak-to-peak value of the real part is the same as for the imaginary part: $\frac{1}{2k\zeta}$. Summing the absolute values of the real part maximum and minimum peaks, we obtain:

$$\frac{1}{4k\zeta(1-\zeta)} + \frac{1}{4k\zeta(1+\zeta)} = \frac{(1+\zeta)+(1-\zeta)}{4k\zeta(1-\zeta)(1+\zeta)} = \frac{2}{4k\zeta\left(1-\zeta^2\right)} \approx \frac{1}{2k\zeta}.$$

This approximation is valid for small ζ values, which is typical for mechanical structures. For example, even with 10% damping ($\zeta = 0.1$), ζ^2 is only 0.01. These frequencies and peaks are identified in Figs. 3.8 and 3.9.

By the Numbers 3.1

Consider the lumped parameter spring-mass-damper system displayed in Fig. 3.10. The harmonic force, $f(t) = Fe^{i\omega t}$, is acting on the system to produce forced vibration. The system natural frequency is 500 Hz, the damping ratio is 0.1, and the stiffness is 1×10^6 N/m.

First, given the system parameters f_n, ζ, and k, we can determine m and c. We obtain the mass using:

$$m = \frac{k}{(2\pi f_n)^2} = \frac{1 \times 10^6}{(2\pi \cdot 500)^2} = 0.1 \text{ kg}.$$

The viscous damping ratio is $c = 2\zeta m\omega_n = 2(0.1)0.1(2\pi \cdot 500) = 63$ N s/m. Let's now sketch the magnitude and phase for this system. For the magnitude plot, we can directly identify the magnitude at forcing frequency values of $\omega = 0$ ($r = 0$) and $\omega = \omega_n$ ($r = 1$). At DC, the magnitude is $\frac{1}{k} = \frac{1}{1\times10^6} = 1 \times 10^{-6}$ m/N $= 100$ μm/100 N.

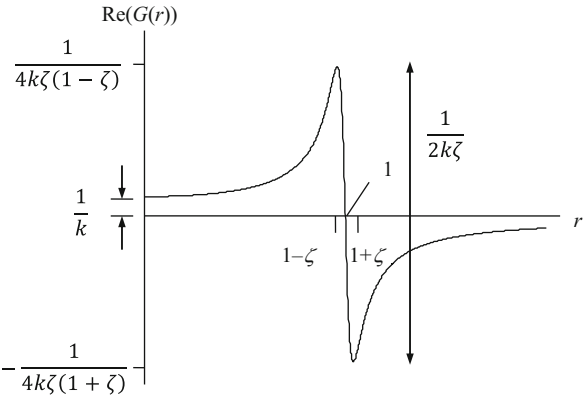

Fig. 3.8 Summary of important points on FRF real part

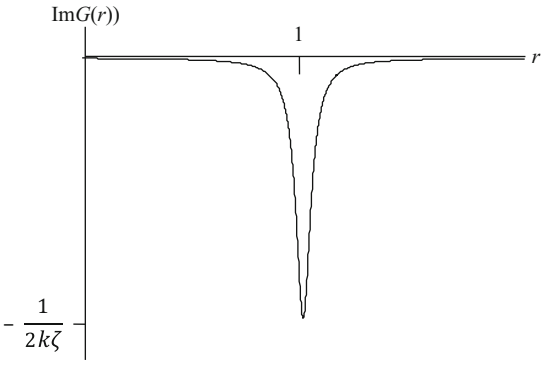

Fig. 3.9 Summary of important points on FRF imaginary part

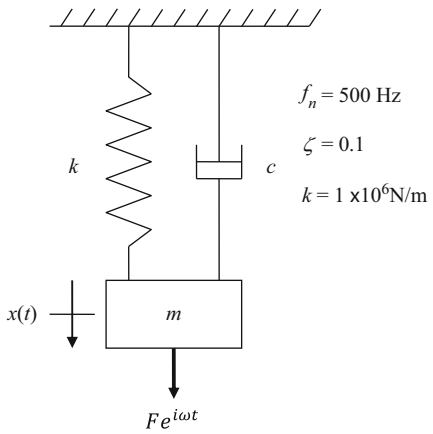

Fig. 3.10 *By the Numbers 3.1*—the example spring-mass-damper system and single degree of freedom models parameters are shown

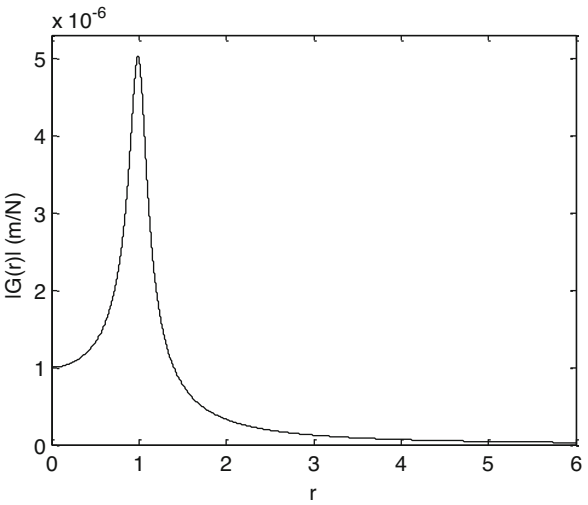

Fig. 3.11 *By the Numbers 3.1*—magnitude plot

This means that we'd get a deflection of approximately the diameter of a human hair if we applied a constant force of 100 N (or 22.5 lb_f). At resonance, where the forcing frequency is equal to the natural frequency, the magnitude is $\frac{1}{2k\zeta} = \frac{1}{2\left(1\times10^6\right)0.1} = 5 \times 10^{-6}$ N/m. Note that the **dynamic flexibility**[2] is five times higher than the **static flexibility** for this system. At a higher frequency, say $r = 5$ where the forcing frequency is $f = 5f_n = 5 \cdot 500 = 2500$ Hz, the magnitude is:

$$|G(5)| = \frac{1}{1 \times 10^6}\sqrt{\frac{1}{\left(1-5^2\right)^2 + (2(0.1)5)^2}} = 4.2 \times 10^{-8}\ \text{N/m} = 4.2\ \mu\text{m}/100\ \text{N}.$$

Now the dynamic flexibility is ~24 times smaller than the static flexibility and ~120 times smaller than the resonant case. This emphasizes the strong dependence of the steady-state response for dynamic systems on the (harmonic) forcing frequency. The magnitude plot is provided in Fig. 3.11.

For the phase plot (Fig. 3.12), we know that the phase is $\phi = 0$ at $\omega = 0$ ($r = 0$), it is $-90°$ at $\omega = \omega_n$ ($r = 1$), and it approaches $-180°$ for large forcing frequencies (r values $\gg 1$). Specifically, we calculate the following.

- For $r = 0$, $\phi(r = 0) = tan^{-1}\left(\frac{-2\zeta r}{1-r^2}\right) = tan^{-1}\left(\frac{0}{1}\right) = 0$.
- For $r = 1$, $\phi(r = 1) = tan^{-1}\left(\frac{-2\zeta}{0}\right) = -90^\circ$. Recognizing that the phase is the inverse tangent of the ratio of the imaginary part to the real part, Fig. 3.13

[2]Flexibility, or compliance, is the inverse of stiffness.

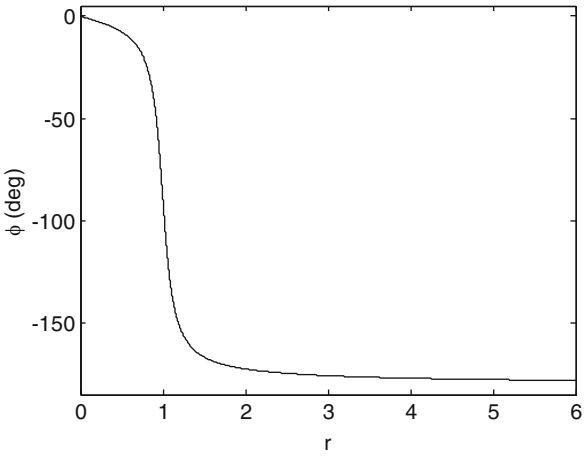

Fig. 3.12 *By the Numbers 3.1*—phase plot

demonstrates this result. Because the real part is zero and the imaginary part is negative, the displacement lags the (real-valued) force by 90°.

- For $r = 5$, $\phi(r = 5) = tan^{-1}\left(\frac{-2(0.1)5}{1-5^2}\right)$. Here we have to exercise caution in calculating the phase. If we simply input this ratio into a calculator and use the $\tan^{-1}$ key/function, we would find that $\phi = 2.4°$ (or 0.04 rad). A positive phase indicates that the displacement has somehow anticipated[3] the force and is leading it in time. This is not possible for our system, so this must not be the correct phase. The error is due to the quadrant dependence of the inverse tangent. Fig. 3.14 shows that the correct phase is $\phi = -(180 - 2.4) = -177.6° = -3.1$ rad. In MATLAB®, the correct result of −3.1 rad is obtained using `atan2(-2*0.1*5, 1-5^2)`.

Next, let's look at the real and imaginary parts of the FRF. The real plot is provided in Fig. 3.15 and the imaginary part in Fig. 3.16. At $\omega = 0$ ($r = 0$), the value is:

$$Re\,(G(0)) = \frac{1}{1 \times 10^6}\left(\frac{(1-0^2)}{(1-0^2)^2 + (2(0.1)0)^2}\right) = 1 \times 10^{-6}\ \text{m/N}.$$

At $\omega = \omega_n$ ($r = 1$), the value of the real part is:

$$Re\,(G(1)) = \frac{1}{1 \times 10^6}\left(\frac{(1-1^2)}{(1-1^2)^2 + (2(0.1)1)^2}\right) = 0.$$

At $\omega = 5\omega_n$ ($r = 5$), the real part is:

[3] Such anticipatory behavior would be exhibited by a noncausal system [2].

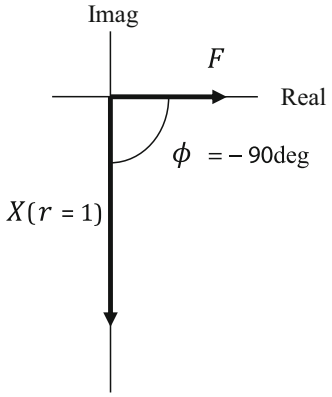

Fig. 3.13 *By the Numbers 3.1*—the displacement lags the force by 90° for $r = 1$

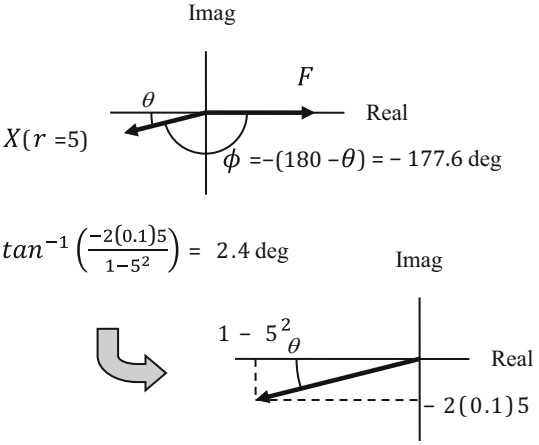

Fig. 3.14 *By the Numbers 3.1*—the displacement lags the force by 177.6° for $r = 5$

$$Re\,(G(5)) = \frac{1}{1 \times 10^6}\left(\frac{\left(1-5^2\right)}{\left(1-5^2\right)^2 + (2(0.1)5)^2}\right) = -4.2 \times 10^{-8}\ \text{m/N}.$$

Let's also determine the real part value at its peaks. For the maximum peak, which occurs approximately at $r = 1 - \zeta = 1 - 0.1 = 0.9$, the value is:

$$Re\,(G(0.9)) = \frac{1}{1 \times 10^6}\left(\frac{\left(1-0.9^2\right)}{\left(1-0.9^2\right)^2 + (2(0.1)0.9)^2}\right) = 2.8 \times 10^{-6}\ \text{m/N}.$$

Note that this result can be approximated using $\frac{1}{4k\zeta(1-\zeta)}$. For the minimum (negative) peak, which occurs at a frequency ratio of approximately $1 + \zeta = 1 + 0.1 = 1.1$, the value is:

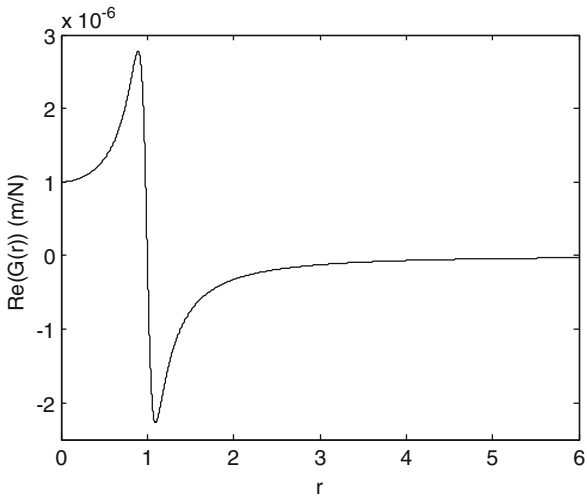

Fig. 3.15 *By the Numbers 3.1*—real part of the FRF

$$Re\left(G(1.1)\right) = \frac{1}{1 \times 10^6}\left(\frac{\left(1 - 1.1^2\right)}{\left(1 - 1.1^2\right)^2 + \left(2(0.1)1.1\right)^2}\right) = -2.3 \times 10^{-6} \text{ m/N}.$$

Similarly, this result can be approximated using $-\frac{1}{4k\zeta(1+\zeta)}$ (Fig. 3.15).

To complete this example, let's plot the Argand diagram, or the real part of the FRF versus the imaginary part of the FRF. The result is provided in Fig. 3.17, where the points for $r = 0$, $r = 1 - \zeta = 1 - 0.1 = 0.9$, $r = 1$, and $r = 1 + \zeta = 1 + 0.1 = 1.1$ are identified by the open circles. For these points, the values of the real and imaginary parts are gives in Table 3.1.

We can see in Fig. 3.17 that the points for $r = 0.9$ and 1.1 do not appear at the Argand "circle" quadrants as we might have expected. They are, after all, supposed to identify the maximum and minimum real part values. The reason for this discrepancy is that using the frequency ratios $r = 1 - \zeta$ and $r = 1 + \zeta$, respectively, to identify the maximum and minimum real part values is an approximation. We can determine the actual r values by differentiating Eq. 3.8 with respect to r and setting this result equal to zero.

$$\frac{d}{dr}\left(\frac{1}{k}\left(\frac{(1 - r^2)}{(1 - r^2)^2 + (2\zeta r)^2}\right)\right) = 0 \tag{3.15}$$

Computing the derivative in Eq. 3.15 yields:

$$\frac{\left((1 - r^2)^2 + (2\zeta r)^2\right)(-2r) - (1 - r^2)(2(1 - r^2)(-2r) + 2(2\zeta r)(2\zeta))}{\left((1 - r^2)^2 + (2\zeta r)^2\right)^2}$$

$$= 0. \tag{3.16}$$

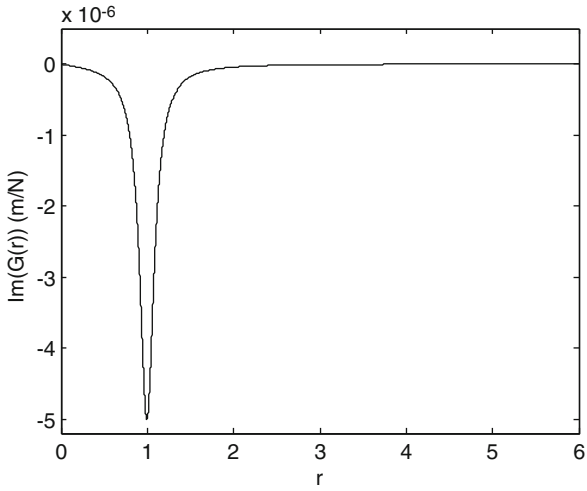

Fig. 3.16 *By the Numbers 3.1*—imaginary part of the FRF

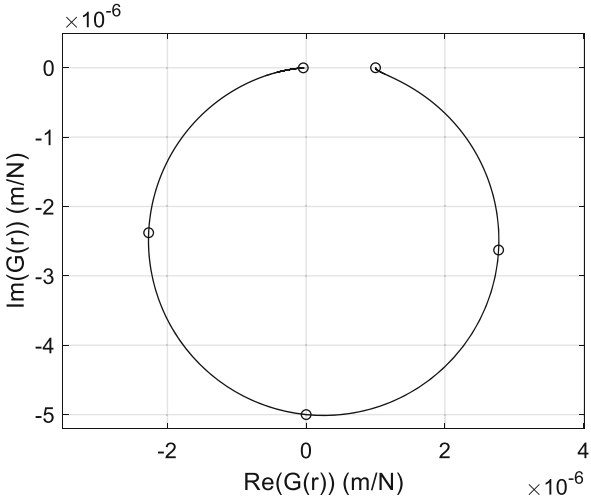

Fig. 3.17 *By the Numbers 3.1*—Argand diagram. The frequency ratios in Table 3.1 are identified by the open circles. Clockwise from the top right circle: $r = 0$, 0.9, 1, 1.1, and 5

Table 3.1 *By the Numbers 3.1*—values of the FRF real and imaginary parts for various frequency ratios (see Fig. 3.17)

r	$Re(G(r))$ (m/N)	$Im(G(r))$ (m/N)
0	1×10^{-6}	0
0.9	2.8×10^{-6}	-2.8×10^{-6}
1	0	-5×10^{-6}
1.1	-2.3×10^{-6}	-2.4×10^{-6}
5	-4.2×10^{-8}	-1.7×10^{-9}

Expanding the numerator and canceling terms gives an equation that is quadratic in r^2:

$$2r^4 - 4r^2 + \left(2 - 8\zeta^2\right) = 0. \tag{3.17}$$

We can obtain the roots, ${r_{1,2}}^2$, of Eq. 3.17 using the quadratic equation:

$${r_{1,2}}^2 = \frac{-(-4) \pm \sqrt{(-4)^2 - 4(2)\left(2 - 8\zeta^2\right)}}{2(2)} = 1 \pm \frac{\sqrt{64\zeta^2}}{4} = 1 \pm 2\zeta. \tag{3.18}$$

For our approximation of $r = 1 \pm \zeta$, the square of this expression gives:

$${r_1}^2 = 1 + 2\zeta + \zeta^2 \text{ and } {r_2}^2 = 1 - 2\zeta + \zeta^2. \tag{3.19}$$

For small ζ, the additional ζ^2 term at the end of the expressions in Eq. 3.19 is negligible. However, as ζ increases, the error in this approximation becomes evident; see Fig. 3.17. Figure 3.18 shows the Argand diagram where the same r values are identified using Eq. 3.18 (rather than the approximation). The code used to generate Fig. 3.18 is provided in MATLAB® MOJO 3.3.

If we look carefully at Fig. 3.18, we see that we are not quite done. In fact, the $r = 1$ point does not exactly identify the minimum value of the FRF imaginary part. This is again an approximation; a good one, but an approximation nonetheless. We can follow the same steps as before, but this time use Eq. 3.9 to determine the proper r value.

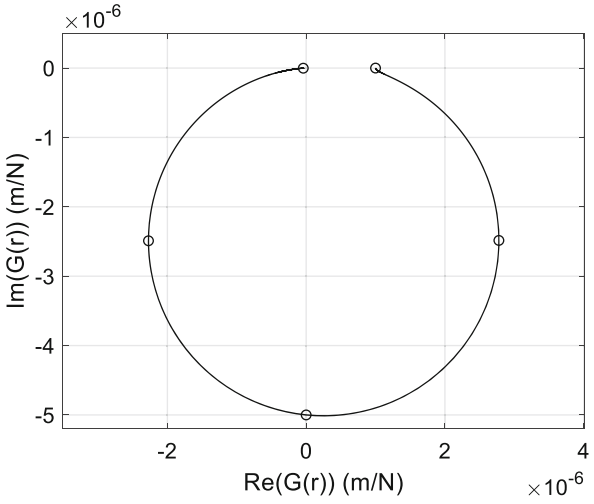

Fig. 3.18 *By the Numbers 3.1*—Argand diagram. The frequency ratios determined using Eq. 3.18 are identified by the open circles. Clockwise from the top right circle: $r = 0$, $\sqrt{0.8}$, 1, $\sqrt{1.2}$, and 5

$$\frac{d}{dr}\left(\frac{1}{k}\left(\frac{-2\zeta r}{(1-r^2)^2+(2\zeta r)^2}\right)\right)=0 \tag{3.20}$$

Calculating the derivative gives:

$$\frac{\left((1-r^2)^2+(2\zeta r)^2\right)(-2\zeta)-(-2\zeta r)(2(1-r^2)(-2r)+2(2\zeta r)(2\zeta))}{\left((1-r^2)^2+(2\zeta r)^2\right)^2}$$

$$=0. \tag{3.21}$$

Expanding the numerator and canceling terms yields:

$$3r^4+\left(4\zeta^2-2\right)r^2-1=0. \tag{3.22}$$

Again using the quadratic equation, we determine the roots to be:

$${r_{1,2}}^2=\frac{\left(2-4\zeta^2\right)\pm 4\sqrt{\zeta^4-\zeta^2+1}}{6}. \tag{3.23}$$

For $\zeta=0.1$, substitution gives:

$${r_{1,2}}^2=\frac{\left(2-4(0.1)^2\right)\pm 4\sqrt{(0.1)^4-(0.1)^2+1}}{6}=\frac{1.96}{6}\pm\frac{4\sqrt{0.9901}}{6}.$$

Using $r^2=\frac{1.96}{6}+\frac{4\sqrt{0.9901}}{6}$, the r value for the minimum imaginary part is 0.995, rather than 1. Note, however, that as ζ approaches zero in Eq. 3.23, r approaches 1 (again using the positive root).

MATLAB® MOJO 3.3

```
% matlab_mojo_3_3.m

clear
close all
clc

% Define variables
r = 0:0.001:6;
k = 1e6;          % N/m

% Define function
zeta1 = 0.1;
real1 = 1/k*(1-r.^2)./((1-r.^2).^2 + (2*zeta1*r).^2);
imag1 = 1/k*(-2*zeta1*r)./((1-r.^2).^2 + (2*zeta1*r).^2);
```

```
figure(1)
plot(real1, imag1, 'k-')
set(gca,'FontSize', 14)
xlabel('Re(G(r)) (m/N)')
ylabel('Im(G(r)) (m/N)')
axis([-2.5e-6 3e-6 -5.2e-6 5e-7])
hold on
grid
axis equal

r_points = [0 sqrt(1-2*zeta1) 1 sqrt(1+2*zeta1) 5];

for cnt = 1:length(r_points)
  r1 = r_points(cnt);
  real_points(cnt) = 1/k*(1-r1^2)/((1-r1^2)^2 + (2*zeta1*r1)^2);
  imag_points(cnt) = 1/k*(-2*zeta1*r1)/((1-r1^2)^2 + (2*zeta1*r1)^2);
end

plot(real_points, imag_points, 'ko')
```

By the Numbers 3.2

Let's consider a second example, now with $m = 1$ kg, $c = 500$ N s/m, $k = 5 \times 10^7$ N/m, and $f = Fe^{i\omega t} = 1e^{i4500t}$ N. See Fig. 3.19. The associated natural frequency is $\omega_n = \sqrt{\frac{5\times10^7}{1}} = 7071.1$ rad/s and the damping ratio is $\zeta = \frac{500}{2\sqrt{5\times10^7(1)}} = 0.035$ (or 3.5%). The forcing frequency is 4500 rad/s, so the frequency ratio is $r = \frac{4500}{7071.1} = 0.636$.

The complex FRF, $G(r)$, for this damped, single degree of freedom system is:

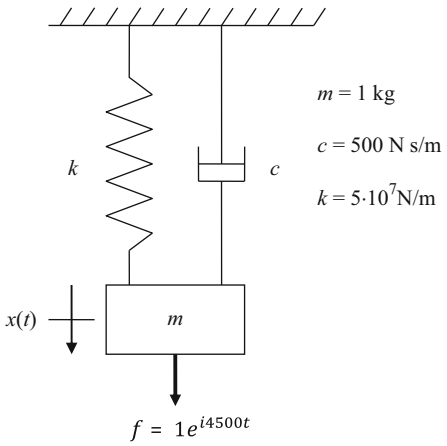

Fig. 3.19 *By the Numbers 3.2*—the single degree of freedom spring-mass-damper system and models parameters are shown

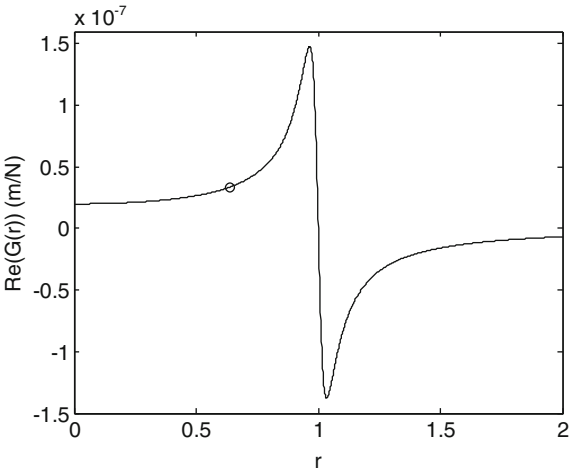

Fig. 3.20 *By the Numbers 3.2*—FRF real part. The $r = 0.636$ point is identified

$$G(0.636) = \frac{1}{5 \times 10^7}\left(\frac{\left(1-(0.636)^2\right) - i2(0.035)(0.636)}{\left(1-(0.636)^2\right)^2 + (2(0.035)(0.636))^2}\right).$$

The real part is shown in Fig. 3.20 and the value for $r = 0.636$ is:

$$\begin{aligned} Re\left(G(0.636)\right) &= \frac{1}{5 \times 10^7}\left(\frac{\left(1-(0.636)^2\right)}{\left(1-(0.636)^2\right)^2 + (2(0.035)(0.636))^2}\right) \\ &= 3.34 \times 10^{-8}\ \text{m/N}. \end{aligned}$$

The real part is shown in Fig. 3.21 and the value for $r = 0.636$ is:

$$\begin{aligned} Im(G(0.636)) &= \frac{1}{5 \times 10^7}\left(\frac{-2(0.035)(0.636)}{\left(1-(0.636)^2\right)^2 + (2(0.035)(0.636))^2}\right) \\ &= -2.5 \times 10^{-9}\ \text{m/N}. \end{aligned}$$

The real and imaginary values of the frequency-domain displacement, $X(0.636)$, are determined by multiplying the FRF by the force magnitude of $F = 1$ N. The real part is:

$$Re\left(X(0.636)\right) = F \cdot Re\left(G(0.636)\right) = 1 \cdot 3.34 \times 10^{-8} = 3.34 \times 10^{-8}\ \text{m}$$

and the imaginary part is:

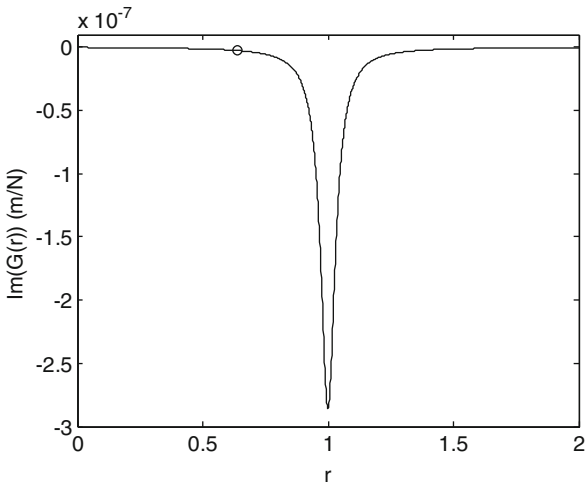

Fig. 3.21 *By the Numbers 3.2*—FRF imaginary part. The $r = 0.636$ point is identified

$$Im(X(0.636)) = F \cdot Im(G(0.636)) = 1 \cdot \left(-2.5 \times 10^{-9}\right) = -2.5 \times 10^{-9} \text{ m}.$$

We can now plot these components of the response in the complex plane. The force and displacement vectors are represented in Fig. 3.22, where the displacement magnitude is:

$$|X(0.636)| = \sqrt{Re\left(G(0.636)\right)^2 + Im(G(0.636))^2} = 3.35 \times 10^{-8} \text{ m}$$

and the phase is:

$$\phi(0.636) = tan^{-1}\left(\frac{Im(G(0.636))}{Re\left(G(0.636)\right)}\right) = -4.28^{\circ} = -0.075 \text{ rad}.$$

Of course we would obtain the same results by applying Eqs. 3.10 and 3.11.

3.4 Defining a Model from a Frequency Response Function Measurement

In Figs. 3.8 and 3.9, we saw that key points from the FRF can be quickly identified based on the peaks in the real and imaginary part plots. What if we were able to perform a measurement to determine the FRF for a particular structure? We could then identify a model to represent the measured system using a **peak picking** approach.

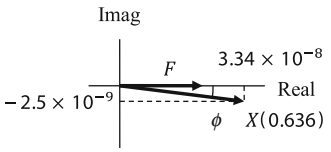

Fig. 3.22 *By the Numbers 3.2*—Argand diagram for $r = 0.636$

$$\phi(0.636) = tan^{-1}\left(\frac{-2.5\times10^{-9}}{3.34\times10^{-8}}\right) = -4.28 \text{ deg}$$

$$|X(0.636)| = \sqrt{(3.34\times10^{-8})^2 + (-2.5\times10^{-9})^2} = 3.35\times10^{-8} \text{ m}$$

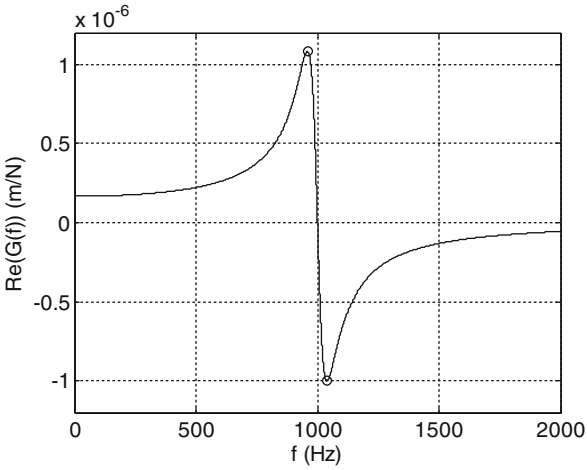

Fig. 3.23 Real part of measured FRF for a test structure

While we won't discuss FRF measurement until Chap. 7, we can still describe the steps necessary to use measurement data to define a single degree of freedom system model. Let's assume that the FRF displayed in Figs. 3.23 (real part) and 3.24 (imaginary part) was obtained from a measurement of a test structure. In the figures, the peaks are identified by circles and the corresponding peak frequencies and values are summarized in Table 3.2.

Defining a single degree of freedom spring-mass-damper model based on the data in Table 3.2 requires five primary steps.

1. The frequency of the minimum imaginary part peak is taken to be the system natural frequency: $f_n = 999.2$ Hz.
2. The real part maximum and minimum peaks occur at approximately $f = f_n(1 - \zeta)$ and $f = f_n(1 + \zeta)$, respectively. Differencing these two frequencies gives:

$$f_n(1+\zeta) - f_n(1-\zeta) = 2\zeta f_n.$$

For the measured FRF, we have that $1039.2 - 959.2 = 80 = 2\zeta f_n$. Since we already know f_n, we can solve for the damping ratio:

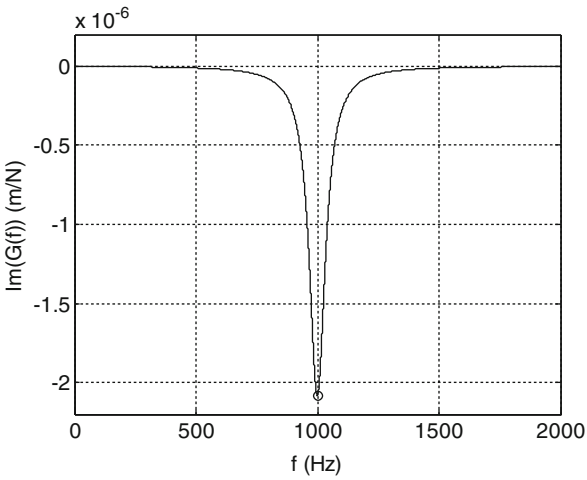

Fig. 3.24 Imaginary part of measured FRF for a test structure

Table 3.2 Frequencies and values of FRF real and imaginary part peaks (the shaded values are not used in the peak picking analysis)

Peak	Frequency (Hz)	Value (m/N)
Real maximum	959.2	1.085×10^{-6}
Real minimum	1039.2	-1.002×10^{-6}
Imaginary minimum	999.2	-2.084×10^{-6}

$$\zeta = \frac{80}{2(999.2)} = 0.04\ (4\%).$$

3. We determine the stiffness from the peak value of the minimum imaginary part. Recall from Fig. 3.9 that the minimum value is $-\frac{1}{2k\zeta}$. We found ζ in step 2, so we can now solve for k.

$$k = \frac{-1}{2(0.04)\left(-2.084 \times 10^{-6}\right)} = 6 \times 10^{6}\ \mathrm{N/m}$$

4. Given the natural frequency and stiffness, we can find the model mass.

$$m = \frac{k}{{\omega_n}^2} = \frac{k}{(2\pi f_n)^2} = \frac{6 \times 10^6}{(2\pi \cdot 999.2)^2} = 0.15 \text{ kg}$$

5. The viscous damping coefficient is then:

$$c = 2\zeta\sqrt{km} = 2(0.04)\sqrt{(6 \times 10^6)0.15} = 75.9 \text{ N s/m}.$$

In a Nutshell
The peak picking strategy is a method of curve-fitting. We have a measured FRF and we are trying to choose model parameters for a single degree of freedom system that has a FRF like the one we measured. There are many curve fitting methods, but the peak picking method uses three easily-identifiable points on the real and imaginary parts of the FRF. This is one reason to choose the real/imaginary FRF representation.

The spring-mass-damper model is shown in Fig. 3.25. Let's now use our model to predict the vibration magnitude if a harmonic force, $f(t) = 1000e^{i\omega_n t}$ N, is applied at the measurement point in the measurement direction. Note that the excitation frequency is equal to the system natural frequency, $\omega_n = 2\pi f_n = 6278$ rad/s. For this resonant condition, the vibration magnitude is:

$$|X| = \frac{F}{2k\zeta} = \frac{1000}{2(6 \times 10^6)0.04} = 2.1 \times 10^{-3} \text{ m} = 2.1 \text{ mm}.$$

If this vibration magnitude is too large, we could attempt to reduce it by:

- increasing the damping

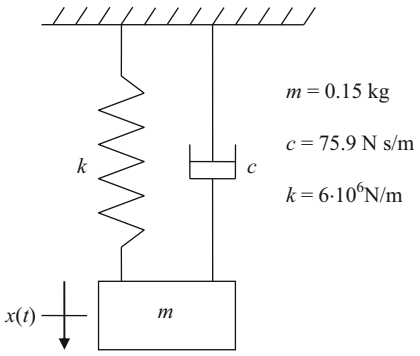

Fig. 3.25 Spring-mass-damper model identified from a measured FRF (Figs. 3.23 and 3.24) using the peak picking approach

- increasing the stiffness—this will serve to not only decrease the magnitude for any forcing function, but will also increase the natural frequency so that the existing force will no longer excite the structure at resonance. If the increase in stiffness is Δk, the new natural frequency will be $\omega_n = \sqrt{\frac{k+\Delta k}{m}}$.

3.5 Rotating Unbalance

A special case of forced vibration is **rotating unbalance**. This occurs when a rotating structure does not possess perfect symmetry in its mass distribution. Common examples include:

- electric motors
- turbines
- automobile wheels
- washing machines.

For the final example, you may have witnessed a washing machine "walk across the floor" during the spin cycle due to an uneven distribution of the wet (heavy) clothes in the drum. To describe this behavior in terms of forced vibration, consider the system shown in Fig. 3.26. An unbalanced mass, m, with an eccentricity (the distance of the unbalanced mass from the center of rotation), e, rotates with an angular speed, ω. The vertical displacement of the mass in Fig. 3.26 is:

$$x + esin(\omega t),$$

where x is the motion of the support structure with a mass of $M - m$. (The total system mass is the sum of the support structure and unbalanced mass, $M - m + m = M$.) The free body diagram for the system is shown in Fig. 3.27. Unlike our previous free body diagrams, this one includes two inertial forces; one for the support structure, $f = (M - m)\ddot{x}$, and one for the rotating unbalanced mass, $f = m\frac{d}{dt^2}(x + esin(\omega t))$. Calculating the derivative gives:

$$f = m\left(\ddot{x} - e\omega^2 \, sin\,(\omega t)\right).$$

Summing the forces to zero in the x direction, $\sum f_x = 0$, gives the equation of motion.

$$(M - m)\ddot{x} + m\left(\ddot{x} - e\omega^2 \, sin\,(\omega t)\right) + c\dot{x} + kx = 0$$

Simplifying and rewriting this equation yields:

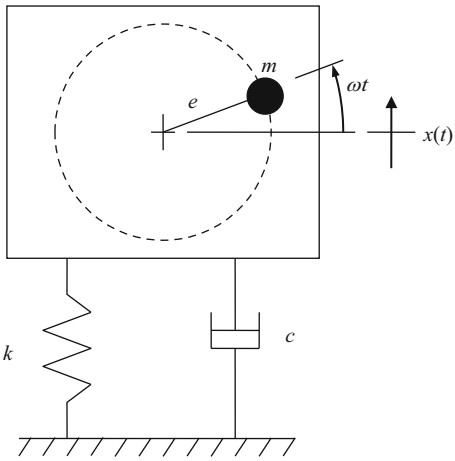

Fig. 3.26 Single degree of freedom model with rotating unbalance

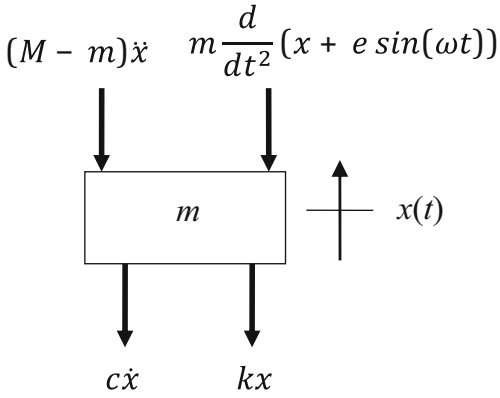

Fig. 3.27 Free body diagram for the rotating unbalance model in Fig. 3.26

$$M\ddot{x} + c\dot{x} + kx = me\omega^2 \sin(\omega t), \tag{3.24}$$

where the right hand side of this equation is a harmonic forcing function with the frequency-dependent magnitude $me\omega^2$. The force amplitude naturally increases with increasing unbalanced mass and eccentricity, but also grows with the square of the rotating frequency.

The magnitude and phase of the corresponding frequency-domain vibration are:

$$|X| = \frac{me\omega^2}{\sqrt{(k - M\omega^2)^2 + (c\omega)^2}} \tag{3.25}$$

and

$$\phi = tan^{-1}\left(\frac{c\omega}{k - M\omega^2}\right). \tag{3.26}$$

As before, we can rewrite these equations to be functions of r and ζ. Here, r is the ratio of the unbalanced mass rotating speed to the natural frequency, $\omega_n = \sqrt{\frac{k}{M}}$. Also, the damping ratio is $\zeta = \frac{c}{2\sqrt{kM}}$. See Eqs. 3.27 and 3.28.

$$|X| = \frac{\frac{m}{M}er^2}{\sqrt{(1 - r^2)^2 + (2\zeta r)^2}} \tag{3.27}$$

$$\phi = tan^{-1}\left(\frac{2\zeta r}{1 - r^2}\right) \tag{3.28}$$

A non-dimensionalized magnitude plot is provided in Fig. 3.28. The vertical axis of $\frac{MX}{me}$ was obtained by moving M, m, and e from the numerator of the right hand side to the left hand side in Eq. 3.27. Responses are provided for $\zeta = 0.01$, 0.05, and 0.1.

In some cases we wish to maintain a vibration magnitude below a certain level to avoid damage to the system, such as bearing damage for a rotating shaft; see Fig. 3.29. In this case, we may need to select a range of acceptable rotating speeds so that this maximum vibration magnitude is not exceeded. In Fig. 3.30, the acceptable rotating speed ranges are $\omega < \omega_1$ and $\omega > \omega_2$. The problem with the second range is that the speed must pass through resonance ($\omega = \omega_n$) in order reach ω_2. This would only be an acceptable alternative if short-term, large vibration magnitudes will not harm the system.

In a Nutshell

Designers of rotating systems use Eq. 3.27. In some instances (such as a jet engine), the rotational speed often changes and the designers attempt to place the natural frequency of the system far above the rotational frequency of the shaft. In this case, the system never operates at resonance. In other situations (like a turbine in a power plant), the rotational speed is held constant over long periods of time (on the order of months). In this case, designers often place the operating speed far above the resonance, so that the vibration amplitude is as small as possible during operation. During start-up, the forcing frequency passes through resonance, but this happens quickly and not very often.

[4]This tether/payload geometry is referred to as a floating element structure in microelectromechanical systems (MEMS) design and has been used for shear stress measurement [3].

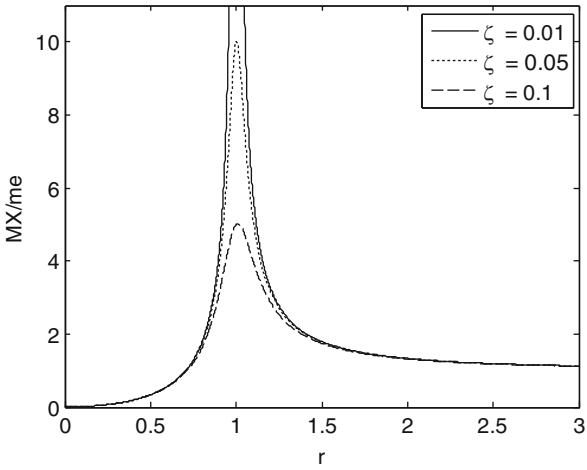

Fig. 3.28 Rotating unbalance frequency-domain vibration response for $\zeta = 0.01$, 0.05, and 0.1

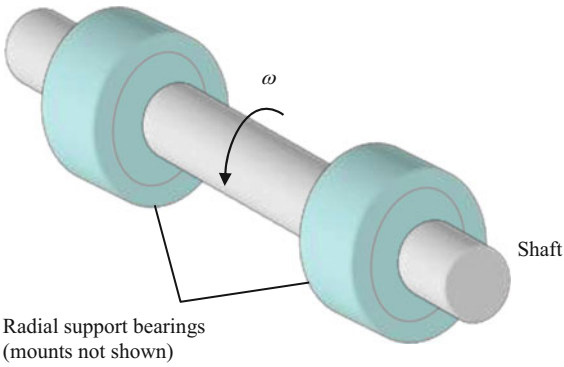

Fig. 3.29 A rotating shaft supported by bearing. Large magnitude rotating unbalance could damage the bearings

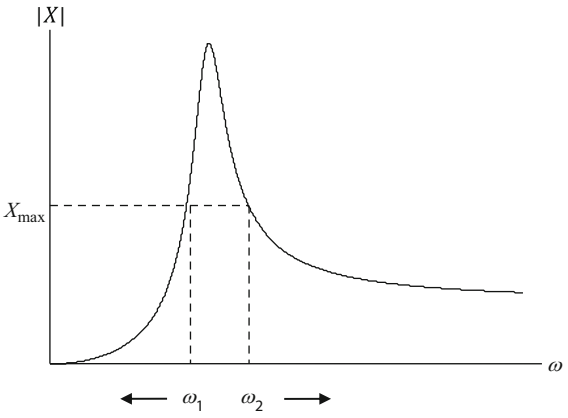

Fig. 3.30 Acceptable speed ranges for a maximum allowable vibration magnitude

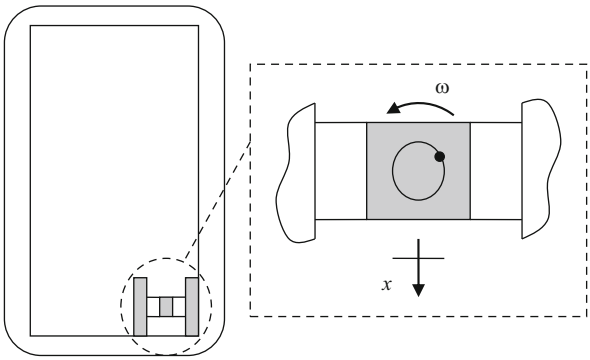

Fig. 3.31 *By the Numbers 3.3*—Unbalanced mass used to produce a cell phone's "silent ring"

By the Numbers 3.3

Let's consider an example. On cell phones, the "silent ring" can be produced using an eccentric mass to provide a force and vibration due to the rotating imbalance. Figure 3.31 shows a small motor with an unbalanced mass supported by four flexible tethers for illustration purposes.[4] The parallel pairs of tethers produce a flexure mechanism that is flexible in the x (vertical) direction, but stiff in the orthogonal (horizontal) direction [4]. For this device, the rotating speed was varied and the following results were obtained.

1. The maximum magnitude of vibration, X, was 1.0 mm.
2. For high frequencies, the magnitude asymptotically approached 0.02 mm = 20 μm (about one-fifth of a human hair's diameter).

Using this information, let's estimate the damping ratio, ζ, for the system. First, we can use the magnitude equation, Eq. 3.27, substitute $r = 1$ for resonance and set the right hand side equal to 1.0 mm.

$$|X| = \frac{\frac{m}{M}e(1)^2}{\sqrt{\left(1-(1)^2\right)^2 + (2\zeta(1))^2}} = \frac{\frac{m}{M}e}{2\zeta} = 1.0 \text{ mm} \tag{3.29}$$

Second, can let $r \to \infty$ in Eq. 3.27 and set the right hand side equal to 0.02 mm.

$$|X| = \frac{\frac{m}{M}e(\infty)^2}{\sqrt{\left(1-(\infty)^2\right)^2 + (2\zeta(\infty))^2}} = \frac{\frac{m}{M}e(\infty)^2}{(\infty)^2} = \frac{m}{M}e = 0.02 \text{ mm} \tag{3.30}$$

Substituting $\frac{m}{M}e = 0.02$ mm from Eq. 3.30 into Eq. 3.29 yields:

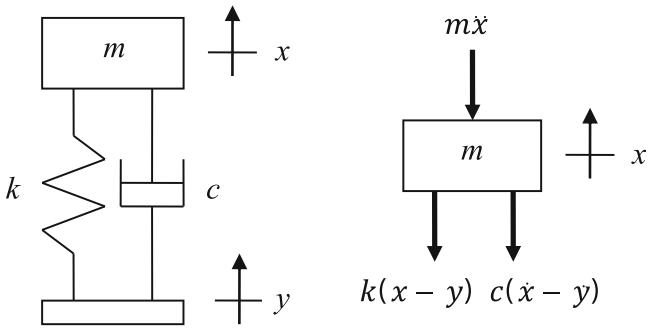

Fig. 3.32 Base motion for a single degree of freedom spring-mass-damper

$$|X| = \frac{0.02}{2\zeta} = 1.0 \text{ mm}. \tag{3.31}$$

Solving for the damping ratio gives $\zeta = 0.01 = 1\%$.

3.6 Base Motion

Base motion is observed when a system (for example, an automobile engine) is excited through elastic supports (such as the engine mounts that connect the engine to the automobile frame). Another example is the motion of an automobile's chassis in response to a wavy road surface.

Let's consider Fig. 3.32, where the motion, $x(t)$, of a single degree of freedom spring-mass-damper system is excited by motion of the structure's base, $y(t)$. The free body diagram for the mass, which is also included in Fig. 3.32, gives the equation of motion:

$$m\ddot{x} + c(\dot{x} - \dot{y}) + k(x - y) = 0. \tag{3.32}$$

We can rewrite Eq. 3.32 to isolate the response (x) terms on the left and the input (y) terms on the right.

$$m\ddot{x} + c\dot{x} + kx = c\dot{y} + ky \tag{3.33}$$

For harmonic base motion, $y(t) = Ye^{i\omega t}$, the response is also harmonic, $x(t) = Xe^{i\omega t}$. Calculating the derivatives of these expressions and substituting in Eq. 3.33 gives:

$$\left(-m\omega^2 + ic\omega + k\right)Xe^{i\omega t} = (ic\omega + k)Ye^{i\omega t}. \tag{3.34}$$

We can now calculate the ratio of the response, X, to the base motion input, Y.

$$\frac{X}{Y} = \frac{ic\omega + k}{-m\omega^2 + ic\omega + k} \tag{3.35}$$

Let's rewrite this equation in the r and ζ notation we've used previously.

$$\frac{X}{Y} = \frac{(k) + i(c\omega)}{(k - m\omega^2) + i(c\omega)} = \frac{\left(\frac{k}{m}\right) + i\left(\frac{c}{m}\omega\right)}{\left(\frac{k}{m} - \omega^2\right) + i\left(\frac{c}{m}\omega\right)} = \frac{\left(\omega_n^2\right) + i(2\zeta\omega_n\omega)}{\left(\omega_n^2 - \omega^2\right) + i(2\zeta\omega_n\omega)} \tag{3.36}$$

Dividing the numerator and denominator by ω_n^2, we obtain:

$$\frac{X}{Y} = \frac{(1) + i\left(2\zeta\frac{\omega}{\omega_n}\right)}{\left(1 - \frac{\omega^2}{\omega_n^2}\right) + i\left(2\zeta\frac{\omega}{\omega_n}\right)} = \frac{1 + i(2\zeta r)}{(1 - r^2) + i(2\zeta r)}. \tag{3.37}$$

We can now rationalize Eq. 3.37.

$$\frac{X}{Y} = \frac{1 + i(2\zeta r)}{(1 - r^2) + i(2\zeta r)} \cdot \frac{(1 - r^2) - i(2\zeta r)}{(1 - r^2) - i(2\zeta r)} = \frac{1 + \left(4\zeta^2 - 1\right)r^2 - i(2\zeta r^3)}{(1 - r^2)^2 + (2\zeta r)^2} \tag{3.38}$$

The real part of Eq. 3.38 is:

$$Re\left(\frac{X}{Y}\right) = \frac{1 + \left(4\zeta^2 - 1\right)r^2}{(1 - r^2)^2 + (2\zeta r)^2}. \tag{3.39}$$

The imaginary part is:

$$Im\left(\frac{X}{Y}\right) = \frac{-2\zeta r^3}{(1 - r^2)^2 + (2\zeta r)^2}. \tag{3.40}$$

The magnitude, which is referred to as the **displacement transmissibility**, is the square root of the sum of the squares of the real and imaginary parts. The displacement transmissibility describes the transfer of the base motion to the mass motion. In many instances, we wish this transmissibility to be low so that the base motion is only weakly transmitted to the degree of freedom of interest.

$$\left|\frac{X}{Y}\right| = \left(\frac{\left(1 + \left(4\zeta^2 - 1\right)r^2\right)^2 + \left(-2\zeta r^3\right)^2}{\left((1 - r^2)^2 + (2\zeta r)^2\right)^2}\right)^{\frac{1}{2}} \tag{3.41}$$

The corresponding phase lag of the mass motion with respect to the base motion is:

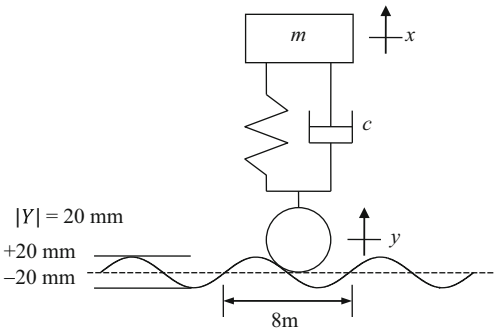

Fig. 3.33 *By the Numbers 3.4*—Base motion example for automobile suspension (not to scale)

$$\phi = tan^{-1}\left(\frac{Im}{Re}\right) = tan^{-1}\left(\frac{-2\zeta r^3}{1+\left(4\zeta^2-1\right)r^2}\right). \tag{3.42}$$

By the Numbers 3.4

The suspension for an automobile can be modeled as a single degree of freedom spring-mass-damper as shown in Fig. 3.32 with a natural frequency of 3 Hz and a damping ratio of 0.5. The natural frequency is based on the combination of the car's mass and the suspension spring's stiffness. The damping comes primarily from the shock absorber. If $y(t)$ represents the motion of the wheel center as it follows the oscillating road surface depicted in Fig. 3.33, determine the magnitude of the automobile's motion, X, when the car is traveling at 60 miles per hour.

The first step in the solution is to determine the forcing frequency, f (in Hz), due to the automobile's motion across the wavy road. The car's speed, v, is:

$$v = 60\frac{miles}{hr}\cdot\frac{1}{3600}\frac{hr}{s}\cdot 5280\frac{ft}{mile}\cdot 12\frac{in}{ft}\cdot 0.0254\frac{m}{in} = 26.8\frac{m}{s}.$$

The forcing frequency is the speed divided by the spatial wavelength of the road's surface:

$$f = \frac{26.8}{8} = 3.35 \text{ Hz}.$$

The frequency ratio is therefore $r = \frac{f}{f_n} = \frac{3.35}{3} = 1.12$. We determine $|X|$ using Eq. 3.41, where $\zeta = 0.5$. A plot of $|X|$ versus r is provided in Fig. 3.34; the operating point is identified by a circle. The code used to produce Fig. 3.34 is provided in MATLAB® MOJO 3.4.

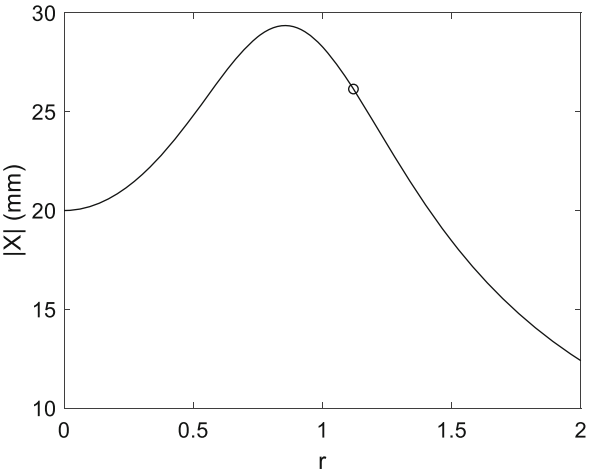

Fig. 3.34 *By the Numbers 3.4*—automobile response, X, to the wavy road input

$$|X| = 20\left(\frac{\left(1+\left(4(0.5)^2-1\right)1.12^2\right)^2+\left(-2(0.5)1.12^3\right)^2}{\left(\left(1-1.12^2\right)^2+\left(2(0.5)1.12\right)^2\right)^2}\right)^{\frac{1}{2}} = 26.1 \text{ mm}$$

We see that the 20 mm road excitation is transmitted as a 26.1 mm magnitude oscillation of the automobile. This amplification occurs because the forcing frequency is near the suspension's natural frequency. At much lower or higher speeds, the vibration level would be less.

MATLAB® MOJO 3.4

```
% matlab_mojo_3_4.m

clear
close all
clc

% Define model dynamics
fn = 3;            % Hz
zeta = 0.5;
Y_mag = 20;          % mm

r = 0:0.001:2;

Re = (1 + (4*zeta^2 - 1)*r.^2)./((1 - r.^2).^2 + (2*zeta*r).^2);
Im = -(2*zeta*r.^3)./((1 - r.^2).^2 + (2*zeta*r).^2);

X_mag = Y_mag*(Re.^2 + Im.^2).^0.5;

figure(1)
plot(r, X_mag, 'k')
```

```
set(gca,'FontSize', 14)
xlabel('r')
ylabel('|X| (mm)')
hold on

index = find(r == 1.12);
plot(r(index), X_mag(index), 'ko')
```

In a Nutshell
"Rumble strips" on a roadway are designed with a spacing that causes large motion of the car body when the car passes over the bumps. One way to minimize the vibration inside the car would be to drive over the rumble strips at a high rate of speed (moving the excitation frequency far above resonance). We do not recommend experimental verification, however.

3.7 Impulse Response

When describing the equation of motion for a single degree of freedom lumped parameter system under forced vibration in Sect. 3.1, we assumed a harmonic force input of the form $f(t) = Fe^{i\omega t}$, where ω is the forcing frequency. This enabled us to define the corresponding FRF and explore its behavior. However, we recognize that not all forces are best described as a harmonic function at a single frequency. In a given situation, the force may be composed of multiple frequencies (e.g., an earthquake), it may be random (i.e., follows an erratic pattern that must be described statistically), or it may be transient. A common transient example is the impulsive force. In Chap. 7, we will explore the use of an impact hammer to excite a structure in order to measure its FRF. Because this is an important measurement technique, let's determine the response of our spring-mass-damper model from Fig. 3.1 to an impulsive input. This input can be defined as:

$$f(t) = \begin{cases} 0, t \leq 0 \\ F, 0 < t < \Delta t \\ 0, t \geq \Delta t \end{cases} \tag{3.43}$$

and is depicted in Fig. 3.35. We see that it has a constant value, F, over the short time interval from 0 to Δt. The solution to the equation of motion, $m\ddot{x} + c\dot{x} + kx = f(t)$, is based on Newton's second law, which tells us that the **impulse** of the force is equal to the change in momentum of the system that it excites. We define the impulse of the force as the area under the force curve; this area is $F\Delta t$ for the function defined in Eq. 3.43, but may be generically described as the product of the average force value and the time interval over which the force is applied (provided the time interval is

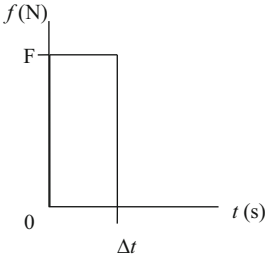

Fig. 3.35 Graphical impulse description

small). If we assume zero initial conditions for the system in Fig. 3.1, its change in momentum is mv_0, where v_0 is the velocity of the mass due to the force application and the initial displacement is still zero. Therefore, $F\Delta t = mv_0$. This is an interesting observation because it enables us to treat this problem as a case of free vibration with a nonzero initial velocity, $v_0 = \frac{F\Delta t}{m}$, and a zero initial displacement.

We have already considered the solution of free vibration for underdamped systems using initial conditions in Sect. 2.4.5. One form for the general response is $x(t) = Xe^{-\zeta\omega_n t}\, sin\left(\sqrt{1-\zeta^2}\omega_n t + \phi\right)$, where:

$$X = \frac{\sqrt{(\dot{x}_0 + \zeta\omega_n x_0)^2 + \left(x_0\sqrt{1-\zeta^2}\omega_n\right)^2}}{\sqrt{1-\zeta^2}\omega_n} \text{ and } \varphi$$
$$= tan^{-1}\left(\frac{x_0\sqrt{1-\zeta^2}\omega_n}{\dot{x}_0 + \zeta\omega_n x_0}\right). \tag{3.44}$$

In a Nutshell
Equation 3.44 is the solution for free vibration of an underdamped single degree of freedom system in terms of the initial conditions. If we have a single degree of freedom system problem and the system is underdamped, then we can use this equation directly to write the resulting motion as a function of time if the initial conditions are known.

For the impulse response, $x_0 = 0$ and $\dot{x}_0 = v_0$, so Eq. 3.44 simplifies to:

$$X = \frac{v_0}{\sqrt{1-\zeta^2}\omega_n} \text{ and } \varphi = 0. \tag{3.45}$$

The system response to the impulse is therefore:

$$x(t) = \frac{v_0}{\sqrt{1-\zeta^2}\omega_n} e^{-\zeta\omega_n t} \sin\left(\sqrt{1-\zeta^2}\omega_n t\right). \tag{3.46}$$

Substituting $v_0 = \frac{F\Delta t}{m}$ gives:

$$x(t) = \frac{F\Delta t}{m\sqrt{1-\zeta^2}\omega_n} e^{-\zeta\omega_n t} \sin\left(\sqrt{1-\zeta^2}\omega_n t\right). \tag{3.47}$$

We can rewrite this equation as $x(t) = F\Delta t \cdot h(t)$, where:

$$h(t) = \frac{1}{m\sqrt{1-\zeta^2}\omega_n} e^{-\zeta\omega_n t} \sin\left(\sqrt{1-\zeta^2}\omega_n t\right) \tag{3.48}$$

is the **impulse response function** for our underdamped spring-mass-damper system.

By the Numbers 3.5

Let's consider the system shown in Fig. 3.1, but now with the Eq. 3.43 force applied to the mass. Let's select a natural frequency of 500 Hz, a damping ratio of 0.05, and a stiffness of 1×10^6 N/m. The mass is, therefore, $m = \frac{k}{(2\pi f_n)^2} = \frac{1\times10^6}{(2\pi\cdot500)^2} = 0.1$ kg. Also, $F = 100$ N and $\Delta t = 1 \times 10^{-3}$ s. Substituting in Eq. 3.47 yields:

$$x(t) = \frac{100\left(1\times10^{-3}\right)}{0.1\sqrt{1-0.05^2}(500\cdot2\pi)} e^{-0.05(500\cdot2\pi)t} \sin\left(\sqrt{1-0.05^2}(500\cdot2\pi)t\right).$$

The vibration response to the impulsive input is displayed in Fig. 3.36. We see that:

- the initial displacement is zero

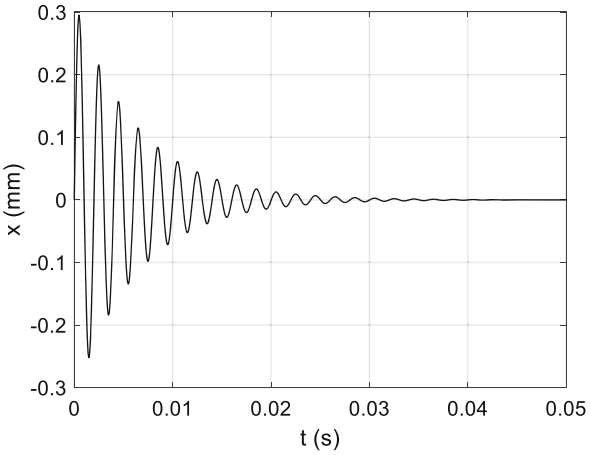

Fig. 3.36 *By the Numbers 3.5*—impulse response for spring-mass-damper system

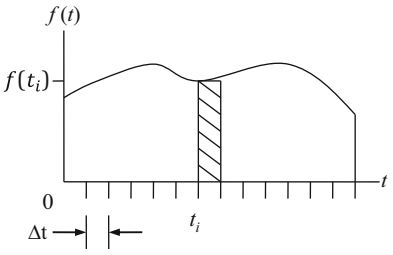

Fig. 3.37 Representation of a general force as a series of impulsive forces

- the force causes a rapid departure from the equilibrium position to a maximum value of 0.295 mm at $t = 4.85 \times 10^{-4}$ s
- the oscillating response exponentially decays to zero over time with a frequency of 500 Hz.

We will explore this further in Sect. 7.4.

We can also use the impulse response function to determine the vibration response for our underdamped single degree of freedom system with zero initial conditions due to a general, nonperiodic input force. If we consider the forcing function shown in Fig. 3.37, we see that it is possible to approximate this profile as n separate impulsive forces. In this case, the force is not applied only at $t = 0$. Rather, it also appears at $t = t_i$, where $i = 1...n$ is the impulse index. The impulse response function can now be written as:

$$h(t - t_i) = \frac{1}{m\sqrt{1 - \zeta^2}\omega_n} e^{-\zeta\omega_n(t-t_i)} \sin\left(\sqrt{1 - \zeta^2}\omega_n(t - t_i)\right) \tag{3.49}$$

and the response to $f(t_i)$ is $x(t_i) = f(t_i)\Delta t \cdot h(t - t_i)$, where Δt is the total time divided by n. The final response for the linear system is simply the sum of all the responses $x(t_i)$. As $\Delta t \to 0$, this sum can be expressed as the **convolution integral**:

$$x(t) = \int_0^t f(\tau)h(t - \tau)d\tau. \tag{3.50}$$

Substitution of Eq. 3.49 into Eq. 3.50 gives:

$$x(t) = \frac{1}{m\sqrt{1 - \zeta^2}\omega_n} e^{-\zeta\omega_n t} \int_0^t f(\tau)e^{\zeta\omega_n\tau} \sin\left(\sqrt{1 - \zeta^2}\omega_n(t - \tau)\right)d\tau. \tag{3.51}$$

Chapter Summary

- The frequency response function relates the harmonic force applied to a system to the resulting vibration as a function of the forcing frequency, ω.

- The largest value of a system's frequency response function occurs at resonance, when the system is forced at its natural frequency ($\omega = \omega_n$).
- The complex-valued frequency response function can be written as its real and imaginary parts or its magnitude and phase.
- A high Q system has low damping and vice versa.
- The dynamic flexibility, or compliance, of a system depends on the excitation frequency.
- A peak picking approach can be applied to a measured frequency response function in order to identify a model that represents the dynamic behavior of the measured system.
- A special case of forced vibration is rotating unbalance, where the force magnitude depends on the unbalanced mass, its eccentricity, and the rotating frequency.
- Base motion is observed when a system is excited through elastic supports.
- As an alternative to a single-frequency harmonic force model, the force may be described as being composed of multiple frequencies, random, or transient.
- An example of a transient force is the impulsive force.
- The impulse response function can be used to identify the behavior of a system due to an impulsive force input.
- The convolution integral can be used to determine the response of a system with zero initial conditions due to a general, nonperiodic input force.

Exercises

1. An apparatus known as a centrifuge is commonly used to separate solutions of different chemical compositions. It operates by rotating at high speeds to separate substances of different densities.

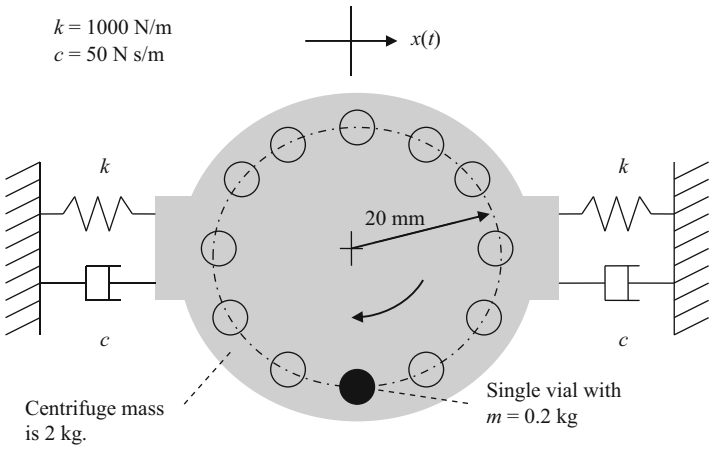

Fig. P3.1 Centrifuge model with a single vial

(a) If a single vial with a mass of 0.2 kg is placed in the centrifuge (see Fig. P3.1) at a distance of 20 mm from the rotating axis, determine the magnitude of the resulting vibration, X (in mm), of the single degree of freedom centrifuge structure. The rotating speed is 200 rpm.
(b) Determine the magnitude of the forcing function (in N) due to the single 0.2 kg vial rotating at 200 rpm.

2. For a single degree of freedom spring-mass-damper system with $m = 2.5$ kg, $k = 6 \times 10^6$ N/m, and $c = 180$ N s/m, complete the following for the case of forced harmonic vibration.

(a) Calculate the undamped natural frequency (in rad/s) and damping ratio.
(b) Sketch the imaginary part of the system FRF versus frequency. Identify the frequency (in Hz) and amplitude (in m/N) of the key features.
(c) Determine the value of the imaginary part of the vibration (in mm) for this system at a forcing frequency of 1500 rad/s if the harmonic force magnitude is 250 N.

3. A single degree of freedom lumped parameter system has mass, stiffness, and damping values of 1.2 kg, 1×10^7 N/m, and 364.4 N s/m, respectively. Generate the following plots of the frequency response function:

(a) magnitude (m/N) vs. frequency (Hz) and phase (°) vs. frequency (Hz)
(b) real part (m/N) vs. frequency (Hz) and imaginary part (m/N) vs. frequency (Hz)
(c) Argand diagram, real part (m/N) vs. imaginary part (m/N).

4. For the single degree of freedom torsional system under harmonic forced vibration (see Fig. P3.4), complete parts (a) through (c) if $J = 40$ kg m^2/rad, $C = 150$ N m s/rad, $K = 5 \times 10^5$ N m/rad, and $T_0 = 65$ N m.

(a) Calculate the undamped natural frequency (rad/s) and damping ratio.
(b) Sketch the Argand diagram (complex plane representation) of $\frac{\theta}{T}(\omega)$. Numerically identify key frequencies (rad/s) and amplitudes (rad/N m).

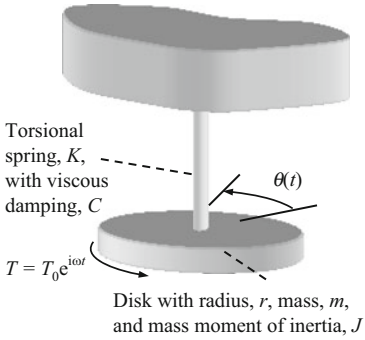

Fig. P3.4 Single degree of freedom torsional system under harmonic forced vibration

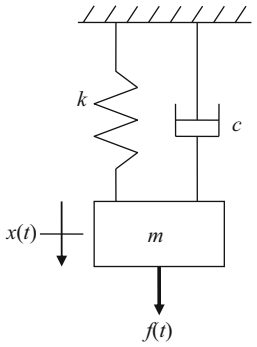

Fig. P3.6 Spring-mass-damper system excited by an impulsive force

(c) Given a forcing frequency of 100 rad/s for the harmonic external torque, determine the phase (in rad) between the torque and corresponding steady-state vibration of the system, θ.

5. For a single degree of freedom spring-mass-damper system subject to forced harmonic vibration with $m = 1$ kg, $k = 1 \times 10^6$ N/m, and $c = 120$ N s/m, complete the following.

   (a) Calculate the damping ratio.
   (b) Write expressions for the real part, imaginary part, magnitude, and phase of the system frequency response function (FRF). These expressions should be written as a function of the frequency ratio, r, stiffness, k, and damping ratio, ζ.
   (c) Plot the real part (in m/N), imaginary part (in m/N), magnitude (in m/N), and phase (in °) of the system frequency response function (FRF) as a function of the frequency ratio, r. Use a range of 0–2 for r (note that $r = 1$ is the resonant frequency). [Hint: for the phase plot, try using the MATLAB® `atan2` function. It considers the quadrant dependence of the $\tan^{-1}$ function.]

6. A single degree of freedom spring-mass-damper system which is initially at rest at its equilibrium position is excited by an impulsive force over a time interval of 1.5 ms; see Fig. P3.6. If the mass is 2 kg, the stiffness is 1×10^6 N/m, and the viscous damping coefficient is 10 N s/m, complete the following.

   (a) Determine the maximum allowable force magnitude if the maximum deflection is to be 1 mm.
   (b) Plot the impulse response function, $h(t)$, for this system. Use a time step size of 0.0001 s.
   (c) Calculate the impulse of the force (N s).

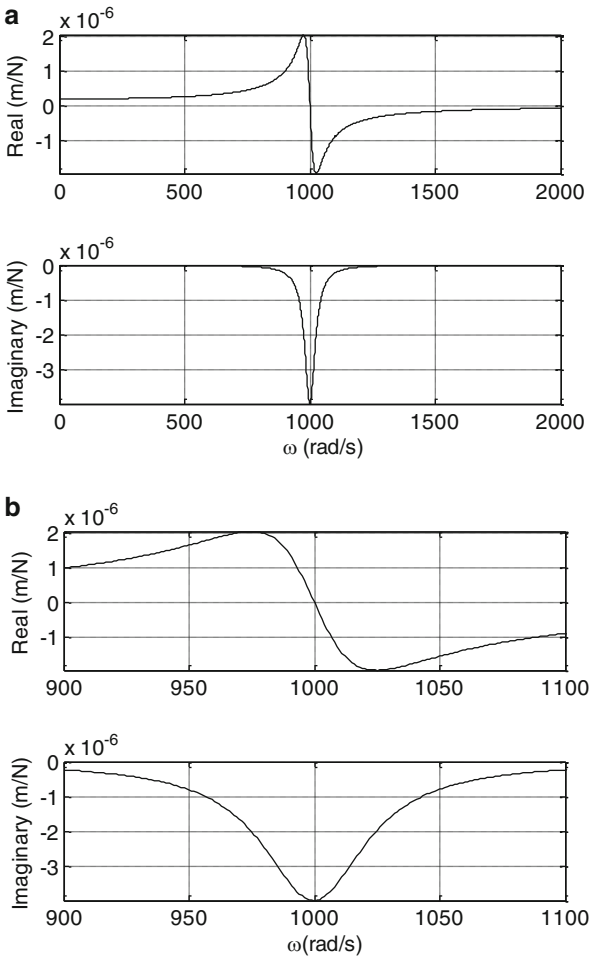

Fig. P3.7 (**a**) Measured FRF. (**b**) Measured FRF (smaller frequency scale)

7. For a single degree of freedom spring-mass-damper system subject to forced harmonic vibration, the following FRF was measured (two figures are provided with different frequency ranges). Using the "peak picking" fitting method, determine m (in kg), k (in N/m), and c (in N s/m) (Fig. P3.7).
8. For a single degree of freedom spring-mass-damper system with $m = 2$ kg, $k = 1 \times 10^7$ N/m, and $c = 200$ N s/m, complete the following for the case of forced harmonic vibration.

   (a) Calculate the natural frequency (in rad/s) and damping ratio.
   (b) Plot the Argand diagram (real part vs. imaginary part of the system FRF).
   (c) Identify the point on the Argand diagram that corresponds to resonance.

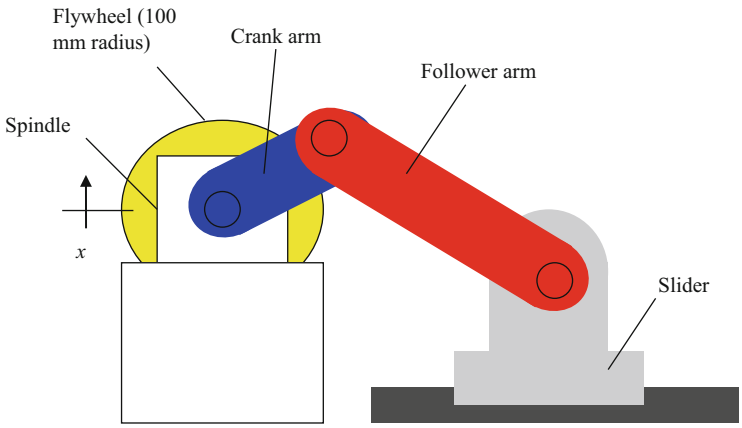

Fig. P3.9 Crank-slider with flywheel

(d) Determine the magnitude of vibration (in m) for this system at a forcing frequency of 2000 rad/s if the harmonic force magnitude is 100 N.

9. In a crank-slider setup, it is desired to maintain a constant rotational speed for driving the crank. Therefore, a flywheel was added to increase the spindle inertia and reduce the speed sensitivity to the driven load. See Fig. P3.9. If the spindle rotating speed is 120 rpm, determine the maximum allowable eccentricity-mass product, *me* (in kg-m), for the flywheel if the spindle vibration magnitude is to be less than 25 μm. The total spindle/flywheel mass is 10 kg, the effective spring stiffness (for the spindle and its support) is 1×10^6 N/m, and the corresponding damping ratio is 0.05 (5%).
   Given your *me* result, comment on the accuracy requirements for the flywheel manufacture (you may assume no rotating unbalance in the spindle).
10. A single degree of freedom spring-mass-damper system with $m = 1.2$ kg, $k = 1 \times 10^7$ N/m, and $c = 364.4$ N s/m is subjected to a forcing function $f(t) = 15e^{i\omega_n t}$ N, where ω_n is the system's natural frequency. Determine the steady-state magnitude (in μm) and phase (in °) of the vibration due to this harmonic force.

References

1. http://en.wikipedia.org/wiki/Slinky
2. Kamen E (1990) Introduction to signals and systems, 2nd edn. Macmillan Publishing Co., New York, NY
3. Xu Z, Naughton J, Lindberg W (2009) 2-D and 3-D numerical modelling of a dynamic resonant shear stress sensor. Comput Fluids 38:340–346
4. Smith S (2000) Flexures: elements of elastic mechanisms. CRC Press, Boca Raton, FL

Chapter 4
Two Degree of Freedom Free Vibration

Since we cannot know all that there is to be known about anything,
we ought to know a little about everything.
—Blaise Pascal

4.1 Equations of Motion

Let's extend our free vibration analysis from Chap. 2 to include two degrees of freedom in the model. This would make sense, for example, if we completed a measurement to determine the frequency response function (FRF) for a system and saw that there were obviously two modes of vibration within the frequency range of interest; see Fig. 4.1.

The two degree of freedom lumped parameter, chain-type model is shown in Fig. 4.2, where damping is neglected for now. The free body diagrams for the upper and lower masses give two equations of motion. Summing the forces in the x_1 direction for the top mass gives:

$$m_1\ddot{x}_1 + k_1x_1 - k_2(x_2 - x_1) = 0,$$

which can be rewritten (by grouping terms) to obtain:

$$m_1\ddot{x}_1 + (k_1 + k_2)x_1 - k_2x_2 = 0. \tag{4.1}$$

Similarly, for the bottom mass we have:

$$m_2\ddot{x}_2 + k_2(x_2 - x_1) = 0$$

or

$$m_2\ddot{x}_2 + k_2x_2 - k_2x_1 = 0. \tag{4.2}$$

T. L. Schmitz, K. S. Smith, *Mechanical Vibrations*,
https://doi.org/10.1007/978-3-030-52344-2_4

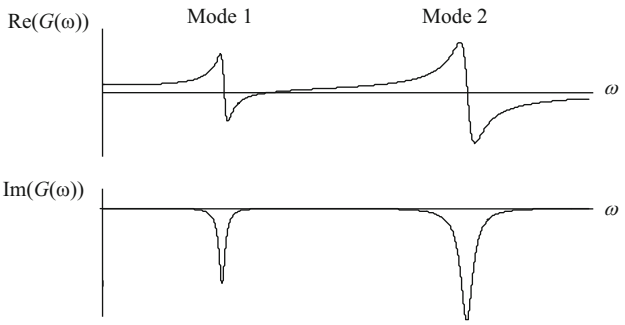

Fig. 4.1 Two mode FRF measurement that justifies a two degree of freedom model

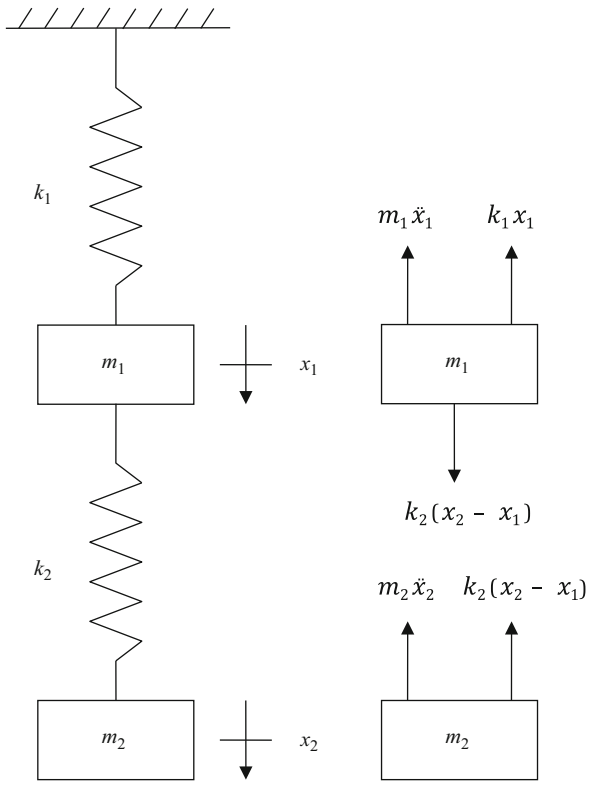

Fig. 4.2 Lumped parameter, chain-type model for an undamped two degree of freedom system

The force in the spring k_2 deserves further discussion. For the lower mass free body diagram in Fig. 4.2, the force is directed up (opposite the x_2 direction) and is written as $k_2(x_2 - x_1)$. This is because the motion of mass m_2 depends on the motion of mass m_1 and vice versa for the chain-type, lumped parameter model. If the position of m_1 was held fixed and m_2 was displaced down by x_2, then the force in the spring k_2 would oppose this motion and its value would be $k_2(x_2 - 0) = k_2x_2$.

However, if both m_1 and m_2 were displaced down by the same amount, Δx, the force in the spring would be $k_2(\Delta x - \Delta x) = 0$. An equal and opposite force is applied to the top mass.

In a Nutshell
It is often useful to consider the effect of the displacement (or velocity or acceleration) of one coordinate while holding the other coordinate (s) motionless.

4.2 Eigensolution for the Equations of Motion

Let's now organize Eqs. 4.1 and 4.2 into matrix form. Equation 4.3 includes two rows in the matrix expressions. The top row describes the behavior of the top coordinate and the bottom row describes the motion of the bottom coordinate. This equation can be more compactly written as shown in Eq. 4.4, where the mass matrix is $m = \begin{bmatrix} m_1 & 0 \\ 0 & m_2 \end{bmatrix}$, the acceleration vector is $\left\{\vec{\ddot{x}}\right\} = \begin{Bmatrix} \ddot{x}_1 \\ \ddot{x}_2 \end{Bmatrix}$, the stiffness matrix is $k = \begin{bmatrix} k_1 + k_2 & -k_2 \\ -k_2 & k_2 \end{bmatrix}$, and the displacement vector is $\left\{\vec{x}\right\} = \begin{Bmatrix} x_1 \\ x_2 \end{Bmatrix}$.

$$\begin{bmatrix} m_1 & 0 \\ 0 & m_2 \end{bmatrix} \begin{Bmatrix} \ddot{x}_1 \\ \ddot{x}_2 \end{Bmatrix} + \begin{bmatrix} k_1 + k_2 & -k_2 \\ -k_2 & k_2 \end{bmatrix} \begin{Bmatrix} x_1 \\ x_2 \end{Bmatrix} = \begin{Bmatrix} 0 \\ 0 \end{Bmatrix} \tag{4.3}$$

$$[m]\left\{\vec{\ddot{x}}\right\} + [k]\left\{\vec{x}\right\} = \{0\} \tag{4.4}$$

We will treat Eq. 4.4 as an **eigenvalue problem** to determine the:

1. **eigenvalues**, which lead to the system's natural frequencies; and
2. **eigenvectors**, or **mode shapes** which describe the characteristic relative motion of the individual degrees of freedom (typically normalized to one of the degrees of freedom). Each mode shape is associated with a particular natural frequency.

In a Nutshell
Eigenvalue problems are found in many areas of engineering. Such problems are called eigenvalue problems because the German word "eigen", which can be translated as "own", "characteristic", or "peculiar to", emphasizes that these values belong to the system model and do not depend on external perturbations [1]. Given the eigensolution, we can then use this information to determine the time-domain response of the system.

Let's begin by assuming harmonic vibration so that we can write a Laplace-domain ($s = i\omega$) form for the solution to the differential equations of motion. The displacement is $x(t) = Xe^{st}$ and the corresponding acceleration is $\ddot{x}(t) = s^2Xe^{st}$. Substitution into Eq. 4.4 gives:

$$[m]s^2\left\{\vec{X}\right\}e^{st} + [k]\left\{\vec{X}\right\}e^{st} = \left[[m]s^2 + [k]\right]\left\{\vec{X}\right\}e^{st} = \{0\}, \tag{4.5}$$

where $\left\{\vec{X}\right\} = \begin{Bmatrix} X_1 \\ X_2 \end{Bmatrix}$. There are two possibilities for satisfying Eq. 4.5. The first is that $\left\{\vec{X}\right\} = \{0\}$. This means that there is no motion and, while this is a valid result, it is not very useful to us. As in the single degree of freedom case, it is referred to as the **trivial solution**. The second possibility is that $[[m]s^2 + [k]] = \{0\}$ and it is the option that we will use to find the eigenvalues. In order for this equation to have non-trivial solutions, it is required that the determinant of the left hand side be equal to zero. This is shown in Eq. 4.6 and is referred to as the **characteristic equation**. The roots of this equation are the eigenvalues.

$$\left|[m]s^2 + [k]\right| = 0 \tag{4.6}$$

For the two degree of freedom model displayed in Fig. 4.2, the corresponding characteristic equation is:

$$\left|\begin{bmatrix} m_1 & 0 \\ 0 & m_2 \end{bmatrix}s^2 + \begin{bmatrix} k_1 + k_2 & -k_2 \\ -k_2 & k_2 \end{bmatrix}\right| = 0. \tag{4.7}$$

As we saw in Sect. 2.4.5, the determinant of a 2×2 matrix is the difference between the product of the on-diagonal terms and the product of the off-diagonal terms, i.e., $(1,1)(2,2) - (1,2)(2,1)$, where these indices identify the (row, column). Rewriting Eq. 4.7 in standard 2×2 form yields:

$$\begin{vmatrix} m_1s^2 + k_1 + k_2 & -k_2 \\ -k_2 & m_2s^2 + k_2 \end{vmatrix} = 0. \tag{4.8}$$

The characteristic equation (determinant) is:

$$\left(m_1s^2 + k_1 + k_2\right)\left(m_2s^2 + k_2\right) - (-k_2)(-k_2) = 0. \tag{4.9}$$

This gives an equation of the form $as^4 + bs^2 + c = 0$, which is quadratic in s^2. Using the quadratic equation, the two roots, s_1^2 and s_2^2, are given by $s_{1,2}^2 = \frac{-b \pm \sqrt{b^2 - 4ac}}{2a}$. These roots, or eigenvalues, are used to determine the system natural frequencies:

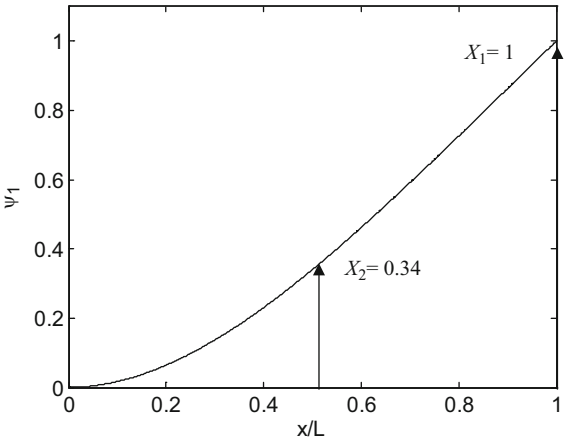

Fig. 4.3 First mode shape for a cantilever beam

$$s_1^2 = -\omega_{n1}^2 \text{ and } s_2^2 = -\omega_{n2}^2, \tag{4.10}$$

where $\omega_{n1} < \omega_{n2}$ by convention (in other words, the roots are ordered such that the first root gives the lowest natural frequency). Using the eigenvalues, we can next determine the eigenvectors, or mode shapes. These represent the relative magnitude and direction for the model's degrees of freedom (coordinates) during vibration.

In a Nutshell

We cannot solve for X_1 and X_2 in Eq. 4.5 once s_1^2 and s_2^2 have been determined. It might look like two equations with two unknowns, but it is not. The s^2 values were found by requiring the determinant to be equal to zero, which means that the two equations are not independent.

Suppose the model in Fig. 4.2 was used to describe the vibrating motion of a cantilever beam. As we discussed in Sect. 1.4, a continuous beam has an infinite number of degrees of freedom. However, in this case, let's assume it is adequate to describe the motion at two locations only: at the mid-point of the beam and at its free end. We'll let x_2 represent the mid-point and x_1 the tip. The first mode shape, ψ_1, for a cantilever beam is provided in Fig. 4.3. The vibration in this mode shape occurs at the first natural frequency, ω_{n1}. The relative magnitudes of vibration at x_1 and x_2 are also shown in Fig. 4.3. We see that the magnitude of vibration at the free end is larger than at the beam's mid-point by a ratio of approximately 1:0.34 for vibration at the first natural frequency, ω_{n1}.

The second mode shape, ψ_2, is displayed in Fig. 4.4. In this case, the motion at x_1 is again larger, but it is out of phase with the motion at x_2. The corresponding ratio is approximately 1:−0.71. Motion in this mode shape occurs at the second natural frequency, ω_{n2}. For the model in Fig. 4.2, we only have two coordinates and therefore wouldn't have any way of knowing the high resolution mode shapes

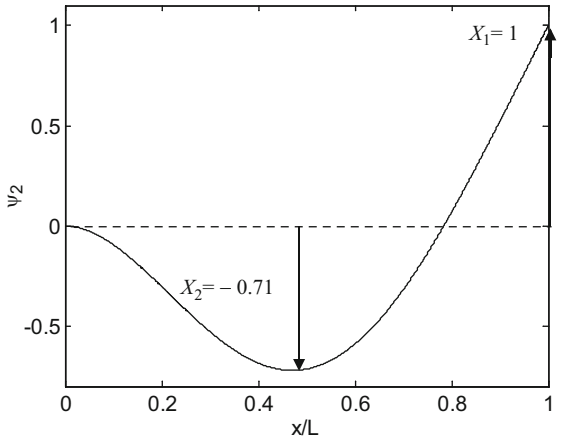

Fig. 4.4 Second mode shape for a cantilever beam

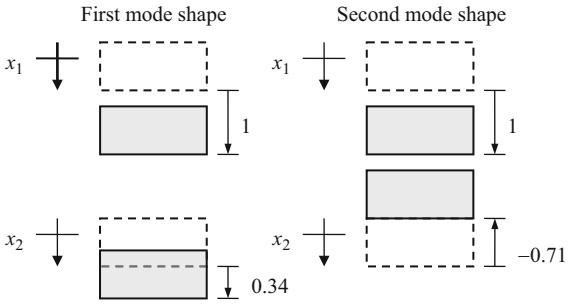

Fig. 4.5 Mode shapes for a two degree of freedom representation of a cantilever beam

given in Figs. 4.3 and 4.4. We can represent the two mode shapes for our two degree of freedom model as shown in Fig. 4.5. As with Figs. 4.3 and 4.4, we will normalize the motion at x_1 to 1 and plot the corresponding magnitude (and direction) for the motion at x_2. The choice to set the vibration magnitude at x_1 to 1 is for convenience; the mode shape only gives the relative motion between coordinates so the scaling is arbitrary. In some cases, it could make more sense to normalize to x_2. We will explore this issue in more detail as we move forward. From Fig. 4.5, we see that the motion at x_2 has a smaller magnitude (the ratio is 1:0.34), but the same direction, when vibrating at ω_{n1} in the first mode shape. For the second mode shape, the motion at x_2 is again smaller than at x_1 (the ratio is 1:−0.71), but now in the opposite direction. This matches the behavior we observed in Figs. 4.3 and 4.4. Note that we have two natural frequencies and mode shapes because our model has two degrees of freedom. For a three degree of freedom model, we'd have three natural frequencies and mode shapes.

Table 4.1 Constants for cantilever beam mode shape calculation in Eq. 4.11 [2]

Mode i	λ_i	σ_i
1	1.87510407	0.734095514
2	4.69409113	1.018467319

In a Nutshell
There are many ways to normalize mode shapes. They can be normalized to a position: scaling so that the mode shape component at a particular coordinate is 1. They may be length normalized: scaling so that the length of the vector is 1. Mode shapes can be scaled in any convenient way because they show relative motion between coordinates, but not the absolute size of motion.

The functions used to plot the mode shapes for beams with various **boundary conditions** (such as free-free, pinned-pinned, and fixed-free) have been tabulated by Blevins [2]. The cantilever, or fixed-free, mode shape function is:

$$\psi_i = \frac{1}{2}\left(cosh\left(\frac{\lambda_i x}{L}\right) - cos\left(\frac{\lambda_i x}{L}\right) - \sigma_i\left(sinh\left(\frac{\lambda_i x}{L}\right) - sin\left(\frac{\lambda_i x}{L}\right)\right)\right), \quad (4.11)$$

where i is the mode shape number, x is the distance along the beam of length L, and the constants λ_i and σ_i are provided in Table 4.1. The code used to produce Figs. 4.3 and 4.4 is provided in MATLAB® MOJO 4.1. Note that Eq. 4.11 is normalized to have a value of one at the free end of the cantilever.

MATLAB® MOJO 4.1

```
% matlab_mojo_4_1.m

clear
close all
clc

% Define variables
L = 1;          % m
x = 0:0.001:L;

% Define first mode shape
lambda = 1.87510407;
sigma = 0.734095514;
psi = (cosh(lambda*x/L) - cos(lambda*x/L) - sigma*(sinh(lambda*x/L) -
sin(lambda*x/L)))/2;

figure(1)
plot(x, psi, 'k-')
set(gca,'FontSize', 14)
axis([0 1 0 1.1])
```

```
xlabel('x/L')
ylabel('\psi_1')

index = find(x == 0.5);
psi(index)

% Define second mode shape
lambda = 4.69409113;
sigma = 1.018467319;
psi = -(cosh(lambda*x/L) - cos(lambda*x/L) - sigma*(sinh(lambda*x/L) -
sin(lambda*x/L)))/2;

figure(2)
plot(x, psi, 'k-')
set(gca,'FontSize', 14)
axis([0 1 -0.8 1.1])
xlabel('x/L')
ylabel('\psi_2')

index = find(x == 0.5);
psi(index)
```

In order to determine the eigenvalues of a system model, we set the determinant of the matrix form for the equations of motion equal to zero; see Eq. 4.6. This means that the two equations (one for each of the two degrees of freedom) are **linearly dependent**. We can think about linear dependence in the following way. If you were given directions from the grocery store to the library that said "go north three blocks and then go west four blocks", this would provide all the necessary information to reach the library. The two statements for the north and west travel cannot be described in terms of the other; they are linearly independent. However, if the directions were augmented to be "go north three blocks and then go west four blocks; the library is five blocks northwest of the grocery store", then the final statement is not independent of the first two. These three statements are linearly dependent because they give redundant information; one of the three is not required [3].

Because the two equations in Eq. 4.6 are linearly dependent, we can select either one to determine the two eigenvectors. They will both give the same result. For the two degree of freedom model in Fig. 4.2, we have:

$$\left[\begin{bmatrix} m_1 & 0 \\ 0 & m_2 \end{bmatrix} s^2 + \begin{bmatrix} k_1 + k_2 & -k_2 \\ -k_2 & k_2 \end{bmatrix}\right] \begin{Bmatrix} X_1 \\ X_2 \end{Bmatrix} = \begin{Bmatrix} 0 \\ 0 \end{Bmatrix}. \tag{4.12}$$

The top row equation, which corresponds to motion of the top mass, is:

$$\left(m_1 s^2 + k_1 + k_2\right) X_1 + (-k_2) X_2 = 0. \tag{4.13}$$

The bottom row equation, which corresponds to motion of the bottom mass, is:

$$(-k_2)X_1 + \left(m_2 s^2 + k_2\right)X_2 = 0. \tag{4.14}$$

We can pick either Eq. 4.13 or 4.14 to determine the two eigenvectors—one eigenvector for s_1^2 and one for s_2^2. We can also choose to normalize our eigenvectors to either coordinate x_1 or x_2. We generally select the coordinate that is of most interest for the particular application (such as the end of the cantilever beam as in the previous example). To normalize to x_1, we need the ratio $\frac{X_2}{X_1}$. Using Eq. 4.13, we have:

$$\frac{X_2}{X_1} = \frac{m_1 s^2 + k_1 + k_2}{k_2}. \tag{4.15}$$

The corresponding eigenvector expression is:

$$\psi_{1,2} = \begin{Bmatrix} \frac{X_1}{X_1} \\ \frac{X_2}{X_1} \end{Bmatrix} = \begin{Bmatrix} 1 \\ \frac{m_1 s_{1,2}^2 + k_1 + k_2}{k_2} \end{Bmatrix}, \tag{4.16}$$

where we substitute s_1^2 to find the first eigenvector, ψ_1, and s_2^2 to find the second eigenvector, ψ_2. As described previously, ψ_1 describes the relative magnitude of the coordinates for vibration at the first natural frequency and ψ_2 describes the relative magnitude of the coordinates for vibration at the second natural frequency. We would obtain exactly the same results using Eq. 4.14. In this case, the ratio is:

$$\frac{X_2}{X_1} = \frac{k_2}{m_2 s^2 + k_2}. \tag{4.17}$$

In order to normalize to x_2, the required ratio is $\frac{X_1}{X_2}$. Using Eq. 4.13, we find that:

$$\frac{X_1}{X_2} = \frac{k_2}{m_1 s^2 + k_1 + k_2}. \tag{4.18}$$

The eigenvector expression for normalization to x_2 is:

$$\psi_{1,2} = \begin{Bmatrix} \frac{X_1}{X_2} \\ \frac{X_2}{X_2} \end{Bmatrix} = \begin{Bmatrix} \frac{k_2}{m_1 s_{1,2}^2 + k_1 + k_2} \\ 1 \end{Bmatrix}. \tag{4.19}$$

Again, substituting s_1^2 gives the first eigenvector, ψ_1, and substituting s_2^2 gives the second eigenvector, ψ_2. We would obtain the same eigenvectors using Eq. 4.14, where the ratio is:

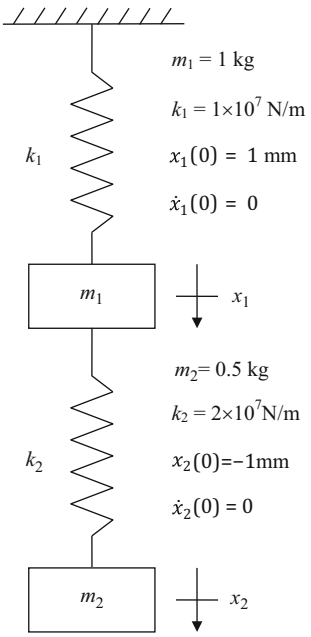

Fig. 4.6 *By the Numbers 4.1*—example two degree of freedom model with parameters and initial conditions

$$\frac{X_1}{X_2} = \frac{m_2 s^2 + k_2}{k_2}. \tag{4.20}$$

For a two degree of freedom system, there are two eigenvectors. The first corresponds to vibration at ω_{n1} and the second to vibration at ω_{n2}. The system vibration (due to some set of initial conditions) occurs in: (1) the first mode shape; (2) the second mode shape; or (3) a linear combination of the two. The latter is the general result, but the final behavior depends on the initial conditions.

In a Nutshell

We've seen that free vibration for a single degree of freedom system always occurs at the system natural frequency. In a two degree of freedom system, the motion may occur at the first natural frequency with the first mode shape, at the second natural frequency with the second mode shape, or in a linear combination of the two modes simultaneously, depending on the initial conditions. No other motions are possible in free vibration.

By the Numbers 4.1

Consider the two degree of freedom system shown in Fig. 4.6. This is the same model we used in Fig. 4.2, so we can write the equations of motion in matrix form directly.

$$\begin{bmatrix} 1 & 0 \\ 0 & 0.5 \end{bmatrix} \begin{Bmatrix} \ddot{x}_1 \\ \ddot{x}_2 \end{Bmatrix} + \begin{bmatrix} 1 \times 10^7 + 2 \times 10^7 & -2 \times 10^7 \\ -2 \times 10^7 & 2 \times 10^7 \end{bmatrix} \begin{Bmatrix} x_1 \\ x_2 \end{Bmatrix} = \begin{Bmatrix} 0 \\ 0 \end{Bmatrix}$$

We should note here that as long as the coordinates are measured with respect to ground, the mass and stiffness matrices are always **symmetric**. In other words, the off-diagonal terms are equal: $m(1,2) = m(2,1)$ and $k(1,2) = k(2,1)$. Alternately, we can write: $m_{12} = m_{21}$ and $k_{12} = k_{21}$ to denote the symmetry. Validating symmetry for the mass and stiffness matrices provides a good check for the equations of motion.

Using the Laplace notion for our (assumed) harmonic solution and substituting gives the characteristic equation:

$$\begin{vmatrix} 1s^2 + 3 \times 10^7 & -2 \times 10^7 \\ -2 \times 10^7 & 0.5s^2 + 2 \times 10^7 \end{vmatrix} = 0.$$

Calculating the determinant gives:

$$\left(1s^2 + 3 \times 10^7\right)\left(0.5s^2 + 2 \times 10^7\right) - \left(-2 \times 10^7\right)\left(-2 \times 10^7\right) = 0.$$

This equation can be expanded and grouped to obtain:

$$0.5s^4 + 3.5 \times 10^7 s^2 + 2 \times 10^{14} = 0.$$

Using the quadratic equation, the roots (eigenvalues) are:

$$\begin{aligned} s_{1,2}^2 &= \frac{-3.5 \times 10^7 \pm \sqrt{\left(3.5 \times 10^7\right)^2 - 4(0.5)2 \times 10^{14}}}{2(0.5)} \\ &= -3.5 \times 10^7 \pm 2.872 \times 10^7. \end{aligned}$$

This gives $s_1^2 = (-3.5 + 2.872) \times 10^7 = -6.28 \times 10^6 = -\omega_{n1}^2$ and the first natural frequency is $\omega_{n1} = 2506$ rad/s. The second eigenvalue is $s_2^2 = (-3.5 - 2.872) \times 10^7 = -6.37 \times 10^7 = -\omega_{n2}^2$ and the second natural frequency is $\omega_{n2} = 7981$ rad/s. Note that $\omega_{n1} < \omega_{n2}$. We can also express these natural frequencies in units of Hz: $f_{n1} = \frac{\omega_{n1}}{2\pi} = 398.8$ Hz and $f_{n2} = \frac{\omega_{n2}}{2\pi} = 1270$ Hz.

To determine the eigenvectors, let's arbitrarily choose the top equation of motion and normalize to coordinate x_2. The eigenvector equation is:

$$\left(1s^2 + 3 \times 10^7\right)X_1 + \left(-2 \times 10^7\right)X_2 = 0$$

and the required ratio is:

$$\frac{X_1}{X_2} = \frac{2 \times 10^7}{1s^2 + 3 \times 10^7}.$$

Substituting $s_1^2 = -6.28 \times 10^6$ gives:

$$\left.\frac{X_1}{X_2}\right|_{s_1^2} = \frac{X_{11}}{X_{21}} = \frac{2 \times 10^7}{1\left(-6.28 \times 10^6\right) + 3 \times 10^7} = 0.843,$$

where the first subscript in $\frac{X_{11}}{X_{21}}$ identifies the coordinate number and the second subscript gives the mode number. Because we normalized to coordinate x_2, the first eigenvector is therefore:

$$\psi_1 = \begin{Bmatrix} \frac{X_{11}}{X_{21}} \\ 1 \end{Bmatrix} = \begin{Bmatrix} 0.843 \\ 1 \end{Bmatrix}.$$

The ratio for the second eigenvector is calculated by substituting $s_2^2 = -6.37 \times 10^7$.

$$\left.\frac{X_1}{X_2}\right|_{s_2^2} = \frac{X_{12}}{X_{22}} = \frac{2 \times 10^7}{1\left(-6.37 \times 10^7\right) + 3 \times 10^7} = -0.593$$

The second eigenvector is:

$$\psi_2 = \begin{Bmatrix} \frac{X_{12}}{X_{22}} \\ 1 \end{Bmatrix} = \begin{Bmatrix} -0.593 \\ 1 \end{Bmatrix}.$$

These mode shapes are demonstrated graphically in Fig. 4.7. For the model type pictured in Fig. 4.6 with the eigenvalues ordered such that $\omega_{n1} < \omega_{n2}$, the vibration

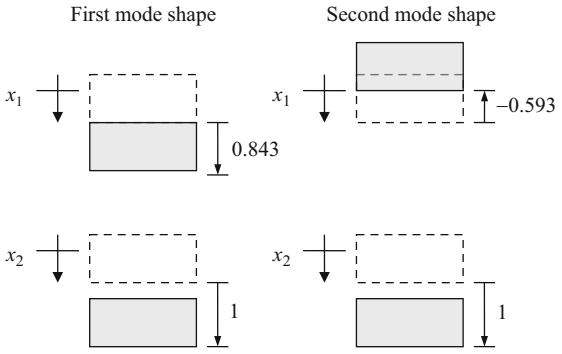

Fig. 4.7 *By the Numbers 4.1*—mode shapes for the example two degree of freedom system

of coordinates x_1 and x_2 are always in phase for the first mode shape and always out of phase for the second mode shape.

How would the mode shapes have changed if he had normalized to coordinate x_1? In this case, we require the ratio:

$$\frac{X_2}{X_1} = \frac{1s^2 + 3 \times 10^7}{2 \times 10^7}.$$

Using the first eigenvalue, $s_1^2 = -6.28 \times 10^6$, we obtain:

$$\frac{X_{21}}{X_{11}} = \frac{1\left(-6.28 \times 10^6\right) + 3 \times 10^7}{2 \times 10^7} = 1.186$$

and the first eigenvector is:

$$\psi_1 = \left\{ \begin{array}{c} 1 \\ \frac{X_{21}}{X_{11}} \end{array} \right\} = \left\{ \begin{array}{c} 1 \\ 1.186 \end{array} \right\}.$$

Note that 1.186 is simply the reciprocal of 0.843, which we calculated when normalizing to x_2. Similarly, if we use the second eigenvalue, $s_2^2 = -6.37 \times 10^7$, we obtain:

$$\frac{X_{22}}{X_{12}} = \frac{1\left(-6.37 \times 10^7\right) + 3 \times 10^7}{2 \times 10^7} = -1.686$$

and the second eigenvector is:

$$\psi_2 = \left\{ \begin{array}{c} 1 \\ \frac{X_{22}}{X_{12}} \end{array} \right\} = \left\{ \begin{array}{c} 1 \\ -1.686 \end{array} \right\}.$$

Again, -1.686 is the reciprocal of -0.593, which we determined by normalizing to x_2.

4.3 Time-Domain Solution

Let's now find the time-domain responses, $x_1(t)$ and $x_2(t)$, for the system in Fig. 4.6 (*By the Numbers 4.1*). As we saw in Eq. 2.12 for the free vibration of single degree of freedom systems, the total response is the sum of all possible solutions. For each of the eigenvalues, there are two roots and, therefore, two solutions. For the first eigenvalue, we have $s_{1a} = +i\omega_{n1}$ and $s_{1b} = -i\omega_{n1}$. For the second eigenvalue,

we have $s_{2a} = +i\omega_{n2}$ and $s_{2b} = -i\omega_{n2}$. For $x_1(t)$, the sum of the harmonic solutions that correspond to these four roots is:

$$x_1(t) = X_{11}e^{i\omega_{n1}t} + X_{11}^* e^{-i\omega_{n1}t} + X_{12}e^{i\omega_{n2}t} + X_{12}^* e^{-i\omega_{n2}t}, \tag{4.21}$$

where the first two terms represent motion of the top coordinate from Fig. 4.6 in the first natural frequency, the second two identify motion in the second natural frequency, and X_{11} and X_{11}^*, as well as X_{12} and X_{12}^*, are complex conjugates (they are identical except for the sign of their imaginary parts). Similarly, the time response $x_2(t)$, which describes the motion of the bottom coordinate, has four terms:

$$x_2(t) = X_{21}e^{i\omega_{n1}t} + X_{21}^* e^{-i\omega_{n1}t} + X_{22}e^{i\omega_{n2}t} + X_{22}^* e^{-i\omega_{n2}t}. \tag{4.22}$$

From *By the Numbers 4.1*, the natural frequencies are $\omega_{n1} = 2506$ rad/s and $\omega_{n2} = 7981$ rad/s. Substituting in Eqs. 4.20 and 4.21 yields:

$$x_1(t) = X_{11}e^{i2506t} + X_{11}^* e^{-i2506t} + X_{12}e^{i7981t} + X_{12}^* e^{-i7981t}$$

and

$$x_2(t) = X_{21}e^{i2506t} + X_{21}^* e^{-i2506t} + X_{22}e^{i7981t} + X_{22}^* e^{-i7981t}.$$

The velocities are determined by calculating the time derivatives.

$$\dot{x}_1(t) = i2506\left(X_{11}e^{i2506t} - X_{11}^* e^{-i2506t}\right) + i7981\left(X_{12}e^{i7981t} - X_{12}^* e^{-i7981t}\right)$$
$$\dot{x}_2(t) = i2506\left(X_{21}e^{i2506t} - X_{21}^* e^{-i2506t}\right) + i7981\left(X_{22}e^{i7981t} - X_{22}^* e^{-i7981t}\right)$$

We can now apply the initial conditions specified in Fig. 4.6.

$$x_1(0) = X_{11} + X_{11}^* + X_{12} + X_{12}^* = 1 \text{ mm}$$
$$x_2(0) = X_{21} + X_{21}^* + X_{22} + X_{22}^* = -1 \text{ mm}$$
$$\dot{x}_1(0) = i2506\left(X_{11} - X_{11}^*\right) + i7981\left(X_{12} - X_{12}^*\right) = 0$$
$$\dot{x}_2(0) = i2506\left(X_{21} - X_{21}^*\right) + i7981\left(X_{22} - X_{22}^*\right) = 0$$

We have a problem, though. There are four equations, but eight unknowns. We can remove this obstacle, however, by applying the eigenvector relationships. From our previous analysis (normalizing to x_2), we found that $\frac{X_{11}}{X_{21}} = 0.843$ and $\frac{X_{12}}{X_{22}} = -0.593$. Rearranging gives $X_{11} = 0.843X_{21}$ and $X_{12} = -0.593X_{22}$. Substituting these relationships gives a system of four equations with four unknowns.

$$0.843X_{21} + 0.843X_{21}^* - 0.593X_{22} - 0.593X_{22}^* = 1 \text{ mm}$$

$$X_{21} + X_{21}^* + X_{22} + X_{22}^* = -1 \text{ mm}$$

$$i2506(0.843)\left(X_{21} - X_{21}^*\right) + i7981(-0.593)\left(X_{22} - X_{22}^*\right) = 0$$

$$i2506\left(X_{21} - X_{21}^*\right) + i7981\left(X_{22} - X_{22}^*\right) = 0$$

We can write these four equations in matrix form.

$$\begin{bmatrix} 0.843 & 0.843 & -0.593 & -0.593 \\ 1 & 1 & 1 & 1 \\ i2112 & -i2112 & -i4733 & i4733 \\ i2506 & -i2506 & i7981 & -i7981 \end{bmatrix} \begin{Bmatrix} X_{21} \\ X_{21}^* \\ X_{22} \\ X_{22}^* \end{Bmatrix} = \begin{Bmatrix} 1 \\ -1 \\ 0 \\ 0 \end{Bmatrix}$$

We need to solve for the magnitude vector composed of X_{21}, X_{21}^*, X_{22}, and X_{22}^*. Like we saw in Sect. 2.4.5, we can invert the A matrix in the $AX = B$ equation to determine $X = A^{-1}B$. We can complete this operation at the MATLAB® command prompt (>>) using the following statements.

```
>> A = [0.843 0.843 -0.593 -0.593;1 1 1 1;i*2112 -i*2112 -i*4733 i*4733;
i*2506 -i*2506 i*7981 -i*7981]

A =

 1.0e+003 *

  0.0008       0.0008       -0.0006       -0.0006
  0.0010       0.0010        0.0010        0.0010
     0 + 2.1120i    0 - 2.1120i    0 - 4.7330i    0 + 4.7330i
     0 + 2.5060i    0 - 2.5060i    0 + 7.9810i    0 - 7.9810i

>> B = [1 -1 0 0]'

B =

   1
  -1
   0
   0
```

The ' operator here indicates that the **transpose** operation is to be performed on the B vector. The transpose operator switches the rows and columns for a matrix. In this case, with only one row, the row becomes the only column. Alternately, B could have been defined using `B = [1; -1; 0; 0]`.

```
>> X = inv(A)*B

X =

  0.1417
  0.1417
 -0.6417
 -0.6417
```

Now that we know X_{21}, X_{21}^*, X_{22}, and X_{22}^*, we can again use the eigenvector relationships to determine X_{11}, X_{11}^*, X_{12}, and X_{12}^*.

$$X_{11} = 0.843X_{21} = 0.843(0.1417) = 0.1195 = X_{11}^*$$
$$X_{12} = -0.593X_{22} = -0.593(-0.6417) = 0.3805 = X_{12}^*$$

The complex conjugates are real-valued and equal in this case because there is no damping in the model. Substituting the coefficients into the original x_1 equation gives:

$$x_1(t) = 0.1195e^{i2506t} + 0.1195e^{-i2506t} + 0.3805e^{i7981t} + 0.3805e^{-i7981t}.$$

Using Eq. 1.12 ($2\,cos\,(\theta) = e^{i\theta} + e^{-i\theta}$), we can rewrite the x_1 time response as:

$$x_1(t) = 0.2390\,cos\,(2506t) + 0.761\,cos\,(7981t),$$

where the first term describes the portion of the motion oscillating at ω_{n1} and the second describes the portion oscillating at ω_{n2}. With a two degree of freedom system, we can have free oscillation in both natural frequencies.

Similarly, for x_2 we have:

$$x_2(t) = 0.1417e^{i2506t} + 0.1417e^{-i2506t} - 0.6417e^{i7981t} - 0.6417e^{-i7981t}.$$

Again applying Eq. 1.12, we can alternately express this result as:

$$x_2(t) = 0.2834\,cos\,(2506t) - 1.2834\,cos\,(7981t).$$

Viewing the time-domain responses for coordinates x_1 and x_2, we see that the two degree of freedom system vibrates in a linear combination of the two mode shapes at the two corresponding natural frequencies. These results are displayed in Fig. 4.8, which was generated using the code in MATLAB® MOJO 4.2.

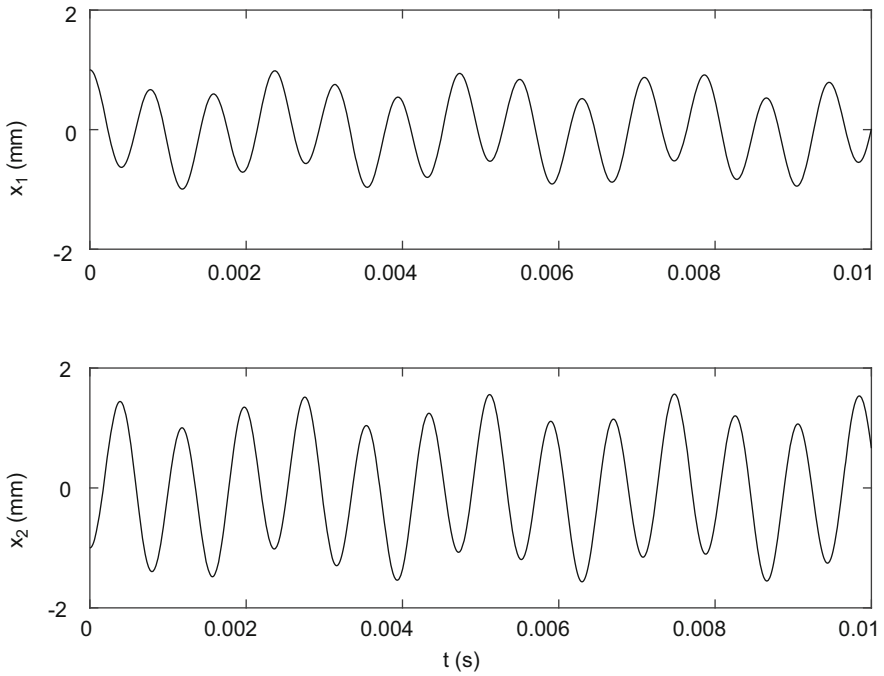

Fig. 4.8 Time-domain responses for the two degrees of freedom system described in Fig. 4.6

MATLAB® MOJO 4.2

```
% matlab_mojo_4_2.m

clear
close all
clc

% Define variables
t = 0:1e-5:0.01;  % s

% Define functions
x1 = 0.2390*cos(2506*t) + 0.761*cos(7981*t);  % mm
x2 = 0.2834*cos(2506*t) - 1.2834*cos(7981*t);

figure(1)
subplot(211)
plot(t, x1, 'k-')
set(gca,'FontSize', 14)
axis([0 0.01 -2 2])
ylabel('x_1 (mm)')
subplot(212)
plot(t, x2, 'k-')
```

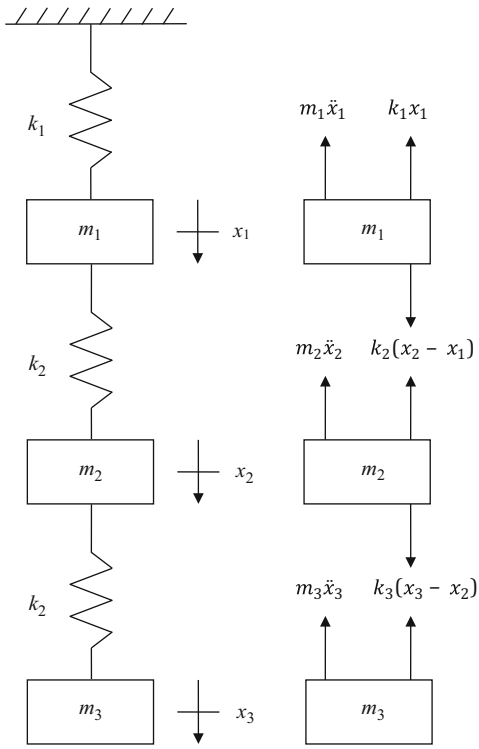

Fig. 4.9 Three degree of freedom system with associated free body diagrams

```
set(gca,'FontSize', 14)
axis([0 0.01 -2 2])
xlabel('t (s)')
ylabel('x_2 (mm)')
```

Now let's consider a three degree of freedom system; see Fig. 4.9. The equations of motion are:

$$\begin{aligned} m_1\ddot{x}_1 + (k_1 + k_2)x_1 - k_2x_2 &= 0 \\ m_2\ddot{x}_2 + (k_2 + k_3)x_2 - k_2x_1 - k_3x_3 &= 0 \\ m_3\ddot{x}_3 + k_3x_3 - k_3x_2 &= 0 \end{aligned} \tag{4.23}$$

for the three masses from top to bottom, respectively. In matrix form, these equations are written as:

$$\begin{bmatrix} m_1 & 0 & 0 \\ 0 & m_2 & 0 \\ 0 & 0 & m_3 \end{bmatrix} \begin{Bmatrix} \ddot{x}_1 \\ \ddot{x}_2 \\ \ddot{x}_3 \end{Bmatrix} + \begin{bmatrix} k_1 + k_2 & -k_2 & 0 \\ -k_2 & k_2 + k_3 & -k_3 \\ 0 & -k_3 & k_3 \end{bmatrix} \begin{Bmatrix} x_1 \\ x_2 \\ x_3 \end{Bmatrix} = \begin{Bmatrix} 0 \\ 0 \\ 0 \end{Bmatrix}, \tag{4.24}$$

where the mass and stiffness matrices are symmetric as we discussed previously. For harmonic vibration, we can assume the solution form $x = Xe^{st}$. Substituting for displacement and acceleration, $\ddot{x} = s^2Xe^{st}$, gives:

$$\left[\begin{bmatrix} m_1 & 0 & 0 \\ 0 & m_2 & 0 \\ 0 & 0 & m_3 \end{bmatrix} s^2 + \begin{bmatrix} k_1 + k_2 & -k_2 & 0 \\ -k_2 & k_2 + k_3 & -k_3 \\ 0 & -k_3 & k_3 \end{bmatrix}\right] \begin{Bmatrix} X_1 \\ X_2 \\ X_3 \end{Bmatrix} e^{st} = \begin{Bmatrix} 0 \\ 0 \\ 0 \end{Bmatrix} \quad (4.25)$$

and the characteristic equation is:

$$\left|\begin{bmatrix} m_1 & 0 & 0 \\ 0 & m_2 & 0 \\ 0 & 0 & m_3 \end{bmatrix} s^2 + \begin{bmatrix} k_1 + k_2 & -k_2 & 0 \\ -k_2 & k_2 + k_3 & -k_3 \\ 0 & -k_3 & k_3 \end{bmatrix}\right| = 0. \quad (4.26)$$

Calculating the determinant, we obtain an equation that is now cubic in s^2 so that we obtain three eigenvalues (i.e., the roots of the characteristic equation): s_1^2, s_2^2, and s_3^2. We use these eigenvalues to determine the three associated eigenvectors. To find the time-domain responses, we can follow the same steps as for the two degree of freedom system. Recall that in order to find X_{11}, X_{12}, X_{21}, and X_{22} (and their complex conjugates), it was necessary to invert a $2^2 \times 2^2 = 4 \times 4$ matrix. For the three degree of freedom system, we would need to invert a $3^2 \times 3^2 = 9 \times 9$ matrix. For large structures, 50 degrees of freedom or more may be necessary to fully describe the complicated system behavior. In this case, we'd have to invert a $50^2 \times 50^2 = 2500 \times 2500$ matrix. The "squared" scaling on our matrix size is clearly computationally unfriendly. Fortunately, there is an alternative to this approach. It is called **modal analysis** and we will discuss it next.

In a Nutshell

Using this approach, we also have a problem computing the determinant and finding the roots of the characteristic equation. For a three degree of freedom system, the characteristic equation is cubic and explicit solutions exist for the roots, similar to the quadratic equation. If we had a four degree of freedom system, however, we'd have to resort to numerical techniques to find the roots. If we had 50 degrees of freedom, then the characteristic equation would have the form $As^{100} + Bs^{98} + \ldots = 0$. This would be difficult to formulate and solve indeed.

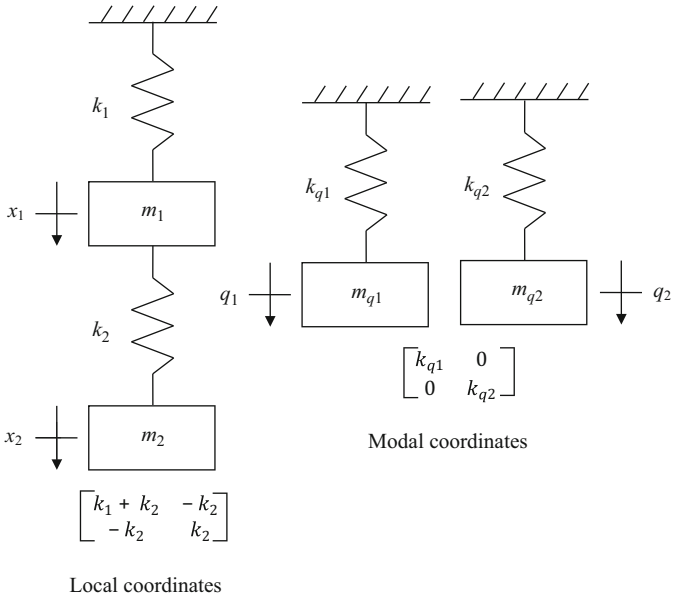

Fig. 4.10 Comparison of local and modal coordinates for a two degree of freedom system

4.4 Modal Analysis

In this approach, the local (i.e., the model or physical) coordinates are transformed into **modal coordinates**. While the modal coordinate system does not have a physical basis, it does provide a coordinate frame where the individual degrees of freedom are uncoupled.

In a Nutshell
There are many choices of coordinates that can be used to describe a physical system. Some of them are "easier" than others to derive and some are more convenient mathematically. The modal coordinate system is mathematically easy because it "decouples" a multiple degree of freedom system into separate single degree of freedom systems.

Figure 4.10 demonstrates the modal coordinate concept, where the local coordinate system gives a stiffness matrix that is coupled. This coupling, or dependence of the response of x_1 on x_2 and vice versa, is manifested by the stiffness matrix with non-zero off-diagonal terms. Alternately, the modal coordinate system yields an uncoupled modal stiffness matrix and two separate single degree of freedom systems; note the new modal coordinates q_1 and q_2 and modal mass and stiffness values identified by the q subscripts in Fig. 4.10. The single degree of freedom free and

forced vibrations solutions we discussed in Chaps. 2 and 3 can therefore by applied individually to each single degree of freedom system. Eureka![1] Once the solutions are determined in modal coordinates, they are transformed back into local coordinates for the final result. In order to convert between the two coordinate systems, the modal matrix, P, is applied. Its columns are the ordered system eigenvectors. The first column is the first eigenvector (that corresponds to the first, lowest natural frequency). The second column is the second eigenvector, and so on. The modal matrix is always a **square matrix**; the number or rows is equal to the number of columns. See Eq. 4.27.

$$P = [\psi_1 \ \ \psi_2 \ \ \ldots] \tag{4.27}$$

Let's complete an example to demonstrate the modal analysis procedure. We'll use a two degree of freedom system that can be described by the two equations of motion:

$$\begin{aligned} 0.05\ddot{x}_1 - 0.05\ddot{x}_2 + 10\dot{x}_1 + 1 \times 10^5 x_1 &= 0 \\ 0.25\ddot{x}_2 - 0.05\ddot{x}_1 + 20\dot{x}_2 + 2 \times 10^5 x_2 &= 0, \end{aligned}$$

which are written in matrix form as:

$$\begin{bmatrix} 0.05 & -0.05 \\ -0.05 & 0.25 \end{bmatrix} \begin{Bmatrix} \ddot{x}_1 \\ \ddot{x}_2 \end{Bmatrix} + \begin{bmatrix} 10 & 0 \\ 0 & 20 \end{bmatrix} \begin{Bmatrix} \dot{x}_1 \\ \dot{x}_2 \end{Bmatrix} + \begin{bmatrix} 1 \times 10^5 & 0 \\ 0 & 2 \times 10^5 \end{bmatrix} \begin{Bmatrix} x_1 \\ x_2 \end{Bmatrix} = \begin{Bmatrix} 0 \\ 0 \end{Bmatrix}.$$

These equations of motion do not represent a chain-type system, as shown in Fig. 4.2. They are coupled in the mass matrix, not the stiffness or damping matrices. However, the modal analysis procedure still works in the same way. The mass, damping, and stiffness matrices are $m = \begin{bmatrix} 0.05 & -0.05 \\ -0.05 & 0.25 \end{bmatrix}$ kg, $c = \begin{bmatrix} 10 & 0 \\ 0 & 20 \end{bmatrix}$ N s/m, and $k = \begin{bmatrix} 1 \times 10^5 & 0 \\ 0 & 2 \times 10^5 \end{bmatrix}$ N/m. The initial conditions are $x_1(0) = x_2(0) = 1$ mm and $\dot{x}_1(0) = \dot{x}_2(0) = 0$ mm/s.

In order to carry out the modal analysis approach, **proportional damping** is required. Mathematically, proportional damping exists if the damping matrix can be written as a linear combination of the mass and stiffness matrices: $[c] = \alpha[m] + \beta[k]$,

[1]The Greek scholar **Archimedes** is historically credited with this interjection. As the story goes, he noticed that the water level rose in proportion to his body's volume when he stepped into a bath. The account continues that he was so excited by this discovery that he ran through the streets of Syracuse naked [4]. Typical engineer!

where α and β are real numbers. Physically, proportional damping means that the individual modes reach their maximum values at the same time. They are either exactly in phase or exactly out of phase. While this is not true for all systems, it is a good approximation for those with low damping (as we typically observe for mechanical structures).

For the example we are considering here, $[c] = \alpha[m] + \beta[k]$ is true when $\alpha = 0$ and $\beta = \frac{1}{1\times10^5}$. Given that the proportional damping requirement is satisfied, we can neglect damping to find the eigensolution. For the eigenvalues, we need the characteristic equation. In this case it is:

$$\left|[m]s^2 + [k]\right| = \left|\begin{bmatrix} 0.05 & -0.05 \\ -0.05 & 0.25 \end{bmatrix} s^2 + \begin{bmatrix} 1\times10^5 & 0 \\ 0 & 2\times10^5 \end{bmatrix}\right| = 0.$$

Calculating the determinant gives $0.01s^4 + 3.5\times10^4 s^2 + 2\times10^{10} = 0$. Using the quadratic equation, the roots are determined using:

$$\begin{aligned} s_{1,2}^2 &= \frac{-3.5\times10^4 \pm \sqrt{\left(3.5\times10^4\right)^2 - 4(0.01)2\times10^{10}}}{2(0.01)} \\ &= -1.75\times10^6 \pm 1.031\times10^6. \end{aligned}$$

The first eigenvalue is $s_1^2 = -1.75\times10^6 + 1.031\times10^6 = -7.19\times10^5 = -\omega_{n1}^2$ and the second eigenvalue is $s_2^2 = -1.75\times10^6 - 1.031\times10^6 = -2.781\times10^6 = -\omega_{n2}^2$. The corresponding natural frequencies are $\omega_{n1} = 847.9$ rad/s and $\omega_{n2} = 1667.6$ rad/s. Note that $\omega_{n1} < \omega_{n2}$. In units of Hz, the natural frequencies are $f_{n1} = \frac{\omega_{n1}}{2\pi} = 134.95$ Hz and $f_{n2} = \frac{\omega_{n2}}{2\pi} = 265.41$ Hz.

To find the eigenvectors we can choose either equation of motion and again neglect damping. The Laplace-domain representation for the equations of motion is:

$$\begin{aligned} \left[[m]s^2 + [\mathrm{k}]\right]\left\{\vec{X}\right\} &= \left[\begin{bmatrix} 0.05 & -0.05 \\ -0.05 & 0.25 \end{bmatrix} s^2 + \begin{bmatrix} 1\times10^5 & 0 \\ 0 & 2\times10^5 \end{bmatrix}\right]\begin{Bmatrix} X_1 \\ X_2 \end{Bmatrix} \\ &= \begin{Bmatrix} 0 \\ 0 \end{Bmatrix}. \end{aligned}$$

Arbitrarily selecting the top equation gives:

$$\left(0.05s^2 + 1\times10^5\right)X_1 - 0.05s^2X_2 = 0.$$

If we wish to normalize to coordinate x_2, we require the ratio:

$$\frac{X_1}{X_2} = \frac{0.05s^2}{0.05s^2 + 1\times10^5}.$$

To find the first eigenvector, ψ_1, substitute $s_1^2 = -7.19\times10^5$ to obtain:

$$\psi_1 = \begin{Bmatrix} \frac{X_{11}}{X_{21}} \\ 1 \end{Bmatrix} = \begin{Bmatrix} \frac{0.05s_1^2}{0.05s_1^2 + 1 \times 10^5} \\ 1 \end{Bmatrix} = \begin{Bmatrix} -0.561 \\ 1 \end{Bmatrix}.$$

This eigenvector represents the relative magnitudes of X_1 and X_2 for vibration at ω_{n1}. The first eigenvector gives motion that is out of phase in this case because the model is not a chain-type system. We find the second eigenvector, ψ_2, by substituting $s_2^2 = -2.781 \times 10^6$ to obtain:

$$\psi_2 = \begin{Bmatrix} \frac{X_{12}}{X_{22}} \\ 1 \end{Bmatrix} = \begin{Bmatrix} \frac{0.05s_2^2}{0.05s_2^2 + 1 \times 10^5} \\ 1 \end{Bmatrix} = \begin{Bmatrix} 3.56 \\ 1 \end{Bmatrix}.$$

We see that the relative motion for vibration at ω_{n2} is in phase and the magnitude of motion at X_1 is 3.56 times larger than the motion at X_2. We can now write the modal matrix, P.

$$P = \begin{bmatrix} -0.561 & 3.56 \\ 1 & 1 \end{bmatrix}$$

The relationship between the local and modal coordinates depends on P.

$$\left\{\vec{x}\right\} = [P]\left\{\vec{q}\right\}, \left\{\dot{\vec{x}}\right\} = [P]\left\{\dot{\vec{q}}\right\}, \text{ and } \left\{\ddot{\vec{x}}\right\} = [P]\left\{\ddot{\vec{q}}\right\} \tag{4.28}$$

To transform from local coordinates to modal coordinates, where the degrees of freedom are uncoupled, we substitute for x and its time derivatives in the system equation of motion using Eq. 4.28.

$$\begin{aligned} [m]\left\{\ddot{\vec{x}}\right\} + [c]\left\{\dot{\vec{x}}\right\} + [k]\left\{\vec{x}\right\} &= \{0\} \\ [m][P]\left\{\ddot{\vec{q}}\right\} + [c][P]\left\{\dot{\vec{q}}\right\} + [k][P]\left\{\vec{q}\right\} &= \{0\} \end{aligned} \tag{4.29}$$

If we now pre-multiply[2] each term in Eq. 4.29 by the transpose of the modal matrix, $P^T = \begin{bmatrix} -0.561 & 3.56 \\ 1 & 1 \end{bmatrix}^T = \begin{bmatrix} -0.561 & 1 \\ 3.56 & 1 \end{bmatrix}$, we obtain the mass, damping, and stiffness matrices in modal coordinates. This process is referred to as **diagonalization**.

[2]Matrix multiplication is not commutative, in general, so the order of multiplication matters. The term pre-multiply means the term appears on the left of the product. The term post-multiply means that the term appears on the right.

$$[P]^T[m][P]\left\{\overrightarrow{\ddot{q}}\right\} + [P]^T[c][P]\left\{\overrightarrow{\dot{q}}\right\} + [P]^T[k][P]\left\{\overrightarrow{q}\right\} = \{0\}$$
$$\left[m_q\right]\left\{\overrightarrow{\ddot{q}}\right\} + \left[c_q\right]\left\{\overrightarrow{\dot{q}}\right\} + \left[k_q\right]\left\{\overrightarrow{q}\right\} = \{0\} \tag{4.30}$$

The modal matrices, $[m_q]$, $[c_q]$, and $[k_q]$, are diagonal matrices—their off-diagonal terms are zero. This yields uncoupled equations of motion.

$$\left[m_q\right] = [P]^T[m][P] = \begin{bmatrix} m_{q1} & 0 \\ 0 & m_{q2} \end{bmatrix} \tag{4.31}$$

$$\left[c_q\right] = [P]^T[c][P] = \begin{bmatrix} c_{q1} & 0 \\ 0 & c_{q2} \end{bmatrix} \tag{4.32}$$

$$\left[k_q\right] = [P]^T[k][P] = \begin{bmatrix} k_{q1} & 0 \\ 0 & k_{q2} \end{bmatrix} \tag{4.33}$$

The two new equations of motion in modal coordinates are:

$$m_{q1}\ddot{q}_1 + c_{q1}\dot{q}_1 + k_{q1}q_1 = 0 \text{ and } m_{q2}\ddot{q}_2 + c_{q2}\dot{q}_2 + k_{q2}q_2 = 0. \tag{4.34}$$

Like the single degree of freedom free vibration systems we studied in Chap. 2, we require the initial conditions in order to solve these differential equations for the time responses $q_1(t)$ and $q_2(t)$. However, we now require these initial conditions to be in modal coordinates. We determine the required initial conditions by rearranging Eq. 4.28. See Eq. 4.35, where the zero subscript denotes the value when the time is zero.

$$\left\{\overrightarrow{q}_0\right\} = [P]^{-1}\left\{\overrightarrow{x}_0\right\} \text{ and } \left\{\overrightarrow{\dot{q}}_0\right\} = [P]^{-1}\left\{\overrightarrow{\dot{x}}_0\right\} \tag{4.35}$$

As we saw in Chap. 2, we can express the damped free vibration response in various forms. One possible form is:

$$q_1(t) = e^{-\zeta_{q1}\omega_{n1}t}(A_1 cos(\omega_{d1}t) + B_1\, sin\,(\omega_{d1}t)), \tag{4.36}$$

which describes motion in the first natural frequency, but note that this motion is not associated with any physical coordinate. In Eq. 4.36, the **modal damping ratio** is $\zeta_{q1} = \frac{c_{q1}}{2\sqrt{m_{q1}k_{q1}}}$ and the modal damped natural frequency is $\omega_{d1} = \omega_{n1}\sqrt{1-\zeta_{q1}^2}$.

For vibration in the second natural frequency, the response is:

$$q_2(t) = e^{-\zeta_{q2}\omega_{n2}t}(A_2\, cos\,(\omega_{d2}t) + B_2\, sin\,(\omega_{d2}t)), \tag{4.37}$$

where $\zeta_{q2} = \frac{c_{q2}}{2\sqrt{m_{q2}k_{q2}}}$ and $\omega_{d2} = \omega_{n2}\sqrt{1-\zeta_{q2}^2}$. To complete the solution, we must transform back into local coordinates.

$$\begin{Bmatrix} x_1 \\ x_2 \end{Bmatrix} = [P]\begin{Bmatrix} q_1 \\ q_2 \end{Bmatrix} \tag{4.38}$$

For our example, we have that $P = \begin{bmatrix} -0.561 & 3.56 \\ 1 & 1 \end{bmatrix}$ and $P^T = \begin{bmatrix} -0.561 & 1 \\ 3.56 & 1 \end{bmatrix}$. The modal mass matrix is then:

$$[m_q] = [P]^T[m][P] = \begin{bmatrix} -0.561 & 1 \\ 3.56 & 1 \end{bmatrix}\begin{bmatrix} 0.05 & -0.05 \\ -0.05 & 0.25 \end{bmatrix}\begin{bmatrix} -0.561 & 3.56 \\ 1 & 1 \end{bmatrix}.$$

Here we have to multiply three matrices. **Matrix multiplication** for 2 × 2 matrices can be completed as shown in Eq. 4.39. For example, the (1,1) term for the product is the first row of the left matrix multiplied in a term-by-term fashion by the first column of the right matrix.

$$\begin{bmatrix} a & b \\ c & d \end{bmatrix}\begin{bmatrix} e & f \\ g & h \end{bmatrix} = \begin{bmatrix} ae+bg & af+bh \\ ce+dg & cf+dh \end{bmatrix} \tag{4.39}$$

Let's now calculate the modal mass matrix. First, we'll multiply the left and middle matrices. Then, we multiply the two remaining matrices.

$$[m_q] = \begin{bmatrix} -0.0781 & 0.2781 \\ 0.128 & 0.072 \end{bmatrix}\begin{bmatrix} -0.561 & 3.56 \\ 1 & 1 \end{bmatrix} = \begin{bmatrix} 0.322 & 0 \\ 0 & 0.528 \end{bmatrix}\text{kg}$$

Similarly, the modal stiffness matrix is:

$$[k_q] = [P]^T[k][P] = \begin{bmatrix} -0.561 & 1 \\ 3.56 & 1 \end{bmatrix}\begin{bmatrix} 1\times10^5 & 0 \\ 0 & 2\times10^5 \end{bmatrix}\begin{bmatrix} -0.561 & 3.56 \\ 1 & 1 \end{bmatrix}.$$

Performing the matrix multiplications yields:[3]

$$[k_q] = \begin{bmatrix} 2.32\times10^5 & 0 \\ 0 & 1.47\times10^6 \end{bmatrix}\text{N/m}.$$

[3]Due to round-off error, the off-diagonal terms in the modal matrices may not be identically zero. However, they will be significantly smaller than the on-diagonal terms.

Because the undamped natural frequencies are the same in local and modal coordinates, we can check our results so far. For the first natural frequency, substitution gives:

$$\omega_{n1} = \sqrt{\frac{k_{q1}}{m_{q1}}} = \sqrt{\frac{2.32 \times 10^5}{0.322}} = 848.8\,\text{rad/s}.$$

The value we obtained from the (local coordinates) eigenvalue was 847.9 rad/s. The difference is due to round-off error, but the results match well enough to validate our modal values. For the second natural frequency, we have:

$$\omega_{n2} = \sqrt{\frac{k_{q2}}{m_{q2}}} = \sqrt{\frac{1.47 \times 10^6}{0.528}} = 1668.6\ \text{rad/s},$$

where the result from the second eigenvalue (determined from local coordinates) was 1667.6 rad/s.

We can calculate the modal damping matrix in two ways. First we can simply perform the matrix multiplications:

$$\begin{aligned}[c_q] = [P]^T[c][P] &= \begin{bmatrix} -0.561 & 1 \\ 3.56 & 1 \end{bmatrix}\begin{bmatrix} 10 & 0 \\ 0 & 20 \end{bmatrix}\begin{bmatrix} -0.561 & 3.56 \\ 1 & 1 \end{bmatrix} \\ &= \begin{bmatrix} 23.15 & 0 \\ 0 & 146.7 \end{bmatrix}\text{N s/m}.\end{aligned}$$

Second, we can use the proportional damping relationship:

$$[c_q] = \alpha[m_q] + \beta[k_q] = 0 \cdot [m_q] + \frac{1}{1 \times 10^4}[k_q] = \begin{bmatrix} 23.15 & 0 \\ 0 & 146.7 \end{bmatrix}\text{N s/m}.$$

We can now calculate the modal damping ratios and corresponding damped natural frequencies.

$$\zeta_{q1} = \frac{c_{q1}}{2\sqrt{m_{q1}k_{q1}}} = \frac{23.5}{2\sqrt{0.322\left(2.32 \times 10^5\right)}} = 0.042$$

$$\zeta_{q2} = \frac{c_{q2}}{2\sqrt{m_{q2}k_{q2}}} = \frac{146.7}{2\sqrt{0.528\left(1.47 \times 10^6\right)}} = 0.083$$

$$\omega_{d1} = \omega_{n1}\sqrt{1 - \zeta_{q1}^2} = 847.2\ \text{rad/s}$$

$$\omega_{d2} = \omega_{n2}\sqrt{1-\zeta_{q2}^2} = 1661.5 \text{ rad/s}$$

As shown in Eqs. 4.36 and 4.37, one form for the underdamped single degree of freedom vibration solution is:

$$q(t) = e^{-\zeta_q \omega_n t}(A cos(\omega_d t) + B sin(\omega_d t)). \tag{4.40}$$

To determine the coefficients we first calculate the velocity and then apply the initial conditions $q(0) = q_0$ and $\dot{q}(0) = \dot{q}_0$. The velocity is:

$$\begin{aligned}\dot{q}(t) = {} & \zeta_q \omega_n e^{-\zeta_q \omega_n t}(A cos(\omega_d t) + B sin(\omega_d t)) \\ & + e^{-\zeta_q \omega_n t}(-\omega_d A sin(\omega_d t) + \omega_d B cos(\omega_d t)).\end{aligned} \tag{4.41}$$

Substituting $t = 0$ in Eqs. 4.40 and 4.41 and using the initial conditions, we obtain Eqs. 4.42 and 4.43.

$$q_1(t) = e^{-\zeta_{q1}\omega_{n1}t}\left(q_{01}\, cos\,(\omega_{d1}t) + \frac{(\dot{q}_{01} + \zeta_{q1}\omega_{n1}q_{01})}{\omega_{d1}}\, sin\,(\omega_{d1}t)\right) \tag{4.42}$$

$$q_2(t) = e^{-\zeta_{q2}\omega_{n2}t}\left(q_{02}\, cos\,(\omega_{d2}t) + \frac{(\dot{q}_{02} + \zeta_{q2}\omega_{n2}q_{02})}{\omega_{d2}} sin(\omega_{d2}t)\right) \tag{4.43}$$

In order to calculate the initial displacement and velocities in modal coordinates, we use Eq. 4.35.

$$\begin{Bmatrix} q_{01} \\ q_{02} \end{Bmatrix} = [P]^{-1}\begin{Bmatrix} x_{01} \\ x_{02} \end{Bmatrix} = \begin{bmatrix} -0.561 & 3.56 \\ 1 & 1 \end{bmatrix}^{-1}\begin{Bmatrix} 1 \\ 1 \end{Bmatrix}$$

$$\begin{Bmatrix} \dot{q}_{01} \\ \dot{q}_{02} \end{Bmatrix} = [P]^{-1}\begin{Bmatrix} \dot{x}_{01} \\ \dot{x}_{02} \end{Bmatrix} = \begin{bmatrix} -0.561 & 3.56 \\ 1 & 1 \end{bmatrix}^{-1}\begin{Bmatrix} 0 \\ 0 \end{Bmatrix}$$

To invert the 2 × 2 modal matrix, we complete three steps: (1) switch the on-diagonal terms; (2) change the signs of the off-diagonal terms; and (3) divide the resulting matrix by the determinant of the original modal matrix.

$$[P]^{-1} = \begin{bmatrix} -0.561 & 3.56 \\ 1 & 1 \end{bmatrix}^{-1} = \frac{\begin{bmatrix} 1 & -3.56 \\ -1 & -0.561 \end{bmatrix}}{-0.561(1) - 3.56(1)} = \begin{bmatrix} -0.243 & 0.864 \\ 0.243 & 0.136 \end{bmatrix}$$

Substitution gives $\begin{Bmatrix} q_{01} \\ q_{02} \end{Bmatrix} = \begin{bmatrix} -0.243 & 0.864 \\ 0.243 & 0.136 \end{bmatrix} \begin{Bmatrix} 1 \\ 1 \end{Bmatrix} = \begin{Bmatrix} 0.621 \\ 0.379 \end{Bmatrix}$ mm.

Because the initial velocities in local coordinates are zero, the initial velocities in modal coordinates are also zero. The modal displacements from Eqs. 4.42 and 4.43 can now be determined.

$$q_1(t) = e^{-35.95t}(0.621\,cos\,(847.2t) + 0.264\,sin\,(847.2t))$$
$$q_2(t) = e^{-139.05t}(0.379\,cos\,(1661.5t) + 0.0317\,sin\,(1661.5t))$$

Finally, we must transform back into local coordinates using Eq. 4.38.

$$\begin{Bmatrix} x_1 \\ x_2 \end{Bmatrix} = \begin{bmatrix} -0.561 & 3.56 \\ 1 & 1 \end{bmatrix} \begin{Bmatrix} q_1 \\ q_2 \end{Bmatrix}$$

Performing the matrix multiplication, we obtain the expressions for x_1 and x_2.
$x_1 = -0.561q_1 + 3.56q_2$ and $x_2 = q_1 + q_2$

We see that x_2 is the sum of the modal contributions q_1 and q_2. This result is obtained because we normalized to coordinate x_2 when we determined the eigenvectors. Substituting for q_1 and q_2 gives the following results. Each response is a linear combination of motion in both damped natural frequencies.

$$x_1(t) = -0.561e^{-35.95t}(0.621\,cos\,(847.2t) + 0.264\,sin\,(847.2t)) + 3.56e^{-139.05t}(0.379\,cos\,(1661.5t) + 0.0317\,sin\,(1661.5t))$$

$$x_2(t) = e^{-35.95t}(0.621\,cos\,(847.2t) + 0.264\,sin\,(847.2t)) + e^{-139.05t}(0.379\,cos\,(1661.5t) + 0.0317\,sin\,(1661.5t))$$

In a Nutshell

We derive the equations of motion in local coordinates, which make physical sense to us. We transform them into modal coordinates, which are mathematically easy, since we already know how to solve single degree of freedom problems. We then transform back to local coordinates to express the final solution. While this may not seem like a big time-saver for two degree of freedom systems, the procedure does not get more complicated as the number of degrees of freedom increases and its benefit becomes clearly apparent.

Let's review the modal analysis steps.

1. Write the equations of motion in matrix form.
2. Verify that proportional damping exists.
3. Neglect damping and write the characteristic equation $|[m]s^2 + [k]| = 0$.

4. Calculate the eigenvalues (i.e., the roots of the characteristic equation). Using the eigenvalues, determine the undamped natural frequencies $s_i^2 = -\omega_{ni}^2$.
5. Select any one of the linearly dependent equations of motion to find the eigenvectors (mode shapes). Normalize to the coordinate of interest (e.g., this may be the location where it is desired to minimize the vibration magnitude).
6. Using the eigenvectors, assemble the modal matrix $P = [\psi_1 \quad \psi_2 \quad \dots]$.
7. Transform the equations of motion into (uncoupled) modal coordinates. The diagonal modal mass, damping, and stiffness matrices are $[m_q] = [P]^T[m][P]$, $[c_q] = [P]^T[c][P]$, and $[k_q] = [P]^T[k][P]$.
8. Write the solutions to the uncoupled (single degree of freedom) equations of motion in modal coordinates. An example solution form is:

$$q(t) = e^{-\zeta_q \omega_n t}\left(q_0 \cos(\omega_d t) + \frac{(\dot{q}_0 + \zeta_q \omega_n q_0)}{\omega_d} \sin(\omega_d t)\right).$$

   Note that the initial conditions must be transformed into modal coordinates to solve the equations of motion.
9. Transform back into local coordinates.

The reason that this approach works is that the eigenvectors possess a very unique property. They are orthogonal with respect to the mass, damping, and stiffness matrices. This is a generalization of the concept of perpendicularity. More information is available in Appendix B.

By the Numbers 4.2

In *By the Numbers 4.1* we determined the time-responses for the two degree of freedom system shown in Fig. 4.6. Let's repeat this example, but now use modal analysis. We'll apply the modal analysis steps we just reviewed.

1. Write the equations of motion in matrix form.

$$\begin{bmatrix} 1 & 0 \\ 0 & 0.5 \end{bmatrix} \begin{Bmatrix} \ddot{x}_1 \\ \ddot{x}_2 \end{Bmatrix} + \begin{bmatrix} 1 \times 10^7 + 2 \times 10^7 & -2 \times 10^7 \\ -2 \times 10^7 & 2 \times 10^7 \end{bmatrix} \begin{Bmatrix} x_1 \\ x_2 \end{Bmatrix} = \begin{Bmatrix} 0 \\ 0 \end{Bmatrix}$$

2. Verify that proportional damping exists.
   There is no damping in this example.
3. Neglect damping and write the characteristic equation.

$$\begin{vmatrix} 1s^2 + 3 \times 10^7 & -2 \times 10^7 \\ -2 \times 10^7 & 0.5s^2 + 2 \times 10^7 \end{vmatrix} = 0.$$

   Calculating and simplifying the determinant gives:

$$0.5s^4 + 3.5 \times 10^7 s^2 + 2 \times 10^{14} = 0.$$

4. Calculate the eigenvalues and determine the undamped natural frequencies.

$$s_{1,2}^2 = \frac{-3.5 \times 10^7 \pm \sqrt{\left(3.5 \times 10^7\right)^2 - 4(0.5)2 \times 10^{14}}}{2(0.5)}$$
$$= -3.5 \times 10^7 \pm 2.872 \times 10^7.$$

The first eigenvalue is:

$$s_1^2 = (-3.5 + 2.872) \times 10^7 = -6.28 \times 10^6 = -\omega_{n1}^2$$

and the first natural frequency is $\omega_{n1} = 2506$ rad/s. The second eigenvalue is:

$$s_2^2 = (-3.5 - 2.872) \times 10^7 = -6.37 \times 10^7 = -\omega_{n2}^2$$

and the second natural frequency is $\omega_{n2} = 7981$ rad/s.

5. Select one of the linearly dependent equations of motion to find the eigenvectors. We'll arbitrarily use the top equation and normalize to x_2. The corresponding ratio is:

$$\frac{X_1}{X_2} = \frac{2 \times 10^7}{1s^2 + 3 \times 10^7}.$$

Substituting the first eigenvalue gives the first eigenvector.

$$\psi_1 = \begin{Bmatrix} \frac{X_{11}}{X_{21}} \\ 1 \end{Bmatrix} = \begin{Bmatrix} 0.843 \\ 1 \end{Bmatrix}$$

Substituting the second eigenvalue gives the second eigenvector.

$$\psi_2 = \begin{Bmatrix} \frac{X_{12}}{X_{22}} \\ 1 \end{Bmatrix} = \begin{Bmatrix} -0.593 \\ 1 \end{Bmatrix}$$

6. Assemble the modal matrix.

$$P = \begin{bmatrix} 0.843 & -0.593 \\ 1 & 1 \end{bmatrix}$$

7. Transform the equations of motion into (uncoupled) modal coordinates. The diagonal modal mass, damping, and stiffness matrices are $[m_q] = [P]^T[m][P]$, $[c_q] = [P]^T[c][P]$, and $[k_q] = [P]^T[k][P]$.

$$[m_q] = \begin{bmatrix} 0.843 & -0.593 \\ 1 & 1 \end{bmatrix}^T \begin{bmatrix} 1 & 0 \\ 0 & 0.5 \end{bmatrix} \begin{bmatrix} 0.843 & -0.593 \\ 1 & 1 \end{bmatrix} = \begin{bmatrix} 1.211 & 0 \\ 0 & 0.852 \end{bmatrix} \text{kg}$$

$$[k_q] = \begin{bmatrix} 0.843 & -0.593 \\ 1 & 1 \end{bmatrix}^T \begin{bmatrix} 3 \times 10^7 & -2 \times 10^7 \\ -2 \times 10^7 & 2 \times 10^7 \end{bmatrix} \begin{bmatrix} 0.843 & -0.593 \\ 1 & 1 \end{bmatrix}$$

$$= \begin{bmatrix} 7.6 \times 10^6 & 0 \\ 0 & 5.43 \times 10^7 \end{bmatrix} \text{N/m}$$

Actually, due to round-off error, the modal stiffness matrix off-diagonal terms were $k_{q12} = 3 \times 10^3$ N/m and $k_{q21} = 3.5 \times 10^4$ N/m after the previous matrix multiplications were completed. However, these values are two to four orders of magnitude smaller than the on-diagonal terms and were neglected.

8. Write the solutions to the uncoupled (single degree of freedom) equations of motion in modal coordinates. The equations of motion are:

$$1.211\ddot{q}_1 + 7.6 \times 10^6 q_1 = 0 \text{ and } 0.852\ddot{q}_2 + 5.43 \times 10^7 q_2 = 0.$$

These equations are now uncoupled and represent two separate single degree of freedom systems. As a check, let's calculate the natural frequencies.

$$\omega_{n1} = \sqrt{\frac{7.6 \times 10^6}{1.211}} = 2505\,\text{rad/s} \text{ and } \omega_{n2} = \sqrt{\frac{5.43 \times 10^7}{0.852}} = 7983\,\text{rad/s}$$

These results match the natural frequencies obtained from the eigenvalues, as they should. Natural frequencies are system properties that do not depend on choice of coordinates. To solve the equations of motion, we require the initial conditions in modal coordinates.

$$q(t) = e^{-\zeta_q \omega_n t}\left(q_0\, cos\,(\omega_d t) + \frac{(\dot{q}_0 + \zeta_q \omega_n q_0)}{\omega_d}\, sin\,(\omega_d t)\right).$$

Note that the initial conditions must be transformed into modal coordinates to solve the equations of motion.

$$\begin{Bmatrix} q_{01} \\ q_{02} \end{Bmatrix} = [P]^{-1} \begin{Bmatrix} x_{01} \\ x_{02} \end{Bmatrix} = \begin{bmatrix} 0.843 & -0.593 \\ 1 & 1 \end{bmatrix}^{-1} \begin{Bmatrix} 1 \\ -1 \end{Bmatrix}$$

The inverse of the modal matrix is:

$$[P]^{-1} = \frac{\begin{bmatrix} 1 & 0.593 \\ -1 & 0.843 \end{bmatrix}}{0.843(1) - (-0.593)1} = \begin{bmatrix} 0.696 & 0.413 \\ -0.696 & 0.587 \end{bmatrix}.$$

The initial displacements are therefore:

$$\begin{Bmatrix} q_{01} \\ q_{02} \end{Bmatrix} = \begin{bmatrix} 0.696 & 0.413 \\ -0.696 & 0.587 \end{bmatrix} \begin{Bmatrix} 1 \\ -1 \end{Bmatrix} = \begin{Bmatrix} 0.283 \\ -1.283 \end{Bmatrix} \text{mm}.$$

The zero initial velocities in modal coordinates give zero initial velocities in modal coordinates.

$$\begin{Bmatrix} \dot{q}_{01} \\ \dot{q}_{02} \end{Bmatrix} = [P]^{-1} \begin{Bmatrix} 0 \\ 0 \end{Bmatrix} = \begin{Bmatrix} 0 \\ 0 \end{Bmatrix}$$

For non damping, one single degree of freedom vibration solution form is:

$$q(t) = q_0 \, cos\,(\omega_n t) + \frac{\dot{q}_0}{\omega_n} \, sin\,(\omega_n t).$$

Substituting the appropriate natural frequencies and initial conditions gives:

$$q_1(t) = 0.283 \, cos\,(2506t)$$

and

$$q_2(t) = -1.283 \, cos\,(7981t).$$

9. Transform back into local coordinates using $\begin{Bmatrix} x_1 \\ x_2 \end{Bmatrix} = \begin{bmatrix} 0.843 & -0.593 \\ 1 & 1 \end{bmatrix} \begin{Bmatrix} q_1 \\ q_2 \end{Bmatrix}$. The results are:

$$x_1(t) = 0.239 \, cos\,(2506t) + 0.761 \, cos\,(7981t) \text{ mm}$$

and

$$x_2(t) = 0.283 \, cos\,(2506t) - 1.283 \, cos\,(7981t) \text{ mm}.$$

Naturally, this is the same result that we obtained from the previous analysis. However, we avoided the need to invert the 4×4 matrix. This is particularly beneficial for models with many more degrees of freedom.

In a Nutshell
Note that the motion of the coordinate to which the mode shapes are normalized is just the sum of the motions expressed in modal coordinates. If you are concerned about the motion of a particular point, simply normalize the mode shapes so that their value is 1 at that coordinate.

Let's conclude the chapter by applying new initial conditions to this example. For the initial conditions provided in Fig. 4.6, we obtained time-domain responses for the two degrees of freedom that were linear combinations of vibration in the two natural frequencies. Could we select initial conditions that would yield vibration in only one natural frequency? The answer is yes. If we choose initial displacements (and zero initial velocities) that match one of the eigenvectors (i.e., the ratios of the magnitude of vibrations between the individual local coordinates), then we'll obtain vibration only in the natural frequency that corresponds to the selected eigenvector.

Let's use local coordinate initial displacements of $x_1(0) = -1.686$ mm and $x_2(0) = -2$ mm. Note that these initial displacements match the ratio provided by the first eigenvector. The initial displacements in modal coordinates are:

$$\begin{Bmatrix} q_{01} \\ q_{02} \end{Bmatrix} = \begin{bmatrix} 0.696 & 0.413 \\ -0.696 & 0.587 \end{bmatrix} \begin{Bmatrix} -1.686 \\ -2 \end{Bmatrix} = \begin{Bmatrix} -2 \\ 0 \end{Bmatrix} \text{mm}$$

and the initial velocities are zero.

The modal coordinate, time-domain solutions in the form $q(t) = q_0 \, cos\,(\omega_n t) + \frac{\dot{q}_0}{\omega_n} \, sin\,(\omega_n t)$ are:

$$q_1(t) = -2 \, cos\,(2506t) \text{ mm}$$

and

$$q_2(t) = 0 \text{ mm}.$$

Transforming back into local coordinates using $\begin{Bmatrix} x_1 \\ x_2 \end{Bmatrix} = \begin{bmatrix} 0.843 & -0.593 \\ 1 & 1 \end{bmatrix} \times \begin{Bmatrix} q_1 \\ q_2 \end{Bmatrix}$ gives:

$$x_1(t) = -1.686 \, cos\,(2506t) \text{ mm}$$

and

$$x_2(t) = -2 \, cos\,(2506t) \text{ mm}.$$

As expected, the time-domain solutions in local coordinates include vibration in only the first natural frequency and the ratio of displacement magnitudes between coordinates x_1 and x_2 matches the first eigenvector.

Chapter Summary

- The eigensolution gives the eigenvalues, which identify the system's natural frequencies, and the eigenvectors, or mode shapes, which describe the relative motion of the individual degrees of freedom.
- The number of eigenvalue/eigenvector pairs is equal to the number of degrees of freedom in the system model.
- The mode shapes are typically normalized to one of the degrees of freedom for the system model since they only provide the ratio of vibration magnitude between coordinates.
- The roots of the characteristic equation are the eigenvalues. The characteristic equation is determined from the equations of motion.
- The eigenvalues are used to determine the eigenvectors. The eigenvalues, and corresponding eigenvectors, are ordered in ascending natural frequency values.
- In modal analysis, the local (model) coordinates are transformed into modal coordinates. The equations of motion are uncoupled in modal coordinates and, therefore, they can each be treated as a single degree of freedom system.
- The modal matrix is used to transform between local and modal coordinates. It is also used to diagonalize the mass, stiffness, and damping matrices. Its columns are the system's eigenvectors (ordered from left to right in the matrix).
- Modal analysis requires proportional damping. Mathematically, proportional damping exists if the damping matrix can be written as a linear combination of the mass and stiffness matrices. Physically, proportional damping means that the individual modes reach their maximum values at the same time.
- The undamped natural frequencies are the same in both local and modal coordinates.
- The selection of initial conditions determines whether the system's time-domain free vibration responses will oscillate in the first natural frequency, second natural frequency, or a linear combination of the two. If the initial displacements (with zero initial velocities) match the ratio provided by one of the eigenvectors, then the system will vibrate only in the natural frequency that corresponds to that eigenvector.

Exercises

1. Given the eigenvalues and eigenvectors for the two degree of freedom system shown in Fig. P4.1, determine the modal matrices m_q (kg), c_q (N s/m), and k_q (N/m).

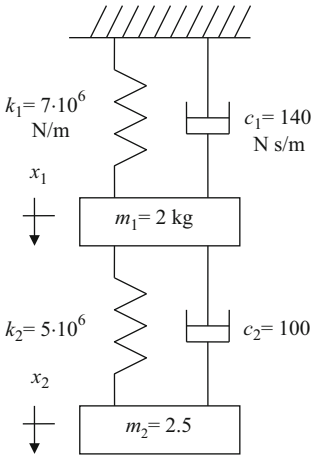

Fig. P4.1 Two degree of freedom spring-mass-damper system

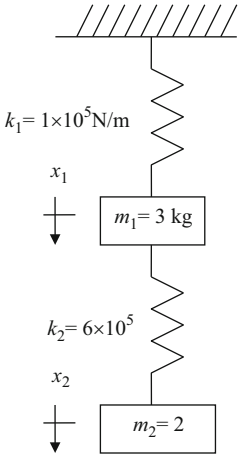

Fig. P4.2 Two degree of freedom spring-mass system

$$s_1{}^2 = -1 \times 10^6 \text{ rad/s}^2$$

$$s_2{}^2 = -7 \times 10^6 \text{ rad/s}^2$$

$$\psi_1 = \begin{Bmatrix} 0.5 \\ 1 \end{Bmatrix} \qquad \psi_2 = \begin{Bmatrix} -2.5 \\ 1 \end{Bmatrix}$$

2. Given the two degree of freedom system in Fig. P4.2, complete the following.
   (a) Write the equations of motion in matrix form.
   (b) Write the system characteristic equation using Laplace notation. Your solution should be a polynomial that is quadratic in s^2 with appropriate numerical coefficients.
   (c) Calculate the natural frequencies (in Hz).

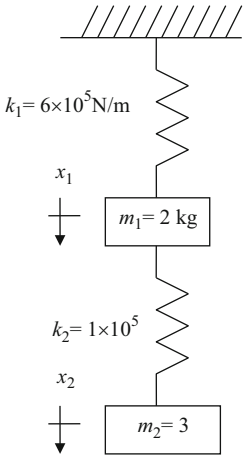

Fig. P4.3 Two degree of freedom spring-mass system

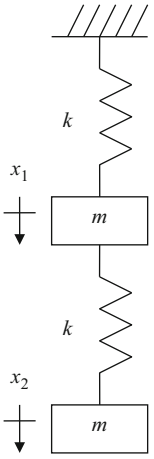

Fig. P4.4 Two degree of freedom spring-mass system

(d) Determine the two mode shapes (normalize to coordinate x_1).

3. Given the two degree of freedom system shown in Fig. P4.3, complete the following.

   (a) Write the equations of motion in matrix form.
   (b) Write the system characteristic equation using Laplace notation. Your solution should be a polynomial that is quadratic in s^2 with appropriate numerical coefficients.
   (c) Determine the natural frequencies (in rad/s).
   (d) Determine the mode shapes (normalize to coordinate x_2).

4. A two degree of freedom spring-mass system is shown in Fig. P4.4. For harmonic free vibration, complete the following if $k = 5 \times 10^6$ N/m and $m = 2$ kg.

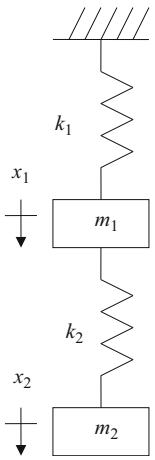

Fig. P4.5 Two degree of freedom spring-mass system

(a) Draw the free body diagram showing the forces on the two masses during vibration.
(b) Write the two equations of motion in matrix form. First show the equations symbolically and then substitute the numerical values for m and k.
(c) Write the characteristic equation for this system. First show the equation symbolically and then substitute the numerical values for m and k.
(d) Determine the numerical roots of the characteristic equation (which is quadratic in s^2). What do these two roots represent?
(e) Determine the two mode shapes for this system. Normalize the mode shapes to coordinate x_1.

5. A two degree of freedom spring-mass system is displayed in Fig. P4.5. For harmonic free vibration, complete the following if $k_1 = 2 \times 10^6$ N/m, $m_1 = 0.8$ kg, $k_2 = 1 \times 10^6$ N/m, and $m_2 = 1.4$ kg. The initial displacements for the system's free vibration are $x_1(0) = 2$ mm and $x_2(0) = 1$ mm and the initial velocities are $\dot{x}_1(0) = 0$ mm/s and $\dot{x}_2(0) = 5$ mm/s.

   (a) Calculate the two natural frequencies and mode shapes. Normalize the mode shapes (eigenvectors) to coordinate x_2.
   (b) Define the modal matrix and determine the modal mass and stiffness matrices.
   (c) Write the uncoupled single degree of freedom time responses for the modal coordinates q_1 and q_2. Use the following form: $q_{1,2}(t) = A_{1,2}\, cos\left(\omega_{n_{1,2}} t\right) + B_{1,2}\, sin\left(\omega_{n_{1,2}} t\right)$ with units of mm.
   (d) Write the time responses for the local coordinates x_1 and x_2 (in mm).
   (e) Plot the time responses for x_1 and x_2 (in mm). Define the time vector as: `t = 0:0.0001:0.2;` (in seconds).

6. For the same system as described in Problem 5, complete the following.

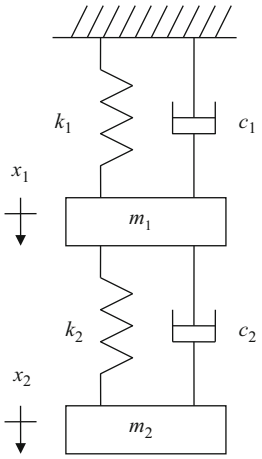

Fig. P4.7 Two degree of freedom spring-mass-damper system under free vibration

(a) The initial displacements for the system's free vibration are $x_1(0) = 0.378$ mm and $x_2(0) = 1$ mm and the initial velocities are $\dot{x}_1(0) = 0$ mm/s and $\dot{x}_2(0) = 0$ mm/s. Plot the time responses for x_1 and x_2 (in mm). Define the time vector as: `t = 0:0.0001:0.2;` (in seconds). What is the vibrating frequency for both $x_1(t)$ and $x_2(t)$? What is special about these initial conditions to give this result?

(b) The initial displacements for the system's free vibration are $x_1(0) = -4.628$ mm and $x_2(0) = 1$ mm and the initial velocities are $\dot{x}_1(0) = 0$ mm/s and $\dot{x}_2(0) = 0$ mm/s. Plot the time responses for x_1 and x_2 (in mm). Define the time vector as: `t = 0:0.0001:0.2;` (in seconds). What is the vibrating frequency for both $x_1(t)$ and $x_2(t)$? What is special about these initial conditions to give this result?

7. A two degree of freedom spring-mass-damper system is shown in Fig. P4.7. For harmonic free vibration, complete the following if $k_1 = 2 \times 10^5$ N/m, $c_1 = 60$ N-s/m, $m_1 = 2.5$ kg, $k_2 = 5.5 \times 10^4$ N/m, $c_2 = 16.5$ N s/m, and $m_2 = 1.2$ kg.

   (a) Verify that proportional damping exists.
   (b) Define the modal matrix and determine the modal mass, stiffness, and damping matrices. Normalize the mode shapes to coordinate x_2.

8. Given the two degree of freedom system in Fig. P4.8, complete the following.

   (a) Write the equations of motion in matrix form.
   (b) Verify that proportional damping exists.
   (c) Determine the roots of the characteristic equation. What do these roots represent?
   (d) Determine the two mode shapes (normalize to coordinate x_1).

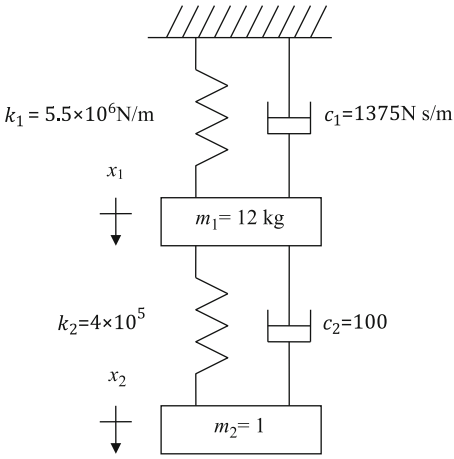

Fig. P4.8 Two degree of freedom spring-mass system

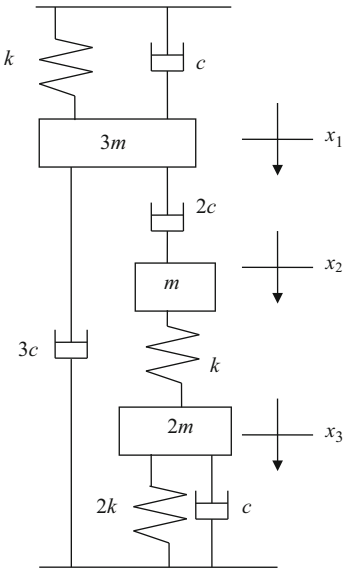

Fig. P4.9 Three degree of freedom spring-mass-damper model

9. Determine the mass, damping, and stiffness matrices in local coordinates for the model shown in Fig. P4.9.
10. Given the mass, damping, and stiffness matrices for the model shown in Fig. P4.9 determined from Problem 9, can proportional damping exist for this system? Justify your answer.

References

1. http://en.wiktionary.org/wiki/eigen
2. Blevins RD (2001) Formulas for natural frequency and mode shape. Table 8-1. Krieger Publishing Co., Malabar, FL
3. http://en.wikipedia.org/wiki/Linear_independence
4. http://en.wikipedia.org/wiki/Eureka_(word)

Chapter 5
Two Degree of Freedom Forced Vibration

Our achievements of today are but the sum total of our thoughts of yesterday.
—Blaise Pascal

5.1 Equations of Motion

Let's extend the two degree of freedom free vibration analysis from Chap. 4 to include externally applied forces so that we can analyze two degree of freedom forced vibration. The general case is that a separate harmonic force is applied at each coordinate; see Fig. 5.1. However, we are considering only linear systems, so we can apply **superposition**. This means that we can determine the system response due to each force separately and then sum the results to find the combined effect.

Using the free body diagrams included in Fig. 5.1, the equations of motion expressed in matrix form are:

$$\begin{bmatrix} m_1 & 0 \\ 0 & m_2 \end{bmatrix} \begin{Bmatrix} \ddot{x}_1 \\ \ddot{x}_2 \end{Bmatrix} + \begin{bmatrix} c_1 + c_2 & -c_2 \\ -c_2 & c_2 \end{bmatrix} \begin{Bmatrix} \dot{x}_1 \\ \dot{x}_2 \end{Bmatrix} + \begin{bmatrix} k_1 + k_2 & -k_2 \\ -k_2 & k_2 \end{bmatrix} \begin{Bmatrix} x_1 \\ x_2 \end{Bmatrix} = \begin{Bmatrix} F_1 e^{i\omega_1 t} \\ F_2 e^{i\omega_2 t} \end{Bmatrix}, \tag{5.1}$$

where the subscripts on the forcing frequencies indicate that they are not necessarily equal. Because the springs and dampers appear together in the Fig. 5.1 model, the damping and stiffness matrices have the same format in Eq. 5.1. This is not always the case, but the mass, damping, and stiffness matrices will be symmetric in all instances, as long as the coordinates are measured with respect to ground.

T. L. Schmitz, K. S. Smith, *Mechanical Vibrations*,
https://doi.org/10.1007/978-3-030-52344-2_5

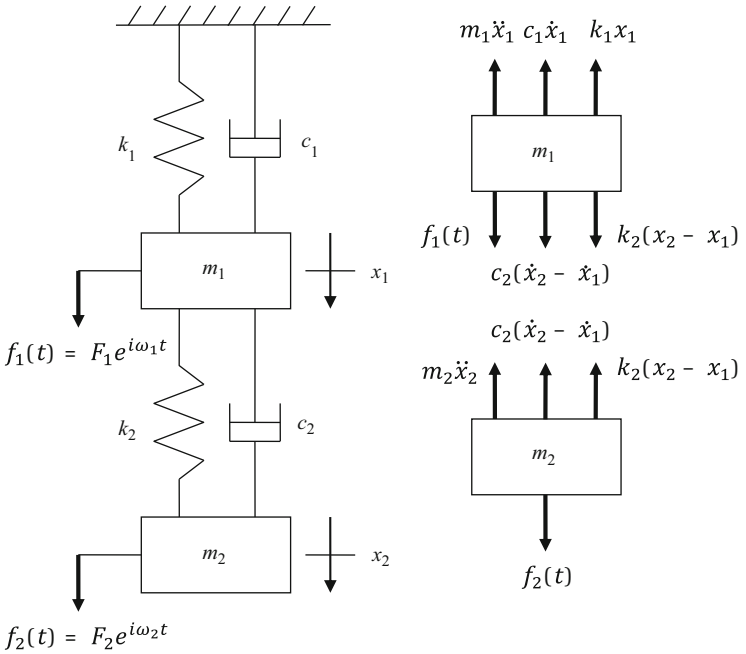

Fig. 5.1 Two degree of freedom chain-type, spring-mass-damper system with harmonic forces $f_1(t)$ and $f_2(t)$ applied at coordinates x_1 and x_2, respectively

In a Nutshell
If the coordinates are measured with respect to ground and the stiffness matrix (for example) is not symmetric, then we have made a perpetual motion machine. Essentially, the energy required to achieve a specified displacement configuration through one loading path (say moving coordinate 1 and then moving coordinate 2) would not be the same as the energy recovered by returning the coordinates to their original position through a different loading path. By loading and unloading through two different paths, energy could be extracted from the system indefinitely. Simply put, when the coordinates are measured with respect to ground, the mass, stiffness, and damping matrices must be symmetric.

For now let's take advantage of superposition and consider only $f_2(t) = F_2 e^{i\omega t}$ (the frequency subscript is removed because there is just one force). Similar to the single degree of freedom forced vibration analysis in Chap. 3 we can assume a harmonic form for the solution which mimics the forcing function $x(t) = Xe^{i\omega t}$. This gives $\dot{x}(t) = i\omega Xe^{i\omega t}$ and $\ddot{x}(t) = (i\omega)^2 Xe^{i\omega t} = -\omega^2 Xe^{i\omega t}$. Substitution in Eq. 5.1 yields:

$$\left[-\omega^2\begin{bmatrix} m_1 & 0 \\ 0 & m_2 \end{bmatrix} + i\omega\begin{bmatrix} c_1+c_2 & -c_2 \\ -c_2 & c_2 \end{bmatrix} + \begin{bmatrix} k_1+k_2 & -k_2 \\ -k_2 & k_2 \end{bmatrix}\right]\begin{Bmatrix} X_1 \\ X_2 \end{Bmatrix} e^{i\omega t} = \begin{Bmatrix} 0 \\ F_2 e^{i\omega t} \end{Bmatrix}. \tag{5.2}$$

In the generic case, we can express Eq. 5.2 as:

$$\left[-\omega^2[m] + i\omega[c] + [k]\right]\left\{\vec{X}\right\}e^{i\omega t} = \left\{\vec{F}\right\}e^{i\omega t}. \tag{5.3}$$

We will apply two methods to solve the system of coupled differential equations represented by Eq. 5.3. In both cases, we will determine the system frequency response functions (FRFs). These FRFs identify the frequency-dependent, steady-state vibration behavior and, because this is our desired result, we will neglect the transients which rapidly decay in general. The first solution method is referred to as **complex matrix inversion**. While this approach is more computationally expensive, it does not require proportional damping. The second method is **modal analysis**, which we introduced in Chap. 4. This method is applicable to systems with any number of degrees of freedom, but proportional damping must be satisfied (or assumed).

5.2 Complex Matrix Inversion

To implement this approach, it is helpful to rewrite Eq. 5.3 in a more compact form; see Eq. 5.4. In this form, the sum of the mass, damping, and stiffness matrices, with the appropriate frequency multipliers on the mass and damping matrices, is represented by the matrix A. To determine the system FRFs, we simply need to invert the complex matrix A. This is demonstrated in Eq. 5.5.

$$\left[-\omega^2[m] + i\omega[c] + [k]\right]\left\{\vec{X}\right\}e^{i\omega t} = [A]\left\{\vec{X}\right\}e^{i\omega t} = \left\{\vec{F}\right\}e^{i\omega t} \tag{5.4}$$

$$\left\{\vec{X}\right\} = [A]^{-1}\left\{\vec{F}\right\} \tag{5.5}$$

For the two degree of freedom system displayed in Fig. 5.1, A is a 2×2 matrix and can be expressed as shown in Eq. 5.6. This matrix is frequency dependent. One way to visualize A is to consider it as a book where each page provides the four a_{ij} values at a particular frequency. The beginning of the book gives the low frequency values and the end gives the high frequency values.

$$[A] = \begin{bmatrix} a_{11} & a_{12} \\ a_{21} & a_{22} \end{bmatrix} = \begin{bmatrix} -\omega^2 m_1 + i\omega(c_1 + c_2) + (k_1 + k_2) & -i\omega c_2 - k_2 \\ -i\omega c_2 - k_2 & -\omega^2 m_2 + i\omega c_2 + k_2 \end{bmatrix} \tag{5.6}$$

As we saw in Sect. 2.4.5, we determine the inverse of the A matrix by switching the on-diagonals, changing the sign of the off-diagonals, and dividing each term by the determinant of A; see Eq. 5.7. In this case, however, we have to repeat the inversion for each frequency value within our range (or **bandwidth**) of interest. For example, we might be interested in a system's response between 0 and 5000 Hz. With a frequency resolution of 1 Hz, we would need to invert A 5001 times.

$$[A]^{-1} = \frac{1}{|A|}\begin{bmatrix} a_{22} & -a_{12} \\ -a_{21} & a_{11} \end{bmatrix} = \frac{1}{(a_{11}a_{22} - a_{12}a_{21})}\begin{bmatrix} a_{22} & -a_{12} \\ -a_{21} & a_{11} \end{bmatrix} = \begin{bmatrix} \alpha_{11} & \alpha_{12} \\ \alpha_{21} & \alpha_{22} \end{bmatrix} \tag{5.7}$$

The four entries in the inverted A matrix are provided in Eqs. 5.8 through 5.11.

$$\alpha_{11} = \frac{-\omega^2 m_2 + i\omega c_2 + k_2}{|A|} \tag{5.8}$$

$$\alpha_{12} = \frac{i\omega c_2 + k_2}{|A|} \tag{5.9}$$

$$\alpha_{21} = \frac{i\omega c_2 + k_2}{|A|} \tag{5.10}$$

$$\alpha_{22} = \frac{-\omega^2 m_1 + i\omega(c_1 + c_2) + (k_1 + k_2)}{|A|} \tag{5.11}$$

Let's assume that the external force is applied to coordinates x_1 only in Fig. 5.1. We can therefore write:

$$\begin{Bmatrix} X_1 \\ X_2 \end{Bmatrix} = \begin{bmatrix} \alpha_{11} & \alpha_{12} \\ \alpha_{21} & \alpha_{22} \end{bmatrix} \begin{Bmatrix} F_1 \\ 0 \end{Bmatrix}. \tag{5.12}$$

Using Eq. 5.12, we can solve for X_1.

$$X_1 = \alpha_{11} F_1 \tag{5.13}$$

From Eq. 5.13, we see that $\alpha_{11} = \frac{X_1}{F_1}$ gives X_1 for a force F_1. This is called a **direct FRF** because the response is measured at the same location where the force is applied (the α_{ij} subscripts match). From the bottom row in Eq. 5.12, we have

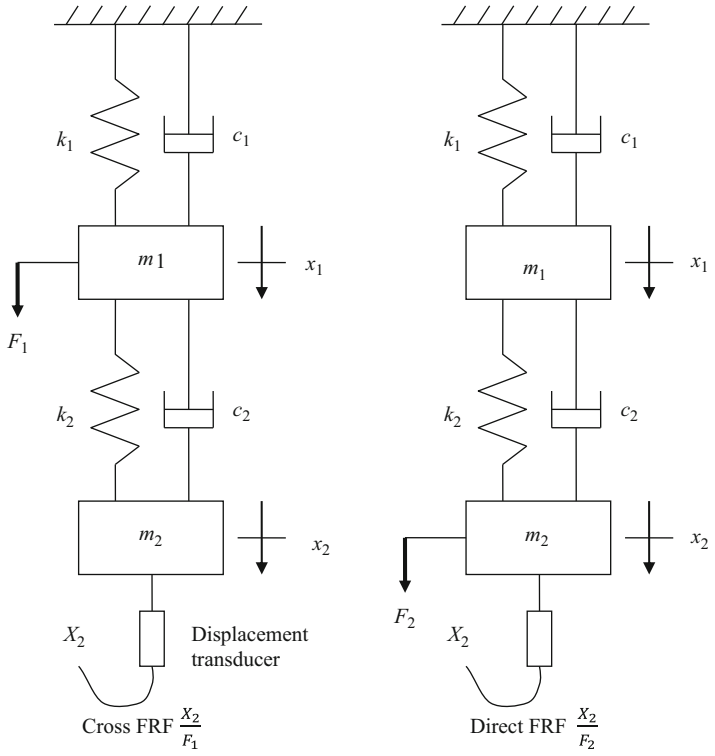

Fig. 5.2 The direct and cross FRFs for coordinate x_2 are shown

$\alpha_{21} = \frac{X_2}{F_1}$, which relates X_2 and F_1. This is a **cross FRF** because the response is measured at a different location than where the force is applied (the α_{ij} subscripts do not match). If the force is applied to coordinates x_2 only in Fig. 5.1, then $\begin{Bmatrix} X_1 \\ X_2 \end{Bmatrix} = \begin{bmatrix} \alpha_{11} & \alpha_{12} \\ \alpha_{21} & \alpha_{22} \end{bmatrix} \begin{Bmatrix} 0 \\ F_2 \end{Bmatrix}$ and we have:

$$X_2 = \alpha_{22} F_2. \tag{5.14}$$

From Eq. 5.14, $\alpha_{22} = \frac{X_2}{F_2}$ is a direct FRF that relates X_2 and F_2. Also, $\alpha_{12} = \frac{X_1}{F_2}$ is a cross FRF that relates X_1 and F_2. The FRFs $\frac{X_2}{F_2}$ and $\frac{X_2}{F_1}$ are depicted in Fig. 5.2. All together, our two degree of freedom system has four direct and cross FRFs (2^2). A three degree of freedom system has nine (3^2).

From Eqs. 5.9 and 5.10, we see that $\alpha_{12} = \alpha_{21}$ because $[A]^{-1}$ is symmetric. This attribute is referred to as **reciprocity** and can be observed by comparing cross FRFs measured on actual systems. Let's consider the cantilever, or fixed-free, beam shown in Fig. 5.3 for two cases. First, a harmonic force is applied at coordinate 1 (the free end) and the response is measured at coordinate 2 somewhere along the beam, let's say the midpoint. Second, the same force is applied at coordinate 2, but the response

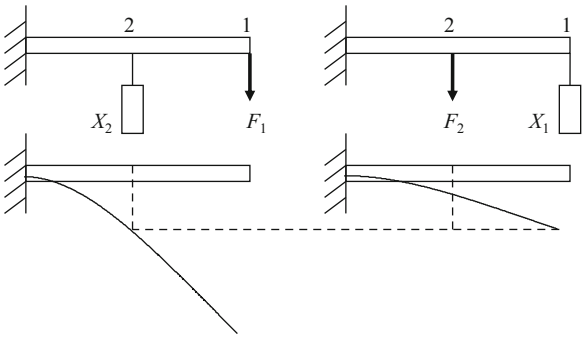

Fig. 5.3 Reciprocity demonstration for cantilever beam cross FRF measurements

is measured at coordinate 1. In the first case, if we measured the response and converted both the force and response into the frequency domain (using the Fourier transform), we would obtain the cross FRF $\frac{X_2}{F_1}$. In the second case, we would determine the cross FRF $\frac{X_1}{F_2}$ from our measurements. Due to reciprocity, these two cross FRFs are equal.

In a Nutshell
Reciprocity will be a handy tool later, when we explore the physical measurement of FRFs. Sometimes it is convenient to switch the excitation and measurement locations; we are free to do so because of this property.

To aid in understanding this concept, Fig. 5.3 depicts the two cases where the forcing frequency is equal to the beam's first (lowest) natural frequency so that it vibrates in the corresponding mode shape (see Sect. 4.2). When the force is applied at the free end, the magnitude of the response is largest everywhere and the corresponding X_2 is obtained. When the force is instead applied at coordinate 2, the response is not so big, but it is largest at the free end where we measure X_1. As shown in the figure, the magnitudes X_1 and X_2 are equal and, therefore, the cross FRFs are equal.

To consider a limiting case, assume that the force is applied at the free end and the response is measured at the fixed end, now labeled as coordinate 2. Because the boundary condition is fixed, no matter what force is applied at the free end (1), the measured response will be zero at the fixed end (2). Therefore, the cross FRF $\frac{X_2}{F_1}$ will be zero for all frequencies. If, on the other hand, the force is applied at the fixed end and the response is measured at the free end, the cross FRF $\frac{X_1}{F_2}$ will still be zero because a force at the base will not serve to excite vibration in the beam. Reciprocity again holds.

To determine the system FRFs by complex matrix inversion, we solve Eq. 5.7 for each frequency within the range of interest. At each frequency, we extract the desired direct or cross FRF from the inverted matrix and then plot the results on a frequency-by-frequency basis. An example is provided in *By the Numbers 5.1*.

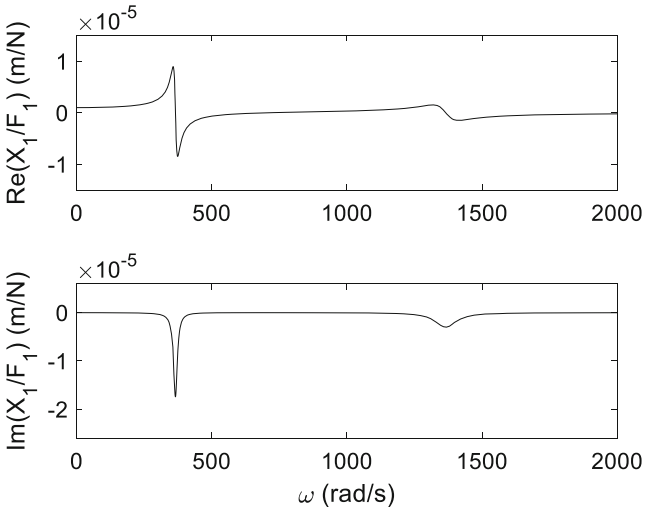

Fig. 5.4 *By the Numbers 5.1*—direct FRF $\frac{X_1}{F_1}$ for the example system

By the Numbers 5.1

Consider the system shown in Fig. 5.1 with $m_1 = 2$ kg, $c_1 = 150$ N s/m, $k_1 = 1 \times 10^6$ N/m, $m_2 = 4$ kg, $c_2 = 50$ N s/m, and $k_2 = 2 \times 10^6$ N/m. Note that proportional damping is not satisfied for this system ($[c] \neq \alpha[m] + \beta[k]$ for any combination of real α and β values). Substitution in Eq. 5.6 gives:

$$[A] = \begin{bmatrix} -\omega^2 \cdot 2 + i\omega \cdot 200 + 3 \times 10^6 & -i\omega \cdot 50 - 2 \times 10^6 \\ -i\omega \cdot 50 - 2 \times 10^6 & -\omega^2 \cdot 4 + i\omega \cdot 50 + 2 \times 10^6 \end{bmatrix}.$$

Computing the inverse of A for a frequency range between 0 and 2000 rad/s gives the four system FRFs. The direct FRF $\frac{X_1}{F_1}$ is shown in Fig. 5.4. Vibration modes are observed at 366 and 1365.5 rad/s for the two degree of freedom system; these are the natural frequencies. The cross FRF $\frac{X_1}{F_2}$ is displayed in Fig. 5.5. We see that the higher frequency mode is inverted; its motion is out of phase with the lower frequency mode. We also see that its magnitude is quite small relative to the lower frequency mode. To better view modes with very different magnitudes in a single plot, a semi-logarithmic representation is often used. In this case, the logarithmic vertical (magnitude) axis is plotted against the linear horizontal (frequency) axis. Figure 5.6 was produced using the MATLAB® command `semilogy`. To complete the story, the corresponding phase is provided in Fig. 5.7. Figures 5.4, 5.5, 5.6, and 5.7 were generated using MATLAB® MOJO 5.1.

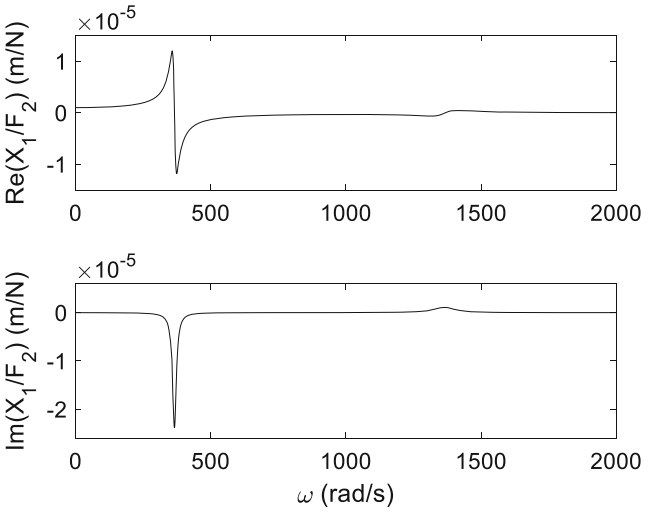

Fig. 5.5 *By the Numbers 5.1*—cross FRF $\frac{X_1}{F_2}$ for the example system

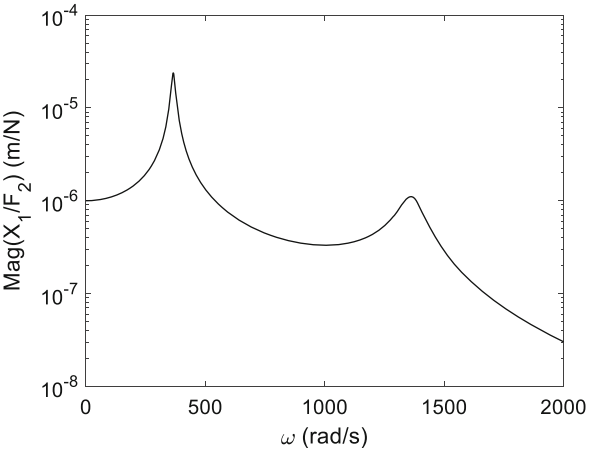

Fig. 5.6 *By the Numbers 5.1*—semi-logarithmic plot of the cross FRF $\frac{X_1}{F_2}$

MATLAB® MOJO 5.1

```
% matlab_mojo_5_1.m

clear
close all
clc

% Define variables
omega = 0:0.5:2000;     % frequency, rad/s
```

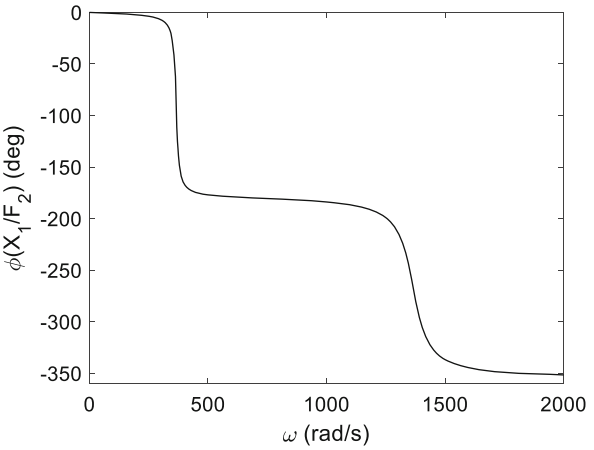

Fig. 5.7 *By the Numbers 5.1*—phase plot of the cross FRF $\frac{X_1}{F_2}$

```
% Define function
for cnt = 1:length(omega)
  w = omega(cnt);
  a11 = -w^2*2 + i*w*200 + 3e6;
  a12 = -i*w*50 - 2e6;
  a21 = a12;
  a22 = -w^2*4 + i*w*50 + 2e6;
  A = [a11 a12; a21 a22];
  inverted_A = inv(A);
  X1_F1(cnt) = inverted_A(1,1);
  X1_F2(cnt) = inverted_A(1,2);
  X2_F1(cnt) = inverted_A(2,1);
  X2_F2(cnt) = inverted_A(2,2);
end

figure(1)
subplot(211)
plot(omega, real(X1_F1), 'k-')
set(gca,'FontSize', 14)
ylabel('Re(X_1/F_1) (m/N)')
axis([0 2000 -1.5e-5 1.5e-5])
subplot(212)
plot(omega, imag(X1_F1), 'k-')
set(gca,'FontSize', 14)
xlabel('\omega (rad/s)')
ylabel('Im(X_1/F_1) (m/N)')
axis([0 2000 -2.6e-5 6e-6])

figure(2)
subplot(211)
plot(omega, real(X1_F2), 'k-')
set(gca,'FontSize', 14)
ylabel('Re(X_1/F_2) (m/N)')
axis([0 2000 -1.5e-5 1.5e-5])
subplot(212)
```

```
plot(omega, imag(X1_F2), 'k-')
set(gca,'FontSize', 14)
xlabel('\omega (rad/s)')
ylabel('Im(X_1/F_2) (m/N)')
axis([0 2000 -2.6e-5 6e-6])

figure(3)
semilogy(omega, abs(X1_F2), 'k-')
set(gca,'FontSize', 14)
xlabel('\omega (rad/s)')
ylabel('Mag(X_1/F_2) (m/N)')

figure(4)
plot(omega, unwrap(angle(X1_F2))*180/pi, 'k-')
set(gca,'FontSize', 14)
xlabel('\omega (rad/s)')
ylabel('\phi(X_1/F_2) (deg)')
ylim([-360 0])
```

5.3 Modal Analysis

Let's next solve the two degree of freedom forced vibration problem using the modal analysis approach. Recall that this method requires that proportional damping exists (or can be assumed). The analysis steps are similar to those we discussed for two degree of freedom free vibration in Sect. 4.4. For the chain-type, spring-mass-damper system shown in Fig. 5.8 we'll consider only $f_2(t)$ for now. We could also determine the response to $f_1(t)$ and add the results using linear superposition. The system equations of motion in matrix form are:

$$[m]\left\{\vec{\ddot{x}}\right\} + [c]\left\{\vec{\dot{x}}\right\} + [k]\left\{\vec{x}\right\} = \left\{\vec{F}\right\}e^{i\omega t}, \tag{5.15}$$

where $[m] = \begin{bmatrix} m_1 & 0 \\ 0 & m_2 \end{bmatrix}$, $[c] = \begin{bmatrix} c_1 + c_2 & -c_2 \\ -c_2 & c_2 \end{bmatrix}$, $[k] = \begin{bmatrix} k_1 + k_2 & -k_2 \\ -k_2 & k_2 \end{bmatrix}$, and $\left\{\vec{F}\right\} = \begin{Bmatrix} 0 \\ F_2 \end{Bmatrix}$. To determine the forced response, we complete the following steps.

In a Nutshell

Because the modal analysis technique is so powerful, we often assume that the damping is proportional even when it is not. In other situations, when we do not know the nature of the damping because a physical incarnation of our design does not exist, we often assume proportional damping during the analysis.

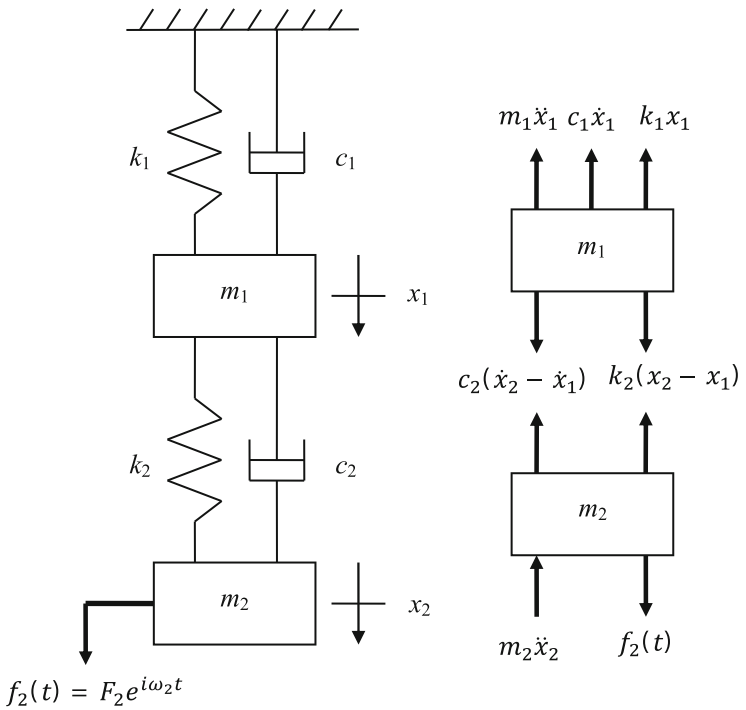

Fig. 5.8 Two degree of freedom system with $f_2(t)$ applied at x_2

1. Verify proportional damping using $[c] = \alpha[m] + \beta[k]$.
2. Ignore damping and the force to find the eigenvalues and eigenvectors.

$$\left[[m]s^2 + [k]\right]\begin{Bmatrix} X_1 \\ X_2 \end{Bmatrix} = \begin{Bmatrix} 0 \\ 0 \end{Bmatrix}, \text{where } \begin{Bmatrix} x_1 \\ x_2 \end{Bmatrix} = \begin{Bmatrix} X_1 \\ X_2 \end{Bmatrix} e^{st} \tag{5.16}$$

Obtain the eigenvalues from the characteristic equation:

$$\left|[m]s^2 + [k]\right| = 0. \tag{5.17}$$

For the two degree of freedom system, the two roots, s_1^2 and s_2^2, are the eigenvalues. These give the natural frequencies $s_1^2 = -\omega_{n1}^2$ and $s_2^2 = -\omega_{n2}^2$, where $\omega_{n1} < \omega_{n2}$. Use either equation of motion and normalize to X_2 (because the force is applied at this location). The eigenvectors are:

$$\psi_1 = \begin{Bmatrix} \left(\frac{X_1}{X_2}\right)_1 \\ 1 \end{Bmatrix} = \begin{Bmatrix} p_1 \\ 1 \end{Bmatrix} \text{ and } \psi_2 = \begin{Bmatrix} \left(\frac{X_1}{X_2}\right)_2 \\ 1 \end{Bmatrix} = \begin{Bmatrix} p_2 \\ 1 \end{Bmatrix}, \tag{5.18}$$

where ψ_1 is evaluated using $s^2 = s_1^2$ and ψ_2 is obtained using $s^2 = s_2^2$.

3. Construct the modal matrix using the eigenvectors.

$$[P] = [\psi_1 \ \ \psi_2] \tag{5.19}$$

Use the modal matrix to transform into modal coordinates and uncouple the equations of motion.

$$\left[m_q\right] = \begin{bmatrix} m_{q1} & 0 \\ 0 & m_{q2} \end{bmatrix} = [P]^T[m][P] \tag{5.20}$$

$$\left[c_q\right] = \begin{bmatrix} c_{q1} & 0 \\ 0 & c_{q2} \end{bmatrix} = [P]^T[c][P] \tag{5.21}$$

$$\left[k_q\right] = \begin{bmatrix} k_{q1} & 0 \\ 0 & k_{q2} \end{bmatrix} = [P]^T[k][P] \tag{5.22}$$

Transform the force vector from local to modal coordinates.

$$\left\{\overline{R}\right\} = \begin{Bmatrix} R_1 \\ R_2 \end{Bmatrix} = [P]^T\left[\overline{F}\right] = \begin{bmatrix} p_1 & p_2 \\ 1 & 1 \end{bmatrix}^T \begin{Bmatrix} 0 \\ F_2 \end{Bmatrix} = \begin{Bmatrix} F_2 \\ F_2 \end{Bmatrix} \tag{5.23}$$

In modal coordinates, the same force is applied to both single degree of freedom systems. Recall that modal coordinates may not make physical sense to us.

4. Write the FRFs for the two single degree of freedom systems in modal coordinates, Q_1 and Q_2. Note that Q_1 and Q_2 are the frequency-domain representations of the time-domain modal coordinates, q_1 and q_2, that we introduced in Sect. 4.4. For the first natural frequency, the FRF is:

$$\frac{Q_1}{R_1} = \frac{1}{k_{q1}}\left(\frac{\left(1 - r_1^2\right) - i\left(2\zeta_{q1}r_1\right)}{\left(1 - r_1^2\right)^2 + \left(2\zeta_{q1}r_1\right)^2}\right), \tag{5.24}$$

where $r_1 = \frac{\omega}{\omega_{n1}}$ and $\zeta_{q1} = \frac{c_{q1}}{2\sqrt{k_{q1}m_{q1}}}$. Plot the real and imaginary parts as shown in Fig. 5.9 and the magnitude and phase as displayed in Fig. 5.10.

For the second natural frequency, the FRF is:

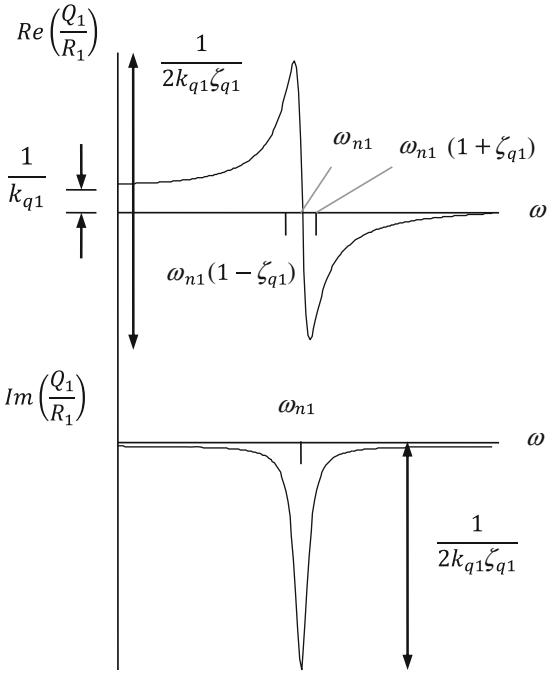

Fig. 5.9 Real and imaginary parts of $\frac{Q_1}{R_1}$ FRF (modal coordinates)

$$\frac{Q_2}{R_2} = \frac{1}{k_{q2}}\left(\frac{\left(1-r_2^2\right)-i\left(2\zeta_{q2}r_2\right)}{\left(1-r_2^2\right)^2+\left(2\zeta_{q2}r_2\right)^2}\right), \tag{5.25}$$

where $r_2 = \frac{\omega}{\omega_{n2}}$ and $\zeta_{q2} = \frac{c_{q2}}{2\sqrt{k_{q2}m_{q2}}}$. The plots are similar to Figs. 5.9 and 5.10.

5. Transform back to local coordinates using:

$$\left\{\vec{X}\right\} = [P]\left\{\vec{Q}\right\} = \begin{bmatrix} p_1 & p_2 \\ 1 & 1 \end{bmatrix}\begin{Bmatrix} Q_1 \\ Q_2 \end{Bmatrix}. \tag{5.26}$$

Using Eq. 5.26, we solve for X_1 and X_2.

$$X_1 = p_1Q_1 + p_2Q_2 \text{ and } X_2 = Q_1 + Q_2 \tag{5.27}$$

The direct FRF is:

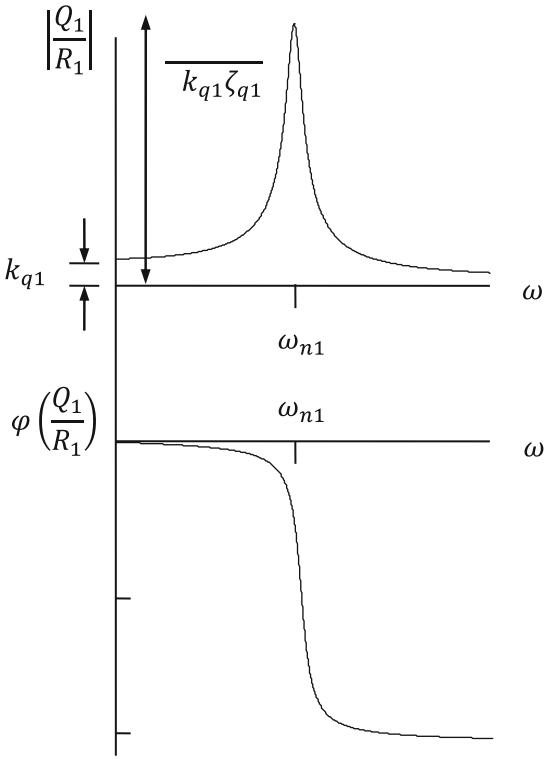

Fig. 5.10 Magnitude and phase of $\frac{Q_1}{R_1}$ FRF (modal coordinates)

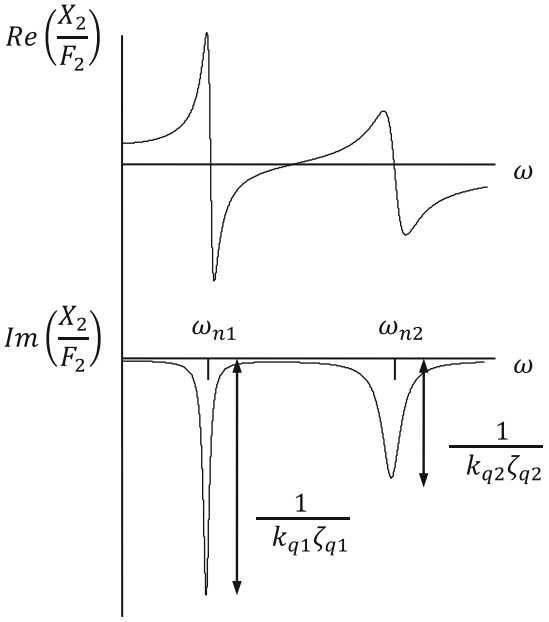

Fig. 5.11 Direct FRF $\frac{X_2}{F_2}$ (local coordinates)

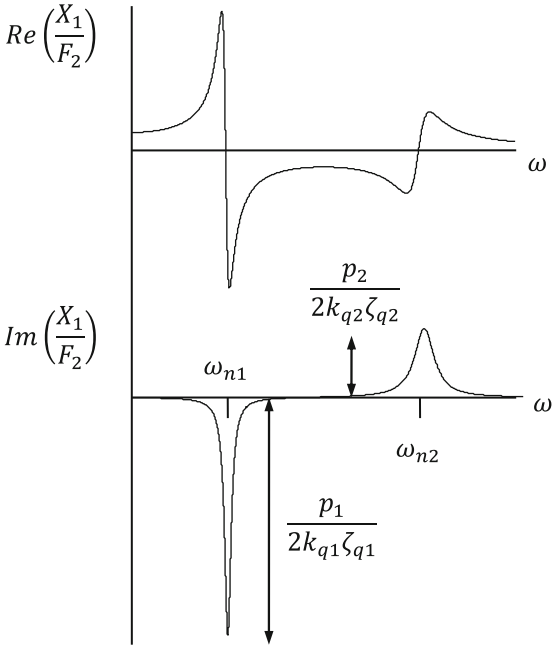

Fig. 5.12 Cross FRF $\frac{X_1}{F_2}$ (local coordinates)

Table 5.1 Modal analysis steps

Step	Action
1	Verify proportional damping.
2	Ignore damping and external force to find the eigenvalues and eigenvectors.
3	Construct the modal matrix using the eigenvectors.
4	Write the FRFs for the single degree of freedom systems in modal coordinates.
5	Transform back to local coordinates.

$$\frac{X_2}{F_2} = \frac{Q_1 + Q_2}{F_2} = \frac{Q_1}{R_1} + \frac{Q_2}{R_2} \tag{5.28}$$

because $R_1 = R_2 = F_2$. The direct FRF at the location where the mode shapes were normalized is the sum of the modal contributions. See Fig. 5.11. The cross FRF is:

$$\frac{X_1}{F_2} = \frac{p_1 Q_1 + p_2 Q_2}{F_2} = p_1 \frac{Q_1}{R_1} + p_2 \frac{Q_2}{R_2}. \tag{5.29}$$

The cross FRF is the sum of the modal contributions scaled by the eigenvectors. See Fig. 5.12.

The five fundamental steps for modal analysis are summarized in Table 5.1.

By the Numbers 5.2

Let's complete an example to demonstrate the steps we've just discussed. For the two degree of freedom model in Fig. 5.8, the parameters are $k_1 = 4 \times 10^5$ N/m, $c_1 = 80$ N s/m, $m_1 = 2$ kg, $k_2 = 6 \times 10^5$ N/m, $c_2 = 120$ N s/m, $m_2 = 1$ kg, and $f_2(t) = 100e^{i\omega t}$ N. The mass, damping, and stiffness matrices are:

$$[m] = \begin{bmatrix} m_1 & 0 \\ 0 & m_2 \end{bmatrix} = \begin{bmatrix} 2 & 0 \\ 0 & 1 \end{bmatrix} \text{ kg},$$

$$[c] = \begin{bmatrix} c_1 + c_2 & -c_2 \\ -c_2 & c_2 \end{bmatrix} = \begin{bmatrix} 200 & -120 \\ -120 & 120 \end{bmatrix} \text{N s/m, and}$$

$$[k] = \begin{bmatrix} k_1 + k_2 & -k_2 \\ -k_2 & k_2 \end{bmatrix} = \begin{bmatrix} 1 \times 10^6 & -6 \times 10^5 \\ -6 \times 10^5 & 6 \times 10^5 \end{bmatrix} \text{N/m}.$$

1. Verify proportional damping. The equality is true when $\alpha = 0$ and $\beta = \frac{1}{5000}$ so proportional damping holds.

$$\begin{bmatrix} 200 & -120 \\ -120 & 120 \end{bmatrix} = \alpha \begin{bmatrix} 2 & 0 \\ 0 & 1 \end{bmatrix} + \beta \begin{bmatrix} 1 \times 10^6 & -6 \times 10^5 \\ -6 \times 10^5 & 6 \times 10^5 \end{bmatrix}$$

2. Ignore damping and the force to find the eigenvalues and eigenvectors.

$$\left[\begin{bmatrix} 2 & 0 \\ 0 & 1 \end{bmatrix} s^2 + \begin{bmatrix} 1 \times 10^6 & -6 \times 10^5 \\ -6 \times 10^5 & 6 \times 10^5 \end{bmatrix} \right] \begin{Bmatrix} X_1 \\ X_2 \end{Bmatrix} = \begin{Bmatrix} 0 \\ 0 \end{Bmatrix}$$

Obtain the eigenvalues from the characteristic equation:

$$\begin{vmatrix} 2s^2 + 1 \times 10^6 & -6 \times 10^5 \\ -6 \times 10^5 & 1s^2 + 6 \times 10^5 \end{vmatrix} = 0, \text{ or}$$

$$\left(2s^2 + 1 \times 10^6\right)\left(1s^2 + 6 \times 10^5\right) - \left(-6 \times 10^5\right)^2$$
$$= 2s^4 + 2.2 \times 10^6 s^2 + 2.4 \times 10^{11} = 0.$$

The roots are $s_1^2 = -122799.81 = -\omega_{n1}^2$ and $s_2^2 = -977200.19 = -\omega_{n2}^2$. The natural frequencies are $\omega_{n1} = 350.43$ rad/s and $\omega_{n2} = 988.53$ rad/s. Alternately, $f_{n1} = 55.77$ Hz and $f_{n2} = 157.33$ Hz. The top equation of motion from the matrix format is $(2s^2 + 1 \times 10^6)X_1 - 6 \times 10^5 X_2 = 0$. In order to normalize the eigenvectors to x_2 (the force location), the required ratio is:

$$\frac{X_1}{X_2} = \frac{6 \times 10^5}{2s^2 + 1 \times 10^6}.$$

Substituting $s_1^2 = -122799.81$ gives the first eigenvector.

$$\psi_1 = \left\{ \begin{array}{c} \left(\dfrac{6 \times 10^5}{2(-122799.81) + 1 \times 10^6} \right) \\ 1 \end{array} \right\} = \left\{ \begin{array}{c} 0.795 \\ 1 \end{array} \right\}$$

Substituting $s_2^2 = -977200.19$ gives the second eigenvector.

$$\psi_2 = \left\{ \begin{array}{c} \left(\dfrac{6 \times 10^5}{2(-977200.19) + 1 \times 10^6} \right) \\ 1 \end{array} \right\} = \left\{ \begin{array}{c} -0.629 \\ 1 \end{array} \right\}$$

3. Construct the modal matrix using the eigenvectors.

$$[P] = \begin{bmatrix} 0.795 & -0.629 \\ 1 & 1 \end{bmatrix}$$

Use the modal matrix to transform into modal coordinates and uncouple the equations of motion.

$$\left[m_q\right] = [P]^T[m][P] = \begin{bmatrix} 2.264 & 0 \\ 0 & 1.791 \end{bmatrix} \text{kg}$$

$$\left[c_q\right] = [P]^T[c][P] = \begin{bmatrix} 55.605 & 0 \\ 0 & 350.088 \end{bmatrix} \text{N s/m}$$

$$\left[k_q\right] = [P]^T[k][P] = \begin{bmatrix} 2.780 \times 10^5 & 0 \\ 0 & 1.750 \times 10^6 \end{bmatrix} \text{N/m}$$

Transform the force vector from local to modal coordinates.

$$\left\{\vec{R}\right\} = \left\{ \begin{array}{c} R_1 \\ R_2 \end{array} \right\} = [P]^T\left[\vec{F}\right] = \begin{bmatrix} 0.795 & -0.629 \\ 1 & 1 \end{bmatrix}^T \left\{ \begin{array}{c} 0 \\ 100 \end{array} \right\} = \left\{ \begin{array}{c} 100 \\ 100 \end{array} \right\} \text{N}$$

4. Write the FRFs for the two single degree of freedom systems in modal coordinates. For the first natural frequency, the FRF is:

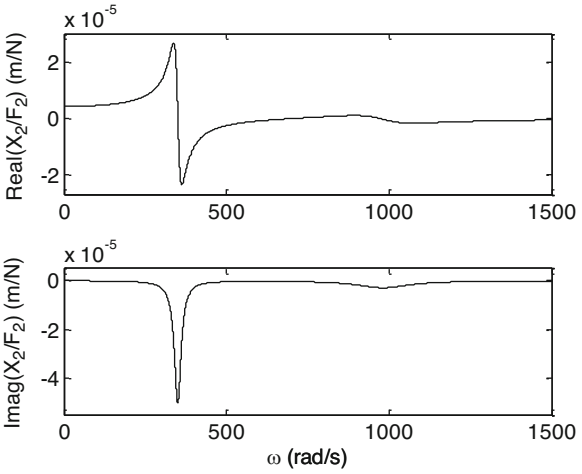

Fig. 5.13 *By the Numbers 5.2*—direct FRF $\frac{X_2}{F_2}$ (local coordinates)

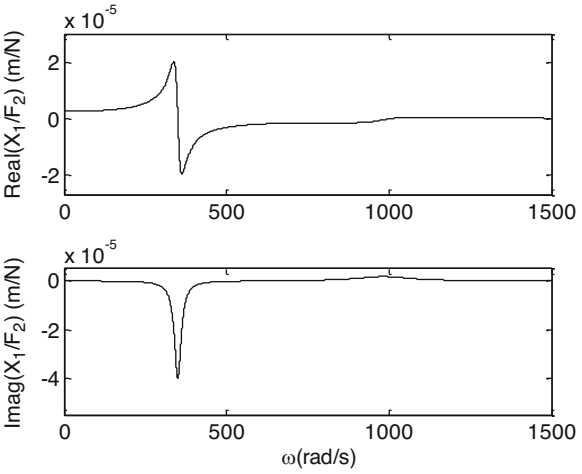

Fig. 5.14 *By the Numbers 5.2*—cross FRF $\frac{X_1}{F_2}$ (local coordinates)

$$\frac{Q_1}{R_1} = \frac{1}{2.780 \times 10^5}\left(\frac{\left(1-r_1^2\right) - i(2(0.0358)r_1)}{\left(1-r_1^2\right)^2 + (2(0.0358)r_1)^2}\right),$$

where $r_1 = \frac{\omega}{350.43}$ and the damping ratio is $\zeta_{q1} = \frac{55.605}{2\sqrt{2.780\times10^5(2.264)}} = 0.0358$. For the second natural frequency, the FRF is:

$$\frac{Q_2}{R_2} = \frac{1}{1.750 \times 10^6}\left(\frac{\left(1 - r_2^2\right) - i(2(0.0989)r_2)}{\left(1 - r_2^2\right)^2 + (2(0.0989)r_2)^2}\right),$$

where $r_2 = \frac{\omega}{988.53}$ and $\zeta_{q2} = \frac{350.088}{2\sqrt{1.750 \times 10^6 (1.791)}} = 0.0989$.

5. Transform back to local coordinates. The direct FRF, $\frac{X_2}{F_2} = \frac{Q_1}{R_1} + \frac{Q_2}{R_2}$, is plotted in Fig. 5.13. The cross FRF, $\frac{X_1}{F_2} = p_1 \frac{Q_1}{R_1} + p_2 \frac{Q_2}{R_2}$, is plotted in Fig. 5.14.

   In Figs. 5.13 and 5.14, the value of the real part at zero frequency ($\omega = 0$) represents the DC compliance (i.e., the inverse of stiffness). For the direct FRF in Fig. 5.13, the value is:

$$\text{Re}\left(\frac{X_2}{F_2}\right)\Big|_{\omega=0} = \frac{1}{k_{q1}} + \frac{1}{k_{q2}} = 4.169 \times 10^{-6} \text{ m/N}. \tag{5.30}$$

   This indicates that the modal stiffness for each mode is added in series to give the local stiffness for the model. For the cross FRF in Fig. 5.14, the DC compliance is:

$$\text{Re}\left(\frac{X_1}{F_2}\right)\Big|_{\omega=0} = \frac{p_1}{k_{q1}} + \frac{p_2}{k_{q2}} = 2.500 \times 10^{-6} \text{ m/N}. \tag{5.31}$$

   Again, the modal stiffness values are added in series, but each is scaled by the appropriate eigenvector. Given the force magnitude F_2, we could use Eqs. 5.30 and 5.31 to determine the real-valued deflections, X_1 and X_2, due to the DC (non-oscillating) force. At any non-zero forcing frequency, the responses are complex-valued and describe the steady-state forced vibration; see Figs. 5.13 and 5.14.

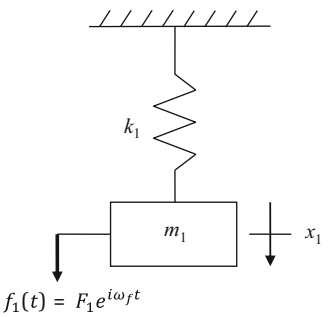

Fig. 5.15 Single degree of freedom, undamped system with the harmonic force $f_1(t) = F_1 e^{i\omega_f t}$ which causes excessive vibration at coordinate x_1

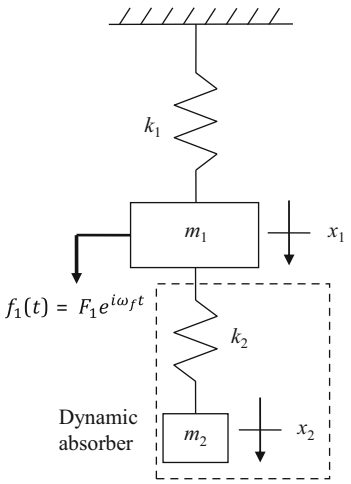

Fig. 5.16 The addition of the dynamic absorber gives a new two degree of freedom system

5.4 Dynamic Absorber

Let's now investigate a special application of complex matrix inversion. Consider the undamped single degree of freedom system subject to forced vibration shown in Fig. 5.15. Let's assume that the magnitude X_1 due to the harmonic force $f_1(t) = F_1 e^{i\omega_f t}$ is too large and causes, for example, mechanical failure, passenger discomfort, manufacturing errors, etc. In order to eliminate this problem, we would like X_1 to ideally be zero at the forcing frequency ω_f. In other words, the magnitude of motion at coordinate x_1 is zero when the system is forced at the frequency ω_f. This result is expressed in Eq. 5.32.

$$\frac{X_1}{F_1} = 0 \text{ at } \omega = \omega_f \tag{5.32}$$

Let's add a second degree of freedom to the system and see what happens. See Fig. 5.16, where the system model is now:

$$\left[-\omega^2 \begin{bmatrix} m_1 & 0 \\ 0 & m_2 \end{bmatrix} + \begin{bmatrix} k_1 + k_2 & -k_2 \\ -k_2 & k_2 \end{bmatrix}\right] \begin{Bmatrix} X_1 \\ X_2 \end{Bmatrix} e^{i\omega_f t} = \begin{Bmatrix} F_1 \\ 0 \end{Bmatrix} e^{i\omega_f t}. \tag{5.33}$$

Equation 5.33 can be more compactly expressed as $[A]\left\{\vec{X}\right\} = \left\{\vec{F}\right\}$. As we saw in Sect. 5.2, we can use complex matrix inversion to determine the system FRFs.

Similar to Eq. 5.8, the direct FRF at coordinate x_1 for the new two degree of freedom system is:

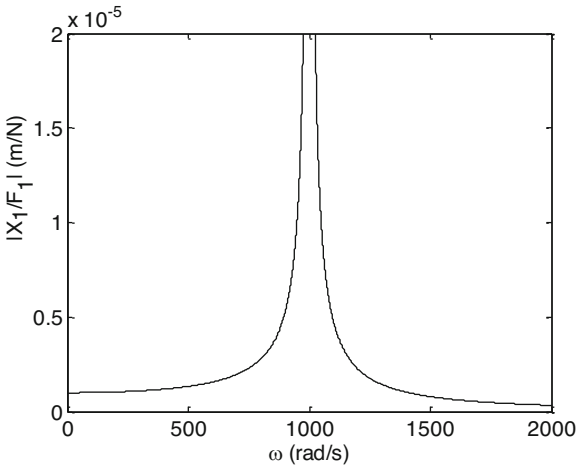

Fig. 5.17 Direct FRF for the original single degree of freedom system

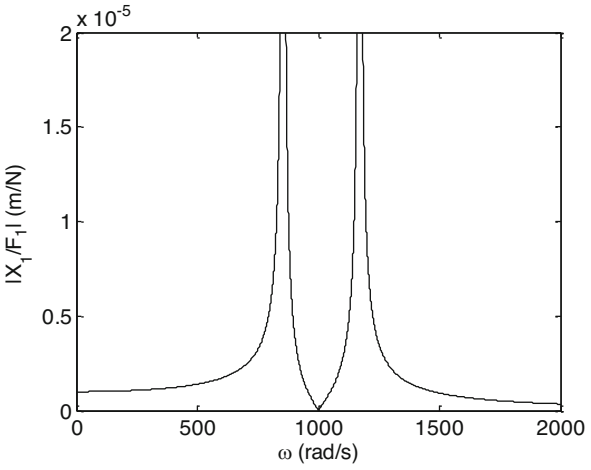

Fig. 5.18 Direct FRF $\frac{X_1}{F_1}$ for the new two degree of freedom system

$$\alpha_{11} = \frac{X_1}{F_1} = \frac{-\omega_f^2 m_2 + k_2}{\left(-\omega_f^2 m_1 + k_1 + k_2\right)\left(-\omega_f^2 m_2 + k_2\right) - \left(-k_2\right)^2}. \tag{5.34}$$

We want this FRF to be zero, so it is required that $-\omega_f^2 m_2 + k_2 = 0$ or:

$$\omega_f = \sqrt{\frac{k_2}{m_2}}. \tag{5.35}$$

When the k_2 and m_2 values for the added spring and mass, together known as a **dynamic absorber,** are selected by applying this design rule, the response at x_1 is

zero, even though $f_1(t) = F_1 e^{i\omega_f t}$ remains. Let's sketch the magnitude plots for the original and new systems. Figure 5.17 shows the original single degree of freedom FRF magnitude with $m_1 = 1$ kg and $k_1 = 1 \times 10^6$ N/m. We see that the response is infinite at resonance in the absence of damping. For this example, we'll assume that the forcing frequency is equal to the natural frequency, $\omega_f = \sqrt{\frac{k_1}{m_1}} = 1000$ rad/s. Clearly, the response would be too large in this case! In Fig. 5.18, the new direct FRF $\frac{X_1}{F_1}$ is shown, where m_2 was selected to be 0.1 kg and the corresponding spring stiffness was $k_2 = \omega_f^2 \cdot m_2 = 1 \times 10^5$ N/m according to Eq. 5.35. The new two degree of freedom system naturally has two modes (and natural frequencies), but the response is zero at $\omega = \omega_f$.

We have now eliminated the vibration at x_1 due to the force f_1 with a frequency of ω_f. What about the motion of the added mass? To answer this question we need the cross FRF $\frac{X_2}{F_1}$. Similar to Eq. 5.10 we have:

$$\alpha_{21} = \frac{X_2}{F_1} = \frac{k_2}{\left(-\omega_f^2 m_1 + k_1 + k_2\right)\left(-\omega_f^2 m_2 + k_2\right) - (-k_2)^2}. \tag{5.36}$$

Expanding the denominator gives:

$$\alpha_{21} = \frac{X_2}{F_1} = \frac{k_2}{m_1 m_2 \omega_f^4 - k_2 m_1 \omega_f^2 - (k_1 + k_2) m_2 \omega_f^2 + k_1 k_2 + k_2^2 - k_2^2}. \tag{5.37}$$

According to the dynamic absorber design rule, $\omega_f^2 = \frac{k_2}{m_2}$. Substituting yields:

$$\alpha_{21} = \frac{X_2}{F_1} = \frac{k_2}{m_1 m_2 \frac{k_2^2}{m_2^2} - k_2 m_1 \frac{k_2}{m_2} - k_1 m_2 \frac{k_2}{m_2} - k_2 m_2 \frac{k_2}{m_2} + k_1 k_2}. \tag{5.38}$$

Simplifying gives:

$$\alpha_{21} = \frac{X_2}{F_1} = \frac{k_2}{\frac{m_1}{m_2} k_2^2 - \frac{m_1}{m_2} k_2^2 - k_1 k_2 - k_2^2 + k_1 k_2} = \frac{k_2}{-k_2^2} = -\frac{1}{k_2}. \tag{5.39}$$

Equation 5.39 can be rewritten as $X_2 = -\frac{F_1}{k_2}$. This tells us that the motion of x_2 is 180° out of phase with x_1. The role of the added spring and mass, therefore, is for its inertial force to counteract the external force at x_1 and cause the vibration to be zero—hence the name, dynamic absorber. It effectively absorbs the external force's energy at ω_f. Equation 5.22 also shows that a stiffer dynamic absorber spring decreases the magnitude of the x_2 vibration. While we may want k_2 to be larger to keep $\frac{X_2}{F_1}$ smaller, we must also satisfy $\omega_f^2 = \frac{k_2}{m_2}$. A larger k_2 means a proportionally larger m_2 and there is typically a practical limit on how much mass can be added as the dynamic absorber.

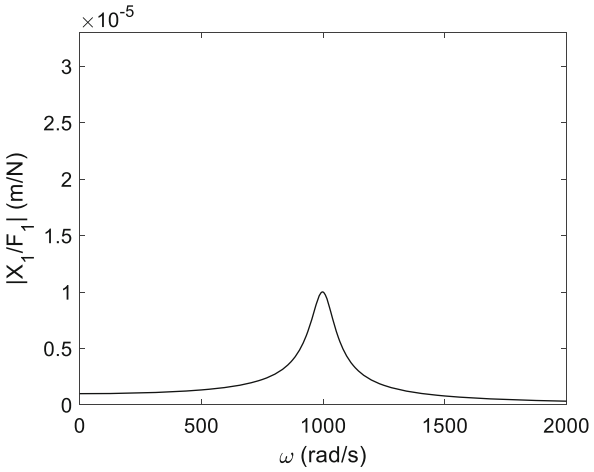

Fig. 5.19 *By the Numbers 5.3*—FRF for the original single degree of freedom damped system

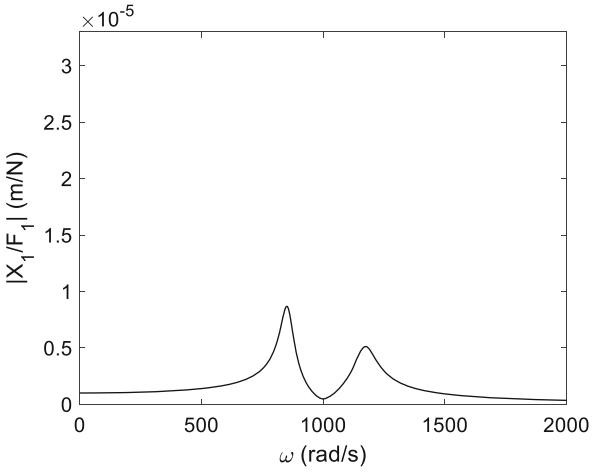

Fig. 5.20 *By the Numbers 5.3*—direct FRF $\frac{X_1}{F_1}$ for the two degree of freedom system with the dynamic absorber added

In a Nutshell

The dynamic absorber is a valuable tool. If we encounter a forced vibration that is too large, we can eliminate it by adding a new spring and mass, which alone would have a natural frequency that matches the forcing frequency. The added mass will move, but the motion of the attachment point will be dramatically reduced. Dynamic absorbers are found, for example, in automobile transmissions, at the top of skyscrapers, on power lines, and in machine tools.

To conclude this section, we should recognize that all systems include some level of damping. We can conveniently analyze the damped system response using

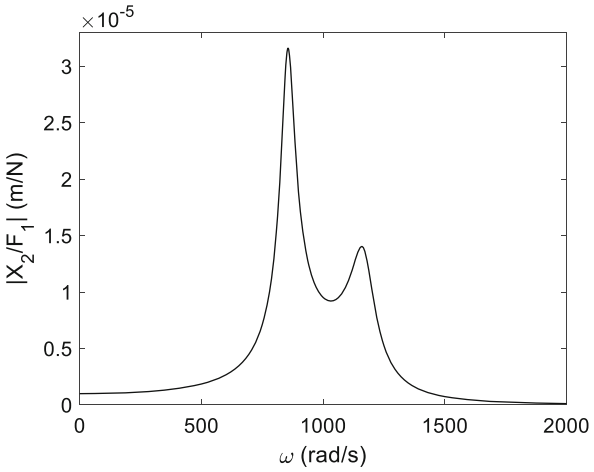

Fig. 5.21 *By the Numbers 5.3*—cross FRF $\frac{X_2}{F_1}$ for the two degree of freedom system with the dynamic absorber added

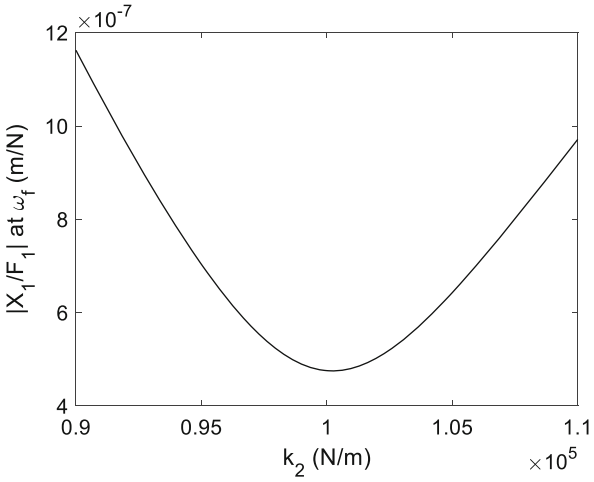

Fig. 5.22 *By the Numbers 5.3*—variation in $\frac{X_1}{F_1}$ magnitude at ω_f for a range of k_2 values near the initial guess

Eqs. 5.8 and 5.10. Given the base system (Fig. 5.15) description, we could tune the dynamic absorber stiffness (assuming its mass was pre-selected) to minimize the response at the forcing frequency. The design rule provided in Eq. 5.35 still provides a reasonable starting point.

By the Numbers 5.3

Let's again consider the Fig. 5.15 system with $m_1 = 1$ kg and $k_1 = 1 \times 10^6$ N/m, but now add the damper $c_1 = 100$ N s/m. This gives a single degree of freedom damping ratio of $\zeta_1 = \frac{c_1}{2\sqrt{k_1 m_1}} = \frac{100}{2\sqrt{1\times10^6(1)}} = 0.05 = 5\,\%$. The FRF is shown in Fig. 5.19, where the damped natural frequency, ω_d, is 998.75 rad/s. We'll specify a forcing function of $f_1(t) = 100e^{i\omega_d t}$ N. If the absorber mass, m_2, is 0.1 kg, then an initial

guess for the absorber spring stiffness is $k_2 = \omega_d^2 \cdot m_2 = 9.975 \times 10^4$ N/m. We'll assume the absorber damping coefficient is $c_2 = 5$ N s/m. The corresponding two degree of freedom system direct FRF $\frac{X_1}{F_1}$ is provided in Fig. 5.20. Its value at the forcing frequency, ω_d, is 4.7565×10^{-7} m/N. The vibration magnitude at x_1 is therefore $X_1 = 4.7565 \times 10^{-7} \cdot 100 = 4.7565 \times 10^{-5}$ m ≈ 48 μm for the 100 N magnitude force. This is quite an improvement over the original single degree of freedom response of $X_1 = 1 \times 10^{-5} \cdot 100 = 1 \times 10^{-3}$ m $= 1$ mm. The cross FRF $\frac{X_2}{F_1}$ for the absorber response is shown in Fig. 5.21. The magnitude at the forcing frequency is $X_2 = 9.5249 \times 10^{-6} \cdot 100 = 9.5249 \times 10^{-4}$ m ≈ 0.952 mm.

While this result is already pretty good, perhaps we can reduce the response at x_1 by adjusting k_2. Figure 5.22 shows the value of $\frac{X_1}{F_1}$ at $\omega = \omega_f$ for the two degree of freedom system as a function of the modified k_2 value. We see that the minimum is obtained when $k_2 = 1.0025 \times 10^5$ N/m. The vibration magnitude for this optimum stiffness is $X_1 = 4.7517 \times 10^{-7} \cdot 100 = 4.7517 \times 10^{-5}$ m, which is again approximately 48 μm. The code used to produce Figs. 5.19, 5.20, 5.21 and 5.22 is provided in MATLAB® MOJO 5.2.

MATLAB® MOJO 5.2

```
% matlab_mojo_5_2.m

clear
close all
clc

% Define variables
omega = 0:0.25:2000;   % rad/s
m1 = 1;          % kg
k1 = 1e6;         % N/m
c1 = 100;         % N s/m
wn1 = sqrt(k1/m1);    % rad/s
zeta1 = 0.05;

% Define function
r = omega/wn1;
mag1 = 1/k1*(1./((1-r.^2).^2 + (2*zeta1*r).^2)).^0.5;

figure(1)
plot(omega, mag1, 'k-')
set(gca,'FontSize', 14)
xlabel('\omega (rad/s)')
ylabel('|X_1/F_1| (m/N)')
axis([0 2000 0 3.3e-5])

index = find(omega == wn1);
mag_original = abs(mag1(index))
```

```
% Dynamic absorber
m2 = 0.1;
wf = wn1;
k2 = wf^2*m2;
c2 = 5;

for cnt = 1:length(omega)
  w = omega(cnt);
  a11 = -w^2*m1 + 1i*w*(c1 + c2) + k1 + k2;
  a12 = -1i*w*c2 - k2;
  a21 = a12;
  a22 = -w^2*m2 + 1i*w*c2 + k2;
  A = [a11 a12; a21 a22];
  inverted_A = inv(A);
  X1_F1(cnt) = inverted_A(1,1);
  X1_F2(cnt) = inverted_A(1,2);
  X2_F1(cnt) = inverted_A(2,1);
  X2_F2(cnt) = inverted_A(2,2);
end

figure(2)
plot(omega, abs(X1_F1), 'k-')
set(gca,'FontSize', 14)
xlabel('\omega (rad/s)')
ylabel('|X_1/F_1| (m/N)')
axis([0 2000 0 3.3e-5])

index = find(omega == wf);
mag_direct = abs(X1_F1(index))
mag_cross = abs(X2_F1(index))

figure(3)
plot(omega, abs(X2_F1), 'k-')
set(gca,'FontSize', 14)
xlabel('\omega (rad/s)')
ylabel('|X_2/F_1| (m/N)')
axis([0 2000 0 3.3e-5])

clear X1_F1

k2_test = 0.9*k2:50:1.1*k2;
for cnt = 1:length(k2_test)
  w = wf;
  k2 = k2_test(cnt);
  a11 = -w^2*m1 + 1i*w*(c1 + c2) + k1 + k2;
  a12 = -1i*w*c2 - k2;
  a21 = a12;
  a22 = -w^2*m2 + 1i*w*c2 + k2;
  A = [a11 a12; a21 a22];
  inverted_A = inv(A);
  X1_F1(cnt) = inverted_A(1,1);
end
```

```
figure(4)
plot(k2_test, abs(X1_F1), 'k-')
set(gca,'FontSize', 14)
xlabel('k_2 (N/m)')
ylabel('|X_1/F_1| at \omega_f (m/N)')
xlim([min(k2_test) max(k2_test)])

index = find(X1_F1 == min(X1_F1));
k2_test(index)
abs(X1_F1(index))
```

Chapter Summary

- Superposition enables the linear system response to each external force to be calculated individually and the results summed to find the overall response.
- Complex matrix inversion can be used to determine the forced response for systems with two (or more) degrees of freedom. While this approach is more computationally expensive than modal analysis, it does not require proportional damping.
- For a direct FRF the response is measured at the same location where the force is applied.
- For a cross FRF the response is measured at a different location than where the force is applied.
- Pairs of cross FRFs with the displacement and force subscripts switched, such as $\frac{X_1}{F_2}$ and $\frac{X_2}{F_1}$, are equal. This is referred to as reciprocity.
- A dynamic absorber may be added to a system to attenuate the original system response at a particular frequency. The dynamic absorber may be realized using a simple spring-mass-damper. The natural frequency of the dynamic absorber is matched to the frequency of interest.

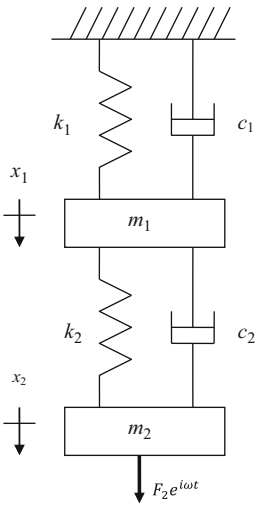

Fig. P5.1 Two degree of freedom spring-mass-damper system under forced vibration

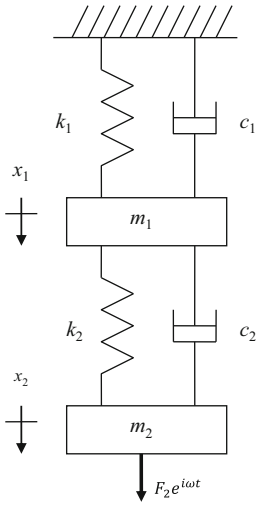

Fig. P5.2 Two degree of freedom spring-mass-damper system under forced vibration

- In modal analysis, the coupled differential equations of motion are uncoupled using the modal matrix, which is composed of the system eigenvectors. Modal analysis requires proportional damping.
- In modal analysis, the direct FRF in local coordinates is the sum of the single degree of freedom FRFs in modal coordinates. The cross FRF is the sum of the modal FRFs scaled by the eigenvectors.

Exercises

1. A two degree of freedom spring-mass-damper system is shown Fig. P5.1. For harmonic forced vibration (due to the external force at coordinate x_2), complete the following if $k_1 = 2 \times 10^5$ N/m, $c_1 = 60$ N s/m, $m_1 = 2.5$ kg, $k_2 = 5.5 \times 10^4$ N/m, $c_2 = 16.5$ N s/m, and $m_2 = 1.2$ kg.
   (a) Verify that proportional damping exists.
   (b) Define the modal matrix and determine the modal mass, stiffness, and damping matrices. Note that the mode shapes should be normalized to the force location.
   (c) Write expressions for the uncoupled single degree of freedom FRFs in modal coordinates, $\frac{Q_1}{R_1}$ and $\frac{Q_2}{R_2}$, and the direct FRF in local coordinates, $\frac{X_2}{F_2}$.
   (d) Plot the real and imaginary parts of the direct FRF, $\frac{X_2}{F_2}$. Units should be m/N for the vertical axis and rad/s for the horizontal (frequency) axis. Use a frequency range of `omega = 0:0.01:500;` (rad/s).

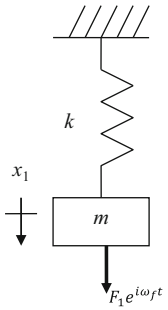

Fig. P5.3 Single degree of freedom system excited by the harmonic forcing function $F_1 e^{i\omega_f t}$

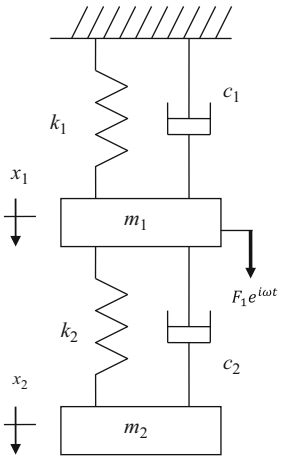

Fig. P5.4 Two degree of freedom spring-mass-damper system under forced vibration

2. A two degree of freedom spring-mass-damper system is shown in Fig. P5.2. For harmonic forced vibration (due to the external force applied at coordinate x_2), complete the following if $k_1 = 8 \times 10^7$ N/m, $c_1 = 1000$ N s/m, $m_1 = 50$ kg, $k_2 = 5 \times 10^7$ N/m, $c_2 = 500$ N s/m, and $m_2 = 12$ kg.

   (a) Show that proportional damping does not exist.
   (b) Write a symbolic expression for the direct FRF $\frac{X_2}{F_2}$ as a function of the frequency, ω, and mass, stiffness, and damping values, $m_{1,2}$, $k_{1,2}$, and $c_{1,2}$. Use the complex matrix inversion approach.
   (c) Write a symbolic expression for the cross FRF $\frac{X_1}{F_2}$ as a function of the frequency, ω, and mass, stiffness, and damping values, $m_{1,2}$, $k_{1,2}$, and $c_{1,2}$. Use the complex matrix inversion approach.
   (d) Plot the real and imaginary parts of the cross FRF, $\frac{X_1}{F_2}$. Units should be m/N for the vertical axis and rad/s for the horizontal (frequency) axis. Use a frequency range of `omega = 0:0.01:3500;` (rad/s).

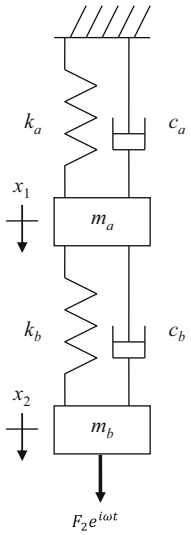

Fig. P5.5 Two degree of freedom spring-mass-damper system under forced vibration

3. Consider the single degree of freedom freedom spring-mass system shown in Fig. P5.3, where $k = 4 \times 10^5$ N/m and $m = 8$ kg. It is being excited by a harmonic forcing function, $F_1 e^{i\omega_f t}$, at a frequency, ω_f.
   (a) If the excitation frequency is 200 rad/s, design a dynamic absorber to eliminate the vibration at coordinate x_1. The only available spring for use in the absorber is identical to the one already used in the system.
   (b) If the 4×10^5 N/m absorber spring is used in conjunction with a 2 kg absorber mass, at what forced excitation frequency (in rad/s) will the steady-state vibration of coordinate x_1 be eliminated?

4. A two degree of freedom spring-mass-damper system is shown in Fig. P5.4. For harmonic forced vibration (due to the external force at coordinate x_1), complete the following if $k_1 = 2 \times 10^5$ N/m, $c_1 = 60$ N s/m, $m_1 = 2.5$ kg, $k_2 = 5.5 \times 10^4$ N/m, $c_2 = 16.5$ N s/m, and $m_2 = 1.2$ kg.
   (a) Verify that proportional damping exists.
   (b) Define the modal matrix and determine the modal mass, stiffness, and damping matrices. Note that the mode shapes should be normalized to the force location.
   (c) Write expressions for the uncoupled single degree of freedom FRFs in modal coordinates, $\frac{Q_1}{R_1}$ and $\frac{Q_2}{R_2}$, and the direct FRF in local coordinates, $\frac{X_1}{F_1}$.
   (d) Plot the real and imaginary parts of the direct FRF, $\frac{X_1}{F_1}$. Units should be m/N for the vertical axis and rad/s for the horizontal (frequency) axis. Use a frequency range of `omega = 0:0.1:500;` (rad/s).

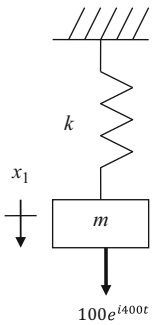

Fig. P5.6 Single degree of freedom system excited by the harmonic forcing function $100e^{i400t}$

5. For the two degree of freedom spring-mass-damper system shown in Fig. P5.5, complete the following if $k_a = 2 \times 10^5$ N/m, $k_b = 5.5 \times 10^4$ N/m, $c_a = 60$ N s/m, $c_b = 16.5$ N s/m, $m_a = 2.5$ kg, and $m_b = 1.2$ kg.
   (a) Obtain the equations of motion in matrix form and transform them into modal coordinates q_1 and q_2. Normalize your eigenvectors to the force location, coordinate x_2. Verify that proportional damping exists.
   (b) Determine the FRFs $\frac{Q_1}{R_1}$, $\frac{Q_2}{R_2}$, and $\frac{X_2}{F_2}$. Express them in equation form and then plot the real and imaginary parts (in m/N) vs. frequency (in rad/s). Use a frequency range of `0:0.1:600;` (rad/s).
6. A dynamic absorber is to be designed to eliminate the vibration at coordinate x_1 for the system shown in Fig. P5.6, where the excitation frequency is 400 rad/s and the force magnitude is 100 N. For the given system constants, determine the values of the mass and spring constant for the dynamic absorber if the magnitude of vibration for the absorber mass is 5 mm.
7. Given the modal mass matrix, $m_q = \begin{bmatrix} 2 & 0 \\ 0 & 2 \end{bmatrix}$ kg, the modal stiffness matrix, $k_q = \begin{bmatrix} 5.858 \times 10^6 & 0 \\ 0 & 3.414 \times 10^7 \end{bmatrix}$ N/m, the modal matrix, $[P] = \begin{bmatrix} 0.707 & -0.707 \\ 1 & 1 \end{bmatrix}$, and the modal damping ratios, $\zeta_{q1} = 0.04$ and $\zeta_{q2} = 0.02$, complete the following.
   (a) Plot the imaginary part (m/N) of the direct FRF $\frac{X_2}{F_2}$. Use a frequency range of `0:0.1:5000;` (rad/s).

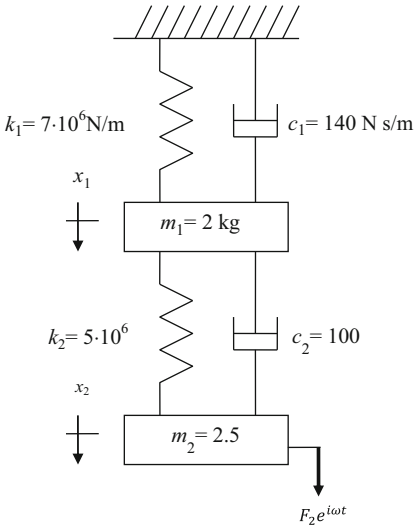

Fig. P5.9 Two degree of freedom spring-mass-damper system under forced vibration

(b) Plot the imaginary part (in m/N) of the cross FRF $\frac{X_1}{F_2}$. Use a frequency range of `0:0.1:5000;` (rad/s).

8. After installation, it was found that a particular machine exhibited excessive vibration due to a harmonic excitation force with a frequency of 100 Hz. A dynamic absorber was designed and added to the original system to attenuate this vibration. If the resulting vibration magnitude of the absorber mass was 2 mm at 100 Hz and the excitation force magnitude was 25 N, determine the stiffness of the spring (N/m) and mass (kg) used to construct the absorber. You may neglect damping in your analysis.
9. Given the eigenvalues and eigenvectors for the two degree of freedom system shown in Fig. P5.9, complete the following.

$$s_1{}^2 = -1 \times 10^6 \text{rad/s}^2 \quad s_2{}^2 = -7 \times 10^6 \text{rad/s}^2$$

$$\psi_1 = \begin{Bmatrix} 0.5 \\ 1 \end{Bmatrix} \quad \psi_2 = \begin{Bmatrix} -2.5 \\ 1 \end{Bmatrix}$$

(a) Determine the modal matrices m_q (kg), c_q (N s/m), and k_q (N/m).
(b) Plot the imaginary part (in m/N) of the cross frequency response function, $\frac{X_1}{F_2}$. Use a frequency range of `0:0.1:3500;` (rad/s).

10. Given the eigenvalues and eigenvectors for the two degree of freedom system shown in Fig. P5.9, determine the DC (zero frequency) compliance for the real part of the direct FRF $\frac{X_2}{F_2}$.

Chapter 6
Model Development by Modal Analysis

Il n'est pas certain que tout soit incertain.
(It is not certain that everything is uncertain.)
—*Blaise Pascal*

6.1 The Backward Problem

In Chaps. 1–5, we assumed a model and then used that model to determine the system response in the time or frequency domain (or both). More often, however, we have an actual dynamic system and would like to build a model that we can use to represent its vibratory behavior in response to some external excitation. For example, in milling operations, the flexibility of the cutting tool-holder-spindle-machine structure (and sometimes the workpiece) determines the limiting axial depth of cut to avoid chatter, a self-excited vibration [1]. In this case, the dynamic response at the free end of the tool (and/or at the cutting location on the workpiece) is measured. Using this measured response, a model in the form of modal parameters can be developed for use in a time-domain simulation[1] of the milling process. How can we work this "backward problem" of starting with a measurement and developing a model? To begin, we need to determine the modal mass, stiffness, and damping values from the measured frequency response function (FRF).

6.2 Peak Picking

6.2.1 Single Degree of Freedom

After performing a measurement to determine the FRF for a physical structure (see Chap. 7), we can use **peak picking** to estimate the modal parameters from the real

[1] In time-domain, or time-marching, simulation, the equations of motion that describe the process behavior are solved at small increments in time using numerical integration [1].

T. L. Schmitz, K. S. Smith, *Mechanical Vibrations*,
https://doi.org/10.1007/978-3-030-52344-2_6

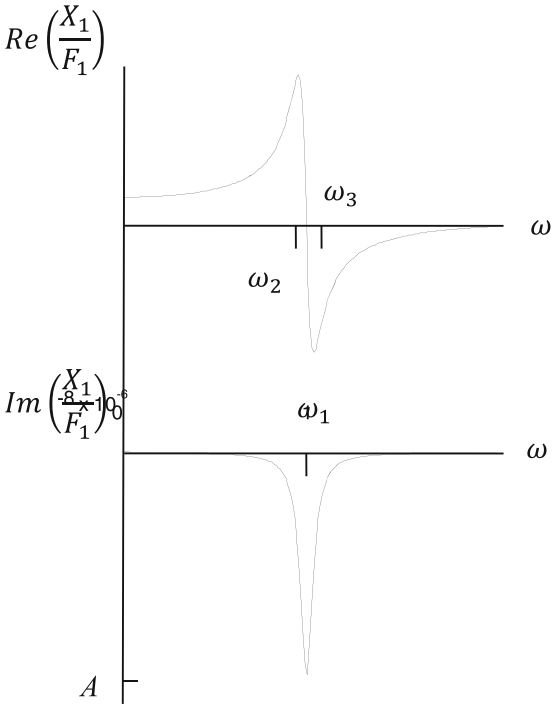

Fig. 6.1 An example FRF measurement is shown. A single mode is included within the measurement bandwidth

and imaginary parts of the FRF. We discussed this previously in Sect. 3.4, but let's review it here and see how it fits into our task of model development.

Figure 6.1 shows a representation of a measured FRF with a single mode within the measurement bandwidth. Therefore, a single degree of freedom model is sufficient to describe this system's dynamic behavior. In the figure, three frequencies, ω_1, ω_2, and ω_3, and one peak value, A, are identified. Frequency ω_1 gives the (undamped) natural frequency, ω_n. Also, ω_2 (from the maximum real part peak) occurs at $\omega_n(1-\zeta_q)$ and ω_3 (from the minimum real part peak) occurs at $\omega_n(1+\zeta_q)$. [As we saw in Sect. 3.4, these approximations yield reasonable results when the damping is low.]

Differencing ω_3 and ω_2 gives:

$$\omega_3 - \omega_2 = \omega_n\left(1+\zeta_q\right) - \omega_n\left(1-\zeta_q\right) = 2\omega_n\zeta_q. \tag{6.1}$$

Because ω_2, ω_3, and ω_n are known, Eq. 6.1 can be solved for ζ_q. See Eq. 6.2.

$$\zeta_q = \frac{\omega_3 - \omega_2}{2\omega_n} \tag{6.2}$$

Next, from the imaginary part minimum peak, we have that $A = \frac{-1}{2k_q\zeta_q}$. Rearranging to solve for the modal stiffness k_q results in:

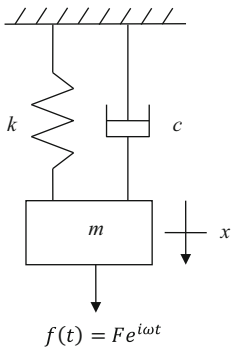

Fig. 6.2 Single degree of freedom model determined from the measurement provided in Fig. 6.1

$$k_q = \frac{-1}{2A\zeta_q}. \tag{6.3}$$

Finally, given that $\omega_n^2 = \frac{k_q}{m_q}$, we can solve for the modal mass m_q using Eq. 6.4, where compatible SI units are rad/s for the natural frequency, N/m for the stiffness, and kg for the mass.

$$m_q = \frac{k_q}{\omega_n^2} \tag{6.4}$$

Now we have the natural frequency, stiffness, mass, and damping ratio for the single degree of freedom system. We can also determine the modal (viscous) damping coefficient using Eq. 6.5.

$$c_q = 2\zeta_q\sqrt{m_q k_q} \tag{6.5}$$

The single degree of freedom FRF represents a special situation. In this case, there is no difference between modal and local coordinates. There is no coordinate transformation required to uncouple the equations of motion because there is only one equation of motion. We can therefore define the single degree of freedom model directly: $k = k_q$, $c = c_q$, and $m = m_q$; see Fig. 6.2. Given this model, we can describe the transient and steady-state vibration for any harmonic forcing function or initial conditions.

In a Nutshell
Using the model developed by peak picking, it is also possible to inexpensively examine "what if" scenarios. What if we could double the damping? What if a dynamic absorber was added? What if the system was exposed to a

(continued)

given time-varying force? Such questions can be easily and quickly evaluated once we have a model of the physical system. Some parts of a model might be easily estimated, such as the mass. However, other parts are vexingly difficult to predict without a measurement, particularly the damping.

6.2.2 *Two Degrees of Freedom*

What if there are two modes within the measurement bandwidth for the direct FRF? The simple answer is that we can again use peak picking, but now we must repeat the process for each of the two modes. Of course a model with two degrees of freedom will now be required as well. Consider the direct FRF measurement data provided in Fig. 6.3—six frequencies and two peak magnitudes are identified. The three frequencies, ω_1, ω_2, and ω_3, and peak value, A, describe the lower frequency mode with a natural frequency of $\omega_{n1} = \omega_1$. The three frequencies, ω_4, ω_5, and ω_6, and peak value, B, describe the higher frequency mode with a natural frequency of $\omega_{n2} = \omega_4$. Recall from Chap. 4 that the natural frequencies are the same in modal and local coordinates, so we do not need to make any distinction regarding the coordinate system (local or modal) for these frequencies.

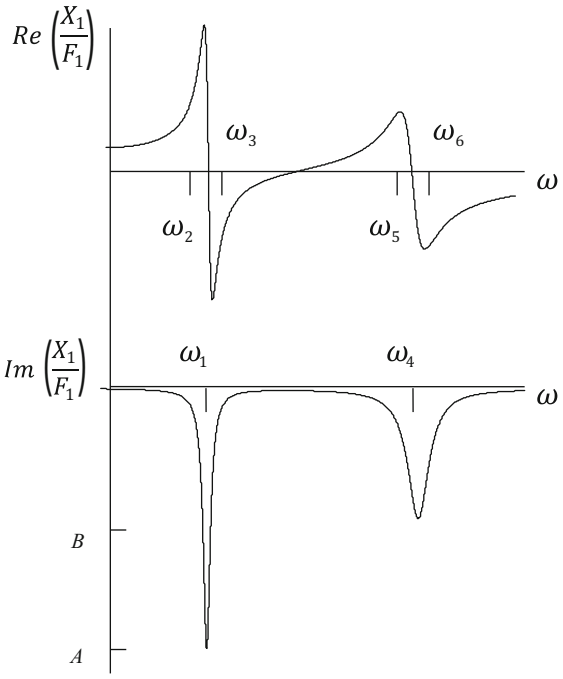

Fig. 6.3 An FRF measurement is displayed where two modes are contained in the measurement bandwidth

For the lower frequency mode, differencing ω_3 and ω_2 gives:

$$\omega_3 - \omega_2 = 2\omega_{n1}\zeta_{q1}.$$

Because ω_2, ω_3, and ω_{n1} are known, this equation can be solved for the modal damping ratio ζ_{q1}.

$$\zeta_{q1} = \frac{\omega_3 - \omega_2}{2\omega_{n1}}$$

From the imaginary part minimum peak, we determine the modal stiffness $k_{q1} = \frac{-1}{2A\zeta_{q1}}$. Next, we can solve for m_{q1} using $m_{q1} = \frac{k_{q1}}{\omega_{n1}^2}$. Finally, the modal damping coefficient is $c_{q1} = 2\zeta_{q1}\sqrt{m_{q1}k_{q1}}$.

For the higher frequency mode, we follow the same steps. Differencing ω_6 and ω_5 gives:

$$\omega_6 - \omega_5 = 2\omega_{n2}\zeta_{q2}.$$

Because ω_5, ω_6, and ω_{n2} are known, we can solve for ζ_{q2}.

$$\zeta_{q2} = \frac{\omega_6 - \omega_5}{2\omega_{n2}}$$

From the imaginary part minimum peak, we have that $k_{q2} = \frac{-1}{2B\zeta_{q2}}$. Next, we determine the modal mass, m_{q2}, using $m_{q2} = \frac{k_{q2}}{\omega_{n2}^2}$. Finally, the modal damping coefficient is $c_{q2} = 2\zeta_{q2}\sqrt{m_{q2}k_{q2}}$.

6.3 Building the Model

The peak picking approach is straightforward to implement, but you may wonder why we can treat the individual modes from a direct FRF measurement separately to find the modal parameters. The answer lies in the "undoing" of the modal analysis steps. Recall that, once we uncoupled the equations of motion to determine the single degree of freedom modal coordinate models, we transformed back to local coordinates by: (1) summing the modal FRFs for the direct FRF; and (2) summing the modal FRFs scaled by the eigenvectors for the cross FRF. In this case, we are beginning with the local coordinate direct FRF measurement, $\frac{X_1}{F_1}$, and determining the modal FRFs, $\frac{Q_1}{R_1}$ and $\frac{Q_2}{R_2}$, by peak picking. The two-mode fit of the direct FRF in local coordinates is simply the sum of the individual modal responses:

$$\frac{X_1}{F_1} = \frac{Q_1}{R_1} + \frac{Q_2}{R_2}.$$

In the peak picking technique, we fit $\frac{Q_1}{R_1}$ and $\frac{Q_2}{R_2}$ separately. From that fitting exercise we defined the modal parameters. In matrix form, they are expressed as $[m_q] = \begin{bmatrix} m_{q1} & 0 \\ 0 & m_{q2} \end{bmatrix}$, $[c_q] = \begin{bmatrix} c_{q1} & 0 \\ 0 & c_{q2} \end{bmatrix}$, and $[k_q] = \begin{bmatrix} k_{q1} & 0 \\ 0 & k_{q2} \end{bmatrix}$ for a two degree of freedom system. Note that we have automatically assumed that proportional damping holds when using this technique for model identification. However, this is a reasonable assumption for most systems because structural damping is typically low.

In order to complete the local coordinate model we need to transform the modal mass, damping, and stiffness matrices into local coordinates. We are already familiar with the "forward" version of this transformation from local (or model) to modal coordinates. For the mass matrices, we have:

$$[m_q] = [P]^T [m][P],$$

where $[P]$ is the modal matrix. Its columns are the system eigenvectors (or mode shapes):

$$[P] = [\psi_1 \ \ \psi_2].$$

To determine the mass matrix in local coordinates, the "backward" form of the coordinate transformation from modal to local coordinates is:

$$[m] = [P]^{-T} [m_q] [P]^{-1},$$

where the "−1" superscript indicates the matrix inverse operation (`inv(P)` in MATLAB®) and the "−T" represents the inverse of the modal matrix transpose (`inv(P')` in MATLAB®). Similarly, the damping and stiffness matrices in local coordinates are determined using:

$$[c] = [P]^{-T} [c_q] [P]^{-1} \quad \text{and} \quad [k] = [P]^{-T} [k_q] [P]^{-1}.$$

For a two degree of freedom model, the modal matrix can be represented as:

$$[P] = [\psi_1 \quad \psi_2] = \begin{bmatrix} 1 & 1 \\ p_1 & p_2 \end{bmatrix},$$

where the first eigenvector, ψ_1, corresponds to vibration at ω_{n1} and the second eigenvector, ψ_2, describes vibration at ω_{n2}. In this case we've normalized to coordinate x_1, so p_1 and p_2 give the ratio $\frac{X_2}{X_1}$. This is a cross FRF, so we must measure not

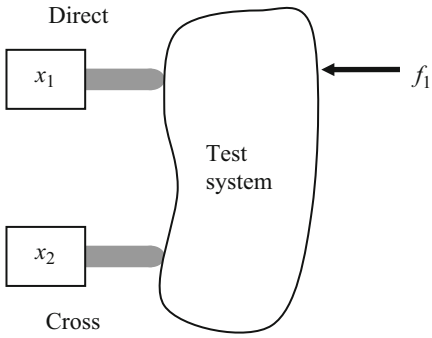

Fig. 6.4 Representation of direct and cross FRF measurements on a physical system

only a direct FRF to determine the modal matrices, but also a cross FRF to identify the modal matrix. In performing these measurements, the force should be applied to the physical system at the location of most interest in the structure's response.

Given the direct and cross FRF measurements, how do we determine p_1 and p_2? To answer this question, we must again return to the modal analysis steps. As we just discussed, the transformation from modal to local coordinates includes a summation of the modal contributions. For the direct FRF we have:

$$\frac{X_1}{F_1} = \frac{Q_1}{R_1} + \frac{Q_2}{R_2}$$

and the transformation for the cross FRF is:

$$\frac{X_2}{F_1} = p_1 \frac{Q_1}{R_1} + p_2 \frac{Q_2}{R_2}.$$

To determine p_1, we use the first (lowest frequency) mode from both the direct and cross FRFs. For the first mode at ω_{n1}, the cross FRF is given by $p_1 \frac{Q_1}{R_1}$ and the direct FRF by $\frac{Q_1}{R_1}$. Taking their ratio enables us to determine p_1; see Eq. 6.6.

$$\left.\frac{\frac{X_2}{F_1}}{\frac{X_1}{F_1}}\right|_{\omega_{n1}} = \frac{p_1 \frac{Q_1}{R_1}}{\frac{Q_1}{R_1}} = p_1 \tag{6.6}$$

Similarly, we determine p_2 from the second mode (with a natural frequency of ω_{n2}) from the direct and cross FRFs. This is shown in Eq. 6.7.

$$\left.\frac{\frac{X_2}{F_1}}{\frac{X_1}{F_1}}\right|_{\omega_{n2}} = \frac{p_2 \frac{Q_1}{R_1}}{\frac{Q_1}{R_1}} = p_2 \tag{6.7}$$

Let's graphically examine this identification of the eigenvectors and, subsequently, the modal matrix. Figure 6.4 shows a schematic of direct and cross FRF

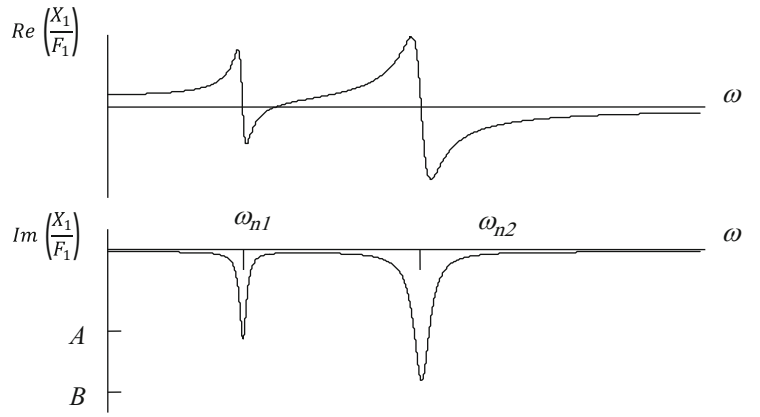

Fig. 6.5 Direct FRF measurement results for the system shown in Fig. 6.4

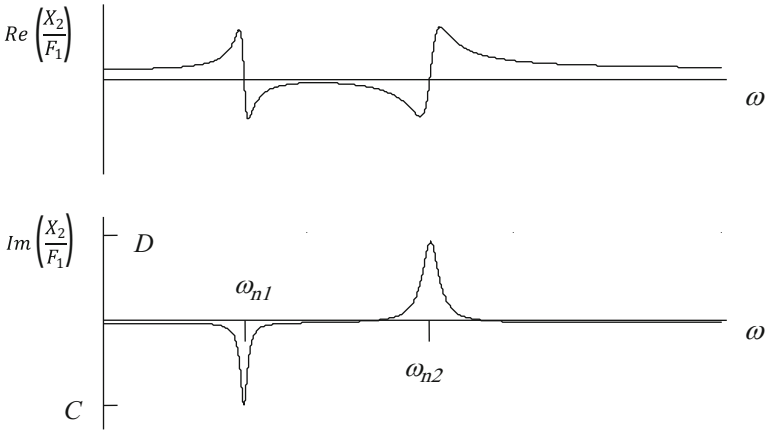

Fig. 6.6 Cross FRF measurement results for the system shown in Fig. 6.4

measurements on a physical system (the "blob" representation). Figures 6.5 and 6.6 display the measurement results. They show the real and imaginary parts of the direct and cross FRFs, respectively. However, the imaginary parts are sufficient to identify the eigenvectors. In the direct FRF (Fig. 6.5), the local minimum values of the imaginary parts are identified: A for the first mode (at ω_{n1}) and B for the second mode (at ω_{n2}). The peak values C and D are identified in the cross FRF (Fig. 6.6). These peak values can be used in Eqs. 6.6 and 6.7. Using Eq. 6.6, we determine p_1 by:

$$\left.\frac{Im\left(\frac{X_2}{F_1}\right)}{Im\left(\frac{X_1}{F_1}\right)}\right|_{\omega_{n1}} = \frac{C}{A} = p_1. \tag{6.8}$$

The value of p_2 is calculated using Eq. 6.7 and the peak heights B and D; see Eq. 6.9. Note that we must pay attention to the sign of these heights. Once p_1 and p_2 are determined, they are substituted into the modal matrix, $[P] = [\psi_1 \quad \psi_2] = \begin{bmatrix} 1 & 1 \\ p_1 & p_2 \end{bmatrix}$.

$$\left.\frac{Im\left(\frac{X_2}{F_1}\right)}{Im\left(\frac{X_1}{F_1}\right)}\right|_{\omega_{n2}} = \frac{D}{B} = p_2 \tag{6.9}$$

In a Nutshell
This technique is often used to visualize the mode shape. First, a direct FRF is measured. Then, using a series of measured cross FRFs, the height of the imaginary peak for the mode of interest (relative to the height of the same mode in the direct measurement) provides the mode shape component at that location. With a little practice, it is possible to quickly describe the mode shape.

By the Numbers 6.1
In order to perform a numerical demonstration of the backward problem solution, let's begin with the forward problem solution by modal analysis for a two degree of freedom spring-mass-damper model (as we discussed in Chap. 5). We'll then use the local coordinate direct and cross FRFs as the starting point for the backward solution. Commençons![2]

The two degree of freedom chain-type model is shown in Fig. 6.7. A harmonic force, $f_1(t)$, is applied at coordinate x_1. Let's follow the five steps we identified in Sect. 5.4 for the forward solution. The parameters for the model in Fig. 6.7 are $k_1 = 8 \times 10^5$ N/m, $c_1 = 160$ N s/m, $m_1 = 3$ kg, $k_2 = 4 \times 10^5$ N/m, $c_2 = 80$ N s/m, $m_2 = 3$ kg, and $f_1(t) = 200e^{i\omega t}$ N. The mass, damping, and stiffness matrices are:

[2] Let's begin!

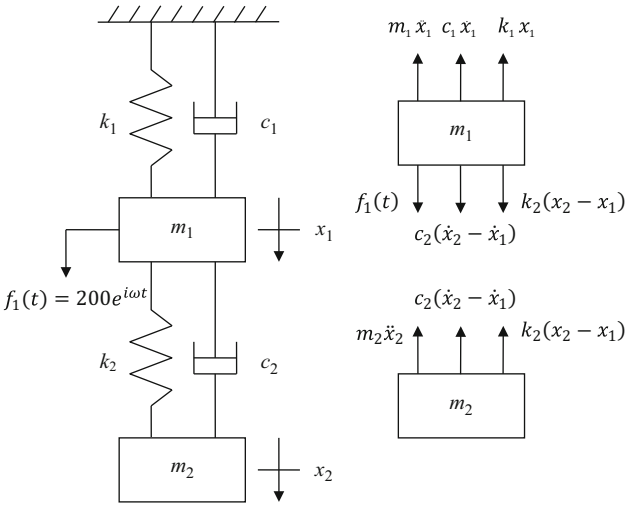

Fig. 6.7 *By the Numbers 6.1*—two degree of freedom model (the free body diagrams for the two masses are also included)

$$[m] = \begin{bmatrix} m_1 & 0 \\ 0 & m_2 \end{bmatrix} = \begin{bmatrix} 3 & 0 \\ 0 & 3 \end{bmatrix} \text{kg},$$

$$[c] = \begin{bmatrix} c_1 + c_2 & -c_2 \\ -c_2 & c_2 \end{bmatrix} = \begin{bmatrix} 240 & -80 \\ -80 & 80 \end{bmatrix} \text{N s/m, and}$$

$$[k] = \begin{bmatrix} k_1 + k_2 & -k_2 \\ -k_2 & k_2 \end{bmatrix} = \begin{bmatrix} 1.2 \times 10^6 & -4 \times 10^5 \\ -4 \times 10^5 & 4 \times 10^5 \end{bmatrix} \text{N/m}.$$

Note that the matrices are symmetric (i.e., the off-diagonal terms are equal). We proceed according to the steps identified in Table 5.1.

1. Verify proportional damping. The equality $[c] = \alpha[m] + \beta[k]$ is true when $\alpha = 0$ and $\beta = \frac{1}{5000}$ so proportional damping holds. We require proportional damping for modal analysis, so this check must be completed for each forward problem solution. For the backward problem, however, we assume that proportional damping exists so no check is applied.

$$\begin{bmatrix} 240 & -80 \\ -80 & 80 \end{bmatrix} = \alpha \begin{bmatrix} 3 & 0 \\ 0 & 3 \end{bmatrix} + \beta \begin{bmatrix} 1.2 \times 10^6 & -4 \times 10^5 \\ -4 \times 10^5 & 4 \times 10^5 \end{bmatrix}$$

2. Ignore damping and the force to find the eigenvalues and eigenvectors.

$$\left[\begin{bmatrix}3 & 0\\ 0 & 3\end{bmatrix}s^2 + \begin{bmatrix}1.2\times10^6 & -4\times10^5\\ -4\times10^5 & 4\times10^5\end{bmatrix}\right]\begin{Bmatrix}X_1\\ X_2\end{Bmatrix} = \begin{Bmatrix}0\\ 0\end{Bmatrix}$$

Obtain the eigenvalues from the characteristic equation:

$$\begin{vmatrix}3s^2 + 1.2\times10^6 & -4\times10^5\\ -4\times10^5 & 3s^2 + 4\times10^5\end{vmatrix} = 0, \text{ or}$$

$$\begin{aligned}&\left(3s^2 + 1.2\times10^6\right)\left(3s^2 + 4\times10^5\right) - \left(-4\times10^5\right)^2\\ &\quad = 9s^4 + 4.8\times10^6 s^2 + 3.2\times10^{11} = 0.\end{aligned}$$

The roots are $s_1^2 = -78104.86 = -\omega_{n1}^2$ and $s_2^2 = -455228.47 = -\omega_{n2}^2$. The natural frequencies are $\omega_{n1} = 279.47$ rad/s ($f_{n1} = 44.48$ Hz) and $\omega_{n2} = 674.71$ rad/s ($f_{n2} = 107.38$ Hz). The bottom (second) equation of motion from the matrix format is $-4 \times 10^5 X_1 + (3s^2 + 4 \times 10^5)X_2 = 0$. In order to normalize the eigenvectors to x_1 (the force location), the required ratio is:

$$\frac{X_2}{X_1} = \frac{4\times10^5}{3s^2 + 4\times10^5}.$$

Substituting $s_1^2 = -78104.86$ gives the first eigenvector.

$$\psi_1 = \begin{Bmatrix}1\\ \left(\dfrac{4\times10^5}{3(-78104.86) + 4\times10^5}\right)\end{Bmatrix} = \begin{Bmatrix}1\\ 2.414\end{Bmatrix}$$

Substituting $s_2^2 = -455228.47$ gives the second eigenvector.

$$\psi_2 = \begin{Bmatrix}1\\ \left(\dfrac{4\times10^5}{3(-45228.47) + 4\times10^5}\right)\end{Bmatrix} = \begin{Bmatrix}1\\ -0.414\end{Bmatrix}$$

3. Construct the modal matrix using the eigenvectors.

$$[P] = \begin{bmatrix}1 & 1\\ 2.414 & -0.414\end{bmatrix}$$

Use the modal matrix to transform into modal coordinates and uncouple the equations of motion.

$$[m_q] = [P]^T[m][P] = \begin{bmatrix} 20.482 & 0 \\ 0 & 3.514 \end{bmatrix} \text{kg}$$

$$[c_q] = [P]^T[c][P] = \begin{bmatrix} 319.95 & 0 \\ 0 & 319.95 \end{bmatrix} \text{N s/m}$$

$$[k_q] = [P]^T[k][P] = \begin{bmatrix} 1.600 \times 10^6 & 0 \\ 0 & 1.600 \times 10^6 \end{bmatrix} \text{N/m}$$

Transform the force vector from local to modal coordinates.

$$\left\{\vec{R}\right\} = \begin{Bmatrix} R_1 \\ R_2 \end{Bmatrix} = [P]^T\left[\vec{F}\right] = \begin{bmatrix} 1 & 2.414 \\ 1 & -0.414 \end{bmatrix}\begin{Bmatrix} 200 \\ 0 \end{Bmatrix} = \begin{Bmatrix} 200 \\ 200 \end{Bmatrix} \text{N}$$

As a check, the single degree of freedom natural frequencies can be calculated using the modal parameters; they are $\omega_{n1} = \sqrt{\frac{k_{q1}}{m_{q1}}} = \sqrt{\frac{1.6\times10^6}{20.482}} = 279.49$ rad/s and $\omega_{n2} = \sqrt{\frac{k_{q2}}{m_{q2}}} = \sqrt{\frac{1.6\times10^6}{3.514}} = 674.78$ rad/s. These values do not match the original natural frequencies (determined from the eigenvalues) exactly due to round-off error, but they do verify that the modal mass and stiffness parameters are correct.

4. Write the FRFs for the two single degree of freedom systems in modal coordinates. For the first natural frequency, the FRF is:

$$\frac{Q_1}{R_1} = \frac{1}{1.600 \times 10^6}\left(\frac{\left(1 - r_1^2\right) - i(2(0.0279)r_1)}{\left(1 - r_1^2\right)^2 + (2(0.0279)r_1)^2}\right),$$

where $r_1 = \frac{\omega}{279.49}$ and the damping ratio is $\zeta_{q1} = \frac{319.95}{2\sqrt{1.600\times10^6(20.482)}} = 0.0279$. For the second natural frequency, the FRF is:

$$\frac{Q_2}{R_2} = \frac{1}{1.600 \times 10^6}\left(\frac{\left(1 - r_2^2\right) - i(2(0.0675)r_2)}{\left(1 - r_2^2\right)^2 + (2(0.0675)r_2)^2}\right),$$

where $r_2 = \frac{\omega}{674.78}$ and $\zeta_{q2} = \frac{319.95}{2\sqrt{1.600\times10^6(3.514)}} = 0.0675$.

5. Transform back to local coordinates. The direct FRF, $\frac{X_1}{F_1} = \frac{Q_1}{R_1} + \frac{Q_2}{R_2}$, is plotted in Fig. 6.8. The cross FRF, $\frac{X_2}{F_1} = p_1\frac{Q_1}{R_1} + p_2\frac{Q_2}{R_2}$, is displayed in Fig. 6.9.

We can now treat Figs. 6.8 and 6.9 as measurement results (0.1 rad/s frequency resolution) and identify the two degree of freedom model that can be used to represent this dynamic system; this is the backward solution. We'll assume a chain-type model format as shown in Fig. 6.7. However, this is not necessary in general; we'll discuss this further in Sect. 6.6. As shown in Figs. 6.3 and 6.6, the peak picking approach requires that we identify six frequencies and four peak

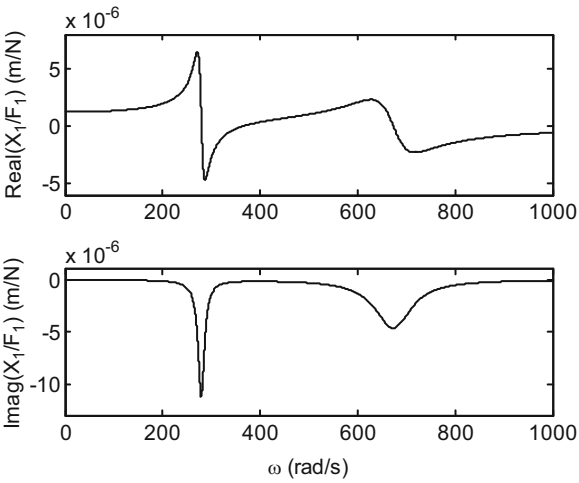

Fig. 6.8 *By the Numbers 6.1*—direct FRF $\frac{X_1}{F_1}$ (local coordinates)

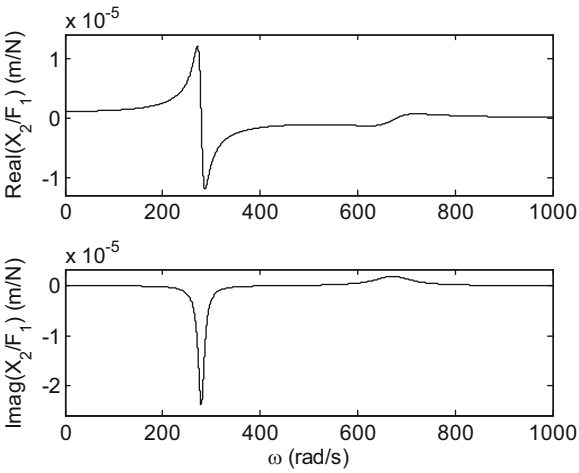

Fig. 6.9 *By the Numbers 6.1*—cross FRF $\frac{X_2}{F_1}$ (local coordinates)

heights; see Figs. 6.10 (direct FRF) and 6.11 (cross FRF). The frequencies and heights are summarized in Table 6.1.

Let's begin with the 279.4 rad/s mode. We determine the modal damping ratio using $\zeta_{q1} = \frac{287.2-271.6}{2(279.4)} = 0.0279$. From the imaginary part minimum peak, A, the modal stiffness is $k_{q1} = \frac{-1}{2\left(-1.125\times10^{-5}\right)0.0279} = 1.593 \times 10^6$ N/m. Next, the modal mass is $m_{q1} = \frac{1.593\times10^6}{279.4^2} = 20.406$ kg. Finally, the modal damping coefficient is $c_{q1} = 2(0.0279)\sqrt{20.406\left(1.593 \times 10^6\right)} = 318.14$ N s/m.

We complete the same calculations for the 673.2 rad/s mode. The modal damping ratio is $\zeta_{q2} = \frac{718.6-628.1}{2(673.2)} = 0.0672$. Using the imaginary part minimum peak, B, the

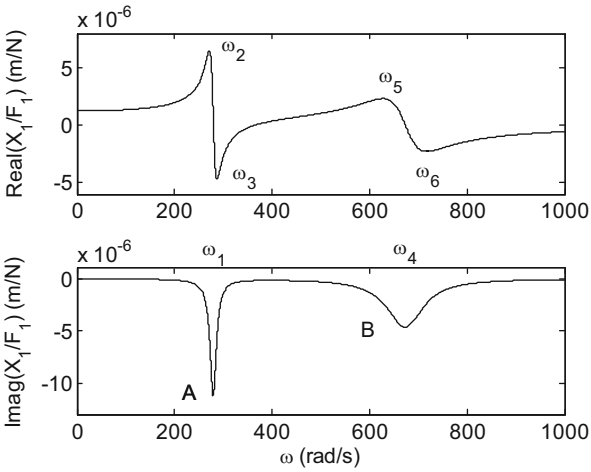

Fig. 6.10 *By the Numbers 6.1*—peak picking frequencies and heights for the direct FRF $\frac{X_1}{F_1}$

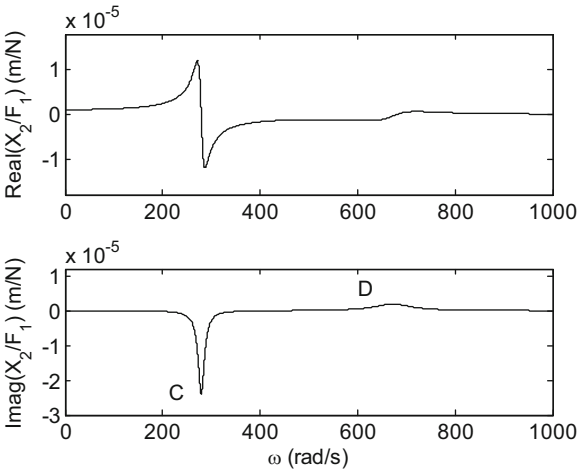

Fig. 6.11 *By the Numbers 6.1*—peak picking heights for the cross FRF $\frac{X_2}{F_1}$

Frequency (rad/s)	Peak height (m/N)
$\omega_1 = 279.4$	$A = -1.125 \times 10^{-5}$
$\omega_2 = 271.6$	$B = -4.639 \times 10^{-6}$
$\omega_3 = 287.2$	$C = -2.396 \times 10^{-5}$
$\omega_4 = 673.2$	$D = 1.911 \times 10^{-6}$
$\omega_5 = 628.1$	
$\omega_6 = 718.6$	

Table 6.1 *By the Numbers 6.1*—peak picking frequencies and heights from Figs. 6.10 and 6.11

modal stiffness is determined by $k_{q2} = \frac{-1}{2\left(-4.639\times10^{-6}\right)0.0672} = 1.604 \times 10^6$ N/m. The modal mass is $m_{q2} = \frac{1.604\times10^6}{673.2^2} = 3.539$ kg and the modal damping coefficient is

$c_{q2} = 2(0.0672)\sqrt{3.539\left(1.604 \times 10^6\right)} = 320.22$ N s/m. We now have all the values required to fully populate the modal mass, damping, and stiffness matrices.

$$\left[m_q\right] = \begin{bmatrix} 20.406 & 0 \\ 0 & 3.539 \end{bmatrix} \text{kg}$$

$$\left[c_q\right] = \begin{bmatrix} 318.14 & 0 \\ 0 & 320.22 \end{bmatrix} \text{N s/m}$$

$$\left[k_q\right] = \begin{bmatrix} 1.593 \times 10^6 & 0 \\ 0 & 1.604 \times 10^6 \end{bmatrix} \text{N/m}$$

Next, we determine the eigenvectors using the peak heights A, B, C, and D. For the lower frequency mode, $p_1 = \frac{C}{A} = \frac{-2.396 \times 10^{-5}}{-1.125 \times 10^{-5}} = 2.130$. For the higher frequency mode, $p_2 = \frac{D}{B} = \frac{1.911 \times 10^{-6}}{-4.639 \times 10^{-5}} = -0.412$. The modal matrix is:

$$[P] = \begin{bmatrix} 1 & 1 \\ 2.130 & -0.412 \end{bmatrix}.$$

The mass, damping, and stiffness matrices in local coordinates are:

$$[m] = [P]^{-T}\left[m_q\right][P]^{-1} = \begin{bmatrix} 3.021 & 0 \\ 0 & 3.707 \end{bmatrix} = \begin{bmatrix} m_1 & 0 \\ 0 & m_2 \end{bmatrix} \text{kg},$$

$$[c] = [P]^{-T}\left[c_q\right][P]^{-1} = \begin{bmatrix} 233.19 & -85.27 \\ -85.27 & 98.79 \end{bmatrix} = \begin{bmatrix} c_1 + c_2 & -c_2 \\ -c_2 & c_2 \end{bmatrix} \text{N s/m, and}$$

$$[k] = [P]^{-T}\left[k_q\right][P]^{-1} = \begin{bmatrix} 1.168 \times 10^6 & -4.272 \times 10^5 \\ -4.272 \times 10^5 & 4.948 \times 10^5 \end{bmatrix}$$

$$= \begin{bmatrix} k_1 + k_2 & -k_2 \\ -k_2 & k_2 \end{bmatrix} \text{N/m}.$$

In a Nutshell

The forms on the right hand side of the local coordinate mass, damping, and stiffness matrices indicate that we had an idea what the model should look like. That is, we assumed a chain type model. If our idea of the model is right, then the local mass, stiffness, and damping matrices should have this form. We don't always know what the model should be, but the measurements guide us. For example, how many modes do we see in the measured FRF? That is how many degrees of freedom are required to represent the physical system in the frequency range we measured and in the locations we measured.

Table 6.2 *By the Numbers 6.1*—results for the backward problem solution

	Original model	Backward solution	Percent error (%)
m_1 (kg)	3	3.021	−0.7
c_1 (N s/m)	160	141.16	11.8
k_1 (N/m)	8×10^5	7.07×10^5	11.6
m_2	3	3.707	−23.6
c_2	80	92.03	−15.0
k_2	4×10^5	4.61×10^5	−15.3

We are almost finished, but need to make an engineering decision. For the damping matrix we have that $c_2 = 98.79$ N s/m from the (2,2) term. For the (1,2) and (2,1) terms, however, $c_2 = 85.27$ N s/m. Let's use the average, $c_2 = \frac{98.79+85.27}{2} = 92.03$ N s/m. From the (1,1) term, then, $c_1 = 233.19 - 92.03 = 141.16$ N s/m. We complete the same analysis for the stiffness values. Using the (1,2), (2,1), and (2,2) values from the stiffness matrix, $k_2 = \frac{4.948\times10^5+4.272\times10^5}{2} = 4.61 \times 10^5$ N/m. Using the (1,1) term, $k_1 = 1.168 \times 10^6 - 4.610 \times 10^5 = 7.07 \times 10^5$ N/m. The original model parameters, backward solution values, and percent differences are provided in Table 6.2. The disagreement is the result of round-off error in both the forwards and backward solutions, assumptions in the peak picking approach, and the engineering decision to use the average c_2 and k_2 values.

6.4 Peak Picking for Multiple Degrees of Freedom

The peak picking method is straightforward to extend to additional degrees of freedom. For the cutting tool-holder-spindle-machine structure mentioned in Sect. 6.1, it is common for many modes to exist in the 0–5000 Hz frequency range. An example direct FRF measurement for a 47 mm diameter shell mill[3] which was clamped in a high-speed spindle is provided in Fig. 6.12. The measurement was performed at the free end of the cutting tool. There are five modes which were selected for fitting. The three frequencies and peak height for each mode are included in Table 6.3. The corresponding modal stiffness and damping ratio are also identified.

The five-mode fit and original data are plotted together in Fig. 6.13; the code used to generate the modal fit is provided in MATLAB® MOJO 6.1. The fit to the direct FRF measurement is simply the sum of the modal contributions:

$$\frac{X_1}{F_1} = \sum_{n=1}^{5} \frac{Q_n}{R_n}. \tag{6.10}$$

MATLAB® MOJO 6.1

[3] Shell mills are typically used to machine large flat surfaces.

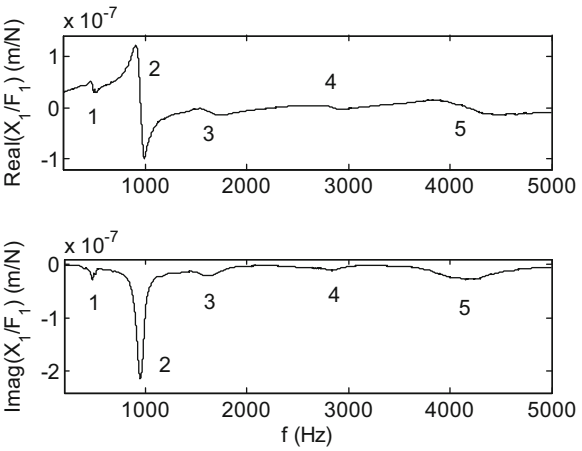

Fig. 6.12 Direct FRF measurement for cutting tool-holder-spindle-machine structure. The modes selected for fitting are identified numerically (1–5)

Table 6.3 Modal fitting parameters for the cutting tool-holder-spindle-machine direct FRF

Mode	f_1 (Hz)	f_2 (Hz)	f_3 (Hz)	Imaginary peak (m/N)	f_n (Hz)	k_q (N/m)	ζ_q
1	480	468	493	-2.89×10^{-8}	480	6.65×10^{8}	0.026
2	950	906	992	-2.14×10^{-7}	950	5.19×10^{7}	0.045
3	1630	1542	1745	-2.13×10^{-8}	1630	3.79×10^{8}	0.062
4	2842	2770	2915	-1.12×10^{-8}	2842	1.72×10^{9}	0.026
5	4150	3823	4500	-2.78×10^{-8}	4150	2.19×10^{8}	0.082

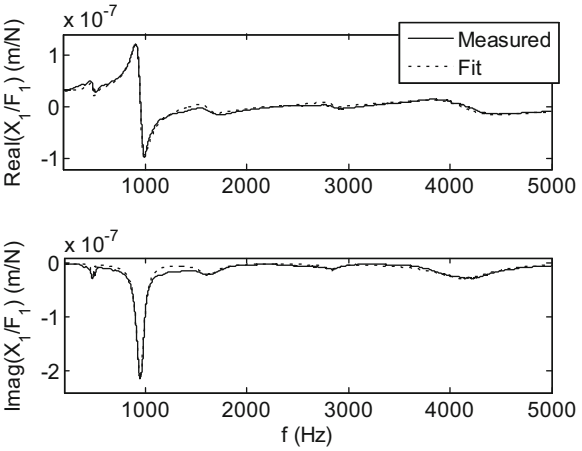

Fig. 6.13 Modal fit to the cutting tool-holder-spindle-machine direct FRF

```
% matlab_mojo_6_1.m

clear
close all
clc

% Modal fit
f = 200:0.2:5000; % Hz
kq = 6.65e8;    % N/m
zetaq = 0.026;
fn = 480;     % Hz
r = f/fn;
real_part = 1/kq*(1-r.^2)./((1-r.^2).^2 + (2*zetaq*r).^2);
imag_part = 1/kq*(-2*zetaq*r)./((1-r.^2).^2 + (2*zetaq*r).^2);
Q1_R1 = real_part + 1i*imag_part;  % m/N

kq = 5.19e7;    % N/m
zetaq = 0.045;
fn = 950;     % Hz
r = f/fn;
real_part = 1/kq*(1-r.^2)./((1-r.^2).^2 + (2*zetaq*r).^2);
imag_part = 1/kq*(-2*zetaq*r)./((1-r.^2).^2 + (2*zetaq*r).^2);
Q2_R2 = real_part + 1i*imag_part;  % m/N

kq = 3.79e8;    % N/m
zetaq = 0.062;
fn = 1630;     % Hz
r = f/fn;
real_part = 1/kq*(1-r.^2)./((1-r.^2).^2 + (2*zetaq*r).^2);
imag_part = 1/kq*(-2*zetaq*r)./((1-r.^2).^2 + (2*zetaq*r).^2);
Q3_R3 = real_part + 1i*imag_part;  % m/N

kq = 1.72e9;    % N/m
zetaq = 0.026;
fn = 2842;     % Hz
r = f/fn;
real_part = 1/kq*(1-r.^2)./((1-r.^2).^2 + (2*zetaq*r).^2);
imag_part = 1/kq*(-2*zetaq*r)./((1-r.^2).^2 + (2*zetaq*r).^2);
Q4_R4 = real_part + 1i*imag_part;  % m/N

kq = 2.19e8;    % N/m
zetaq = 0.082;
fn = 4150;     % Hz
r = f/fn;
real_part = 1/kq*(1-r.^2)./((1-r.^2).^2 + (2*zetaq*r).^2);
imag_part = 1/kq*(-2*zetaq*r)./((1-r.^2).^2 + (2*zetaq*r).^2);
Q5_R5 = real_part + 1i*imag_part;  % m/N

X1_F1 = Q1_R1 + Q2_R2 + Q3_R3 + Q4_R4 + Q5_R5;

figure(1)
subplot(211)
plot(f, real(X1_F1), 'k:')
set(gca,'FontSize', 14)
```

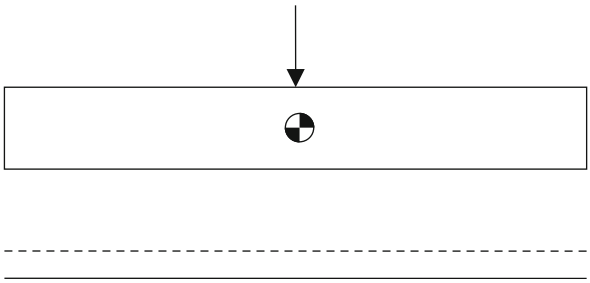

Fig. 6.14 Translational rigid body mode

```
axis([200 5000 -12e-8 14e-8])
ylabel('Real(X_1/F_1) (m/N)')
subplot(212)
plot(f, imag(X1_F1), 'k:')
axis([200 5000 -24e-8 1e-8])
set(gca,'FontSize', 14)
xlabel('f (Hz)')
ylabel('Imag(X_1/F_1) (m/N)')
```

In a Nutshell
There are other curve fitting methods, of course. The peak picking technique described here is easy to visualize and works well provided that the modes are well separated. Naturally, the modal parameters are sensitive to the peaks used in the curve fitting.

6.5 Mode Shape Measurement

It is often of interest to determine the mode shapes (eigenvectors) for a structure, even in the absence of building a model. This can give insight into: (1) the source of a particular natural frequency; and (2) how the structure might be modified to reduce the magnitude of a particular mode.[4]

Consider the steel rod from the **beam experimental platform (BEP).**[5] What if this beam was not clamped in the platform, but was floating in space instead? In this case, the boundary conditions would be free-free; there would be no external restrictions on the beam's motion. Let's discuss the mode shapes for this free-free beam. First, there are two **rigid body modes**. Second, there are an infinite number of **bending modes** for the continuous beam.[6]

[4]One structural modification technique we've already discussed is the addition of a dynamic absorber (Sect. 5.4).

[5]The BEP was introduced in Sect. 2.6.

[6]There are also other modes of vibration, but we'll discuss these in Chap. 8.

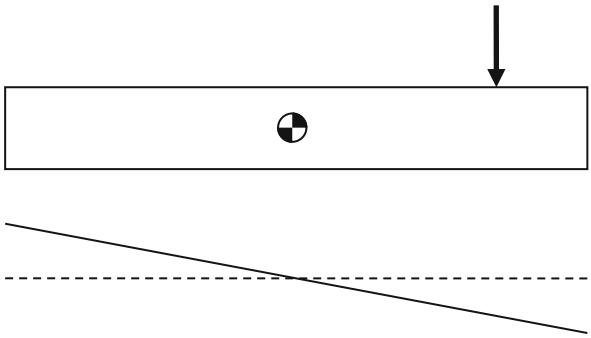

Fig. 6.15 Rotational rigid body mode

Table 6.4 Constants for the free-free beam mode shape calculation in Eq. 6.11 [2]

Mode i	λ_i	σ_i
1	4.73004074	0.982502215
2	7.85320462	1.000777312

One of the rigid body modes is depicted in Fig. 6.14. This mode is a translation of the rigid beam due to a constant (zero frequency, or DC) force applied at the center of mass. The corresponding rigid body mode frequency is zero because the beam does not actually oscillate. The other rigid body mode is represented in Fig. 6.15. It is a rotation of the rigid beam due to a constant force that is not applied at the center of mass. The vibration frequency is again zero because there is no relative motion of points along the beam, only the rigid body rotation.

The bending modes for a free-free, uniform cross-section beam can be described analytically [2]. The mode shape function that describes the relative vibration magnitudes at locations, x, along the beam length, l, is:

$$\psi_i = \frac{1}{2}\left(cosh\left(\frac{\lambda_i x}{l}\right) + cos\left(\frac{\lambda_i x}{l}\right) - \sigma_i\left(sinh\left(\frac{\lambda_i x}{l}\right) + sin\left(\frac{\lambda_i x}{l}\right)\right)\right), \quad (6.11)$$

where $i = 1, 2, 3, \ldots$ is the mode shape number and the constants λ_i and σ_i for the first two modes are provided in Table 6.4. The first two mode shapes, which have been normalized to the end of the beam ($x = 0$), are displayed in Fig. 6.16.

We see in Fig. 6.16 that there are points where the mode shapes change sign and, therefore, pass through zero. These points are referred to as **nodes** and identify locations along the beam where the vibration response (at the corresponding natural frequency) is zero regardless of the force magnitude. Note, however, that the locations of the two nodes for the first mode, which describes the beam's shape for vibration at the first natural frequency, do not coincide with the locations of the three nodes for the second mode, which corresponds to vibration at the second natural frequency.[7] Because the beam's response to an external force is the

[7]The number of nodes is equal to $i + 1$ for a free-free beam.

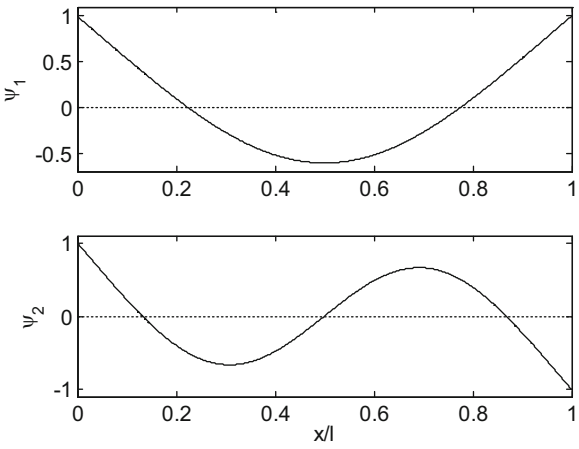

Fig. 6.16 The first two bending mode shapes for a free-free beam

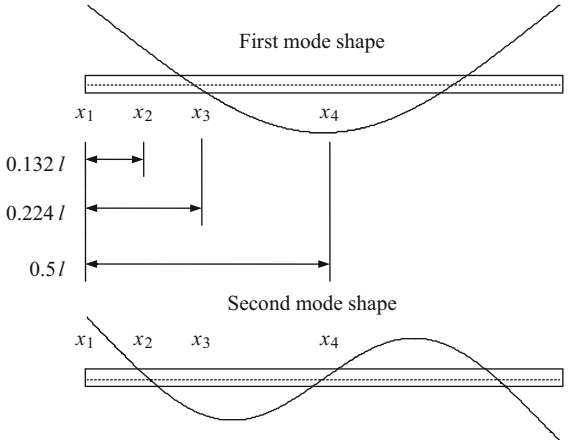

Fig. 6.17 Direct and cross FRF measurement locations for the free-free steel rod

superposition of all the modes, there is still motion at all points along the beam, in general, when it is excited.

For the steel rod from the BEP (12.7 mm diameter, 153 mm long), let's assume that we placed the beam on a very flexible support, such as a block of soft foam, to mimic free-free boundary conditions[8] and then measured the direct FRF at location 1 and the cross FRFs at locations 2–4. These locations are identified in Fig. 6.17, where 2 (at $\frac{x}{l} = 0.132$) and 4 (at $\frac{x}{l} = 0.5$) are nodes for ψ_2 and 3 (at $\frac{x}{l} = 0.224$) is a node for ψ_1. If we applied the force at location 1 for each measurement, then the four FRFs would be $\frac{X_1}{F_1}$, $\frac{X_2}{F_1}$, $\frac{X_3}{F_1}$, and $\frac{X_4}{F_1}$. The imaginary parts of these FRFs are displayed in Fig. 6.18, where the measurement bandwidth only includes the first two modes.

[8]Because the foam base is much more flexible than the beam, free-free conditions are approximated. Alternately, we could support the beam using flexible bungee cords. Both techniques are applied in practice.

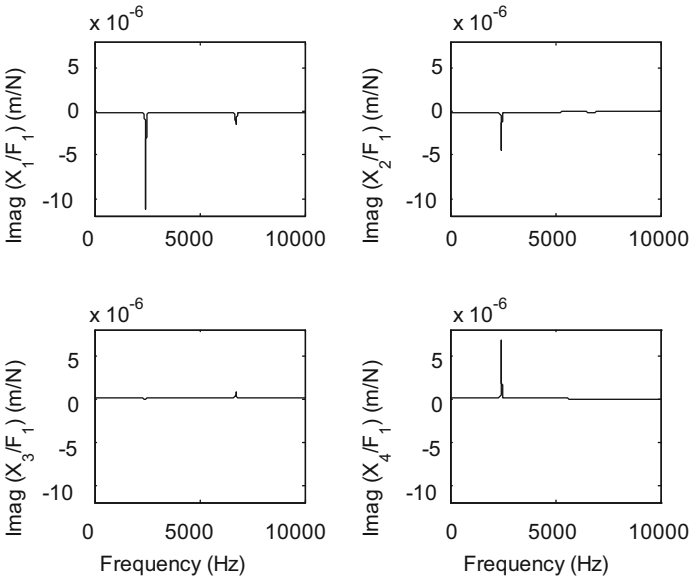

Fig. 6.18 (**a**) The imaginary parts of the four direct and cross FRFs for the free-free steel rod viewed at full scale. (**b**) The imaginary parts of the four direct and cross FRFs for the free-free steel rod viewed at a reduced scale to show the second mode

For the first mode at a natural frequency of 2446 Hz, we notice two distinct behaviors. First, the peak height at location 3 is zero. This demonstrates an important consideration for experimental identification of mode shapes—if the transducer is positioned or the force is applied at or near a node, then the response will have a magnitude that is close to (or equal to) zero for the mode shape that includes that node at the selected measurement location. Because the node locations are not known in advance, many measurements are typically required on a given structure to adequately describe all the mode shapes within the measurement bandwidth. Second, the sign of the peak height switches between locations 2 and 4. The motion at these points is out of phase when the beam vibrates in the first mode shape. For the second mode at 6741 Hz, we see a zero response at both locations 2 and 4. Also, the peak heights switch sign between locations 1 and 3. These sign switches and height variations with measurement location correspond directly to the eigenvector identification approach we detailed in Sect. 6.3.

Next, let's insert the rod in the BEP with an overhang length of 130 mm so that it now has fixed-free boundary conditions (it is a cantilever beam). The first three mode shapes are shown in Fig. 6.19[9] These are described using the mode shape function in Eq. 6.12. The mode shapes are normalized to the beam's free end and the constants λ_i and σ_i ($i = 1$–3) are provided in Table 6.5.

[9]The number of nodes is equal to $i - 1$ for a fixed-free beam.

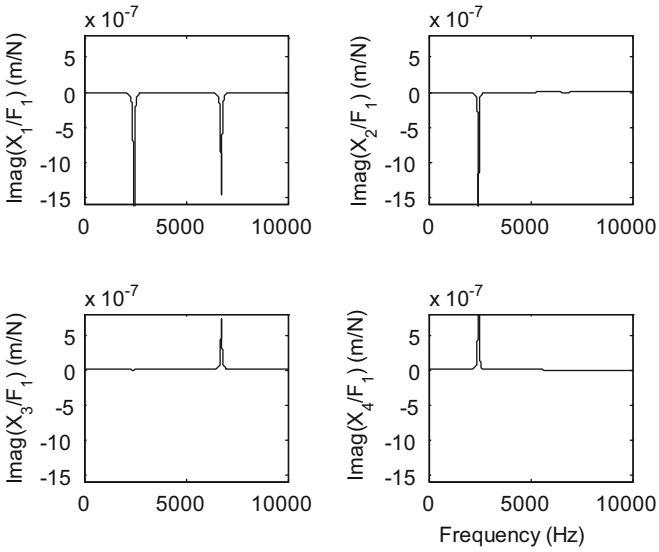

Fig. 6.19 The first three bending mode shapes for a fixed-free beam

Table 6.5 Constants for the fixed-free beam mode shape calculation in Eq. 6.12 [2]

Mode i	λ_i	σ_i
1	1.87510407	0.734095514
2	4.69409113	1.018467319
3	7.85475744	0.999224497

$$\psi_i = \frac{1}{2}\left(cosh\left(\frac{\lambda_i x}{l}\right) - cos\left(\frac{\lambda_i x}{l}\right) - \sigma_i\left(sinh\left(\frac{\lambda_i x}{l}\right) - sin\left(\frac{\lambda_i x}{l}\right)\right)\right) \quad (6.12)$$

We'll select three measurement locations along the beam's axis as shown in Fig. 6.20: $x_1 = l$, $x_2 = \frac{l}{2}$, and $x_3 = \frac{l}{4}$ (this location is near a node for the third mode shape); the force is applied at x_1. The imaginary parts of the direct and cross FRFs are displayed in Fig. 6.21a, b. Because there are three modes within the measurement bandwidth and we performed measurements at three locations, we can identify the eigenvectors and modal matrix for the three degree of freedom system. This is actually a requirement for modal analysis. The number of measurement locations and, therefore, the number of direct and cross FRFs must always be equal to the number of degrees of freedom (i.e., the number of modes selected for modeling). This produces a square modal matrix.[10] Using the peak heights *A* through *I* identified in Fig. 6.21, the modal matrix is:

[10]In a square matrix the number of rows and columns is the same.

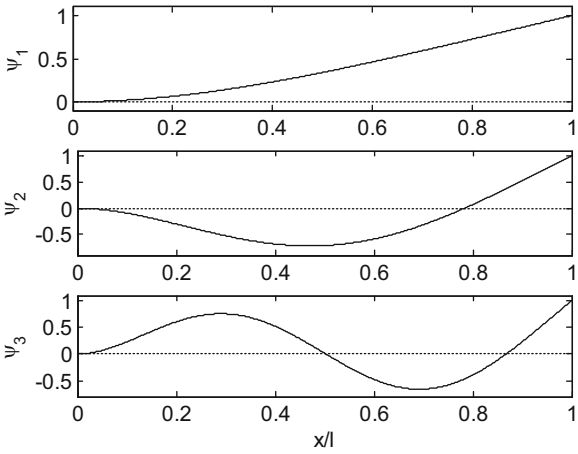

Fig. 6.20 Direct and cross FRF measurement locations for the BEP fixed-free steel rod

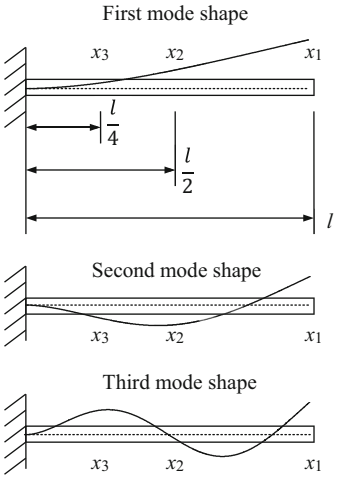

Fig. 6.21 (**a**) The imaginary parts of the three direct and cross FRFs for the BEP fixed-free steel rod (full scale). The peak heights *A*, *D*, and *G* are labeled. (**b**) The imaginary parts of the three direct and cross FRFs for the BEP fixed-free steel rod (reduced scale). The peak heights *B*, *C*, *E*, *F*, *H*, and *I* are labeled

$$P = \begin{bmatrix} \frac{A}{A} = 1 & \frac{B}{B} = 1 & \frac{C}{C} = 1 \\ \frac{D}{A} & \frac{E}{B} & \frac{F}{C} \\ \frac{G}{A} & \frac{H}{B} & \frac{I}{C} \end{bmatrix} = \begin{bmatrix} 1 & 1 & 1 \\ 0.3395 & -0.7137 & 0.0197 \\ 0.0973 & -0.4173 & 0.7245 \end{bmatrix}, \qquad (6.13)$$

where the eigenvectors are normalized to the beam's free end.

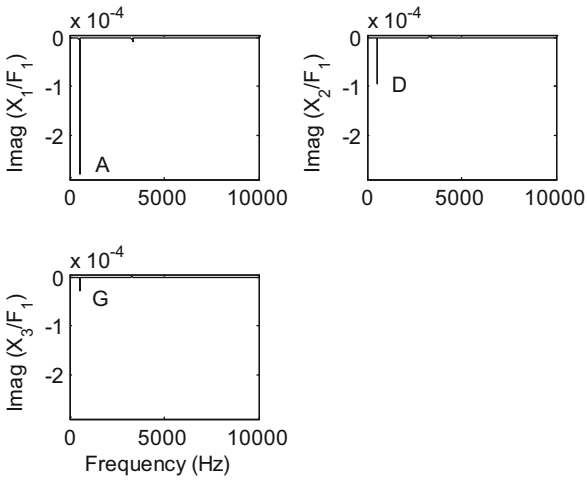

Fig. 6.22 Potential model for describing an automobile's suspension behavior

6.6 Shortcut Method for Determining Mass, Stiffness, and Damping Matrices

So far we've only discussed the chain-type spring-mass-damper model shown in Fig. 6.7 for the backward problem solution. Of course there may be situations where the structure's design and/or behavior warrant another model type. For example, an automobile's suspension response may be better described using the model shown in Fig. 6.22, which includes a rigid, massless bar, two concentrated masses, two degrees of freedom, and two springs and viscous dampers.

Let's next describe a shortcut method that can applied to determine the local coordinate mass, damping, and stiffness matrices for lumped parameter models, such as those shown in Figs. 6.7 and 6.22. We'll begin with Fig. 6.7 since we have already identified the matrices using the free body diagrams. In the shortcut method, the force required to give a unit acceleration to the coordinate in question, while holding the other coordinate(s) motionless, is used to determine the on-diagonal terms in the mass matrix. The force that is required to hold the other coordinate(s) motionless defines the off-diagonal terms. Similarly, the damping matrix is determined using the force required to give a unit velocity and the stiffness matrix is identified using the force required to give a unit displacement.

The mass matrix for the two degree of freedom model has four terms: two on-diagonals, m_{11} and m_{22}, and two off-diagonals, m_{12} and m_{21}.

$$m = \begin{bmatrix} m_{11} & m_{12} \\ m_{21} & m_{22} \end{bmatrix}$$

To determine the mass matrix we neglect the influence of the springs, dampers, and external forces. Let's begin with the m_{11} on-diagonal term. We need to find the force, $f_{m_{11}}$, required to give coordinate x_1 a unit acceleration, $\ddot{x}_1 = 1$, while holding

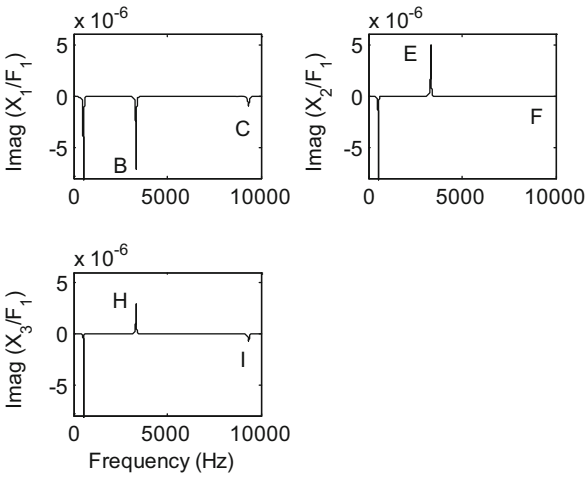

Fig. 6.23 Force balance for determining m_{11}

the other coordinate, x_2, motionless. When we remove the springs and dampers, the two coordinates are not connected so the analysis is simple. The forces are shown in Fig. 6.23. Summing the forces in the x_1 direction to zero gives:

$$f_{m_{11}} = m_1 \ddot{x}_1 = m_1(1) = m_1.$$

The m_{11} on-diagonal term is therefore m_1. The m_{12} off-diagonal term is the force, $f_{m_{12}}$, required to hold x_2 stationary while giving x_1 a unit acceleration. In the absence of the springs and dampers, no force is necessary to restrict x_2 as shown in Fig. 6.24. Therefore, the force summation in the x_2 direction gives:

$$f_{m_{12}} = 0.$$

We find the other on-diagonal term, m_{22}, by applying a unit acceleration to x_2 while holding x_1 motionless. Using Fig. 6.25, the required force is:

$$f_{m_{22}} = m_2 \ddot{x}_2 = m_2(1) = m_2.$$

The m_{21} off-diagonal term is the force, $f_{m_{21}}$, required to hold x_1 fixed while giving x_2 a unit acceleration. It is calculated using Fig. 6.26. We find that $f_{m_{21}} = 0$. We didn't actually need to calculate $f_{m_{21}}$, however. Because the mass matrix is symmetric, we know that $f_{m_{21}} = f_{m_{12}}$. However, it serves as a good check to ensure that our $f_{m_{12}}$ calculation was correct. We can now populate the mass matrix for Fig. 6.7.

$$m = \begin{bmatrix} m_{11} & m_{12} \\ m_{21} & m_{22} \end{bmatrix} = \begin{bmatrix} m_1 & 0 \\ 0 & m_2 \end{bmatrix}$$

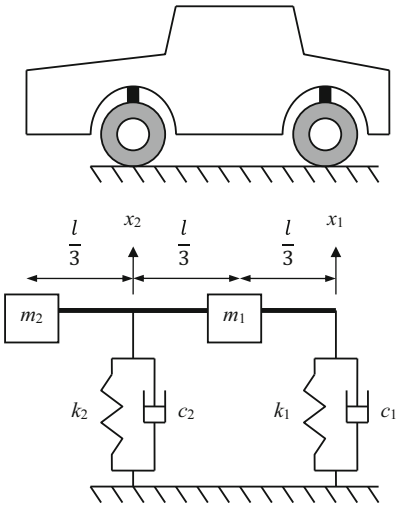

Fig. 6.24 Force balance for determining m_{12}

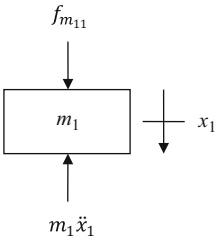

Fig. 6.25 Force balance for determining m_{22}

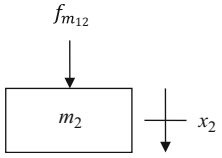

Fig. 6.26 Force balance for determining m_{21}

Of course this is the same result we obtained previously. To determine the stiffness matrix, we neglect the masses, dampers, and external forces.

$$k = \begin{bmatrix} k_{11} & k_{12} \\ k_{21} & k_{22} \end{bmatrix}$$

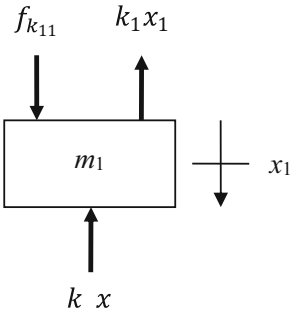

Fig. 6.27 Force balance for determining k_{11}

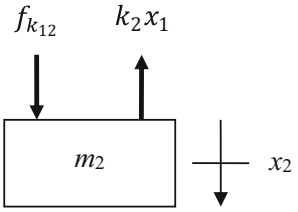

Fig. 6.28 Force balance for determining k_{12}

To find k_{11}, we need the force, $f_{k_{11}}$, required to give coordinate x_1 a unit displacement, $x_1 = 1$, while holding the other coordinate, x_2, motionless. The free body diagram is provided in Fig. 6.27. Summing the forces in the x_1 direction gives:

$$f_{k_{11}} = k_1x_1 + k_2x_1 = k_1(1) + k_2(1) = k_1 + k_2.$$

The off-diagonal term, k_{12}, is the force required to hold x_2 stationary while giving x_1 a unit displacement. Using Fig. 6.28, we see that:

$$f_{k_{12}} = -k_2x_1 = -k_2(1) = -k_2.$$

We determine k_{22} from the force, $f_{k_{22}}$, required to give coordinate x_2 a unit displacement while holding x_1 stationary. The free body diagram is displayed in Fig. 6.29. The force summation in the x_2 direction gives:

$$f_{k_{22}} = k_2x_2 = k_2(1) = k_2.$$

Finally, we find k_{21} from the force required to hold x_1 fixed while giving x_2 a unit displacement. See Fig. 6.30, where the force balance requires that $f_{k_{21}} = -k_2$, which satisfies our symmetry requirement. The system stiffness matrix is:

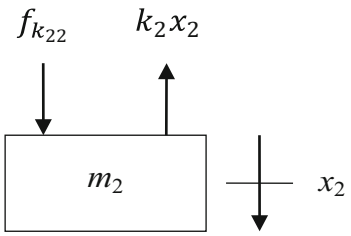

Fig. 6.29 Force balance for determining k_{22}

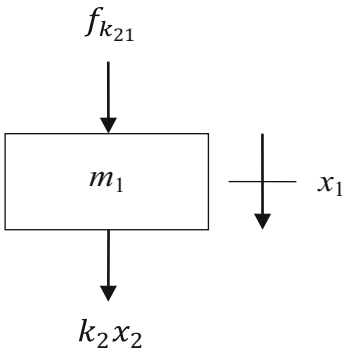

Fig. 6.30 Force balance for determining k_{21}

$$k = \begin{bmatrix} k_{11} & k_{12} \\ k_{21} & k_{22} \end{bmatrix} = \begin{bmatrix} k_1 + k_2 & -k_2 \\ -k_2 & k_2 \end{bmatrix},$$

which agrees with our previous result using the free body diagrams. We could complete the analysis for damping by applying a unit velocity and neglecting the springs, masses, and external forces, but we can see from Fig. 6.7 that the dampers are located at the same physical locations as the springs. Therefore, the damping matrix will have the same form as the stiffness matrix.

6.6.1 Linearized Pendulum

Let's next use the shortcut method for the **linearized pendulum**. We'll begin with the traditional free body diagram analysis and then follow it with the new shortcut method. The pendulum, relevant geometry, and free body diagram are shown in Fig. 6.31. As seen in Sect. 2.5.2, we can sum the moments, M, about O, using the force components that are perpendicular to the massless rod. Because we are summing about O, the reaction components at the pivot may be neglected. Also, the free body diagram includes d'Alembert's inertial moment, $J\ddot{\theta} = ml^2\ddot{\theta}$, with the mass moment of inertia, J, so that $\sum M_O = 0$.

The moment sum about O from Fig. 6.31 is:

$$\sum M_O = J\ddot{\theta} + k\delta cos(\theta) \cdot a + mgsin(\theta) \cdot l = 0. \tag{6.14}$$

Substituting $J = ml^2$ and $\delta = asin(\theta)$ gives:

$$ml^2\ddot{\theta} + ka^2\, cos\,(\theta)\, sin\,(\theta) + mglsin(\theta) = 0. \tag{6.15}$$

For small angles, we can approximate using $sin(\theta) \approx \theta$ and $cos(\theta) \approx 1$. Substitution yields:

$$ml^2\ddot{\theta} + ka^2\theta + mgl\theta = ml^2\ddot{\theta} + \left(ka^2 + mgl\right)\theta = 0. \tag{6.16}$$

We can convert to small horizontal displacements, x, of the pendulum mass by again applying the small angle approximation. See Fig. 6.32, where $x = lsin(\theta) \approx l\theta$ and, subsequently, $\ddot{x} \approx l\ddot{\theta}$ for a constant rod length. Rewriting Eq. 6.16 in terms of x gives:

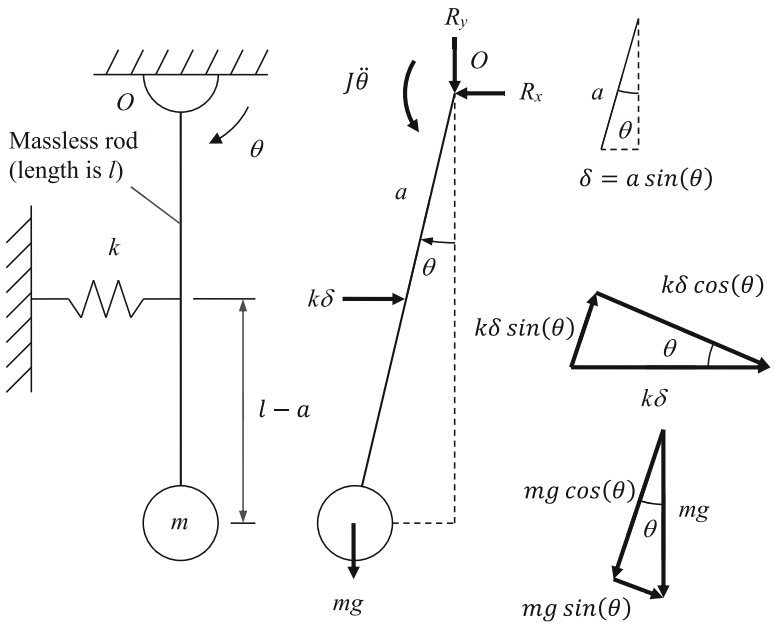

Fig. 6.31 Linearized pendulum and its free body diagram

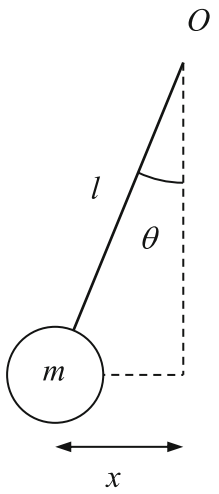

Fig. 6.32 Relationship between small angles, θ, and horizontal displacements, x, of the pendulum mass

$$ml^2\frac{\ddot{x}}{l}+\left(ka^2+mgl\right)\frac{x}{l}=ml\ddot{x}+\left(\frac{ka^2}{l}+mg\right)x=m\ddot{x}+\left(\frac{ka^2}{l^2}+\frac{mg}{l}\right)x$$
$$=0. \tag{6.17}$$

Now let's use the shortcut method. To find the mass term for the single degree of freedom equation of motion, we need to determine the force, f_m, required to give the pendulum mass a unit (horizontal) acceleration. Figure 6.33 shows the forces, where the spring is neglected. Summing the moments about O gives:

$$\sum M_O = f_m l - m\ddot{x}l = f_m l - m(1)l = f_m l - ml = 0. \tag{6.18}$$

Simplifying Eq. 6.18 gives $f_m = m$. To determine the stiffness term, we find the force, f_k, required to give the pendulum mass a unit displacement. In this case, we neglect the inertial influence of the mass in the free body diagram, but must include the gravitational effects; see Fig. 6.34. Summing the moments about O gives:

$$\sum M_O = f_k l - k\left(x\frac{a}{l}\right)a - mg\frac{x}{l}l = f_k l - k\left(\frac{a}{l}\right)a - mg$$
$$= f_k l - k\frac{a^2}{l} - mg. \tag{6.19}$$

Note that the displacement at the spring is not $x = 1$. Rather, it is scaled by the distance from the pivot O and is $x\frac{a}{l} = \frac{a}{l}$ for a unit displacement x. Solving for f_k from Eq. 6.19 gives the stiffness term:

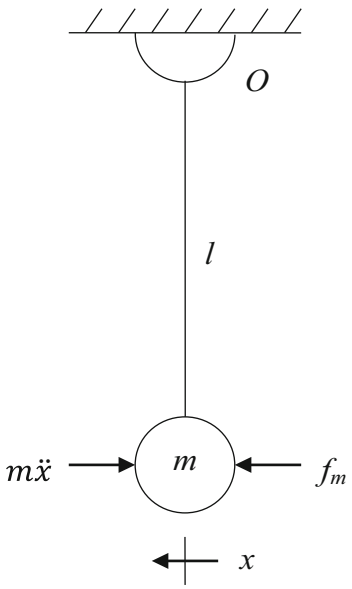

Fig. 6.33 Force balance to determine the mass term

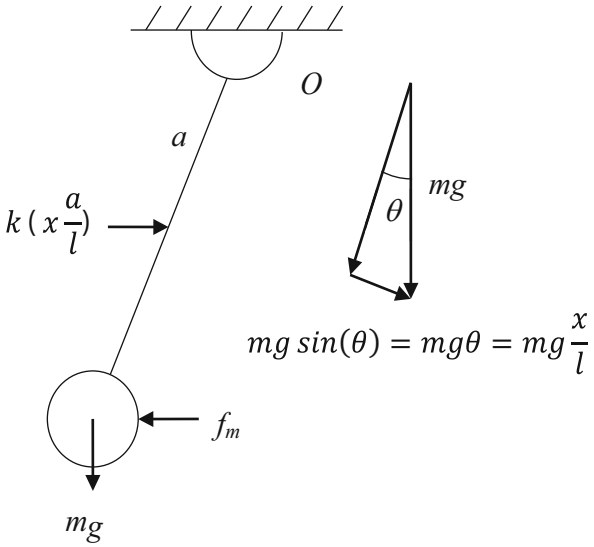

Fig. 6.34 Force balance to determine the stiffness term

$$f_k = \frac{ka^2}{l^2} + \frac{mg}{l}. \tag{6.20}$$

As expected, substitution in the differential equation of motion gives the same result that we obtained from the free body diagram approach; see Eq. 6.17.

6.6.2 Automobile Suspension Model

Let's conclude this section (and chapter) by determining the mass, damping, and stiffness matrices for the automobile suspension model shown in Fig. 6.22. We'll begin with the 2×2 mass matrix for the two degree of freedom system. We determine m_{11} from the force, $f_{m_{11}}$, required to apply a unit acceleration to x_1 while holding x_2 stationary. The force balance is shown in Fig. 6.35, where the motionless x_2 is represented as a pivot for the rigid, massless bar. The accelerations at the two masses are both $\frac{\ddot{x}_1}{2} = \frac{1}{2}$ because they are half the distance from the pivot relative to x_1. Summing the moments (clockwise moments are taken to be positive) about the x_2 pivot gives:

$$\begin{aligned}\sum M &= -f_{m_{11}} \cdot \frac{2l}{3} + m_1 \frac{\ddot{x}_1}{2} \cdot \frac{l}{3} + m_2 \frac{\ddot{x}_1}{2} \cdot \frac{l}{3} \\ &= -f_{m_{11}} \cdot \frac{2l}{3} + m_1 \frac{1}{2} \cdot \frac{l}{3} + m_2 \frac{1}{2} \cdot \frac{l}{3} = 0.\end{aligned} \tag{6.21}$$

Dividing by $\frac{l}{3}$ and solving for $f_{m_{11}}$ yields:

$$f_{m_{11}} = \frac{m_1 + m_2}{4}. \tag{6.22}$$

The off-diagonal term m_{12} is the force that is necessary to hold x_2 motionless. The forces are displayed in Fig. 6.36. The force summation is:

$$\sum f = f_{m_{11}} + f_{m_{12}} - m_1 \frac{\ddot{x}_1}{2} + m_2 \frac{\ddot{x}_1}{2} = f_{m_{11}} + f_{m_{12}} - m_1 \frac{1}{2} + m_2 \frac{1}{2} = 0. \tag{6.23}$$

Solving Eq. 6.23 for $f_{m_{12}}$ gives:

$$f_{m_{12}} = -f_{m_{11}} + \frac{m_1}{2} - \frac{m_2}{2}. \tag{6.24}$$

Substituting for $f_{m_{11}}$ from Eq. 6.22 gives the final expression for $f_{m_{12}}$.

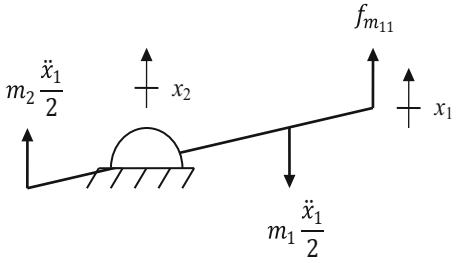

Fig. 6.35 Force balance to determine m_{11}

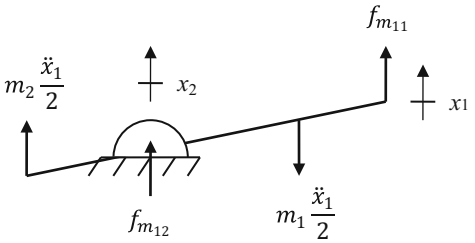

Fig. 6.36 Force balance to determine m_{12}

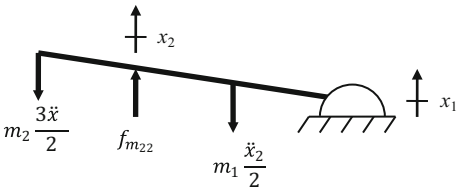

Fig. 6.37 Force balance to determine m_{22}

$$f_{m_{12}} = -\left(\frac{m_1 + m_2}{4}\right) + \frac{m_1}{2} - \frac{m_2}{2} = \frac{m_1 - 3m_2}{4} \tag{6.25}$$

We'll next find m_{22} by applying a unit acceleration to x_2 while holding x_1 stationary. The corresponding forces are shown in Fig. 6.37. The moment summation about the x_1 pivot is:

$$\begin{aligned} \sum M &= f_{m_{22}} \cdot \frac{2l}{3} - m_1 \frac{\ddot{x}_1}{2} \cdot \frac{l}{3} - m_2 \frac{3\ddot{x}_1}{2} \cdot \frac{3l}{3} \\ &= f_{m_{22}} \cdot \frac{2l}{3} - m_1 \frac{1}{2} \cdot \frac{l}{3} - m_2 \frac{3}{2} \cdot \frac{3l}{3} = 0. \end{aligned} \tag{6.26}$$

Dividing by $\frac{l}{3}$ and solving for $f_{m_{22}}$ leads to Eq. 6.27.

$$f_{m_{22}} = \frac{m_1 + 9m_2}{4} \tag{6.27}$$

Let's find m_{21} as a check on our m_{12} result. It is the force required to hold x_1 fixed while applying the unit acceleration to x_2. The forces are displayed in Fig. 6.38 and the force summation gives:

$$\sum f = f_{m_{21}} + f_{m_{22}} - m_1 \frac{\ddot{x}_2}{2} + m_2 \frac{3\ddot{x}_2}{2} = f_{m_{21}} + f_{m_{22}} - m_1 \frac{1}{2} - m_2 \frac{3}{2} = 0. \tag{6.28}$$

Solving for $f_{m_{21}}$ and substituting for $f_{m_{22}}$ yields the m_{21} value; see Eq. 6.29. As anticipated, it matches the m_{12} result provided in Eq. 6.25. The mass matrix is

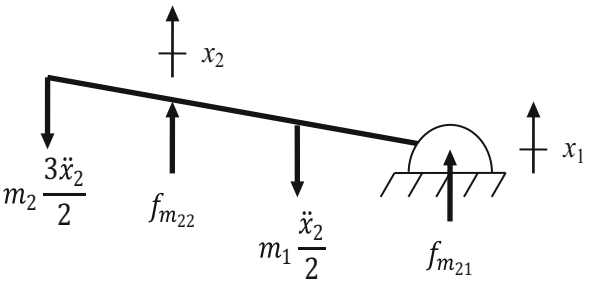

Fig. 6.38 Force balance to determine m_{21}

provided in Eq. 6.30. We note that it is symmetric and, because the off-diagonals are non-zero, the equations of motion are coupled through the mass matrix.

$$f_{m_{21}} = -\left(\frac{m_1 + 9m_2}{4}\right) + \frac{m_1}{2} + \frac{3m_2}{2} = \frac{m_1 - 3m_2}{4} \tag{6.29}$$

$$m = \begin{bmatrix} m_{11} & m_{12} \\ m_{21} & m_{22} \end{bmatrix} = \begin{bmatrix} \frac{m_1 + m_2}{4} & \frac{m_1 - 3m_2}{4} \\ \frac{m_1 - 3m_2}{4} & \frac{m_1 + 9m_2}{4} \end{bmatrix} \tag{6.30}$$

Now let's populate the stiffness matrix. For the k_{11} on-diagonal term, we need the force required to give a unit displacement to x_1 while holding x_2 stationary. The forces are shown in Fig. 6.39. The moment sum about the motionless x_2 is given by:

$$\sum M = -f_{k_{11}} \cdot \frac{2l}{3} + k_1 x_1 \cdot \frac{2l}{3} = -f_{k_{11}} \cdot \frac{2l}{3} + k_1 \cdot \frac{2l}{3} = 0. \tag{6.31}$$

Dividing by $\frac{2l}{3}$ and solving for $f_{k_{11}}$ gives the stiffness k_{11}.

$$f_{k_{11}} = k_1 \tag{6.32}$$

The off-diagonal term k_{12} is the force required to hold x_2 motionless. See Fig. 6.40, where the force summation yields:

$$\sum f = f_{k_{11}} + f_{k_{12}} - k_1 x_1 = f_{k_{11}} + f_{k_{12}} - k_1 = 0. \tag{6.33}$$

Substituting k_1 for $f_{k_{11}}$ in Eq. 6.33 enables us to determine the k_{12} stiffness.

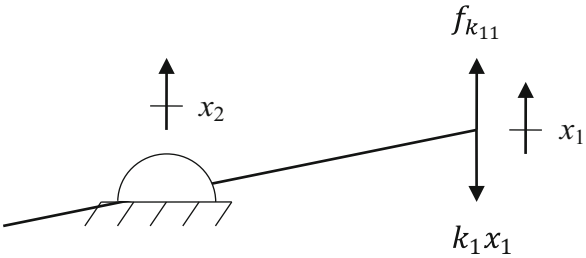

Fig. 6.39 Force balance to determine k_{11}

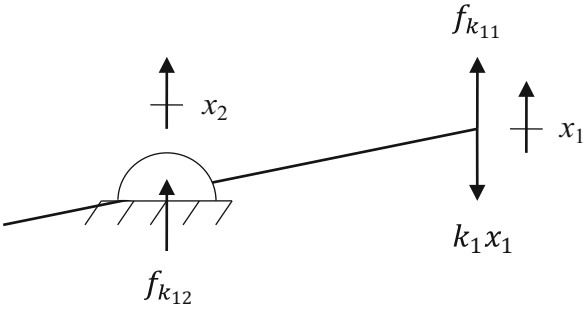

Fig. 6.40 Force balance to determine k_{12}

$$f_{k_{12}} = 0 \tag{6.34}$$

The other on-diagonal term, k_{22}, is determined from the force required to give a unit displacement to x_2 while holding x_1 fixed. The forces are displayed in Fig. 6.41. Summing the moments about x_1 gives:

$$\sum M = f_{k_{22}} \cdot \frac{2l}{3} - k_2 x_2 \cdot \frac{2l}{3} = f_{k_{22}} \cdot \frac{2l}{3} - k_2 \cdot \frac{2l}{3} = 0. \tag{6.35}$$

We solve Eq. 6.35 for $f_{k_{22}}$ to determine k_{22}.

$$f_{k_{22}} = k_2 \tag{6.36}$$

The off-diagonal term, k_{21}, is the force required to hold x_1 stationary. Summing the forces in Fig. 6.42 and substituting for $f_{k_{22}}$ provides the desired result.

$$\begin{aligned} \sum f = f_{k_{21}} + f_{k_{22}} - k_2 x_2 = f_{k_{21}} + f_{k_{22}} - k_2 = 0 \\ f_{k_{21}} = -f_{k_{22}} + k_2 = -k_2 + k_2 = 0 \end{aligned} \tag{6.37}$$

The final stiffness matrix is:

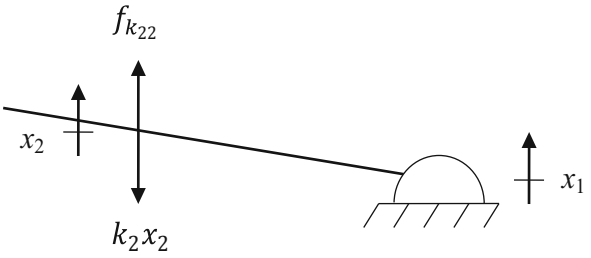

Fig. 6.41 Force balance to determine k_{22}

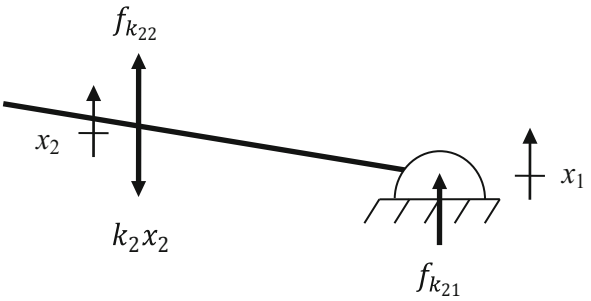

Fig. 6.42 Force balance to determine k_{21}

$$k = \begin{bmatrix} k_{11} & k_{12} \\ k_{21} & k_{22} \end{bmatrix} = \begin{bmatrix} k_1 & 0 \\ 0 & k_2 \end{bmatrix}. \tag{6.38}$$

Because the dampers are appear at the same locations as the springs, the damping matrix is:

$$c = \begin{bmatrix} c_{11} & c_{12} \\ c_{21} & c_{22} \end{bmatrix} = \begin{bmatrix} c_1 & 0 \\ 0 & c_2 \end{bmatrix}. \tag{6.39}$$

Chapter Summary

- In practice, it is commonly required that we have an actual dynamic system and would like to build a model that we can use to represent its vibratory behavior.
- The first step in the "backward problem" of starting with a measurement and developing a model is identifying the modal parameters for each of the modes selected for fitting.
- We can use peak picking to determine the modal parameters from the real and imaginary parts of a measured FRF.
- For a measured direct FRF, each mode can be fit independently to find the modal parameters.

- We assume that proportional damping holds when performing the modal fits to the measured FRF.
- We determine the eigenvectors from the ratios of the peak heights between the cross and direct FRFs. The imaginary parts are used to find the peak heights.
- For structures with free-free boundary conditions, rigid body modes exist.
- Nodes are points of zero deflection on the mode shapes.
- The number of direct and cross FRFs must be equal to the number of modeled modes (degrees of freedom) in order to obtain a square modal matrix.
- Alternative lumped-parameter model types were introduced.
- A shortcut method for identifying the mass, damping, and stiffness matrices for lumped parameter models was described. The on-diagonal and off-diagonal terms were treated separately.

Exercises

1. For a single degree of freedom spring-mass-damper system subject to forced harmonic vibration, the measured FRF is displayed in Figs. P6.1a and P6.1b. Using the peak picking method, determine m (in kg), k (in N/m), and c (in N s/m).
2. The direct and cross FRFs for the two degree of freedom system shown in Fig. P6.2a are provided in Figs. P6.2b and P6.2c.

   (a) If the modal damping ratios are $\zeta_{q1} = 0.01$ and $\zeta_{q2} = 0.016$, determine the modal stiffness values k_{q1} and k_{q2} (N/m) by peak picking.
   (b) Determine the mode shapes by peak picking.

3. A FRF measurement was completed to give the two degree of freedom response shown in Fig. P6.3. Use the peak picking approach to identify the modal mass, stiffness, and damping parameters for the two modes. Arrange your results in the 2×2 modal matrices m_q, c_q, and k_q.
4. A FRF measurement was completed to give the two degree of freedom response shown in Fig. P6.4 (a limited frequency range is displayed to aid in the peak picking activity).

   (a) Use the peak picking approach to identify the modal mass, stiffness, and damping parameters for the two modes. Arrange your results in the 2×2 modal matrices m_q, c_q, and k_q.
   (b) The FRF "measurement" in part a) was defined using the following MATLAB® code.

Fig. P6.1a Measured FRF

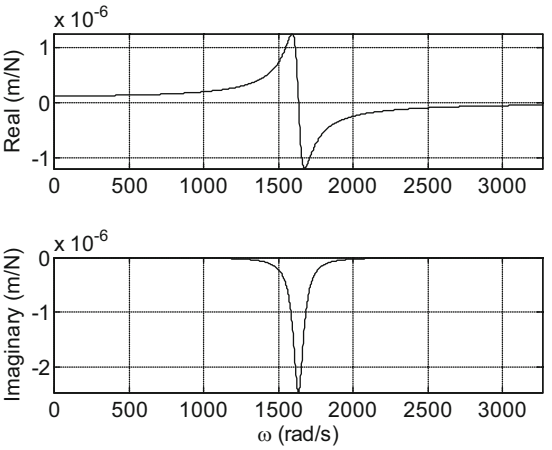

Fig. P6.1b Measured FRF (smaller frequency scale)

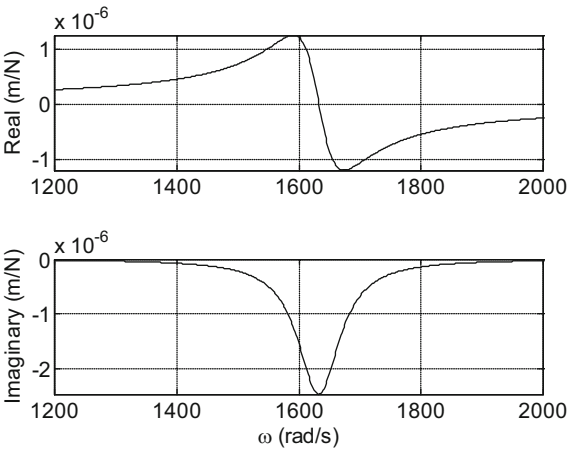


```
kq1 = 6e6;        % N/m
kq2 = 6e6;        % N/m
omega_n1 = 475*2*pi;  % rad/s
omega_n2 = 525*2*pi;
zetaq1 = 0.04;
zetaq2 = 0.04;

omega = 0:1000*2*pi;  % rad/s
r1 = omega/omega_n1;
r2 = omega/omega_n2;

realQ1_R1 = 1/kq1*(1-r1.^2)./((1-r1.^2).^2 + (2*zetaq1*r1).^2);
imagQ1_R1 = 1/kq1*(-2*zetaq1*r1)./((1-r1.^2).^2 + (2*zetaq1*r1).
^2);
```

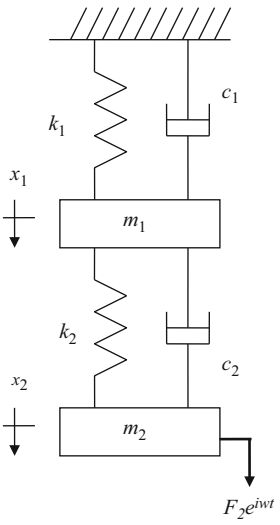

Fig. P6.2a Two degree of freedom spring-mass-damper system under forced vibration

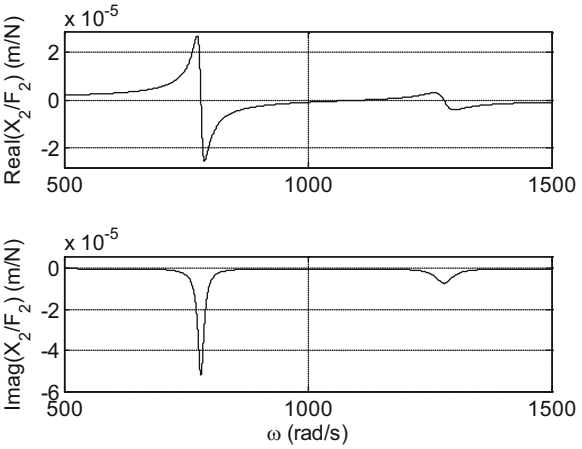

Fig. P6.2b Direct FRF $\frac{X_2}{F_2}$

```
   realQ2_R2 = 1/kq2*(1-r2.^2)./((1-r2.^2).^2 + (2*zetaq2*r2).^2);
   imagQ2_R2 = 1/kq2*(-2*zetaq2*r2)./((1-r2.^2).^2 + (2*zetaq2*r2).
^2);

   realX1_F1 = realQ1_R1 + realQ2_R2;
   imagX1_F1 = imagQ1_R1 + imagQ2_R2;

   freq = omega/2/pi;

   figure(1)
   subplot(211)
   plot(freq, realX1_F1, 'k')
   set(gca,'FontSize', 14)
```

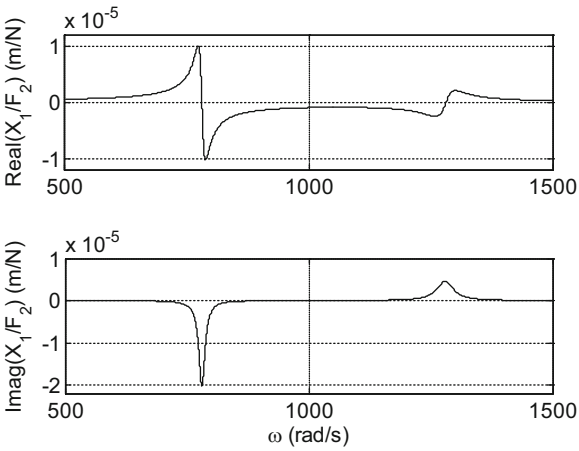

Fig. P6.2c Cross FRF $\frac{X_1}{F_2}$

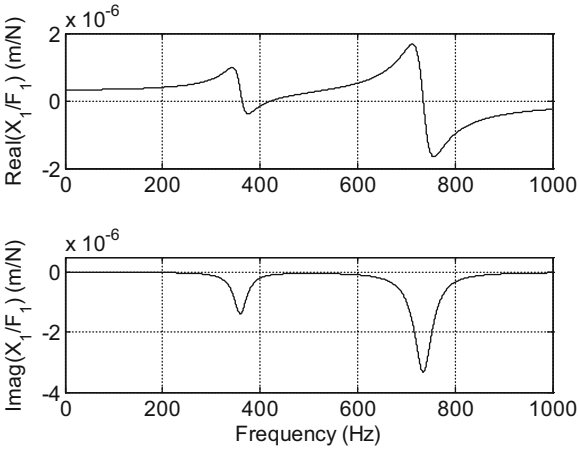

Fig. P6.3 Measured direct FRF for two degree of freedom system

```
axis([200 800 -2e-6 2e-6])
ylabel('Real({X_1}/{F_1}) (m/N)')
grid
subplot(212)
plot(freq, imagX1_F1, 'k')
set(gca,'FontSize', 14)
axis([200 800 -3e-6 5e-7])
xlabel('Frequency (Hz)')
ylabel('Imag({X_1}/{F_1}) (m/N)')
grid
```

Plot your modal fit together with the measured FRF and comment on their agreement.

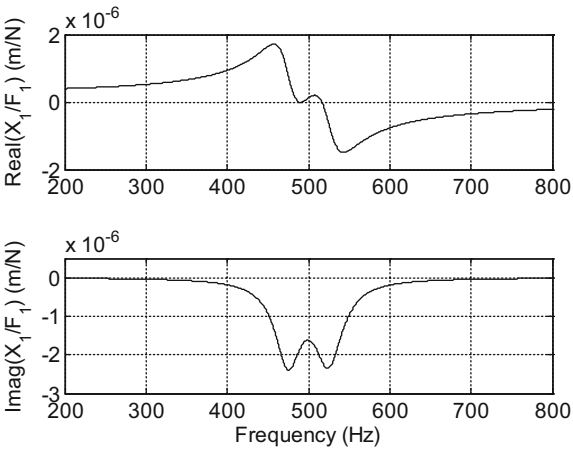

Fig. P6.4 FRF measurement for two degree of freedom system

5. Figures P6.5a, P6.5b, P6.5c, P6.5d, and P6.5e show direct, $\frac{X_1}{F_1}$, and cross FRFs, $\frac{X_2}{F_1}$ through $\frac{X_5}{F_1}$, measured on a fixed-free beam. They were measured at the beam's free end and in 20 mm increments towards its base; see Fig. P6.5f. Determine the mode shape associated with the 200 Hz natural frequency.

   When plotting the mode shape, normalize the free end response at coordinate x_1 to 1 (this is normalizing the mode shape to x_1) and show the relative amplitudes at the other coordinates x_2 through x_5. See Fig. P6.5f
6. For the same fixed-free beam as Problem 5, the measurement bandwidth was increased so that the first three modes were captured. Again, the direct, $\frac{X_1}{F_1}$, and cross FRFs, $\frac{X_2}{F_1}$ through $\frac{X_5}{F_1}$, were measured. The imaginary part of the direct FRF for the entire bandwidth is shown in Fig. P6.6a. The three natural frequencies are 200, 550, and 1250 Hz.

   Use Figs. P6.6b, P6.6c, P6.6d, P6.6e, and P6.6f to identify the mode shape that corresponds to the 1250 Hz natural frequency. Plot your results using the same approach described in Problem 5.
7. Find the mass matrix (in local coordinates) for the two degree of freedom system displayed in Fig. P6.7 using the shortcut method described in Sect. 6.6 if $m_1 = 10$ kg and $m_2 = 12$ kg.
8. Find the stiffness matrix (in local coordinates) for the two degree of freedom system displayed in Fig. P6.7 using the shortcut method described in Sect. 6.6 if $k_1 = 2 \times 10^5$ N/m, $k_2 = 2 \times 10^5$ N/m, and $k_3 = 1 \times 10^5$ N/m.
9. Find the mass matrix (in local coordinates) for the two degree of freedom system displayed in Fig. P6.9 using the shortcut method described in Sect. 6.6 if $m_1 = 10$ kg and $m_2 = 12$ kg.

10. Find the stiffness matrix (in local coordinates) for the two degree of freedom system displayed in Fig. P6.9 using the shortcut method described in Sect. 6.6 if $k_1 = 2 \times 10^5$ N/m, $k_2 = 2 \times 10^5$ N/m.

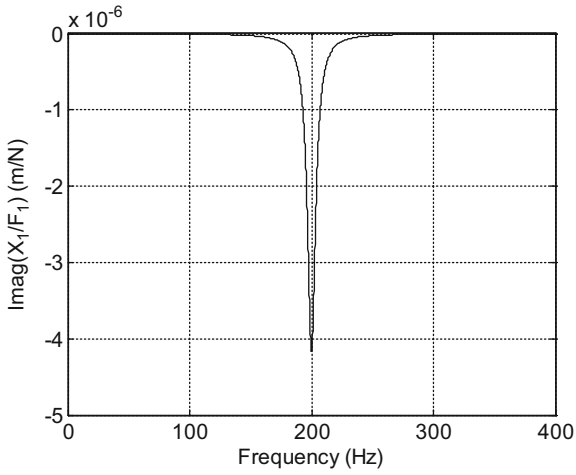

Fig. P6.5a Direct FRF $\frac{X_1}{F_1}$

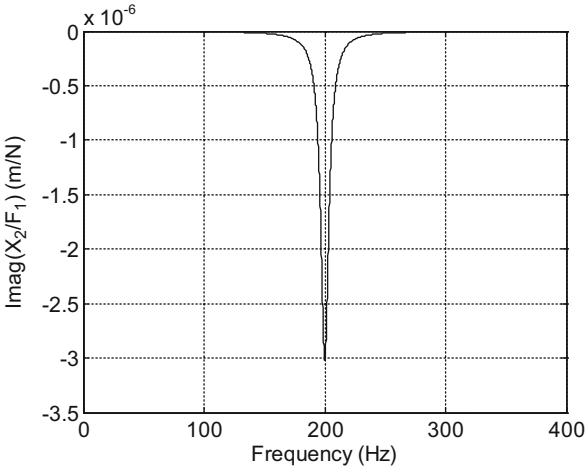

Fig. P6.5b Cross FRF $\frac{X_2}{F_1}$

Fig. P6.5c Cross FRF $\frac{X_3}{F_1}$

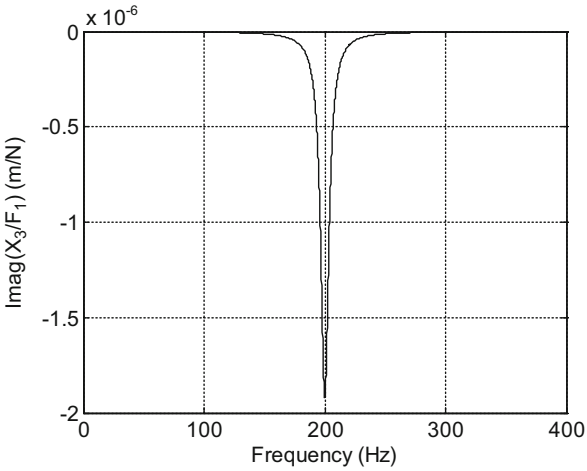

Fig. P6.5d Cross FRF $\frac{X_4}{F_1}$

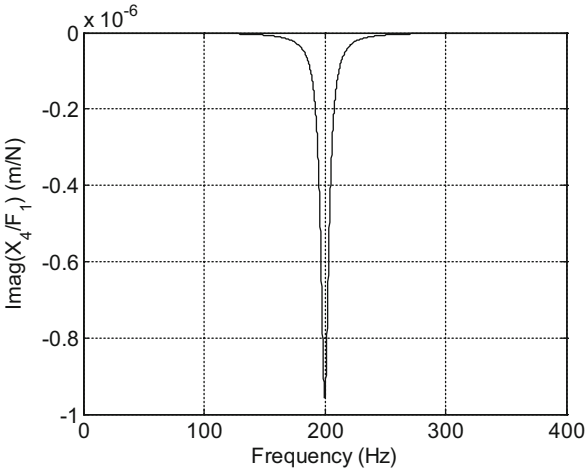

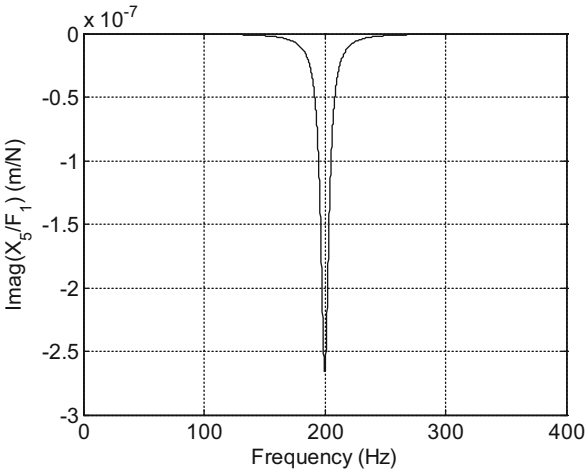

Fig. P6.5e Cross FRF $\frac{X_5}{F_1}$

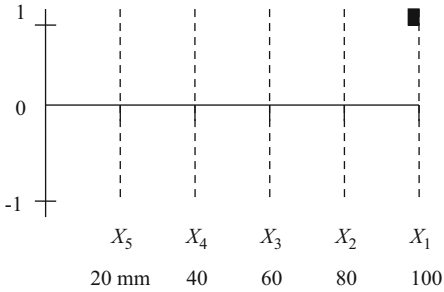

Fig. P6.5f Coordinates for direct and cross FRF measurements

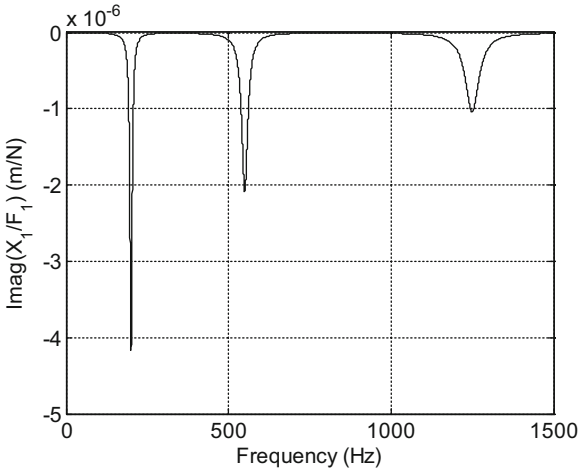

Fig. P6.6a Direct FRF $\frac{X_1}{F_1}$

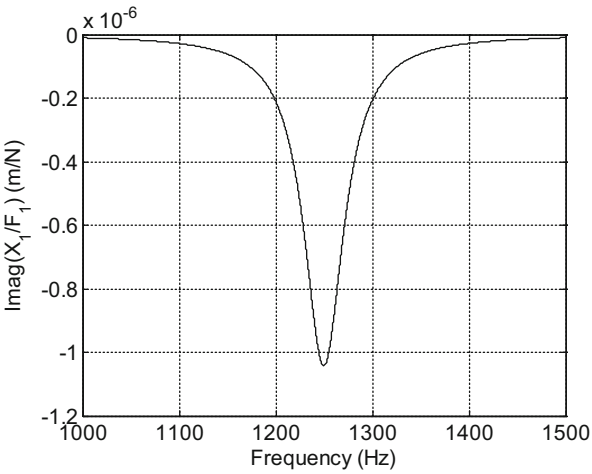

Fig. P6.6b Direct FRF $\frac{X_1}{F_1}$ (mode 3 only)

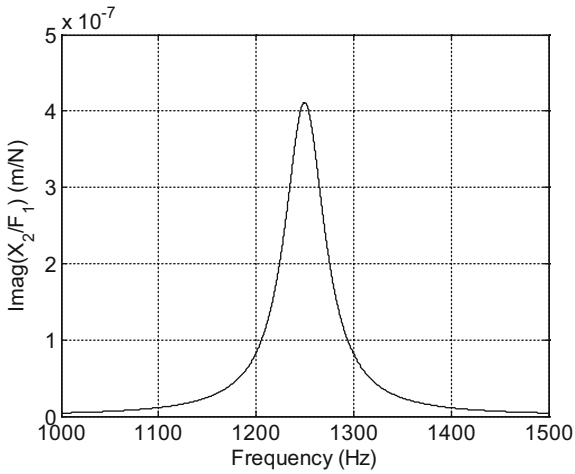

Fig. P6.6c Cross FRF $\frac{X_2}{F_1}$

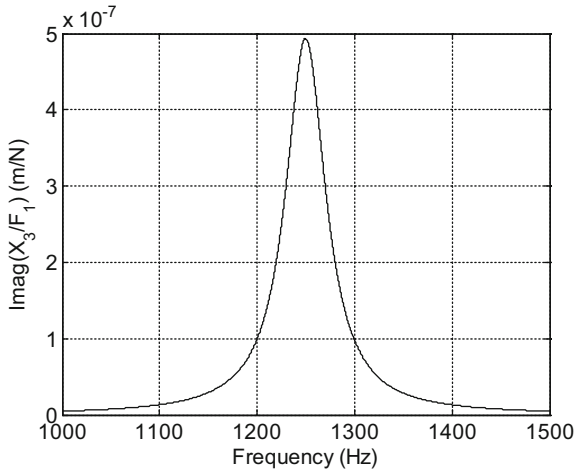

Fig. P6.6d Cross FRF $\frac{X_3}{F_1}$

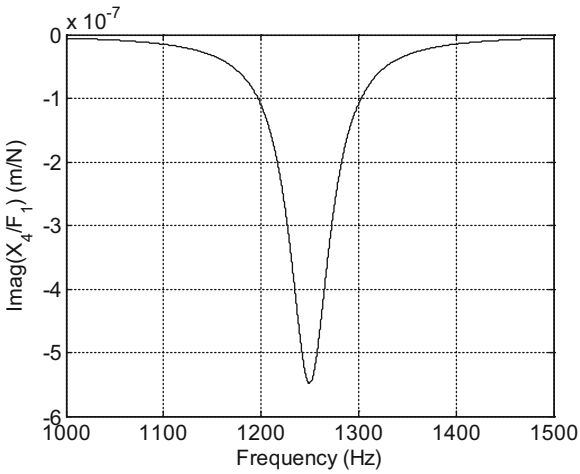

Fig. P6.6e Cross FRF $\frac{X_4}{F_1}$

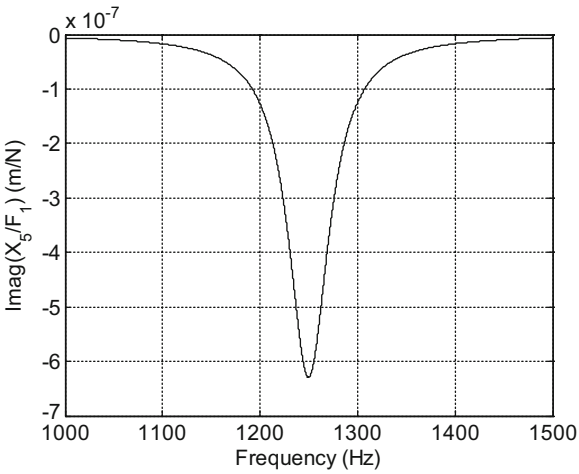

Fig. P6.6f Cross FRF $\frac{X_5}{F_1}$

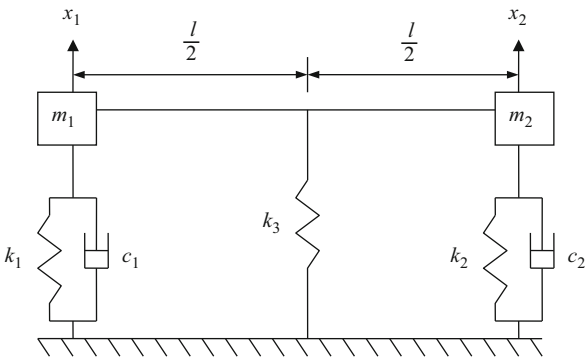

Fig. P6.7 Two degree of freedom system with a rigid, massless bar connecting the two masses, m_1 and m_2

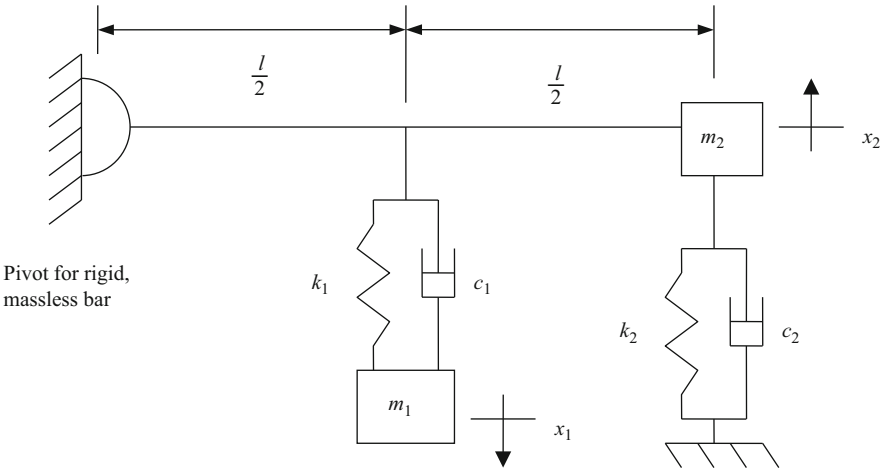

Fig. P6.9 Two degree of freedom system with a rigid, massless bar connecting the mass, m_2, to a fixed pivot

References

1. Schmitz, T. and Smith, K.S., 2019, Machining dynamics: frequency response to improved productivity, 2nd ed, Springer, New York
2. Blevins RD (2001) Formulas for natural frequency and mode shape. Krieger Publishing Co, Malabar, FL, Table 8-1

Chapter 7
Measurement Techniques

> Man is but a reed, the most feeble thing in nature, but he is a thinking reed.
> —*Blaise Pascal*

7.1 Frequency Response Function Measurement

In Chap. 6 we solved the "backward problem" of starting with frequency response function (FRF) measurements and developing a model. However, we did not describe the measurement procedure. The basic hardware required to measure FRFs is:

- a mechanism for known force input across the desired frequency range (or **bandwidth**)
- a transducer for vibration measurement, again with the required bandwidth
- a **dynamic signal analyzer** to record the time-domain force and vibration inputs and convert these into the desired FRF.

A dynamic signal analyzer includes input channels for the time-domain force and vibration signals and computes the Fourier transform of these signals to convert them to the frequency domain. It then calculates the complex-valued ratio of the frequency-domain vibration signal to the frequency-domain force signal; this ratio is the FRF. A schematic of the setup is provided in Fig. 7.1. It includes the time-domain force and vibration (which may take the form of displacement, x, velocity, $\dot{x}$, or acceleration, $\ddot{x}$) inputs and amplifiers for each. The amplifiers are used to increase the magnitude of the signals. The force and vibration are continuous in time, or **analog**. However, recording these signals with the analyzer requires sampling them at small time intervals, or digitizing them. This process is completed using an analog-to-digital converter (ADC). These **digital** signals are then used in the FRF calculation by the dynamic signal analyzer. Based on the vibration input type, the FRF may be expressed as:

T. L. Schmitz, K. S. Smith, *Mechanical Vibrations*,
https://doi.org/10.1007/978-3-030-52344-2_7

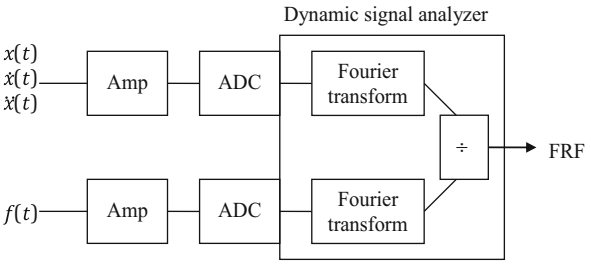

Fig. 7.1 Schematic of FRF measurement setup

- receptance or compliance—the ratio of displacement to force
- mobility—the ratio of velocity to force
- accelerance or inertance—the ratio of acceleration to force.

7.2 Force Input

There are three common types of force excitation. These include:

- fixed frequency sine wave—The FRF is determined one frequency at a time. At each frequency within the desired bandwidth, the sinusoidal force is applied, the response to the force input is averaged over a short time interval, and the FRF is calculated. This is referred to as a **sine sweep test**.
- random signal—The frequency content of the random signal may be broadband (**white noise**) or truncated to a limited range (**pink noise**). Averaging over a fixed period of time is again applied, but all the frequencies within the selected bandwidth are excited in a single test.
- impulse—A short duration impact is used to excite the structure and the corresponding response is measured. This approach enables a broad range of frequencies to be excited in a single, short test. Multiple tests are typically averaged in the frequency domain to improve **coherence**, or the correlation between the force and vibration signals.

To generate these different forces, two common types of force input hardware are applied:

- **shaker** (similar to a speaker)—These systems include a harmonically driven armature and a base. The armature may be actuated along its axis by a magnetic coil or hydraulic force. The magnetic coil, or electrodynamic, configurations can provide excitation frequencies of tens of kHz with force levels from tens to thousands of Newtons (increased force typically means a lower frequency range). Hydraulic shakers offer high force with the potential for a static preload (i.e., the average, or mean, force is not zero), but relatively lower frequency

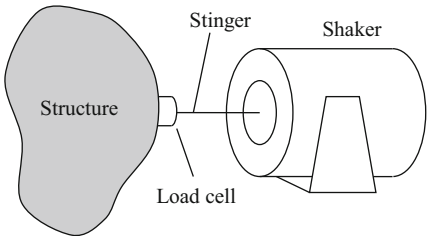

Fig. 7.2 Shaker setup

Fig. 7.3 Example impact hammers. A 150 mm steel ruler is included in the photograph to provide scale

ranges. In either case, the force is often applied to the structure of interest through a **stinger**, or a slender rod that supports axial tension and compression, but not bending or shear. This insures that the force is applied in a single direction only. A load cell is incorporated in the setup to measure the input force. See Fig. 7.2. One consideration is that this load cell adds mass to the system under test, which can alter the FRF for structures with low modal mass values. Finally, the shaker must be isolated from the structure to prevent reaction forces due to the shaker motion from being transmitted through the shaker base to the structure.

- **impact hammer**—An impact hammer incorporates a force transducer located at a metal, plastic, or rubber tip to measure the force input during a hammer strike. When a hammer is used in conjunction with a vibration transducer, the measurement procedure is referred to as **impact testing**. The energy input to the structure is a function of the hammer mass; a larger mass provides more energy (the linear momentum is the product of mass and velocity). Therefore, many sizes are available. Examples are displayed in Fig. 7.3. Also, the excitation bandwidth of

the force input depends on the mass and tip stiffness. Stiffer tips tend to excite a wider frequency range, but also spread the input energy over this wider range. Softer tips concentrate the energy over a lower frequency range. This is discussed further in Sect. 7.4. Hard plastic and metal tips provide higher stiffness, while rubber tips give reduced stiffness.

In a Nutshell
Impact testing excites the structure with many frequencies, all at the same time. The Fourier transform provides a way to separate them. This type of testing increased in popularity when computers became available to handle the computational load. Prior to that time, shaker measurements dominated.

7.3 Vibration Measurement

Vibration transducers are available in both non-contact and contact types. While non-contact transducers, such as **capacitance probes** and **laser vibrometers**, are preferred because they do not affect the system dynamics, contacting types, such as **accelerometers**, are often more convenient to implement. As a compromise, low mass accelerometers may be used to minimize the influence on the test structure. They are attached at the location of interest using wax, adhesive, a magnet, or a threaded stud and then removed when the testing is completed. Let's now discuss these different transducers in more detail.

7.3.1 Capacitance Probe

Noncontact capacitive sensors measure changes in capacitance, the ability of a body to hold an electrical charge. When a voltage is applied to two conductors separated by some distance, an electric field is produced between them and positive and negative charges collect on each conductor. If the polarity of the voltage is reversed, then the charges also reverse.

Capacitive sensors use an alternating voltage which causes the charges to continually reverse their positions. This charge motion generates an alternating electric current which is detected by the sensor. The amount of current flow is determined by the capacitance, which depends on the surface area of the conductors, the distance between them, and the dielectric constant of the material between them (such as air). The capacitance, C, is directly proportional to the surface area, A, and inversely proportional to the distance, d, between them. A larger surface area and smaller distance produces a larger current. For two parallel plate conductors, the capacitance is given by:

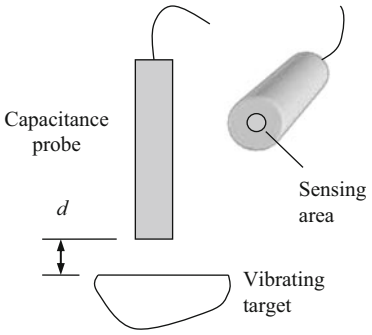

Fig. 7.4 Capacitance probe configuration for vibration measurement

$$C = \varepsilon_r \varepsilon_0 \frac{A}{d}, \tag{7.1}$$

where ε_r is the dielectric constant (or static relative permittivity) and ε_0 is the electric constant (or vacuum permittivity). The value of the dielectric constant is 1 in vacuum and the electric constant is 8.854187817... $\times$ 10^{-12} A·s/(V·m).

Typically, the probe is one of the conductors and the measurement target is the other. If the sizes of the sensor and the target and dielectric constant of the material between them are assumed to be constant, then any change in capacitance is due to a change in the distance between the probe and the target [1]. A common capacitance probe configuration is displayed in Fig. 7.4.

In a Nutshell
A capacitance gage requires that the target is a conductor. If the target is not flat and parallel to the tip of the probe, then the distance-capacitance relationship must be calibrated using the target. The capacitance gage makes a relative measurement and there must be a suitable mounting structure for the probe—that is, we do not want to measure the FRF of a flexible probe mount when we are trying to measure the FRF of the structure.

7.3.2 Laser Vibrometer

A vibrometer performs non-contact vibration measurements using the Dopper shift[1] of a laser beam's frequency that occurs due to the motion of the target surface. The vibrometer's output is generally an analog voltage that is directly proportional to the component of the target's velocity in the laser beam direction. A schematic of a vibrometer is shown in Fig. 7.5. In the figure, the laser head emits a single frequency, f_0. A portion of this beam is redirected using a beam splitter and serves as a reference

[1]You may recognize this Doppler frequency shift as the increase in the pitch (frequency) of an approaching automobile's horn and subsequent drop in pitch after the automobile passes you.

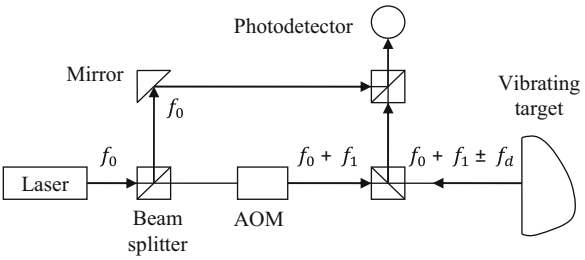

Fig. 7.5 Laser vibrometer schematic

signal. The remainder continues to an acousto-optic modulator (AOM) which upshifts the light frequency to $f_0 + f_1$. When this test beam is reflected from the target surface, it is Doppler shifted by f_d, where the Doppler frequency is directly proportional to the target velocity. The frequency-shifted measurement signal is recombined with the reference signal and the corresponding interference signal is incident on a photodetector. The photodetector current is then used to determine the time-dependent target velocity.

Given the target velocity and excitation force as inputs, the dynamic signal analyzer calculates their frequency-domain ratio, or mobility, $\frac{V}{F}(\omega)$, as the output. To convert from mobility to receptance, $\frac{X}{F}(\omega)$, we simply divide by the product, $i\omega$. To understand this frequency-domain integration, let's write the harmonic displacement as $x(t) = Xe^{i\omega t}$. The corresponding velocity is $\dot{x}(t) = i\omega Xe^{i\omega t} = i\omega \cdot x(t)$. The conversion from mobility to receptance is therefore given by:

$$\frac{X}{F}(\omega) = \frac{X}{V}\frac{V}{F} = \frac{1}{i\omega}\frac{V}{F}. \tag{7.2}$$

7.3.3 Accelerometer

Accelerometers for structural vibration measurement typically use the **piezoelectric**[2] effect to generate a voltage signal that is proportional to acceleration. A schematic is provided in Fig. 7.6. An accelerometer includes, at minimum, a seismic mass, piezoelectric material, and package that is connected to the structure under test. The piezoelectric material may be quartz, tourmaline, barium titanate ($BaTiO_3$), or lead zirconate titanate ($Pb[Zr_xTi_{1-x}]O_3$, $0 < x < 1$, or PZT) and produces a charge when strained by the inertial force applied by the mass during motion of the base. The corresponding voltage is equal to this charge divided by the piezoelectric material's capacitance. The output voltage is proportional to the inertial force and, therefore, the acceleration.[3] As shown in Fig. 7.1, the voltage is carried to the

[2]The prefix piezo is derived from the Greek word *piezein*, which translates "to squeeze".

[3]This follows from Newton's second law, $F = ma$.

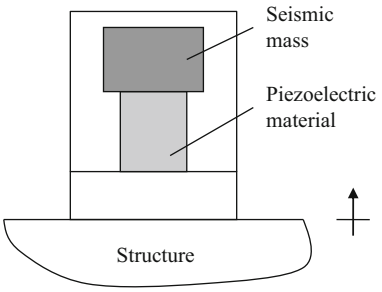

Fig. 7.6 Accelerometer schematic

Fig. 7.7 Example accelerometers

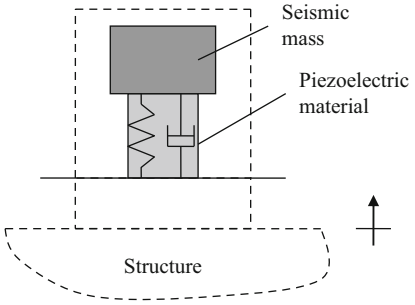

Fig. 7.8 Representation of an accelerometer as a spring-mass-damper system

dynamic signal analyzer by a cable, which can have a capacitance on the same order as the piezoelectric material. The increased capacitance decreases the voltage for a given charge. In order to eliminate this effect (and reduce the measurement noise), an amplifier is usually located within the accelerometer package. Example accelerometers are pictured in Fig. 7.7.

If we think of the piezoelectric material as having finite stiffness and damping which resist the deformation (strain) imposed by the seismic mass, then we can represent the accelerometer as shown in Fig. 7.8. This emphasizes that the accelerometer is a dynamic system itself with its own natural frequency that could affect the

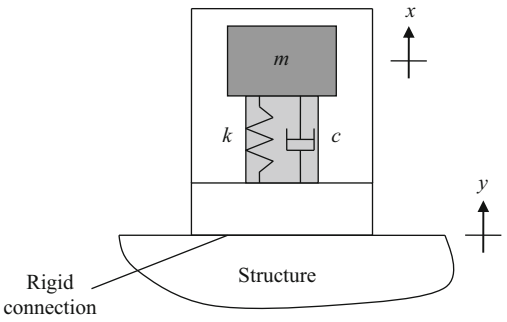

Fig. 7.9 Schematic used to determine the equation of motion for an accelerometer attached to a vibrating structure

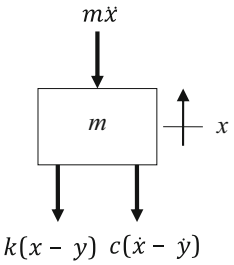

Fig. 7.10 Free body diagram for the accelerometer's seismic mass with a moving base structure

measurement result. For this reason, accelerometers are designed to have high natural frequencies (nearly 100 kHz for low mass versions).

The spring-mass-damper accelerometer representation shown in Fig. 7.9 can be used to determine the equation of motion due to motion of the base structure to which the accelerometer is attached. In the figure, m is the seismic mass, k and c are the piezoelectric material's spring stiffness and viscous damping coefficient, y is the test structure displacement, and x is the seismic mass displacement. The free body diagram for the mass is provided in Fig. 7.10. The equation of motion from the force balance in the x direction is:

$$m\ddot{x} + c(\dot{x} - \dot{y}) + k(x - y) = 0. \tag{7.3}$$

This is an example of **base motion** as we discussed in Sect. 3.6. Let's rewrite Eq. 7.3 by substituting $z = x - y$ and $\dot{z} = \dot{x} - \dot{y}$. This gives:

$$m\ddot{x} + c\dot{z} + kz = 0. \tag{7.4}$$

If we now let $\ddot{z} = \ddot{x} - \ddot{y}$, then $\ddot{x} = \ddot{z} + \ddot{y}$. Replacing $\ddot{x}$ and rewriting yields:

$$m\ddot{z} + c\dot{z} + kz = -m\ddot{y}. \tag{7.5}$$

If the structure is experiencing harmonic vibration, then we can write $y(t) = Ye^{i\omega t}$. The corresponding acceleration of the structure is $\ddot{y} = -\omega^2 Ye^{i\omega t}$. If we also let z

$(t) = Ze^{i\omega t}$, calculate the velocity and acceleration, and substitute in Eq. 7.5, then we have:

$$\left(-m\omega^2 + ic\omega + k\right)Ze^{i\omega t} = m\omega^2 Ye^{i\omega t}. \tag{7.6}$$

Equation 7.6 can be written as a ratio of the output (relative vibration) to the input (base structure motion):

$$\frac{Z}{Y} = \frac{m\omega^2}{-m\omega^2 + ic\omega + k} = \frac{m\omega^2}{(k - m\omega^2) + i(c\omega)} = \frac{\omega^2}{\left(\frac{k}{m} - \omega^2\right) + i\left(\frac{c}{m}\omega\right)}. \tag{7.7}$$

From Chap. 2, we know that $\frac{k}{m} = {\omega_n}^2$ and $\frac{c}{m} = 2\zeta\omega_n$. Substituting gives:

$$\frac{Z}{Y} = \frac{\omega^2}{\left(\omega_n^2 - \omega^2\right) + i(2\zeta\omega_n\omega)} = \frac{\frac{\omega^2}{\omega_n^2}}{\left(1 - \frac{\omega^2}{\omega_n^2}\right) + i\left(2\zeta\frac{\omega}{\omega_n}\right)}. \tag{7.8}$$

Replacing $\frac{\omega}{\omega_n}$ with the frequency ratio, r, results in:

$$\frac{Z}{Y} = \frac{r^2}{(1 - r^2) + i(2\zeta r)}. \tag{7.9}$$

To eliminate the imaginary part from the denominator, we can multiply both the numerator and denominator by $(1 - r^2) - i(2\zeta r)$.

$$\frac{Z}{Y} = \frac{r^2}{(1 - r^2) + i(2\zeta r)} \cdot \frac{(1 - r^2) - i(2\zeta r)}{(1 - r^2) - i(2\zeta r)} = \frac{r^2((1 - r^2) - i(2\zeta r))}{(1 - r^2)^2 + (2\zeta r)^2} \tag{7.10}$$

The real part of Eq. 7.10 is:

$$\frac{Z}{Y} = \frac{r^2(1 - r^2)}{(1 - r^2)^2 + (2\zeta r)^2} \tag{7.11}$$

and the imaginary part is:

$$\frac{Z}{Y} = \frac{r^2(-2\zeta r)}{(1 - r^2)^2 + (2\zeta r)^2}. \tag{7.12}$$

The magnitude is the square root of the sum of the squares of the real and imaginary parts.

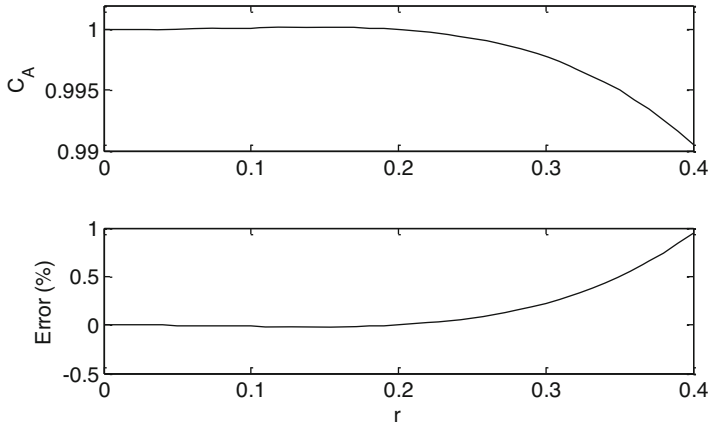

Fig. 7.11 Equation 7.14 coefficient, C_A, plotted versus the frequency ratio, r, for a damping ratio of 0.7. The percent error between 1 and the frequency-dependent C_A value is also shown

$$\left|\frac{Z}{Y}\right| = \sqrt{Re^2 + Im^2} = \sqrt{\frac{(r^2)^2(1-r^2)^2 + (r^2)^2(-2\zeta r)^2}{\left((1-r^2)^2 + (2\zeta r)^2\right)^2}}$$

$$\left|\frac{Z}{Y}\right| = \sqrt{\frac{(r^2)^2\left((1-r^2)^2 + (2\zeta r)^2\right)}{\left((1-r^2)^2 + (2\zeta r)^2\right)^2}} = \sqrt{\frac{(r^2)^2}{\left((1-r^2)^2 + (2\zeta r)^2\right)}} = \frac{r^2}{\sqrt{(1-r^2)^2 + (2\zeta r)^2}} \tag{7.13}$$

Let's replace r^2 with $\frac{\omega^2}{\omega_n^2}$ and rearrange to obtain:

$$\omega_n^2|Z| = \frac{1}{\sqrt{(1-r^2)^2 + (2\zeta r)^2}}\omega^2|Y|. \tag{7.14}$$

In this equation, $\omega^2|Y|$ represents the base structure's acceleration. The coefficient on this acceleration, $C_A = \frac{1}{\sqrt{(1-r^2)^2+(2\zeta r)^2}}$, defines the bandwidth, or useful frequency range, of the accelerometer. When $r = 0$, the coefficient is 1. Depending on ζ, however, C_A deviates from 1 as r increases. The result of this C_A variation is that the frequency content of the structure's acceleration is not uniformly scaled in the measurement signal; the scaling is frequency dependent. To avoid this effect, the accelerometer bandwidth is limited to a frequency range where C_A is nearly constant. Figure 7.11 displays the variation in C_A with r for $\zeta = 0.7$; the percent error between 1 and the actual value, $(1 - C_A) \cdot 100\%$, is also shown. We observe that for $r < 0.2$ the deviation of C_A from 1 is negligible [1]. This means that the valid frequency

range for an accelerometer with $\zeta = 0.7$ is from zero to approximately one-fifth of its natural frequency. A higher (first) natural frequency for an accelerometer therefore provides a wider measurement bandwidth.

Because the accelerometer produces a voltage that is proportional to acceleration, we obtain the accelerance, $\frac{A}{F}(\omega)$, from the dynamic signal analyzer when it calculates the frequency-domain ratio of the accelerometer response to the input force. In order to determine the receptance, $\frac{X}{F}(\omega)$, we follow a similar approach to that described in Sect. 7.3.2 for the vibrometer's mobility data. If the harmonic displacement is written as $x(t) = Xe^{i\omega t}$, then the acceleration is described by $\ddot{x}(t) = (i\omega)^2 Xe^{i\omega t} = -\omega^2 Xe^{i\omega t}$. Therefore, the displacement and acceleration are related by $-\omega^2$. See Eq. 7.15.

$$\frac{X}{F}(\omega) = -\frac{1}{\omega^2}\frac{A}{F} \tag{7.15}$$

This frequency-domain double integration is straightforward to complete, but, like the vibrometer, the zero frequency ($\omega = 0$) information is lost due to the division by zero. For this reason, accelerometers are not well-suited to measuring quasi-static, or slowly changing, signals.

7.4 Impact Testing

As we discussed in Sect. 7.2, impact testing can be used to determine the FRF for a structure. In this approach an instrumented hammer is used to excite the structure and a transducer is used to record the resulting vibration. We'll explore this technique using time-domain simulation (Euler integration) of the displacement due to the impulsive force input. Time-domain simulation provides an alternative to the analytical impulse response function we discussed in Sect. 3.7.

Let's model the case shown in Fig. 7.12 where a single degree of freedom spring-mass-damper is excited by a hammer impact with a triangular force profile, $f(t)$. The hammer initially contacts the structure at t_1, the force reaches its maximum value at t_2, and contact is lost at t_3. The differential equation of motion for this case is:

$$m\ddot{x} + c\dot{x} + kx = f(t). \tag{7.16}$$

We can obtain a numerical solution to Eq. 7.16 using Euler integration. As described in Sect. 2.5.2, the displacement is determined at small intervals in time, dt, by numerical (Euler) integration from acceleration to velocity and then velocity to displacement. We begin by solving for acceleration in Eq. 7.17:

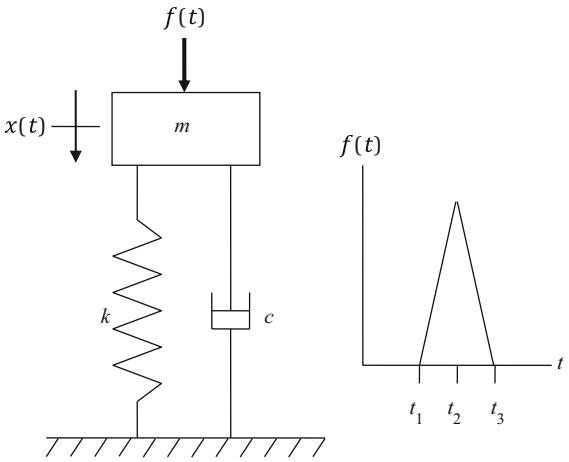

Fig. 7.12 Single degree of freedom spring-mass-damper system excited by an impact force

$$\ddot{x} = \frac{f(t) - c\dot{x} - kx}{m}. \tag{7.17}$$

The current acceleration value depends on the instantaneous values of the time-dependent force, velocity, and displacement. For the first time step in the simulation, the velocity and displacement are defined by the initial conditions. For all subsequent time steps, these are the values from the previous time step. Given the acceleration, the current velocity is determined using:

$$\dot{x} = \dot{x} + \ddot{x}dt. \tag{7.18}$$

In this equation, the velocity on the right hand side is the value from the previous time step (or the initial condition for the first simulation time step) and the acceleration is the value determined using Eq. 7.17. Using this velocity, the current displacement is:

$$x = x + \dot{x}dt, \tag{7.19}$$

where the displacement on the right hand side of the equation is again the value from the previous time step. This process is repeated over many time steps to determine the system response. An important consideration for accurate Euler integration is the size of the time step. If the value is too large, inaccurate results are obtained. As a rule of thumb, it is generally acceptable to set dt to be at least ten times smaller than the period corresponding to the highest natural frequency for the system in question.

By the Numbers 7.1

Consider a system with a damped natural frequency of $f_d = 1000$ Hz. The corresponding period of vibration for free vibration is $\tau = \frac{1}{f_d} = \frac{1}{1000} = 1 \times 10^{-3}$ s.

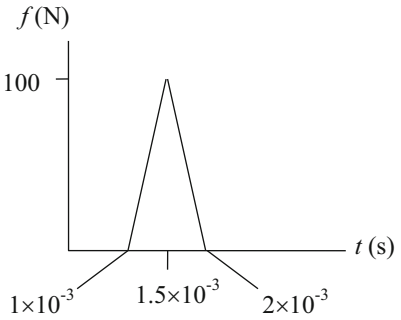

Fig. 7.13 *By the Numbers 7.2*—force profile for exciting the single degree of freedom system pictured in Fig. 7.12

The maximum dt value for simulation is $dt = \frac{\tau}{10} = 1 \times 10^{-4}$ s. Smaller values are naturally acceptable (dividing the time constant by 50 or 100, for example), but there is a tradeoff between improved numerical accuracy and execution time. At some point, smaller time steps do not improve the accuracy and only serve to increase the simulation time.

By the Numbers 7.2

Let's use Euler integration to determine the displacement of the single degree of freedom spring-mass-damper system displayed in Fig. 7.12 due to the triangular force profile shown in Fig. 7.13. For the single degree of freedom spring-mass-damper system, we'll use $m = 1$ kg, $k = 1 \times 10^6$ N/m, and $c = 80$ N s/m. Therefore, the undamped natural frequency is $\omega_n = \sqrt{\frac{k}{m}} = \sqrt{\frac{1\times10^6}{1}} = 1000$ rad/s, the damping ratio is $\zeta = \frac{c}{2\sqrt{km}} = \frac{80}{2\sqrt{1\times10^6(1)}} = 0.04$, the damped natural frequency is $\omega_d = \omega_n\sqrt{1-\zeta^2} = 1000\sqrt{1-0.04^2} = 998.4$ rad/s, and the corresponding period of vibration is $\tau = \frac{1}{f_d} = \frac{2\pi}{\omega_d} = \frac{2\pi}{998.4} = 6.29 \times 10^{-3}$ s. The maximum simulation step size for this vibration period is $dt = \frac{\tau}{10} = 6.3 \times 10^{-4}$. We'll choose a smaller, more conservative time step of 5×10^{-5} s and carry out the simulation for 0.15 s (3000 points).

We can complete the Euler integration described in Eqs. 7.17–7.19 using a `for` loop in MATLAB®. For each iteration in the `for` loop, we must: (1) define the time-dependent force; (2) calculate the acceleration; (3) calculate the velocity; and (4) calculate the displacement. The code is provided in MATLAB® MOJO 7.1 and the results are plotted in Fig. 7.14. We see that the 100 N impact force causes an exponentially decaying oscillation with a peak value of 46.1 μm at $t = 0.003$ s. This lags the peak force time of 0.0015 s. The second peak height of 35.9 μm occurs at $t = 0.0093$ s. Using this information, we can verify the damped natural frequency and damping ratio.

First, the period of free vibration is the difference between the two peak times, $\tau = 0.0093 - 0.003 = 0.0063$. The corresponding oscillating frequency is $\omega_d = \frac{2\pi}{\tau} = \frac{2\pi}{0.0063} = 997$ rad/s. Second, we can estimate the damping ratio using the

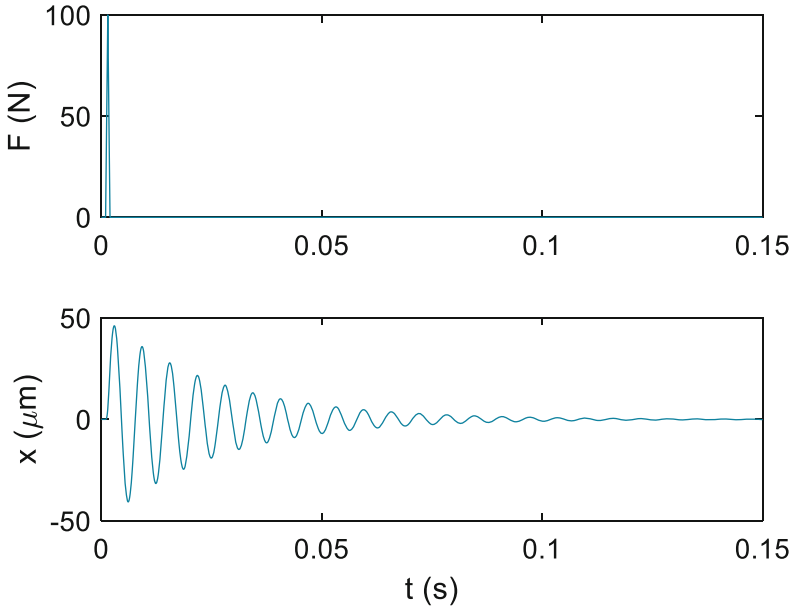

Fig. 7.14 *By the Numbers 7.2*—time-domain response of the single degree of freedom system to the force profile in Fig. 7.13. The displacement was calculated using Euler integration

logarithmic decrement, δ. By Eq. 2.81, $\delta = ln\,\frac{x_1}{x_2} = ln\,\frac{46.1}{35.9} = 0.25$. According to Eq. 2.86, the damping ratio is then $\zeta = \sqrt{\frac{\delta^2}{4\pi^2+\delta^2}} = \sqrt{\frac{0.25^2}{4\pi^2+0.25^2}} = 0.04$. These values verify the simulation results.

MATLAB® MOJO 7.1

```
% matlab_mojo_7_1.m

clear
close all
clc

% Define model
k = 1e6;       % N/m
m = 1;         % kg
c = 80;        % N s/m
fmax = 100;    % N

dt = 5e-5;     % s
total_time = 1;   % s
points = round(total_time/dt);

% Initial conditions
dx = 0;
x = 0;
```

```
% Predefine vectors used in the 'for' loop
time = zeros(points, 1);
displacement = zeros(points, 1);
force = zeros(points, 1);

for cnt = 1:points
  t = cnt*dt;

  % Define impulse
  if t < 1e-3
    f = 0;
  elseif t >= 1e-3 && t <= 1.5e-3
    f = (t-1e-3)*fmax/0.5e-3;      % N
  elseif t > 1.5e-3 && t <= 2e-3
    f = fmax - fmax/0.5e-3*(t-1.5e-3);
  else
    f = 0;
  end

  % Perform Euler integration
  ddx = (f - c*dx - k*x)/m;
  dx = dx + ddx*dt;
  x = x + dx*dt;

  % Write results to vectors
  force(cnt) = f;
  displacement(cnt) = x;
  time(cnt) = t;
end

figure(1)
subplot(211)
plot(time, force)
set(gca,'FontSize', 14)
xlim([0 0.15])
ylabel('F (N)')
subplot(212)
plot(time, displacement*1e6)
set(gca,'FontSize', 14)
xlim([0 0.15])
xlabel('t (s)')
ylabel('x (\mum)')
```

Now that we have the (simulated) time response of a system due to an impact force, we can perform the function of the dynamic signal analyzer and calculate the FRF. To do this we need to calculate the discrete Fourier transform of the time-domain displacement and force signals.[4] We can use the MATLAB® function `fft` to

[4]The discrete Fourier transform is applied because our inputs are sampled; they are not continuous in time.

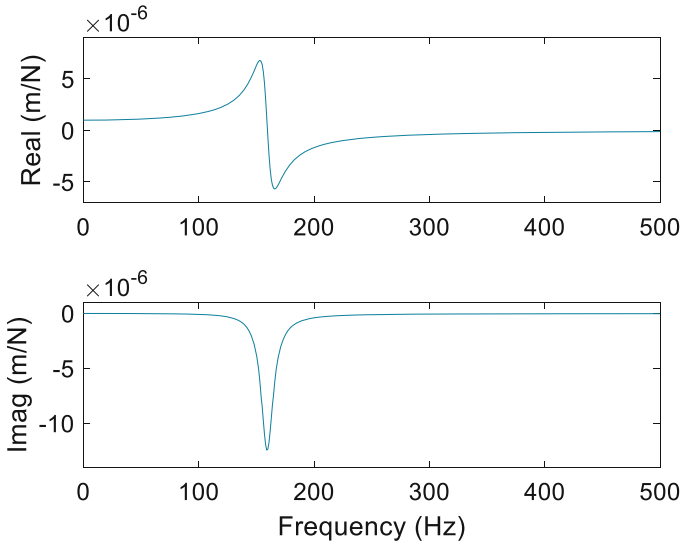

Fig. 7.15 *By the Numbers 7.2*—FRF for the time-domain response displayed in Fig. 7.14

do this. The following code is appended to MATLAB® MOJO 7.1 in order to determine the complex-valued force transform, `F`, and displacement transform, `X`. The FRF is their ratio; see Fig. 7.15.

```
% Calculate Fourier transform of force
F = fft(force);                    % m
freq = (0:1/(dt*points):(1-1/(2*points))/dt)';    % Hz
F = F(1:round(points/2+1), :);
freq = freq(1:round(points/2+1), :);

% Calculate Fourier transform of displacement
X = fft(displacement);                % m
X = X(1:round(points/2+1), :);

FRF = X./F;

figure(2)
subplot(211)
plot(freq, real(FRF))
axis([0 500 -7e-6 9e-6])
ylabel('Real (m/N)')
subplot(212)
plot(freq, imag(FRF))
axis([0 500 -1.4e-5 1e-6])
xlabel('Frequency (Hz)')
ylabel('Imag (m/N)')
```

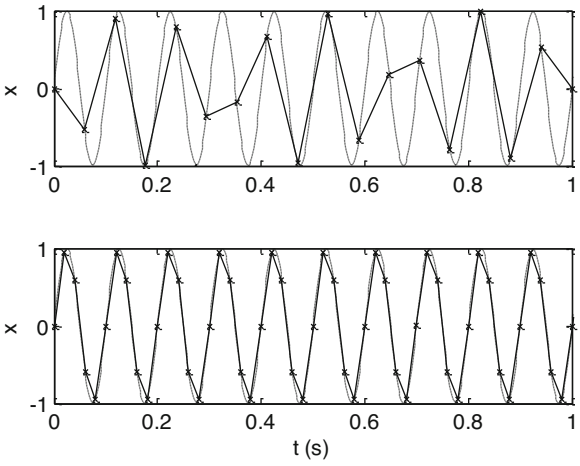

Fig. 7.16 Time-domain example of aliasing. The 10 Hz signal (dotted line) is sampled at 17 Hz in the top panel. Because the signal frequency is greater than the Nyquist frequency ($\frac{f_s}{2} = \frac{17}{2} = 8.5$ Hz), aliasing occurs. For a 50 Hz sampling frequency with a Nyquist frequency of 25 Hz (bottom panel), the signal is captured accurately

In the preceding code, we note that the `fft` function does not return the corresponding frequency vector. This is defined separately as `freq` and depends on both the sampling interval, `dt`, and the number of points, `points`, in the time-domain signals. The frequency resolution for the FRF depends on the ratio `1/(dt*points)`. It is increased (i.e., the frequency step size is decreased) by increasing the number of points in the signals for a fixed **sampling frequency**, $f_s = \frac{1}{dt}$. This is achieved by collecting data over a longer time interval.

We also note that the frequency vector is defined over an interval from zero to half the sampling frequency. This is based on the **Nyquist-Shannon sampling theorem**, which states that only signals with frequencies up to half the sampling frequency, $\frac{f_s}{2}$, can be reconstructed from the sampled data. If a signal with frequencies higher than $\frac{f_s}{2}$ (referred to as the **Nyquist frequency**) is sampled, then the data will be **aliased** and incorrect frequency content will be obtained in the Fourier transform. This is demonstrated in Figs. 7.16 and 7.17. In Fig. 7.16 a sine wave with a unit magnitude and oscillating frequency of 10 Hz is sampled at 17 Hz (top panel) and 50 Hz (bottom panel). It is clear that the 17 Hz sampling frequency is insufficient to capture the behavior of the 10 Hz signal. To see the effect in the frequency domain, the discrete Fourier transform of the sampled signals is provided in Fig. 7.17, which displays the transform magnitudes. We see that when the 10 Hz sine wave is sampled at 17 Hz, the apparent frequency is the difference between the two frequencies, $17 - 10 = 7$ Hz. The signal is aliased because its frequency exceeds the Nyquist frequency of $\frac{f_s}{2} = \frac{17}{2} = 8.5$ Hz. When the same 10 Hz sine wave is sampled at 50 Hz, we observe the expected 10 Hz peak with a unit magnitude. When the maximum frequency content of a signal is unknown (which is generally the case), an analog **anti-aliasing filter** is applied. This removes content from the continuous signal that exceeds the Nyquist frequency prior to sampling.

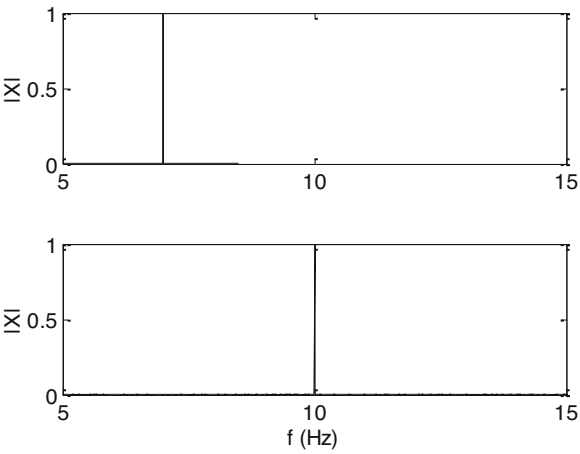

Fig. 7.17 Frequency-domain example of aliasing. In the top panel, the result of sampling a 10 Hz signal with a 17 Hz sampling frequency is shown. The apparent frequency in the aliased signal is their difference, $17 - 10 = 7$ Hz. The Fourier transform magnitude for a sampling frequency of 50 Hz is displayed in the bottom panel. The correct result is obtained

In a Nutshell

We have to sample at least twice the frequency of the highest frequency we hope to see. If we want to see a 500 Hz signal, then we need to sample at least 1000 times per second. In practice, we would like to sample much faster than that. Once the sampling frequency is chosen, then an anti-aliasing filter is used to remove signals beyond our measurement range.

Let's next compare the frequency content of two hammer impacts. We stated in Sect. 7.2 that the impulse excitation bandwidth depends on the hammer mass and tip stiffness. We choose a stiffer tip tend to excite a wider frequency range and a softer tip to concentrate the energy over a lower frequency range. Let's model the impacts as half-period sine waves and calculate the corresponding frequency content using the discrete Fourier transform. Figure 7.18 shows two example impacts. Both have a maximum value of 100 N, but the total impact durations differ by a factor of 10. A shorter duration of 0.5 ms represents a stiff tip and a longer duration of 5 ms represents a softer tip. The frequency-domain force magnitudes for the two impacts are provided in Fig. 7.19, where the signals were sampled at 50 kHz for a total of $2^{12} = 4096$ points. We see that the shorter duration impact excites a wider frequency range, but with a lower force level than the longer impact. Note that it is this broad frequency range excitation that makes the impact test a popular choice for FRF measurement. With a single hammer impact, the response over a wide range of frequencies is obtained. For the stiff tip spectrum shown in Fig. 7.19, modes with natural frequencies of up to 2000 Hz would be effectively excited. The softer tip can only excite modes with natural frequencies up to about 200 Hz, but introduces approximately 10 times more force into these low frequency modes.

To conclude this section, let's observe the results of an impact test completed on the beam experimental platform (BEP) that was introduced in Sect. 2.6. For these

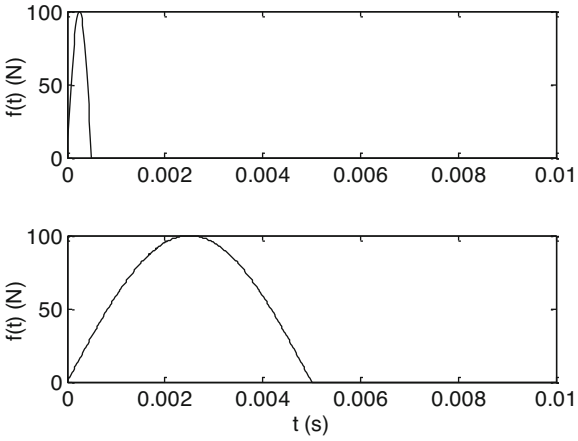

Fig. 7.18 Two example force impacts

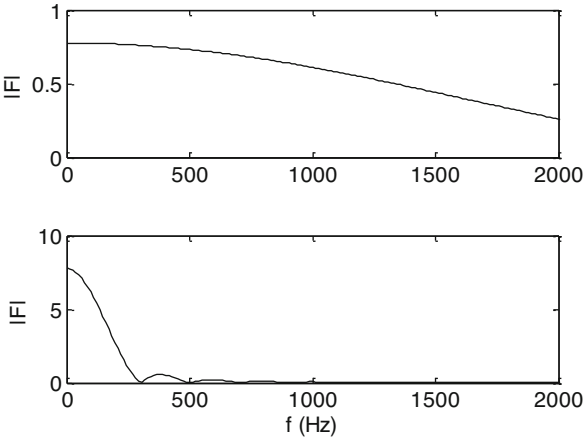

Fig. 7.19 Discrete Fourier transforms of the two force impacts in Fig. 7.18. The top panel shows the 0.5 ms duration impact magnitude and the bottom panel displays the 5 ms duration impact magnitude

measurements, a low mass accelerometer was attached to the free end of the clamped rod and it was excited using a small impact hammer as shown in Fig. 7.20. The extended length of the steel rod was 130 mm. The direct FRF obtained by exciting and measuring at the rod's free end is provided in Fig. 7.21. We observe a single mode with a natural frequency of 463.9 Hz within the 1000 Hz measurement bandwidth. Therefore, if the vibration behavior only up to 1000 Hz is of interest, then the BEP could be modeled as a single degree of freedom system. (As discussed in the next section, other modes actually exist at higher frequencies outside the measurement bandwidth.) The low frequency behavior observed in Fig. 7.21 is due to the double integration of the accelerance as described in Sect. 7.3.3.

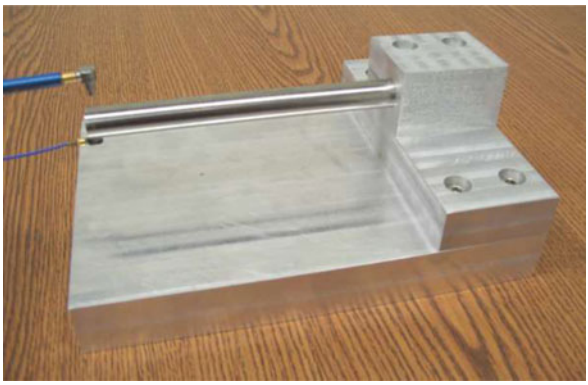

Fig. 7.20 Impact testing setup for the BEP

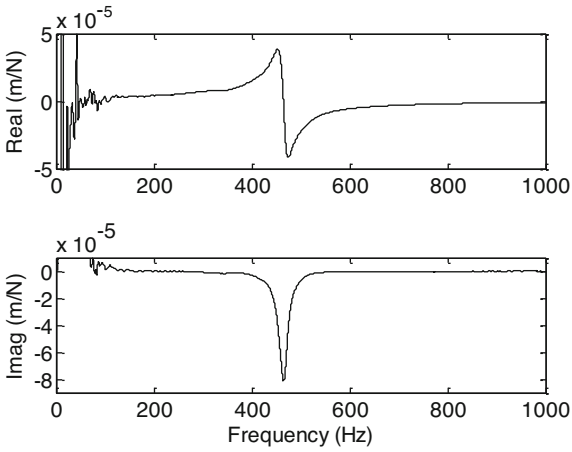

Fig. 7.21 Direct FRF measured at the free end of the BEP's clamped rod

7.5 Modal Truncation

Because FRF measurements always have a finite frequency range and elastic bodies possess an infinite number of degrees of freedom (with increasing natural frequencies), there are necessarily modes that exist outside the measurement range. While all the modes affect the measurement, when we identify a model of the system using peak picking we only consider the effects of the individual modes within the measurement bandwidth that we selected for fitting. Omitting the higher frequency modes affects the accuracy of the modal fit, particularly the real part of the FRF. This is referred to as **modal truncation**. Equations 7.20 and 7.21, which describe the real and imaginary parts of a single degree of freedom FRF, are included here to demonstrate the effect.

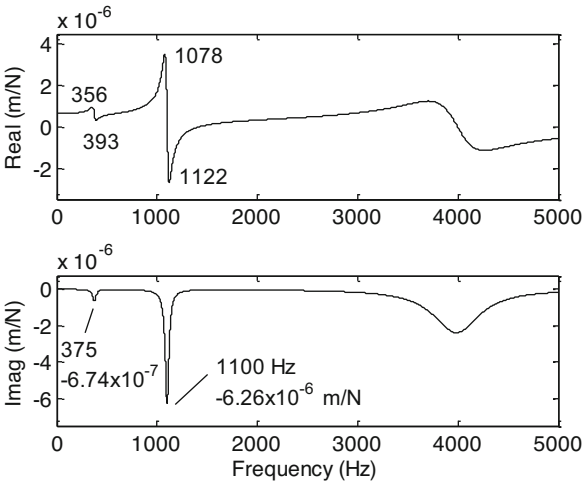

Fig. 7.22 *By the Numbers 7.3*—measured direct FRF. The peak picking values are listed within the 2000 Hz measurement bandwidth. A 5000 Hz frequency range is provided to show the truncated 4000 Hz mode

$$Re\left(\frac{X}{F}\right) = \frac{1}{k}\left(\frac{1-r^2}{(1-r^2)^2 + (2\zeta r)^2}\right) \tag{7.20}$$

$$Im\left(\frac{X}{F}\right) = \frac{1}{k}\left(\frac{-2\zeta r}{(1-r^2)^2 + (2\zeta r)^2}\right) \tag{7.21}$$

We see that when the frequency ratio $r = \frac{\omega}{\omega_n}$ is large, or the forcing frequency ω is very high and outside the measurement range, the denominator for the right parenthetical terms in these two equations becomes very large and the response approaches zero. However, when r is very small, the parenthetical term in the real part approaches a value of 1 and the parenthetical term in the imaginary part approaches zero. Therefore, the value of the real part approaches $\frac{1}{k}$ as r approaches zero.[5] Neglecting the modes beyond the measurement bandwidth and, therefore, the associated $\frac{1}{k}$ contribution for each, leads to errors in the vertical location of the modal fit's real part. This is demonstrated in By the Numbers 7.3.

By the Numbers 7.3

An example FRF is provided in Fig. 7.22. We will presume that the measurement bandwidth was 2000 Hz, although a 5000 Hz frequency range is shown for the purposes of this demonstration. Within the 2000 Hz range, two modes are visible and peak picking can be applied to determine the associated modal parameters. Using the values from the figure, the modal stiffness, mass, and damping matrix terms may be determined as shown in Sect. 6.2.

[5]This $\frac{1}{k}$ term can be referred to as the DC compliance.

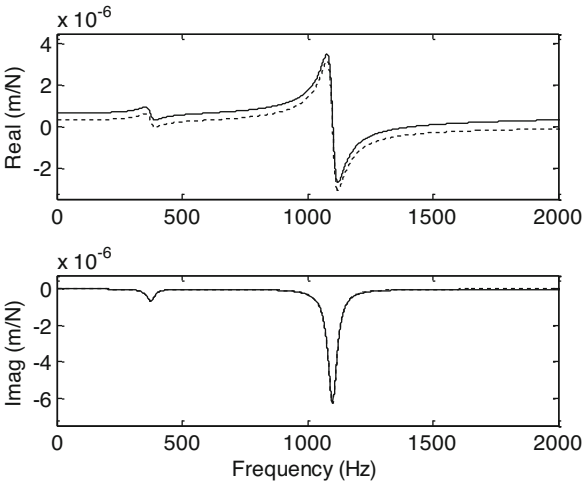

Fig. 7.23 *By the Numbers 7.3*—result of modal fitting. An offset in the real part of the fit (dotted line) is observed because the DC compliance of the 4000 Hz mode is not included

$$\zeta_{q1} = \frac{393 - 356}{2 \cdot 375} = 0.049 \quad \zeta_{q2} = \frac{1122 - 1078}{2 \cdot 1100} = 0.020$$

$$k_{q1} = \frac{-1}{2 \cdot 0.049 \cdot \left(-6.74 \times 10^{-7}\right)} = 1.50 \times 10^7 \text{ N/m}$$

$$k_{q2} = \frac{-1}{2 \cdot 0.020 \cdot \left(-6.26 \times 10^{-6}\right)} = 3.99 \times 10^6 \text{ N/m}$$

$$m_{q1} = \frac{1.50 \times 10^7}{(375 \cdot 2\pi)^2} = 2.70 \text{ kg} \quad m_{q2} = \frac{3.99 \times 10^6}{(1100 \cdot 2\pi)^2} = 0.084 \text{ kg}$$

$$c_{q1} = 2 \cdot 0.049 \sqrt{1.50 \times 10^7 \cdot 2.70} = 624 \text{ N s/m}$$

$$c_{q2} = 2 \cdot 0.020 \sqrt{3.99 \times 10^6 \cdot 0.084} = 23.2 \text{ N s/m}$$

The fit to the measured direct FRF is determined by summing the two contributions in modal coordinates using:

$$\frac{X}{F} = \frac{Q_1}{R_1} + \frac{Q_2}{R_2} = \frac{1}{k_{q1}} \left(\frac{(1 - {r_1}^2) - i\left(2\zeta_{q1} r_1\right)}{(1 - {r_1}^2)^2 + \left(2\zeta_{q1} r_1\right)^2} \right) + \frac{1}{k_{q2}} \left(\frac{(1 - {r_2}^2) - i\left(2\zeta_{q2} r_2\right)}{(1 - {r_2}^2)^2 + \left(2\zeta_{q2} r_2\right)^2} \right),$$

where $r_1 = \frac{f}{375}$ and $r_2 = \frac{f}{1100}$ and f is given in Hz. It is seen in Fig. 7.23 that, although the shape of the two modes within the 2000 Hz bandwidth are correctly identified, there is a noticeable offset in the real part of the fit. It appears too stiff (i.e., it is located below the measured FRF) because the DC compliance due to the 4000 Hz mode has not been considered. Because this mode is outside the measurement frequency range, it is not possible to fit the mode and determine the appropriate modal parameters. However, given the visible offset in Fig. 7.23, the combined

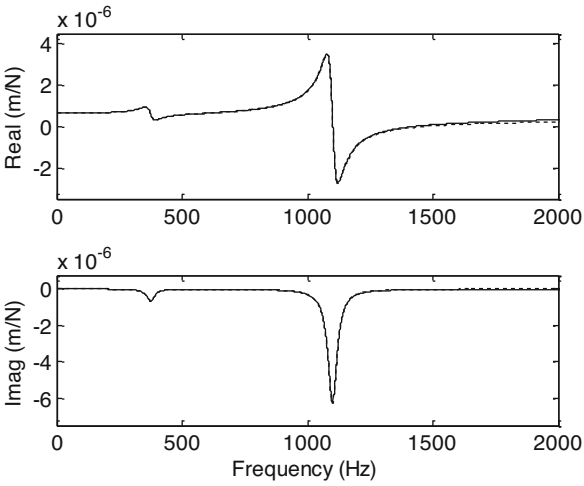

Fig. 7.24 *By the Numbers 7.3*—result of modal fitting with the addition of a DC compliance term to compensate for the truncated mode

contributions of truncated modes can be included by adding an effective DC compliance term to the fit. Specifically, for this example, the fit could be rewritten as:

$$\frac{X}{F} = \frac{1}{k} + \frac{Q_1}{R_1} + \frac{Q_2}{R_2},$$

where the $\frac{Q_j}{R_j}$ terms ($j = 1, 2$) are obtained through peak picking as described previously and the $\frac{1}{k}$ value is selected to move the fit to a vertical overlap with the measured FRF. If a value of $k = 3 \times 10^6$ N/m is applied here, the fit is improved and the result shown in Fig. 7.24 is obtained. Note that this stiffness value is equal to the modal stiffness of the 4000 Hz mode shown in Fig. 7.22 (for completeness, the modal damping ratio for this mode is 0.07). The code used to produce the Figs. 7.22, 7.23, and 7.24 is provided in MATLAB® MOJO 7.2.

MATLAB® MOJO 7.2

```
% matlab_mojo_7_2.m

clear
close all
clc

% Define modal parameters for the "measured" FRF
fn1 = 375;      % Hz
wn1 = fn1*2*pi;   % rad/s
zetaq1 = 0.05;
kq1 = 1.5e7;     % N/m

fn2 = 1100;     % Hz
wn2 = fn2*2*pi;   % rad/s
```

```
zetaq2 = 0.02;
kq2 = 4e6;      % N/m

fn3 = 4000;     % Hz
wn3 = fn3*2*pi;   % rad/s
zetaq3 = 0.07;
kq3 = 3e6;      % N/m

% Define the measured FRF
w = (0:0.2:5000)'*2*pi;   % frequency, rad/s
r1 = w/wn1;
r2 = w/wn2;
r3 = w/wn3;
FRF = 1/kq1*((1-r1.^2) - i*(2*zetaq1*r1))./((1-r1.^2).^2 +
(2*zetaq1*r1).^2) + 1/kq2*((1-r2.^2) - i*(2*zetaq2*r2))./((1-r2.^2).
^2 + (2*zetaq2*r2).^2) + 1/kq3*((1-r3.^2) - i*(2*zetaq3*r3))./((1-r3.
^2).^2 + (2*zetaq3*r3).^2);

figure(1)
subplot(211)
plot(w/2/pi, real(FRF), 'k')
ylim([-3.5e-6 4.5e-6])
set(gca,'FontSize', 14)
ylabel('Real (m/N)')
subplot(212)
plot(w/2/pi, imag(FRF), 'k')
ylim([-7.5e-6 7.5e-7])
set(gca,'FontSize', 14)
xlabel('Frequency (Hz)')
ylabel('Imag (m/N)')

figure(2)
subplot(211)
plot(w/2/pi, real(FRF), 'k')
axis([0 2000 -3.5e-6 4.5e-6])
set(gca,'FontSize', 14)
ylabel('Real (m/N)')
hold on
subplot(212)
plot(w/2/pi, imag(FRF), 'k')
axis([0 2000 -7.5e-6 7.5e-7])
set(gca,'FontSize', 14)
xlabel('Frequency (Hz)')
ylabel('Imag (m/N)')
hold on

figure(3)
subplot(211)
plot(w/2/pi, real(FRF), 'k')
axis([0 2000 -3.5e-6 4.5e-6])
set(gca,'FontSize', 14)
ylabel('Real (m/N)')
```

```
hold on
subplot(212)
plot(w/2/pi, imag(FRF), 'k')
axis([0 2000 -7.5e-6 7.5e-7])
set(gca,'FontSize', 14)
xlabel('Frequency (Hz)')
ylabel('Imag (m/N)')
hold on

% Perform fit
fn1 = 375;     % Hz
wn1 = fn1*2*pi;   % rad/s
zetaq1 = (393 - 356)*2*pi/(2*wn1);
kq1 = 1/(2*zetaq1*6.74e-7);

fn2 = 1100;     % Hz
wn2 = fn2*2*pi;   % rad/s
zetaq2 = (1122 - 1078)*2*pi/(2*wn2);
kq2 = 1/(2*zetaq2*6.26e-6);

r1 = w/wn1;
r2 = w/wn2;
FRF1 = 1/kq1*((1-r1.^2) - 1i*(2*zetaq1*r1))./((1-r1.^2).^2 +
(2*zetaq1*r1).^2); % mode 1
FRF2 = 1/kq2*((1-r2.^2) - 1i*(2*zetaq2*r2))./((1-r2.^2).^2 +
(2*zetaq2*r2).^2); % mode 2
FRF = FRF1 + FRF2; % modal fit

figure(2)
subplot(211)
plot(w/2/pi, real(FRF), 'k:')
subplot(212)
plot(w/2/pi, imag(FRF), 'k:')

% Add correction for modal truncation
k = 3e6;       % N/m
FRF = 1/k + FRF1 + FRF2; % new modal fit

figure(3)
subplot(211)
plot(w/2/pi, real(FRF), 'k:')
subplot(212)
plot(w/2/pi, imag(FRF), 'k:')
```

Chapter Summary

- FRF measurement requires a mechanism for force input, a transducer to measure the vibration, and a dynamic signal analyzer to compute the vibration to force ratio of the Fourier-transformed signals.

- The FRF may take the form of receptance (displacement), mobility (velocity), or accelerance (acceleration) depending on the vibration measurement technique.
- Force input types include fixed frequency sine waves, random noise, and impulses. These forces can be produced using a shaker or impact hammer.
- Example vibration transducers include capacitance probes, laser vibrometers, and accelerometers. The latter is a contact-type measurement.
- The response of an accelerometer to a structure's motion is an example of base motion.
- Accelerance and mobility can be converted to receptance in the frequency domain using the measurement frequency vector.
- Euler (numerical) integration can be used to solve the differential equation of motion for arbitrary force inputs, including the force impulse in impact testing.
- Care must be exercised in sampling continuous signals to avoid aliasing.
- In modal truncation, modes that exist outside the measurement range affect the accuracy of the modal fit to the measured FRF.

Exercises

1. Complete the following statements.
   (a) Receptance is the frequency-domain ratio of _____ to _____.
   (b) Mobility is the frequency-domain ratio of _____ to _____.
   (c) Accelerance is the frequency-domain ratio of _____ to _____.
2. Find three commercial suppliers of impact hammers for modal testing.
3. Find three commercial suppliers of dynamic signal analyzers for modal testing.
4. Digital data acquisition is to be used to record vibration signals for a particular system. If the highest anticipated frequency in the measurements is 5000 Hz, select the minimum sampling frequency.
5. An impact test was completed using an instrumented hammer to excite a structure and an accelerometer to measure the vibration response.
   (a) Show how to convert from the acceleration-to-force frequency response function (i.e., accelerance) that was obtained to a displacement-to-force frequency response function (i.e., receptance).
   (b) What information is lost in this conversion?
6. As described in Sects. 7.2 and 7.4, FRFs are often measured using impact testing. In this approach an instrumented hammer is used to excite the structure and a transducer is used to record the resulting vibration.

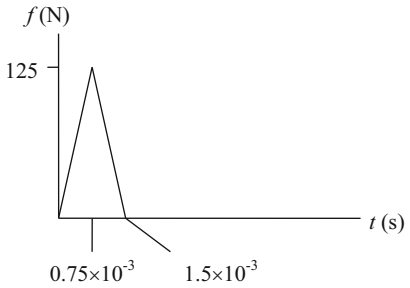

Fig. P7.6 Impulsive force profile for impact test

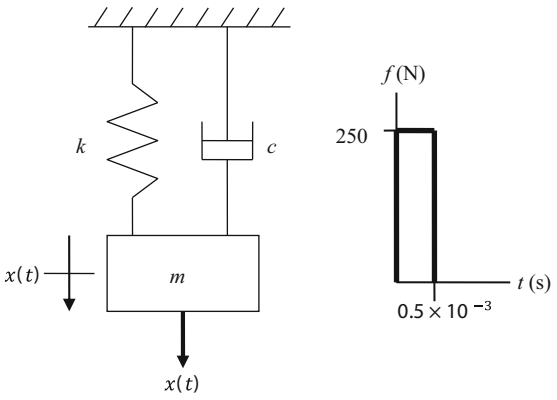

Fig. P7.8 Spring-mass-damper system excited by an impulsive force

Use Euler integration to determine the displacement due to the triangular impulsive force profile shown in Fig. P7.6. The force excites a single degree of freedom spring-mass-damper system with $m = 2$ kg, $k = 1.1 \times 10^6$ N/m, and $c = 83$ N s/m. For the Euler integration, use a time step of 1×10^{-5} s and carry out your simulation for 0.2 s (20,000 points).

(a) Plot both the force (N) versus time (s) and displacement (μm) versus time.
(b) Determine the maximum displacement (in μm) and the time at which this displacement occurs.

7. For a particular measurement application, an accelerometer must be selected with a bandwidth, or useful frequency range, of 5000 Hz. If the allowable deviation in the scaling coefficient $C_A = \frac{1}{\sqrt{(1-r^2)^2+(2\zeta r)^2}}$ is $\pm 1\%$ and the damping ratio is known to be 0.65, determine the minimum required natural frequency of the accelerometer.
8. A single degree of freedom spring-mass-damper system which is initially at rest at its equilibrium position is excited by an impulsive force with a magnitude of 250 N over a time interval of 0.5 ms; see Fig. P7.8. If the mass is 3 kg, the stiffness is 3×10^6 N/m, and the viscous damping coefficient is 120 N s/m, complete the following.

(a) Determine $x(t)$ using Eq. 3.44. Plot the response (in μm) over a time period of 0.3 s with a step size of 1×10^{-4} s in the time vector.
(b) Determine $x(t)$ using Euler integration. Use a time step of 1×10^{-4} s and carry out your simulation for 0.3 s (30,000 points). Plot $x(t)$ (in μm) versus time.

9. Determine the FRF for the system described in Problem 8 using Euler integration to calculate the time-domain displacement due to the impulsive input force. To increase the FRF frequency resolution, use a total simulation time of 1 s. Given the time-domain displacement and force vectors, use the MATLAB® function `fft` to calculate the complex-valued force transform, `F`, and displacement transform, `X`. Plot the real and imaginary parts (in m/N) of their ratio, `X/F`, versus frequency (in Hz). Use axis limits of `axis([0 500 -5e-6 5e-6])` for the real plot and axis limits of `axis([0 500 -1e-5 1e-6])` for the imaginary plot.
10. The existence of modes with frequencies higher than the measurement bandwidth leads to an effect referred to as _____ when performing a modal fit to the measured FRF.

Reference

1. http://www.lionprecision.com/tech-library/technotes/cap-0020-sensor-theory.html

Chapter 8
Continuous Beam Modeling

Continuity in everything is unpleasant.
—*Blaise Pascal*

8.1 Beam Bending

In Chaps. 1–5 we discussed the solution of discrete, lumped parameter models. For multiple degree of freedom systems, we employed modal analysis to enable us to transform the coupled equations of motion in local (model) coordinates into modal coordinates. In this coordinate frame, the equations of motion were uncoupled and we could apply single degree of freedom solution techniques. In Chap. 6 we shifted our attention to the "backwards problem", which is representative of a common task for vibration engineers. In this problem, we begin with measurements of an existing structure and use this information to develop a model. We again used discrete models to describe the system behavior.

An alternative to lumped parameter models is continuous models. In this case, the mass is distributed throughout the structure, rather than localized at the model coordinates. This modeling approach can be very effective and can offer good accuracy. As an example, the modal truncation effects we discussed in Sect. 7.5 are non-existent when a continuous model that includes the effects of all modes is implemented.

In a Nutshell
Continuous solutions can be derived for many simple geometries. These solutions offer insight into the way that vibrating systems behave and describe the distributed mass, stiffness, and damping elements that are often encountered. Continuous models become complicated for any but the simplest systems, but it is useful to understand the parallels between the continuous and the discrete parameter models. In addition, the continuous models form the basis for deriving finite element representations, a useful technique for discretizing continuous systems.

T. L. Schmitz, K. S. Smith, *Mechanical Vibrations*,
https://doi.org/10.1007/978-3-030-52344-2_8

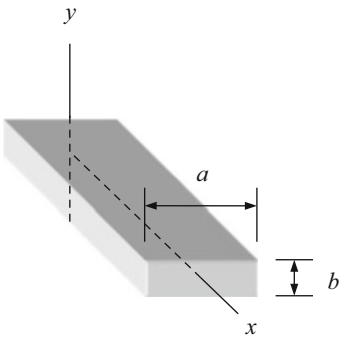

Fig. 8.1 Coordinate definitions for continuous beam transverse deflection. The deflection, y, depends on the location along the beam axis, x

To begin this discussion, let's consider the bending of beams using **Euler-Bernoulli beam theory** and see how we can expand the analysis to derive the vibration response. The fundamental relationship between the transverse deflection, y, and a load per unit length, q, applied to a **beam**[1] with constant cross-section and material properties is provided in Eq. 8.1. In this equation E is the elastic modulus, I is the second moment of area, and x is the (continuous) position along the beam. Figure 8.1 displays the x and y coordinate axes for a rectangular beam. In this case, the second moment of area is $I = \frac{ab^3}{12}$.

$$\frac{q}{EI} = \frac{d^4y}{dx^4} \tag{8.1}$$

To determine the static (non-vibratory) deflection of a continuous beam under a selected loading condition, we integrate Eq. 8.1 four successive times. Let's apply the loading condition shown in Fig. 8.2, where a simply supported[2] beam with length l is loaded by a force per unit length, w. Due to symmetry, the reaction force, $\frac{wl}{2}$, is the same at both ends. Equation 8.1 can be rewritten as shown in Eq. 8.2 for this case.

$$\frac{q}{EI} = \frac{d^4y}{dx^4} = \frac{-w}{EI} \tag{8.2}$$

Integrating Eq. 8.2 gives Eq. 8.3, where C_1 is the integration constant and V is the position-dependent shear force acting on the beam.

$$\frac{V}{EI} = \frac{d^3y}{dx^3} = \frac{-w}{EI}x + C_1 \tag{8.3}$$

[1] A beam can be described as a structure where one dimension is much larger than the other two dimensions.

[2] A simply supported beam is pinned at one end and has a rolling support at the other.

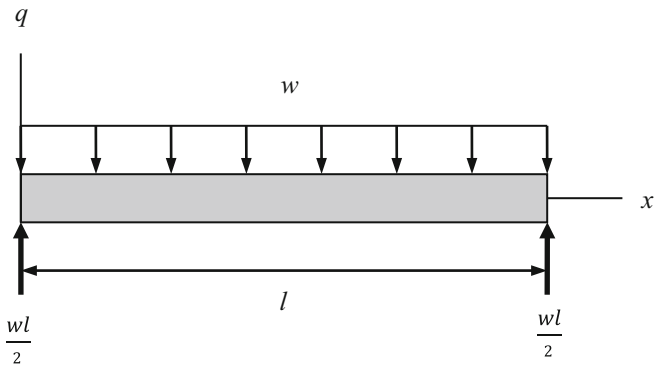

Fig. 8.2 Simply supported beam loaded by the force per unit length, w

Integrating a second time yields the moment, M, equation shown in Eq. 8.4. Now there are two integration constants.

$$\frac{M}{EI} = \frac{d^2y}{dx^2} = \frac{-w^2}{2EI}x + C_1x + C_2 \tag{8.4}$$

The third integration gives the beam slope, θ. See Eq. 8.5.

$$\theta = \frac{dy}{dx} = \frac{-w^3}{6EI}x + \frac{C_1x^2}{2} + C_2x + C_3 \tag{8.5}$$

Finally, the deflection equation is obtained by a fourth integration as shown in Eq. 8.6.

$$y = \frac{-w^4}{24EI}x + \frac{C_1x^3}{6} + \frac{C_2x^2}{2} + C_3x + C_4 \tag{8.6}$$

In order to obtain the deflection profile from Eq. 8.6, we must determine the four integration constants. We identify these using the beam's **boundary conditions**. For the simply supported beam in Fig. 8.2, the following boundary conditions apply.

1. The shear force at the left end ($x = 0$) is equal to the reaction force. We can express this relationship as

$$\frac{V}{EI}\Big|_{x=0} = \frac{wl}{2EI} \tag{8.7}$$

2. The ends points of the beam are free to rotate so the moment at the left end is zero

$$\left.\frac{M}{EI}\right|_{x=0} = 0 \tag{8.8}$$

3. The slope at the beam's midpoint is zero due to symmetry

$$\theta|_{x=\frac{l}{2}} = 0 \tag{8.9}$$

4. The deflection at the left end is zero.

$$y|_{x=0} = 0 \tag{8.10}$$

Substitution of Eqs. 8.7–8.10 into Eqs. 8.3–8.6 and simultaneous solution yields the following four relationships for the beam in Fig. 8.2.

$$\frac{V}{EI} = \frac{w}{EI}\left(\frac{l}{2} - x\right) \tag{8.11}$$

$$\frac{M}{EI} = \frac{w}{2EI}\left(lx - x^2\right) \tag{8.12}$$

$$\theta = \frac{w}{24EI}\left(6lx^2 - 4x^3 - l^3\right) \tag{8.13}$$

$$y = \frac{w}{24EI}\left(2lx^3 - l^3x - x^4\right) \tag{8.14}$$

When implementing Euler-Bernoulli beam theory, there are two underlying assumptions: (1) shear deformations are negligible; and (2) planar cross-sections remain planar and normal to the beam axis during deformation. These assumptions limit the accuracy of the model when the beam is not long and slender (approximately ten times longer, or more, than the largest cross-sectional dimension).

By the Numbers 8.1

Let's determine the shear force, moment, slope, and deflection diagrams for a steel, 10 mm (0.01 m) square cross-section, simply supported beam with a length of 200 mm (0.2 m). The loading conditions follow Fig. 8.2 with $w = 100$ N/m. We'll assume a steel modulus of 200 GPa. The area moment of inertia is determined for the square cross-section using:

$$I = \frac{(0.01)^4}{12} = 8.3 \times 10^{-10}\ \text{m}^4.$$

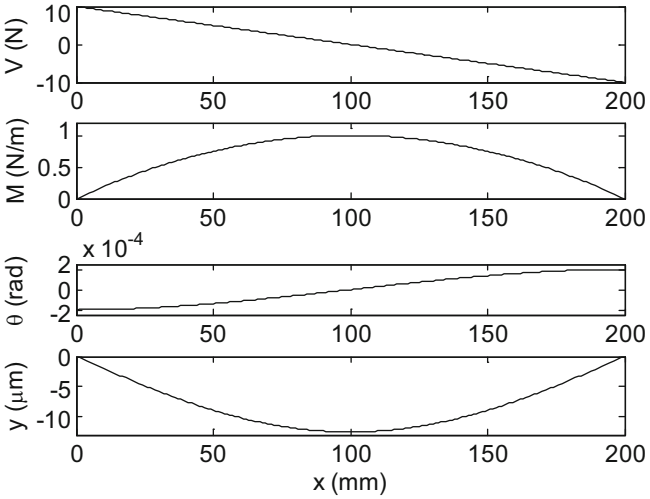

Fig. 8.3 *By the Numbers 8.1*—shear force, moment, slope, and deflection diagrams for the simply supported steel beam subjected to self-loading

The results are shown in Fig. 8.3. We see that the maximum deflection of 12.5 μm occurs at the beam midpoint. The code used to produce Fig. 8.3 is provided in MATLAB® MOJO 8.1.

MATLAB® MOJO 8.1

```
% matlab_mojo_8_1.m

clear
close all
clc

% Define beam parameters
s = 10e-3;      % m
E = 200e9;      % N/m^2
I = s^4/12;     % m^4
w = 100;        % N/m
l = 200e-3;     % m
x = 0:1e-3:l;   % m

% Shear force
V = w*(l/2 - x);
% Moment
M = w*(l*x - x.^2);
% Slope
theta = w/(24*E*I)*(6*l*x.^2 - 4*x.^3 - l^3);
% Deflection
y = w/(24*E*I)*(2*l*x.^3 - l^3*x - x.^4);
```

```
figure(1)
subplot(411)
plot(x*1e3, V, 'k')
set(gca,'FontSize', 14)
ylabel('V (N)')
subplot(412)
plot(x*1e3, M, 'k')
set(gca,'FontSize', 14)
ylim([0 1.2])
ylabel('M (N/m)')
subplot(413)
plot(x*1e3, theta, 'k')
set(gca,'FontSize', 14)
ylim([-2.5e-4 2.5e-4])
ylabel('\theta (rad)')
subplot(414)
plot(x*1e3, y*1e6, 'k')
set(gca,'FontSize', 14)
ylim([-13 0])
xlabel('x (mm)')
ylabel('y (\mum)')
```

8.2 Transverse Vibration Equation of Motion

While the analysis in Sect. 8.1 is useful, it only gives the static solution. It does not describe the dynamic, or vibratory, behavior of a beam. For the beam vibration we need to determine the time-dependent deflection. We'll now build on the previous analysis to determine the required differential equation of motion for the beam. Let's begin with Fig. 8.4, which shows the forces and moments acting on a section of a vibrating Euler-Bernoulli beam with an infinitesimal length, ∂x.

According to Newton's second law, the sum of the forces in the y direction is equal to the product of the section mass and acceleration, $\sum F_y = m\frac{\partial^2 y}{\partial t^2}$. See Eq. 8.15, where the mass is rewritten as the product of the density, ρ, cross-sectional area, A, and section length, ∂x.

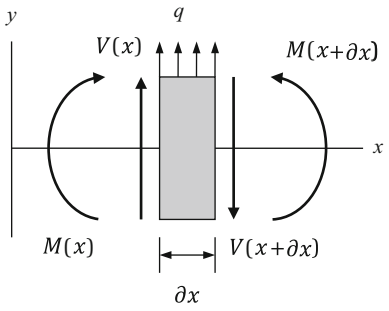

Fig. 8.4 Forces and moments acting on a small section of a vibrating Euler-Bernoulli beam

$$q\partial x + V(x) - V(x + \partial x) = \rho A \partial x \frac{\partial^2 y}{\partial t^2} \tag{8.15}$$

We can rewrite Eq. 8.15 by substituting $\partial V = V(x + \partial x) - V(x)$ and dividing each term by ∂x. The result is provided in Eq. 8.16.

$$q - \frac{\partial V}{\partial x} = \rho A \frac{\partial^2 y}{\partial t^2} \tag{8.16}$$

From Eq. 8.3, the shear force is $V = EI\frac{\partial^3 y}{\partial x^3}$. Calculating the partial derivative with respect to x gives:

$$\frac{\partial V}{\partial x} = EI \frac{\partial^4 y}{\partial x^4}. \tag{8.17}$$

Substituting Eq. 8.17 into Eq. 8.16 gives the differential equation of motion for the transverse vibration of a uniform cross-section Euler-Bernoulli beam.

$$\rho A \frac{\partial^2 y}{\partial t^2} + EI \frac{\partial^4 y}{\partial x^4} = q \tag{8.18}$$

For free vibration, the external transverse load q is zero so we can write:

$$\rho A \frac{\partial^2 y}{\partial t^2} + EI \frac{\partial^4 y}{\partial x^4} = 0. \tag{8.19}$$

8.3 Frequency Response Function for Transverse Vibration

Our next task is to determine the beam's frequency response function using Eq. 8.19. A general solution to this equation is:

$$y(x, t) = Y(x)\, sin\,(\omega t), \tag{8.20}$$

where $Y(x)$ is a function that describes the position-dependent vibration behavior and ω is frequency [1]. Let's calculate the required partial derivatives of Eq. 8.20 that appear in Eq. 8.19.

$$\frac{\partial^2 y}{\partial t^2} = Y(x)\left(-\omega^2\right) sin\,(\omega t) \tag{8.21}$$

$$\frac{\partial^4 y}{\partial x^4} = \frac{\partial^4 Y}{\partial x^4} \sin(\omega t) \tag{8.22}$$

Substituting Eqs. 8.21 and 8.22 into Eq. 8.19 gives:

$$\left(\rho A\left(-\omega^2 Y\right) + EI\frac{\partial^4 Y}{\partial x^4}\right) \sin(\omega t) = 0. \tag{8.23}$$

Rewriting Eq. 8.23 yields:

$$\frac{\partial^4 Y}{\partial x^4} - \omega^2 \frac{\rho A}{EI} Y = 0. \tag{8.24}$$

Letting $\lambda^4 = \omega^2 \frac{\rho A}{EI}$, we now have:

$$\frac{\partial^4 Y}{\partial x^4} - \lambda^4 Y = 0. \tag{8.25}$$

The time-dependence of Eq. 8.19 has been eliminated in Eq. 8.25. In addition, frequency has been introduced through the λ^4 term. A general solution to this new equation is:

$$Y(x) = A\cos(\lambda x) + B\sin(\lambda x) + C\cosh(\lambda x) + D\sinh(\lambda x). \tag{8.26}$$

To determine the coefficients A, B, C, and D, we must apply the beam's boundary conditions. Given these coefficients, the continuous beam's direct and cross FRFs can be determined. In the next two sections, we'll derive the FRFs for beams with fixed-free (cantilever) and free-free boundary conditions.

In a Nutshell
The sinh and cosh functions are the hyperbolic sine and hyperbolic cosine, respectively. These functions are not often encountered by most engineers, but they are analogs of the more familiar sine and cosine functions and they frequently appear in continuous structure solutions. They are defined by $\sinh(x) = \frac{1}{2}(e^x - e^{-x})$ and $\cosh(x) = \frac{1}{2}(e^x + e^{-x})$.

8.3.1 Fixed-Free Beam

Figure 8.5 shows a fixed-free beam. In order to determine the FRF at the free end, coordinate 1, we need to apply a force, $f_1 = F\sin(\omega t)$, at this location. Note that the force and vibration, $y(x, t) = Y(x)\sin(\omega t)$, expressions both have the same sinusoidal form. The cantilever base coordinate is labeled as 2.

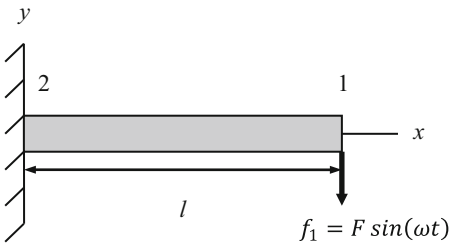

Fig. 8.5 Fixed-free beam model with a harmonic force applied at the free end

We need to identify four boundary conditions for this beam in order to determine the coefficients A though D in Eq. 8.26. For the free end, where $x = l$, no moment is supported (it is free to rotate), so we can modify Eq. 8.4 to be:

$$\frac{M}{EI}\Big|_{x=l} = \frac{d^2y}{dx^2}\Big|_{x=l} = 0. \tag{8.27}$$

We know that the shear force at the free end is $f_1 = Fsin(\omega t)$ so we can define the corresponding boundary condition (see Eq. 8.3).

$$\frac{V}{EI}\Big|_{x=l} = \frac{d^3y}{dx^3}\Big|_{x=l} = -\frac{F}{EI}\,sin\,(\omega t) \tag{8.28}$$

At the fixed end, $x = 0$, both the deflection and the slope are zero. You can visualize this by considering the shape of a swimming pool's diving board when you stand at the free end.

$$\frac{dy}{dx}\Big|_{x=0} = 0 \tag{8.29}$$

$$y|_{x=0} = 0 \tag{8.30}$$

Let's now use Eqs. 8.27–8.30 to determine the coefficients in Eq. 8.26. At $x = 0$, we obtain:

$$Y(0) = Acos(0) + Bsin(0) + Ccosh(0) + Dsinh(0) = A + C = 0 \tag{8.31}$$

and

$$\frac{\partial Y}{\partial x}(0) = \lambda(-Asin(0) + Bcos(0) + Csinh(0) + Dcosh(0)) = \lambda(B + D)$$
$$= 0. \tag{8.32}$$

These two equations specify that $A = -C$ and $B = -D$. At $x = l$, applying the boundary conditions gives:

$$\frac{\partial^2 Y}{\partial x^2}(l) = \lambda^2(-Acos(\lambda l) - Bsin(\lambda l) + Ccosh(\lambda l) + Dsinh(\lambda l)) = 0 \tag{8.33}$$

and

$$\begin{aligned}\frac{\partial^3 Y}{\partial x^3}(l) &= \lambda^3(Asin(\lambda l) - Bcos(\lambda l) + Csinh(\lambda l) + Dcosh(\lambda l)) \\ &= -\frac{F}{EI}\, sin\,(\omega t).\end{aligned} \tag{8.34}$$

Using the relationships determined from Eqs. 8.31 and 8.32, we can substitute for A and B in Eqs. 8.33 and 8.34 to obtain a system of two equations with two unknowns.

$$Ccos(\lambda l) + Dsin(\lambda l) + Ccosh(\lambda l) + Dsinh(\lambda l) = 0 \tag{8.35}$$

$$-Csin(\lambda l) + Dcos(\lambda l) + Csinh(\lambda l) + Dcosh(\lambda l) = -\frac{F}{\lambda^3 EI}\, sin\,(\omega t) \tag{8.36}$$

Combining terms in these two equations yields:

$$C(\,cos\,(\lambda l) + \,cosh\,(\lambda l)) + D(\,sin\,(\lambda l) + \,sinh\,(\lambda l)) = 0 \tag{8.37}$$

and

$$C(-\,sin\,(\lambda l) + \,sinh\,(\lambda l)) + D(\,cos\,(\lambda l) + \,cosh\,(\lambda l)) = -\frac{F}{\lambda^3 EI}\, sin\,(\omega t). \tag{8.38}$$

Let's arrange Eqs. 8.37 and 8.38 into matrix form.

$$\begin{bmatrix} cos\,(\lambda l) + \,cosh\,(\lambda l) & sin\,(\lambda l) + \,sinh\,(\lambda l) \\ -\,sin\,(\lambda l) + \,sinh\,(\lambda l) & cos\,(\lambda l) + \,cosh\,(\lambda l) \end{bmatrix} \begin{Bmatrix} C \\ D \end{Bmatrix} = \begin{Bmatrix} 0 \\ -\frac{F}{\lambda^3 EI}\, sin\,(\omega t) \end{Bmatrix} \tag{8.39}$$

There are a number of solution methods available for Eq. 8.39. We could apply matrix inversion, for example. However, let's use **Cramer's rule** to determine C and D [2]. To describe this technique, let's rewrite Eq. 8.39 in generic form:

$$\begin{bmatrix} a_{11} & a_{12} \\ a_{21} & a_{22} \end{bmatrix} \begin{Bmatrix} x_1 \\ x_2 \end{Bmatrix} = \begin{Bmatrix} b_1 \\ b_2 \end{Bmatrix}. \tag{8.40}$$

According to Cramer's rule, we determine x_1 and x_2 using ratios of determinants as shown in Eqs. 8.41 and 8.42.

$$x_1 = \frac{\begin{vmatrix} b_1 & a_{12} \\ b_2 & a_{22} \end{vmatrix}}{\begin{vmatrix} a_{11} & a_{12} \\ a_{21} & a_{22} \end{vmatrix}} = \frac{b_1 a_{22} - b_2 a_{12}}{a_{11} a_{22} - a_{21} a_{12}} \tag{8.41}$$

$$x_2 = \frac{\begin{vmatrix} a_{11} & b_1 \\ a_{21} & b_2 \end{vmatrix}}{\begin{vmatrix} a_{11} & a_{12} \\ a_{21} & a_{22} \end{vmatrix}} = \frac{a_{11} b_2 - a_{21} b_1}{a_{11} a_{22} - a_{21} a_{12}} \tag{8.42}$$

Using Eqs. 8.39 and 8.41, we can determine C.

$$C = \frac{\begin{vmatrix} 0 & sin\,(\lambda l) + sinh\,(\lambda l) \\ -\dfrac{F}{\lambda^3 EI} sin\,(\omega t) & cos\,(\lambda l) + cosh\,(\lambda l) \end{vmatrix}}{\begin{vmatrix} cos\,(\lambda l) + cosh\,(\lambda l) & sin\,(\lambda l) + sinh\,(\lambda l) \\ -sin\,(\lambda l) + sinh\,(\lambda l) & cos\,(\lambda l) + cosh\,(\lambda l) \end{vmatrix}} \tag{8.43}$$

$$C = \frac{\frac{F}{\lambda^3 EI}(\,sin\,(\lambda l) + sinh\,(\lambda l))}{(\,cos\,(\lambda l) + cosh\,(\lambda l))^2 - (-sin\,(\lambda l) + sinh\,(\lambda l))(\,sin\,(\lambda l) + sinh\,(\lambda l))} sin\,(\omega t) \tag{8.44}$$

$$C = \frac{F(\,sin\,(\lambda l) + sinh\,(\lambda l))}{2\lambda^3 EI(1 + cos\,(\lambda l)\,cosh\,(\lambda l))} sin\,(\omega t) \tag{8.45}$$

Using Eqs. 8.39 and 8.42, we can find D.

$$D = \frac{\begin{vmatrix} cos\,(\lambda l) + cosh\,(\lambda l) & 0 \\ -sin\,(\lambda l) + sinh\,(\lambda l) & -\dfrac{F}{\lambda^3 EI} sin\,(\omega t) \end{vmatrix}}{\begin{vmatrix} cos\,(\lambda l) + cosh\,(\lambda l) & sin\,(\lambda l) + sinh\,(\lambda l) \\ -sin\,(\lambda l) + sinh\,(\lambda l) & cos\,(\lambda l) + cosh\,(\lambda l) \end{vmatrix}} \tag{8.46}$$

$$D = \frac{-\frac{F}{\lambda^3 EI}(\cos(\lambda l) + \cosh(\lambda l))}{(\cos(\lambda l) + \cosh(\lambda l))^2 - (-\sin(\lambda l) + \sinh(\lambda l))(\sin(\lambda l) + \sinh(\lambda l))} \sin(\omega t) \tag{8.47}$$

$$D = -\frac{F(\cos(\lambda l) + \cosh(\lambda l))}{2\lambda^3 EI(1 + \cos(\lambda l)\cosh(\lambda l))} \sin(\omega t) \tag{8.48}$$

To find Y_1 due to the harmonic force f_1 (see Fig. 8.5), we substitute for A, B, C, and D and let $x = l$ in Eq. 8.26.

$$Y_1 = A\cos(\lambda l) + B\sin(\lambda l) + C\cosh(\lambda l) + D\sinh(\lambda l) \tag{8.49}$$

$$Y_1 = -C\cos(\lambda l) - D\sin(\lambda l) + C\cosh(\lambda l) + D\sinh(\lambda l) \tag{8.50}$$

$$Y_1 = C(-\cos(\lambda l) + \cosh(\lambda l)) + D(-\sin(\lambda l) + \sinh(\lambda l)) \tag{8.51}$$

$$Y_1 = \frac{F(\sin(\lambda l) + \sinh(\lambda l))}{2\lambda^3 EI(1 + \cos(\lambda l)\cosh(\lambda l))} \sin(\omega t)(-\cos(\lambda l) + \cosh(\lambda l)) - \frac{F(\cos(\lambda l) + \cosh(\lambda l))}{2\lambda^3 EI(1 + \cos(\lambda l)\cosh(\lambda l))} \sin(\omega t)(-\sin(\lambda l) + \sinh(\lambda l)) \tag{8.52}$$

Expanding and simplifying Eq. 8.52 gives:

$$Y_1 = \frac{\sin(\lambda l)\cosh(\lambda l) - \cos(\lambda l)\sinh(\lambda l)}{\lambda^3 EI(1 + \cos(\lambda l)\cosh(\lambda l))} F\sin(\omega t). \tag{8.53}$$

Because $f_1 = F\sin(\omega t)$, the direct FRF at the beam's free end is:

$$\frac{Y_1}{F_1} = \frac{\sin(\lambda l)\cosh(\lambda l) - \cos(\lambda l)\sinh(\lambda l)}{\lambda^3 EI(1 + \cos(\lambda l)\cosh(\lambda l))}, \tag{8.54}$$

where $\lambda^4 = \omega^2 \frac{\rho A}{EI}$. This gives the frequency dependence.

What about the cross FRF, $\frac{Y_2}{F_1}$, for the fixed-free beam? This is the response at the base due to the harmonic force at the free end. Our intuition should tell us that the cross FRF is zero since, by definition, the base does not move regardless of the force input. Let's verify this using Eq. 8.26. At $x = 0$ we have:

$$Y_2 = Acos(0) + Bsin(0) + Ccosh(0) + Dsinh(0) = A + C. \tag{8.55}$$

However, based on the boundary conditions (Eq. 8.31) we already know that $A = -C$. Substitution in Eq. 8.55 gives $Y_2 = 0$. Therefore, $\frac{Y_2}{F_1} = 0$ as expected.

8.3.2 Free-Free Beam

A free-free beam is displayed in Fig. 8.6. To determine the FRF at the right end, coordinate 1 ($x = l$), we apply a force, $f_1 = Fsin(\omega t)$, at this location. The left end is coordinate 2 ($x = 0$). The boundary conditions at the right end are:

$$\left.\frac{M}{EI}\right|_{x=l} = \left.\frac{d^2y}{dx^2}\right|_{x=l} = 0 \tag{8.56}$$

and

$$\left.\frac{V}{EI}\right|_{x=l} = \left.\frac{d^3y}{dx^3}\right|_{x=l} = -\frac{F}{EI}\,sin\,(\omega t). \tag{8.57}$$

At the left end, $x = 0$, the beam is again free to rotate, but there is no shear force so we have:

$$\left.\frac{M}{EI}\right|_{x=0} = \left.\frac{d^2y}{dx^2}\right|_{x=0} = 0 \tag{8.58}$$

and

$$\left.\frac{V}{EI}\right|_{x=0} = \left.\frac{d^3y}{dx^3}\right|_{x=0} = 0. \tag{8.59}$$

Let's next use the four boundary conditions described by Eqs. 8.56–8.59 to determine the coefficients in Eq. 8.26. At $x = 0$, we obtain:

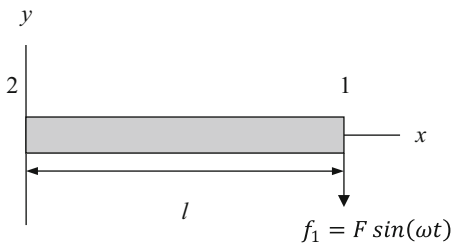

Fig. 8.6 Free-free beam model with a harmonic force applied at coordinate 1

$$\frac{\partial^2 Y}{\partial x^2}(0) = \lambda^2(-Acos(0) - Bsin(0) + Ccosh(0) + Dsinh(0))$$
$$= \lambda^2(-A + C) = 0 \tag{8.60}$$

and

$$\frac{\partial^3 Y}{\partial x^3}(0) = \lambda^3(Asin(0) - Bcos(0) + Csinh(0) + Dcosh(0)) = \lambda^3(-B + D)$$
$$= 0. \tag{8.61}$$

From these two equations, we see that $A = C$ and $B = D$. At $x = l$, applying the boundary conditions gives:

$$\frac{\partial^2 Y}{\partial x^2}(l) = \lambda^2(-Acos(\lambda l) - Bsin(\lambda l) + Ccosh(\lambda l) + Dsinh(\lambda l)) = 0 \tag{8.62}$$

and

$$\frac{\partial^3 Y}{\partial x^3}(l) = \lambda^3(Asin(\lambda l) - Bcos(\lambda l) + Csinh(\lambda l) + Dcosh(\lambda l))$$
$$= -\frac{F}{EI}\, sin\,(\omega t). \tag{8.63}$$

Substituting for A and B in Eqs. 8.62 and 8.63 yields a system of two equations with two unknowns.

$$-Ccos(\lambda l) - Dsin(\lambda l) + Ccosh(\lambda l) + Dsinh(\lambda l) = 0 \tag{8.64}$$

$$Csin(\lambda l) - Dcos(\lambda l) + Csinh(\lambda l) + Dcosh(\lambda l) = -\frac{F}{\lambda^3 EI}\, sin\,(\omega t) \tag{8.65}$$

Combining terms gives:

$$C(-\,cos\,(\lambda l) + \,cosh\,(\lambda l)) + D(-\,sin\,(\lambda l) + \,sinh\,(\lambda l)) = 0 \tag{8.66}$$

and

$$C(\,sin\,(\lambda l) + \,sinh\,(\lambda l)) + D(-\,cos\,(\lambda l) + \,cosh\,(\lambda l)) = -\frac{F}{\lambda^3 EI}\, sin\,(\omega t). \tag{8.67}$$

Arranging Eqs. 8.66 and 8.67 into matrix form results in Eq. 8.68.

$$\begin{bmatrix} -\cos(\lambda l) + \cosh(\lambda l) & -\sin(\lambda l) + \sinh(\lambda l) \\ \sin(\lambda l) + \sinh(\lambda l) & -\cos(\lambda l) + \cosh(\lambda l) \end{bmatrix} \begin{Bmatrix} C \\ D \end{Bmatrix} = \begin{Bmatrix} 0 \\ -\frac{F}{\lambda^3 EI} \sin(\omega t) \end{Bmatrix} \tag{8.68}$$

Using Cramer's rule, we determine C.

$$C = \frac{\begin{vmatrix} 0 & -\sin(\lambda l) + \sinh(\lambda l) \\ -\frac{F}{\lambda^3 EI} \sin(\omega t) & -\cos(\lambda l) + \cosh(\lambda l) \end{vmatrix}}{\begin{vmatrix} -\cos(\lambda l) + \cosh(\lambda l) & -\sin(\lambda l) + \sinh(\lambda l) \\ \sin(\lambda l) + \sinh(\lambda l) & -\cos(\lambda l) + \cosh(\lambda l) \end{vmatrix}} \tag{8.69}$$

$$C = \frac{\frac{F}{\lambda^3 EI}(-\sin(\lambda l) + \sinh(\lambda l))}{(-\cos(\lambda l) + \cosh(\lambda l))^2 - (\sin(\lambda l) + \sinh(\lambda l))(-\sin(\lambda l) + \sinh(\lambda l))} \sin(\omega t) \tag{8.70}$$

$$C = \frac{F(-\sin(\lambda l) + \sinh(\lambda l))}{2\lambda^3 EI(1 - \cos(\lambda l)\cosh(\lambda l))} \sin(\omega t) \tag{8.71}$$

Let's now calculate D.

$$D = \frac{\begin{vmatrix} -\cos(\lambda l) + \cosh(\lambda l) & 0 \\ \sin(\lambda l) + \sinh(\lambda l) & -\frac{F}{\lambda^3 EI} \sin(\omega t) \end{vmatrix}}{\begin{vmatrix} -\cos(\lambda l) + \cosh(\lambda l) & -\sin(\lambda l) + \sinh(\lambda l) \\ \sin(\lambda l) + \sinh(\lambda l) & -\cos(\lambda l) + \cosh(\lambda l) \end{vmatrix}} \tag{8.72}$$

$$D = \frac{-\frac{F}{\lambda^3 EI}(-\cos(\lambda l) + \cosh(\lambda l))}{(-\cos(\lambda l) + \cosh(\lambda l))^2 - (\sin(\lambda l) + \sinh(\lambda l))(-\sin(\lambda l) + \sinh(\lambda l))} \sin(\omega t) \tag{8.73}$$

$$D = \frac{F(\cos(\lambda l) - \cosh(\lambda l))}{2\lambda^3 EI(1 - \cos(\lambda l)\cosh(\lambda l))} \sin(\omega t) \tag{8.74}$$

To find Y_1 due to the harmonic force f_1 (see Fig. 8.6), we substitute for A, B, C, and D and let $x = l$ in Eq. 8.26.

$$Y_1 = Acos(\lambda l) + Bsin(\lambda l) + Ccosh(\lambda l) + Dsinh(\lambda l) \tag{8.75}$$

$$Y_1 = Ccos(\lambda l) + Dsin(\lambda l) + Ccosh(\lambda l) + Dsinh(\lambda l) \tag{8.76}$$

$$Y_1 = C(\,cos\,(\lambda l) + \,cosh\,(\lambda l)) + D(\,sin\,(\lambda l) + \,sinh\,(\lambda l)) \tag{8.77}$$

$$Y_1 = \frac{F(-\,sin\,(\lambda l) + \,sinh\,(\lambda l))}{2\lambda^3 EI(1 - \,cos\,(\lambda l)\,cosh\,(\lambda l))}\,sin\,(\omega t)(\,cos\,(\lambda l) + \,cosh\,(\lambda l)) + \frac{F(\,cos\,(\lambda l) - \,cosh\,(\lambda l))}{2\lambda^3 EI(1 - \,cos\,(\lambda l)\,cosh\,(\lambda l))}\,sin\,(\omega t)(\,sin\,(\lambda l) + \,sinh\,(\lambda l)) \tag{8.78}$$

Expanding and simplifying Eq. 8.78 gives:

$$Y_1 = \frac{cos\,(\lambda l)\,sinh\,(\lambda l) - \,sin\,(\lambda l)\,cosh\,(\lambda l)}{\lambda^3 EI(1 - \,cos\,(\lambda l)\,cosh\,(\lambda l))}Fsin(\omega t). \tag{8.79}$$

The direct FRF at the beam's free end is:

$$\frac{Y_1}{F_1} = \frac{cos\,(\lambda l)\,sinh\,(\lambda l) - \,sin\,(\lambda l)\,cosh\,(\lambda l)}{\lambda^3 EI(1 - \,cos\,(\lambda l)\,cosh\,(\lambda l))}. \tag{8.80}$$

For the cross FRF, $\frac{Y_2}{F_1}$, we require the expression for Y_2. This is the response at coordinate 2 due to the harmonic force at coordinate 1. At $x = 0$ we have:

$$Y_2 = Acos(0) + Bsin(0) + Ccosh(0) + Dsinh(0) = A + C. \tag{8.81}$$

Based on the free boundary condition (Eq. 8.60) we know that $A = C$. Therefore, $Y_2 = 2C$. Using Eq. 8.71, we obtain:

$$Y_2 = \frac{(-\,sin\,(\lambda l) + \,sinh\,(\lambda l))}{\lambda^3 EI(1 - \,cos\,(\lambda l)\,cosh\,(\lambda l))}Fsin(\omega t). \tag{8.82}$$

The cross FRF is finally:

$$\frac{Y_2}{F_1} = \frac{(-\sin(\lambda l) + \sinh(\lambda l))}{\lambda^3 EI(1 - \cos(\lambda l)\cosh(\lambda l))}. \tag{8.83}$$

8.4 Solid Damping in Beam Models

At this point we have not yet included damping in our continuous beam transverse vibration FRFs. As we discussed in Sect. 2.4, various damping models are available. These include: viscous damping, which relates the damping force to velocity; Coulomb damping, which represents the energy dissipation due to dry sliding between two surfaces; and **solid damping**, which occurs due to internal energy dissipation within the material of the vibrating body. Viscous damping is convenient mathematically, but solid damping makes the most intuitive sense for modeling the vibration of continuous beams.

Solid damping is included in the differential equation of motion as a complex stiffness term. For the differential equation of forced harmonic motion, we include the unitless solid damping factor, η, as:

$$m\ddot{x} + k(1 + i\eta)x = Fe^{i\omega t}. \tag{8.84}$$

In our continuous beam model, this material-dependent damping is conveniently incorporated in the elastic modulus which, together with the second moment of area and beam length, defines the beam's stiffness. The new **complex modulus**, E_s, is:

$$E_s = E(1 + i\eta). \tag{8.85}$$

Damping is therefore incorporated in the continuous beam FRFs by replacing E with E_s. Note that this substitution also holds for $\lambda^4 = \omega^2 \frac{\rho A}{E_s I}$.

Let's now explore the relationship between η and the viscous damping ratio, ζ. For the forced harmonic motion described by Eq. 8.84, we can assume a solution of the form $x(t) = Xe^{i\omega t}$. Substitution yields:

$$\left(-m\omega^2 + k(1 + i\eta)\right)Xe^{i\omega t} = Fe^{i\omega t}. \tag{8.86}$$

Rearranging to identify the FRF gives:

$$\frac{X}{F}(\omega) = \frac{1}{k - m\omega^2 + ik\eta}. \tag{8.87}$$

The value at resonance,[3] where $\omega = \omega_n$, is:

$$\frac{X}{F}(\omega_n) = \frac{1}{k - m\omega_n^2 + ik\eta} = \frac{1}{k - m\frac{k}{m} + ik\eta} = \frac{1}{ik\eta}. \tag{8.88}$$

The corresponding FRF magnitude is $\frac{1}{k\eta}$. For viscous damping, we can complete an equivalent analysis. The differential equation of motion is now:

$$m\ddot{x} + c\dot{x} + kx = Fe^{i\omega t}. \tag{8.89}$$

Again assuming a solution of the form $x(t) = Xe^{i\omega t}$ gives:

$$\left(-m\omega^2 + i\omega c + k\right)Xe^{i\omega t} = Fe^{i\omega t}. \tag{8.90}$$

The FRF is:

$$\frac{X}{F}(\omega) = \frac{1}{-m\omega^2 + i\omega c + k}. \tag{8.91}$$

As we saw in Sect. 3.2, we can rewrite this equation as:

$$\frac{X}{F}(\omega) = \frac{1}{k}\left(\frac{1}{\left(1 - \left(\frac{\omega}{\omega_n}\right)^2\right) + i2\zeta\left(\frac{\omega}{\omega_n}\right)}\right). \tag{8.92}$$

At resonance, the FRF value is:

$$\frac{X}{F}(\omega_n) = \frac{1}{k}\left(\frac{1}{\left(1 - \left(\frac{\omega_n}{\omega_n}\right)^2\right) + i2\zeta\left(\frac{\omega_n}{\omega_n}\right)}\right) = \frac{1}{i2k\zeta}. \tag{8.93}$$

The FRF magnitude at resonance for viscous damping is therefore $\frac{1}{2k\zeta}$. Equating this result with the resonant magnitude for solid damping gives the relationship between η and ζ at resonance.

$$\zeta = \frac{\eta}{2} \tag{8.94}$$

[3] We consider the resonant case because this is where damping has the most significant effect. Its influence is less at frequencies far from resonance.

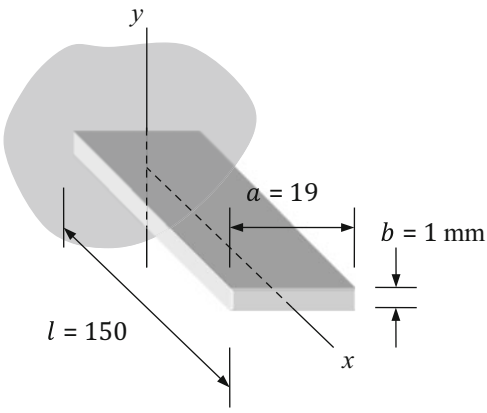

Fig. 8.7 *By the Numbers 8.2*—dimensions for a steel machinist's scale with fixed-free boundary conditions

Solid damping factors are quite low. For steel alloys, typical values are between 0.001 and 0.002. According to Eq. 8.93, the equivalent damping ratio at resonance is 0.0005–0.001 (0.05–0.1%). These small values emphasize that most damping in structures is introduced at the connections between individual beam members rather than within the beams themselves.

By the Numbers 8.2

Let's consider an example fixed-free beam and calculate the direct FRF at its free end. We'll use the dimensions and material properties for a typical steel ruler/machinist's scale; see Fig. 8.7. For the steel beam, we'll use an elastic modulus of 200 GPa and a density of 7800 kg/m^3. The second moment of area is:

$$I = \frac{ab^3}{12} = \frac{0.019(0.001)^3}{12} = 1.583 \times 10^{-12}\ \text{m}^4$$

and the cross-sectional area, A, is:

$$A = ab = 0.019(0.001) = 1.9 \times 10^{-5}\ \text{m}^2.$$

To plot the free end direct FRF we use Eq. 8.54 and replace E with the complex modulus $E_s = E(1 + i\eta)$ from Eq. 8.85.

$$\frac{Y_1}{F_1} = \frac{sin\,(\lambda l)\,cosh\,(\lambda l) - cos\,(\lambda l)\,sinh\,(\lambda l)}{\lambda^3 E(1 + i\eta)I(1 + cos\,(\lambda l)\,cosh\,(\lambda l))} \tag{8.95}$$

Let's choose a solid damping factor of 0.01 for display purposes. Even though this value is approximately an order of magnitude too large, it reduces the "sharpness" of the real and imaginary parts of the FRF and enables us to view them more clearly. Figure 8.8 shows the first three bending modes for a bandwidth of 1200 Hz;

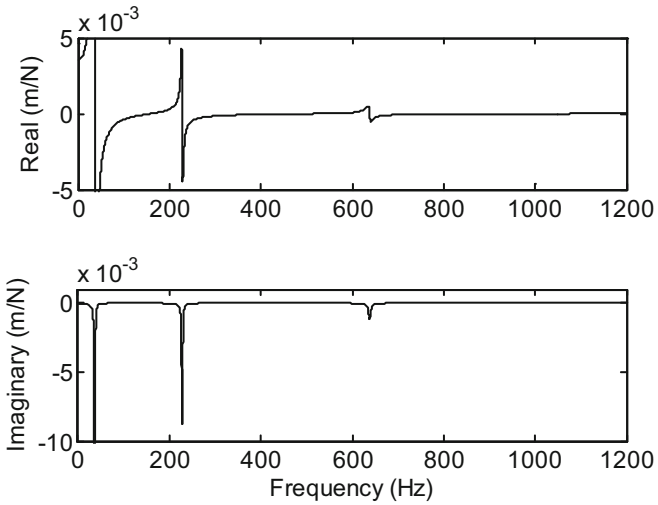

Fig. 8.8 *By the Numbers 8.2*—direct FRF for the free end of the beam depicted in Fig. 8.7

note that the scale was selected to be able to observe the third mode. If we increased the frequency range, we would see additional modes.[4] These first three modes, which appear at 36.4, 227.8, and 637.9 Hz, correspond to the first three bending mode shapes shown in Fig. 6.19.

For Euler-Bernoulli beams, a closed-form expression for the natural frequencies has been developed for various boundary conditions [3]. See Eq. 8.96, where $i = 1$, 2, 3... indicates the natural frequency numbers in ascending order.

$$f_{n,i} = \frac{\beta_i^2}{2\pi l^2}\sqrt{\frac{EI}{\rho A}}\,(\text{Hz}) \tag{8.96}$$

For the fixed-free beam in this example, the β_i values are provided in Table 8.1 [3]. Substitution of the beam geometry and material properties gives the same first three natural frequencies we determined using Figs. 8.8 and 8.9.

The direct FRF is presented in a semi-logarithmic format in Fig. 8.9. We again observe the resonant peaks at 36.4, 227.8, and 637.9 Hz, but we also see local minima at 159.4, 516.6, and 1077.8 Hz. These are referred to as **anti-resonant frequencies** and represent frequencies where the beam response is small even for a large force input. While this definition sounds similar to the node description provided in Sect. 6.5, in this case we are describing frequencies, not spatial locations (nodes), where the response is small. The code used to produce Figs. 8.8 and 8.9 is provided in MATLAB® MOJO 8.2.

MATLAB® MOJO 8.2

[4]For a continuous beam there are an infinite number of modes for an infinite bandwidth.

Table 8.1 β_i values for fixed-free Euler-Bernoulli beam natural frequency calculations [3]

i	β_i
1	1.87510107
2	4.69409113
3	7.85475744
4	10.99554073
5	14.13716839
>5	$\frac{\pi}{2}(2i-1)$

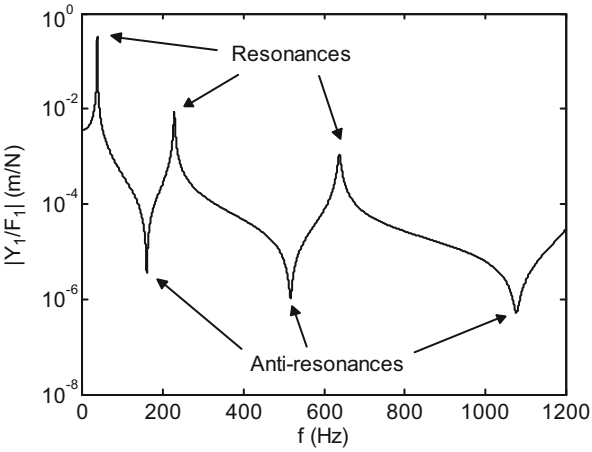

Fig. 8.9 *By the Numbers 8.2*—semi-logarithmic plot of the direct FRF for the free end of the beam depicted in Fig. 8.7

```
% matlab_mojo_8_2.m

clear
close all
clc

f = 1:0.1:1200;     % Hz
omega = f*2*pi;     % rad/s

% Define beam
a = 19e-3;          % m
b = 1e-3;           % m
l = 150e-3;         % m
E = 2e11;           % N/m^2
density = 7800;     % kg/m^3
eta = 0.01;
I = a*b^3/12;       % m^4
EI = E*I;           % N-m^2
EI = EI*(1+1i*eta);   % N-m^2
A = a*b;            % m^2

lambda = (omega.^2*density*A/EI).^0.25;
```

```
% Direct FRF for the free end of the fixed-free beam
Y1_F1 = (sin(lambda*l).*cosh(lambda*l)-cos(lambda*l).*sinh
(lambda*l))./(lambda.^3*EI.*(1+cos(lambda*l).*cosh(lambda*l)));

figure(1)
subplot(211)
plot(f, real(Y1_F1), 'k')
set(gca,'FontSize', 14)
ylim([-0.005 0.005])
ylabel('Real (m/N)')
subplot(212)
plot(f, imag(Y1_F1), 'k')
set(gca,'FontSize', 14)
ylim([-0.01 0.001])
xlabel('Frequency (Hz)')
ylabel('Imaginary (m/N)')

figure(2)
semilogy(f, abs(Y1_F1), 'k')
set(gca,'FontSize', 14)
xlabel('f (Hz)')
ylabel('|Y_1/F_1| (m/N)')
```

What would happen if we increased the width of the beam in Fig. 8.7? Let's consider a 20% increase so that $a = 0.019(1.2) = 0.0228$ m. The beam stiffness depends on the modulus (unchanged), length (unchanged), and second moment of area. The new second moment of area is:

$$I = \frac{ab^3}{12} = \frac{0.0228(0.001)^3}{12} = 1.9 \times 10^{-12}\ \text{m}^4.$$

Because the stiffness increases with I, we might anticipate that the natural frequencies will increase with a. The new direct FRF, together with the previous result from Fig. 8.8 (dotted line), is provided in Fig. 8.10. Surprisingly, the natural frequencies did not change! While the wider beam is indeed stiffer, it is also heavier. These effects serve to offset each other so that the natural frequencies are not affected. We can observe this in Eq. 8.96. Substituting for I and A (based on the rectangular beam in Fig. 8.7), we see that a cancels.

$$f_{n,i} = \frac{\beta_i^2}{2\pi l^2}\sqrt{\frac{E\frac{ab^3}{12}}{\rho ab}} = \frac{\beta_i^2}{2\pi l^2}\sqrt{\frac{E\frac{b^2}{12}}{\rho}}\ (\text{Hz}), \tag{8.97}$$

The same result is obtained from Eq. 8.95. The roots of the denominator give the natural frequencies and these roots depend on the product:

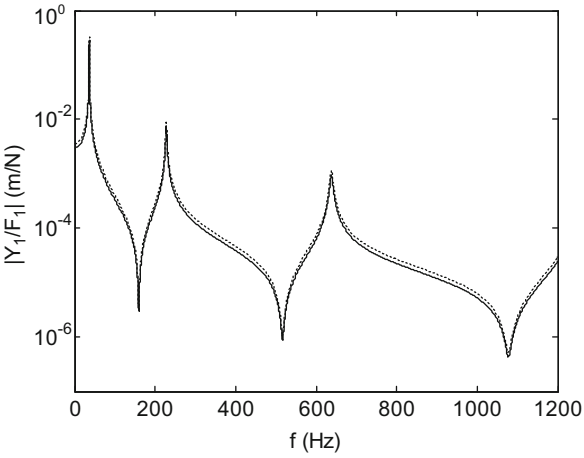

Fig. 8.10 *By the Numbers 8.2*—direct FRF for the beam with a 20% width increase (the dotted line shows the FRF for the original width)

$$\lambda l = \left(\omega^2 \frac{\rho A}{E_s I}\right)^{\frac{1}{4}} l = \left(\omega^2 \frac{\rho ab}{E_s \frac{ab^3}{12}}\right)^{\frac{1}{4}} l = \left(\omega^2 \frac{\rho}{E_s \frac{b^2}{12}}\right)^{\frac{1}{4}} l.$$

Again, the natural frequencies of the rectangular beam do not depend on a after substituting and simplifying. While the resonant peaks appear at the same frequencies for both FRFs in Fig. 8.10, the new FRF with the increased width is stiffer (its FRF appears below the original FRF). The source of the change in magnitude is also observed using Eq. 8.95. We see that I appears in the denominator. It does not change the roots, but does serve to scale the FRF. As I (and the denominator) increases with a, the magnitude decreases.

8.5 Rotation Frequency Response Functions

In Sects. 8.3.1 and 8.3.2 we derived the transverse vibration FRFs, $\frac{Y}{F}$, for beams with fixed-free and free-free boundary conditions. We are not limited to these boundary conditions of course. We can complete the same analysis using the boundary conditions summarized in Table 8.2. In this table we see one unfamiliar entry—the boundary condition due to a harmonic bending couple is included. Let's now extend our analysis to consider not only transverse deflection, $y(x, t)$, but also rotation of the beam in the bending plane, $\theta(x, t)$; see Fig. 8.11.

To determine the rotation FRF, $\frac{\Theta_1}{F_1}$, for a fixed-free beam, we return to Eq. 8.26 and substitute $A = -C$ and $B = -D$ (from Eqs. 8.31 and 8.32).

Table 8.2 Boundary conditions for beam FRF calculations

End description	Boundary conditions
Fixed	$y = 0, \frac{\partial y}{\partial x} = 0$
Free	$\frac{\partial^2 y}{\partial x^2} = 0, \frac{\partial^3 y}{\partial x^3} = 0$
Pinned	$y = 0, \frac{\partial^2 y}{\partial x^2} = 0$
Sliding	$\frac{\partial y}{\partial x} = 0, \frac{\partial^3 y}{\partial x^3} = 0$
Harmonic force $Fsin(\omega t)$	$\frac{\partial^3 y}{\partial x^3} = -\frac{F}{EI} sin(\omega t)$
Harmonic bending couple $Msin(\omega t)$	$\frac{\partial^2 y}{\partial x^2} = \frac{M}{EI} sin(\omega t)$

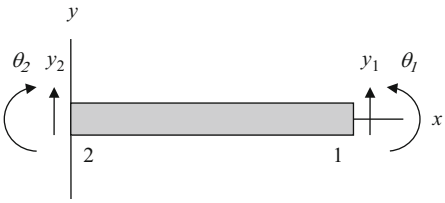

Fig. 8.11 Coordinates for both transverse deflection and rotation vibration in the bending plane

$$Y = C(-cos(\lambda x) + cosh(\lambda x)) + D(-sin(\lambda x) + sinh(\lambda x)) \tag{8.98}$$

We obtain rotation by differentiating Y with respect to x, $\Theta = \frac{dY}{dx}$. We then evaluate this expression at $x = l$ (coordinate 1) and substitute for C and D from Eqs. 8.45 and 8.48. Finally, we divide this expression by F_1. The result is provided in Eq. 8.99.

$$\frac{\Theta_1}{F_1} = \frac{sin(\lambda L) sinh(\lambda L)}{\lambda^2 EI(1 + cos(\lambda L) cosh(\lambda L))} \tag{8.99}$$

In addition to the deflection and rotation responses due to a harmonic force, we can also determine the responses due to a harmonic bending couple, $\frac{Y_1}{M_1}$ and $\frac{\Theta_1}{M_1}$. We find these terms by applying the harmonic bending couple $M_1 = Msin(\omega t)$ at coordinate 1 as shown in Fig. 8.12. The boundary conditions at coordinate 2 ($x = 0$) are $y = 0$ and $\frac{\partial y}{\partial x} = 0$. The boundary conditions at coordinate 1 ($x = l$) are $\frac{\partial^2 y}{\partial x^2} = \frac{M}{EI} sin(\omega t)$ and $\frac{\partial^3 y}{\partial x^3} = 0$. We find the coefficients A, B, C, and D from Eq. 8.26 in the same manner as described previously.

At $x = 0$, the situation is identical to the force application case shown in Fig. 8.5 so we obtain $A = -C$ and $B = -D$. At $x = l$, we first use $\frac{\partial^2 y}{\partial x^2} = \frac{M}{EI} sin(\omega t)$ as demonstrated in Eq. 8.100.

$$\left.\frac{\partial^2 y}{\partial x^2}\right|_{x=l} = \lambda^2 \begin{pmatrix} -Acos(\lambda l) - Bsin(\lambda l) + \\ Ccosh(\lambda l) + Dsinh(\lambda l) \end{pmatrix} = \frac{M}{EI} sin(\omega t) \tag{8.100}$$

Substitution for A and B in Eq. 8.100 gives:

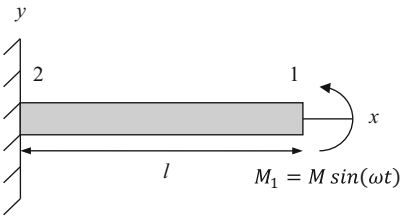

Fig. 8.12 Fixed-free beam with a harmonic bending couple applied at the free end

$$C(\,cos\,(\lambda L) + \,cosh\,(\lambda L)) + D(\,sin\,(\lambda L) + \,sinh\,(\lambda L)) = \frac{M}{\lambda^2 EI}\,sin\,(\omega t). \quad (8.101)$$

We next apply $\frac{\partial^3 y}{\partial x^3} = 0$ (at $x = l$) and substitute for A and B to get:

$$C(-\,sin\,(\lambda L) + \,sinh\,(\lambda L)) + D(\,cos\,(\lambda L) + \,cosh\,(\lambda L)) = 0. \quad (8.102)$$

Expressing Eqs. 8.101 and 8.102 in matrix form yields:

$$\begin{bmatrix} cos\,(\lambda L) + cosh\,(\lambda L) & sin\,(\lambda L) + sinh\,(\lambda L) \\ -\,sin\,(\lambda L) + sinh\,(\lambda L) & cos\,(\lambda L) + cosh\,(\lambda L) \end{bmatrix} \begin{Bmatrix} C \\ D \end{Bmatrix} = \begin{Bmatrix} \frac{M}{\lambda^2 EI} \\ 0 \end{Bmatrix} sin\,(\omega t). \quad (8.103)$$

Applying Cramer's rule, we solve for C and D.

$$C = \frac{M(\,cos\,(\lambda L) + \,cosh\,(\lambda L))}{2\lambda^2 EI(1 + \,cos\,(\lambda L)\,cosh\,(\lambda L))}\,sin\,(\omega t) \quad (8.104)$$

$$D = -\frac{M(-\,sin\,(\lambda L) + \,sinh\,(\lambda L))}{2\lambda^2 EI(1 + \,cos\,(\lambda L)\,cosh\,(\lambda L))}\,sin\,(\omega t) \quad (8.105)$$

We find Y_1 by substituting Eqs. 8.104 and 8.105, together with the relationships $A = -C$ and $B = -D$, in Eq. 8.26. We also set $x = l$. The result is provided in Eq. 8.106.

$$Y_1 = -\left(\frac{(\,cos\,(\lambda L) + \,cosh\,(\lambda L))(\,cos\,(\lambda L) - \,cosh\,(\lambda L))}{2\lambda^2 EI(1 + \,cos\,(\lambda L)\,cosh\,(\lambda L))} + \frac{(\,sin\,(\lambda L) - \,sinh\,(\lambda L))(\,sin\,(\lambda L) - \,sinh\,(\lambda L))}{2\lambda^2 EI(1 + \,cos\,(\lambda L)\,cosh\,(\lambda L))} \right) M sin(\omega t) \quad (8.106)$$

We obtain the $\frac{Y_1}{M_1}$ FRF at the free end of the fixed-free beam by dividing Eq. 8.106 by M_1 and simplifying; see Eq. 8.107. A comparison of Eqs. 8.107 and 8.99 shows us that the $\frac{Y_1}{M_1}$ and $\frac{\Theta_1}{F_1}$ FRFs are identical.

$$\frac{Y_1}{M_1} = \frac{-\left(\begin{array}{c}\frac{(\cos(\lambda L)+\cosh(\lambda L))(\cos(\lambda L)-\cosh(\lambda L))}{2\lambda^2 EI(1+\cos(\lambda L)\cosh(\lambda L))}+ \\ \frac{(\sin(\lambda L)-\sinh(\lambda L))(\sin(\lambda L)-\sinh(\lambda L))}{2\lambda^2 EI(1+\cos(\lambda L)\cosh(\lambda L))}\end{array}\right) M\sin(\omega t)}{M\sin(\omega t)}$$

$$\frac{Y_1}{M_1} = -\left(\begin{array}{c}\frac{(\cos(\lambda L)+\cosh(\lambda L))(\cos(\lambda L)-\cosh(\lambda L))}{2\lambda^2 EI(1+\cos(\lambda L)\cosh(\lambda L))}+ \\ \frac{(\sin(\lambda L)-\sinh(\lambda L))(\sin(\lambda L)-\sinh(\lambda L))}{2\lambda^2 EI(1+\cos(\lambda L)\cosh(\lambda L))}\end{array}\right) \tag{8.107}$$

$$\frac{Y_1}{M_1} = \frac{\sin(\lambda L)\sinh(\lambda L)}{\lambda^2 EI(1+\cos(\lambda L)\cosh(\lambda L))}$$

To determine the $\frac{\Theta_1}{M_1}$ FRF, we return to Eq. 8.26 and substitute $A = -C$ and $B = -D$ (from Eqs. 8.31 and 8.32).

$$Y = (C(-\cos(\lambda x)+\cosh(\lambda x)) + D(-\sin(\lambda x)+\sinh(\lambda x))) \tag{8.108}$$

We then find $\frac{\Theta_1}{M_1}$ by: (1) differentiating Y with respect to x to obtain rotation $\Theta = \frac{dY}{dx}$; (2) evaluating this expression at $x = l$; and (3) substituting for C and D from Eqs. 8.104 and 8.105; and (4) dividing this result by M_1. See Eq. 8.109.

$$\frac{\Theta_1}{M_1} = \frac{\sin(\lambda L)\cosh(\lambda L)+\cos(\lambda L)\sinh(\lambda L)}{\lambda EI(1+\cos(\lambda L)\cosh(\lambda L))} \tag{8.109}$$

This process can be repeated for any of the boundary conditions shown in Table 8.2. The FRFs for fixed-free and free-free boundary conditions are summarized in Table 8.3, where both direct and cross FRFs are included for the free-free beam. As discussed previously, no cross FRFs are shown for the fixed-free beam because the response at the free end is zero for any excitation at the fixed end and the response is always zero at the fixed end.

8.6 Transverse Vibration FRF Measurement Comparisons

8.6.1 Fixed-Free Beam

To apply the FRFs defined in Table 8.3, let's compare these models with measurements completed using the BEP. In Sect. 7.4, we performed an impact test on the

Table 8.3 Euler-Bernoulli beam FRFs for fixed-free and free-free boundary conditions [1]

$\frac{Y_2}{F_2}$	$\frac{\Theta_2}{F_2}, \frac{Y_2}{M_2}$	$\frac{Y_1}{F_2}, \frac{Y_2}{F_1}$	$\frac{\Theta_1}{F_2}, \frac{Y_2}{M_1}$	$\frac{\Theta_2}{M_2}$	$\frac{\Theta_2}{F_1}, \frac{Y_1}{M_2}$	$\frac{\Theta_1}{M_2}, \frac{\Theta_2}{M_1}$	$\frac{Y_1}{F_1}$	$\frac{\Theta_1}{F_1}, \frac{Y_1}{M_1}$	$\frac{\Theta_1}{M_1}$
Free-free									
$\frac{-c_1}{\lambda^3 c_7}$	$\frac{-c_2}{\lambda^2 c_7}$	$\frac{c_3}{\lambda^3 c_7}$	$\frac{c_4}{\lambda^2 c_7}$	$\frac{c_5}{\lambda c_7}$	$\frac{-c_4}{\lambda^2 c_7}$	$\frac{c_6}{\lambda c_7}$	$\frac{-c_1}{\lambda^3 c_7}$	$\frac{c_2}{\lambda^2 c_7}$	$\frac{c_5}{\lambda c_7}$
Fixed-free									
							$\frac{-c_1}{\lambda^3 c_8}$	$\frac{c_2}{\lambda^2 c_8}$	$\frac{c_5}{\lambda c_8}$

Terms c_1 through c_8	
$c_1 = \cos(\lambda l)\sinh(\lambda l) - \sin(\lambda l)\cosh(\lambda l)$	$c_5 = \cos(\lambda l)\sinh(\lambda l) + \sin(\lambda l)\cosh(\lambda l)$
$c_2 = \sin(\lambda l)\sinh(\lambda l)$	$c_6 = \sin(\lambda l) + \sinh(\lambda l)$
$c_3 = \sin(\lambda l) - \sinh(\lambda l)$	$c_7 = E_s I(\cos(\lambda l)\cosh(\lambda l) - 1)$
$c_4 = \cos(\lambda l) - \cosh(\lambda l)$	$c_8 = E_s I(\cos(\lambda l)\cosh(\lambda l) + 1)$

Coordinate 2 is the fixed end for the fixed-free beam

BEP with the cantilevered steel rod extended 130 mm beyond the base; the measurement setup is displayed in Fig. 7.20. Let's now model the rod as a fixed-free beam with a length of 130 mm and compare the analytical prediction with the measured result (shown previously in Fig. 7.21).

The relevant equation from Table 8.2 is:

$$\frac{Y_1}{F_1} = \frac{\sin(\lambda l)\cosh(\lambda l) - \cos(\lambda l)\sinh(\lambda l)}{\lambda^3 E(1+i\eta)I(\cos(\lambda l)\cosh(\lambda l)+1)},$$

where $\lambda^4 = \omega^2 \frac{\rho A}{E(1+i\eta)I}$. The beam in this case is a 12.7 mm diameter cylinder so the second moment of area is:

$$I = \frac{\pi d^4}{64} = \frac{\pi(0.0127)^4}{64} = 1.277 \times 10^{-9}\ \mathrm{m}^4$$

and the cross-sectional area, A, is:

$$A = \frac{\pi d^2}{4} = \frac{\pi(0.0127)^2}{4} = 1.267 \times 10^{-4}\ \mathrm{m}^2.$$

For the steel rod, we can use $\rho = 7800\ \mathrm{kg/m}^3$ and $E = 200$ GPa. The measured (dotted line) and predicted (solid line) FRFs are shown in Fig. 8.13. The solid damping factor was selected to be 0.034 to match the measured and predicted FRF magnitudes. Given this very large solid damping factor (a reasonable value of 0.001–0.002 was suggested for steel in Sect. 8.4) and the natural frequency mismatch (the predicted natural frequency is too high), we can make an observation about the BEP setup. A reasonable explanation for the experimental behavior is that the split-clamp used to secure the rod in the BEP holder does not provide an ideal fixed boundary condition. Small relative motion between the rod and base at the

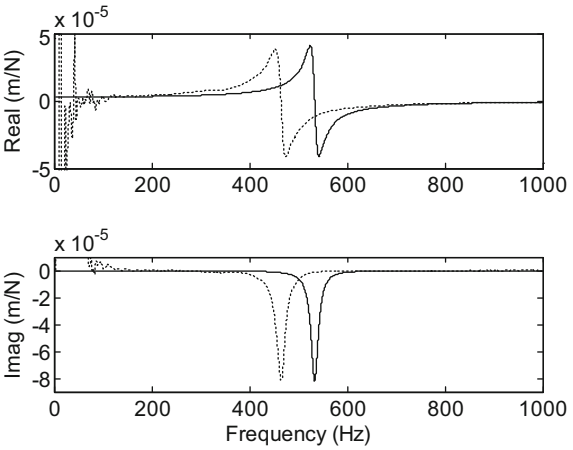

Fig. 8.13 Comparison between measured (dotted line) and predicted (solid line) fixed-free FRFs on the BEP

split-clamp connection would explain the additional damping. Also, the effective beam length may be slightly more than the measured value of 130 mm due to the radius/chamfer at the edge of the hole used to clamp the rod. This result is not unique; in practice, it is quite difficult to realize a fixed boundary condition.

8.6.2 Free-Free Beam

Let's now remove the steel rod from the BEP and measure its response alone (the rod's length is 152.5 mm). We can approximate free-free boundary conditions by supporting the rod on a soft foam base as shown in Fig. 8.14. The appropriate FRF equation from Table 8.3 is now:

$$\frac{Y_1}{F_1} = \frac{sin\,(\lambda l)\,cosh\,(\lambda l) - cos\,(\lambda l)\,sinh\,(\lambda l)}{\lambda^3 E(1+i\eta)I(\,cos\,(\lambda l)\,cosh\,(\lambda l)+1)}.$$

A comparison between the measured (dotted line) and predicted (solid line) FRFs is provided in Fig. 8.15 (5000 Hz measurement bandwidth). The solid damping factor for the prediction is 0.003. This significantly reduced value supports our theory that the clamping conditions for the rod served as a primary source of energy dissipation (damping) for the fixed-free setup. We do note, however, that $\eta = 0.003$ is still slightly larger than the anticipated value. In this case, it is the foam base that contributes the additional damping.

If we examine the FRFs in Fig. 8.15 carefully, we observe a behavior unique to free-free FRFs. The absolute value of the real parts gets very large as the frequency approaches zero. This is due to **rigid body modes** of the free-free beam. As we discussed in Sect. 6.5, if we imagine the rod floating in space, then applying a force

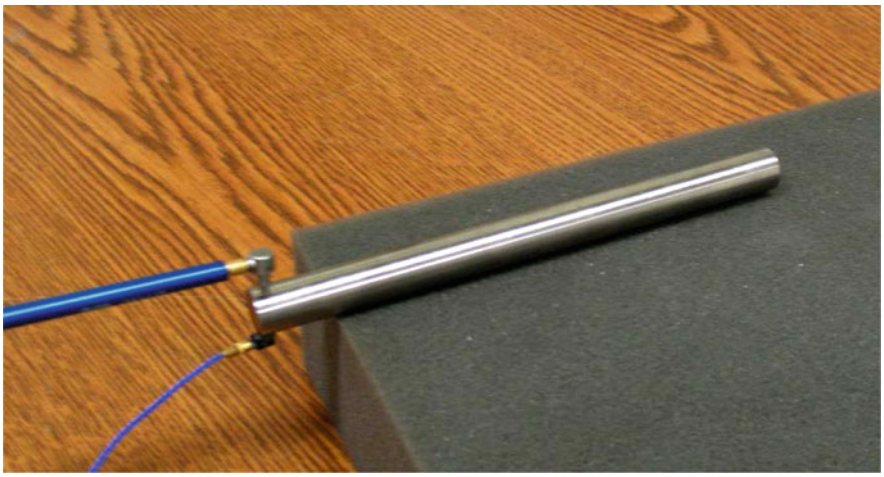

Fig. 8.14 Experimental impact testing setup for the free-free beam measurement

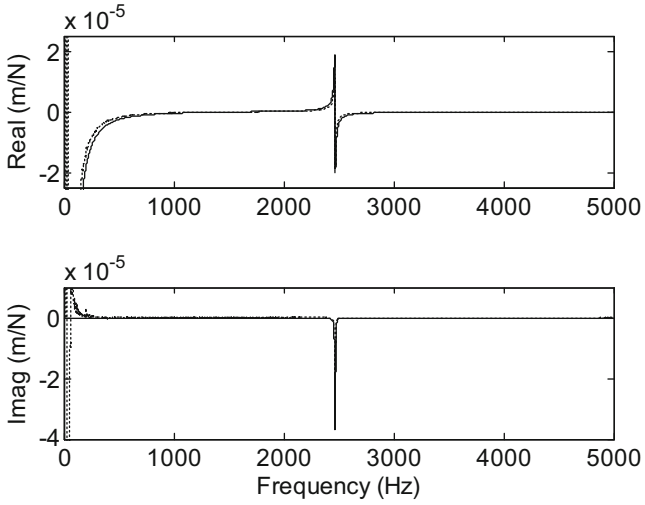

Fig. 8.15 Comparison between measured (dotted line) and predicted (solid line) free-free FRFs

at the center of mass will cause it to translate as a rigid body in the direction of the force. Alternately, applying a force at any other location will also cause it to rotate, again as a rigid body. Because there is no oscillation associated with these modes, they occur at zero frequency and are real-valued. Note that the free-free FRF expressions in Table 8.3 include these rigid body modes (as seen in the Fig. 8.15 prediction).

8.6.3 Natural Frequency Uncertainty

As a final consideration regarding the prediction of a beam's dynamic behavior, we need to recognize that, because the inputs for any model are uncertain (the true value of any quantity is never known), the output inherently includes uncertainty. As we discussed in Sect. 2.4.7, we can perform a first-order Taylor series expansion of the model (provided an analytical expression is available) to determine the output uncertainty as a function of the input uncertainties. In this way, we propagate the input uncertainties through the model to find the output uncertainty. Let's consider the sensitivity of the natural frequency equation shown in Eq. 8.96 to the beam's length. To do so, let's rewrite Eq. 8.96 to isolate the beam length, l:

$$f_{n,i} = \frac{1}{l^2}\frac{\beta_i^2}{2\pi}\sqrt{\frac{EI}{\rho A}}\,(\text{Hz}).$$

For the free-free beam discussed in Sect. 8.6.2, the β_i values are provided in Table 8.4 [3]. While there is uncertainty associated with E, I, ρ, A, if we consider only l, then the natural frequency uncertainty is determined using:

$$u^2(f_{n,i}) = \left(\frac{\partial f_{n,i}}{\partial l}\right)^2 u^2(l) = \left(\frac{-2}{l^3}\frac{\beta_i^2}{2\pi}\sqrt{\frac{EI}{\rho A}}\right)^2 u^2(l),$$

where $u(l)$ is the beam length uncertainty (the square of the uncertainty, $u^2(l)$, is referred to as the **variance**) and the average (or mean) values of the input variables are applied to evaluate the natural frequency uncertainty. For the free-free 12.7 mm diameter steel rod with a nominal length of 152.5 mm and an associated uncertainty of 0.1 mm, the uncertainty in the first natural frequency is $u(f_{n,1}) = 3.2$ Hz. This value represents one standard deviation and means that we would expect our predicted natural frequency to be within ±3.2 Hz of the true value 68% of the time for a normal (or **Gaussian distribution**). The relationships between error, uncertainty, the measured/predicted value, and the (unknown) true value are

Table 8.4 β_i values for free-free Euler-Bernoulli beam natural frequency calculations [3]

i	β_i
1	4.73004074
2	7.85320462
3	10.9956078
4	14.1371655
5	17.2787597
>5	$\frac{\pi}{2}(2i+1)$

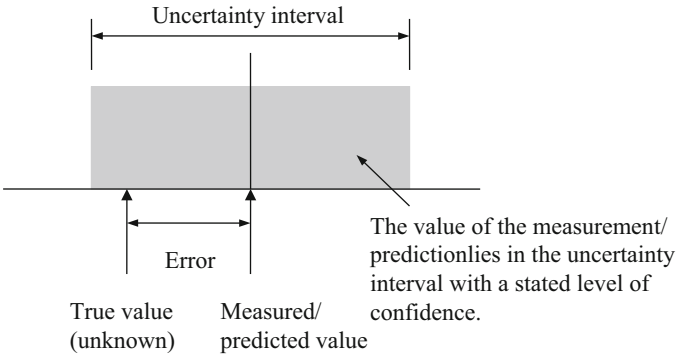

Fig. 8.16 Relationships between error, uncertainty, the measured/predicted value, and the unknown true value

presented graphically in Fig. 8.16.[5] A complete measurement/prediction description must include not only the mean value, but also the associated uncertainty.

8.7 Torsion Vibration

The equation of motion for a uniform beam with a circular cross-section under torsion vibration is provided in Eq. 8.110, where G is the beam's shear modulus and $\varphi(x,t)$ is the rotation about the beam's axis. The following assumptions apply: (1) radial lines extending from the beam center to its outer diameter remain straight after an external torque is applied; and (2) shear is the only significant stress [1].

$$G\frac{\partial^2\varphi}{\partial x^2} = \rho\frac{\partial^2\varphi}{\partial t^2} \tag{8.110}$$

For harmonic torsion vibration due to an external torque $Tsin(\omega t)$, a general solution to Eq. 8.110 is given by $\varphi(x,t) = \Phi(x)\ sin\ (\omega t)$, where $\Phi(x)$ is a function that describes the position-dependent vibration behavior and ω is the forcing frequency (rad/s). Calculating the second-order partial derivatives of this general solution with respect to x and t and substituting in Eq. 8.110 yields Eq. 8.111, where the $sin(\omega t)$ term appears on both sides of the equality and is not shown.

[5]The authors credit Dr. W.T. Estler (retired, National Institute of Standards and Technology) with this figure.

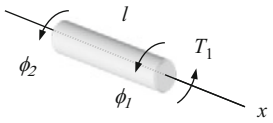

Fig. 8.17 Circular cross-section free-free beam with a torque applied at coordinate ϕ_1

$$G\frac{\partial^2 \Phi}{\partial x^2} = \left(-\omega^2 \rho\right)\Phi \tag{8.111}$$

A general solution to Eq. 8.111 is given in Eq. 8.112, where $\lambda = \omega\sqrt{\frac{\rho}{G}}$. Using this equation, we can determine the rotation FRFs for a free-free beam due to an external torque. Two boundary conditions are required. First, $\frac{\partial \Phi}{\partial x} = 0$ at a free boundary. Second, for an external torque application at the beam's end, $\frac{\partial \Phi}{\partial x} = \frac{T}{GJ}\, sin\,(\omega t)$, where T is the harmonic torque magnitude and J is the second polar moment of area for the beam's cross-section. This boundary condition follows from the relationship between the shear stress, τ, at a radius r and the shear strain, γ, $\tau = G\gamma$, or $\frac{Tr}{J} = rG\frac{d\varphi}{dx}$.

$$\Phi(x) = Acos(\lambda x) + Bsin(\lambda x) \tag{8.112}$$

In Fig. 8.17 an external torque $T_1 = Tsin(\omega t)$ is applied at the right end of the free-free beam, labeled as coordinate ϕ_1, where $x = l$ and l is the beam length ($x = 0$ at the left end of the beam). The corresponding boundary conditions are provided in Eq. 8.113.

$$\left.\frac{\partial \Phi}{\partial x}\right|_{x=0} = 0 \quad \left.\frac{\partial \Phi}{\partial x}\right|_{x=l} = \frac{T}{GJ}\sin(\omega t) \tag{8.113}$$

We determine the coefficients A and B in Eq. 8.112 by calculating $\frac{\partial \Phi}{\partial x}$ and applying the two boundary conditions from Eq. 8.113. This gives $A = \frac{-T}{GJ\lambda sin(\lambda l)}\, sin\,(\omega t)$ and $B = 0$. Substitution of these coefficient values in Eq. 8.112 gives Eq. 8.114.

$$\Phi(x) = \frac{-T}{GJ\lambda sin(\lambda l)}\, cos\,(\lambda x)\, sin\,(\omega t) \tag{8.114}$$

Finally, we write the direct torsion FRF at coordinate 1, $\frac{\Phi_1}{T_1}$, as shown in Eq. 8.115 by substituting $T_1 = Tsin(\omega t)$. Similarly, we find the cross FRF, $\frac{\Phi_2}{T_1}$, by substituting $x = 0$ in Eq. 8.114; see Eq. 8.116.

$$\frac{\Phi_1}{T_1} = \frac{-\,cos\,(\lambda l)}{GJ\lambda sin(\lambda l)} = \frac{-\,cot\,(\lambda l)}{GJ\lambda} \tag{8.115}$$

$$\frac{\Phi_2}{T_1} = \frac{-\cos(\lambda \cdot 0)}{GJ\lambda \sin(\lambda l)} = \frac{-1}{GJ\lambda \sin(\lambda l)} = \frac{-\csc(\lambda l)}{GJ\lambda} \tag{8.116}$$

To determine the direct and cross FRFs due to a torque applied at the other end of the beam, $\frac{\Phi_2}{T_2}$ and $\frac{\Phi_1}{T_2}$, we repeat the process. These results are given in Eqs. 8.117 and 8.118. In order to introduce damping in the component responses, we again incorporate solid damping, but this time using a complex shear modulus $G_s = G(1 + i\eta)$. Note that λ is a function of G as well.

$$\frac{\Phi_2}{T_2} = \frac{-\cot(\lambda l)}{GJ\lambda} \tag{8.117}$$

$$\frac{\Phi_1}{T_2} = \frac{-\csc(\lambda l)}{GJ\lambda} \tag{8.118}$$

8.8 Axial Vibration

The equation of motion for a uniform cross-section beam[6] under axial, or longitudinal, vibration is provided in Eq. 8.119, where γ is the deflection along the beam axis and **Poisson effects** are neglected[7] [1].

$$E\frac{\partial^2 \gamma}{\partial x^2} = \rho \frac{\partial^2 \gamma}{\partial t^2} \tag{8.119}$$

Because the equation of motion has the same form as Eq. 8.110 for torsion, the free-free receptance development is similar to that provided in Sect. 8.7. For the free-free beam of length l shown in Fig. 8.18, the application of a harmonic axial force $p_1 = P\sin(\omega t)$ enables us to determine the FRFs $\frac{\Gamma_1}{P_1}$ and $\frac{\Gamma_2}{P_1}$. See Eqs. 8.120 and 8.121, where $\lambda = \omega\sqrt{\frac{\rho}{E}}$. As before, determining the FRFs requires that two boundary conditions be applied. In this case, these are $\frac{\partial \Gamma}{\partial x} = 0$ at a free end and $\frac{\partial \Gamma}{\partial x} = \frac{P}{EA}\sin(\omega t)$ for an external axial force application at the beam's end, where A is the beam's cross-sectional area. The latter boundary conditions follows from the relationship between the axial stress, σ, and axial strain, ε, $\sigma = E\varepsilon$, or $\frac{P}{A} = E\frac{d\gamma}{dx}$. The other two FRFs for the beam in Fig. 8.14 are determined by applying p_2 to γ_2. See Eqs. 8.122 and 8.123. Again, in order to introduce damping in the component

[6]The beam's cross-section is not required to be circular as in the torsion vibration analysis in Sect. 8.7.

[7]This means that the beam's expansion and contraction in the directions normal to the oscillating axial deflection are ignored.

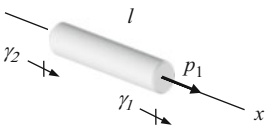

Fig. 8.18 Free-free beam with an axial force p_1 applied at coordinate γ_1

responses, we apply solid damping by replacing the elastic modulus with the complex elastic modulus $E_s = E(1 + i\eta)$. Note that λ is a function of E as well.

$$\frac{\Gamma_1}{P_1} = \frac{-\cot(\lambda l)}{EA\lambda} \tag{8.120}$$

$$\frac{\Gamma_2}{P_1} = \frac{-\csc(\lambda l)}{EA\lambda} \tag{8.121}$$

$$\frac{\Gamma_2}{P_2} = \frac{-\cot(\lambda l)}{EA\lambda} \tag{8.122}$$

$$\frac{\Gamma_1}{P_2} = \frac{-\csc(\lambda l)}{EA\lambda} \tag{8.123}$$

By the Numbers 8.3

Let's now compare the transverse deflection, torsion, and axial FRFs for a cylindrical beam. We'll consider a 10 mm diameter steel beam that is 500 mm long with free-free boundary conditions. Steel's material properties are $\rho = 7800$ kg/m^3, $E = 200$ GPa, Poisson's ratio is $\nu = 0.29$, and $G = \frac{E}{2(1+\nu)}$. Also, for the cylindrical beam, $A = \frac{\pi d^2}{4}$, $I = \frac{\pi d^4}{64}$, and $J = \frac{\pi d^2}{32}$. For plotting purposes, let's select $\eta = 0.01$. The relevant FRF equations are Eq. 8.80 for transverse deflection, Eq. 8.115 for torsion, and Eq. 8.120 for axial deflection. The FRFs are plotted using a semi-logarithmic scale in Figs. 8.19, 8.20, and 8.21. We see that the axial deflection natural frequencies are higher than the torsion natural frequencies which are, in turn, higher than the transverse deflection natural frequencies. We can also note that the increasing magnitude as the responses approach zero frequency is due to the rigid body modes for the free-free beam. The code used to produce Figs. 8.19, 8.20, and 8.21 is provided in MATLAB® MOJO 8.3.

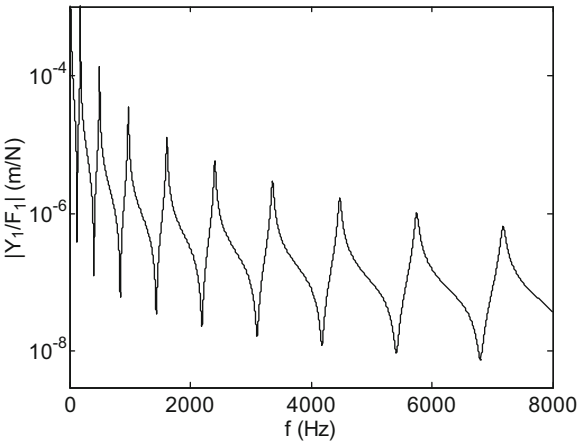

Fig. 8.19 *By the Numbers 8.3*—semi-logarithmic plot of the transverse deflection FRF for the 10 mm diameter, 500 mm long free-free steel beam

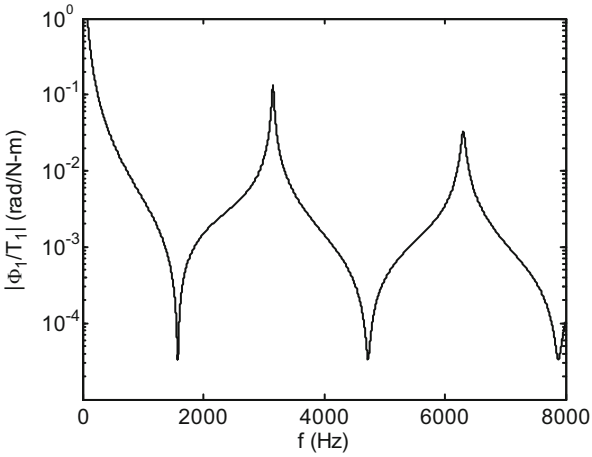

Fig. 8.20 *By the Numbers 8.3*—semi-logarithmic plot of the torsion FRF for the 10 mm diameter, 500 mm long free-free steel beam

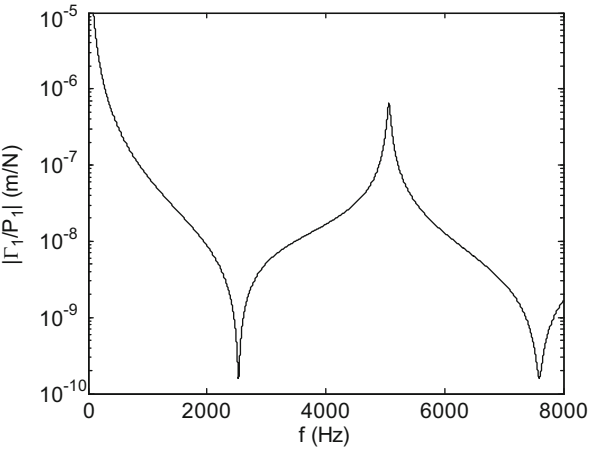

Fig. 8.21 *By the Numbers 8.3*—semi-logarithmic plot of the axial deflection FRF for the 10 mm diameter, 500 mm long free-free steel beam

MATLAB® MOJO 8.3

```
% matlab_mojo_8_3.m

clear
close all
clc

f = 1:0.1:8000;     % Hz
omega = f*2*pi;     % rad/s

% Define beam
d = 10e-3;        % m
l = 500e-3;       % m
E = 2e11;        % N/m^2
nu = 0.29;
G = E/(2*(1+nu));    % N/m^2
density = 7800;     % kg/m^3
eta = 0.01;
A = pi*d^2/4;      % m^2
I = pi*d^4/64;     % m^4
J = pi*d^4/32;     % m^4
E = E*(1+1i*eta);    % N-m^2
G = G*(1+1i*eta);    % N-m^2

% Free-free beam FRFs
% Transverse deflection FRF
lambda = (omega.^2*density*A/(E*I)).^0.25;
Y1_F1 = (cos(lambda*l).*sinh(lambda*l)-sin(lambda*l).*cosh
(lambda*l))./(lambda.^3*E*I.*(1-cos(lambda*l).*cosh(lambda*l)));

figure(1)
semilogy(f, abs(Y1_F1), 'k')
set(gca,'FontSize', 14)
ylim([3e-9 1e-3])
xlabel('f (Hz)')
ylabel('|Y_1/F_1| (m/N)')

% Torsion FRF
lambda = omega*(density/G)^0.5;
Phi1_T1 = -cot(lambda*l)./(G*J*lambda);

figure(2)
semilogy(f, abs(Phi1_T1), 'k')
ylim([1e-5 1])
set(gca,'FontSize', 14)
xlabel('f (Hz)')
ylabel('|\Phi_1/T_1| (rad/N-m)')

% Axial deflection FRF
lambda = omega*(density/E)^0.5;
Gamma1_P1 = -cot(lambda*l)./(E*A*lambda);
```

```
figure(3)
semilogy(f, abs(Gamma1_P1), 'k')
ylim([1e-10 1e-5])
set(gca,'FontSize', 14)
xlabel('f (Hz)')
ylabel('|\Gamma_1/P_1| (m/N)')
```

8.9 Timoshenko Beam Model

While the closed-form Euler-Bernoulli beam transverse vibration FRFs provided in Table 8.3 are convenient to apply, accurate solutions are obtained only for beams which exhibit small cross sectional area-to-length ratios (i.e., long slender beams). An alternative for beams that do not meet this criterion is the **Timoshenko beam model** [4]. The corresponding differential equation is given by:

$$\left(\frac{\partial^2 y}{\partial t^2} + \frac{EI}{\rho A}\frac{\partial^4 y}{\partial x^4}\right) + \left(\frac{\rho I}{\widehat{k}AG}\frac{\partial^4 y}{\partial t^4} + \frac{EI}{\widehat{k}AG}\frac{\partial^4 y}{\partial x^2 \partial t^2}\right) - \left(\frac{I}{A}\frac{\partial^4 y}{\partial x^2 \partial t^2}\right) = 0, \quad (8.124)$$

where $\widehat{k}$ is a shape factor that depends on the beam cross section [5]. Equation 8.124 is grouped into three sections (i.e., three parenthetical expressions). We see that the first section matches the Euler-Bernoulli beam equation provided in Eq. 8.19. The second and third sections account for shear deformations and rotary inertia, respectively. While these additional terms improve the model accuracy (particularly at higher frequencies), the tradeoff is that a closed-form solution to Eq. 8.124 is not available. Finite element calculations may be applied, but at the expense of increased computation time; see Chap. 9.

Chapter Summary

- In continuous models, the mass is distributed throughout the structure, rather than localized at the coordinates as in discrete models.
- Euler-Bernoulli beam theory can be used to derive transverse deflection FRFs for continuous cross-section beams.
- The beam's boundary conditions, such as fixed, free, or pinned, determine the FRF behavior.
- Solid damping can be incorporated in continuous beam FRFs using a complex modulus.
- The solid damping factor is equal to two times the viscous damping ratio at resonance.
- Anti-resonant frequencies represent frequencies where the beam response is small even for a large force input.
- Rotation FRFs are related to the transverse beam FRFs and describe the harmonic rotation of a beam within the bending plane due to a harmonic force or moment.

- Torsion FRFs describe the ratio of the frequency-domain rotation about the beam's axis to a harmonic torque applied to the beam.
- Axial FRFs, which provide the axial deflection response due to a harmonic axial force, have a similar form to torsion FRFs.
- The Timoshenko beam model may be implemented when the accuracy of the Euler-Bernoulli beam model is not adequate.

Exercises

1. Consider a uniform cross-section fixed-free (i.e., clamped-free or cantilever) beam.
   (a) Sketch the first bending mode shape (lowest natural frequency).
   (b) Sketch the second mode shape (next lowest natural frequency).
   (c) On your sketches in parts (a) and (b), identify any node location(s).
2. In describing beam vibrations using Euler-Bernoulli beam theory, we derived the equation of motion $\frac{\partial^4 Y}{\partial x^4} - \lambda^4 Y = 0$.
   (a) In the equation of motion, what does x represent physically?
   (b) In the equation of motion, what does Y represent physically?
   (c) Write the equation for λ (it replaces several other variables) and describe what each variable represents (include the SI units).
3. Consider a fixed-free beam. The general solution to the equation of motion can be written as $Y(x) = Acos(\lambda x) + Bsin(\lambda x) + Ccosh(\lambda x) + Dsinh(\lambda x)$. To determine the four coefficients, A through D, four boundary conditions are required. Write the four boundary conditions (in the table) as a function of x and y for the beam shown in Fig. P8.3.

at $x = 0$	at $x = L$
1.	3.
2.	4.

4. Consider the free-sliding beam shown in Fig. P8.4a. Direct and cross FRFs were measured at six locations and the imaginary parts are provided for the frequency interval near its second bending natural frequency of 350 Hz in Figs. P8.4b, P8.4c, P8.4d, P8.4e, P8.4f, and P8.4g. Given the FRF data, sketch the mode shape corresponding to the second natural frequency. Normalize the mode shape to a value of 1 at the free end.
5. Complete the following for the transverse deflection of a free-free cylindrical beam. The beam's diameter is 15 mm diameter steel and it is 480 mm long. The

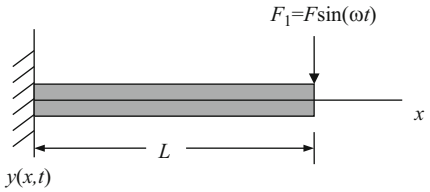

Fig. P8.3 Fixed-free beam model

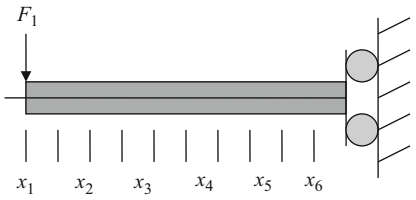

Fig. P8.4a Free-sliding beam model

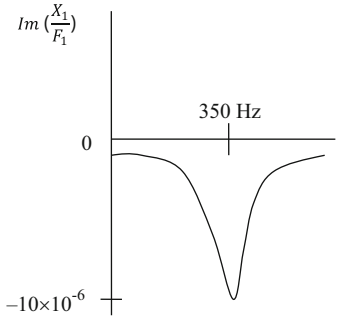

Fig. P8.4b Direct FRF $\frac{X_1}{F_1}$ for the free-sliding beam

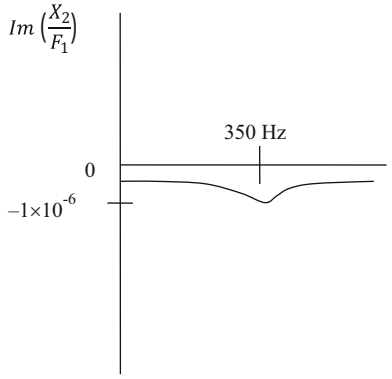

Fig. P8.4c Cross FRF $\frac{X_2}{F_1}$ for the free-sliding beam

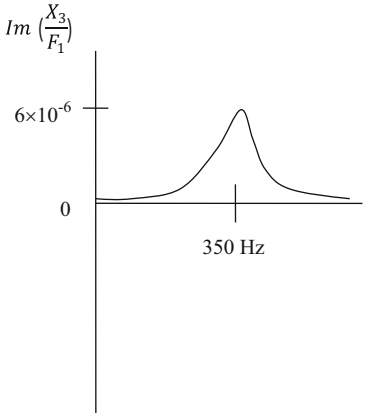

Fig. P8.4d Cross FRF $\frac{X_3}{F_1}$ for the free-sliding beam

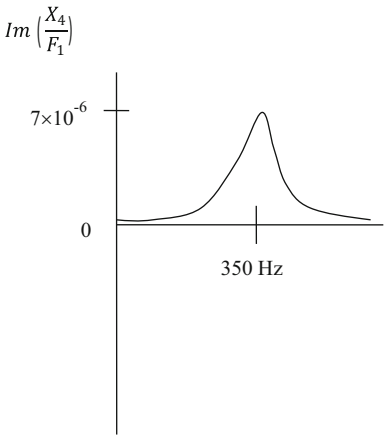

Fig. P8.4e Cross FRF $\frac{X_4}{F_1}$ for the free-sliding beam

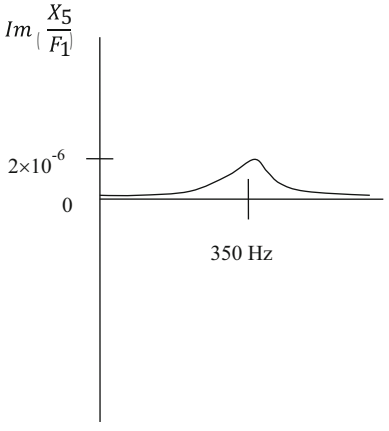

Fig. P8.4f Cross FRF $\frac{X_5}{F_1}$ for the free-sliding beam

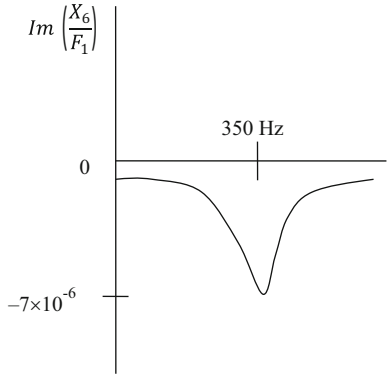

Fig. P8.4g Cross FRF $\frac{X_6}{F_1}$ for the free-sliding beam

beam material 6061-T6 aluminum with $\rho = 2700$ kg/m^3, $E = 70$ GPa, $\nu = 0.35$, $G = \frac{E}{2(1+\nu)}$, and $\eta = 0.002$.

(a) Plot the transverse deflection FRF over a frequency range of 10,000 Hz. Use a semi-logarithmic scale.
(b) How many modes are captured in this bandwidth (excluding the rigid body modes)?
(c) What is the natural frequency of the first (non-rigid) bending mode?

6. Complete the following for the torsion vibration of a free-free cylindrical beam. The beam's diameter is 15 mm diameter steel and it is 480 mm long. The beam material 6061-T6 aluminum with $\rho = 2700$ kg/m^3, $E = 70$ GPa, $\nu = 0.35$, $G = \frac{E}{2(1+\nu)}$, and $\eta = 0.002$.

(a) Plot the torsion FRF over a frequency range of 10,000 Hz. Use a semi-logarithmic scale.
(b) How many modes are captured in this bandwidth (excluding the rigid body mode)?
(c) What is the natural frequency of the first (non-rigid) torsion mode?

7. Complete the following for the axial vibration of a free-free cylindrical beam. The beam's diameter is 15 mm diameter steel and it is 480 mm long. The beam material 6061-T6 aluminum with $\rho = 2700$ kg/m^3, $E = 70$ GPa, $\nu = 0.35$, $G = \frac{E}{2(1+\nu)}$, and $\eta = 0.002$.

(a) Plot the axial FRF over a frequency range of 10,000 Hz. Use a semi-logarithmic scale.
(b) How many modes are captured in this bandwidth (excluding the rigid body mode)?
(c) What is the natural frequency of the first (non-rigid) torsion mode?

8. Consider the transverse vibration of a free-free cylindrical beam. If the diameter of a solid beam is d, determine the outer diameter, d_o, of a hollow beam with the

same length and material properties to give the same natural frequencies as the solid beam if the inner diameter, d_i, is one-half of the outer diameter, $d_i = 0.5d_o$.

9. For a 25 mm diameter 6061-T6 aluminum rod ($\rho = 2700$ kg/m^3 and $E = 70$ GPa,) with a nominal length of 190 mm and an associated uncertainty of 0.2 mm, determine the uncertainty in the second bending natural frequency, $u(f_{n,2})$ (in Hz) if free-free boundary conditions are imposed. You may neglect the uncertainty in E, ρ, and d.
10. The Timoshenko beam model is more accurate than the Euler-Bernoulli beam model because it includes the effects of _____ and _____.

References

1. Bishop R, Johnson D (1960) The mechanics of vibration. Cambridge University Press, Cambridge
2. Chapra S, Canale R (1985) Numerical methods for engineers with personal computer applications. McGraw-Hill, New York, NY, Section 7.1
3. Blevins RD (2001) Formulas for natural frequency and mode shape. Krieger Publishing, Malabar, FL, Table 8.1
4. Weaver W Jr, Timoshenko S, Young D (1990) Vibration problems in engineering, 5th edn. Wiley, New York, Section 5.12
5. Hutchinson J (2001) Shear coefficients for Timoshenko beam theory. J Appl Mech 68:87–92

Chapter 9
Finite Element Introduction

Little things console us because little things afflict us.
—*Blaise Pascal*

9.1 Introduction

In this chapter we introduce the topic of finite element analysis for beam vibration. In Chap. 8 we described continuous models based on Euler-Bernoulli beam theory. This is a reasonable approach for a simple geometry, such as the cylindrical shaft in a small DC electric motor, but is more difficult to implement for a more complex structure, such as a gas turbine fan. In this case, finite element analysis provides a common option for vibration studies. Rather than a continuous cross-section model, the geometry is discretized into small elements. The mass and stiffness matrices for the elements are then defined and assembled to provide a numerical solution for the behavior of the entire structure. In this chapter, we focus on axial and bending vibrations of beams that are discretized into elements along their lengths. We derive the associated stiffness and mass matrices and then show how the element matrices are combined to describe the entire beam. Finally, we arrange these matrices into the corresponding differential equations of motion and solve them to obtain the eigenvalues and frequency response functions, or FRFs. While our scope is limited to simple beam geometries, it provides a foundation that can be used for more complex structures.

In a Nutshell
Many software packages exist for finite element analysis of mechanical structures. Training for the use of these software packages often focusses on how to run the software, enter the geometry, plotting the results, and so on. Mechanical engineers will do a better job using the software with an understanding of what is going on "behind the scenes", and that is what this chapter is all about.

T. L. Schmitz, K. S. Smith, *Mechanical Vibrations*,
https://doi.org/10.1007/978-3-030-52344-2_9

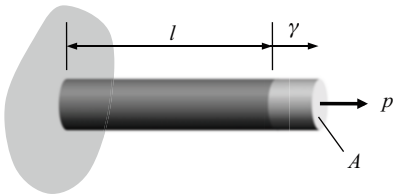

Fig. 9.1 Axial element with length, l, and cross-sectional area, A. The force p causes a change in length γ. The circular cross-section is for demonstration purposes only; any shape is acceptable

Finite element analysis leads to multiple degree of freedom mass and stiffness matrices, similar to the those we derived for the two degree of freedom lumped parameter models in Chaps. 4 and 5. In finite element analysis, the behaviors of continuous elements are described at their ends, which are rigidly connected to the ends of other elements.

Remember that eigenvalues are related to natural frequencies, the frequencies at which the system oscillates during free vibration. Each eigenvalue has a corresponding eigenvector, or mode shape. The way that the natural frequencies and mode shapes combine in free vibration depends on initial conditions. The FRFs, on the other hand, describe the magnitude and phase (or, equivalently, the real and imaginary parts) of the forced vibration as a function of the exciting frequency. We'll see these topics emerge during our finite element discussion.

9.2 Axial Element

In this section we consider an axial element that supports axial forces only; no lateral forces or moments are considered. The axial strain, ε, for the Fig. 9.1 element is:

$$\varepsilon = \frac{\gamma}{l}, \tag{9.1}$$

where γ is the change in element length due to an external axial force, p, and l is the original length. For elastic deformation,[1] the stress, σ, is related to the strain by the elastic modulus, E.

$$\sigma = E\varepsilon \tag{9.2}$$

Because the uniaxial stress is the ratio of the axial force to the cross-sectional area, A, perpendicular to the force direction, we substitute in Eq. 9.2 to obtain Eq. 9.3.

[1] In other words, the element returns to its original length when the force is removed.

Fig. 9.2 Axial element for the generic case with displacement γ_1 and force p_1 at the left end and displacement γ_2 and force p_2 at the right end

Fig. 9.3 Axial element with displacement γ_1 and force p_1 at the left end and the right end fixed ($\gamma_2 = 0$) with force p_2

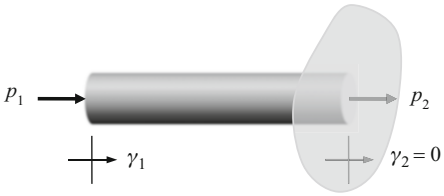

$$\frac{p}{A} = E\frac{\gamma}{l} \tag{9.3}$$

Rearranging gives us the linear relationship between p and γ, which is the element stiffness, k. We see that this resistance to deformation depends on the elastic modulus, area, and length. A larger elastic modulus or cross-sectional area increases the stiffness, while a larger length decreases the stiffness.

$$p = \left(\frac{EA}{l}\right)\gamma = k\gamma \tag{9.4}$$

For the generic case, we must describe displacements and forces at each end of the axial element. This is displayed in Fig. 9.2, where we've labeled the left end as 1 and the right end as 2. Because there are two axial forces and two axial displacements, the four stiffness terms, k_{ij} $(i, j = 1, 2)$, that relate them may be organized in a matrix format. In the Eq. 9.5 2×2 **stiffness matrix**, the first subscript indicates the row and the second the column.

$$\begin{Bmatrix} p_1 \\ p_2 \end{Bmatrix} = \begin{bmatrix} k_{11} & k_{12} \\ k_{21} & k_{22} \end{bmatrix} \begin{Bmatrix} \gamma_1 \\ \gamma_2 \end{Bmatrix} \tag{9.5}$$

To determine the four stiffness values, let's proceed by column. For the left column, we are relating the axial forces to γ_1, so let's set γ_2 equal to zero. We accomplish this by fixing the right end of the axial element (i.e., it does not move so the strain is zero); see Fig. 9.3. From the top row of Eq. 9.5, we have that:

$$p_1 = k_{11}\gamma_1 + k_{12}\gamma_2 = k_{11}\gamma_1 + k_{12} \cdot 0 = k_{11}\gamma_1. \tag{9.6}$$

We can now solve for k_{11}, where we've substituted using Eq. 9.4 for the final expression.

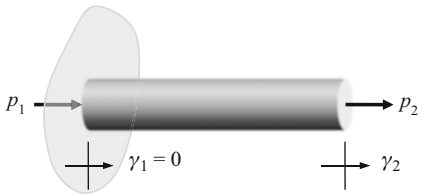

Fig. 9.4 Axial element with displacement γ_2 and force p_2 at the right end and the left end fixed ($\gamma_1 = 0$) with force p_1

$$k_{11} = \frac{p_1}{\gamma_1} = k = \frac{EA}{l} \tag{9.7}$$

From the bottom row of Eq. 9.5, we have that:

$$p_2 = k_{21}\gamma_1 + k_{22}\gamma_2 = k_{21}\gamma_1 + k_{22} \cdot 0 = k_{21}\gamma_1 \tag{9.8}$$

and

$$k_{21} = \frac{p_2}{\gamma_1}. \tag{9.9}$$

If we sum the forces in the axial direction from Fig. 9.3 we find that $p_1 + p_2 = 0$, or $p_2 = -p_1$, for static equilibrium. Substituting for p_2 in Eq. 9.9 gives:

$$k_{21} = \frac{-p_1}{\gamma_1} = -k = -\frac{EA}{l}. \tag{9.10}$$

For the right column, we are relating the axial forces to γ_2, so we set γ_1 equal to zero in this case. We now fix the left end of the axial element; see Fig. 9.4. From the top row of Eq. 9.5, we have that:

$$p_1 = k_{11}\gamma_1 + k_{12}\gamma_2 = k_{11} \cdot 0 + k_{12}\gamma_2 = k_{12}\gamma_2. \tag{9.11}$$

We can now solve for k_{12}, where we've substituted $p_1 = -p_2$.

$$k_{12} = -\frac{p_2}{\gamma_2} = -k = -\frac{EA}{l} \tag{9.12}$$

From the bottom row of Eq. 9.5, we have that:

$$p_2 = k_{21}\gamma_1 + k_{22}\gamma_2 = k_{21} \cdot 0 + k_{22}\gamma_2 = k_{22}\gamma_2 \tag{9.13}$$

and

$$k_{22} = \frac{p_2}{\gamma_2} = k = \frac{EA}{l}. \tag{9.14}$$

We can now populate the stiffness matrix in Eq. 9.5; see Eq. 9.15. We note that this matrix is symmetric (i.e., the off-diagonal terms, $-k$, are equal).

$$\begin{Bmatrix} p_1 \\ p_2 \end{Bmatrix} = \begin{bmatrix} k & -k \\ -k & k \end{bmatrix} \begin{Bmatrix} \gamma_1 \\ \gamma_2 \end{Bmatrix} = k \begin{bmatrix} 1 & -1 \\ -1 & 1 \end{bmatrix} \begin{Bmatrix} \gamma_1 \\ \gamma_2 \end{Bmatrix}$$
$$= \frac{EA}{l} \begin{bmatrix} 1 & -1 \\ -1 & 1 \end{bmatrix} \begin{Bmatrix} \gamma_1 \\ \gamma_2 \end{Bmatrix} \tag{9.15}$$

In a Nutshell
The stiffness matrix makes physical sense. You can think about it by asking what forces on the ends would be required to cause a certain deflection pattern. The on-diagonal elements are the forces required to cause a unit displacement of one node while the other node is held motionless. The off-diagonal elements are the forces required to hold the other node motionless. In other words, the on-diagonal term k_{11} is the force necessary to move γ_1 one unit in the positive direction, while γ_2 is held motionless. The off-diagonal term k_{12} is the force required to hold γ_2 motionless while γ_1 moves one unit. The second row can be derived by giving a unit displacement to γ_2 while holding γ_1 motionless. If the coordinates are measured with respect to ground, the stiffness matrix will always be symmetric.

We'll now turn our attention to the Fig. 9.2 axial element **mass matrix**. We have a bit of work to do to get there. Let's begin!

In Sect. 2.2, we saw that the kinetic energy of a lumped parameter, moving mass is $KE = \frac{1}{2}mv^2$. We will use this relationship again, but must now consider the distributed mass for the axial beam element. This requires that we integrate over the element length:

$$KE = \frac{1}{2}\frac{1}{l}\int_0^l m\dot{\gamma}^2 dx, \tag{9.16}$$

where m is the element mass, and $\dot{\gamma}$ is the time derivative of the change in axial length, or velocity. With a uniform mass distribution, we move m outside the integral to obtain Eq. 9.17, where $\frac{m}{l}$ is the mass per unit length.

$$KE = \frac{1}{2}\frac{m}{l}\int_0^l \dot{\gamma}^2 dx \tag{9.17}$$

The change in length at any point along the element is:

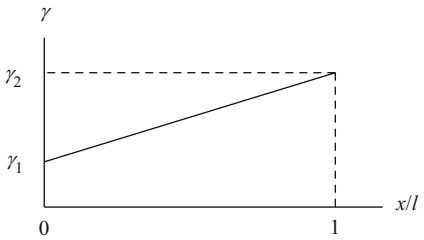

Fig. 9.5 Graphical representation of the axial displacement as a function of location along the beam axis (normalized to the beam length)

$$\gamma = \gamma_1\left(1 - \frac{x}{l}\right) + \gamma_2\left(\frac{x}{l}\right). \tag{9.18}$$

The Eq. 9.18 relationship is displayed graphically in Fig. 9.5. For example, if $\gamma_1 = 0$ (i.e., the left end of the element is fixed), then we have a change in length that increases linearly from 0 to $\gamma = \gamma_2\left(\frac{x}{l}\right) = \gamma_2\left(\frac{l}{l}\right) = \gamma_2$ at the right end. Substituting Eq. 9.18 in Eq. 9.17 gives:

$$KE = \frac{1}{2}\frac{m}{l}\int_0^l \left(\dot{\gamma}_1\left(1 - \frac{x}{l}\right) + \dot{\gamma}_2\left(\frac{x}{l}\right)\right)^2 dx. \tag{9.19}$$

Expanding gives:

$$KE = \frac{1}{2}\frac{m}{l}\int_0^l \left(\dot{\gamma}_1{}^2\left(1 - \frac{x}{l}\right)^2 + \dot{\gamma}_2{}^2\left(\frac{x}{l}\right)^2 + 2\dot{\gamma}_1\dot{\gamma}_2\left(1 - \frac{x}{l}\right)\left(\frac{x}{l}\right)\right) dx. \tag{9.20}$$

Expanding again yields:

$$KE = \frac{1}{2} \times \frac{m}{l}\int_0^l \left(\dot{\gamma}_1{}^2\left(1 - \frac{2x}{l} + \left(\frac{x}{l}\right)^2\right) + \dot{\gamma}_2{}^2\left(\frac{x}{l}\right)^2 + 2\dot{\gamma}_1\dot{\gamma}_2\left(\frac{x}{l} - \left(\frac{x}{l}\right)^2\right)\right) dx. \tag{9.21}$$

Integrating gives:

$$KE = \frac{1}{2}\frac{m}{l}\left[\dot{\gamma}_1{}^2\left(x - \frac{x^2}{l} + \frac{x^3}{3l^2}\right) + \dot{\gamma}_2{}^2\left(\frac{x^3}{3l^2}\right) + 2\dot{\gamma}_1\dot{\gamma}_2\left(\frac{x^2}{2l} - \frac{x^3}{3l^2}\right)\right]_0^l. \tag{9.22}$$

Evaluating over the integration limits results in:

$$KE = \frac{1}{2}\frac{m}{l}\left(\begin{array}{r}\left[\dot{\gamma}_1{}^2\left(l - l + \frac{l}{3}\right) + \dot{\gamma}_2{}^2\left(\frac{l}{3}\right) + 2\dot{\gamma}_1\dot{\gamma}_2\left(\frac{l}{2} - \frac{l}{3}\right)\right] - \\ \left[\dot{\gamma}_1{}^2(0) + \dot{\gamma}_2{}^2(0) + 2\dot{\gamma}_1\dot{\gamma}_2(0)\right]\end{array}\right). \tag{9.23}$$

Combining terms gives:

$$KE = \frac{1}{2}\frac{m}{l}\left[\dot{\gamma}_1{}^2\left(\frac{l}{3}\right) + \dot{\gamma}_2{}^2\left(\frac{l}{3}\right) + 2\dot{\gamma}_1\dot{\gamma}_2\left(\frac{l}{6}\right)\right]. \tag{9.24}$$

Finally, we eliminate l, simplify, and rearrange to obtain:

$$KE = \frac{1}{6}m\left[\dot{\gamma}_1{}^2 + \dot{\gamma}_1\dot{\gamma}_2 + \dot{\gamma}_2{}^2\right]. \tag{9.25}$$

We can now use this kinetic energy expression to determine the 2 × 2 mass matrix for the two degree of freedom axial element in Fig. 9.2. The mass matrix relates the axial forces to the axial accelerations, $\ddot{\gamma}$.

$$\left\{\begin{array}{c} p_1 \\ p_2 \end{array}\right\} = \left[\begin{array}{cc} m_{11} & m_{12} \\ m_{21} & m_{22} \end{array}\right]\left\{\begin{array}{c} \ddot{\gamma}_1 \\ \ddot{\gamma}_2 \end{array}\right\} \tag{9.26}$$

To find the four mass matrix entries, we apply the **Euler-Lagrange equation**:

$$p_i = \frac{d}{dt}\frac{\partial KE}{\partial \dot{\gamma}_i}, \quad i = 1, 2. \tag{9.27}$$

For $i = 1$, we obtain the following.

$$p_1 = \frac{d}{dt}\left(\frac{\partial}{\partial \dot{\gamma}_1}\left(\frac{1}{6}m\left[\dot{\gamma}_1{}^2 + \dot{\gamma}_1\dot{\gamma}_2 + \dot{\gamma}_2{}^2\right]\right)\right) \tag{9.28}$$

$$p_1 = \frac{d}{dt}\left(\frac{1}{6}m(2\dot{\gamma}_1 + \dot{\gamma}_2)\right) = \frac{d}{dt}\left(\frac{1}{3}m\dot{\gamma}_1 + \frac{1}{6}m\dot{\gamma}_2\right) \tag{9.29}$$

$$p_1 = \frac{1}{3}m\ddot{\gamma}_1 + \frac{1}{6}m\ddot{\gamma}_2 \tag{9.30}$$

Similarly, for $i = 2$, we obtain Eqs. 9.31–9.33.

$$p_2 = \frac{d}{dt}\left(\frac{\partial}{\partial \dot{\gamma}_2}\left(\frac{1}{6}m\left[\dot{\gamma}_1{}^2 + \dot{\gamma}_1\dot{\gamma}_2 + \dot{\gamma}_2{}^2\right]\right)\right) \tag{9.31}$$

$$p_2 = \frac{d}{dt}\left(\frac{1}{6}m(\dot{\gamma}_1 + 2\dot{\gamma}_2)\right) = \frac{d}{dt}\left(\frac{1}{6}m\dot{\gamma}_1 + \frac{1}{3}m\dot{\gamma}_2\right) \tag{9.32}$$

$$p_2 = \frac{1}{6}m\ddot{\gamma}_1 + \frac{1}{3}m\ddot{\gamma}_2 \tag{9.33}$$

Substitution in Eq. 9.26 gives the symmetric mass matrix.

$$\begin{Bmatrix} p_1 \\ p_2 \end{Bmatrix} = \begin{bmatrix} \frac{1}{3}m & \frac{1}{6}m \\ \frac{1}{6}m & \frac{1}{3}m \end{bmatrix} \begin{Bmatrix} \ddot{\gamma}_1 \\ \ddot{\gamma}_2 \end{Bmatrix} = \frac{m}{6}\begin{bmatrix} 2 & 1 \\ 1 & 2 \end{bmatrix} \begin{Bmatrix} \ddot{\gamma}_1 \\ \ddot{\gamma}_2 \end{Bmatrix} \tag{9.34}$$

In a Nutshell

Why is the mass matrix derivation so much more complicated than the stiffness matrix? In the stiffness matrix, the element acted like a lumped parameter spring and our task was simply to determine the spring constant. In the mass matrix, this is not so. The mass is distributed throughout the element and different parts of the element have different accelerations. The mass matrix derived here indicates the force-acceleration behavior of the end points of the element, based on the mass distribution in between. As long as the coordinates are measured with respect to ground, the mass matrix will also be symmetric.

We can now combine the mass and stiffness matrices to write the equation of motion for undamped longitudinal vibration of the two degree of freedom axial element. At this point, we have not placed a constraint on either end, so Eq. 9.35 represents free-free boundary conditions. In Eq. 9.35, ρAl has been substituted for m in the mass matrix, where ρ is the element density.

$$\frac{\rho Al}{6}\begin{bmatrix} 2 & 1 \\ 1 & 2 \end{bmatrix} \begin{Bmatrix} \ddot{\gamma}_1 \\ \ddot{\gamma}_2 \end{Bmatrix} + \frac{EA}{l}\begin{bmatrix} 1 & -1 \\ -1 & 1 \end{bmatrix} \begin{Bmatrix} \gamma_1 \\ \gamma_2 \end{Bmatrix} = \begin{Bmatrix} p_1 \\ p_2 \end{Bmatrix} \tag{9.35}$$

Solution of this equation of motion provides the time-dependent axial displacements at the element ends due to the external forces. Let's now model a beam with two axial elements and three displacements. See Fig. 9.6.

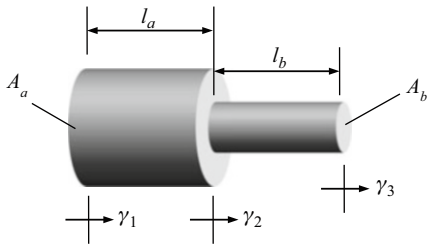

Fig. 9.6 Two-element beam model with displacements γ_1, γ_2, and γ_3. The cross-sectional area and length for the left element are A_a and l_a. They are A_b and l_b for the right element

In a Nutshell
Once the mass and stiffness matrices exist, the analysis is no different than the lumped parameter case, except that a finite element model may have thousands (or millions!) of degrees of freedom. The computational power required is often a limiting factor on the size of the model (i.e., the number of finite elements).

We'll consider both elements to be made from the same material with elastic modulus, E, and density, ρ, but with different lengths and cross-sectional areas. The individual mass matrices are:

$$\frac{\rho A_a l_a}{6}\begin{bmatrix} 2 & 1 \\ 1 & 2 \end{bmatrix} \quad \text{and} \quad \frac{\rho A_b l_b}{6}\begin{bmatrix} 2 & 1 \\ 1 & 2 \end{bmatrix}. \tag{9.36}$$

The individual stiffness matrices are:

$$\frac{EA_a}{l_a}\begin{bmatrix} 1 & -1 \\ -1 & 1 \end{bmatrix} \quad \text{and} \quad \frac{EA_b}{l_b}\begin{bmatrix} 1 & -1 \\ -1 & 1 \end{bmatrix}. \tag{9.37}$$

We must assemble these individual matrices into a new equation of motion that includes all three displacements. The mass and stiffness matrices are now 3×3 because the Fig. 9.6 model has three degrees of freedom. Also, there are no external forces in Fig. 9.6, so the right hand side of Eq. 9.38 is zero.

$$\begin{bmatrix} m_{11} & m_{12} & m_{13} \\ m_{21} & m_{22} & m_{23} \\ m_{31} & m_{32} & m_{33} \end{bmatrix}\begin{Bmatrix} \ddot{\gamma}_1 \\ \ddot{\gamma}_2 \\ \ddot{\gamma}_3 \end{Bmatrix} + \begin{bmatrix} k_{11} & k_{12} & k_{13} \\ k_{21} & k_{22} & k_{23} \\ k_{31} & k_{32} & k_{33} \end{bmatrix}\begin{Bmatrix} \gamma_1 \\ \gamma_2 \\ \gamma_3 \end{Bmatrix} = \begin{Bmatrix} 0 \\ 0 \\ 0 \end{Bmatrix} \tag{9.38}$$

To obtain the nine entries in the 3×3 mass and stiffness matrices, we must superimpose the original 2×2 matrices. The overlay result is presented in Eq. 9.39, where the upper left 2×2 portion of the matrices comes from the left element and the lower right 2×2 portion comes from the right element of Fig. 9.6.

$$\frac{\rho}{6}\begin{bmatrix} 2A_a l_a & A_a l_a & 0 \\ A_a l_a & 2A_a l_a + 2A_b l_b & A_b l_b \\ 0 & A_b l_b & 2A_b l_b \end{bmatrix}\begin{Bmatrix} \ddot{\gamma}_1 \\ \ddot{\gamma}_2 \\ \ddot{\gamma}_3 \end{Bmatrix} + E\begin{bmatrix} \frac{A_a}{l_a} & -\frac{A_a}{l_a} & 0 \\ -\frac{A_a}{l_a} & \frac{A_a}{l_a}+\frac{A_b}{l_b} & -\frac{A_b}{l_b} \\ 0 & -\frac{A_b}{l_b} & \frac{A_b}{l_b} \end{bmatrix}\begin{Bmatrix} \gamma_1 \\ \gamma_2 \\ \gamma_3 \end{Bmatrix} = \begin{Bmatrix} 0 \\ 0 \\ 0 \end{Bmatrix} \tag{9.39}$$

We observe that the superposition results in a sum of two mass and stiffness entries at the (2, 2) position and that the (1, 3) and (3, 1) positions of the square matrices are zero. Also, the new matrices remain symmetric.

In a Nutshell

The matrices for a single element or for multiple joined elements only differ by size. We have two coordinates (one at the left end and one right end) for a single element. When two elements are joined, we have four coordinates, but because the motion of the right end of the left beam and the motion of the left end of the right beam must be the same, so we only require three coordinates to fully describe the behavior.

Let's now consider a special case of Fig. 9.6, where the two elements have equal lengths, l, and cross-sectional areas, A. The equation of motion is now given by Eq. 9.40.

$$\frac{\rho A l}{6}\begin{bmatrix} 2 & 1 & 0 \\ 1 & 4 & 1 \\ 0 & 1 & 2 \end{bmatrix}\begin{Bmatrix} \ddot{\gamma}_1 \\ \ddot{\gamma}_2 \\ \ddot{\gamma}_3 \end{Bmatrix} + \frac{EA}{l}\begin{bmatrix} 1 & -1 & 0 \\ -1 & 2 & -1 \\ 0 & -1 & 1 \end{bmatrix}\begin{Bmatrix} \gamma_1 \\ \gamma_2 \\ \gamma_3 \end{Bmatrix} = \begin{Bmatrix} 0 \\ 0 \\ 0 \end{Bmatrix} \tag{9.40}$$

Next, let's fix the left end of the beam so that we have fixed-free boundary conditions; see Fig. 9.7. This is equivalent to setting $\gamma_1 = 0$. In doing so, we eliminate the first row and column of the 3×3 matrices in Eq. 9.40. The corresponding equation of motion has 2×2 matrices as shown in Eq. 9.41.

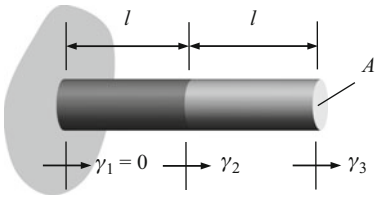

Fig. 9.7 Two-element beam model with displacements γ_1, γ_2, and γ_3. The cross-sectional areas and lengths are equal for the two elements and the left end is fixed so that $\gamma_1 = 0$

$$\frac{\rho Al}{6}\begin{bmatrix}4 & 1\\ 1 & 2\end{bmatrix}\begin{Bmatrix}\ddot{\gamma}_2\\ \ddot{\gamma}_3\end{Bmatrix}+\frac{EA}{l}\begin{bmatrix}2 & -1\\ -1 & 1\end{bmatrix}\begin{Bmatrix}\gamma_2\\ \gamma_3\end{Bmatrix}=\begin{Bmatrix}0\\ 0\end{Bmatrix} \tag{9.41}$$

This equation presents us with the same format we used for free vibration of the two degree of freedom lumped parameter, chain type system in Sect. 4.2, except that the off-diagonal terms are no longer zero in the mass matrix. We can again solve the **eigenvalue problem** to determine the two natural frequencies. Assuming harmonic motion, we substitute $\gamma_i = \Gamma_i e^{st}$ and $\ddot{\gamma}_i = s^2\Gamma_i e^{st}$, $i = 1, 2$, to obtain Eq. 9.42.

$$\begin{bmatrix}\frac{4\rho Al}{6}s^2+\frac{2EA}{l} & \frac{\rho Al}{6}s^2-\frac{EA}{l}\\ \frac{\rho Al}{6}s^2-\frac{EA}{l} & \frac{2\rho Al}{6}s^2+\frac{EA}{l}\end{bmatrix}\begin{Bmatrix}\Gamma_2\\ \Gamma_3\end{Bmatrix}=\begin{Bmatrix}0\\ 0\end{Bmatrix} \tag{9.42}$$

To calculate the eigenvalues, ${s_1}^2$ and ${s_2}^2$, we use the determinant of Eq. 9.42.

$$\begin{vmatrix}\frac{2\rho Al}{3}s^2+\frac{2EA}{l} & \frac{\rho Al}{6}s^2-\frac{EA}{l}\\ \frac{\rho Al}{6}s^2-\frac{EA}{l} & \frac{\rho Al}{3}s^2+\frac{EA}{l}\end{vmatrix}=0 \tag{9.43}$$

As we discussed in Sect. 2.4.5, the determinant of a 2×2 matrix is the product of the on-diagonal terms minus the product of the off-diagonal terms.

$$\left(\frac{2\rho Al}{3}s^2+\frac{2EA}{l}\right)\left(\frac{\rho Al}{3}s^2+\frac{EA}{l}\right)-\left(\frac{\rho Al}{6}s^2-\frac{EA}{l}\right)\left(\frac{\rho Al}{6}s^2-\frac{EA}{l}\right)=0 \tag{9.44}$$

Expanding and simplifying Eq. 9.44 gives the following.

$$\frac{2}{9}(\rho Al)^2s^4+\frac{4}{3}E\rho A^2s^2+2\left(\frac{EA}{l}\right)^2-\frac{1}{36}(\rho Al)^2s^4+\frac{2}{6}E\rho A^2s^2-\left(\frac{EA}{l}\right)^2=0 \tag{9.45}$$

$$\frac{7}{36}(\rho Al)^2s^4+\frac{5}{3}E\rho A^2s^2+\left(\frac{EA}{l}\right)^2=0 \tag{9.46}$$

Applying the quadratic equation to Eq. 9.46, we obtain the two eigenvalues.

$$s_1{}^2 = \frac{-\frac{5}{3}E\rho A^2 + \sqrt{\frac{25}{9}E^2\rho^2A^4 - 4\frac{7}{36}\rho^2A^2l^2\frac{E^2A^2}{l^2}}}{\frac{14}{36}(\rho Al)^2} = -0.6492\frac{EA}{\rho Al^2} \tag{9.47}$$

$$s_2{}^2 = \frac{-\frac{5}{3}E\rho A^2 - \sqrt{\frac{25}{9}E^2\rho^2A^4 - 4\frac{7}{36}\rho^2A^2l^2\frac{E^2A^2}{l^2}}}{\frac{14}{36}(\rho Al)^2} = -7.9223\frac{EA}{\rho Al^2} \tag{9.48}$$

Using $s_1{}^2 = -\omega_{n1}{}^2$ and $s_2{}^2 = -\omega_{n2}{}^2$, we determine the two natural frequencies.

$$\omega_{n1} = 0.8057\sqrt{\frac{EA}{\rho Al^2}} \tag{9.49}$$

$$\omega_{n2} = 2.8147\sqrt{\frac{EA}{\rho Al^2}} \tag{9.50}$$

Let's conclude this example by comparing the two-element model natural frequencies in Eqs. 9.49 and 9.50 to the exact solution provided in Eq. 9.51, where $L = 2l$ for this case (see Fig. 9.7).

$$\omega_{ni} = (2(i-1)+1)\frac{\pi}{2}\sqrt{\frac{EA}{\rho AL^2}} \tag{9.51}$$

Substituting $i = 1$ and $i = 2$ in Eq. 9.51, we obtain the first two natural frequencies.

$$\omega_{n1} = \frac{\pi}{2}\sqrt{\frac{EA}{\rho A(2l)^2}} = 0.7854\sqrt{\frac{EA}{\rho Al^2}} \tag{9.52}$$

$$\omega_{n2} = \frac{3\pi}{2}\sqrt{\frac{EA}{\rho A(2l)^2}} = 2.3562\sqrt{\frac{EA}{\rho Al^2}} \tag{9.53}$$

We see that the two-element model overestimates the natural frequencies. However, as we add more elements, while maintaining the same overall length, the agreement improves. Let's explore this convergence by calculating the frequency response functions for both free-free and fixed-free boundary conditions.

In a Nutshell
This illustrates a basic principle of finite element modeling. It is an approximation. We want to be as accurate as we need to be, but using too many elements leads to problems with numerical accuracy and computational resources. How do we know how many elements to use? Typically, we look at a few different models with differing numbers of elements. If the models agree (converge) within our required tolerance, then we believe that the model is close enough and we do not required additional elements to describe the structure's dynamic behavior.

Returning to Eq. 9.40 for the uniform cross-section free-free beam, we have the equation of motion:

$$[M]\{\ddot{\gamma}\} + [K]\{\gamma\} = \{p\}, \tag{9.54}$$

where

$$[M] = \frac{\rho Al}{6}\begin{bmatrix} 2 & 1 & 0 \\ 1 & 4 & 1 \\ 0 & 1 & 2 \end{bmatrix}, \quad \{\ddot{\gamma}\} = \begin{Bmatrix} \ddot{\gamma}_1 \\ \ddot{\gamma}_2 \\ \ddot{\gamma}_3 \end{Bmatrix}, \quad [K] = \frac{EA}{l}\begin{bmatrix} 1 & -1 & 0 \\ -1 & 2 & -1 \\ 0 & -1 & 1 \end{bmatrix}, \quad \{\gamma\} = \begin{Bmatrix} \gamma_1 \\ \gamma_2 \\ \gamma_3 \end{Bmatrix}, \quad \text{and} \quad \{p\} = \begin{Bmatrix} p_1 \\ p_2 \\ p_3 \end{Bmatrix}.$$

Substituting $\gamma = \Gamma e^{st}$, $\ddot{\gamma} = s^2\Gamma e^{st}$, and $p = Pe^{st}$ and rearranging gives:

$$\{\Gamma\}e^{st} = \left[[M]s^2 + [K]\right]^{-1}\{P\}e^{st}. \tag{9.55}$$

Setting $s = i\omega$ and dropping the exponent from both sides of Eq. 9.55, we obtain:

$$\{\Gamma\} = \left[-[M]\omega^2 + [K]\right]^{-1}\{P\}. \tag{9.56}$$

We refer to the inverted matrix as the **dynamic matrix**, $[D] = [-[M]\omega^2 + [K]]$. Using this matrix, we define the beam FRFs. For example, the corner entries in the 3×3 matrix give the end (or tip) direct FRFs, h_{ii}, $i = 1, 3$, and cross FRFs, h_{ij}, $i = 1, 3$ and $j = 3, 1$.

$$[D]^{-1} = \left[-[M]\omega^2 + [K]\right]^{-1} = \begin{bmatrix} h_{11} & h_{12} & h_{13} \\ h_{21} & h_{22} & h_{23} \\ h_{31} & h_{32} & h_{33} \end{bmatrix} \tag{9.57}$$

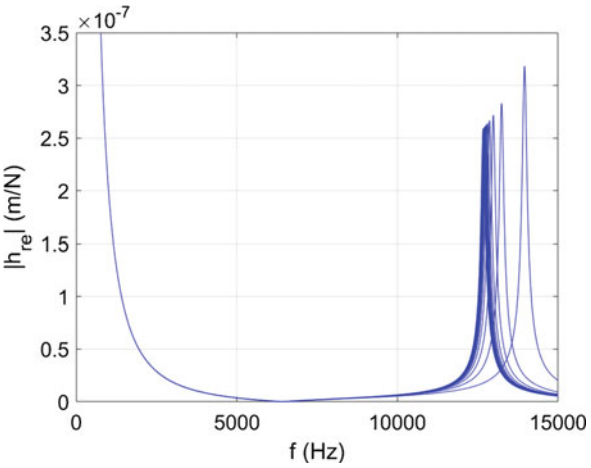

Fig. 9.8 *By the Numbers 9.1*—the free-free boundary condition h_{re} magnitude is plotted for the number of elements, n, from 2 to 25. The right (highest frequency) response is for $n = 2$

In Eq. 9.57, the $h_{33} = \frac{\Gamma_3}{P_3}(\omega)$ entry is the direct FRF at the right end due to a harmonic force with magnitude P_3 and frequency ω.

In a Nutshell
The math here is the same as it was for the lumped parameter models in Chaps. 2–5.

By the Numbers 9.1
Using MATLAB® MOJO 9.1, let's compare the right end direct FRF, h_{re}, natural frequencies for free-free boundary conditions as we add elements. We'll consider the first axial mode only for a 10 mm diameter, 200 mm long steel beam with $E = 200$ GPa and $\rho = 7800$ kg/m^3. The FRF magnitudes for the number of elements, n, from 2 to 25 are displayed in Fig. 9.8. Note that the large response at small frequencies is due to the free-free boundary conditions and the associated rigid body mode (i.e., linear translation, no oscillation) and that we've incorporated damping using the complex modulus as described in Sect. 8.4. The variation in the first natural frequency with n is shown in Fig. 9.9.

MATLAB® MOJO 9.1

```
% matlab_mojo_9_1.m

clear
close all
clc
warning off
```

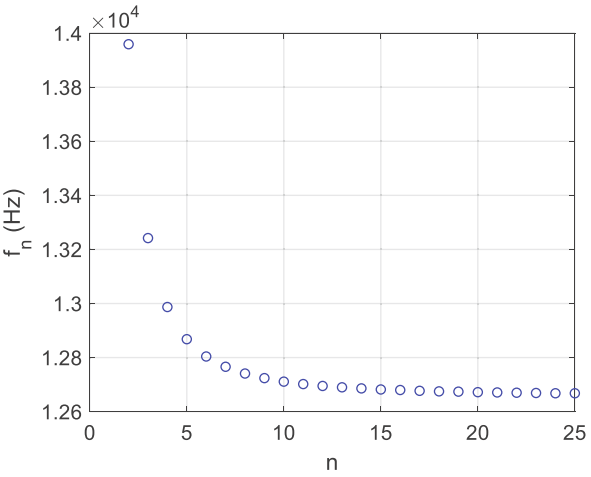

Fig. 9.9 *By the Numbers 9.1*—variation in the first natural frequency for the free-free boundary condition h_{re} with the number of elements in the model, n

```
f = 1:15000; % Hz
E = 200e9; % Pa
eta = 0.01; % -
L = 200e-3; % m
rho = 7800; % kg/m^3
d = 10e-3; % m
A = pi*d^2/4; % m^2
maxn = 25;

% Create vector for natural frequencies
fn = zeros(1, (maxn-1));

% Calculate FRFs for two elements
n = 2;
[h11, h22, h12, h21] = axial_free_free(f, E, eta, L, rho, A, n);

% Plot results
figure(1)
plot(f, abs(h22), 'b')
set(gca,'FontSize', 14)
xlabel('f (Hz)')
ylabel('|h_{re}| (m/N)')
ylim([0 3.5e-7])
grid
hold on

% Identify first natural frequency for two-element solution
index = find(imag(h22) == min(imag(h22)));
fn(1) = f(index);

% Repeat for additional elements
for cnt = 3:maxn
```

```
 n = cnt;
 [h11, h22, h12, h21] = axial_free_free(f, E, eta, L, rho, A, n);

 figure(1)
 plot(f, abs(h22), 'b')

 index = find(imag(h22) == min(imag(h22)));
 fn(cnt-1) = f(index);
end

figure(2)
plot((2:maxn), fn, 'bo')
set(gca,'FontSize', 14)
xlabel('n')
ylabel('f_n (Hz)')
grid

% axial_free_free.m

% This function uses n axial beam elements to determine end receptances
for
% a free-free beam.
% Input variables are: f, frequency, Hz
% E, elastic modulus, N/m^2
% eta, solid damping, -
% L, beam length, m
% rho, density, kg/m^3
% A, cross sectional area, m^2
% n, number of elements

function [h11, h22, h12, h21] = axial_free_free(f, E, eta, L, rho, A, n)
l = L/n; % length of each finite element, m
E = E*(1 + 1i*eta); % complex modulus, N/m^2

% Matrices for single axial element
% Mass matrix
M = rho*A*l/6*[2 1;1 2];
% Stiffness matrix
K = E*A/l*[1 -1;-1 1];

Mtemp2 = M;
Ktemp2 = K;

% Build full mass and stiffness matrices
for cnt = 2:n
 % Concatenate left element matrices with required zeros
 right = zeros(cnt, 1);
 bottom = zeros(1, (cnt+1));
 % Mass matrix
 temp = cat(2, M, right);
 Mtemp1 = cat(1, temp, bottom);
 % Stiffness matrix
```

```
temp = cat(2, K, right);
Ktemp1 = cat(1, temp, bottom);

% Concatenate right element matrices with required zeros
left = zeros(cnt, 1);
top = zeros(1, (cnt+1));
% Mass matrix
temp = cat(2, left, Mtemp2);
Mtemp2 = cat(1, top, temp);
% Stiffness matrix
temp = cat(2, left, Ktemp2);
Ktemp2 = cat(1, top, temp);

% Add two matrices
M = Mtemp1 + Mtemp2;
K = Ktemp1 + Ktemp2;
end

% Initialize receptance vectors
h11 = zeros(1,length(f));
h12 = zeros(1,length(f));
h21 = zeros(1,length(f));
h22 = zeros(1,length(f));

% Calculate required direct and cross receptances for ends of beam
for cnt = 1:length(f)
w = f(cnt)*2*pi; % frequency, rad/s
temp_matrix = (-M*w^2 + K);
D = eye(size(temp_matrix))/temp_matrix;

h11(cnt) = D(1,1);
h12(cnt) = D(1,(n+1));
h21(cnt) = D((n+1),1);
h22(cnt) = D((n+1),(n+1));

clear D;
end
```

By the Numbers 9.2

In MATLAB® MOJO 9.2, we compare h_{re} natural frequencies for fixed-free boundary conditions as we again add elements. We'll consider the first axial mode only for the same 10 mm diameter, 200 mm long steel beam with $E = 200$ GPa and $\rho = 7800$ kg/m^3. The magnitudes for n from 2 to 25 are displayed in Fig. 9.10. The variation in the first natural frequency with n is shown in Fig. 9.11. We see that the natural frequency converges to 6331 Hz. This is close to the 6330 Hz result from Eq. 9.52.

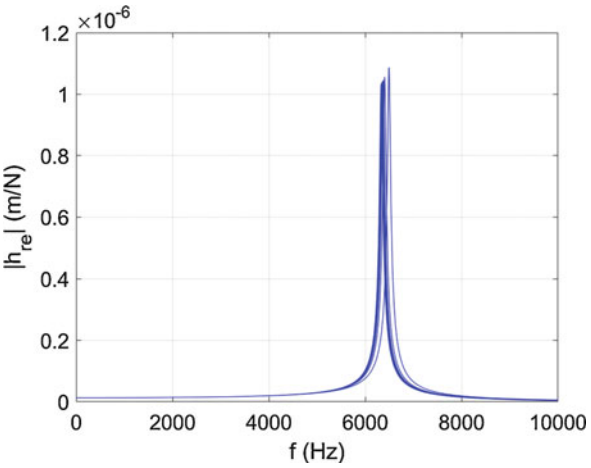

Fig. 9.10 *By the Numbers 9.2*—the fixed-free boundary condition h_{re} magnitude is plotted for the number of elements, n, from 2 to 25. The right (highest frequency) response is for $n = 2$

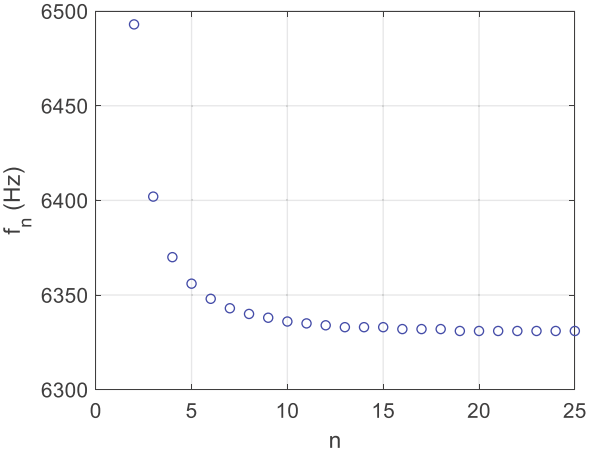

Fig. 9.11 *By the Numbers 9.2*—variation in the first natural frequency for the fixed-free boundary condition h_{re} with the number of elements in the model, n

MATLAB® MOJO 9.2

```
% matlab_mojo_9_2.m

clear
close all
clc
warning off

f = 0:10000; % Hz
E = 200e9; % Pa
eta = 0.01; % -
L = 200e-3; % m
rho = 7800; % kg/m^3
d = 10e-3; % m
```

```
A = pi*d^2/4; % m^2
maxn = 25;

% Create vector for natural frequencies
fn = zeros(1, (maxn-1));

% Calculate FRFs for two elements
n = 2;
[h11, h22, h12, h21] = axial_fixed_free(f, E, eta, L, rho, A, n);

% Plot results
figure(1)
plot(f, abs(h22), 'b')
set(gca,'FontSize', 14)
xlabel('f (Hz)')
ylabel('|h_{re}| (m/N)')
ylim([0 1.2e-6])
grid
hold on

% Identify first natural frequency for two-element solution
index = find(imag(h22) == min(imag(h22)));
fn(1) = f(index);

% Repeat for additional elements
for cnt = 3:maxn
 n = cnt;

 [h11, h22, h12, h21] = axial_fixed_free(f, E, eta, L, rho, A, n);

 figure(1)
 plot(f, abs(h22), 'b')
 index = find(imag(h22) == min(imag(h22)));
 fn(cnt-1) = f(index);
end

figure(2)
plot((2:maxn), fn, 'bo')
set(gca,'FontSize', 14)
xlabel('n')
ylabel('f_n (Hz)')
grid

fn_exact = pi/2*sqrt(E*A/(rho*A*L^2))/2/pi

% axial_fixed_free.m

% This program uses n axial beam elements to determine end receptances
for
% a fixed-free beam.
% Input variables are: f, frequency, Hz
```

```
% E, elastic modulus, N/m^2
% eta, solid damping, -
% L, beam length, m
% rho, density, kg/m^3
% A, cross sectional area, m^2
% n, number of elements

function [h11, h22, h12, h21] = axial_fixed_free(f, E, eta, L, rho, A, n)
l = L/n; % length of each finite element, m
E = E*(1 + 1i*eta); % complex modulus, N/m^2

% Matrices for single axial element
% Mass matrix
M = rho*A*l/6*[2 1;1 2];
% Stiffness matrix
K = E*A/l*[1 -1;-1 1];

Mtemp2 = M;
Ktemp2 = K;

% Build full mass and stiffness matrices
for cnt = 2:n
 % Concatenate left element matrices with required zeros
 right = zeros(cnt, 1);
 bottom = zeros(1, (cnt+1));
 % Mass matrix
 temp = cat(2, M, right);
 Mtemp1 = cat(1, temp, bottom);
 % Stiffness matrix
 temp = cat(2, K, right);
 Ktemp1 = cat(1, temp, bottom);

 % Concatenate right element matrices with required zeros
 left = zeros(cnt, 1);
 top = zeros(1, (cnt+1));
 % Mass matrix
 temp = cat(2, left, Mtemp2);
 Mtemp2 = cat(1, top, temp);
 % Stiffness matrix
 temp = cat(2, left, Ktemp2);
 Ktemp2 = cat(1, top, temp);

 % Add two matrices
 M = Mtemp1 + Mtemp2;
 K = Ktemp1 + Ktemp2;
end

% Remove first row and column from M and K matrices to convert free-free
% beam to fixed-free beam (coordinate 1 at left end is fixed)
[row, col] = size(M);
Mtemp = zeros((row -1), (col - 1));
Ktemp = Mtemp;
```

```
for cnt1 = 2:row
 for cnt2 = 2:col
 Mtemp((cnt1 - 1), (cnt2 - 1)) = M(cnt1, cnt2);
 Ktemp((cnt1 - 1), (cnt2 - 1)) = K(cnt1, cnt2);
 end
end

M = Mtemp;
K = Ktemp;
% Coordinate 1 is now the right end of the first element that attaches to
the
% fixed left end of the beam.

% Initialize receptance vectors
h11 = zeros(1,length(f));
h12 = zeros(1,length(f));
h21 = zeros(1,length(f));
h22 = zeros(1,length(f));

% Calculate required direct and cross receptances for right end of beam
(2)
% and right end of the first element that attaches to the
% fixed left end of the beam (1).
for cnt = 1:length(f)
 w = f(cnt)*2*pi; % frequency, rad/s
 temp_matrix = (-M*w^2 + K);
 D = eye(size(temp_matrix))/temp_matrix;

 h11(cnt) = D(1,1);
 h12(cnt) = D(1,n);
 h21(cnt) = D(n,1);
 h22(cnt) = D(n,n);

 clear D;
end
```

By the Numbers 9.3

In MATLAB® MOJO 9.3, we compare the 25-element free-free boundary condition h_{re} result from *By the Numbers 9.1* with the analytical solution from Sect. 8.8. The two axial FRFs are displayed in Fig. 9.12. The results are indistinguishable at this scale. The magnified version in Fig. 9.13 shows that the analytical h_{re} natural frequency is 12,659 Hz and the finite element h_{re} natural frequency is 12,667.5 Hz. The difference is −0.07%.

MATLAB® MOJO 9.3

```
% matlab_mojo_9_3.m

clear
close all
```

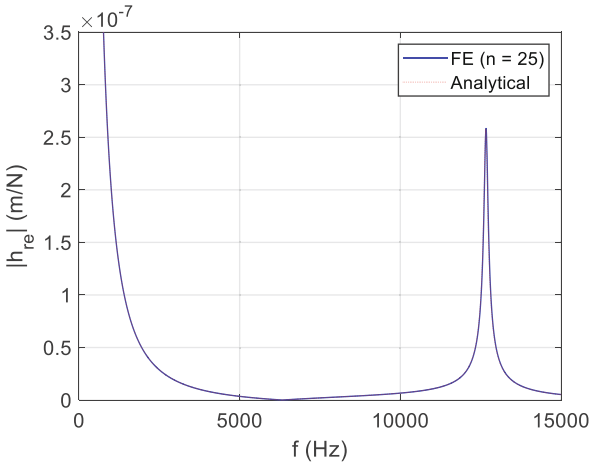

Fig. 9.12 *By the Numbers 9.3*—the free-free boundary condition h_{re} magnitude is plotted for the finite element (FE) result with $n = 25$ and the analytical result from Sect. 8.8

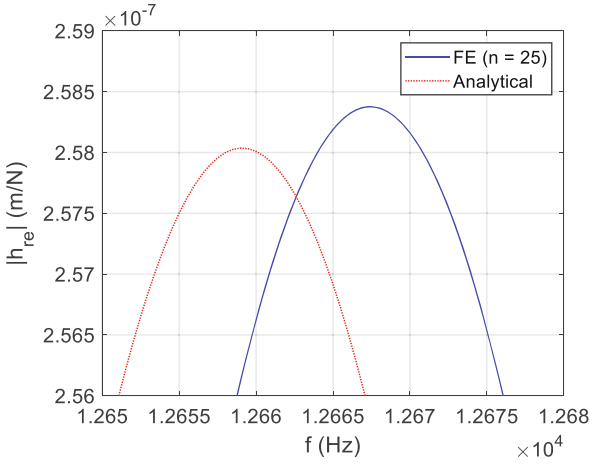

Fig. 9.13 *By the Numbers 9.3*—a magnified view of Fig. 9.12 is displayed to highlight the small difference in natural frequencies

```
clc
warning off

f = 1:0.5:15000; % Hz
E = 200e9; % Pa
eta = 0.01; % -
L = 200e-3; % m
rho = 7800; % kg/m^3
d = 10e-3; % m
A = pi*d^2/4; % m^2
maxn = 25;

% Finite element solution
% Calculate FRFs for 25 elements
```

```
n = 25;
[h11, h22, h12, h21] = axial_free_free(f, E, eta, L, rho, A, n);

% Plot results
figure(1)
plot(f, abs(h22), 'b')
set(gca,'FontSize', 14)
xlabel('f (Hz)')
ylabel('|h_{re}| (m/N)')
ylim([0 3.5e-7])
grid
hold on

% Analytical solution
omega = f*2*pi; % rad/s
E = E*(1+1i*eta); % N-m^2
lambda = omega*(rho/E)^0.5;
Gamma1_P1 = -cot(lambda*L)./(E*A*lambda);

plot(f, abs(Gamma1_P1), 'r:')
legend('FE (n = 25)', 'Analytical')

figure(2)
plot(f, abs(h22), 'b', f, abs(Gamma1_P1), 'r:')
set(gca,'FontSize', 14)
xlabel('f (Hz)')
ylabel('|h_{re}| (m/N)')
axis([12650 12680 2.56e-7 2.59e-7])
grid
legend('FE (n = 25)', 'Analytical')

% axial_free_free.m

% This function uses n axial beam elements to determine end receptances
for
% a free-free beam.
% Input variables are: f, frequency, Hz
% E, elastic modulus, N/m^2
% eta, solid damping, -
% L, beam length, m
% rho, density, kg/m^3
% A, cross sectional area, m^2
% n, number of elements

function [h11, h22, h12, h21] = axial_free_free(f, E, eta, L, rho, A, n)
l = L/n;  % length of each finite element, m
E = E*(1 + 1i*eta); % complex modulus, N/m^2

% Matrices for single axial element
% Mass matrix
M = rho*A*l/6*[2 1;1 2];
```

```
% Stiffness matrix
K = E*A/l*[1 -1;-1 1];

Mtemp2 = M;
Ktemp2 = K;

% Build full mass and stiffness matrices
for cnt = 2:n
 % Concatenate left element matrices with required zeros
 right = zeros(cnt, 1);
 bottom = zeros(1, (cnt+1));
 % Mass matrix
 temp = cat(2, M, right);
 Mtemp1 = cat(1, temp, bottom);
 % Stiffness matrix
 temp = cat(2, K, right);
 Ktemp1 = cat(1, temp, bottom);

 % Concatenate right element matrices with required zeros
 left = zeros(cnt, 1);
 top = zeros(1, (cnt+1));
 % Mass matrix
 temp = cat(2, left, Mtemp2);
 Mtemp2 = cat(1, top, temp);
 % Stiffness matrix
 temp = cat(2, left, Ktemp2);
 Ktemp2 = cat(1, top, temp);

 % Add two matrices
 M = Mtemp1 + Mtemp2;
 K = Ktemp1 + Ktemp2;
end

% Initialize receptance vectors
h11 = zeros(1,length(f));
h12 = zeros(1,length(f));
h21 = zeros(1,length(f));
h22 = zeros(1,length(f));

% Calculate required direct and cross receptances for ends of beam
for cnt = 1:length(f)
 w = f(cnt)*2*pi; % frequency, rad/s
 temp_matrix = (-M*w^2 + K);
 D = eye(size(temp_matrix))/temp_matrix;

 h11(cnt) = D(1,1);
 h12(cnt) = D(1,(n+1));
 h21(cnt) = D((n+1),1);
 h22(cnt) = D((n+1),(n+1));

 clear D;
end
```

In a Nutshell
It is generally not good practice to make just one finite element model and then stop. Although we are often happy that we made a model with no software errors and that we got a result that seems to make sense, that is not enough. It is important to check whether the model is sufficiently accurate enough, so checking the convergence is important.

9.3 Transverse Element

In this section we consider transverse vibration of a beam element. We'll no longer consider axial forces, but will now include lateral forces and bending moments at both ends. See Fig. 9.14, where we have two coordinates, one each for displacement, y, and rotation, θ, at both ends for a total of four coordinates that define the transverse beam element behavior. The forces, f, and moments, m, are also identified. Note that this model only considers the forces and moments in a single plane. If we return to Eq. 8.1 from Euler-Bernoulli beam theory (reproduced here as Eq. 9.58 for convenience), we see that integrating three times gives the cubic polynomial function, y, in Eq. 9.59 that describes the transverse deflection.

$$\frac{q}{EI} = \frac{d^4y}{dx^4} \tag{9.58}$$

$$y = C_1x^3 + C_2x^2 + C_3x + C_4 \tag{9.59}$$

The corresponding rotation function is:

$$\frac{dy}{dx} = \theta = 3C_1x^2 + 2C_2x + C_3. \tag{9.60}$$

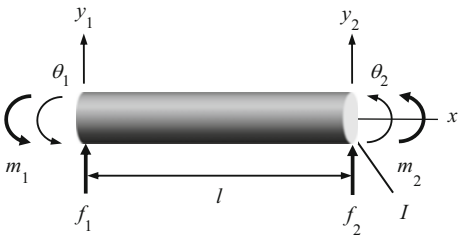

Fig. 9.14 Transverse element with length, l, and cross-sectional second moment of area, I. The lateral forces, f, and moments, m, cause transverse deflection, y, and rotation, θ. The circular cross-section is for demonstration purposes only; any shape is acceptable

To find C_i, $i = 1$ to 4, we apply generic boundary conditions at both ends (tips) of the beam; see Eqs. 9.61–9.64. These represent the unknown displacements and rotations displayed in Fig. 9.13.

$$y|_{x=0} = y_1 \tag{9.61}$$

$$\left.\frac{dy}{dx}\right|_{x=0} = \theta_1 \tag{9.62}$$

$$y|_{x=l} = y_2 \tag{9.63}$$

$$\left.\frac{dy}{dx}\right|_{x=l} = \theta_2 \tag{9.64}$$

Applying these boundary conditions, we obtain:

$$y|_{x=0} = C_1 \cdot 0 + C_2 \cdot 0 + C_3 \cdot 0 + C_4 = y_1 \tag{9.65}$$

$$\left.\frac{dy}{dx}\right|_{x=0} = 3C_1 \cdot 0 + 2C_2 \cdot 0 + C_3 = \theta_1 \tag{9.66}$$

$$y|_{x=l} = C_1 l^3 + C_2 l^2 + C_3 l + C_4 = y_2 \tag{9.67}$$

$$\left.\frac{dy}{dx}\right|_{x=l} = 3C_1 l^2 + 2C_2 l + C_3 = \theta_2 \tag{9.68}$$

From Eqs. 9.65 and 9.66, we determine C_4 and C_3.

$$C_4 = y_1 \tag{9.69}$$

$$C_3 = \theta_1 \tag{9.70}$$

Substituting in Eq. 9.67 gives:

$$y|_{x=l} = C_1 l^3 + C_2 l^2 + \theta_1 l + y_1 = y_2. \tag{9.71}$$

Substituting in Eq. 9.68 gives:

$$\left.\frac{dy}{dx}\right|_{x=l} = 3C_1 l^2 + 2C_2 l + \theta_1 = \theta_2. \tag{9.72}$$

Let's consider Eqs. 9.71 and 9.72 together and rearrange them to isolate the unknowns on the left hand side.

$$C_1 l^3 + C_2 l^2 = -y_1 - \theta_1 l + y_2 \tag{9.73}$$

$$3C_1 l^2 + 2C_2 l = -\theta_1 + \theta_2 \tag{9.74}$$

Solving Eq. 9.74 for C_1, we obtain:

$$C_1 = \frac{-\theta_1 + \theta_2 - 2C_2 l}{3l^2}. \tag{9.75}$$

Substituting for C_1 in Eq. 9.73 gives:

$$\frac{-\theta_1 + \theta_2 - 2C_2 l}{3l^2} l^3 + C_2 l^2 = -y_1 - \theta_1 l + y_2. \tag{9.76}$$

Solving Eq. 9.76 for C_2 (after a bit of algebra) yields:

$$C_2 = -\frac{3}{l^2}(y_1 - y_2) - \frac{1}{l}(2\theta_1 + \theta_2). \tag{9.77}$$

We substitute this result into Eq. 9.75 to determine C_1 (again, after algebraic manipulations).

$$C_1 = \frac{2}{l^3}(y_1 - y_2) + \frac{1}{l^2}(\theta_1 + \theta_2) \tag{9.78}$$

We now substitute Eqs. 9.69, 9.70, 9.77, and 9.78 in Eq. 9.59 to find y, the beam's lateral deflection at any location, x, given the four generic boundary conditions.

$$y = \left(\frac{2}{l^3}(y_1 - y_2) + \frac{1}{l^2}(\theta_1 + \theta_2)\right)x^3 + \left(-\frac{3}{l^2}(y_1 - y_2) - \frac{1}{l}(2\theta_1 + \theta_2)\right)x^2 + \theta_1 x + y_1 \tag{9.79}$$

We next organize Eq. 9.79 to write it in terms of the four boundary conditions. The cubic polynomial multipliers on y_i and θ_i, $i = 1, 2$ in Eq. 9.80 are referred to as the **interpolation (or shape) functions** for the transverse beam element [1].

$$y = \frac{1}{l^3}\left(2x^3 - 3x^2 l + l^3\right)y_1 + \frac{1}{l^3}\left(x^3 l - 2x^2 l^2 + x l^3\right)\theta_1 + \frac{1}{l^3}\left(-2x^3 + 3x^2 l\right)y_2 + \frac{1}{l^3}\left(x^3 l - x^2 l^2\right)\theta_2 \tag{9.80}$$

In a Nutshell

Interestingly, other shape functions will also work. These shape functions make sense when we think of the element as a beam, but we could, of course, imagine other shapes. Finite element software contains many choices for element shapes and similar derivations were made for them to create the associated mass and stiffness matrices.

Using Euler-Bernoulli beam theory (Sect. 8.1), we relate the transverse displacement, y, to the shear (transverse) forces and bending moments using Eqs. 9.81–9.84 and Fig. 9.13.

$$f_1 = V = EI\frac{d^3y}{dx^3}\bigg|_{x=0} \tag{9.81}$$

$$f_2 = -V = -EI\frac{d^3y}{dx^3}\bigg|_{x=l} \tag{9.82}$$

$$m_1 = -M = -EI\frac{d^2y}{dx^2}\bigg|_{x=0} \tag{9.83}$$

$$m_2 = M = EI\frac{d^2y}{dx^2}\bigg|_{x=l} \tag{9.84}$$

For Eqs. 9.81–9.84, we've used the standard sign convention for V and M provided in Fig. 8.4. Let's now calculate the required derivatives.

$$\frac{dy}{dx} = \frac{1}{l^3}\left(6x^2 - 6xl\right)y_1 + \frac{1}{l^3}\left(3x^2 l - 4xl^2 + l^3\right)\theta_1 + \frac{1}{l^3}\left(-6x^2 + 6xl\right)y_2 + \frac{1}{l^3} \times \left(3x^2 l - 2xl^2\right)\theta_2 \tag{9.85}$$

$$\frac{d^2y}{dx^2} = \frac{1}{l^3}(12x - 6l)y_1 + \frac{1}{l^3}\left(6xl - 4l^2\right)\theta_1 + \frac{1}{l^3}(-12x + 6l)y_2 + \frac{1}{l^3} \times \left(6xl - 2l^2\right)\theta_2 \tag{9.86}$$

$$\frac{d^3y}{dx^3} = \frac{1}{l^3}(12)y_1 + \frac{1}{l^3}(6l)\theta_1 + \frac{1}{l^3}(-12)y_2 + \frac{1}{l^3}(6l)\theta_2 \tag{9.87}$$

Substituting Eq. 9.87 in Eq. 9.81 provides the relationship between f_1 and the beam end displacements and rotations.

$$f_1 = \frac{EI}{l^3}(12y_1 + 6l\theta_1 - 12y_2 + 6l\theta_2) \tag{9.88}$$

Similarly, we find f_2 by substituting Eq. 9.87 in Eq. 9.82.

$$f_2 = \frac{EI}{l^3}(-12y_1 - 6l\theta_1 + 12y_2 - 6l\theta_2) \tag{9.89}$$

We determine m_1 by substituting Eq. 9.86 in Eq. 9.83 and setting $x = 0$.

$$\begin{aligned} m_1 &= -\frac{EI}{l^3} \\ &\quad \times \left((12 \cdot 0 - 6l)y_1 + \left(6 \cdot 0 \cdot l - 4l^2\right)\theta_1 + (-12 \cdot 0 + 6l)y_2 + \left(6 \cdot 0 \cdot l - 2l^2\right)\theta_2\right) \\ &= -\frac{EI}{l^3}\left(-6ly_1 - 4l^2\theta_1 + 6ly_2 - 2l^2\theta_2\right) \end{aligned} \tag{9.90}$$

Finally, we obtain m_2 by substituting Eq. 9.86 in Eq. 9.84 and setting $x = l$.

$$\begin{aligned} m_2 &= \frac{EI}{l^3}\left((12l - 6l)y_1 + \left(6l^2 - 4l^2\right)\theta_1 + (-12l + 6l)y_2 + \left(6l^2 - 2l^2\right)\theta_2\right) \\ &= \frac{EI}{l^3}\left(6ly_1 + 2l^2\theta_1 - 6ly_2 + 4l^2\theta_2\right) \end{aligned} \tag{9.91}$$

We now combine Eqs. 9.88–9.91 in matrix form to obtain the transverse beam element 4×4 **stiffness matrix**.

$$\begin{Bmatrix} f_1 \\ f_2 \\ m_1 \\ m_2 \end{Bmatrix} = \frac{EI}{l^3}\begin{bmatrix} 12 & 6l & -12 & 6l \\ 6l & 4l^2 & -6l & 2l^2 \\ -12 & -6l & 12 & -6l \\ 6l & 2l^2 & -6l & 4l^2 \end{bmatrix}\begin{Bmatrix} y_1 \\ \theta_1 \\ y_2 \\ \theta_2 \end{Bmatrix} \tag{9.92}$$

Specifically, the stiffness matrix is:

$$K = \frac{EI}{l^3}\begin{bmatrix} 12 & 6l & -12 & 6l \\ 6l & 4l^2 & -6l & 2l^2 \\ -12 & -6l & 12 & -6l \\ 6l & 2l^2 & -6l & 4l^2 \end{bmatrix}. \tag{9.93}$$

In a Nutshell
Some of the elements in the stiffness matrix relate forces to linear displacements, some relate moments to rotational displacements, and some cross between linear and rotational coordinates.

We note, once again, that the stiffness matrix is symmetric (i.e., $k_{ij} = k_{ji}$, $i, j = 1$ to 4, $i \neq j$). To calculate the corresponding **mass matrix**, we return to Eq. 9.17 and replace $\dot{\gamma}$ with $\dot{y} = \frac{dy}{dt}$. We begin by calculating the time derivative of Eq. 9.80.

$$\dot{y} = \frac{1}{l^3}\left(2x^3 - 3x^2 l + l^3\right)\dot{y}_1 + \frac{1}{l^3}\left(x^3 l - 2x^2 l^2 + x l^3\right)\dot{\theta}_1 + \frac{1}{l^3}\left(-2x^3 + 3x^2 l\right)\dot{y}_2 + \frac{1}{l^3}\left(x^3 l - x^2 l^2\right)\dot{\theta}_2 \tag{9.94}$$

For Eq. 9.17, we require $\dot{y}^2$ so let's calculate it next. After simplification, we obtain Eq. 9.95.

$$\begin{aligned} \dot{y}^2 = \frac{1}{l^6}\big[&\left(4x^6 - 12x^5 l + 9x^4 l^2 + 4x^3 l^3 - 6x^2 l^4 + l^6\right)\dot{y}_1{}^2 + \left(x^6 l^2 - 4x^5 l^3\right. \\ &+6x^4 l^4 - 4x^3 l^5 + x^2 l^6)\dot{\theta}_1{}^2 + \left(4x^6 - 12x^5 l + 9x^4 l^2\right)\dot{y}_2{}^2 \\ &+ \left(x^6 l^2 - 2x^5 l^3 + x^4 l^4\right)\dot{\theta}_2{}^2 \\ &+ \left(4x^6 l - 14x^5 l^2 + 16x^4 l^3 - 4x^3 l^4 - 4x^2 l^5 + 2x l^6\right)\dot{y}_1\dot{\theta}_1 \\ &+ \left(-8x^6 + 24x^5 l - 18x^4 l^2 - 4x^3 l^3 + 6x^2 l^4\right)\dot{y}_1\dot{y}_2 \\ &+ \left(4x^6 l - 10x^5 l^2 + 6x^4 l^3 + 2x^3 l^4 - 2x^2 l^5\right)\dot{y}_1\dot{\theta}_2 \\ &+ \left(-4x^6 l + 14x^5 l^2 - 16x^4 l^3 + 6x^3 l^4\right)\dot{y}_2\dot{\theta}_1 \\ &+ \left(-4x^6 l + 10x^5 l^2 - 6x^4 l^3\right)\dot{y}_2\dot{\theta}_2 \\ &+ \left(2x^6 l^2 - 6x^5 l^3 + 6x^4 l^4 - 2x^3 l^5\right)\dot{\theta}_1\dot{\theta}_2\big] \end{aligned} \tag{9.95}$$

We now integrate Eq. 9.95 over the element length, l, to enable substitution in the Eq. 9.17 kinetic energy expression.

$$\int_0^l \dot{y}^2 dx = \frac{1}{l^6}\left[\left(\frac{4}{7}x^7 - \frac{12}{6}x^6 l + \frac{9}{5}x^5 l^2 + \frac{4}{4}x^4 l^3 - \frac{6}{3}x^3 l^4 + x l^6\right)\dot{y}_1{}^2\right.$$
$$+\left(\frac{1}{7}x^7 l^2 - \frac{4}{6}x^6 l^3 + \frac{6}{5}x^5 l^4 - \frac{4}{4}x^4 l^5 + \frac{1}{3}x^3 l^6\right)\dot{\theta}_1{}^2$$
$$+\left(\frac{4}{7}x^7 - \frac{12}{6}x^6 l + \frac{9}{5}x^5 l^2\right)\dot{y}_2{}^2 + \left(\frac{1}{7}x^7 l^2 - \frac{2}{6}x^6 l^3 + \frac{1}{5}x^5 l^4\right)\dot{\theta}_2{}^2$$
$$+\left(\frac{4}{7}x^7 l - \frac{14}{6}x^6 l^2 + \frac{16}{5}x^5 l^3 - \frac{4}{4}x^4 l^4 - \frac{4}{3}x^3 l^5 + \frac{2}{2}x^2 l^6\right)\dot{y}_1\dot{\theta}_1$$
$$+\left(-\frac{8}{7}x^7 + \frac{24}{6}x^6 l - \frac{18}{5}x^5 l^2 - \frac{4}{4}x^4 l^3 + \frac{6}{3}x^3 l^4\right)\dot{y}_1\dot{y}_2$$
$$+\left(\frac{4}{7}x^7 l - \frac{10}{6}x^6 l^2 + \frac{6}{5}x^5 l^3 + \frac{2}{4}x^4 l^4 - \frac{2}{3}x^3 l^5\right)\dot{y}_1\dot{\theta}_2$$
$$+\left(-\frac{4}{7}x^7 l + \frac{14}{6}x^6 l^2 - \frac{16}{5}x^5 l^3 + \frac{6}{4}x^4 l^4\right)\dot{y}_2\dot{\theta}_1$$
$$+\left(-\frac{4}{7}x^7 l + \frac{10}{6}x^6 l^2 - \frac{6}{5}x^5 l^3\right)\dot{y}_2\dot{\theta}_2$$
$$\left.+\left(\frac{2}{7}x^7 l^2 - \frac{6}{6}x^6 l^3 + \frac{6}{5}x^5 l^4 - \frac{2}{4}x^4 l^5\right)\dot{\theta}_1\dot{\theta}_2\right]_0^l \tag{9.96}$$

After evaluating over the integration limits and combining terms, we obtain Eq. 9.97.

$$\int_0^l \dot{y}^2 dx = \frac{1}{l^6}\left[\left(\frac{78}{210}l^7\right)\dot{y}_1{}^2 + \left(\frac{1}{105}l^9\right)\dot{\theta}_1{}^2 + \left(\frac{13}{35}l^7\right)\dot{y}_2{}^2 + \left(\frac{1}{105}l^9\right)\dot{\theta}_2{}^2 + \left(\frac{11}{105}l^8\right)\dot{y}_1\dot{\theta}_1\right.$$
$$+\left(\frac{9}{35}l^7\right)\dot{y}_1\dot{y}_2 + \left(\frac{-13}{210}l^8\right)\dot{y}_1\dot{\theta}_2 + \left(\frac{13}{210}l^8\right)\dot{y}_2\dot{\theta}_1 + \left(\frac{-11}{105}l^8\right)\dot{y}_2\dot{\theta}_2$$
$$\left.+\left(\frac{-1}{70}l^9\right)\dot{\theta}_1\dot{\theta}_2\right] \tag{9.97}$$

We next calculate the kinetic energy for the transverse vibration beam element.

$$KE = \frac{1}{2}\frac{m}{l}\int_0^l \dot{y}^2 dx = \frac{m}{420}\left[78\dot{y}_1{}^2 + 2l^2\dot{\theta}_1{}^2 + 78\dot{y}_2{}^2 + 2l^2\dot{\theta}_2{}^2 + 22l\dot{y}_1\dot{\theta}_1 + 54\dot{y}_1\dot{y}_2\right.$$
$$\left.-13l\dot{y}_1\dot{\theta}_2 + 13l\dot{y}_2\dot{\theta}_1 - 22l\dot{y}_2\dot{\theta}_2 - 3l^2\dot{\theta}_1\dot{\theta}_2\right] \tag{9.98}$$

We are now (finally) ready to calculate the mass matrix that relates the forces and moments to linear and rotational accelerations for the transverse vibration beam element.

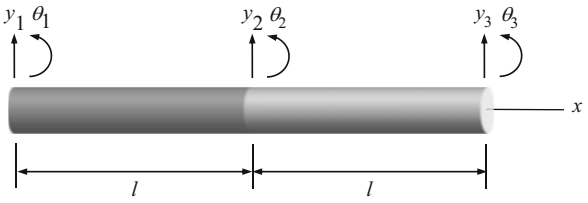

Fig. 9.15 Beam model with two transverse elements. The overall beam length is $2l$, so the two identical elements each have a length l. The model has six total coordinates

$$\begin{Bmatrix} f_1 \\ f_2 \\ m_1 \\ m_2 \end{Bmatrix} = \begin{bmatrix} m_{11} & m_{12} & m_{13} & m_{14} \\ m_{21} & m_{22} & m_{23} & m_{24} \\ m_{31} & m_{32} & m_{33} & m_{34} \\ m_{41} & m_{42} & m_{43} & m_{44} \end{bmatrix} \begin{Bmatrix} \ddot{y}_1 \\ \ddot{\theta}_1 \\ \ddot{y}_2 \\ \ddot{\theta}_2 \end{Bmatrix} \tag{9.99}$$

We determine the first row in the mass matrix using the Euler-Lagrange equation (Eq. 9.17) together with Eq. 9.98.

$$\begin{aligned} f_1 &= \frac{d}{dt}\frac{\partial KE}{\partial \dot{y}_1} = \frac{d}{dt}\frac{m}{420}\left[2 \cdot 78\dot{y}_1 + 22l\dot{\theta}_1 + 54\dot{y}_2 - 13l\dot{\theta}_2\right] \\ &= \frac{m}{420}\left[156\ddot{y}_1 + 22l\ddot{\theta}_1 + 54\ddot{y}_2 - 13l\ddot{\theta}_2\right] \end{aligned} \tag{9.100}$$

By repeating this step for f_2, m_1, and m_2, we obtain the remaining three rows of the 4×4 mass matrix, M, where we've substituted ρAl for the element mass, m, in Eq. 9.101. Because this matrix is based on the same displacement function (Eq. 9.80) used for the stiffness matrix, it is referred to as the **consistent mass matrix** [2, 3].

$$M = \frac{\rho Al}{420}\begin{bmatrix} 156 & 22l & 54 & -13l \\ 22l & 4l^2 & 13l & -3l^2 \\ 54 & 13l & 156 & -22l \\ -13l & -3l^2 & -22l & 4l^2 \end{bmatrix} \tag{9.101}$$

In a Nutshell
The math is more complicated, but the transverse element mass matrix calculation is the same, in principle, as the axial element derivation.

Let's now consider two elements for a single beam model; see Fig. 9.15. The two-element beam has six degrees of freedom, y_1, θ_1, y_2, θ_2, y_3, and θ_3. The corresponding forces and moments are: f_1, m_1, f_2, m_2, f_3, and m_3. The overlap for the two elements in the model stiffness matrix is presented in Eq. 9.102. The mass matrix is provided in Eq. 9.103. In both cases, we see that the upper left 4×4 portion

of the 6 × 6 matrix belongs to the left element and the lower right 4 × 4 portion belongs to the (identical) right element. They overlap in the central 2 × 2 portion where the sums appear. The superposition also gives a 2 × 2 matrix of zeros at the upper right and lower left corners. The equation of motion is shown in Eq. 9.104.

$$K = \frac{EI}{l^3}\begin{bmatrix} 12 & 4l & -12 & 6l & 0 & 0 \\ 6l & 4l^2 & -6l & 2l^2 & 0 & 0 \\ -12 & -6l & 12+12 & -6l+4l & -12 & 6l \\ 6l & 2l^2 & -6l+6l & 4l^2+4l^2 & -6l & 2l^2 \\ 0 & 0 & -12 & -6l & 12 & -6l \\ 0 & 0 & 6l & 2l^2 & -6l & 4l^2 \end{bmatrix} \tag{9.102}$$

$$M = \frac{\rho Al}{420} \times \begin{bmatrix} 156 & 22l & 54 & -13l & 0 & 0 \\ 22l & 4l^2 & 13l & -3l^2 & 0 & 0 \\ 54 & 13l & 156+156 & -22l+22l & 54 & -13l \\ -13l & -3l^2 & -22l+22l & 4l^2+4l^2 & 13l & -3l^2 \\ 0 & 0 & 54 & -6l+13l & 156 & -22l \\ 0 & 0 & -13l & 2l^2-3l^2 & -22l & 4l^2 \end{bmatrix} \tag{9.103}$$

Table 9.1 Beam end FRFs for two-element transverse vibration model

	Left end			Right end	
Direct	$h_{11} = \frac{y_1}{f_1}$	$h_{12} = \frac{\theta_1}{f_1}$	Cross	$h_{15} = \frac{y_3}{f_1}$	$h_{16} = \frac{\theta_3}{f_1}$
	$h_{21} = \frac{y_1}{m_1}$	$h_{22} = \frac{\theta_1}{m_1}$		$h_{25} = \frac{y_3}{m_1}$	$h_{26} = \frac{\theta_3}{m_1}$
Cross	$h_{51} = \frac{y_1}{f_3}$	$h_{52} = \frac{\theta_1}{f_3}$	Direct	$h_{55} = \frac{y_3}{f_3}$	$h_{56} = \frac{\theta_3}{f_3}$
	$h_{61} = \frac{y_1}{m_3}$	$h_{62} = \frac{\theta_1}{m_3}$		$h_{65} = \frac{y_3}{m_3}$	$h_{66} = \frac{\theta_3}{m_3}$

$$\frac{\rho Al}{420}\begin{bmatrix} 156 & 22l & 54 & -13l & 0 & 0 \\ 22l & 4l^2 & 13l & -3l^2 & 0 & 0 \\ 54 & 13l & 156+156 & -22l+22l & 54 & -13l \\ -13l & -3l^2 & -22l+22l & 4l^2+4l^2 & 13l & -3l^2 \\ 0 & 0 & 54 & -6l+13l & 156 & -22l \\ 0 & 0 & -13l & 2l^2-3l^2 & -22l & 4l^2 \end{bmatrix}\begin{Bmatrix} \ddot{y}_1 \\ \ddot{\theta}_1 \\ \ddot{y}_2 \\ \ddot{\theta}_2 \\ \ddot{y}_3 \\ \ddot{\theta}_3 \end{Bmatrix}+$$

$$\frac{EI}{l^3}\begin{bmatrix} 12 & 4l & -12 & 6l & 0 & 0 \\ 6l & 4l^2 & -6l & 2l^2 & 0 & 0 \\ -12 & -6l & 12+12 & -6l+4l & -12 & 6l \\ 6l & 2l^2 & -6l+6l & 4l^2+4l^2 & -6l & 2l^2 \\ 0 & 0 & -12 & -6l & 12 & -6l \\ 0 & 0 & 6l & 2l^2 & -6l & 4l^2 \end{bmatrix}\begin{Bmatrix} y_1 \\ \theta_1 \\ y_2 \\ \theta_2 \\ y_3 \\ \theta_3 \end{Bmatrix} = \begin{Bmatrix} f_1 \\ m_1 \\ f_2 \\ m_2 \\ f_3 \\ m_3 \end{Bmatrix} \tag{9.104}$$

As we explored in Sect. 9.2, we increase the model accuracy as we increase the number of elements. For n elements, the number of degrees of freedom for the transverse beam model is $(2n + 2)$ and the size of the full mass and stiffness matrices is $(2n + 2) \times (2n + 2)$. Note that the mass and stiffness matrices are always square and symmetric.

In the same way as the axial element, we determine the beam FRFs, $h_{ij}(\omega)$, using the **dynamic matrix**, $[D] = [-[M]\omega^2 + [K]]$. For the two-element example, the inverted 6×6 dynamic matrix is presented in Eq. 9.105. Note that each entry in this matrix is a different FRF; it may be helpful to think of the Eq. 9.105 matrix as a book where only the top page is seen (for the lowest frequency). Higher frequencies are given by the additional book pages, one frequency per page from lowest to highest as you flip from front to back.

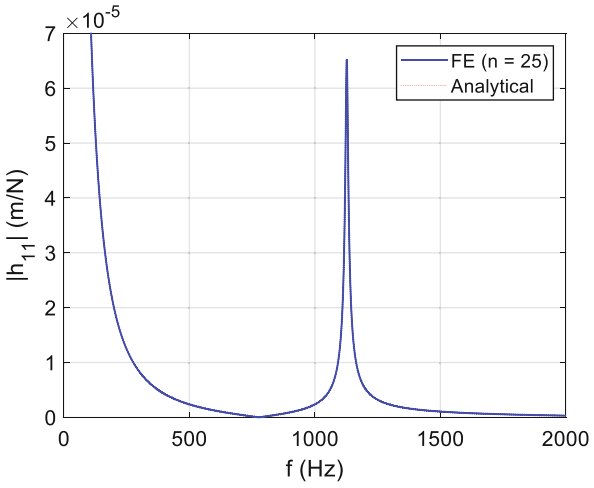

Fig. 9.16 *By the Numbers 9.4*—the free-free boundary condition $h_{11} = \frac{y_1}{f_1}$ magnitude is plotted for the finite element (FE) result with $n = 25$ and the analytical result from Sect. 8.5

$$[D]^{-1} = \left[-[M]\omega^2 + [K]\right]^{-1}$$

$$= \begin{bmatrix} h_{11} & h_{12} & h_{13} & h_{14} & h_{15} & h_{16} \\ h_{21} & h_{22} & h_{23} & h_{24} & h_{25} & h_{26} \\ h_{31} & h_{32} & h_{33} & h_{34} & h_{35} & h_{36} \\ h_{41} & h_{42} & h_{43} & h_{44} & h_{45} & h_{46} \\ h_{51} & h_{52} & h_{53} & h_{54} & h_{55} & h_{56} \\ h_{61} & h_{62} & h_{63} & h_{64} & h_{65} & h_{66} \end{bmatrix} \tag{9.105}$$

In Eq. 9.105, The corner 2×2 entries provide the beam end FRFs. These are explicitly identified in Table 9.1, where we have both translational and rotational FRFs.

By the Numbers 9.4

In MATLAB® MOJO 9.4, we calculate the 25-element free-free boundary condition left end FRF, $h_{11} = \frac{y_1}{f_1}$, for a 10 mm diameter, 200 mm long steel beam with $E = 200$ GPa and $\rho = 7800$ kg/m^3. The FRF magnitude for the finite element model ($n = 25$) is compared to the analytical solution from Sect. 8.5 (Table 8.3) in Fig. 9.16. The results are identical. Note that the large response at small frequencies is due to the free-free boundary conditions and the associated rigid body modes (i.e., linear translation and rotation about the center of mass, no oscillation) and that we've incorporated damping using the complex modulus as described in Sect. 8.4.

MATLAB® MOJO 9.4

```
% matlab_mojo_9_4.m

clear
close all
clc
warning off

f = 1:0.1:2000; % Hz
E = 200e9; % Pa
eta = 0.01; % -
L = 200e-3; % m
rho = 7800; % kg/m^3
d = 10e-3; % m
I = pi*d^4/64; % m^4
A = pi*d^2/4; % m^2

% Finite element solution
% Calculate FRFs for 25 elements
n = 25;
[h11, l11, n11, p11, h22, l22, n22, p22, h12, l12, n12, p12, h21, l21, n21,
p21] = transverse_free_free(f, E, I, eta, L, rho, A, n);

% Plot results
figure(1)
plot(f, abs(h11), 'b')
set(gca,'FontSize', 14)
xlabel('f (Hz)')
ylabel('|h_{11}| (m/N)')
ylim([0 7e-5])
grid
hold on

% Analytical solution
omega = f*2*pi; % rad/s
E = E*(1+1i*eta); % N-m^2
EI = E*I;
lambda = (omega.^2*rho*A/EI).^0.25;
h11 = -(cos(lambda*L).*sinh(lambda*L) - sin(lambda*L).*cosh
(lambda*L))./(lambda.^3.*(EI*(cos(lambda*L).*cosh(lambda*L)-1)));

plot(f, abs(h11), 'r:')
legend('FE (n = 25)', 'Analytical')

% transverse_free_free.m

% This function uses n transverse beam elements to determine end FRFs for
% a free-free beam.
% Input variables are: f, frequency, Hz
% E, elastic modulus, N/m^2
```

```
% I, second moment of area, m^4
% eta, solid damping, -
% L, beam length, m
% rho, density, kg/m^3
% A, cross sectional area, m^2
% n, number of elements

function [h11, l11, n11, p11, h22, l22, n22, p22, h12, l12, n12, p12, h21,
l21, n21, p21] = transverse_free_free(f, E, I, eta, L, rho, A, n)
l = L/n; % length of each, m
E = E*(1 + 1i*eta); % complex modulus, N/m^2
EI = E*I;

% Single element matrices for beam with transverse bending
% Mass matrix
M = rho*A*l/420*[156 22*l 54 -13*l; 22*l 4*l^2 13*l -3*l^2; 54 13*l
156 -22*l; -13*l -3*l^2 -22*l 4*l^2];

% Stiffness matrix
K = EI/(l^3)*[12 6*l -12 6*l; 6*l 4*l^2 -6*l 2*l^2; -12 -6*l 12 -6*l; 6*l
2*l^2 -6*l 4*l^2];

Mtemp2 = M;
Ktemp2 = K;

% Build full mass and stiffness matrices
for cnt = 2:n
 % Concatenate left element matrices with required zeros
 right = zeros(cnt*2, 2);
 bottom = zeros(2, (cnt+1)*2);
 % Mass matrix
 temp = cat(2, M, right);
 Mtemp1 = cat(1, temp, bottom);
 % Stiffness matrix
 temp = cat(2, K, right);
 Ktemp1 = cat(1, temp, bottom);

 % Concatenate right element matrices with required zeros
 left = zeros(cnt*2, 2);
 top = zeros(2, (cnt+1)*2);
 % Mass matrix
 temp = cat(2, left, Mtemp2);
 Mtemp2 = cat(1, top, temp);
 % Stiffness matrix
 temp = cat(2, left, Ktemp2);
 Ktemp2 = cat(1, top, temp);

 % Add two matrices
 M = Mtemp1 + Mtemp2;
 K = Ktemp1 + Ktemp2;
end
```

```
% Initialize FRF vectors
h11 = zeros(1,length(f));
l11 = zeros(1,length(f));
n11 = zeros(1,length(f));
p11 = zeros(1,length(f));
h12 = zeros(1,length(f));
l12 = zeros(1,length(f));
n12 = zeros(1,length(f));
p12 = zeros(1,length(f));
h21 = zeros(1,length(f));
l21 = zeros(1,length(f));
n21 = zeros(1,length(f));
p21 = zeros(1,length(f));
h22 = zeros(1,length(f));
l22 = zeros(1,length(f));
n22 = zeros(1,length(f));
p22 = zeros(1,length(f));

% Calculate required direct and cross FRFs for beam ends
for cnt = 1:length(f)
 w = f(cnt)*2*pi; % frequency, rad/s
 temp_matrix = (-M*w^2 + K);
 D = eye(size(temp_matrix))/temp_matrix; % dynamic matrix

 h11(cnt) = D(1,1);
 l11(cnt) = -D(1,2);
 n11(cnt) = -D(2,1);
 p11(cnt) = D(2,2);

 h12(cnt) = D(1,2*(n+1)-1);
 l12(cnt) = -D(1,2*(n+1));
 n12(cnt) = -D(2,2*(n+1)-1);
 p12(cnt) = D(2,2*(n+1));

 h21(cnt) = D(2*(n+1)-1,1);
 l21(cnt) = -D(2*(n+1)-1,2);
 n21(cnt) = -D(2*(n+1),1);
 p21(cnt) = D(2*(n+1),2);

 h22(cnt) = D(2*(n+1)-1,2*(n+1)-1);
 l22(cnt) = -D(2*(n+1)-1,2*(n+1));
 n22(cnt) = -D(2*(n+1),2*(n+1)-1);
 p22(cnt) = D(2*(n+1),2*(n+1));

 clear D;
end
```

In a Nutshell
From this point on, finite element analysis is primarily bookkeeping. When restricted to a plane, each beam-type element has six degrees of freedom (a transverse displacement, an axial displacement, and a rotation in the plane, at each of its two ends). The mass and stiffness matrices are assembled by superimposing and adding terms at rigid connections of coordinates. Extending this into three-dimensional space adds more coordinates, so that a beam-type element would have 12 coordinates (degrees of freedom) with three translations and three rotations at each end. Conceptually, it is not more difficult to understand, but we have to rely on software to help us keep track of the numbering, assembly, boundary conditions, and so on. In addition, consideration of symmetry and implementation of efficient numbering strategies can reduce the computational burden; this is important considerations as the size of the model grows (i.e., the number of elements increases).

Chapter Summary
- In finite element analysis, the model geometry is discretized into small elements.
- The mass and stiffness matrices for the elements are defined and assembled to provide a numerical solution for the dynamic behavior of the entire model.
- An axial element was defined to describe axial deflections of a beam.
- A transverse element was defined to describe transverse deflections and bending rotations of a beam.
- Both elements have corresponding stiffness and mass matrices.
- As additional elements are added, the stiffness and mass matrices are combined to obtain full model matrices.
- These matrices are used to define the corresponding differential equations of motion and numerically solved to obtain the model frequency response functions.

Exercises

1. Consider a cylindrical rod with a diameter of 10 mm and a length of 100 mm. One is end is fixed and the other is free. A 500 N axial load is applied at the free end. See Fig. P9.1. Determine the aluminum rod's change in length (μm) if its elastic modulus is 70 GPa.
2. Populate the 2×2 stiffness matrix for the axial element that represents a cylindrical aluminum rod with a diameter of 10 mm, length of 100 mm, and elastic modulus of 70 GPa. Substitute the numerical stiffness values (N/m).
3. Populate the 2×2 mass matrix for the axial element that represents a cylindrical aluminum rod with a diameter of 10 mm, length of 100 mm, and density of 2700 kg/m^3. Substitute the numerical mass values (kg).

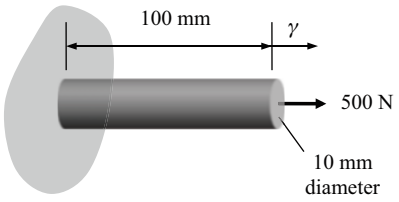

Fig. P9.1 Aluminum rod with 500 N axial force

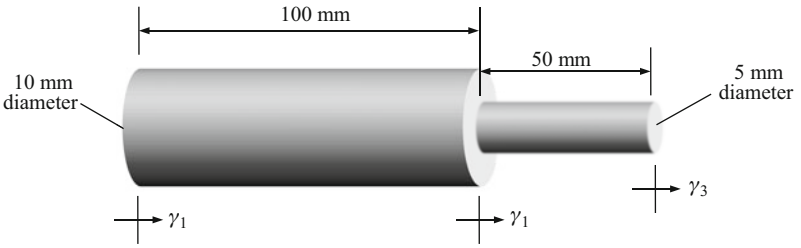

Fig. P9.2 Two cylindrical rods joined end-to-end

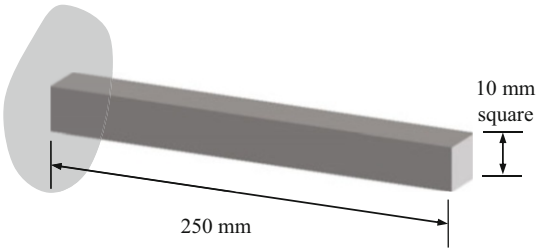

Fig. P9.3 Square cross-section steel beam with fixed-free boundary conditions

4. Let a first cylindrical rod with a diameter of 10 mm and a length of 100 mm be joined end-to-end to a second cylindrical rod with a diameter of 5 mm and a length of 50 mm. See Fig. P9.2. If the elastic modulus is 70 GPa and the density is 2700 kg/m^3 for both aluminum rods, write the 3 $\times$ 3 stiffness matrix (N/m).
5. Determine the first axial natural frequency for the fixed-free steel beam shown in Fig. P9.3. The elastic modulus is 205 GPa and the density is 7800 kg/m^3. Use 20 elements for the finite element model.
6. Plot the four interpolation (or shape) functions from Eq. 9.80. For the horizontal axis, use $\frac{x}{l}$ with limits from 0 to 1. For the vertical axis, use limits of -0.25 to 1.25.
7. Populate the 4 $\times$ 4 stiffness matrix (N/m) for the transverse beam element that represents a cylindrical aluminum rod with a diameter of 10 mm, a length of 100 mm, and an elastic modulus of 70 GPa.
   Is the stiffness generally higher or lower than the axial element for the same geometry and material from Problem 2?

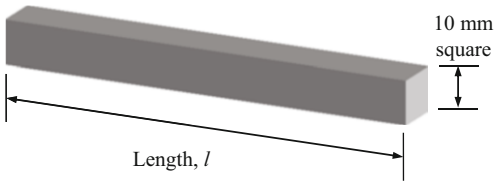

Fig. P9.4 Free-free boundary condition steel beam with square cross-section

8. Populate the 4 × 4 mass matrix (kg) for the transverse beam element that represents a cylindrical aluminum rod with a diameter of 10 mm, a length of 100 mm, and a density of 2700 kg/m^3.
9. Consider the free-free boundary condition steel beam displayed in Fig. P9.4, where the elastic modulus is 200 GPa and the density is 7800 kg/m^3. For a finite element model with 25 transverse elements, determine the length so that the first bending natural frequency is 1500 Hz.
10. Plot the left end FRF for the 25 finite element model that represents a 10 mm diameter, 150 mm long cylindrical beam with free-free boundary conditions. Use an elastic modulus of 69 GPa, a density of 2750 kg/m^3, and solid damping factors of $\eta = \{0.005, 0.01, 0.02\}$. Plot the magnitudes for all three FRFs in a single figure.

References

1. Logan DL (2011) A first course in the finite element method. Cengage Learning, Boston, Chapter 4.
2. Archer JS (1963) Consistent mass matrix for distributed mass systems. J Struct Div 89 (4):161–178
3. Thomson WT, Dahleh MD (1998) Theory of vibration with applications, 5th edn. Prentice-Hall, Inc., Upper Saddle River, Chapter 10.

Chapter 10
Receptance Coupling

I have made this letter longer than usual,
only because I have not had the time to make it shorter.
—*Blaise Pascal*

10.1 Introduction

In Chaps. 1–9 we discussed discrete and continuous beam models that can be used to describe the behavior of vibrating systems. We also detailed experimental techniques that we can use to identify these models. In this chapter, we will introduce an approach to combine models or measurements of individual components in order to predict the assembly's frequency response function (FRF). This method is referred to as receptance coupling [1]; recall from Sect. 7.1 that a receptance is a type of FRF.

In a Nutshell
Receptance coupling enables the connection of measurements to measurements, models to models, or models to measurements. Sometimes it is easy to make the measurements and sometimes it is difficult or impossible, such as when the component to be added only exists as a model.

10.2 Two Component Rigid Coupling

Let's begin with the rigid coupling of two **components, or substructures**. Our goal is to predict the direct and cross FRFs for the **assembly** based on the direct and cross FRFs for the two components. As a practical example, we could consider performing experiments to identify the free-free FRFs for an airplane's wing and fuselage separately and then coupling the wing to the fuselage mathematically to predict the response for the entire structure. This concept is demonstrated in Fig. 10.1, where the two components, I and II, are rigidly coupled to form the assembly III. Note that the direct and cross FRFs for the two components I and II could be derived from:

T. L. Schmitz, K. S. Smith, *Mechanical Vibrations*,
https://doi.org/10.1007/978-3-030-52344-2_10

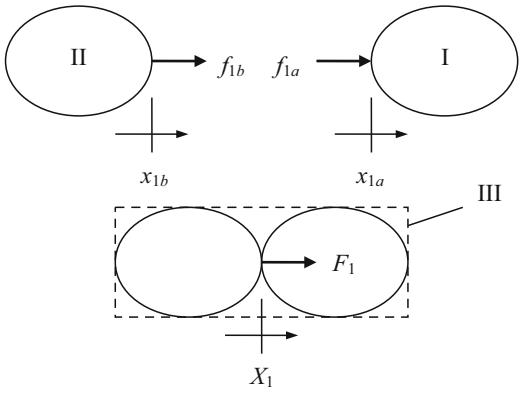

Fig. 10.1 Rigid coupling of components I and II to form assembly III. The force F_1 is applied to the assembly in order to determine H_{11}

(1) measurements; (2) discrete models; or (3) continuous beam models. The coupling coordinates are x_{1a} and x_{1b} for the two substructures I and II, respectively. The corresponding assembly coordinate, X_1, is located at the same physical location as x_{1a} and x_{1b} after they are joined.[1] An attractive aspect of receptance coupling is that the component FRFs are only required at the coupling locations and any point where the assembly response is to be predicted. Therefore, the assembly's direct receptance at X_1 due to a harmonic force applied at that location, $H_{11} = \frac{X_1}{F_1}$, can be fully described using the direct component receptances $h_{1a1a} = \frac{x_{1a}}{f_{1a}}$ and $h_{1b1b} = \frac{x_{1b}}{f_{1b}}$ obtained from harmonic forces applied to the components at x_{1a} and x_{1b}, respectively.

In a Nutshell

Recall that the FRFs (H_{11}, h_{1a1a}, and h_{1b1b}) are complex functions of frequency. At each frequency, the FRF has the form $a + ib$. The function may be continuous (e.g., based on a beam model) or it may be discrete (i.e., a measurement known only at a number of frequencies over the measurement frequency range).

To determine the assembly response, we must first describe the **compatibility condition**, $x_{1b} - x_{1a} = 0$, which represents the **rigid coupling** between component coordinates x_{1a} and x_{1b}. We can therefore write $x_{1b} = x_{1a} = X_1$ due to our decision to locate assembly coordinate X_1 at the (rigid) coupling point. We must also define the **equilibrium condition**, $f_{1a} + f_{1b} = F_1$, which equates the internal (component) and external (assembly) forces. Let's substitute for the displacements in the compatibility equation.

[1] We will follow this lower case/upper case notation to differentiate between component and assembly coordinates throughout the chapter.

$$\begin{aligned} x_{1b} - x_{1a} &= 0 \\ h_{1b1b} f_{1b} - h_{1a1a} f_{1a} &= 0 \end{aligned} \tag{10.1}$$

We next use the equilibrium condition, rewritten as $f_{1a} = F_1 - f_{1b}$, to eliminate f_{1a} in Eq. 10.1. Rearranging enables us to solve for f_{1b}.

$$\begin{aligned} h_{1b1b} f_{1b} - h_{1a1a} F_1 + h_{1a1a} f_{1b} &= 0 \\ (h_{1a1a} + h_{1b1b}) f_{1b} &= h_{1a1a} F_1 \\ f_{1b} &= (h_{1a1a} + h_{1b1b})^{-1} h_{1a1a} F_1 \end{aligned} \tag{10.2}$$

Now that we have f_{1b}, we can again use the equilibrium condition to determine f_{1a}.

$$\begin{aligned} f_{1a} &= F_1 - f_{1b} \\ f_{1a} &= \left(1 - (h_{1a1a} + h_{1b1b})^{-1} h_{1a1a}\right) F_1 \end{aligned} \tag{10.3}$$

We solve for H_{11} as shown in Eq. 10.4. This equation gives the direct assembly response at the coupling coordinate, X_1, as a function of the component receptances. These frequency-dependent, complex-valued receptances may have any number of modes. There are no restrictions on the relationship between the number of modes and coordinates as with modal analysis (i.e., we saw in Sect. 6.5 that the number of modeled modes and coordinates must be equal to obtain square matrices when using modal analysis).

$$H_{11} = \frac{X_1}{F_1} = \frac{x_{1a}}{F_1} = \frac{h_{1a1a} f_{1a}}{F_1} = h_{1a1a} - h_{1a1a}(h_{1a1a} + h_{1b1b})^{-1} h_{1a1a} \tag{10.4}$$

Is a Nutshell

Coupling FRFs requires that the mathematical operations (such as addition or multiplication) be completed in a frequency-by-frequency manner. For example, if h_{1a1a} is given by $a + ib$ and h_{1b1b} is $c + id$ at frequency ω_1, then $(h_{1a1a} + h_{1b1b}) = (a + c) + i(b + d)$ at ω_1. It is therefore required that the component FRFs are defined at the same frequency values. Inverting an FRF means that we compute $\frac{1}{a+ib}$ at each particular frequency. This inversion is completed by rationalizing the complex number (i.e., multiplying the numerator and denominator by its complex conjugate). The result at the selected frequency is $\frac{a-ib}{a^2+b^2}$, which has a real part $\frac{a}{a^2+b^2}$ and an imaginary part $\frac{-b}{a^2+b^2}$. This computation is repeated at every frequency. Multiplying two FRFs means that we multiply the two complex numbers at each frequency, $(a + ib)(c + id) = (ac - bd) + i(bc + ad)$.

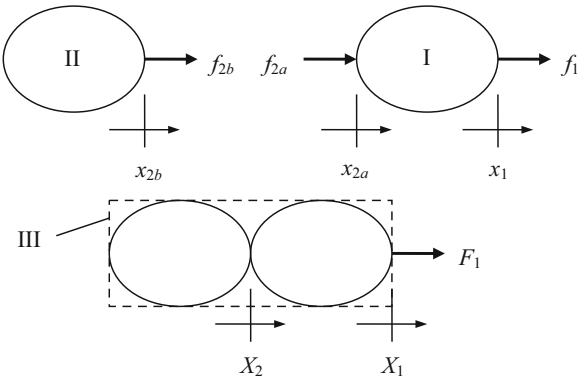

Fig. 10.2 Example showing rigid coupling of components I and II to form assembly III. The force F_1 is applied to the assembly at coordinate X_1 in order to determine H_{11} and H_{21}

Similarly, we can predict the assembly response at another coordinate, not coincident with the coupling point, by defining the component receptance at the desired location. Consider Fig. 10.2, where the direct assembly response at X_1 is again desired, but this location is now at another point on component I. We again assume x_1 and X_1 are collocated before and after coupling. The new coupling coordinates at the rigid coupling point are x_{2a} and x_{2b}. The component direct and cross receptances corresponding to Fig. 10.2 are $h_{11} = \frac{x_1}{f_1}$, $h_{2a2a} = \frac{x_{2a}}{f_{2a}}$, $h_{12a} = \frac{x_1}{f_{2a}}$, and $h_{2a1} = \frac{x_{2a}}{f_1}$ for I, and $h_{2b2b} = \frac{x_{2b}}{f_{2b}}$ for II. The compatibility condition for the rigid coupling is $x_{2b} - x_{2a} = 0$ and we can therefore write $x_{2a} = x_{2b} = X_2$. Also, $x_1 = X_1$. The equilibrium conditions are $f_{2a} + f_{2b} = 0$ (because there is no external force at the coupling point in this case) and $f_1 = F_1$.

To determine $H_{11} = \frac{X_1}{F_1}$, we'll first write the component displacements. For I, we now have two forces acting on the body, so the frequency-domain displacements are:

$$x_1 = h_{11} f_1 + h_{12a} f_{2a} \quad \text{and} \quad x_{2a} = h_{2a1} f_1 + h_{2a2a} f_{2a}. \tag{10.5}$$

For II, we have $x_{2b} = h_{2b2b} f_{2b}$. Substitution into the compatibility condition gives:

$$x_{2b} - x_{2a} = h_{2b2b} f_{2b} - h_{2a1} f_1 - h_{2a2a} f_{2a} = 0. \tag{10.6}$$

We apply the equilibrium conditions to replace f_1 with F_1 and eliminate f_{2a} ($f_{2a} = -f_{2b}$).

$$h_{2b2b} f_{2b} - h_{2a1} F_1 + h_{2a2a} f_{2b} = 0 \tag{10.7}$$

This enables us to group terms and solve for f_{2b}. Specifically, we have that $f_{2b} = (h_{2a2a} + h_{2b2b})^{-1} h_{2a1} F_1$. Therefore, we can also write $f_{2a} = -(h_{2a2a} + h_{2b2b})^{-1} h_{2a1} F_1$. Substitution of this force value into the H_{11} expression gives us the desired result; see Eq. 10.8. Again, the assembly response is written as a function of the direct (h_{11}, h_{2a2a}, and h_{2b2b}) and cross (h_{12a} and h_{2a1}) receptances for the two components.

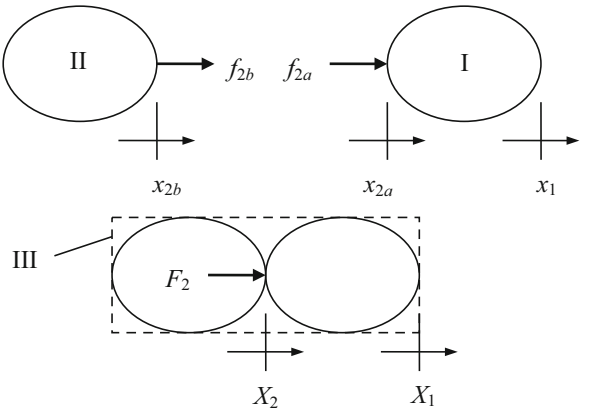

Fig. 10.3 Example showing rigid coupling of components I and II to form assembly III. The force F_2 is applied to the assembly at coordinate X_2 in order to determine H_{22} and H_{12}

$$H_{11} = \frac{X_1}{F_1} = \frac{x_1}{F_1} = \frac{h_{11}f_1 + h_{12a}f_{2a}}{F_1} = \frac{h_{11}f_1 - h_{12a}(h_{2a2a} + h_{2b2b})^{-1}h_{2a1}F_1}{F_1}$$
$$H_{11} = \frac{h_{11}F_1 - h_{12a}(h_{2a2a} + h_{2b2b})^{-1}h_{2a1}F_1}{F_1} = h_{11} - h_{12a}(h_{2a2a} + h_{2b2b})^{-1}h_{2a1} \tag{10.8}$$

We can also use f_{2a} to determine the cross receptance H_{21}. See Eq. 10.9.

$$H_{21} = \frac{X_2}{F_1} = \frac{x_{2a}}{F_1} = \frac{h_{2a1}f_1 + h_{2a2a}f_{2a}}{F_1} = \frac{h_{2a1}f_1 - h_{2a2a}(h_{2a2a} + h_{2b2b})^{-1}h_{2a1}F_1}{F_1}$$
$$H_{21} = \frac{h_{2a1}F_1 - h_{2a2a}(h_{2a2a} + h_{2b2b})^{-1}h_{2a1}F_1}{F_1} = h_{2a1} - h_{2a2a}(h_{2a2a} + h_{2b2b})^{-1}h_{2a1} \tag{10.9}$$

We determine the direct and cross receptances, H_{22} and H_{12}, respectively, by applying a force to the assembly coordinate X_2. See Fig. 10.3. The component receptances are again $h_{11} = \frac{x_1}{f_1}$, $h_{2a2a} = \frac{x_{2a}}{f_{2a}}$, $h_{12a} = \frac{x_1}{f_{2a}}$, and $h_{2a1} = \frac{x_{2a}}{f_1}$ for I and $h_{2b2b} = \frac{x_{2b}}{f_{2b}}$ for II. The compatibility condition for the rigid coupling remains as $x_{2b} - x_{2a} = 0$. However, the equilibrium condition is $f_{2a} + f_{2b} = F_2$ because the force is applied to the coupling coordinate.

To determine $H_{22} = \frac{X_2}{F_2}$, we begin by writing the component displacements. For I, the displacements are:

$$x_1 = h_{12a}f_{2a} \quad \text{and} \quad x_{2a} = h_{2a2a}f_{2a}. \tag{10.10}$$

For II, we have $x_{2b} = h_{2b2b}f_{2b}$. Substitution in the compatibility condition gives:

$$h_{2b2b}f_{2b} - h_{2a2a}f_{2a} = 0. \tag{10.11}$$

We apply the equilibrium condition, $f_{2a} = F_2 - f_{2b}$, to eliminate f_{2a} in Eq. 10.11.

$$h_{2b2b}f_{2b} - h_{2a2a}F_2 + h_{2a2a}f_{2b} = 0 \tag{10.12}$$

This enables us to group terms and solve for f_{2b}. We find that $f_{2b} = (h_{2a2a} + h_{2b2b})^{-1}h_{2a2a}F_2$. Again using the equilibrium condition, we can write $f_{2a} = (1 - (h_{2a2a} + h_{2b2b})^{-1}h_{2a2a})F_2$. Equation 10.13 gives the desired H_{22} expression.

$$H_{22} = \frac{X_2}{F_2} = \frac{x_{2a}}{F_2} = \frac{h_{2a2a}f_{2a}}{F_2} = \frac{h_{2a2a}\left(1 - (h_{2a2a} + h_{2b2b})^{-1}h_{2a2a}\right)F_2}{F_2}$$
$$H_{22} = \frac{h_{2a2a}F_2 - h_{2a2a}(h_{2a2a} + h_{2b2b})^{-1}h_{2a2a}F_2}{F_2} = h_{2a2a} - h_{2a2a}(h_{2a2a} + h_{2b2b})^{-1}h_{2a2a} \tag{10.13}$$

We use f_{2a} to find the cross receptance H_{12} as well. See Eq. 10.14.

$$H_{12} = \frac{X_1}{F_2} = \frac{x_1}{F_2} = \frac{h_{12a}f_{2a}}{F_2} = \frac{h_{12a}\left(1 - (h_{2a2a} + h_{2b2b})^{-1}h_{2a2a}\right)F_2}{F_2} \tag{10.14}$$
$$H_{12} = h_{12a} - h_{12a}(h_{2a2a} + h_{2b2b})^{-1}h_{2a2a}$$

10.3 Two Component Flexible Coupling

Let's continue with the system shown in Fig. 10.1, but now couple the two components through a linear spring, described by the constant k. This case is depicted in Fig. 10.4 and represents the situation where the connection between two components is not rigid. As an example, perhaps the joint is a bolted connection where the elastic deformation of the bolts due to an external harmonic force acts as a spring that couples the two components; see Fig. 10.5. In Fig. 10.4 the component receptances are $h_{1a1a} = \frac{x_{1a}}{f_{1a}}$ and $h_{1b1b} = \frac{x_{1b}}{f_{1b}}$ and the equilibrium condition is $f_{1a} + f_{1b} = F_{1a}$. These are analogous to the rigid coupling case. However, the compatibility condition now becomes:

$$k(x_{1b} - x_{1a}) = -f_{1b}. \tag{10.15}$$

for the **flexible coupling** case. This relationship follows Hooke's law, $F = kx$.

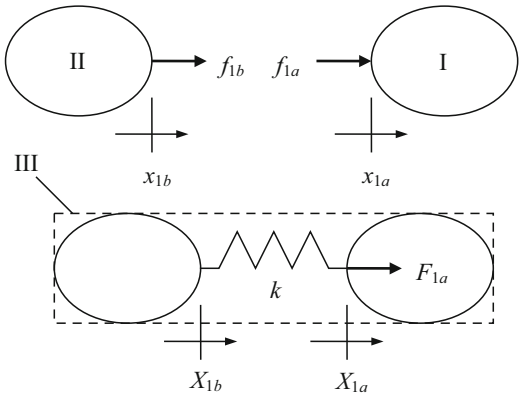

Fig. 10.4 Flexible coupling of components I and II to form assembly III. The force F_{1a} is applied to the assembly at coordinate X_{1a} in order to determine H_{1a1a} and H_{1b1a}

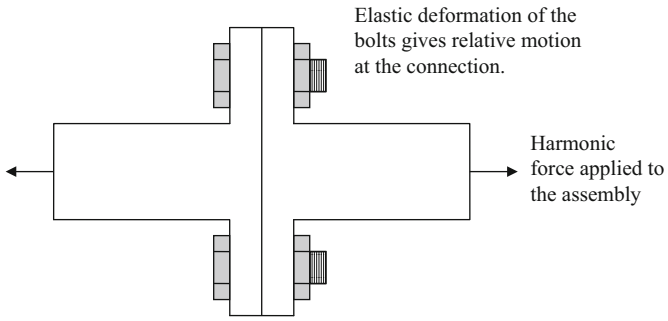

Fig. 10.5 A bolted connection where the elastic strain in the bolts due to the applied harmonic force effectively serves as a spring that connects the two components

In a Nutshell
We recognize that components cannot, in practice, be rigidly connected. Sometimes rigid connection is a good approximation, but when it is not, connection through a spring is often more accurate.

Because the component and assembly coordinates are coincident, we have that $x_{2a} = X_{2a}$ and $x_{2b} = X_{2b}$. To determine $H_{1a1a} = \frac{X_{1a}}{F_{1a}}$, we first substitute the component displacements in the compatibility condition. See Eq. 10.16.

$$k(h_{1b1b}f_{1b} - h_{1a1a}f_{1a}) = -f_{1b} \tag{10.16}$$

Using the equilibrium condition, $f_{1a} = F_{1a} - f_{1b}$, we can eliminate f_{1a} to obtain the equation for f_{1b}.

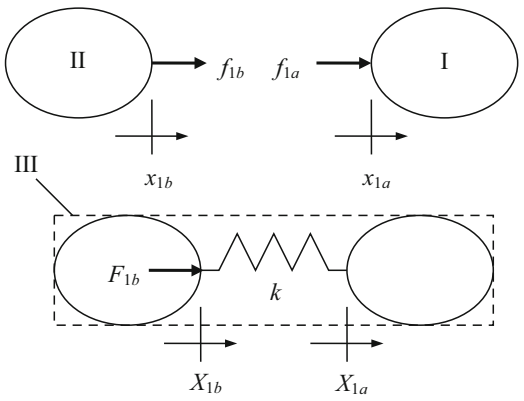

Fig. 10.6 Flexible coupling of components I and II to form assembly III. The force F_{1b} is applied to the assembly at coordinate X_{1b} in order to determine H_{1b1b} and H_{1a1b}

$$\begin{aligned} k(h_{1b1b}f_{1b} - h_{1a1a}F_{1a} + h_{1a1a}f_{1b}) &= -f_{1b} \\ kh_{1b1b}f_{1b} - kh_{1a1a}F_{1a} + kh_{1a1a}f_{1b} &= -f_{1b} \\ \left(h_{1a1a} + h_{1b1b} + \frac{1}{k}\right)f_{1b} &= h_{1a1a}F_{1a} \\ f_{1b} &= \left(h_{1a1a} + h_{1b1b} + \frac{1}{k}\right)^{-1} h_{1a1a}F_{1a} \end{aligned} \tag{10.17}$$

Using f_{1b} and the equilibrium condition, we find that $f_{1a} = \left(1 - \left(h_{1a1a} + h_{1b1b} + \frac{1}{k}\right)^{-1} h_{1a1a}\right)F_{1a}$. Substitution then yields the direct assembly receptance H_{1a1a} as shown in Eq. 10.18. We can see that this equation simplifies to Eq. 10.4 as k approaches infinity (rigid connection).

$$\begin{aligned} H_{1a1a} = \frac{X_{1a}}{F_{1a}} = \frac{x_{1a}}{F_{1a}} = \frac{h_{1a1a}f_{1a}}{F_{1a}} &= \frac{h_{1a1a}\left(1 - \left(h_{1a1a} + h_{1b1b} + \frac{1}{k}\right)^{-1} h_{1a1a}\right)F_{1a}}{F_{1a}} \\ H_{1a1a} &= h_{1a1a} - h_{1a1a}\left(h_{1a1a} + h_{1b1b} + \frac{1}{k}\right)^{-1} h_{1a1a} \end{aligned} \tag{10.18}$$

The cross receptance due to the force F_{1a} is provided in Eq. 10.19.

$$\begin{aligned} H_{1b1a} = \frac{X_{1b}}{F_{1a}} = \frac{x_{1b}}{F_{1a}} = \frac{h_{1b1b}f_{1b}}{F_{1a}} &= \frac{h_{1b1b}\left(h_{1a1a} + h_{1b1b} + \frac{1}{k}\right)^{-1} h_{1a1a}F_{1a}}{F_{1a}} \\ H_{1b1a} &= h_{1b1b}\left(h_{1a1a} + h_{1b1b} + \frac{1}{k}\right)^{-1} h_{1a1a} \end{aligned} \tag{10.19}$$

As shown in Fig. 10.6, we can alternately apply the assembly force to coordinate X_{1b}. The component receptances and displacements are unchanged, but the

equilibrium condition is $f_{1a} + f_{1b} = F_{1b}$. Similarly, we modify the compatibility condition to be:

$$k(x_{1a} - x_{1b}) = -f_{1a}. \tag{10.20}$$

Substitution for the component displacements and f_{1b} (from the equilibrium condition) yields the expression for f_{1a}.

$$\begin{aligned} k(h_{1a1a}f_{1a} - h_{1b1b}F_{1b} + h_{1b1b}f_{1a}) &= -f_{1a} \\ kh_{1a1a}f_{1a} - kh_{1b1b}F_{1b} + kh_{1b1b}f_{1a} &= -f_{1a} \\ \left(h_{1a1a} + h_{1b1b} + \frac{1}{k}\right)f_{1a} &= h_{1b1b}F_{1b} \\ f_{1a} &= \left(h_{1a1a} + h_{1b1b} + \frac{1}{k}\right)^{-1} h_{1b1b}F_{1b} \end{aligned} \tag{10.21}$$

Again applying the equilibrium condition, $f_{1b} = F_{1b} - f_{1a}$, we obtain $f_{1b} = \left(1 - \left(h_{1a1a} + h_{1b1b} + \frac{1}{k}\right)^{-1} h_{1b1b}\right)F_{1b}$. Substitution then gives the assembly direct and cross receptances due to F_{1b}.

$$H_{1b1b} = \frac{X_{1b}}{F_{1b}} = \frac{x_{1b}}{F_{1b}} = \frac{h_{1b1b}f_{1b}}{F_{1b}} = \frac{h_{1b1b}\left(1 - \left(h_{1a1a} + h_{1b1b} + \frac{1}{k}\right)^{-1} h_{1b1b}\right)F_{1b}}{F_{1b}}$$

$$H_{1b1b} = h_{1b1b} - h_{1b1b}\left(h_{1a1a} + h_{1b1b} + \frac{1}{k}\right)^{-1} h_{1b1b} \tag{10.22}$$

$$H_{1a1b} = \frac{X_{1a}}{F_{1b}} = \frac{x_{1a}}{F_{1b}} = \frac{h_{1a1a}f_{1a}}{F_{1b}} = \frac{h_{1a1a}\left(h_{1a1a} + h_{1b1b} + \frac{1}{k}\right)^{-1} h_{1b1b}F_{1b}}{F_{1b}}$$

$$H_{1a1b} = h_{1a1a}\left(h_{1a1a} + h_{1b1b} + \frac{1}{k}\right)^{-1} h_{1b1b} \tag{10.23}$$

Similar to the rigid connection example depicted in Fig. 10.2, we can again add another coordinate, not located at the coupling location, and apply the external force at that point. See Fig. 10.7. The component displacements are again $x_1 = h_{11}f_1 + h_{12a}f_{2a}$ and $x_{2a} = h_{2a1}f_1 + h_{2a2a}f_{2a}$ for substructure I and $x_{2b} = h_{2b2b}f_{2b}$ for substructure II. The equilibrium conditions are $f_{2a} + f_{2b} = 0$ and $f_1 = F_1$. The compatibility condition is:

$$k(x_{2b} - x_{2a}) = -f_{2b}. \tag{10.24}$$

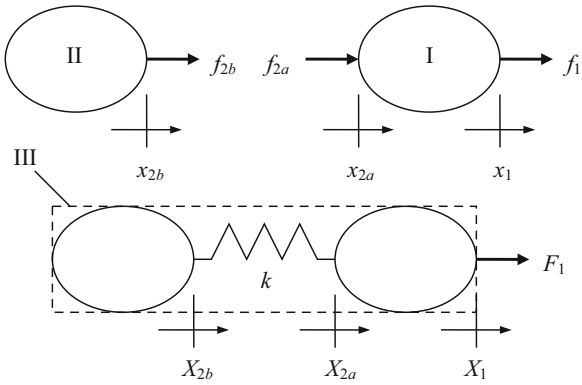

Fig. 10.7 Flexible coupling of components I and II to form assembly III. The force F_1 is applied to the assembly at coordinate X_1 in order to determine H_{11}, H_{2a1}, and H_{2b1}

As before, the component and assembly coordinates are coincident, so we have that $x_1 = X_1$, $x_{2a} = X_{2a}$, and $x_{2b} = X_{2b}$. To determine $H_{11} = \frac{X_1}{F_1}$, we first substitute the component displacements in the compatibility condition. See Eq. 10.25.

$$k(h_{2b2b}f_{2b} - h_{2a1}f_1 - h_{2a2a}f_{2a}) = -f_{2b} \tag{10.25}$$

Using the equilibrium conditions, we can eliminate f_{2a} and replace f_1 with F_1 to obtain the equation for f_{2b}.

$$\begin{aligned} k(h_{2b2b}f_{2a} - h_{2a1}F_1 + h_{2a2a}f_{2b}) &= -f_{2b} \\ kh_{2b2b}f_{2b} - kh_{2a1}F_1 + kh_{2a2a}f_{2b} &= -f_{2b} \\ \left(h_{2a2a} + h_{2b2b} + \frac{1}{k}\right)f_{2b} &= h_{2a1}F_1 \\ f_{2b} &= \left(h_{2a2a} + h_{2b2b} + \frac{1}{k}\right)^{-1} h_{2a1}F_1 \end{aligned} \tag{10.26}$$

Applying the equilibrium condition $f_{2a} = -f_{2b}$, we obtain:

$$f_{2a} = -\left(h_{2a2a} + h_{2b2b} + \frac{1}{k}\right)^{-1} h_{2a1}F_1. \tag{10.27}$$

This enables us to write the direct and cross receptances as shown in Eqs. 10.28 and 10.29, respectively. We note that these equations simplify to the rigid coupling results provided in Eqs. 10.8 and 10.9 as k approaches infinity. The assembly cross receptance at coordinate X_{2b} is given by Eq. 10.30.

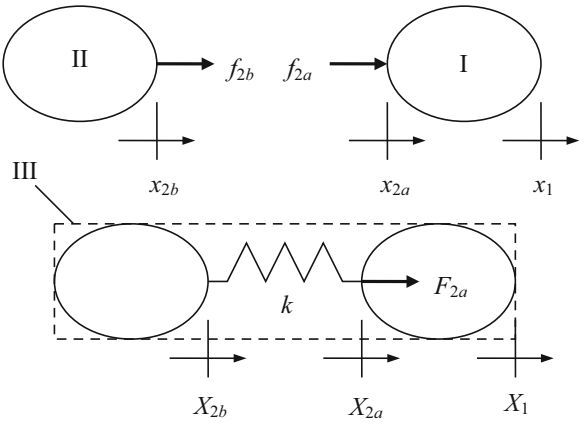

Fig. 10.8 Flexible coupling of components I and II to form assembly III. The force F_{2a} is applied to the assembly at coordinate X_{2a} in order to determine H_{2a2a}, H_{2b2a}, and H_{12a}

$$H_{11} = \frac{X_1}{F_1} = \frac{x_1}{F_1} = \frac{h_{11}f_1 + h_{12a}f_{2a}}{F_1} = \frac{h_{11}f_1 - h_{12a}\left(h_{2a2a} + h_{2b2b} + \frac{1}{k}\right)^{-1}h_{2a1}F_1}{F_1}$$

$$H_{11} = \frac{h_{11}F_1 - h_{12a}\left(h_{2a2a} + h_{2b2b} + \frac{1}{k}\right)^{-1}h_{2a1}F_1}{F_1} = h_{11} - h_{12a}\left(h_{2a2a} + h_{2b2b} + \frac{1}{k}\right)^{-1}h_{2a1} \tag{10.28}$$

$$H_{2a1} = \frac{X_{2a}}{F_1} = \frac{x_{2a}}{F_1} = \frac{h_{2a1}f_1 + h_{2a2a}f_{2a}}{F_1} = \frac{h_{2a1}F_1 - h_{2a2a}\left(h_{2a2a} + h_{2b2b} + \frac{1}{k}\right)^{-1}h_{2a1}F_1}{F_1}$$

$$H_{2a1} = h_{2a1} - h_{2a2a}\left(h_{2a2a} + h_{2b2b} + \frac{1}{k}\right)^{-1}h_{2a1} \tag{10.29}$$

$$H_{2b1} = \frac{X_{2b}}{F_1} = \frac{x_{2b}}{F_1} = \frac{h_{2b2b}f_{2b}}{F_1} = \frac{h_{2b2b}\left(h_{2a2a} + h_{2b2b} + \frac{1}{k}\right)^{-1}h_{2a1}F_1}{F_1}$$

$$H_{2b1} = h_{2b2b}\left(h_{2a2a} + h_{2b2b} + \frac{1}{k}\right)^{-1}h_{2a1} \tag{10.30}$$

Let's now apply the external force, F_{2a}, to coordinate X_{2a} as shown in Fig. 10.8 in order to determine the assembly receptances H_{2a2a}, H_{2b2a}, and H_{12a}. The component displacements are $x_1 = h_{12a}f_{2a}$ and $x_{2a} = h_{2a2a}f_{2a}$ for substructure I and $x_{2b} = h_{2b2b}f_{2b}$ for substructure II. The equilibrium condition is $f_{2a} + f_{2b} = F_{2a}$ and the compatibility condition is:

$$k(x_{2b} - x_{2a}) = -f_{2b}. \tag{10.31}$$

We first determine the force f_{2b} by substituting the component displacements in Eq. 10.31 and replacing f_{2a} with $F_{2a} - f_{2b}$.

$$\begin{aligned} k(h_{2b2b}f_{2b} - h_{2a2a}F_{2a} + h_{2a2a}f_{2b}) &= -f_{2b} \\ kh_{2b2b}f_{2b} - kh_{2a2a}F_{2a} + kh_{2a2a}f_{2b} &= -f_{2b} \\ \left(h_{2a2a} + h_{2b2b} + \frac{1}{k}\right)f_{2b} &= h_{2a2a}F_{2a} \\ f_{2b} &= \left(h_{2a2a} + h_{2b2b} + \frac{1}{k}\right)^{-1} h_{2a2a}F_{2a} \end{aligned} \tag{10.32}$$

Again using the equilibrium condition we find the equation for f_{2a}.

$$f_{2a} = F_{2a} - f_{2b} = \left(1 - \left(h_{2a2a} + h_{2b2b} + \frac{1}{k}\right)^{-1} h_{2a2a}\right)F_{2a} \tag{10.33}$$

The direct and cross receptances for this situation (depicted in Fig. 10.8) are provided in Eqs. 10.34–10.36.

$$\begin{aligned} H_{2a2a} = \frac{X_{2a}}{F_{2a}} = \frac{x_{2a}}{F_{2a}} = \frac{h_{2a2a}f_{2a}}{F_{2a}} &= \frac{h_{2a2a}\left(1 - \left(h_{2a2a} + h_{2b2b} + \frac{1}{k}\right)^{-1} h_{2a2a}\right)F_{2a}}{F_{2a}} \\ H_{2a2a} &= h_{2a2a} - h_{2a2a}\left(h_{2a2a} + h_{2b2b} + \frac{1}{k}\right)^{-1} h_{2a2a} \end{aligned} \tag{10.34}$$

$$\begin{aligned} H_{2b2a} = \frac{X_{2b}}{F_{2a}} = \frac{x_{2b}}{F_{2a}} = \frac{h_{2b2b}f_{2b}}{F_{2b}} &= \frac{h_{2b2b}\left(h_{2a2a} + h_{2b2b} + \frac{1}{k}\right)^{-1} h_{2a2a}F_{2a}}{F_{2a}} \\ H_{2b2a} &= h_{2b2b}\left(h_{2a2a} + h_{2b2b} + \frac{1}{k}\right)^{-1} h_{2a2a} \end{aligned} \tag{10.35}$$

$$\begin{aligned} H_{12a} = \frac{X_1}{F_{2a}} = \frac{x_1}{F_{2a}} = \frac{h_{12a}f_{2a}}{F_{2a}} &= \frac{h_{12a}\left(1 - \left(h_{2a2a} + h_{2b2b} + \frac{1}{k}\right)^{-1} h_{2a2a}\right)F_{2a}}{F_{2a}} \\ H_{12a} &= h_{12a} - h_{12a}\left(h_{2a2a} + h_{2b2b} + \frac{1}{k}\right)^{-1} h_{2a2a} \end{aligned} \tag{10.36}$$

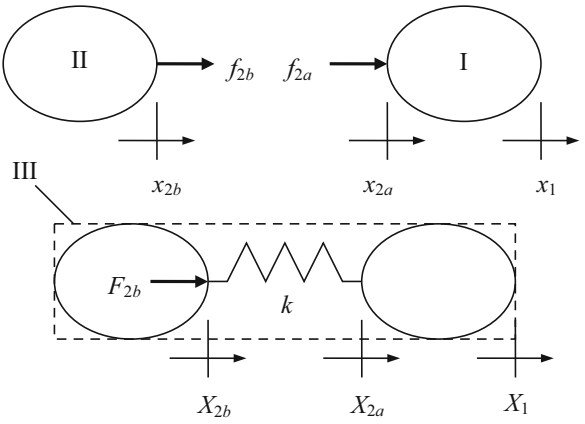

Fig. 10.9 Flexible coupling of components I and II to form assembly III. The force F_{2b} is applied to the assembly at coordinate X_{2b} in order to determine H_{2b2b}, H_{2a2b}, and H_{12b}

In a Nutshell
While these computations are straightforward, they are more complicated than the rigid connection case. Increased accuracy often comes at the expense of increased computational complexity. The essence of engineering is to determine the required accuracy of the measurement/model/desired outcome and proceeding accordingly.

Our final scenario for the two component flexible coupling is shown in Fig. 10.9. Here, we apply the external force F_{2b} to coordinate X_{2b} to obtain the direct and cross assembly receptances H_{2b2b}, H_{2a2b}, and H_{12b}. The component displacements are the same as the previous case: $x_1 = h_{12a}f_{2a}$ and $x_{2a} = h_{2a2a}f_{2a}$ for substructure I and $x_{2b} = h_{2b2b}f_{2b}$ for substructure II. However, the equilibrium condition is modified to be $f_{2a} + f_{2b} = F_{2b}$ and the compatibility condition is rewritten as:

$$k(x_{2a} - x_{2b}) = -f_{2a}. \tag{10.37}$$

We find f_{2a} by substituting the component displacements in Eq. 10.37 and replacing f_{2b} with $F_{2a} - f_{2a}$.

$$\begin{aligned} k(h_{2a2a}f_{2a} - h_{2b2b}F_{2b} + h_{2b2b}f_{2a}) &= -f_{2a} \\ kh_{2a2a}f_{2a} - kh_{2b2b}F_{2b} + kh_{2b2b}f_{2a} &= -f_{2a} \\ \left(h_{2a2a} + h_{2b2b} + \frac{1}{k}\right)f_{2a} &= h_{2b2b}F_{2b} \\ f_{2a} &= \left(h_{2a2a} + h_{2b2b} + \frac{1}{k}\right)^{-1} h_{2b2b}F_{2b} \end{aligned} \tag{10.38}$$

Again using the equilibrium condition we find the equation for f_{2b}.

$$f_{2b} = F_{2b} - f_{2a} = \left(1 - \left(h_{2a2a} + h_{2b2b} + \frac{1}{k}\right)^{-1} h_{2b2b}\right) F_{2b} \tag{10.39}$$

The direct and cross receptances for the case shown in Fig. 10.9 are given in Eqs. 10.40–10.42.

$$H_{2b2b} = \frac{X_{2b}}{F_{2b}} = \frac{x_{2b}}{F_{2b}} = \frac{h_{2b2b} f_{2b}}{F_{2b}} = \frac{h_{2b2b}\left(1 - \left(h_{2a2a} + h_{2b2b} + \frac{1}{k}\right)^{-1} h_{2b2b}\right) F_{2b}}{F_{2b}}$$
$$H_{2b2b} = h_{2b2b} - h_{2b2b}\left(h_{2a2a} + h_{2b2b} + \frac{1}{k}\right)^{-1} h_{2b2b} \tag{10.40}$$

$$H_{2a2b} = \frac{X_{2a}}{F_{2b}} = \frac{x_{2a}}{F_{2b}} = \frac{h_{2a2a} f_{2a}}{F_{2b}} = \frac{h_{2a2a}\left(h_{2a2a} + h_{2b2b} + \frac{1}{k}\right)^{-1} h_{2b2b} F_{2b}}{F_{2b}}$$
$$H_{2a2b} = h_{2a2a}\left(h_{2a2a} + h_{2b2b} + \frac{1}{k}\right)^{-1} h_{2b2b} \tag{10.41}$$

$$H_{12b} = \frac{X_1}{F_{2b}} = \frac{x_1}{F_{2b}} = \frac{h_{12a} f_{2a}}{F_{2a}} = \frac{h_{12a}\left(h_{2a2a} + h_{2b2b} + \frac{1}{k}\right)^{-1} h_{2b2b} F_{2b}}{F_{2b}}$$
$$H_{12b} = h_{12a}\left(h_{2a2a} + h_{2b2b} + \frac{1}{k}\right)^{-1} h_{2b2b} \tag{10.42}$$

10.4 Two Component Flexible-Damped Coupling[2]

As we discussed in Sect. 1.3, damping is always present in mechanical systems. Therefore, as a final step in our receptance coupling of components I and II to predict the assembly III response, we can expand the model in Fig. 10.7 to include viscous damping at the coupling interface. See Fig. 10.10. If we again consider the bolted connection in Fig. 10.5, the elastic deflection of the bolts could cause rubbing between the bolts and their mating surfaces. This would lead to energy dissipation that we could model as viscous damping.

The expressions for the component displacements and equilibrium conditions remain unchanged relative to the flexible coupling derivation when we add damping. However, the compatibility condition is now:

[2]The authors gratefully acknowledge the contributions of Dr. T. Burns, National Institute of Standards and Technology, in developing the damping analysis.

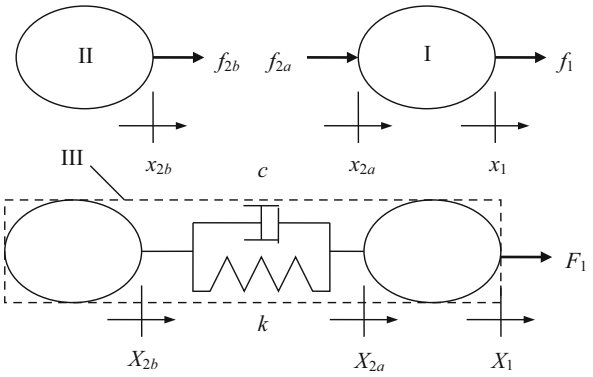

Fig. 10.10 Viscously damped, flexible coupling of components I and II to form assembly III. As with the flexible coupling case, the force F_1 is applied to the assembly at coordinate X_1 in order to determine H_{11}, H_{2a1}, and H_{2b1}

$$k(x_{2b} - x_{2a}) + i\omega c(x_{2b} - x_{2a}) = -f_{2b}, \tag{10.43}$$

where we have assumed harmonic motion so that the velocity-dependent damping forces can be express in the form $i\omega cx$. Equation 10.43 can be rewritten as:

$$(k + i\omega c)(x_{2b} - x_{2a}) = -f_{2b}. \tag{10.44}$$

If we substitute the complex, frequency-dependent variable k' for $(k + i\omega c)$, then we see that the compatibility equation takes the same form as shown in Eq. 10.24. Therefore, we can simply replace k in Eq. 10.28 with k' to obtain Eq. 10.45. This defines the direct FRF at coordinate X_1 on assembly III in Fig. 10.10. The same substitution can be made in the other assembly receptances derived for the two component flexible coupling in order to obtain the two component flexible-damped coupling results.

$$H_{11} = h_{11} - h_{12a}\left(h_{2a2a} + h_{2b2b} + \frac{1}{k'}\right)^{-1} h_{2a1} \tag{10.45}$$

Before proceeding with a numerical example in the next section, we present Table 10.1 which summarizes the receptance coupling equations developed in the previous sections.

10.5 Comparison of Assembly Modeling Techniques

Let's now complete an example where we compare receptance coupling to the modal analysis and complex matrix inversion methods we discussed in Chap. 5. As shown in Fig. 10.11, two single degree of freedom spring-mass-damper systems, I and II, are to be connected using the spring, k_c, to form the new two degree of freedom assembly, III. The assembled system's equations of motion are determined using the appropriate free body diagrams. The matrix representation of these equations, after

Table 10.1 Direct and cross receptances for two component coupling

	Component coordinates		Receptances			
R/F	I	II	D/C		Fig.	Eq.
R	x_{1a}	x_{1b}	D	$H_{11} = h_{1a1a} - h_{1a1a}(h_{1a1a} + h_{1b1b})^{-1} h_{1a1a}$	10.1	10.4
R	x_1, x_{2a}	x_{2b}	D	$H_{11} = h_{11} - h_{12a}(h_{2a2a} + h_{2b2b})^{-1} h_{2a1}$	10.2	10.8
			C	$H_{21} = h_{2a1} - h_{2a2a}(h_{2a2a} + h_{2b2b})^{-1} h_{2a1}$		10.9
			D	$H_{22} = h_{2a2a} - h_{2a2a}(h_{2a2a} + h_{2b2b})^{-1} h_{2a2a}$	10.3	10.13
			C	$H_{12} = h_{12a} - h_{12a}(h_{2a2a} + h_{2b2b})^{-1} h_{2a2a}$		10.14
F	x_{1a}	x_{1b}	D	$H_{1a1a} = h_{1a1a} - h_{1a1a}\left(h_{1a1a} + h_{1b1b} + \frac{1}{k}\right)^{-1} h_{1a1a}$	10.4	10.18
			C	$H_{1b1a} = h_{1b1b}\left(h_{1a1a} + h_{1b1b} + \frac{1}{k}\right)^{-1} h_{1a1a}$		10.19
			D	$H_{1b1b} = h_{1b1b} - h_{1b1b}\left(h_{1a1a} + h_{1b1b} + \frac{1}{k}\right)^{-1} h_{1b1b}$	10.6	10.22
			C	$H_{1a1b} = h_{1a1a}\left(h_{1a1a} + h_{1b1b} + \frac{1}{k}\right)^{-1} h_{1b1b}$		10.23
F	x_1, x_{2a}	x_{2b}	D	$H_{11} = h_{11} - h_{12a}\left(h_{2a2a} + h_{2b2b} + \frac{1}{k}\right)^{-1} h_{2a1}$	10.7	10.28
			C	$H_{2a1} = h_{2a1} - h_{2a2a}\left(h_{2a2a} + h_{2b2b} + \frac{1}{k}\right)^{-1} h_{2a1}$		10.29
			C	$H_{2b1} = h_{2b2b}\left(h_{2a2a} + h_{2b2b} + \frac{1}{k}\right)^{-1} h_{2a1}$		10.30
			D	$H_{2a2a} = h_{2a2a} - h_{2a2a}\left(h_{2a2a} + h_{2b2b} + \frac{1}{k}\right)^{-1} h_{2a2a}$	10.8	10.34
			C	$H_{2b2a} = h_{2b2b}\left(h_{2a2a} + h_{2b2b} + \frac{1}{k}\right)^{-1} h_{2a2a}$		10.35
			C	$H_{12a} = h_{12a} - h_{12a}\left(h_{2a2a} + h_{2b2b} + \frac{1}{k}\right)^{-1} h_{2a2a}$		10.36
			D	$H_{2b2b} = h_{2b2b} - h_{2b2b}\left(h_{2a2a} + h_{2b2b} + \frac{1}{k}\right)^{-1} h_{2b2b}$	10.9	10.40
			C	$H_{2a2b} = h_{2a2a}\left(h_{2a2a} + h_{2b2b} + \frac{1}{k}\right)^{-1} h_{2b2b}$		10.41
			C	$H_{12b} = h_{12a}\left(h_{2a2a} + h_{2b2b} + \frac{1}{k}\right)^{-1} h_{2b2b}$		10.42

The connection type is either rigid, R, or flexible, F. The receptance type is either direct, D, or cross, C. The corresponding figure and equation numbers are also included

substituting the assumed harmonic form of the solution, is provided in Eq. 10.46. This equation takes the form:

$$\left(s^2[m] + s[c] + [k]\right)\left\{\vec{X}\right\}e^{st} = \left\{\vec{F}\right\}e^{st},$$

where we've used the Laplace variable s to represent the product $i\omega$ and $[m]$, $[c]$, and $[k]$ are the assembly's lumped parameter mass, damping, and stiffness matrices in local coordinates, respectively.

$$\left(s^2\begin{bmatrix} m_1 & 0 \\ 0 & m_2 \end{bmatrix} + s\begin{bmatrix} c_1 & 0 \\ 0 & c_2 \end{bmatrix} + \begin{bmatrix} k_1 + k_c & -k_c \\ -k_c & k_2 + k_c \end{bmatrix}\right)\begin{Bmatrix} X_{1a} \\ X_{1b} \end{Bmatrix} = \begin{Bmatrix} 0 \\ F_{1b} \end{Bmatrix}$$

$$\begin{bmatrix} m_1 s^2 + c_1 s + (k_1 + k_c) & -k_c \\ -k_c & m_2 s^2 + c_2 s + (k_2 + k_c) \end{bmatrix}\begin{Bmatrix} X_{1a} \\ X_{1b} \end{Bmatrix} = \begin{Bmatrix} 0 \\ F_{1b} \end{Bmatrix} \tag{10.46}$$

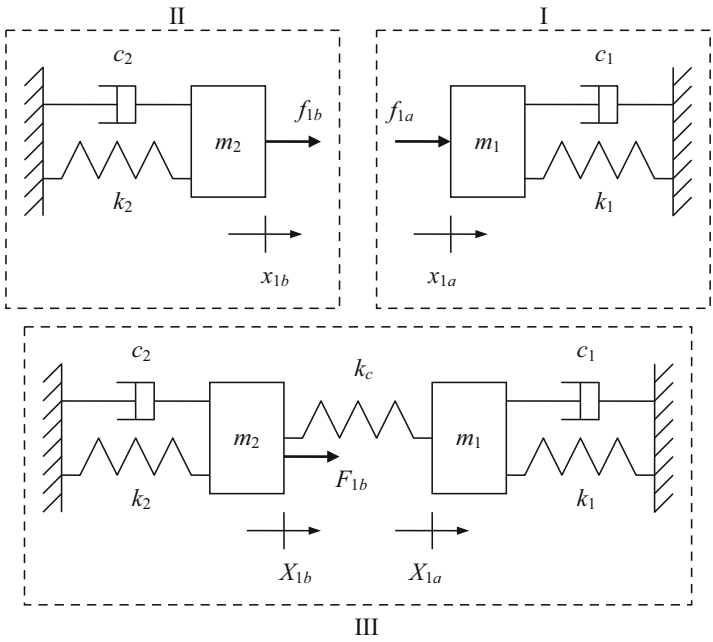

Fig. 10.11 Flexible coupling of spring-mass-damper systems I and II to form the two degree of freedom assembly III

10.5.1 Modal Analysis

We can use the equations of motion shown in Eq. 10.46 to find the modal solution for the assembled system. If we assume that proportional damping exists (i.e., $[c] = \alpha[m] + \beta[k]$, where α and β are real numbers), damping can be neglected in the modal solution. Note that this solution is also independent of the external force, F_{1b}. We write the characteristic equation for this system as shown in Eq. 10.47. The quadratic roots of this fourth order equation, ${s_1}^2$ and ${s_2}^2$, give the two eigenvalues (${s_1}^2 = -{\omega_{n1}}^2$ and ${s_2}^2 = -{\omega_{n2}}^2$, where $\omega_{n1} < \omega_{n2}$) for the two degree of freedom system.

$$\begin{gathered}\left(m_1 s^2 + (k_1 + k_c)\right)\left(m_2 s^2 + (k_2 + k_c)\right) - {k_c}^2 = 0 \\ m_1 m_2 s^4 + (m_1(k_2 + k_c) + m_2(k_1 + k_c))s^2 + (k_1 + k_c)(k_2 + k_c) - {k_c}^2 = 0\end{gathered} \tag{10.47}$$

Substitution of these eigenvalues into either of the original equations of motion, again neglecting damping and the external force, yields the eigenvectors (mode

shapes). Note that the eigenvectors must be normalized to the force location (coordinate X_{1b} in this case). Selecting the top equation from Eq. 10.46, for example, gives:

$$\frac{X_{1a}}{X_{1b}} = \frac{k_c}{m_1 s^2 + (k_1 + k_c)}. \tag{10.48}$$

The mass, damping, and stiffness matrices are diagonalized using the modal matrix (composed of columns of the eigenvectors), P, defined in Eq. 10.49.

$$P = \begin{bmatrix} \frac{X_{1a}}{X_{1b}}\left(s_1{}^2\right) & \frac{X_{1a}}{X_{1b}}\left(s_2{}^2\right) \\ 1 & 1 \end{bmatrix} \tag{10.49}$$

Specifically, we have that:

$$\begin{aligned} \left[m_q\right] &= [P]^T[m][P] = \begin{bmatrix} m_{q1} & 0 \\ 0 & m_{q2} \end{bmatrix}, \\ \left[c_q\right] &= [P]^T[c][P] = \begin{bmatrix} c_{q1} & 0 \\ 0 & c_{q2} \end{bmatrix}, \text{and} \\ \left[k_q\right] &= [P]^T[k][P] = \begin{bmatrix} k_{q1} & 0 \\ 0 & k_{q2} \end{bmatrix}. \end{aligned}$$

Based on these modal mass, damping, and stiffness values, we calculate the associated damping ratios, $\zeta_{q1,2} = \frac{c_{q1,2}}{2\sqrt{k_{q1,2}m_{q1,2}}}$. The modal solution for the direct FRF at coordinate X_{1b} of the assembled system is then expressed as shown in Eq. 10.50, where $r_{1,2} = \frac{\omega}{\omega_{n1,2}}$. As we discussed in Chap. 5, the direct FRF is the sum of the modal contributions.

$$\begin{aligned} H_{1b1b} &= \frac{X_{1b}}{F_{1b}} \\ &= \frac{1}{k_{q1}}\left(\frac{(1 - r_1{}^2) - i\left(2\zeta_{q1}r_1\right)}{(1 - r_1{}^2)^2 + \left(2\zeta_{q1}r_1\right)^2}\right) + \frac{1}{k_{q2}}\left(\frac{(1 - r_2{}^2) - i\left(2\zeta_{q2}r_2\right)}{(1 - r_2{}^2)^2 + \left(2\zeta_{q2}r_2\right)^2}\right) \end{aligned} \tag{10.50}$$

10.5.2 Complex Matrix Inversion[3]

Equation 10.46 can be compactly written as $[A]\left\{\vec{X}\right\} = \left\{\vec{F}\right\}$. As shown in Sect. 5.2, complex matrix inversion is carried out using $\left\{\vec{X}\right\}\left\{\vec{F}\right\}^{-1} = [A]^{-1}$ to determine the assembly's direct and cross FRFs. The inverted $[A]$ matrix for this two degree of freedom example is:

$$[A]^{-1} = \frac{\begin{bmatrix} a_{22} & -a_{12} \\ -a_{21} & a_{11} \end{bmatrix}}{a_{11} \cdot a_{22} - a_{12} \cdot a_{21}} = \frac{\begin{bmatrix} -\omega^2 m_2 + i\omega c_2 + (k_2 + k_c) & k_c \\ k_c & -\omega^2 m_1 + i\omega c_1 + (k_1 + k_c) \end{bmatrix}}{(-\omega^2 m_1 + i\omega c_1 + (k_1 + k_c))(-\omega^2 m_2 + i\omega c_2 + (k_2 + k_c)) - {k_c}^2},$$

where we've replaced s with $i\omega$ relative to Eq. 10.46. The individual terms in the inverted $[A]$ matrix are:

$$[A]^{-1} = \begin{bmatrix} \frac{X_{1a}}{F_{1a}} & \frac{X_{1a}}{F_{1b}} \\ \frac{X_{1b}}{F_{1a}} & \frac{X_{1b}}{F_{1b}} \end{bmatrix} = \begin{bmatrix} H_{1a1a} & H_{1a1b} \\ H_{1b1a} & H_{1b1b} \end{bmatrix}. \tag{10.51}$$

10.5.3 Receptance Coupling

This case is displayed in Fig. 10.12 and is the same as the two-component flexible coupling example shown in Fig. 10.6. Replacing k with k_c in Eq. 10.22, we obtain Eq. 10.52.

$$\begin{aligned} \frac{X_{1b}}{F_{1b}} = \frac{x_{1b}}{F_{1b}} = \frac{h_{1b1b} f_{1b}}{F_{1b}} &= \frac{h_{1b1b}\left(1 - \left(h_{1a1a} + h_{1b1b} + \frac{1}{k_c}\right)^{-1} h_{1b1b}\right) F_{1b}}{F_{1b}} \\ \frac{X_{1b}}{F_{1b}} = H_{1b1b} &= h_{1b1b} - h_{1b1b}\left(h_{1a1a} + h_{1b1b} + \frac{1}{k_c}\right)^{-1} h_{1b1b} \end{aligned} \tag{10.52}$$

[3] As discussed in Sect. 5.2, complex matrix inversion, rather than modal analysis, is applied when the damping may not be proportional.

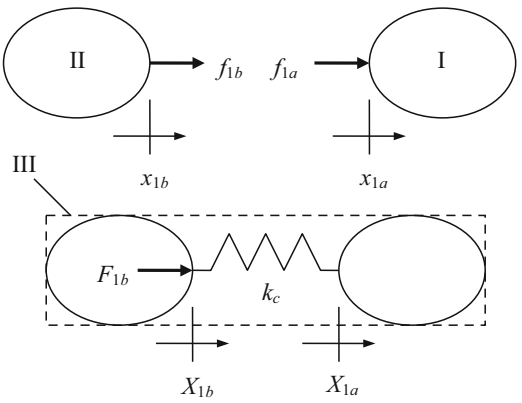

Fig. 10.12 Receptance coupling representation of joining spring-mass-damper systems I and II to form the two degree of freedom assembly III

Table 10.2 Mass, damping, and stiffness values for the two degree of freedom system in Fig. 10.11

Parameter	Value
m_1	3 kg
c_1	200 N s/m
k_1	2×10^6 N/m
m_2	2 kg
c_2	100 N s/m
k_2	1×10^6 N/m
k_c	5×10^5 N/m

To compare the three methods, we apply the mass, damping, and stiffness values shown in Table 10.2 to the model displayed in Fig. 10.11. We note that proportional damping exists ($\alpha = 0$ and $\beta = 1 \times 10^{-4}$) for the selected system, so the modal approach may be applied. The code used to produce Fig. 10.13, which displays both the component receptances and the assembly receptance computed using the three methods, is provided in MATLAB® MOJO 10.1. The frequency-dependent differences between the complex matrix inversion result, which was obtained through vector manipulations by calculating the H_{1b1b} result directly:

$$H_{1b1b} = \frac{-\omega^2 m_1 + i\omega c_1 + (k_1 + k_c)}{(-\omega^2 m_1 + i\omega c_1 + (k_1 + k_c))(-\omega^2 m_2 + i\omega c_2 + (k_2 + k_c)) - {k_c}^2},$$

and the modal and receptance coupling method results are displayed in Fig. 10.14. It is seen that the errors introduced by the modal method (top) are approximately 4×10^{13} times greater than the errors associated with the receptance technique (bottom). The differences between the three techniques are introduced by numerical round-off errors in the mathematical manipulations. However, the improved numerical accuracy obtained with receptance coupling (vector manipulations) over modal coupling (matrix manipulations) is another benefit of the receptance coupling approach.

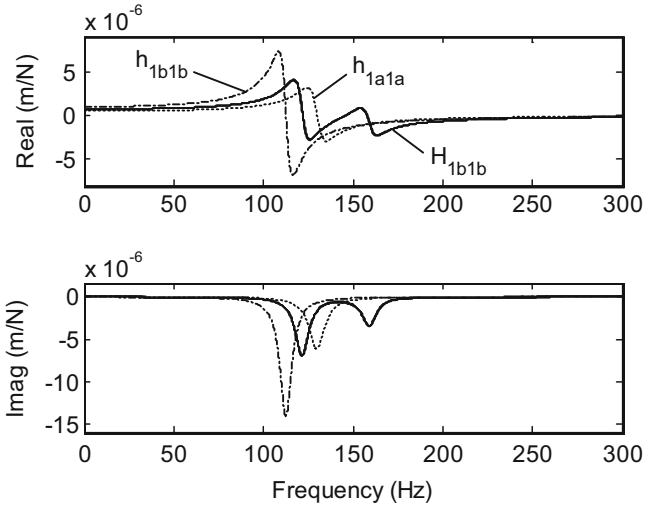

Fig. 10.13 Comparison of three methods for H_{1b1b} calculation. It is seen that the modal analysis, complex matrix inversion, and receptance coupling methods nominally agree (superimposed solid lines). The component receptances, h_{1a1a} and h_{1b1b}, are also shown

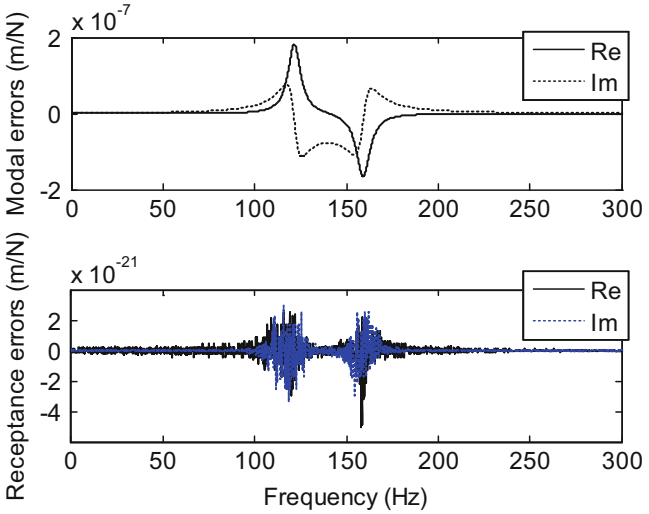

Fig. 10.14 Real and imaginary parts of the difference between complex matrix inversion and modal analysis (top) and real and imaginary parts of difference between complex matrix inversion and receptance coupling (bottom). Receptance coupling agrees more closely

In a Nutshell

Our comparison presumes that the receptances are accurately known. If they are obtained from measurements, this may not be the case. Measured FRFs are only known with finite frequency and amplitude resolution. Large modes require more digital bits to represent them and small modes may fall below the amplitude resolution (and not appear in the measurement). For high measurement bandwidths with reduced frequency resolution, modes with very low damping (and a corresponding narrow frequency range) may be misrepresented as well.

MATLAB® MOJO 10.1

```
% matlab_mojo_10_1.m

clear
close all
clc

% Define parameters in local coordinates
m1 = 3;       % kg
c1 = 200;      % N s/m
k1 = 2e6;      % N/m

m2 = 2;       % kg
c2 = 100;      % N s/m
k2 = 1e6;      % N/m

kc = 5e5;      % N/m

% Define I and II FRFs
w = (0:0.1:300)'*2*pi; % frequency, rad/s
FRF_I = 1./(-w.^2*m1 + 1i*w*c1 + k1);
FRF_II = 1./(-w.^2*m2 + 1i*w*c2 + k2);

% Receptance coupling
FRF_III_rc = FRF_II - FRF_II./(FRF_I + FRF_II + 1/kc).*FRF_II;

% Modal analysis
s_squared = roots([(m1*m2) (m1*(k2+kc)+m2*(k1+kc)) ((k1+kc)*(k2+kc)-
kc^2)]);
s1_squared = s_squared(1);
s2_squared = s_squared(2);
% Order natural frequencies so that wn1 < wn2
if s1_squared < s2_squared
  temp = s1_squared;
  s1_squared = s2_squared;
  s2_squared = temp;
end
```

```
wn1 = sqrt(-s1_squared);
wn2 = sqrt(-s2_squared);

p1 = kc/(m1*s1_squared + (k1+kc));
p2 = kc/(m1*s2_squared + (k1+kc));

% Local matrices
m = [m1 0; 0 m2];
c = [c1 0; 0 c2];
k = [k1+kc -kc; -kc k2+kc];

% Modal matrices
P = [p1 p2; 1 1];
mq = P'*m*P;
cq = P'*c*P;
kq = P'*k*P;

mq1 = mq(1,1);
mq2 = mq(2,2);
cq1 = cq(1,1);
cq2 = cq(2,2);
kq1 = kq(1,1);
kq2 = kq(2,2);

zetaq1 = cq1/(2*sqrt(kq1*mq1));
zetaq2 = cq2/(2*sqrt(kq2*mq2));

r1 = w/wn1;
r2 = w/wn2;

FRF_III_modal = 1/kq1*((1-r1.^2) - 1i*(2*zetaq1*r1))./((1-r1.^2).^2 +
(2*zetaq1*r1).^2) + 1/kq2*((1-r2.^2) - 1i*(2*zetaq2*r2))./((1-r2.
^2).^2 + (2*zetaq2*r2).^2);

% Complex matrix inversion
FRF_III_inversion = (-w.^2*m1 + 1i*w*c1 + k1 + kc)./((-w.^2*m1 + 1i*w*c1
+ k1 + kc).*(-w.^2*m2 + 1i*w*c2 + k2 + kc) - kc^2);

figure(1)
subplot(211)
plot(w/2/pi, real(FRF_I), 'k:', w/2/pi, real(FRF_II), 'k-.', w/2/pi,
real(FRF_III_rc), 'k', w/2/pi, real(FRF_III_modal), 'k', w/2/pi, real
(FRF_III_inversion), 'k')
ylim([-8e-6 9e-6])
set(gca,'FontSize', 14)
ylabel('Real (m/N)')
subplot(212)
plot(w/2/pi, imag(FRF_I), 'k:', w/2/pi, imag(FRF_II), 'k-.', w/2/pi,
imag(FRF_III_rc), 'k', w/2/pi, imag(FRF_III_modal), 'k', w/2/pi, imag
(FRF_III_inversion), 'k')
ylim([-16e-6 16e-7])
set(gca,'FontSize', 14)
```

```
xlabel('Frequency (Hz)')
ylabel('Imag (m/N)')

% Calculate differences
diff_modal = FRF_III_inversion - FRF_III_modal;
diff_rc = FRF_III_inversion - FRF_III_rc;

figure(2)
subplot(211)
plot(w/2/pi, real(diff_modal), 'k', w/2/pi, imag(diff_modal), 'k:')
legend('Re', 'Im')
ylim([-2e-7 2e-7])
set(gca,'FontSize', 14)
ylabel('Modal errors (m/N)')
subplot(212)
plot(w/2/pi, real(diff_rc), 'k', w/2/pi, imag(diff_rc), 'b:')
legend('Re', 'Im')
ylim([-6e-21 4e-21])
set(gca,'FontSize', 14)
xlabel('Frequency (Hz)')
ylabel('Receptance errors (m/N)')
```

10.6 Advanced Receptance Coupling[4]

In the previous sections we only considered transverse deflections, x_i and X_i, for the components and assembly due to internal and external forces, f_j and F_j. However, as we saw in Sects. 8.5 and 9.3 we must also consider **rotations** about lines perpendicular to the beam axis, θ_i and Θ_i, and **bending moments** (or couples), m_j and M_j, to completely describe the transverse dynamic behavior of beams.[5] To begin this discussion, let's consider the solid cylinder-prismatic cantilever beam assembly shown in Fig. 10.13. To determine the assembly dynamics, all four bending receptances must be included in the component descriptions (i.e., displacement-to-force, h_{ij}, displacement-to-couple, l_{ij}, rotation-to-force, n_{ij}, and rotation-to-couple, p_{ij}).

Let's now summarize the steps required to predict the Fig. 10.15 assembly receptances.

[4]The authors gratefully acknowledge contributions from Dr. T. Burns, National Institute of Standards and Technology, Dr. M. Davies, University of North Carolina at Charlotte, and Dr. G.S. Duncan, Valparaiso University, to the development of the Sect. 10.6 receptance coupling analysis.

[5]We will not consider axial or torsional vibrations in this analysis.

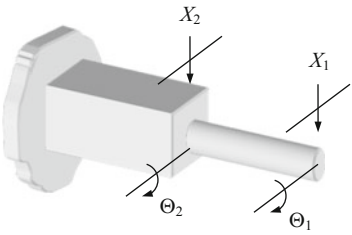

Fig. 10.15 Rigid coupling of solid cylinder and prismatic beam to form a cantilevered assembly

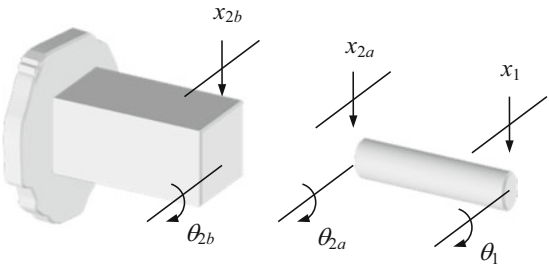

Fig. 10.16 Solid cylinder and prismatic beam components used to form cantilevered assembly

1. Define the components and coordinates for the model. In this example, we can select two components: a prismatic beam with fixed-free (or cantilever) boundary conditions and a cylinder with free-free (or unsupported) boundary conditions; see Fig. 10.16.
2. Determine the component receptances. We can use either measurements or models. For the models, an elegant choice is the closed-form receptances for flexural vibrations of uniform Euler-Bernoulli beams with free, fixed, sliding, and pinned boundary conditions that we discussed in Chap. 8 [1]. Of course, the Timoshenko beam model [2] may also be applied when increased accuracy is required, but we will leave the details of this analysis to a more advanced course. For measurements, we can follow the procedures outlined in Chap. 7.
3. Based on the model from step 1, express the assembly receptances as a function of the component receptances. As demonstrated in Sects. 10.2–10.4, we determine the assembly receptances using the component displacements/rotations, equilibrium conditions, and compatibility conditions.

We begin the analysis of the system shown in Figs. 10.15 and 10.16 by writing the component receptances. Note that we have placed coordinates at the prediction location (1) and coupling locations ($2a$ and $2b$) on the two components. For the cylinder, we have the following direct receptances at the coordinate 1 end:

$$h_{11} = \frac{x_1}{f_1} \quad l_{11} = \frac{x_1}{m_1} \quad n_{11} = \frac{\theta_1}{f_1} \quad p_{11} = \frac{\theta_1}{m_1}. \tag{10.53}$$

The corresponding cross receptances at the same location are:

$$h_{12a} = \frac{x_1}{f_{2a}} \quad l_{12a} = \frac{x_1}{m_{2a}} \quad n_{12a} = \frac{\theta_1}{f_{2a}} \quad p_{12a} = \frac{\theta_1}{m_{2a}}. \tag{10.54}$$

At coordinate $2a$ on the cylinder, the direct and cross receptances are written as shown in Eqs. 10.55 and 10.56, respectively.

$$h_{2a2a} = \frac{x_{2a}}{f_{2a}} \quad l_{2a2a} = \frac{x_{2a}}{m_{2a}} \quad n_{2a2a} = \frac{\theta_{2a}}{f_{2a}} \quad p_{2a2a} = \frac{\theta_{2a}}{m_{2a}} \tag{10.55}$$

$$h_{2a1} = \frac{x_{2a}}{f_1} \quad l_{2a1} = \frac{x_{2a}}{m_1} \quad n_{2a1} = \frac{\theta_{2a}}{f_1} \quad p_{2a1} = \frac{\theta_{2a}}{m_1} \tag{10.56}$$

Similarly, for the prismatic cantilever beam, the direct receptances at the coupling location $2b$ are described by Eq. 10.57.

$$h_{2b2b} = \frac{x_{2b}}{f_{2b}} \quad l_{2b2b} = \frac{x_{2b}}{m_{2b}} \quad n_{2b2b} = \frac{\theta_{2b}}{f_{2b}} \quad p_{2b2b} = \frac{\theta_{2b}}{m_{2b}} \tag{10.57}$$

To simplify notation, the component receptances can be compactly represented in matrix form as shown in Eqs. 10.58–10.61 for the cylinder and Eq. 10.62 for the prismatic beam:

$$\begin{Bmatrix} x_1 \\ \theta_1 \end{Bmatrix} = \begin{bmatrix} h_{11} & l_{11} \\ n_{11} & p_{11} \end{bmatrix} \begin{Bmatrix} f_1 \\ m_1 \end{Bmatrix} \quad \text{or} \quad \{u_1\} = [R_{11}]\{q_1\}, \tag{10.58}$$

$$\begin{Bmatrix} x_{2a} \\ \theta_{2a} \end{Bmatrix} = \begin{bmatrix} h_{2a2a} & l_{2a2a} \\ n_{2a2a} & p_{2a2a} \end{bmatrix} \begin{Bmatrix} f_{2a} \\ m_{2a} \end{Bmatrix} \quad \text{or} \quad \{u_{2a}\} = [R_{2a2a}]\{q_{2a}\}, \tag{10.59}$$

$$\begin{Bmatrix} x_1 \\ \theta_1 \end{Bmatrix} = \begin{bmatrix} h_{12a} & l_{12a} \\ n_{12a} & p_{12a} \end{bmatrix} \begin{Bmatrix} f_{2a} \\ m_{2a} \end{Bmatrix} \quad \text{or} \quad \{u_1\} = [R_{12a}]\{q_{2a}\}, \tag{10.60}$$

$$\begin{Bmatrix} x_{2a} \\ \theta_{2a} \end{Bmatrix} = \begin{bmatrix} h_{2a1} & l_{2a1} \\ n_{2a1} & p_{2a1} \end{bmatrix} \begin{Bmatrix} f_1 \\ m_1 \end{Bmatrix} \quad \text{or} \quad \{u_{2a}\} = [R_{2a1}]\{q_1\}, \quad \text{and} \tag{10.61}$$

$$\begin{Bmatrix} x_{2b} \\ \theta_{2b} \end{Bmatrix} = \begin{bmatrix} h_{2b2b} & l_{2b2b} \\ n_{2b2b} & p_{2b2b} \end{bmatrix} \begin{Bmatrix} f_{2b} \\ m_{2b} \end{Bmatrix} \quad \text{or} \quad \{u_{2b}\} = [R_{2b2b}]\{q_{2b}\}, \tag{10.62}$$

where R_{ij} is the **generalized receptance matrix** that describes both translational and rotational component behavior [3–5] and u_i and q_j are the corresponding **generalized**

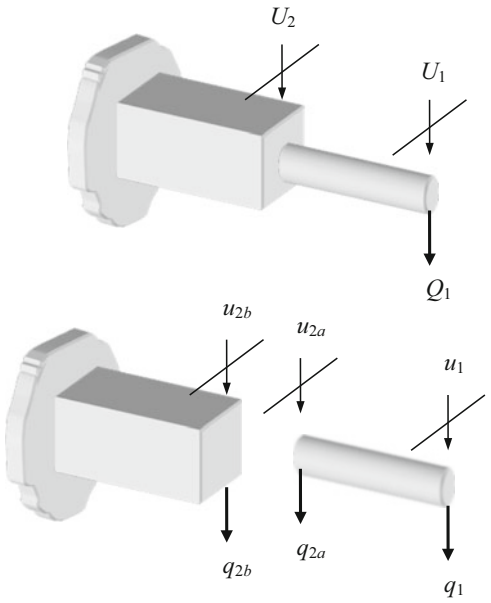

Fig. 10.17 Receptance coupling model for determining G_{11} and G_{21}. Rigid coupling is assumed

displacement/rotation and **force/couple** vectors. To visualize R_{ij}, we can think of each frequency-dependent 2×2 R_{ij} matrix as a page in a book where each page represents a different frequency value. Flipping through the book from front to back scans the frequency values from low to high through the modeled, or measured, bandwidth. Naturally, all receptances in the coupling analysis must be based on the same frequency vector (resolution and range).

We write the component receptances using the new notation as $u_1 = R_{11}q_1 + R_{12a}q_{2a}$ and $u_{2a} = R_{2a1}q_1 + R_{2a2a}q_{2a}$ for the cylinder and $u_{2b} = R_{2b2b}q_{2b}$ for the prismatic beam. If we apply a rigid connection between the two components, the compatibility condition is $u_{2b} - u_{2a} = 0$. Additionally, if we again specify that the component and assembly coordinates are at the same physical locations, then we have that $u_1 = U_1$ and $u_{2a} = u_{2b} = U_2$ (due to the rigid coupling).

We can write the assembly receptances as shown in Eq. 10.63, which again incorporates the generalized notation:

$$\begin{Bmatrix} U_1 \\ U_2 \end{Bmatrix} = \begin{bmatrix} G_{11} & G_{12} \\ G_{21} & G_{22} \end{bmatrix} \begin{Bmatrix} Q_1 \\ Q_2 \end{Bmatrix}, \tag{10.63}$$

where $U_i = \begin{Bmatrix} X_i \\ \Theta_i \end{Bmatrix}$, $G_{ij} = \begin{bmatrix} H_{ij} & L_{ij} \\ N_{ij} & P_{ij} \end{bmatrix}$, and $Q_j = \begin{Bmatrix} F_j \\ M_j \end{Bmatrix}$. To determine the assembly receptance at the free end of the cylinder, G_{11}, we apply Q_1 to coordinate U_1 as shown in Fig. 10.17, where the generalized U_i and u_i vectors are shown

schematically as "displacements", although we recognize that they describe both transverse deflection and rotation. The associated equilibrium conditions are $q_{2a} + q_{2b} = 0$ and $q_1 = Q_1$. By substituting the component displacements/rotations and equilibrium conditions into the compatibility condition, we obtain the expression for q_{2b} shown in Eq. 10.64. The component force q_{2a} is then determined from the equilibrium condition $q_{2a} = -q_{2b}$. The expression for G_{11} is given by Eq. 10.65. We find the corresponding cross receptance matrix, G_{21}, in a similar manner; see Eq. 10.66. Note that G_{11} and G_{21} comprise the first column of the receptance matrix in Eq. 10.63.

$$\begin{aligned} &u_{2b} - u_{2a} = 0 \\ &R_{2b2b}q_{2b} - R_{2a1}q_1 - R_{2a2a}q_{2a} = 0 \\ &(R_{2a2a} + R_{2b2b})q_{2b} - R_{2a1}Q_1 = 0 \\ &q_{2b} = (R_{2a2a} + R_{2b2b})^{-1}R_{2a1}Q_1 \end{aligned} \tag{10.64}$$

$$G_{11} = \frac{U_1}{Q_1} = \frac{u_1}{Q_1} = \frac{R_{11}q_1 + R_{12a}q_{2a}}{Q_1} = \frac{R_{11}Q_1 - R_{12a}(R_{2a2a} + R_{2b2b})^{-1}R_{2a1}Q_1}{Q_1}$$

$$G_{11} = R_{11} - R_{12a}(R_{2a2a} + R_{2b2b})^{-1}R_{2a1} = \begin{bmatrix} H_{11} & L_{11} \\ N_{11} & P_{11} \end{bmatrix} \tag{10.65}$$

$$G_{21} = \frac{U_2}{Q_1} = \frac{u_{2a}}{Q_1} = \frac{R_{2a1}q_1 + R_{2a2a}q_{2a}}{Q_1} = \frac{R_{2a1}Q_1 - R_{2a2a}(R_{2a2a} + R_{2b2b})^{-1}R_{2a1}Q_1}{Q_1}$$

$$G_{21} = R_{2a1} - R_{2a2a}(R_{2a2a} + R_{2b2b})^{-1}R_{2a1} = \begin{bmatrix} H_{21} & L_{21} \\ N_{21} & P_{21} \end{bmatrix} \tag{10.66}$$

To find the receptances in the second column of Eq. 10.63, we apply Q_2 at U_2, as shown in Fig. 10.18. The component receptances are $u_1 = R_{12a}q_{2a}$ and $u_{2a} = R_{2a2a}q_{2a}$ for the cylinder, and $u_{2b} = R_{2b2b}q_{2b}$ for the prismatic beam. For the rigid connection, the compatibility condition is again $u_{2b} - u_{2a} = 0$. The equilibrium condition is $q_{2a} + q_{2b} = Q_2$. By substituting the component displacements/rotations and equilibrium condition into the compatibility condition, we obtain the expression for q_{2b} shown in Eq. 10.67. The component force q_{2a} is then determined from the equilibrium condition $q_{2a} = Q_2 - q_{2b}$. The expression for G_{22} is provided by Eq. 10.68. We find the corresponding cross receptance matrix, G_{12}, in a similar manner as shown in Eq. 10.69.

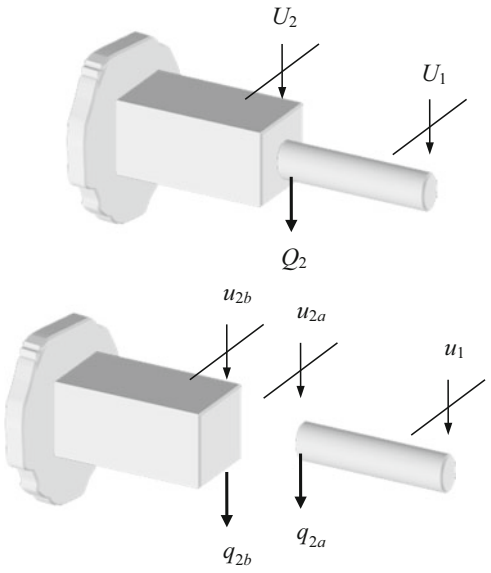

Fig. 10.18 Receptance coupling model for determining G_{22} and G_{12}. Rigid coupling is assumed

$$\begin{aligned}
&u_{2b} - u_{2a} = 0\\
&R_{2b2b}q_{2b} - R_{2a2a}q_{2a} = 0\\
&R_{2b2b}q_{2b} - R_{2a2a}Q_2 + R_{2a2a}q_{2b} = 0\\
&(R_{2a2a} + R_{2b2b})q_{2b} - R_{2a2a}Q_2 = 0\\
&q_{2b} = (R_{2a2a} + R_{2b2b})^{-1}R_{2a2a}Q_2
\end{aligned} \tag{10.67}$$

$$\begin{aligned}
G_{22} &= \frac{U_2}{Q_2} = \frac{u_{2a}}{Q_2} = \frac{R_{2a2a}q_{2a}}{Q_2} = \frac{R_{2a2a}\left(1 - (R_{2a2a} + R_{2b2b})^{-1}R_{2a2a}\right)Q_2}{Q_2}\\
G_{22} &= R_{2a2a} - R_{2a2a}(R_{2a2a} + R_{2b2b})^{-1}R_{2a2a} = \begin{bmatrix} H_{22} & L_{22} \\ N_{22} & P_{22} \end{bmatrix}
\end{aligned} \tag{10.68}$$

$$\begin{aligned}
G_{12} &= \frac{U_1}{Q_2} = \frac{u_1}{Q_2} = \frac{R_{12a}q_{2a}}{Q_2} = \frac{R_{12a}\left(1 - (R_{2a2a} + R_{2b2b})^{-1}R_{2a2a}\right)Q_2}{Q_2}\\
G_{12} &= R_{12a} - R_{12a}(R_{2a2a} + R_{2b2b})^{-1}R_{2a2a} = \begin{bmatrix} H_{12} & L_{12} \\ N_{12} & P_{12} \end{bmatrix}
\end{aligned} \tag{10.69}$$

We see that the procedure to model the systems with both displacements and rotations is analogous to the examples provided in Sections 10.2–10.4. Let's again summarize the receptance terms in tabular form; see Table 10.3. Due to the clear

Table 10.3 Direct and cross receptances for generalized two component coupling

	Substructure coordinates		Receptances			
R/F	I	II	D/C		Fig.	Eq.
R	u_1, u_{2a}	u_{2b}	D	$G_{11} = R_{11} - R_{12a}(R_{2a2a} + R_{2b2b})^{-1}R_{2a1}$	10.17	10.65
			C	$G_{21} = R_{2a1} - R_{2a2a}(R_{2a2a} + R_{2b2b})^{-1}R_{2a1}$		10.66
			D	$G_{22} = R_{2a2a} - R_{2a2a}(R_{2a2a} + R_{2b2b})^{-1}R_{2a2a}$	10.18	10.68
			C	$G_{12} = R_{12a} - R_{12a}(R_{2a2a} + R_{2b2b})^{-1}R_{2a2a}$		10.69

The connection type is rigid, R. The receptance type is direct, D, or cross, C. The figure and equation numbers are also included. Similarities to the corresponding entries in Table 10.1 are evident

similarities to Table 10.1, we will not derive the receptances for the other two component coupling cases. The only consideration is that for non-rigid coupling, we replace the scalar stiffness term, $\frac{1}{k}$, from the displacement-to-force analyses with the matrix expression $\left[\widetilde{k}\right]^{-1}$, where:

$$\left[\widetilde{k}\right] = \begin{bmatrix} k_{xf} & k_{\theta f} \\ k_{xm} & k_{\theta m} \end{bmatrix}.$$

The subscripts for the stiffness matrix entries indicate their function. For example, $k_{\theta f}$ represents resistance to rotation due to an applied force. As shown in Eq. 10.45, these four real-valued stiffness terms are augmented by the corresponding damping expressions if viscous damping is included at the coupling location [6]. The new complex, frequency-dependent stiffness matrix is:

$$\left[\widetilde{k}'\right] = \begin{bmatrix} k_{xf} + i\omega c_{xf} & k_{\theta f} + i\omega c_{\theta f} \\ k_{xm} + i\omega c_{xm} & k_{\theta m} + i\omega c_{\theta m} \end{bmatrix}.$$

In a Nutshell
More information about the dynamic behavior of a system enables improved modeling accuracy. Measurement of rotational FRFs is more complicated than the measurement of translational FRFs, but their inclusion increases the model fidelity.

10.7 Assembly Receptance Prediction

In Sect. 10.6, we provided the building blocks for assembly receptance predictions. In this section, we'll detail coupling examples to demonstrate their implementation.

10.7.1 Free-Free Beam Coupled to Rigid Support

As a test of the receptance coupling procedure, let's couple a free-free beam to a rigid support (i.e., a wall) to verify that it matches the fixed-free beam response we derived in Sect. 8.3.1. As described in Sect. 10.6, we have three primary tasks to complete in order to predict the assembly response. First, we must define the components and coordinates for the model. Here we have two components: a uniform beam with free-free boundary conditions and a rigid support (which exhibits zero receptances); see Fig. 10.19. Second, we need to determine the component receptances. We will apply the Euler-Bernoulli beam receptances provided in Table 8.3. Third, based on the selected model, we express the assembly receptances as a function of the component receptances as shown in Table 10.3.

Let's define the free-free beam to be a solid steel cylinder with a diameter of 10 mm and a length of 125 mm. The elastic modulus is 200 GPa and the density is 7800 kg/m^3. We'll select the solid damping factor to be 0.01 for plotting purposes, but in practice a value closer to 0.001 would be more realistic. The free-free cylinder's direct and cross receptance equations are provided in Table 8.3, while the wall receptances are zero. To calculate λ, we need the frequency vector ω (rad/s), cross sectional area, A, and second moment of area, I. We'll use a frequency range of 5000 Hz with a resolution of 0.1 Hz. The variables A and I are defined in Eqs. 10.70 and 10.71 for the cylinder, where d is the cylinder diameter. The displacement-to-force direct receptance for the free-free cylinder, h_{11}, is shown in Fig. 10.20. We see a first bending natural frequency of 2884.9 Hz. The rigid body behavior is exhibited as the rapid decrease in the real part as the frequency approaches zero.

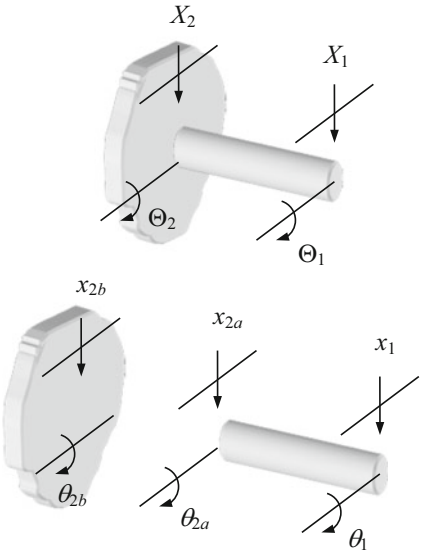

Fig. 10.19 Rigid coupling of a free-free cylinder to a wall

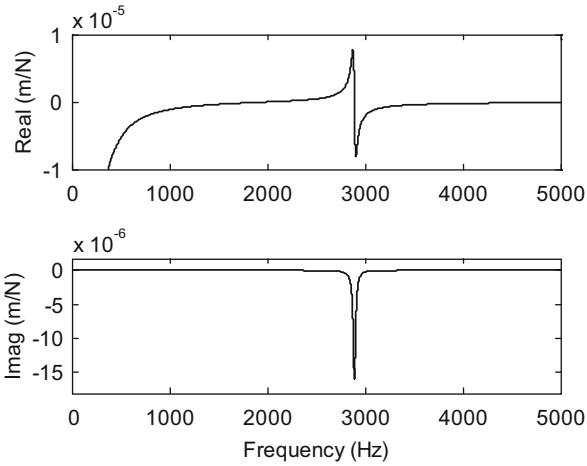

Fig. 10.20 Free-free receptance, h_{11}, for 10 mm diameter by 125 mm long steel cylinder

$$A = \frac{\pi d^2}{4} \tag{10.70}$$

$$I = \frac{\pi d^4}{64} \tag{10.71}$$

To rigidly couple the free-free cylinder to the wall, we apply Eq. 10.65:

$$G_{11} = \begin{bmatrix} H_{11} & L_{11} \\ N_{11} & P_{11} \end{bmatrix} = R_{11} - R_{12a}(R_{2a2a} + R_{2b2b})^{-1} R_{2a1},$$

where the generalized receptance matrices R_{11}, R_{12a}, R_{2a2a}, and R_{2a1} correspond to the free-free cylinder and R_{2b2b} characterizes the wall response. The code provided in MATLAB® MOJO 10.2 is used to complete the receptance coupling procedure. The results are displayed in Figs. 10.21 and 10.22. Figure 10.21 shows the assembly H_{11} response from the $G_{11}(1,1)$ position (solid line). The dotted line in the figure is the clamped-free response, $H_{11} = \frac{-c_1}{\lambda^3 c_8}$, from Table 8.3. We see that the two curves are identical and the rigid body behavior is no longer present due to the coupling conditions. A limited frequency range is displayed in Fig. 10.22 to enable closer comparison of the first bending mode. However, all bending modes are included in the Euler-Bernoulli beam receptances. The frequency range is increased in Fig. 10.23 to show the first two assembly bending modes. The vertical axis (response magnitude) is logarithmic in this plot because the second mode magnitude is much smaller than the first. Again, we observe exact agreement between the receptance coupling result (solid) and clamped-free receptance (dotted). Figure 10.23 displays not only the two resonant peaks at 453.4 and 2841.4 Hz, but also the anti-resonance

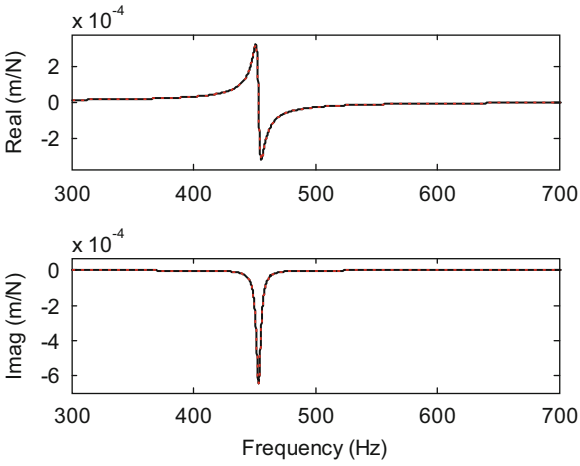

Fig. 10.21 Comparison of H_{11} receptance coupling result (solid line) and fixed-free response (dotted) for 10 mm diameter by 125 mm long steel cylinder

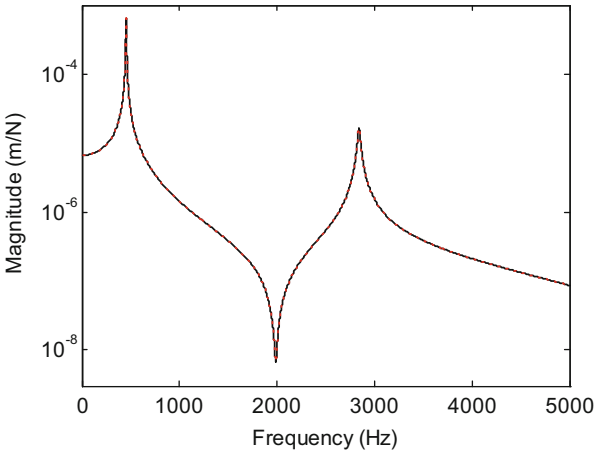

Fig. 10.22 Semi-logarithmic plot showing the first two bending modes for H_{11} tip receptances obtained from: (1) rigid coupling of free-free beam to wall (solid line); and (2) fixed-free response (dotted)

at 1988.1 Hz. At this frequency, the response is very small, even for large input force magnitudes.

The rotation-to-couple free end receptance determined from the rigid free-free beam coupling to the wall is also calculated using the code in MATLAB® MOJO 10.2. This $G_{11}(2,2)$ entry is shown in Fig. 10.23 (solid line). The fixed-free response (dotted line) from Table 8.3, $P_{11} = \frac{c_5}{\lambda c_8}$, again agrees with the receptance coupling result. We also see that the first mode natural frequency matches the H_{11} result (453.4 Hz), but the magnitude is quite different; note the new units of rad/(N m).

We've already noted that the assembly cross receptances, G_{12} and G_{21}, and the direct receptances at the fixed end, G_{22}, are zero. We can verify this by direct application of Eqs. 10.66, 10.68, and 10.69. For the fixed end direct receptance, Eq. 10.68 simplifies as shown in Eq. 10.72.

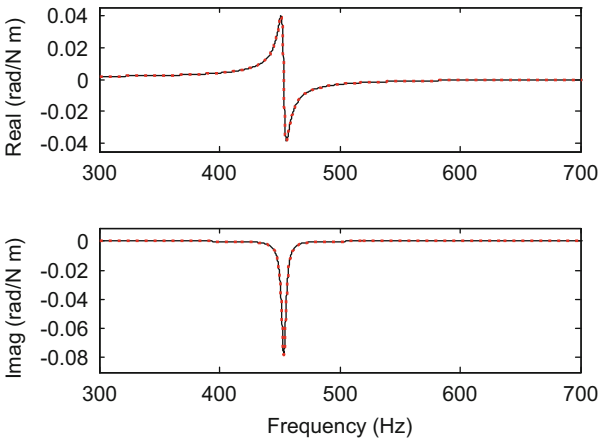

Fig. 10.23 Comparison of P_{11} receptance coupling result (solid line) and fixed-free response (dotted) for 10 mm diameter by 125 mm long steel cylinder

$$
\begin{aligned}
G_{22} &= R_{2a2a} - R_{2a2a}(R_{2a2a} + R_{2b2b})^{-1} R_{2a2a} \\
G_{22} &= R_{2a2a} - R_{2a2a}\left(R_{2a2a} + \begin{bmatrix} 0 & 0 \\ 0 & 0 \end{bmatrix}\right)^{-1} R_{2a2a} \\
G_{22} &= R_{2a2a} - R_{2a2a}(R_{2a2a})^{-1} R_{2a2a} = R_{2a2a} - R_{2a2a} = 0
\end{aligned}
\tag{10.72}
$$

Similar results are obtained for the cross receptances in Eqs. 10.66 and 10.69 when substituting $R_{2b2b} = \begin{bmatrix} 0 & 0 \\ 0 & 0 \end{bmatrix}$.

MATLAB® MOJO 10.2

```
% matlab_mojo_10_2.m

clear
close all
clc

% Define free-free cylinder receptances
w = (1:0.1:5000)*2*pi;    % frequency, rad/s
E = 200e9;              % elastic modulus, N/m^2
d = 10e-3;              % diameter, m
L = 125e-3;              % length, m
I = pi*d^4/64;             % 2nd moment of area, m^4
rho = 7800;              % density, kg/m^3
A = pi*d^2/4;             % cross sectional area, m^2
eta = 0.01;              % solid damping factor
EI = E*I*(1+1i*eta);      % complex stiffness, N-m^2
lambda = (w.^2*rho*A/EI).^0.25;
c1 = cos(lambda*L).*sinh(lambda*L) - sin(lambda*L).*cosh(lambda*L);
c2 = sin(lambda*L).*sinh(lambda*L);
c3 = sin(lambda*L) - sinh(lambda*L);
c4 = cos(lambda*L) - cosh(lambda*L);
```

```
c5 = cos(lambda*L).*sinh(lambda*L) + sin(lambda*L).*cosh(lambda*L);
c6 = sin(lambda*L) + sinh(lambda*L);
c7 = EI*(cos(lambda*L).*cosh(lambda*L)-1);
c8 = EI*(cos(lambda*L).*cosh(lambda*L)+1);

h11 = -c1./(lambda.^3.*c7);
l11 = c2./(lambda.^2.*c7);
n11 = l11;
p11 = c5./(lambda.*c7);

h2a2a = -c1./(lambda.^3.*c7);
l2a2a = -c2./(lambda.^2.*c7);
n2a2a = l2a2a;
p2a2a = c5./(lambda.*c7);

h12a = c3./(lambda.^3.*c7);
l12a = -c4./(lambda.^2.*c7);
n12a = c4./(lambda.^2.*c7);
p12a = c6./(lambda.*c7);

h2a1 = h12a;
l2a1 = n12a;
n2a1 = l12a;
p2a1 = p12a;

% Define wall receptances
h2b2b = zeros(1, length(w));
l2b2b = zeros(1, length(w));
n2b2b = zeros(1, length(w));
p2b2b = zeros(1, length(w));

% Calculate assembly receptances
for cnt = 1:length(w)
  % Define generalized receptance matrices
  % Free-free cylinder
  R11 = [h11(cnt) l11(cnt); n11(cnt) p11(cnt)];
  R12a = [h12a(cnt) l12a(cnt); n12a(cnt) p12a(cnt)];
  R2a2a = [h2a2a(cnt) l2a2a(cnt); n2a2a(cnt) p2a2a(cnt)];
  R2a1 = [h2a1(cnt) l2a1(cnt); n2a1(cnt) p2a1(cnt)];

  % Rigid wall
  R2b2b = [h2b2b(cnt) l2b2b(cnt); n2b2b(cnt) p2b2b(cnt)];

  % Generalized assembly receptance matrix
  G11 = R11 - R12a/(R2a2a + R2b2b)*R2a1;

  % Individual terms in G11
  H11(cnt) = G11(1,1);
  L11(cnt) = G11(1,2);
  N11(cnt) = G11(2,1);
  P11(cnt) = G11(2,2);
end
```

```
% Define fixed-free cylinder receptances
H11cf = -c1./(lambda.^3.*c8);
L11cf = c2./(lambda.^2.*c8);
N11cf = L11cf;
P11cf = c5./(lambda.*c8);

figure(1)
subplot(211)
plot(w/2/pi, real(h11), 'k')
ylim([-1e-5 1e-5])
set(gca,'FontSize', 14)
ylabel('Real (m/N)')
subplot(212)
plot(w/2/pi, imag(h11), 'k')
ylim([-1.8e-5 1.8e-6])
set(gca,'FontSize', 14)
xlabel('Frequency (Hz)')
ylabel('Imag (m/N)')

figure(2)
subplot(211)
plot(w/2/pi, real(H11), 'k', w/2/pi, real(H11cf), 'r:')
axis([300 700 -3.75e-4 3.75e-4])
set(gca,'FontSize', 14)
ylabel('Real (m/N)')
subplot(212)
plot(w/2/pi, imag(H11), 'k', w/2/pi, imag(H11cf), 'r:')
axis([300 700 -7e-4 7e-5])
set(gca,'FontSize', 14)
xlabel('Frequency (Hz)')
ylabel('Imag (m/N)')

figure(3)
semilogy(w/2/pi, abs(H11), 'k', w/2/pi, abs(H11cf), 'r:')
ylim([3e-9 1e-3])
set(gca,'FontSize', 14)
xlabel('Frequency (Hz)')
ylabel('Magnitude (m/N)')

figure(4)
subplot(211)
plot(w/2/pi, real(P11), 'k', w/2/pi, real(P11cf), 'r:')
axis([300 700 -0.045 0.045])
set(gca,'FontSize', 14)
ylabel('Real (rad/(N-m))')
subplot(212)
plot(w/2/pi, imag(P11), 'k', w/2/pi, imag(P11cf), 'r:')
axis([300 700 -0.09 0.009])
set(gca,'FontSize', 14)
xlabel('Frequency (Hz)')
ylabel('Imag (rad/(N-m))')
```

10.7.2 Free-Free Beam Coupled to Fixed-Free Beam

Let's now consider the case depicted in Fig. 10.15. A 10 mm diameter by 100 mm long steel cylinder (free-free boundary conditions) is to be rigidly coupled to a fixed-free 50 mm by 50 mm by 200 mm long steel prismatic beam. The steel elastic modulus, density, and solid damping factor are 200 GPa, 7800 kg/m^3, and 0.01, respectively. (Again, we selected the solid damping value to be artificially high for display purposes.) The analysis is the same as described in Sect. 10.7.1 except that the R_{2b2b} receptances are no longer zero. They are now defined as shown in Table 8.3 for a fixed-free beam, $h_{2b2b} = \frac{-c_1}{\lambda^3 c_8}$, $l_{2b2b} = n_{2b2b} = \frac{c_2}{\lambda^2 c_8}$, and $p_{2b2b} = \frac{c_5}{\lambda c_8}$. We'll again use a frequency range of 5000 Hz with a resolution of 0.1 Hz to calculate λ. The variables A and I are defined in Eqs. 10.73 and 10.74 for the square prismatic beam, where s is the side length of 50 mm. The displacement-to-force direct receptance for the free-free cylinder, h_{11}, is shown in Fig. 10.24 (solid line). The fixed-free square beam tip receptance, h_{2b2b}, is also displayed (dotted line). We see a first bending natural frequency of 4507.6 Hz for the free-free beam. The fixed-free beam has a first bending frequency of 1022.5 Hz.

$$A = s^2 \tag{10.73}$$

$$I = \frac{s^4}{12} \tag{10.74}$$

The application of Eq. 10.65 to this scenario using the code provided in MATLAB® MOJO 10.3 gives Fig. 10.25, which shows H_{11} for the assembly. We see two modes within the 1500 Hz frequency range: one at 1045.2 Hz, near the original fixed-free

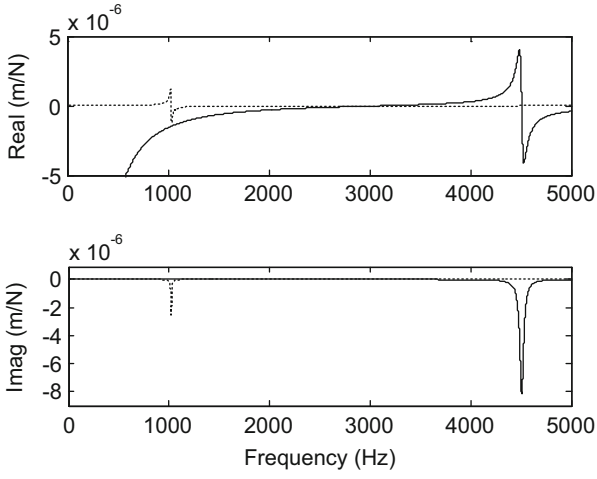

Fig. 10.24 Free-free receptance, h_{11}, for 10 mm diameter by 100 mm long steel cylinder (solid line) and fixed-free receptance, h_{2b2b}, for 50 mm square by 200 mm long steel prismatic beam (dotted line)

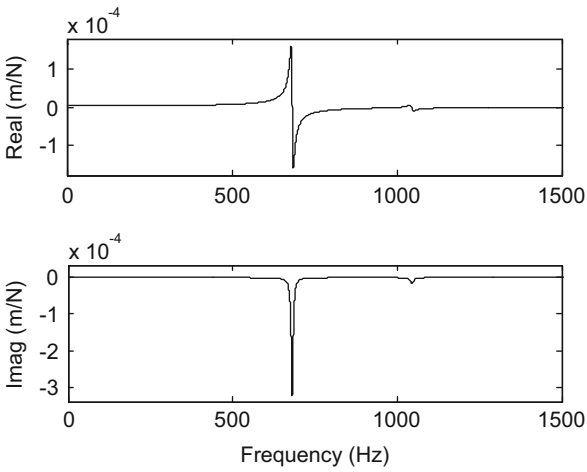

Fig. 10.25 Assembly displacement-to-force tip receptance H_{11} for the rigidly coupled cylinder and prismatic beam shown in Fig. 10.15

response, and a second more flexible mode at 680.9 Hz due to the now coupled cylinder. Because the prismatic beam is much stiffer than the cylinder, it appears to serve as a nearly rigid support for the cylinder. This may lead us to believe that approximating the assembly as a cylinder clamped to a wall is adequate. However, let's investigate what happens if we modify the prismatic beam to reduce its first bending frequency to a value near the fixed-free cylinder's first bending frequency.

MATLAB® MOJO 10.3

```
% matlab_mojo_10_3.m

clear
close all
clc

% Define free-free cylinder receptances
w = (1:0.1:5000)*2*pi;    % frequency, rad/s
E = 200e9;              % elastic modulus, N/m^2
d = 10e-3;              % diameter, m
L = 100e-3;              % length, m
I = pi*d^4/64;             % 2nd moment of area, m^4
rho = 7800;              % density, kg/m^3
A = pi*d^2/4;             % cross sectional area, m^2
eta = 0.01;              % solid damping factor
EI = E*I*(1+1i*eta);     % complex stiffness, N-m^2
lambda = (w.^2*rho*A/EI).^0.25;
c1 = cos(lambda*L).*sinh(lambda*L) - sin(lambda*L).*cosh(lambda*L);
c2 = sin(lambda*L).*sinh(lambda*L);
c3 = sin(lambda*L) - sinh(lambda*L);
c4 = cos(lambda*L) - cosh(lambda*L);
c5 = cos(lambda*L).*sinh(lambda*L) + sin(lambda*L).*cosh(lambda*L);
c6 = sin(lambda*L) + sinh(lambda*L);
```

```
c7 = EI*(cos(lambda*L).*cosh(lambda*L)-1);
c8 = EI*(cos(lambda*L).*cosh(lambda*L)+1);

h11 = -c1./(lambda.^3.*c7);
l11 = c2./(lambda.^2.*c7);
n11 = l11;
p11 = c5./(lambda.*c7);

h2a2a = -c1./(lambda.^3.*c7);
l2a2a = -c2./(lambda.^2.*c7);
n2a2a = l2a2a;
p2a2a = c5./(lambda.*c7);

h12a = c3./(lambda.^3.*c7);
l12a = -c4./(lambda.^2.*c7);
n12a = c4./(lambda.^2.*c7);
p12a = c6./(lambda.*c7);

h2a1 = h12a;
l2a1 = n12a;
n2a1 = l12a;
p2a1 = p12a;

% Define fixed-free prismatic beam receptances
E = 200e9;          % elastic modulus, N/m^2
s = 50e-3;          % square side, m
L = 200e-3;          % length, m
I = s^4/12;          % 2nd moment of area, m^4
rho = 7800;          % density, kg/m^3
A = s^2;           % cross sectional area, m^2
eta = 0.01;          % solid damping factor
EI = E*I*(1+1i*eta);     % complex stiffness, N-m^2
lambda = (w.^2*rho*A/EI).^0.25;
c1 = cos(lambda*L).*sinh(lambda*L) - sin(lambda*L).*cosh(lambda*L);
c2 = sin(lambda*L).*sinh(lambda*L);
c3 = sin(lambda*L) - sinh(lambda*L);
c4 = cos(lambda*L) - cosh(lambda*L);
c5 = cos(lambda*L).*sinh(lambda*L) + sin(lambda*L).*cosh(lambda*L);
c6 = sin(lambda*L) + sinh(lambda*L);
c7 = EI*(cos(lambda*L).*cosh(lambda*L)-1);
c8 = EI*(cos(lambda*L).*cosh(lambda*L)+1);
h2b2b = -c1./(lambda.^3.*c8);
l2b2b = c2./(lambda.^2.*c8);
n2b2b = l2b2b;
p2b2b = c5./(lambda.*c8);

% Calculate assembly receptances
for cnt = 1:length(w)
  % Define generalized receptance matrices
  % Free-free cylinder
  R11 = [h11(cnt) l11(cnt); n11(cnt) p11(cnt)];
  R12a = [h12a(cnt) l12a(cnt); n12a(cnt) p12a(cnt)];
```

```
  R2a2a = [h2a2a(cnt) l2a2a(cnt); n2a2a(cnt) p2a2a(cnt)];
  R2a1 = [h2a1(cnt) l2a1(cnt); n2a1(cnt) p2a1(cnt)];

  % Prismatic beam
  R2b2b = [h2b2b(cnt) l2b2b(cnt); n2b2b(cnt) p2b2b(cnt)];

  % Generalized assembly receptance matrix
  G11 = R11 - R12a/(R2a2a + R2b2b)*R2a1;

  % Individual terms in G11
  H11(cnt) = G11(1,1);
  L11(cnt) = G11(1,2);
  N11(cnt) = G11(2,1);
  P11(cnt) = G11(2,2);
end

figure(1)
subplot(211)
plot(w/2/pi, real(h11), 'k', w/2/pi, real(h2b2b), 'k:')
ylim([-5e-6 5e-6])
set(gca,'FontSize', 14)
ylabel('Real (m/N)')
subplot(212)
plot(w/2/pi, imag(h11), 'k', w/2/pi, imag(h2b2b), 'k:')
ylim([-9e-6 9e-7])
set(gca,'FontSize', 14)
xlabel('Frequency (Hz)')
ylabel('Imag (m/N)')

figure(2)
subplot(211)
plot(w/2/pi, real(H11), 'k')
axis([0 1500 -1.8e-4 1.8e-4])
set(gca,'FontSize', 14)
ylabel('Real (m/N)')
subplot(212)
plot(w/2/pi, imag(H11), 'k')
axis([0 1500 -3.4e-4 3.4e-5])
set(gca,'FontSize', 14)
xlabel('Frequency (Hz)')
ylabel('Imag (m/N)')
```

Figure 10.26 displays h_{11} for the free-free cylinder (solid line), as well as h_{2b2b} for a longer (250 mm) fixed-free prismatic beam (dotted line). The cylinder's first bending natural frequency remains at 4507.6 Hz for the free-free boundary conditions. However, the first bending frequency for the extended fixed-free beam is reduced to 654.4 Hz. Figure 10.27 shows H_{11} for the cylinder rigidly coupled to the 50 mm square by 250 mm long prismatic beam. The response is now quite different than the assembly receptance shown in Fig. 10.25 for the 200 mm long prismatic beam. Even though the cylinder is coupled to a more flexible base (i.e., a longer

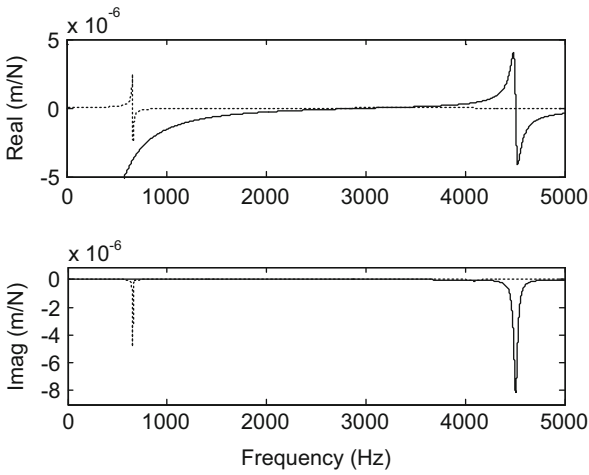

Fig. 10.26 Free-free receptance, h_{11}, for 10 mm diameter by 100 mm long steel cylinder (solid line) and clamped-free receptance, h_{2b2b}, for 50 mm square by 250 mm long steel prismatic beam (dotted line)

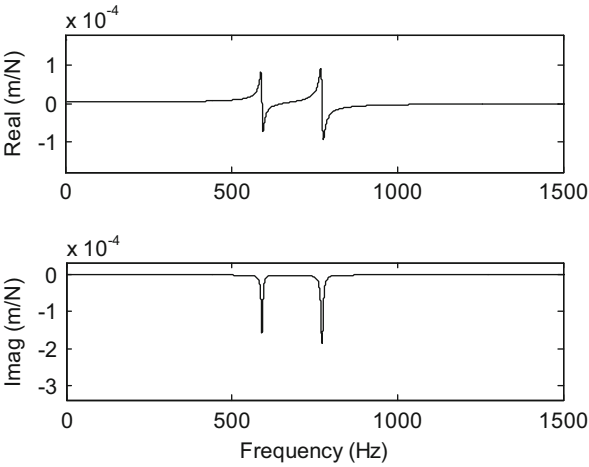

Fig. 10.27 The displacement-to-force tip receptance, H_{11}, for rigid coupling of the 10 mm diameter by 100 mm long cylinder to the 50 mm square by 250 mm long prismatic beam is displayed

fixed-free beam), the assembly response has a smaller peak magnitude. The minimum imaginary value for the new assembly is -1.865×10^{-4} m/N, while the corresponding value for the shorter (and stiffer) prismatic beam assembly was -3.222×10^{-4} m/N; this represents a 42% compliance[6] reduction. The compliance reduction, or, equivalently, the stiffness increase, is due to interaction between the two beams in a manner analogous to the dynamic absorber we discussed in Sect. 5.4. When the fixed-free prismatic beam's natural frequency is near the coupled cylinder's natural frequency, some energy is able to "pass through" the cylinder and excite the stiffer base. The result is that the energy is more equally partitioned between the two modes and the assembly response appears stiffer [7]. An electrical

[6]Compliance is the inverse of stiffness.

equivalent is the impedance matching strategy used at cable connections. For example, it is common to use 50 Ω terminations at all connections to encourage signal transmission and avoid reflection.

10.7.3 Comparison Between Model and BEP Measurement

In Sect. 8.6.1, we compared an Euler-Bernoulli fixed-free beam prediction to a measurement completed on the BEP. The impact test carried out on the BEP is described in Sect. 7.4, where the 12.7 mm diameter cantilevered steel rod was extended 130 mm beyond the base (see Fig. 7.20). Now let's model the extended portion of the steel rod as a free-free beam and couple it to a rigid support (wall) to predict the fixed-free response of the assembly. We can then compare the prediction to the measurement result (see Fig. 7.21).

For the 12.7 mm diameter rod, the second moment of area is:

$$I = \frac{\pi d^4}{64} = \frac{\pi(0.0127)^4}{64} = 1.277 \times 10^{-9}\,\mathrm{m}^4$$

and the cross-sectional area, A, is:

$$A = \frac{\pi d^2}{4} = \frac{\pi(0.0127)^2}{4} = 1.267 \times 10^{-4}\,\mathrm{m}^2.$$

For the steel rod, let's use $\rho = 7800$ kg/m^3, $E = 200$ GPa, and $\eta = 0.002$. The coupling proceeds as detailed in MATLAB® MOJO 10.2, but with the new rod dimensions. Figure 10.28 shows H_{11} for the rod rigidly coupled to the wall. We observe that the fixed-free prediction has a natural frequency that is too high and the damping is too low. As discussed in Sect. 8.6.1, the split-clamp used to secure the rod in the BEP holder does not provide an ideal fixed boundary condition. In order to incorporate the flexibility and damping in the clamping interface into the receptance coupling model, we can modify Eq. 10.65 using the complex stiffness matrix defined in Sect. 10.6:

$$\left[\widetilde{k}'\right] = \begin{bmatrix} k_{xf} + i\omega c_{xf} & k_{\theta f} + i\omega c_{\theta f} \\ k_{xm} + i\omega c_{xm} & k_{\theta m} + i\omega c_{\theta m} \end{bmatrix}.$$

The modified Eq. 10.65 used to predict H_{11} is:

$$G_{11} = R_{11} - R_{12a}\left(R_{2a2a} + R_{2b2b} + \left[\widetilde{k}'\right]^{-1}\right)^{-1} R_{2a1}. \tag{10.75}$$

If the complex stiffness matrix is specified to be:

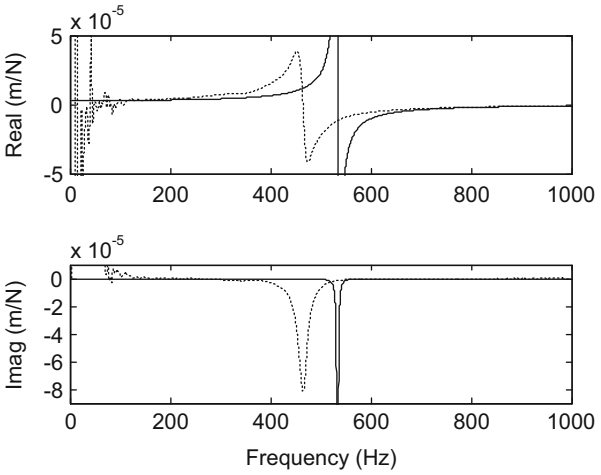

Fig. 10.28 Comparison between the free-free boundary condition rod rigidly coupled to a wall (solid line) and the BEP measurement (dotted line)

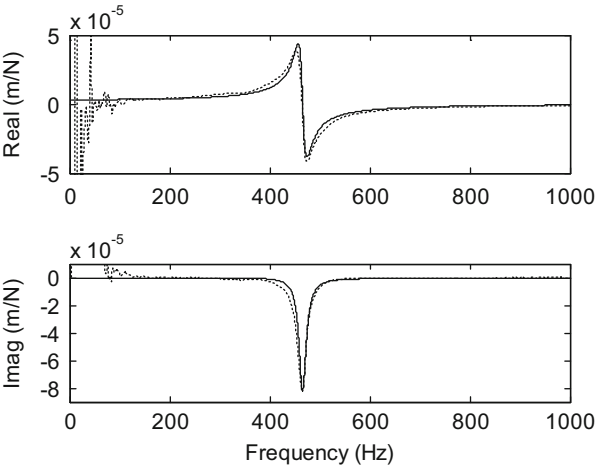

Fig. 10.29 Comparison between the free-free boundary condition rod coupled to a wall using a flexible-damped connection (solid line) and the BEP measurement (dotted line)

$$\left[\widetilde{k}'\right] = \begin{bmatrix} 3 \times 10^6 + i\omega 70 & 3.5 \times 10^5 + i\omega 20 \\ 3.5 \times 10^5 + i\omega 20 & 2 \times 10^3 + i\omega 5 \end{bmatrix},$$

the result displayed in Fig. 10.29 is obtained. We see that the additional flexibility and damping at the connection between the free-free rod and wall improves the agreement between the model and measurement. The code used to carry out this receptance coupling exercise is provided in MATLAB® MOJO 10.4.

MATLAB® MOJO 10.4

```
% matlab_mojo_10_4.m

clear
close all
clc

% Define free-free cylinder receptances
w = (1:0.1:1000)*2*pi;    % frequency, rad/s
E = 200e9;          % elastic modulus, N/m^2
d = 12.7e-3;         % diameter, m
L = 130e-3;         % length, m
I = pi*d^4/64;        % 2nd moment of area, m^4
rho = 7800;         % density, kg/m^3
A = pi*d^2/4;         % cross sectional area, m^2
eta = 0.002;         % solid damping factor
EI = E*I*(1+1i*eta);     % complex stiffness, N-m^2
lambda = (w.^2*rho*A/EI).^0.25;
c1 = cos(lambda*L).*sinh(lambda*L) - sin(lambda*L).*cosh(lambda*L);
c2 = sin(lambda*L).*sinh(lambda*L);
c3 = sin(lambda*L) - sinh(lambda*L);
c4 = cos(lambda*L) - cosh(lambda*L);
c5 = cos(lambda*L).*sinh(lambda*L) + sin(lambda*L).*cosh(lambda*L);
c6 = sin(lambda*L) + sinh(lambda*L);
c7 = EI*(cos(lambda*L).*cosh(lambda*L)-1);
c8 = EI*(cos(lambda*L).*cosh(lambda*L)+1);

h11 = -c1./(lambda.^3.*c7);
l11 = c2./(lambda.^2.*c7);
n11 = l11;
p11 = c5./(lambda.*c7);

h2a2a = -c1./(lambda.^3.*c7);
l2a2a = -c2./(lambda.^2.*c7);
n2a2a = l2a2a;
p2a2a = c5./(lambda.*c7);

h12a = c3./(lambda.^3.*c7);
l12a = -c4./(lambda.^2.*c7);
n12a = c4./(lambda.^2.*c7);
p12a = c6./(lambda.*c7);

h2a1 = h12a;
l2a1 = n12a;
n2a1 = l12a;
p2a1 = p12a;

% Define wall receptances
h2b2b = zeros(1, length(w));
l2b2b = zeros(1, length(w));
```

```
n2b2b = zeros(1, length(w));
p2b2b = zeros(1, length(w));

% Calculate assembly receptances
for cnt = 1:length(w)
  % Define generalized receptance matrices
  % Free-free cylinder
  R11 = [h11(cnt) l11(cnt); n11(cnt) p11(cnt)];
  R12a = [h12a(cnt) l12a(cnt); n12a(cnt) p12a(cnt)];
  R2a2a = [h2a2a(cnt) l2a2a(cnt); n2a2a(cnt) p2a2a(cnt)];
  R2a1 = [h2a1(cnt) l2a1(cnt); n2a1(cnt) p2a1(cnt)];

  % Rigid wall
  R2b2b = [h2b2b(cnt) l2b2b(cnt); n2b2b(cnt) p2b2b(cnt)];

  % Complex connection stiffness
  k = [3e6 + 1i*w(cnt)*70 3.5e5 + 1i*w(cnt)*20; 3.5e5 + 1i*w(cnt)*20 2e3 +
1i*w(cnt)*5];
  invk = inv(k);

  % Generalized assembly receptance matrix
  G11 = R11 - R12a/(R2a2a + R2b2b + invk)*R2a1;

  % Individual terms in G11
  H11(cnt) = G11(1,1);
  L11(cnt) = G11(1,2);
  N11(cnt) = G11(2,1);
  P11(cnt) = G11(2,2);
end

figure(1)
subplot(211)
plot(w/2/pi, real(H11), 'k')
axis([0 1000 -5e-5 5e-5])
set(gca,'FontSize', 14)
ylabel('Real (m/N)')
subplot(212)
plot(w/2/pi, imag(H11), 'k')
axis([0 1000 -9e-5 1e-5])
set(gca,'FontSize', 14)
xlabel('Frequency (Hz)')
ylabel('Imag (m/N)')
```

In a Nutshell
The ability to mathematically predict dynamic system behavior, to experimentally measure dynamic system behavior, and to combine measurements and computations is a powerful tool. The objective of this book is the description and demonstration of these techniques and illustration of their wide application range.

Chapter Summary
- The vibrating behavior of structures can be described using discrete models, continuous beam models, or measurements.
- The responses of individual components, or substructures, can be combined using receptance coupling to predict the assembly's response.
- The coupling between components can be rigid, flexible, or flexible with damping.
- The receptance coupling approach can incorporate not only transverse deflections due to forces, but also rotations and bending couples.

Exercises

1. Determine the direct frequency response function, $\frac{X_2}{F_2}$, for the two degree of freedom system shown in Fig. P10.1 using receptance coupling. Express your final result as a function of m, c, k, and the excitation frequency, ω. You may assume a harmonic forcing function, $F_2 e^{i\omega t}$, is applied to coordinate X_2.
2. Determine the direct frequency response function, $\frac{X_1}{F_1}$, for the two degree of freedom system shown in Fig. P10.2 using receptance coupling. Express your final result as a function of m, c, k, and the excitation frequency, ω. You may assume a harmonic forcing function, $F_1 e^{i\omega t}$, is applied to coordinate X_1.
3. Use receptance coupling to rigidly join two free-free beams and find the free-free assembly's displacement-to-force tip receptance. Both steel cylinders are described by the following parameters: 12.7 mm diameter, 100 mm length, 200 GPa elastic modulus, and 7800 kg/m^3 density. Assume a solid damping factor of 0.0015. Once you have determined the assembly response, verify your

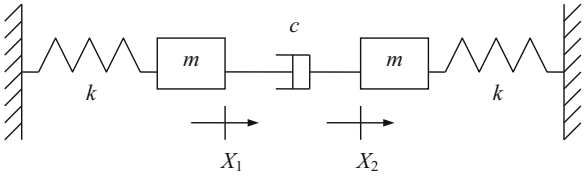

Fig. P10.1 Two degree of freedom assembly

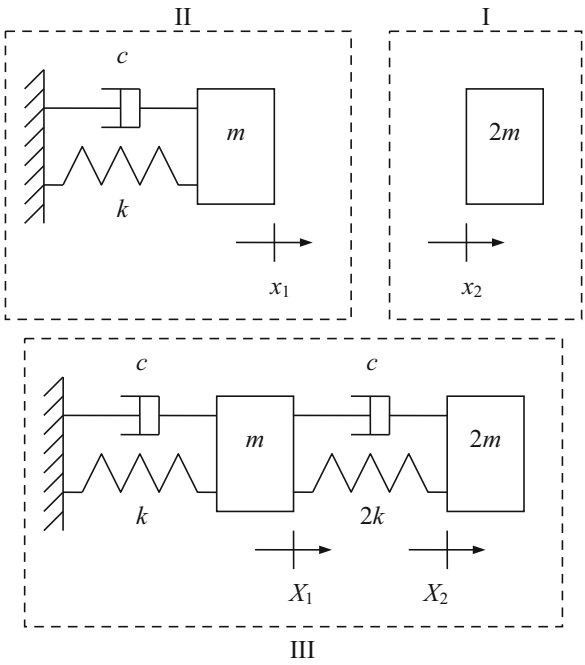

Fig. P10.2 Flexible damped coupling of mass (I) to spring-mass-damper (II) to form the two degree of freedom assembly III

result against the displacement-to-force tip receptance for a 12.7 mm diameter, 200 mm long free-free steel cylinder with the same material properties. Select a frequency range that encompasses the first three bending modes and display your results as the magnitude (in m/N) versus frequency (in Hz) using a semi-logarithmic scale.

4. Plot the displacement-to-force tip receptance for a sintered carbide cylinder with free-free boundary conditions. The beam is described by the following parameters: 19 mm diameter, 150 mm length, 550 GPa elastic modulus, and 15,000 kg/m^3 density. Assume a solid damping factor of 0.002. Select a frequency range that encompasses the first three bending modes and display your results as magnitude (m/N) vs. frequency (Hz) in a semi-logarithmic format.
5. Determine the fixed-free displacement-to-force tip receptance for a sintered carbide cylinder by coupling the free-free receptances to a rigid wall (with zero receptances). The beam is described by the following parameters: 19 mm diameter, 150 mm length, 550 GPa elastic modulus, and 15,000 kg/m^3 density. Assume a solid damping factor of 0.002. Select a frequency range that encompasses the first two bending modes and display your results as magnitude (m/N) vs. frequency (Hz) in a semi-logarithmic format. Verify your result by comparing it to the displacement-to-force tip receptance for a fixed-free beam with the same dimensions and material properties.

6. For a rigid coupling between two component coordinates x_{1a} and x_{1b}, the compatibility condition is _____.
7. For a flexible coupling (spring stiffness k) between two component coordinates x_{1a} and x_{1b}, the compatibility condition is _____. An external force is applied to the assembly at coordinate X_{1a}.
8. For a flexible-damped coupling (spring stiffness k and damping coefficient c) between two component coordinates x_{1a} and x_{1b}, the compatibility condition is _____. An external force is applied to the assembly at coordinate X_{1a}.
9. What are the units for the rotation-to-couple receptance, p_{ij}, used to describe the transverse vibration of beams?
10. What are the (identical) units for the displacement-to-couple, l_{ij}, and rotation-to-force, n_{ij}, receptances used to describe the transverse vibration of beams?

References

1. Bishop R, Johnson D (1960) The mechanics of vibration. Cambridge University Press, Cambridge
2. Weaver W Jr, Timoshenko S, Young D (1990) Vibration problems in engineering, 5th edn. Wiley, New York
3. Burns T, Schmitz T (2004) Receptance coupling study of tool-length dependent dynamic absorber effect. In: Proceedings of American Society of Mechanical Engineers International Mechanical Engineering Congress and Exposition, IMECE2004-60081, Anaheim, CA
4. Burns T, Schmitz T (2005) A study of linear joint and tool models in spindle-holder-tool receptance coupling. In: Proceedings of 2005 American Society of Mechanical Engineers International Design Engineering Technical Conferences and Computers and Information in Engineering Conference, DETC2005-85275, Long Beach, CA
5. Park S, Altintas Y, Movahhedy M (2003) Receptance coupling for end mills. Int J Mach Tools Manuf 43:889–896
6. Schmitz T, Powell K, Won D, Duncan GS, Sawyer WG, Ziegert J (2007) Shrink fit tool holder connection stiffness/damping modeling for frequency response prediction in milling. Int J Mach Tools Manuf 47(9):1368–1380
7. Duncan GS, Tummond M, Schmitz T (2005) An investigation of the dynamic absorber effect in high-speed machining. Int J Mach Tools Manuf 45:497–507

Appendix A: Beam Experimental Platform

The beam experimental platform (BEP) is used throughout the text to demonstrate various concepts in mechanical vibrations. The BEP is composed of a base plate, a holder, and a rod; see Fig. A.1. The base plate and holder are aluminum and can be machined using the dimensions provided in Fig. A.2. The rod is a 12.7 mm diameter, 152.5 mm long high-speed steel tool blank.

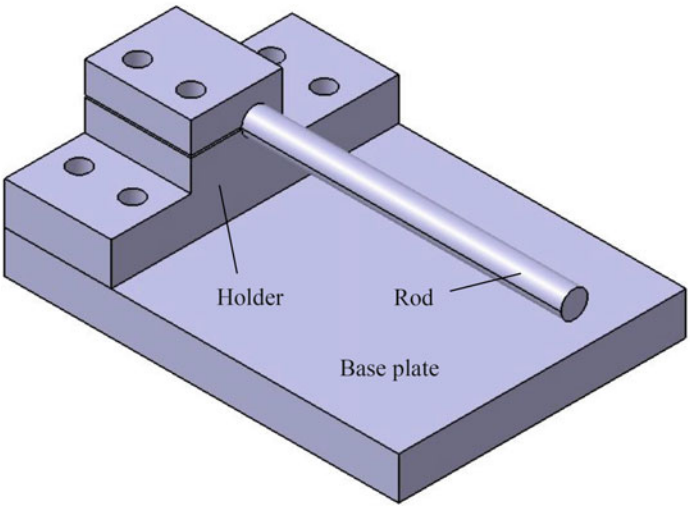

Fig. A.1 BEP components

T. L. Schmitz, K. S. Smith, *Mechanical Vibrations*,
https://doi.org/10.1007/978-3-030-52344-2

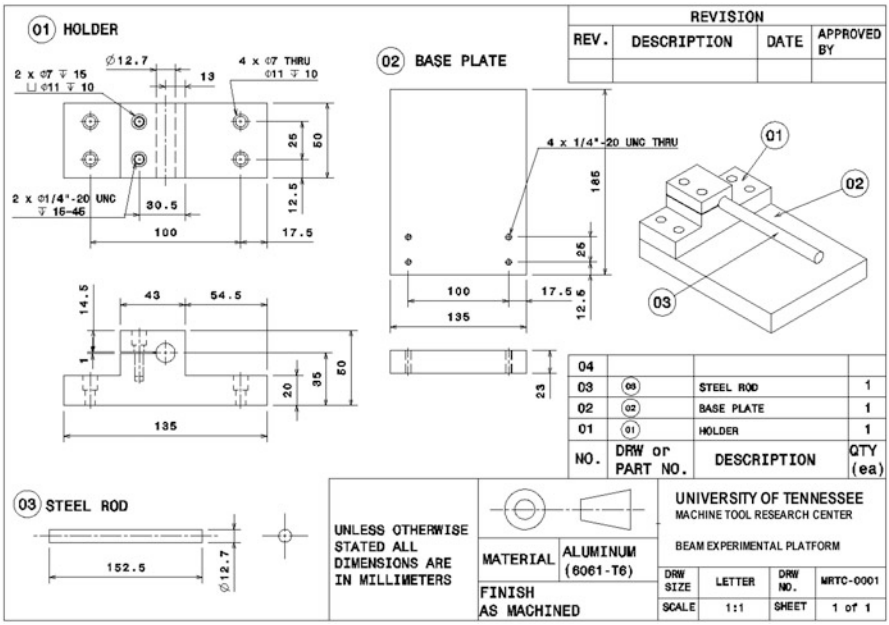

Fig. A.2 BEP dimensions

Appendix B: Orthogonality of Eigenvectors

The orthogonality of eigenvectors with respect to the system mass and stiffness matrices is the basis for modal analysis. In general, we can say that two vectors are perpendicular if their scalar, or dot, product is zero. Consider the two vectors:

$$[U] = \begin{Bmatrix} u_{11} \\ u_{21} \end{Bmatrix} \quad \text{and} \quad [V] = \begin{Bmatrix} v_{11} \\ v_{21} \end{Bmatrix} \tag{B.1}$$

Their dot product is:

$$[U] \cdot [V] = [U]^T [V] = \{u_{11} \;\; u_{21}\} \begin{Bmatrix} v_{11} \\ v_{21} \end{Bmatrix} = u_{11} v_{11} + u_{21} v_{21}. \tag{B.2}$$

This product is zero if the vectors are perpendicular. Orthogonality can be considered a generalization of the concept of perpendicularity.

From Chap. 4, we have seen that we can write the matrix form of the system equations of motion $([m]s^2 + [k])\left\{\vec{X}\right\}e^{st} = \{0\}$ if we assume harmonic vibration. We used the characteristic equation, $|[m]s^2 + [k]| = 0$, to find the eigenvalues, ${s_1}^2$ and ${s_2}^2$. We then substituted the eigenvalues into either of the linearly dependent equations of motion to find the eigenvectors, or mode shapes. Using ${s_1}^2 = -{\omega_{n1}}^2$, we can write:

$$\left(-[m]{\omega_{n1}}^2 + [k]\right)\{\psi_1\} = \{0\}, \tag{B.3}$$

where ψ_1 is the corresponding mode shape. Equation B.3 can be expanded to:

$$-{\omega_{n1}}^2[m]\{\psi_1\} + [k]\{\psi_1\} = \{0\}. \tag{B.4}$$

T. L. Schmitz, K. S. Smith, *Mechanical Vibrations*,
https://doi.org/10.1007/978-3-030-52344-2

Premultiplying Eq. B.4 by the transpose of the second mode shape ψ_2, which corresponds to vibration at ω_{n2}, yields:

$$-{\omega_{n1}}^2\{\psi_2\}^T[m]\{\psi_1\} + \{\psi_2\}^T[k]\{\psi_1\} = 0. \tag{B.5}$$

Performing the transpose operation on Eq. B.5 gives:

$$-{\omega_{n1}}^2\{\psi_1\}^T[m]\{\psi_2\} + \{\psi_1\}^T[k]\{\psi_2\} = 0, \tag{B.6}$$

where the transpose properties $([A][B])^T = [B]^T[A]^T$ and $([A]^T)^T = [A]$ (using matrices of appropriate dimensions) have been applied.

Completing the same operations using ${s_2}^2 = -{\omega_{n2}}^2$ gives:

$$-{\omega_{n2}}^2\{\psi_1\}^T[m]\{\psi_2\} + \{\psi_1\}^T[k]\{\psi_2\} = 0. \tag{B.7}$$

Taking the difference of Eqs. B.6 and B.7 yields:

$$\left({\omega_{n2}}^2 - {\omega_{n1}}^2\right)\{\psi_1\}^T[m]\{\psi_2\} = 0. \tag{B.8}$$

Provided ${\omega_{n2}}^2 \neq {\omega_{n1}}^2$, then $\{\psi_1\}^T[m]\{\psi_2\} = 0$. Substituting this result into either Eq. B.6 or Eq. B.7 gives $\{\psi_1\}^T[k]\{\psi_2\} = 0$. Collecting these results, we obtain the orthogonality conditions shown in Eqs. B.9–B.12, where the products in Eqs. B.10 and B.12 are not necessarily zero.

$$\begin{aligned}\{\psi_1\}^T[m]\{\psi_2\} &= 0\\ \{\psi_2\}^T[m]\{\psi_1\} &= 0\end{aligned} \tag{B.9}$$

$$\begin{aligned}\{\psi_1\}^T[m]\{\psi_1\} &= m_{q1}\\ \{\psi_2\}^T[m]\{\psi_2\} &= m_{q2}\end{aligned} \tag{B.10}$$

$$\begin{aligned}\{\psi_1\}^T[k]\{\psi_2\} &= 0\\ \{\psi_2\}^T[k]\{\psi_1\} &= 0\end{aligned} \tag{B.11}$$

$$\begin{aligned}\{\psi_1\}^T[k]\{\psi_1\} &= k_{q1}\\ \{\psi_2\}^T[k]\{\psi_2\} &= k_{q2}\end{aligned} \tag{B.12}$$

Using the modal matrix, $[P] = [\psi_1 \quad \psi_2]$, and the orthogonality conditions we obtain the diagonalized modal mass and stiffness matrices:

$$[P]^T[m][P] = \begin{bmatrix} \{\psi_1\}^T[m]\{\psi_1\} & \{\psi_1\}^T[m]\{\psi_2\} \\ \{\psi_2\}^T[m]\{\psi_1\} & \{\psi_2\}^T[m]\{\psi_2\} \end{bmatrix} = \begin{bmatrix} m_{q1} & 0 \\ 0 & m_{q2} \end{bmatrix} = \begin{bmatrix} m_q \end{bmatrix} \tag{B.13}$$

and

$$[P]^T[k][P] = \begin{bmatrix} \{\psi_1\}^T[k]\{\psi_1\} & \{\psi_1\}^T[k]\{\psi_2\} \\ \{\psi_2\}^T[k]\{\psi_1\} & \{\psi_2\}^T[k]\{\psi_2\} \end{bmatrix} = \begin{bmatrix} k_{q1} & 0 \\ 0 & k_{q2} \end{bmatrix} = \begin{bmatrix} k_q \end{bmatrix}. \tag{B.14}$$

These diagonal modal mass and stiffness matrices uncouple the equations of motion and enable the solution of independent single degree of freedom systems in modal coordinates. The individual modal contributions can then be transformed back into local (model) coordinates as discussed in Chap. 4.

Index

T. L. Schmitz, K. S. Smith, *Mechanical Vibrations*,
https://doi.org/10.1007/978-3-030-52344-2